Effects of rainfall event characteristics and vegetation regeneration on post-fire hillslope erosion

by

Alexis Lee-Hin Pang

Master of Science (Merit)

A thesis submitted for the degree of Doctor of Philosophy at

Monash University in 2019

School of Earth, Atmosphere and Environment

Faculty of Science, Monash University

ACKNOWLEDGEMENTS

I wish to acknowledge my supervisors, without whom I would not have been able to complete this PhD journey: Associate Professor David Dunkerley, Dr. Xuan Zhu and Dr. Dushmanta Dutta.

David, I cannot thank you enough for your unending patience, perseverance and understanding towards me. Thanks for bringing your wisdom, knowledge and experience to advise me on my research journey, while giving me the freedom to explore and experiment, learn and develop. You are just brilliant, and I can only hope to be like you some day.

Xuan, thank you for always being so friendly, encouraging and supportive throughout my candidature. Dushmanta, thank you for initially taking me on as your PhD student to start me on my PhD journey.

I would also like to thank Dr. Tony Weatherley, my work supervisor at the University of Melbourne. Tony, thank you for your generous support and flexibility with time while I completed this thesis on a part-time basis.

For permission to conduct the field research at the Alpine National Park, I would like to acknowledge the former Department of Sustainability and Environment (DSE) (now the Department of Environment, Land, Water and Planning - DELWP) with the support of Parks Victoria for granting the Research Permit No. 10005900 under the National Parks Act 1975.

I have also been blessed by my family members who helped me stay sane and focused on completing my PhD. To Sharon, my wonderful wife, your love and unwavering support kept me motivated on this long, arduous journey for all of us. Thanks for always taking care of things at home while I worked on my thesis, and ensuring that I was always well-nourished. To my sons Asher and Callum, your love and exuberance have always refreshed me, and filled me with joy and pride, keeping me going.

To my mum, Ng Chai Lan, you have always supported my academic endeavours. The completion of this thesis is certainly one of the fruits of your selfless love, support and encouragement all through the years.

To my mother-in-law, Loh Tick Choo, thank you too for your help and support that has at many times been given quietly behind the scenes, but also very valuable to me.

Finally, I thank God for the multitude of blessings I have received in the various forms of people, places, opportunities and experiences; the spiritual sustenance during the difficult times, and the opportunity to study the beautiful complexity of nature.

To God be the Glory

In loving memory of

Pang Lye Teck

(1939 – 2002)

Thanks Dad, for everything

ABSTRACT

In southeast Australia, exacerbated hillslope soil erosion rates immediately following severe wildfires in dry eucalypt forests cause widespread environmental and human impacts. The post-fire vegetation regeneration that follows brings these landscapes into *intermediate* conditions (nominally five to seven years post-fire) where substantial but incomplete recovery of the "original" plant canopy, mid and ground-strata has occurred. Furthermore, heterophylly of many eucalypt species imply that juvenile, post-fire foliage could modulate rainfall differently from mature, climax-stage (long-unburnt) foliage. Compared to the short-term (i.e. zero to two years post-fire) timeframe, little is known about the operation of hillslope hydrological and geomorphological processes under intermediate conditions.

This PhD research sought to examine, with a fresh perspective, the complex interactions of climate, rainfall, vegetation, terrain and soil factors, and consequent hillslope erosion processes under intermediate post-fire conditions, through a case study of a hillslope in the Licola region, southeast Australia that was severely burnt in the 2006/7 Great Divide Fires. The main questions driving the research were: (i) How do inter and intra-event rainfall characteristics influence hillslope erosion processes in the study area? (ii) How does intermediate post-fire dry-sclerophyll forest modulate rainfall vis-à-vis open-field rainfall, and what are the resultant impacts on throughfall fraction and throughfall splash erosion? (iii) What are the composite impacts of rainfall and post-fire vegetation factors on hillslope sediment and litter fluxes?

Field data was collected in six measurement periods (denoted A to F) spanning ten months across different seasons in 2012, within which rainfall, splash erosion, throughfall and hillslope erosion rates were simultaneously monitored. High temporal resolution rainfall data from standard tipping-bucket raingauges were acquired and analyzed. Sand-filled splash

cups were deployed to measure and compare splash energy between open-field and under-canopy conditions. Throughfall Integrating Funnels (TIFs) were used to compare open-field and under-canopy water volumes and determine throughfall fractions. Six unbounded sediment fences (SFs) were installed to quantify the resultant rates of litter, gravel and soil erosion, composing the gross hillslope material fluxes. Laboratory experiments were undertaken to elucidate detailed on-leaf dynamics of water drops to uncover the differences in drop-size distributions between juvenile (orbicular shaped) and mature (ovate-lanceolate shaped) foliage of *Eucalyptus polyanthemos*, and with those of open-field rainfall.

Analysis of rainfall events found that Periods A (summer), B (autumn) and F (late-spring) had the most intra-event high-intensity episodes (e.g. ≥ 20 mm h^{-1}) at 22, 20 and 9 minutes that could have contributed significantly to the overall hillslope erosion rates. Periods A and F displayed day:night event start time ratios of 4.60 and 2.83 respectively, indicating the dominance of convection-related rainfall generation mechanisms as well as suggesting possible abstraction of erosive energies through intra-event evaporative losses.

Throughfall fractions varied from 0.60 (Period E, late winter to spring) to 0.91 (Period D, winter) with a value of 1.17 recorded for Period F that may have resulted from "canopy funnelling" effects. Throughfall:rainfall erosivity ratios ranged from 1.34 (Period D) to 2.04 (Period C, late autumn to winter), showing how intermediate post-fire eucalypt canopy enhanced drop erosivity through rainfall modulation processes. Laboratory studies showed how different on-leaf water dynamics between juvenile and mature leaf shapes generated distinct drop-size distributions (DSDs) with median drop-sizes of 3.81 mm and 4.16 mm respectively.

Average sediment flux rate per metre contour per mm of rainfall was 2.2 g soil m^{-1} mm^{-1} rainfall. Overall rainfall erosion rate (mass of soil eroded in grams per mm of primitive-event rainfall) was 19.6 g mm^{-1}. Periods A and F had the highest erosion rates (35.4 and 27.7

g mm^{-1} respectively). Period E had the most muted erosion rates at 12.2 g mm^{-1}. Erosion responses to different one-minute rainfall intensity thresholds varied with individual sediment fences. SFs 1 and 2 had strongest soil erosion response to the 5 mm h^{-1} threshold. In contrast, SFs 3 and 4 responded best at 40 mm h^{-1}, and SFs 5 and 6 responded optimally at 10 mm h^{-1} and 20 mm h^{-1} respectively. The findings from this research provide a useful set of baseline data to which future studies on various soils and landscapes, altered vegetation structures and compositions, and changing regional climatic conditions, could be compared.

In addition to the empirical work, this research contributed conceptual developments for post-fire erosion science in the forms of: (i) alternative post-fire recovery trajectories; (ii) anisotropic patterns of post-fire vegetation recovery, hydrology and erosion on steep terrain in the context of connectivity theory; and (iii) Dynamic Zones of Influence (DZI) framework which incorporates spatio-temporal variations in throughfall at the individual plant (under-canopy) and hillslope (inter-canopy) scales. This case study has also contributed more broadly to the domains of biogeomorphology and ecohydrology.

Future research directions include: (i) multi-year, multi-site monitoring studies to account for broad-scale spatio-temporal variability; (ii) further examination of the temporal structures of rainfall and throughfall and their hydrological and erosional consequences; (iii) the dynamic effects of wind on canopy interception and modulation of rainfall; (iv) studying on-leaf water dynamics of a wider range of leaves from different *Eucalypt* (e.g. *E. melliodora* and *E. macrorhyncha*) and non-*Eucalypt* (e.g. *Acacia melanoxylon*) species; (v) investigating the effects of various root features, as well as tree throw, on hillslope processes and evolution; (vi) computer-based modelling work; and (vii) controlled laboratory experiments for the various hillslope processes under consideration.

Declaration

This thesis contains no material which has been accepted for the award of any other degree or diploma at any university or equivalent institution and that, to the best of my knowledge and belief, this thesis contains no material previously published or written by another person, except where due reference is made in the text of the thesis.

Signature:

Name: ALEXIS LEE-HIN PANG

Date: 31 MARCH 2019

TABLE OF CONTENTS

LIST OF FIGURES

LIST OF TABLES

LIST OF PLATES

OUTLINE OF THESIS

This thesis presents a field-based study of post-fire hillslope erosion dynamics operating in the intermediate (5 – 10 years) post-fire period where substantial but incomplete vegetation regeneration has occurred. The structure of the thesis is as follows:

Chapter One: Introduction

This chapter outlines the research by presenting the aims and rationale of the study, followed by the key research gaps, context of the study and theoretical framework. These address the need for post-fire erosion science to develop more detailed understanding of rainfall-canopy interactions and their consequential geomorphological and hydrological effects of the resultant splash and runoff erosion. The research questions driving the work in this thesis are presented with reference to the discussed research gaps. The scope and limitations of the present study are also briefly discussed. The main hypotheses are: (i) post-fire hillslope erosion still active in intermediate recovery (5 – 10 years postfire) phase; (ii) post-fire hillslope erosion dynamics are distinctive from those operating in the immediate post-fire period because of unique rainfall-canopy interactions; (iii) rainfall event variations are a major factor controlling intermediate post-fire erosion; (iv) intermediate eucalypt canopies dominated by juvenile leaf forms have distinctive drop-size spectra compared to mature leaf forms and open rainfall. The examination of (i) to (iv) will focus on their implications on our current understanding of post-fire hillslope splash and runoff processes under intermediate conditions and contribute to theoretical development in hillslope geomorphology and hydrology.

Chapter Two: Literature Review

This chapter presents a review of post-fire erosion in key regions of the world such as the western United States, the Mediterranean and southeast Australia. This is followed by a discussion of the salient gaps in post-fire erosion research that may be found across or

specific to individual regions. Theoretical connections relevant to post-fire erosion are also established and developed. The main argument of the literature review is the growing need to study the dynamics and change trajectories of hillslope hydrological and geomorphological processes in the period 5 to 10 years post-fire. In dry eucalypt forests, the process dynamics are mainly controlled by the variable combinations and characteristics of individual vegetation strata (canopy, mid-stratum, shrub and ground levels) ground litter cover and soil surfaces. These do not all recover at the same rate, nor do they necessarily recover in the same direction. This means that post-fire erosion rates, even when they decrease as vegetation "recovery" occurs, are the result of factor interactions across several vegetation layers that are more complex than may be commonly perceived. Hence, the Dynamic Zones of Interaction (DZI) framework is introduced to integrate and explain the spatio-temporal complexity of these post-fire processes on hillslopes.

Chapter Three: Site description

Detailed description of the study area, site location and characteristics, including information on the climate, weather, soils, geology, topography and vegetation, and post-fire regional and on-site observations is provided. The site was distinctive in the study of post-fire erosion in that even though there had been substantial recovery of eucalypt forest canopy and ground litter cover in some instances, much of the soil surface remained bare and vulnerable to erosion by splash and surface runoff. Furthermore, the juvenile eucalyptus foliage dominated canopy of post-fire regrowth, the thin, gravelly and highly erodible sandy loam soils and the steep terrain of the area, presented good opportunities to contribute new knowledge about intermediate post-fire erosion conditions and processes that would be generalizable to regions with similar soil, vegetation, topography and climate.

Chapter Four: Methodology

This chapter describes and discusses the research approach accompanied by the methodologies applied. The field research apparatus and layout are also described. The main intention was to measure hillslope material (sediment and organic litter) flux simultaneously with rainfall characteristics, throughfall fractions and splash erosion. This involved the setup of six sediment fences (SFs), installation of twenty throughfall integrating funnels (TIFs), twenty sand-filled splash cups and one tipping-bucket pluviometer. Complementing these field measurements was a series of laboratory experiments that developed a low-cost dyed filter paper technique for the measurement of drop sizes, and then examined differences in drop-size distributions (DSD) between juvenile and mature *Eucalyptus polyanthemos* leaves. This served to provide further insights into how intermediate post-fire vegetation canopies modulate rainfall, generate distinct DSDs and subsequently influence splash and runoff erosional processes on hillslopes. Chapters Five, Six and Seven then follow, presenting the results and analyses for rainfall, throughfall effects due to canopy modulation, and then finally hillslope materials respectively. These have been arranged to follow the logical order of hillslope hydrological and erosional processes.

Chapter Five: Rainfall

Rainfall drives hillslope erosion both directly and indirectly (via canopy hydrological partitioning and modulation). Thus, careful, detailed measurement of rainfall characteristics is needed to reveal the complexities of hillslope erosion processes, particularly under intermediate post-fire conditions. This chapter describes the methodologies involved in the collection and processing of rainfall data for the study site. Following this, data such as rainfall depth and intensity metrics, experienced by the study site are examined in detail, in view of the importance of rainfall as the main driving factor for canopy processes, hillslope hydrology and erosion. Recent advancements in rainfall measurement, erosion modelling, rainfall simulation experiments and field observations have pointed to the centrality of storm structure in influencing hillslope hydrology and erosion; it is also highly likely that canopy interception and modulation processes and effects would vary as well, especially in forests. To enable the analyses of storm structures, high temporal resolution data are essential.

Chapter Six: Throughfall

Plant canopies partly transform rainfall into throughfall, and the resultant sub-canopy hydrology and geomorphological processes cause soil, organic matter and litter changes, and plant growth processes. Because post-fire "recovery" is primarily vegetation re-growth and establishment of new plant canopies and strata, throughfall processes and effects have to be examined in addition to rainfall characteristics discussed in Chapter Five. This chapter describes the methodologies for the collection, processing and analysis of throughfall data. The results for throughfall fraction and erosivity are presented and analyzed with respect to the rainfall metrics presented in Chapter Five. The examination of throughfall processes is extended by the description and discussion of drop-size spectra generated by juvenile and mature *Eucalyptus polyanthemos* leaves.

Chapter Seven: Hillslope material flux

Hillslope erosion has been a major problem in the field area in the post-fire period (see Chapter Three). While substantial vegetation recovery would have occurred by the intermediate post-fire phase, active downslope movement of sediments and litter would still occur, albeit under conditions more complex than the immediate post-fire phase, due to the dynamic interplay between open, exposed patches, rainfall modulation by the partial plant canopy, the under-canopy soil and litter patches, and the wide range of rainfall events; DZIs (see Chapter Two). Chapter Seven presents the methodologies, results and analysis for the characteristics of sediment erosion and litter movements at the study hillslope. The results are analysed and discussed in light of the rainfall characteristics and throughfall dynamics presented in the Chapters Five and Six.

Chapter Eight: Conclusion

In this chapter, the complex dynamics of post-fire hillslope processes under intermediate vegetation recovery are discussed with reference to the findings presented across the chapters on rainfall, throughfall and sediments. An integrated discussion is presented to consider the dislodgement and transport of hillslope sediments in these conditions, with considerations of how hillslope hydrology is influenced by vegetation regeneration. This will be done by integrating the DZI concept presented in Chapter Two. Canopy modulation of rainfall mediates the volumes and rates of water reaching the ground (soil and litter) surface with the modulating effects expanding with the canopy zonal growth. The interspaces become sites of active runoff-runon depending on ground cover conditions, and the resultant anisotropy and asymmetry of impacts on sloping land are important considerations. The threshold rainfall intensities required to entrain and transport sediment and litter would generally increase at the broader annual timescale, but also interact with the local soil availability and erodibility, ground cover and surface conditions, canopy conditions and upslope vegetation and soils

processes. The upslope-facing, under-canopy patches of sediment and litter accumulation cause heightened infiltration leading to positive feedback to support plant growth. In parallel, the under-canopy micrometeorological conditions shift from very exposed in the immediate post-fire period, to semi-sheltered conditions in the intermediate post-fire situation (e.g. 5 to 10 years after fire), and then onwards to a quasi-equilibrium state. Important links of this research to the literature on post-fire erosion science, and closely-related discipline areas such as biogeomorphology and ecohydrology, are established.

In the final section, the key findings and conceptual development of the research are highlighted. The avenues of investigation in this line of research are by no means exhausted. The limitations of this research are discussed, and important future research directions for post-fire erosion science, especially in the light of projected global and regional (i.e. southeast Australian) climate changes, are identified.

CHAPTER ONE: INTRODUCTION

1.1. Aims and objectives of research

The overall aim of this research was to investigate and contribute knowledge on post-fire hillslope hydro-geomorphic processes operating in intermediate, regenerating dry sclerophyll forests in southeast Australia. The intermediate phase examined in this research refers broadly to the seral stages of vegetation succession where vegetation regrowth at one or more strata has occurred substantially but is still incomplete – usually five to ten years after fire occurrence (DeBano et al., 1998). Thus far, there has been a paucity of work done to examine the hydrological and geomorphic factors and processes occurring in this complex, transitional post-fire phase. Dry eucalypt forests have unique post-fire seral stage vegetation structures and assemblages due to their fire-adapted and resilient physiological characteristics and reproductive strategies (Clarke et al., 2015). They therefore have interestingly distinct eco-hydrological relationships (Bowman and Boggs, 2006) that differ noticeably from those that operate in other fire-prone parts of the world such as the Mediterranean (Shakesby, 2011) and the western United States (Williams et al., 2014). This research conducted a case study of a representative intermediate post-fire dry sclerophyll eucalypt forest hillslope site, focusing on key processes of: (a) rainfall event characteristics driving hillslope processes; (b) vegetation effects of the recovering canopy modulating rainfall; and (c) hillslope sediment and litter fluxes resulting from the interaction of rainfall and vegetation factors. The main objective of this research was therefore to develop vignettes into the factors and functioning of these key processes to enable better understanding of post-fire erosion five years after severe fire where intermediate vegetation conditions dominate.

1.2. Background and related research gaps

1.2.1. Effects of plant canopies on slope processes

The primary impact of wildfires on forests is the damage to and destruction of plant biomass, especially leaves and twigs, and organic litter at the mineral soil surface. This is due to the fuels consumed in the combustion process and the high radiant heat generated causing damage to plant parts through thermolysis. Tree mortality may also occur at various spatial extents. Where fires have been particularly severe, plant canopies of the dominant and substrata can be completely removed in the immediate post-fire period, after which recovery over the ensuing months and years would commence from "zero". In this section, we shall briefly consider how plant canopies affect the operation of hillslope hydrological and erosion processes. Plant canopies perform important mediating roles in the hydrological balance and partitioning at the hillslope scale, and subsequent operation of any erosional agents and processes. This is primarily done through the process of interception when precipitation (normally rainfall) arrives at, and encounters, the plant canopy. This then leads to the hydrological partitioning of water into storage on plant parts (leaves, branches and stems) and flows such as stemflow (Crockford and Richardson, 2000; Dunkerley, 2014a; Dunkerley, 2014b). Losses from the canopy back to the atmosphere through evaporation can be substantial (Dunkerley, 2008c). Water drops exiting leaves (leaf drip) and other plant parts (branch drip) (Herwitz, 1987) descend as released throughfall (Dunkerley, 2010a; Geddes and Dunkerley, 1999), usually when canopy storage is exceeded. Free throughfall is un-intercepted precipitation falling through gaps in the plant canopy (Nanko et al., 2006). Hence, throughfall is a composite of the free and released throughfall components. Even though interception is an essential ecohydrological process, it remains one of the most underestimated and understudied processes of the hydrological cycle (Tsiko et al., 2012). Notably, it has been demonstrated that eucalypt species (e.g. *Eucalyptus macrorhyncha*) in

dry sclerophyll forests in southeast Australia have a distinctly lower interception (11.4% of total rainfall) and maximum canopy storage capacity (0.39 mm) compared to pine plantations (18.3% of total rainfall intercepted; maximum canopy storage capacity 2.0 mm) (Crockford and Richardson, 1990a; Crockford and Richardson, 1990b; Crockford and Richardson, 1990c; Crockford and Richardson, 1990d). For southeast Australian wet sclerophyll forests dominated by *Eucalyptus regnans F. Mueller,* Vertessy et al. (1996) estimated cumulative throughfall at 86.5% of gross rainfall over 17.5 years. Differences in interception rates, canopy storage and throughfall fractions between different plant canopies help to explain why Feller (1981) found that wet sclerophyll (*E. regnans*) forests had highest streamflows compared to dry sclerophyll (*E. obliqua*) forests and pine (*Pinus radiata*) plantations (lowest streamflow, highest interception losses). For the wet tropical rainforests of northern Queensland, McJannet et al. (2007) reported interception losses of 19-20%, 24-27% and 6% for lowland rainforests, lower montane and upper montane forests respectively.

In north Asia, Toba and Ohta (2005) found that Siberian boreal forests had higher interception ratios (0.2 to 0.3) compared to Japanese coniferous (0.15) and broadleaf (0.2) forests, even though the plant area index (PAI) for the Japanese forests was higher. These differences were attributed to the higher-order influence of meteorological conditions. On the other hand, Li et al. (2016) demonstrated the importance of both leaf and branch characteristics in explaining the distinctive canopy interception characteristics between young broadleaf and needle tree species in Northern China. Whelan and Anderson (1996) found that throughfall of Norway spruce (*Picea abies*) plantation in southwest England ranged between 33.3% and 61% across six measurement periods between Dec 1994 and Feb 1995. For savannah vegetation in Zimbabwe, Africa, Tsiko et al. (2012) reported average canopy interception at 25% of total rainfall with an additional 12% contributed at the forest floor due to interception by ground-level vegetation (Thatching grass) and leaf litter.

Plant canopies not only influence the volume of water that arrives at the ground surface; they also modify the rates and drop sizes of water arriving through and via the canopy, resulting in various possible *throughfall spectra* (distinct drop-size distributions) depending on the rainfall event characteristics (e.g. depth, duration, intensity) and the plant genera, species and growth stages (Pypker et al., 2005; Pypker et al., 2011). Spatial and temporal variations of throughfall spectra have also been recently demonstrated (Mululo Sato et al., 2011; Nanko et al., 2016a). Throughfall spectra variations caused by the abovementioned factors have been found to exert significant controls on splash erosion processes on hillslope surfaces (Bouten et al., 1992; Brandt, 1989; Calder, 2001; Geißler et al., 2012a; Geißler et al., 2012b; Nanko et al., 2008; Nanko et al., 2011; Staelens et al., 2006; Vis, 1986; Wakiyama et al., 2010; Zimmermann et al., 2007). All the eucalypt forests cited thus far were likely to have been characterized by mature foliage forms, being long undisturbed by wildfires. In this research, the throughfall spectra of differentially-shaped juvenile and mature leaves of a common Eucalyptus species in dry sclerophyll forest are examined, and their possible impacts on post-fire erosion is discussed; there has been no known previous work on this topic.

Reduction of rainfall volumes, distribution and dissipation of raindrop energy by plant canopies have been found to be instrumental in controlling soil erosion rates. Their destruction or removal frequently leads to abrupt increases in erosion rates by several orders of magnitude from the vegetated "normal" (Williams et al., 2014). Furthermore, the 'hydrologic vulnerability' of landscapes has be conceptualized as the integrated outcome of the relative dominance and spatial arrangements of hydrologically "stable" canopy areas and vulnerable inter-canopy areas; and the connectivity of these landscape elements (Pierson et al., 2010), although it could be argued that under-canopy spaces can also be hydrologically "vulnerable". Therefore, the destruction of plant canopies and other vegetation strata by

moderate to severe wildfires radically reduces the canopy interception processes that would normally mitigate against direct rainfall impacts on bare soil surfaces, causing heightened hydrologic and erosional vulnerability (Pierson et al., 2010). It should however be highlighted that much post-fire erosion research has focused on the prominently heightened erosion rates typically observed in the first few years after fire, and insufficient work has been done on the canopy effects of post-fire intermediate-stage vegetation on hillslope hydrology and erosion.

1.2.2. Wildfire impacts on soils, hydrology and erosion

Wildfires have long been recognized as a distinct and significant hydrological and geomorphic agent (Shakesby and Doerr, 2006) which can have sudden and enduring impacts on the soil, ecology, microclimate and hydrology of the catchments in which they occur (Certini, 2005). It should be recognized however that wildfires play an instrumental role in the natural operation of ecological systems, for example in plant communities such as *Eucalyptus regnans* dominant wet sclerophyll forests of southeast Australia, where fire-induced seed-fall and germination on suitably bare ash-beds are essential for successful population rejuvenation (Ashton and Chinner, 1999; McCarthy et al., 1999) or soil microbial communities of Mediterranean forest soils (Rodríguez et al., 2017). Severe fires cause substantial or complete defoliation and mortality of vegetation; they also alter soil physical, chemical and biological properties and result in distinct and accelerated operation of hillslope hydrological and erosional processes. Direct and indirect effects include: (i) sudden and increased exposure to rainsplash erosion due to burning of protective vegetation and litter cover at most or all levels of the vegetation structure (Prosser and Williams, 1998); (ii) increased overland flow erosion due to increased surface smoothness and connectivity with the loss of ground-level vegetation and litter (Shakesby and Doerr, 2006); (iii) development of surface or subsurface soil hydrophobicity leading to reduced surface or subsurface

11

infiltration rates and capacities, and higher rates of overland flow (DeBano, 2000; Doerr et al., 2004); (iv) development of soil surface seals due to structural change from raindrop impacts or deposition of ash and fine material clogging soil pores of the topsoil (Larsen et al., 2009) although this can rapidly change over months with successive rainfall events and coupled with quick recovery of ground-level vegetation (Onda et al., 2008) Where moderate to severe fires have occurred, the fire-affected soil surfaces suddenly become exposed to direct solar radiation, rainfall and wind. This disruptive shift from the vegetated pre-fire conditions renders soil surfaces highly vulnerable to erosion by water in the immediate and intermediate post-fire periods. Meteorological conditions at the micro, local and regional scales are also altered in part due to decreased albedo, heightened sensible heat flux and evaporative water losses (Gleason and Nolin, 2016) and hence affect the patterns, processes and rates of post-fire ecological recovery (Meng et al., 2015).

Despite widespread recognition of the significant impacts of wildfires on hydrology and erosion (Prosser and Williams, 1998), the recent expansion of post-fire erosion research has revealed much variability and non-linearity in post-fire erosion and hydrologic responses due to complex interactions between the heterogeneous alterations made to land surfaces and environmental factors (Shakesby and Doerr, 2006). Indeed, Shakesby (2013) has encouraged researchers to critically evaluate twenty-five years' worth of 'established truths' to drive renewed work on understanding and predicting post-fire erosion. Furthermore, unique hydro-climatic, geomorphic and ecological contexts of fire-prone regions around the world necessitate the treatment of these regions and their sub-regions as distinct species of a common environmental perturbation (Moody et al., 2013; Shakesby, 2013; Shakesby et al., 2007). Work done in these regions (southeast Australia, the Mediterranean and western United States) is reviewed in Chapter Two.

Southeastern Australia is considered to be one of the most fire-prone regions of the world (Bureau of Meteorology, 2010) alongside the western United States and the Mediterranean. In the past 15 years, three major wildfires have occurred in southeast Australia: (i) the 2003 Eastern Victorian (Alpine) fires which burnt approximately 1.3 million ha of land, most of which were parks and forest; (ii) the 2006-2007 Great Divide (North and South) fires which burnt approximately 1 million ha of public land; and (iii) the 2009 'Black Saturday' fires which saw close to 430,000 ha of land directly affected, and with 173 lives lost with severe damage or disruptions to almost 78 communities in the region (Department of Sustainability and Environment, 2009). This high-frequency and severity fire regime applicable at the regional scale means that many parts of the landscape are vulnerable to severe erosion at the decadal scale. This heightened vulnerability is likely to be sustained for long durations of perhaps 10 years or more, if areas sustain repeated fires before full vegetation recovery is achieved even where rapid post-fire regrowth typical of many fire-adapted plants of the dry eucalypt forests of southeast Australia, occur. For instance, Leitch et al. (1983) studied post-fire erosion and nutrient losses in the Warburton region of Victoria after the 1983 Ash Wednesday fires and suggested the likelihood of dry sclerophyll forests remaining in a highly erosive state for several months or even longer due to the erosion-related retardation of vegetation recovery associated with diminished soil fertility, exacerbating fertility gradients and vegetation distribution differences between ridge and gully sites in the landscape.

It has been commonly suggested that southeast Australian eucalypt forests have a distinctive resilience enabled by largely innate ecological factors that contribute to rapid reductions in post-fire erosion rates vis-à-vis observed rates in other regions in the world. This is mainly attributed to the rapid re-growth of fire-tolerant plants of the *Eucalyptus* genus, the widespread development of litter dam-microterrace complexes and high levels of

13

bioturbation activity, even in relatively short time periods after fire (Shakesby et al., 2007). However, this is likely to be applicable in rather specific conditions and at limited scales, and negligible at the broader landscape scale. Therefore, a larger volume of evidence through further regionally-specific research is needed for conclusions to be made across such a wide variety of vegetation formations, topographical conditions, pedological characteristics and hydro-climatic contexts. Litter dam-microterrace complexes may not readily form in steep terrain where material can be readily transported downslope; these may be further limited where few microtopographic depressions or fallen logs exist to create initial trapping of litter, and where plant damage by severe fires severely limit the supply of fresh litter to constitute any significant accumulations dependent on positive feedback processes. Cross-scale considerations also apply because rapid declines measured at the coarse catchment scale do not necessarily mean minimal hillslope erosion rates. Sediment and litter may be temporarily detained behind barriers (e.g. stems of trees and shrubs or exposed rocks/boulders) along the hillslopes. Furthermore, post-fire regeneration processes and concomitant changes in erosion rates within this region need to be studied in the varying contexts of the major vegetation formations such as wet and dry sclerophyll forests, woodlands and shrublands, and their sub-formations. For example, key wet sclerophyll species such as *Eucalyptus regnans* (Mountain Ash) are obligate seeders while dry sclerophyll species such as *Eucalyptus polyanthemos* (Red Box) and *Eucalyptus melliodora* (Yellow Box) are facultative resprouters (Clarke et al., 2015; Pausas and Keeley, 2014).

Previous studies conducted in southeast Australia on post-fire hydrological and erosional responses have provided some useful insights into the variable and heterogeneous responses of catchments in terms of water yield, sediment and solute movements, and stream water quality (Doerr et al., 2004; Lane et al., 2007; Nyman et al., 2011; Shakesby et al., 2003; Shakesby et al., 2007; Smith and Dragovich, 2008; Smith et al., 2011; Tomkins et al., 2008;

14

Townsend and Douglas, 2004). However, the picture is far from complete and several knowledge gaps remain. The preponderance of catchment-scale studies has meant a paucity of research at the hillslope and plot scales examining processes, interactions and effects of detailed rainfall characteristics and vegetation regeneration during the intervening intermediate recovery time period (5 to 10 years) between the immediate and short-term (0 to 2 years) and complete recovery (10 to 15 or more years) timeframes, despite the key importance of these two factors in controlling hillslope processes. Shakesby et al. (2007) emphasized the rapid post-fire recovery of eucalypt vegetation and litter accumulation in southeast Australia, and Prosser and Williams (1998) noted that eucalypt vegetation took 4 to 5 years and litter loads 7 years to recover, thereby estimating this duration as the recovery window for erosion resistance. However, recovery of water yield from mixed-species ash forest (*E. regnans* and *E. viminalis* dominant) has been estimated to occur over timescales of one order or more (100 to 150 years) (Kuczera, 1987) (see Figure 1-1) than the above-mentioned recovery rates of vegetation, and by extension, soil erosion. These slow rates of recovery have been attributed to the much higher consumptive water use of vigorously growing juvenile plants in competition for environmental resources, compared to the much lower water uptake of tall mature stands of *E. regnans* due to lower transpiration rates (Vertessy et al., 2001) at these "climax" vegetation states (Dunin et al., 2007). Indeed, any inferred reduction in soil erosion rates might be attributed to the substantive water uptake of regenerating plants post-fire, rather than decreases in erosional vulnerability *per se*.
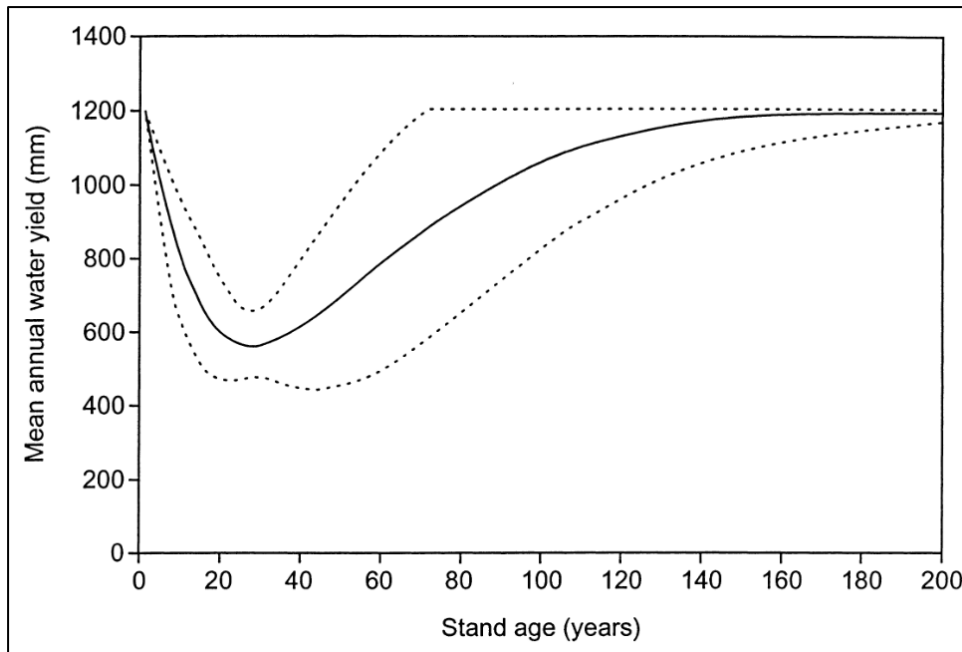
Figure 1-1. Mean annual water yield (mm) with stand age (years) after disturbance such as severe wildfire; after Kuczera (1987). The dashed lines indicate the 95% confidence limits for the modelled relationship. Source: Vertessy et al. (2001).

Therefore, although gross erosion rates may not be high at the catchment scale indicating a high-level of "recovery", hillslope sediments may still be rather mobile and attenuated in interim traps; "sinks" along various topographic and vegetative barriers (de Vente et al., 2007). Furthermore, the implication from Kuczera (1987) is that the vegetative cover of the various strata in this long recovery stage – the intermediate stage, would be intrinsically distinct quantitatively and qualitatively from that of the "mature" stage.

Much work in Australia and abroad has focused on severe erosion rates – sudden spikes in the immediate post-fire period, usually resulting from "large" rainfall events which are coarsely identified based on the total event depth and duration (Shakesby et al., 2007). However, there has been growing evidence that intra-event intensity variations and inter-event relationships impact upon the activation and operation of canopy and hillslope hydrological processes (e.g. interception and throughfall; splash processes and runoff generation) (Dunkerley, 2014b; Dunkerley, 2015a; Dunkerley, 2008c; Nel et al., 2016; Parsons and Stone, 2006; Wang et al., 2016b), and these need to be integrated into existing

soil erosion models such as EUROSEM and RUSLE2 (Khaleghpanah et al., 2016). However, widespread application of this more nuanced treatment of this key driver by closely examining intra-event intensity variations and inter-event relationships, to post-fire erosion science has thus far been sparse, particularly when thinking about intermediate post-fire vegetation conditions (Moody et al., 2013).

In addition to ongoing questions about rainfall event characteristics and their effects in the post-fire erosion context, there is presently insufficient understanding of how the distinct characteristics of post-fire vegetation regeneration of eucalypt trees and forests through epicormic budding (Meier et al., 2012b) and lignotuber regrowth, alongside the re-growth of associated shrubs and ground-level vegetation and litter in this 'regional variant' (Shakesby et al., 2007), influence splash erosion and overland flow erosion on burnt hillslopes. As vegetation regeneration progresses substantially one or more years after extreme defoliation from severe wildfires into intermediate stages, rainfall becomes increasingly modulated by the re-grown foliage which is likely to exert effects that are distinct from either the climax vegetation stage or the bare immediate post-fire stage; altered processes would include canopy interception and storage, throughfall fraction, rates and drop characteristics (such as sizes, arrival rates, spatial distribution and resultant kinetic energy), and surface runoff-run-on. The heterophyllic nature of many eucalypt species (Brooker and Kleinig, 2006; Jacobs, 1955; Penfold and Willis, 1961), with unique juvenile leaf forms dominating post-fire regeneration canopies several years following fire damage, raises further interesting questions on whether leaf shapes and areas contribute significantly to rainfall modulation processes and effects. Additionally, any litter layer recovery means that splash and runoff processes undergo further modification on the hillslope surfaces. Indeed, litter, being of low density can be quite mobile on steep terrain. Presently, however, much of the work done in southeast Australia has focused on the causes of spatial and temporal

heterogeneity in the development of soil hydrophobicity due to low-intensity prescribed fire and the resultant soil erosion processes and rates, e.g. Cawson et al. (2016); Cawson et al. (2012) and ongoing concerns about water quality due to post-fire sedimentation (Smith et al., 2011). Also, there has generally been more emphasis on wet sclerophyll forests which are more important economically (logging) and hydrologically (major water catchment areas) than dry sclerophyll forests; see for example Smith et al. (2011), Sheridan et al. (2007) and Sheridan et al. (2011), even though these vegetation formations are much more important in areal extent in southeast Australia. Furthermore, many dry eucalypt tree species are widely used in revegetation and landscaping efforts in both rural and urban contexts (Livesley et al., 2014; Spooner and Smallbone, 2009).

In the light of the present state of knowledge about post-fire hillslope processes in southeast Australia, and the significance of frequent wildfires in triggering geomorphic perturbations in this region and the outlined knowledge gaps, there is a need to build more empirically-based knowledge about the complex and interesting rainfall-vegetation factors and effects on hillslope processes on intermediate-stage regenerating dry sclerophyll forests. The need for this research gap to be addressed is illustrated in Figure 1-2.
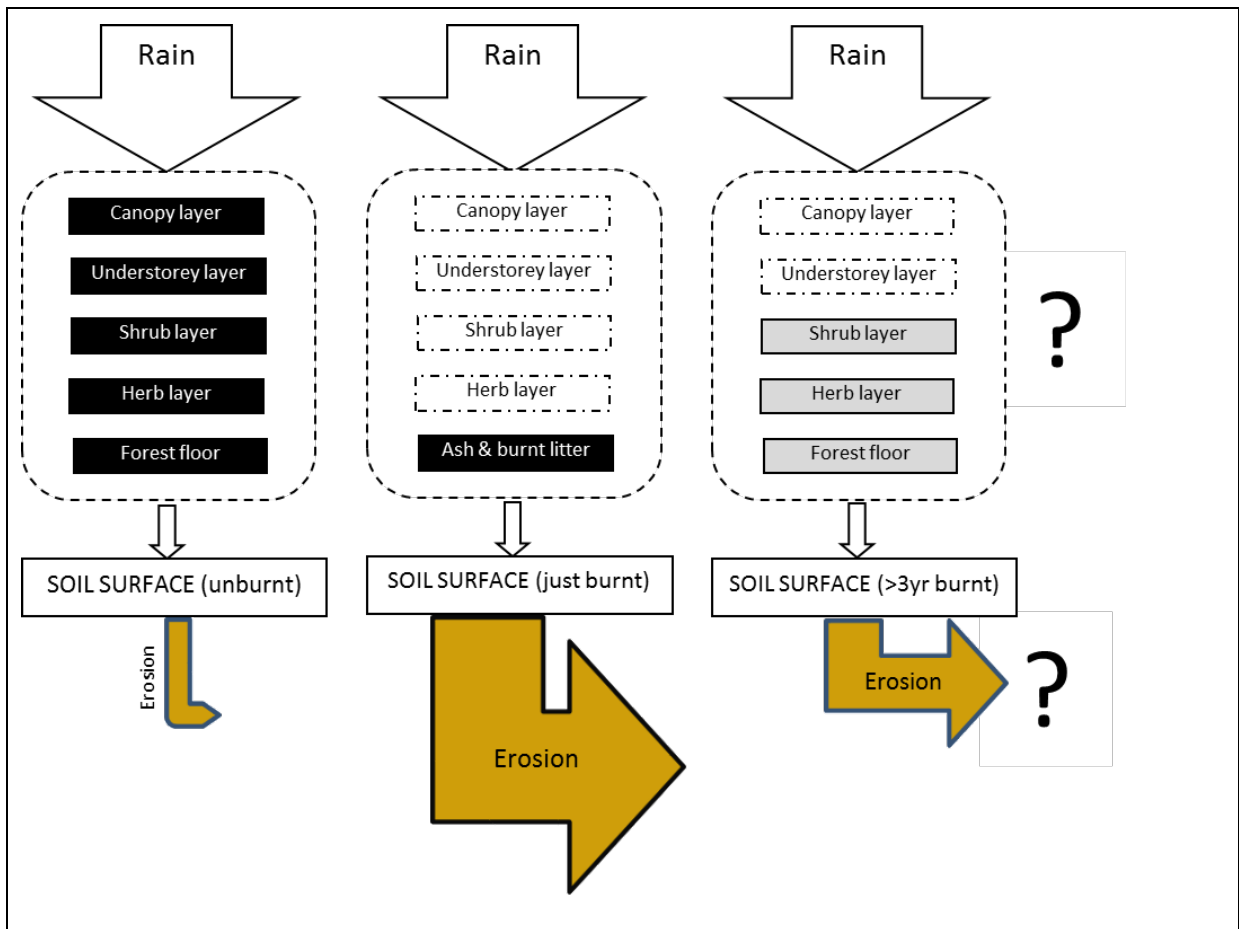
Figure 1-2. Illustration of the research gaps in post-fire erosion science for intermediate post-fire (partial recovery) conditions, particularly for Australian dry eucalypt forests.

The present research was conducted in the Licola area, a steep upland region at the foothills of the Great Dividing Range covered by dry sclerophyll eucalypt forest in the southern fall of the Alpine national park in Victoria, southeast Australia. This region experienced widespread and severe wildfires between Dec 2006 and Jan 2007 (Flinn et al., 2008a) that had a global as well as regional-scale impacts on atmospheric chemistry and physics (Dirksen et al., 2009). Various rainfall events during the post-fire period caused severe soil erosion and debris-flows that denuded the exposed hillslopes in the region, and contributed to severe flooding and landslides (Tryhorn et al., 2008). Much of the eroded sediments were delivered to the Wellington and Macalister Rivers, and many of the environmental problems associated with the rapid soil erosion and flash-flooding such as infrastructure damage, disruptions to water supply quality and reduced dam capacity (ABC

19

News, 2010), have occurred and some issues have persisted. Details of the megafire, its effects on the study site and post-fire hydrological, geomorphological and ecological impacts are presented in Chapter Three. In 2012, five years after the fire, the dry sclerophyll forests had seen substantial but partial recovery of canopy and ground cover, making the area suitable for fieldwork investigations to address the research gaps highlighted above. With the exception of work by Nyman et al. (2011) to identify the occurrence of post-fire debris flows in this area and the broader region, there is no other scientific study of post-fire hillslope erosion dynamics in this area. The fieldwork presented in this thesis involved the simultaneous measurement of rainfall-throughfall volumes and erosivities under intermediate post-fire forest canopy, coupled with collection of hillslope sediment and litter fluxes across six sediment fences; through six data collection periods in 2012.

This study examines the dynamic interactions between vegetation and erosion in post-fire conditions, and is in line with the innovative research area at the interface between ecology and geomorphology identified by Osterkamp et al. (2012). In particular, the knowledge generated from this study contributes to nascent field of biogeomorphology (Rice et al., 2012). It is with this biogeomorphological framework that we examine the concepts and processes applicable to post-fire erosion science, in the next section.

1.3. Post-fire recovery – conceptual considerations

1.3.1. Hillslope erosion – key factors

The key factors that determine the characteristics of erosion by splash and overland flow on hillslopes are rainfall, vegetation, soils and topography (see Figure 1-3). These four key factors have multiple elements within them that variably influence hillslope erosion processes. However, rainfall is the most variable and unpredictable over human timeframes, while topography is the least variable and slowest to change. Various interactions between these factors are also present and need to be considered in the complex processes and outcomes of hillslope erosion. The consequences of the erosion; sediment and litter removal from upslope areas and their deposition at downslope positions (or transfer into the riverine system) would then constitute feedback loops to the main factors of vegetation, soil and topography. Indeed, interactions between the altered land surface and atmospheric processes may also affect meteorological conditions such as temperature, humidity and rainfall (Evans et al., 2010).
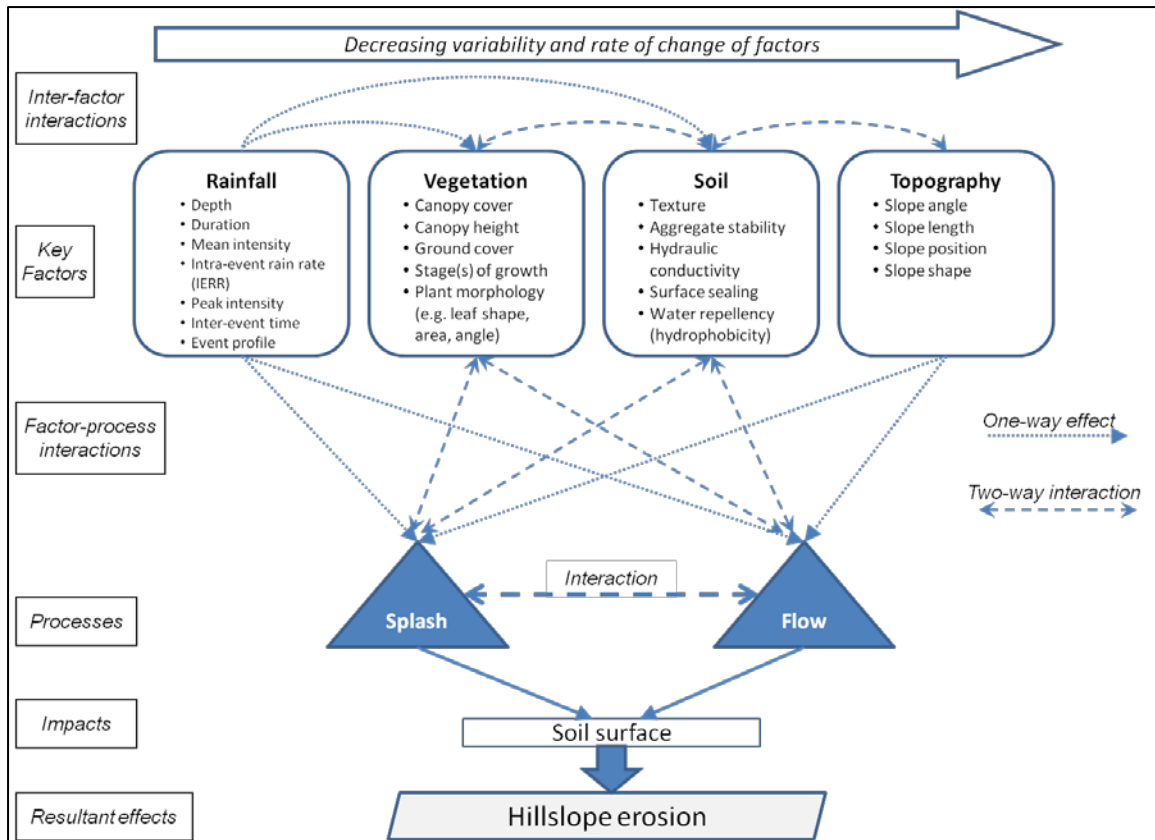
Figure 1-3. Conceptual framework for study on post-fire hillslope erosion.

In the context of the impacts of fires on hillslope erosion, vegetation undergoes the most dramatic changes that substantially alter the hydrological pathways and partitions that lead to the variable operation of splash and overland flow erosion. Post-fire vegetation recovery is also known to be a prime factor for the reduction in post-fire sediment supply levels, and can vary substantially in space and time, depending on local conditions. Soils can undergo significant changes due to the heating effects of fire, deposition of ash and burnt litter and sudden exposure to direct rainsplash and solar radiation. Rainfall and throughfall are the primary controlling drivers of erosion processes (Calder, 2001; Dunkerley, 2012; Nanko et al., 2016a; Parsons and Stone, 2006), and can be highly variable in their characteristics and resultant impacts for any study area. As vegetation regenerates in the post-fire recovery period, the rainfall modulating effect of the vegetation increases and changes (Calder, 2001; Crockford and Richardson, 2000; Levia et al., 2017; Nanko et al., 2016b; Wakiyama et al., 2010). Topography, at the hillslope scale, exerts general controls over the

distribution of water at and below the ground surface and thus also influences vegetation growth and soil re-distribution (erosion, transport and/or deposition) (Gonzalez-Bonorino and Osterkamp, 2004; Larsen and MacDonald, 2007). Micro-topography at the slope segment scale determines the detailed distribution and movement of water at the soil surface by guiding and concentrating overland flow to specific pathways, thus exerting self-reinforcing, positive feedback effects (Asadi et al., 2007; Berg and Azuma, 2010; Bryan, 2000; Parsons, 2006).

1.3.2. Post-fire vegetation and erosion recovery

Vegetation exerts a primary control over the development and movement of hillslope soils (Amundson et al., 2015). Prosser and Williams (1998) proposed a conceptual framework to describe the hypothetical effect of fire on runoff and erosion, whereby landscape resistance to erosion; the inverse of hydrologic vulnerability (Pierson et al., 2010), recovers within a 'window of disturbance' following an exponential function as it "relaxes" from a low to high pre-fire resistance; runoff and erosion rates and impacts being strongly dependent on the depth and intensity of rainfall events that occur during this intermediate period where post-fire vegetation recovery is underway (Figure 1-4). However, the duration of the window of disturbance can be highly variable, depending on the nature and extent of changes to soil and vegetation, ranging from a few months to several years (Prosser and Williams, 1998).
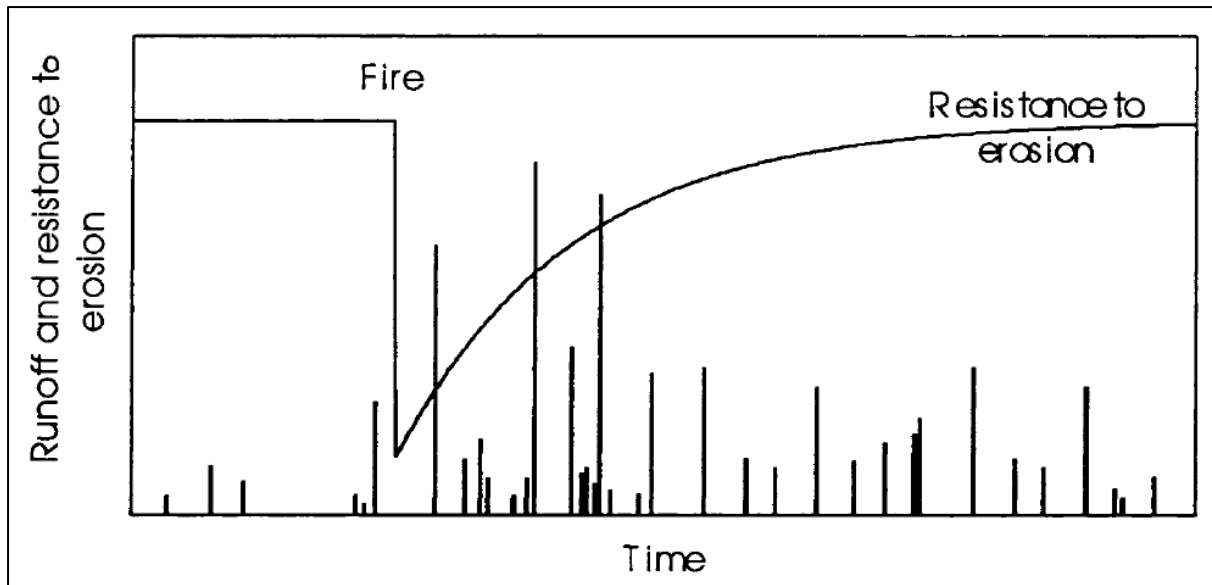
Figure 1-4. Hypothetical effect of fire on runoff and erosion resistance, and their changes with gross vegetation recovery with time. Source: Prosser and Williams (1998).

While this framework is broadly acceptable at the conceptual level, the presumed monotonic recovery of erosion resistance masks considerable uncertainties and complexities. Indeed, much past and present thinking about system changes appear to be constrained within a paradigm focused on convergence and "recovery" towards a stable "climax" state, whereas non-linear systems theory and complexity in many different natural systems directs us to re-conceptualize divergence, dynamic stability and different possible "end-states" as the norm, rather than the exception (Phillips, 2017). Departing from more common deterministic and mechanistic approaches, Jones et al. (2014) studied wildfire occurrences and rainfall events as independent stochastic processes in terms of their spatial extent, duration and temporal distribution of occurrences, and quantified the intersection between storm events and burnt areas. Indeed, wildfires are more likely to occur in periods of drought and therefore the likelihood of geomorphically-significant rainfall events is reduced in the immediate and short-term post-fire period; the importance of aeolian processes during intensely dry conditions remains an area to be comprehensively explored. Therefore, while the potential for severe erosion to occur is present, the actualization of this potential is reduced – this is quite

applicable to ENSO-dominated hydro-climatic regions such as southeast Australia which can cause regional suppression of uplift and stable atmospheric conditions prevailing for substantial time periods.

In Figure 1-5, three alternative scenarios departing from the singular, generalized recovery trajectory shown in Figure 1-5(a) are presented. Truncated recovery is illustrated in Figure 1-5(b); this would occur where fire recurs before "complete" recovery stage has been attained. In the present high fire-prone region, and in the broader context of warmer, drying trends in southeast Australia (less rain-days, but with higher intensity events), this is a distinct possibility, has increased likelihood with the scale and extent of megafires, and evidenced by the double-burnt areas, first noted in the 2003 Eastern Victorian Alpine Fires (Williams et al., 2008) and then the 2006/7 fires (Flinn et al., 2008a) (see Chapter Three for details). The potential erosional response would be high, being prematurely "reset" and therefore vulnerable to rainfall events for a long duration after the very first fire.

Prolonged recovery is shown in Figure 1-5(c); wildfires are likely to be more severe and of greater extent during drought periods. The 2006/7 fires occurred in the midst of the Millennium Drought (Flinn et al., 2008a). With intense water scarcity coupled with heat stress particularly during the summer months, vegetation recovery of various strata of the original formation would be retarded. In the meantime, enhanced litterfall could continue to contribute to fuel accumulation and vulnerability further outbreaks of fire. This would mean lowered resistance and extended erosional vulnerability to rainfall events that would have not necessarily caused much erosion under the original recovery trajectory, within the same hypothetical time window (cf. Figure 1-5a). Transitioned recovery, as seen in Figure 1-5(d) could be caused by a distinct shift in the floristics and vegetation structure giving different (higher/lower) erosion resistance resulting from different combinations of plant characteristics; from the "original" Figure 1-5(a). It has been postulated that changes in fire

regimes associated with climate change; alteration of the initial post-fire floristic compositions could lead to shifted, alternative "climax" vegetation assemblages (Bradstock, 2008; Lindenmayer et al., 2011; Purdie and Slatyer, 1976) due to the high dependence of many shrub and herb species on the seedbanks in residual ash and soil for recolonization. These could occur at the broad scale, with post-fire erosion processes affecting seed availability and distribution together with in-migration of different/alien plant species (including weedy types) due to wind or animal dispersion.

These three scenarios are by no means exhaustive in the possibilities, but serve to illustrate various divergent outcomes. Furthermore, combinations of Figures 1-5(b-d) are possible; for example, the recurrence of fire prior to full recovery - (b), could push the ecosystem into alternative floristic compositions - (d), especially where some species and communities may not have achieved reproductive maturity, or where the second fire destroyed resprouting plant organs or any viable seedbanks.
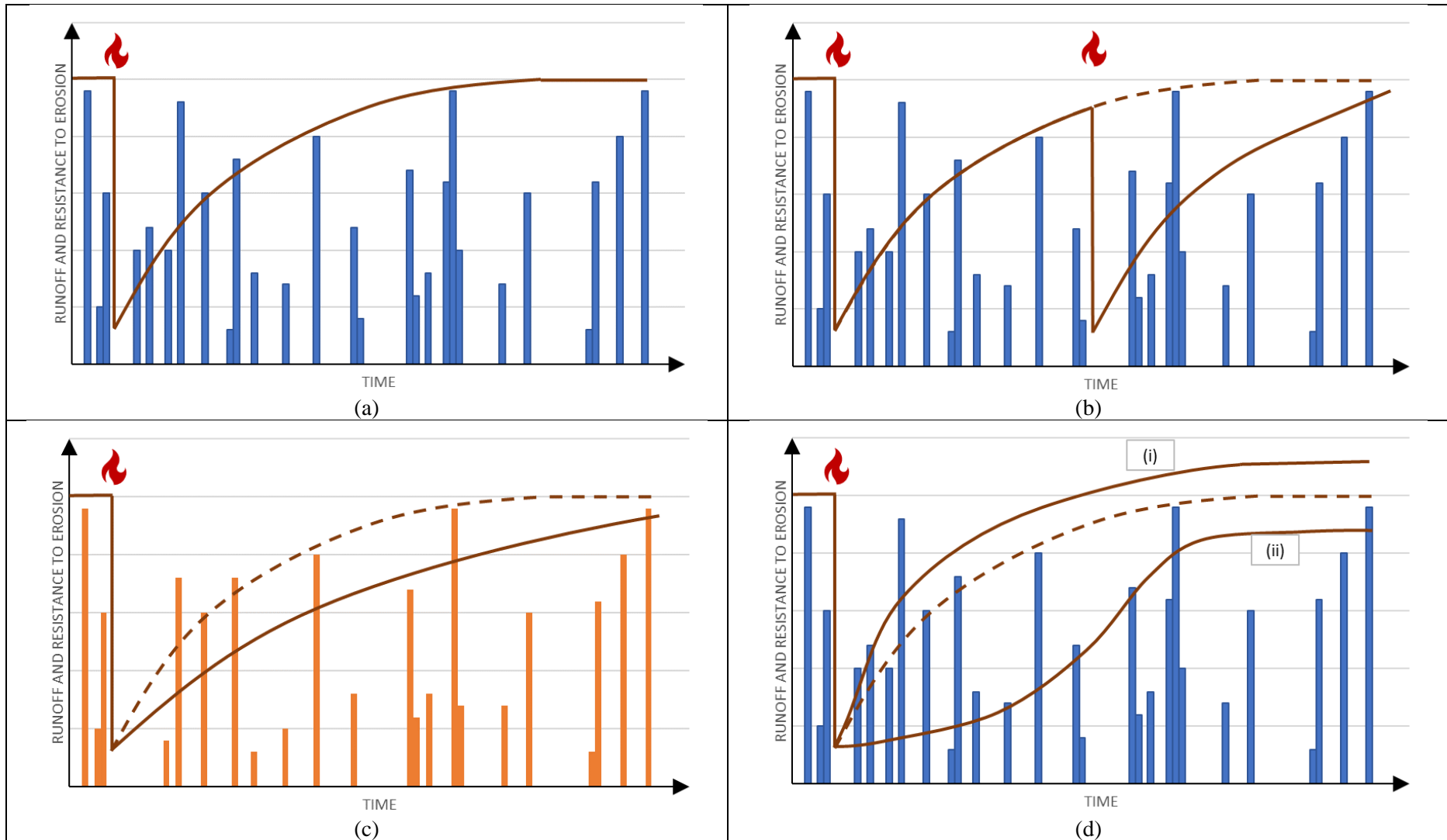
Figure 1-5. Different post-fire recovery trajectories. (a) "Standard" pathway after Prosser and Williams (1998); (b) Truncated recovery due to fire recurrence prior to complete recovery; (c) Prolonged recovery due to effects of drought (note reduced effective rainfall events); (d) Transitioned recovery due to alternative floristics leading to (i) increased or (ii) reduced erosion resistance. Dotted lines represent "original" pathway.

Post-fire erosion science has increasingly found that consideration must be given to the hydro-climatic, ecological (in particular, vegetation-related), geomorphological and edaphic conditions specific to each of the regions and subregions within these fire-prone regions of southeast Australia, the Mediterranean and western United States. Hence, the post-fire "window of disturbance" as proposed by Prosser and Williams (1998) needs to be investigated more robustly to build more sophisticated models of process-based understanding, across multiple spatial and temporal scales (Shakesby et al., 2016).

1.3.3. Dry sclerophyll eucalypt forests after severe fire on steep hillslopes

Post-fire recovery of forest vegetation should be distinguished from that of rangelands (e.g. grasslands, shrublands and woodlands) because of the existence of two or more strata that recover at different rates. These strata-based differences are likely to be higher especially after extensive destruction by moderate to severe fires (Cawson et al., 2012; Cawson et al., 2013; Doerr et al., 2006; Hammill and Bradstock, 2006; Keeley, 2009; Rhoades et al., 2011; Santín et al., 2015; Shakesby and Doerr, 2006) in Australian dry eucalypt forests. Consequently, the hillslope erosion responses would also be distinctive. Figure 1-6 illustrates a possible sequence of post-fire vegetation recovery of the various strata, and the erosional-depositional processes and patterns after severe fire on steeply-sloping dry sclerophyll eucalypt forest hillslopes typically found in many uplands of southeast Australia (Florence, 2004; Gill and Zylstra, 2005; Specht, 1970; Williams and Woinarski, 1997).

The initial open forest canopy with grassy-shrubby understorey and widespread litter cover is illustrated in Figure 1-6(a); also shown in Plate 3-2. Mature foliage is likely to dominate in the eucalypt canopy layer. Because of the substantial plant and litter cover close to the ground, soil erosion rates would be minimal. A large, severe fire event burning through the forest would see most of the litter, grasses, shrubs, twigs and leaves completely consumed, leaving bare tree trunks and branches with an exposed soil layer with a highly

vulnerable veneer of ash and scorched foliage as shown in Figure 1-6(b), and suitably illustrated in Figure 2-1 (iv-vi); a strongly hydrophobic subsurface layer is also likely to develop in the soil profile (Shakesby et al., 2007). In the immediate post-fire period, soil erosion will be very active if rainfall occurs; being enhanced by the presence of ash, and possibly subsurface hydrophobicity that contributes to rapid saturation of the thin soil layers above it (Gabet and Sternberg, 2008). Much erosion would occur over the large canopy interspaces and persistent bare soil surfaces resulting from early post-fire erosion episodes. Small but significant amounts of eroded soil would be re-deposited behind barriers such as tree trunks and roots, rocks and small topographic hollows. The top 5 to 10 cm of the original soil profile could be rapidly stripped rapidly away by highly interconnected sheetflow (Pierson et al., 2010; Williams et al., 2016; Williams et al., 2014) and thin debris flows (Gabet, 2003; Gabet and Sternberg, 2008). With such steep terrain, rapid colluvial processes such as dry ravel could also be active, causing sediment "pulses" in the absence of rainfall or fluvially-induced processes (Roering and Gerber, 2005).

If rainfall of significant depth and/or intensity is received, high erosion rates will likely occur and continue into the early post-fire recovery period as described by Prosser and Williams (1998) and Shakesby et al. (2007) (see Figure 1-5). A depleted and infertile soil layer would now be exposed. Any understorey regeneration would be slow because they would have to be from the existing (depleted) seed bank, or re-introduced via wind or animal dispersal; respectively termed autochthonous and allochthonous sources (Huxel et al., 2002). Therefore, any interception effect by these strata would be minimal. However, most of the fire-adapted eucalypt trees would not have been killed, even though they were significantly scorched and defoliated. These trees would commence regeneration from the epicormis (budding) or lignotubers (sprouting) even just weeks after fire, where local environmental conditions have stabilized. This epicormic sprouting (Meier et al., 2012b) would lead to a

"fuzzy", trunk and branch-aligned canopy profile and Leaf Area Index (LAI) quite different from the original forest canopy, as illustrated in Figure 1-6(a) (Crockford and Richardson, 2000; Holder, 2016; Vertessy et al., 2001), exhibiting high spatial heterogeneity with foliage and litter densities high at or around the stem bases of re-growing trees and shrubs. This would mean that in the intermediate-stages of dry eucalypt forest post-fire recovery, ground and lower-level strata cover would lag-behind the tree-associated middle/upper-level strata. Recovery of the litter layer would also be retarded, as biomass accumulation and subsequent litterfall from senescing foliage operate with substantial time lags after post-fire eucalypt regrowth.

(a) Pre-fire conditions	(b) Immediate post-fire conditions
(c) Early post-fire vegetation recovery (1 year)	(d) Intermediate post-fire vegetation recovery (e.g. 5 years)
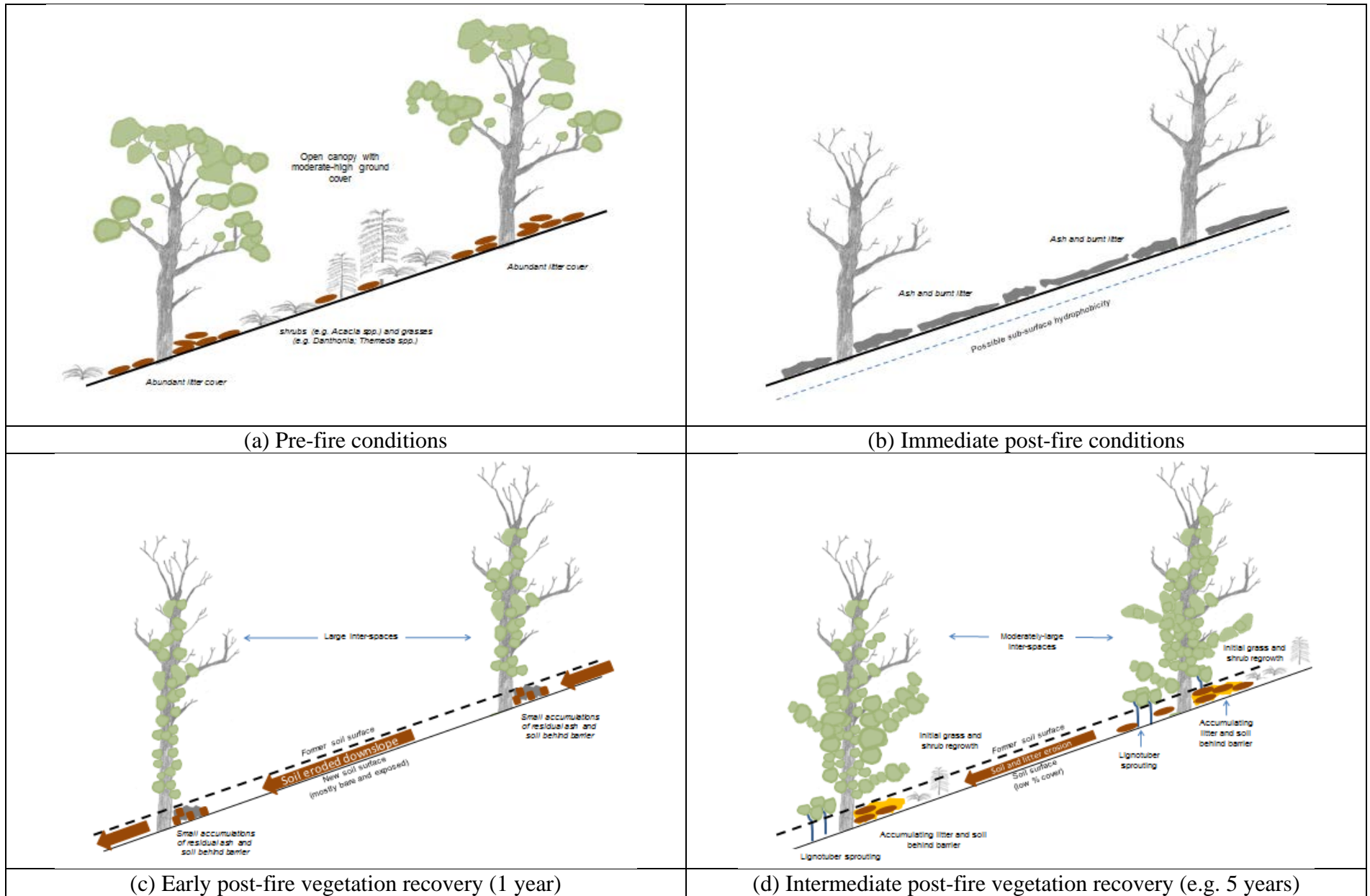
Figure 1-6. Suggested phases of post-fire erosion on dry sclerophyll eucalypt forests on steep terrain.

The intermediate post-fire recovery stage for these forests would nominally commence around three to five years post-fire. These conditions are illustrated in Figure 1-6(d) and exemplified by the study area (Plates 3-3, 3-4 and 3-10). Substantial regrowth of the eucalypts and ground/lower strata shrubs and grasses would have occurred, although it is still incomplete. By this time, the spatial colonization (Christophe et al., 2003) of the trees would see clear extension of branches outwards from the main stem, accompanied by some vertical extension as well. Lignotuber sprouting would also ensue from the lignotuber parts unaffected by fire (Fairman et al., 2015; Purdie and Slatyer, 1976; Shakesby et al., 2007). This creates a narrow shrubby layer centered around the main stem of the tree. A distinct, narrow trunk-biased canopy profile with multiple layers of eucalypt foliage therefore develops and persists in this intermediate phase of post-fire regrowth that is likely to see interception and throughfall effects distinctively different from long unburnt forests.

Because of the steep slopes, the transit of litter and soil through the interspaces will be rapid, with much concentration of litter and eroded soil just upslope of barriers such as the base of tree trunks, roots and rocks. These patches would also be where the seeds of grasses and shrubs would germinate. Therefore, much spatial heterogeneity would be seen in the distribution of protected soil surfaces (undercanopy) contrasting with the persistence of almost bare, hydrologically vulnerable interspaces, even in the intermediate post-fire vegetation phase. The post-fire progression of vegetative re-growth can be viewed through the conceptual framework of the Dynamic Zones of Interaction (DZI) approach discussed in Chapter Two.

From the phases presented in Figure 1-6, it is argued that post-fire hillslopes can remain hydrologically vulnerable for several years after fire because ground cover percentages continue to be low; while a recovering canopy may afford some hydrologic stability under it (Pierson et al., 2010; Williams et al., 2016). Although somewhat counter-

intuitive, the splash erosion potential from throughfall could instead be intensified (Geißler et al., 2012b; Nanko et al., 2008; Nanko et al., 2011), leaving ground litter cover as the only protective layer attenuating the potentially erosive forces (Geddes and Dunkerley, 1999; Ghahramani et al., 2011; Larsen et al., 2009). If sub-canopy litter is removed through erosion or degraded, for instance through fuel-reduction burns, the underlying soil could be strongly eroded or compacted by splash processes. This is also possible with moderate-intensity fires where ground and lower-strata live/dead vegetation are consumed, but with minimal canopy damage (Prosser and Williams, 1998). Coupled with the situation where juvenile leaf forms dominate in post-fire re-growth, large released throughfall drops could result in intensified splash erosion on bare soil surfaces. The resultant hillslope splash and overland flow erosion processes can therefore be seen as the integrated outcome of the quasi-independent recovery of the various strata, each with its own pace and pathway of recovery proceeding through the "window of disturbance" (Prosser and Williams, 1998). Presently, minimal work has been done to examine the rainfall and vegetation factors and processes operating under intermediate conditions described in Figure 1-6(d) (see also Figure 1-2).

1.4. Research questions

The previous sections have outlined the main concepts and research gaps relevant to post-fire erosion in dry sclerophyll eucalypt forests of southeast Australia. The main areas to be addressed include the need to better understand the interactions between rainfall characteristics, canopy processes and the subsequent impacts on hillslope erosion in intermediate post-fire vegetation conditions.

The research questions were as follows:

(i) How do inter and intra-event rainfall characteristics influence hillslope erosion processes in the study area?

(ii) How does intermediate post-fire dry-sclerophyll forest modulate rainfall vis-à-vis open-field rainfall, and what are the resultant impacts on throughfall fraction and throughfall splash erosion?

(iii) What are the composite impacts of rainfall and post-fire vegetation factors on hillslope sediment and litter fluxes?

1.5. Scope of study

This study was implemented at the plot and hillslope scales, and effects on catchment-wide hydrology and sediment yield may not be ascertained directly. Therefore, relationships found in the process of conducting this research should be extrapolated to the broader catchment scale with much caution. Nevertheless, the scale of this study provides important insights into the key processes occurring during the intermediate (5 to 10 years) post-fire condition, and will contribute to better understanding of water and sediment responses at the catchment scale.

Field evidence and observation of steep slopes, skeletal, gravelly soils and the regular occurrences of rocky outcrops at the study site indicated that erosional processes were very likely to be governed by Hortonian processes (see Chapter Three). Therefore, any influence

from subsurface or groundwater processes (Poesen et al., 2003; Valentin et al., 2005) would be minimal. This study recognized that a comprehensive set of soil properties, such as aggregate stability, texture, hydraulic conductivity, surface crusting (presence, absence, extent) and water repellence (hydrophobicity) are likely to be important in the analysis of soil erosion by splash and overland flow. It is also acknowledged that much work has been done in past decades to develop detailed understanding of the formation, effects and deterioration of soil hydrophobicity that has been widely observed to arise as a result of the heating effects of fire on soil which cause the vaporization of organic compounds and the concentrated re-condensation at the surface or near-surface subsoil layer (Letey, 2001); hydrophobicity has also been attributed to the physical impacts of raindrops that cause the compaction of the topmost soil layer, the clogging of the topsoil pores by fine particles dislodged by rainsplash, or particular combinations of microtopography, particle size and packing density (Doerr et al., 2007).

While the causes of the development of hydrophobicity was not the focus of the present study, it was envisioned that the understanding gained from this research would complement the substantial body of knowledge of post-fire soil hydrophobicity to enable a broader and refreshed understanding of post-fire hydrological and geomorphological processes (Moody et al., 2013; Shakesby, 2013; Shakesby et al., 2016). It was also likely that any hydrophobic layers in the study site would have been degraded or removed in the substantial erosion of surface soil horizons associated with storm events in the immediate post-fire period (Certini, 2005; Doerr et al., 2000; Gabet, 2003), and therefore would not be a significant factor in erosion processes in the intermediate post-fire period (Larsen et al., 2009). Furthermore, many long unburnt "eucalypt soils" have been known to be naturally hydrophobic (Doerr et al., 2000; Shakesby et al., 2007) and therefore indicate that wildfire-

induced hydrophobicity is just one of the many causes for the often observed accelerated post-fire erosion rates (Shakesby, 2013; Shakesby et al., 2000).

Having established the key aspects of this research, we now turn to the literature review of previous studies and theoretical domains relevant to post-fire erosion science in Chapter Two.

CHAPTER TWO: LITERATURE REVIEW

In this chapter, I survey key fire-prone regions and their corresponding studies to evaluate the current state of knowledge about the specific roles of vegetation in controlling post-fire erosion across different forests in southeast Australia to discuss the pertinent intra and supra-regional research gaps for the study of post-fire erosion. The importance of this knowledge domain is important because projected changes in global and regional climates are likely to result in increased risks and occurrences of wildfire. Firstly, I present a brief survey of post-fire erosion work in the western United States and the Mediterranean, two other major fire-prone regions of the world. The western United States is where post-fire erosion science developed, and much ongoing scientific development and innovation is ongoing. Hence, there is a need to survey the knowledge gained from work done in this region to inform the present research. The Mediterranean region has built-up a substantial body of knowledge in the past four decades and gives valuable insights into heightened post-fire erosion risks associated with vegetation transitions resulting from a long history of anthropogenic modification, land abandonment, and a general rise in fire risks and severity. Notably, the latter has been attributed to the rather rapid expansion of *Eucalyptus globulus* plantations in the Mediterranean countries such as Portugal (Catry et al., 2013; Mirra et al., 2017). Nevertheless, these regions are widely seen to be distinctive from one another, and from southeast Australia that has unique vegetation, landscapes and hydro-climatic regimes (Shakesby, 2013; Shakesby et al., 2016; Shakesby et al., 2007), even though they are similarly susceptible to wildfires.

The broad understanding of these two key regions is then followed by a more detailed examination of post-fire erosion in southeast Australian dry sclerophyll eucalypt forests where the main research gap emphasized is the need to garner better insights into intermediate phase post-fire hillslope and plot-scale hydrology and erosion dynamics. I then

propose a Dynamic Zones of Influence (DZI) framework which emphasizes the importance of vegetation-related influences on soil, water, nutrients and erosion-deposition processes (Dunkerley, 2000) to drive future work in post-fire ecohydrology and ecogeomorphology. Finally, I consider the increasingly important line of research on how erosion processes are strongly affected by intra-event rainfall variations and discuss the possible implications on post-fire hillslope erosional processes under intermediate vegetation conditions, the focus of my research.

In this chapter, I argue for a tighter, ecohydrologically-framed coupling of the processes of vegetation change and post-fire erosion studies in southeast Australian eucalypt forests which are distinct from other fire-prone vegetation formations in the western United States and the Mediterranean. As outlined in Chapter One, this entails detailed examination of complex, interacting factors and outcomes further into the post-fire 'window of disturbance' (Prosser and Williams, 1998; Shakesby and Doerr, 2006), the intermediate phase when vegetation recovery has advanced substantially, albeit incompletely, to exert significant controls over hillslope hydrology and erosion. This is usually around 5 to 10 years post-fire for Australian dry sclerophyll eucalypt forests. Indeed, the absence of vegetative cover in the immediate and near post-fire period and the associated hydrological and geomorphological processes should be seen as an exception, rather than the norm (Amundson et al., 2015), the significance of these processes within the narrow timeframe notwithstanding. Overlain onto post-fire vegetation "recoveries" are projected ecological impacts of climate change that have clear potential to result in transitions to "alternative" floristic compositions across different hydroclimatic regions, and therefore vegetation structures that are different from the "original" vegetation assemblage. These relate primarily to increases in fire-frequency, potentially keeping many fire-prone forests in seral stages, increased rainfall event intensities with concomitant lower event frequency, and increased transpiration demands of flora on soil

moisture with increased CO_2 concentration. Furthermore, the influences of human activities on fire occurrence, frequency, extent and impacts have increased (Kinoshita et al., 2016). In recent times, workers have also started to analyse how intra-event variations in natural rainfall events lead to variations in canopy hydrological partitioning, throughfall rates and drop-size distribution (Nanko et al., 2016a; Nanko et al., 2011; Nanko et al., 2016b) which impact upon stemflow (Dunkerley, 2014a), splash erosion (Geißler et al., 2012a), infiltration and runoff generation (Dunkerley, 2012). The combined effect of all these factors on post-fire hydrological partitioning and hillslope hydrology and erosion in southeast Australian dry sclerophyll eucalypt forests remains largely unknown and therefore needs further investigation.

The importance of understanding post-fire hydrologic and geomorphic processes has been borne out by the large number of studies on their causes and effects at various scales, in the wildfire-prone regions of the western United States, the Mediterranean and southeast Australia. This can be attributed to the clear connections between post-fire erosion and their consequent environmental and human impacts. Moderate to severe wildfires tend to lead to sharply heightened rates of soil erosion because of (i) loss of protective vegetative cover at all structural levels, including ground-level plant material such as grasses, forbs and organic litter leading to direct exposure to rainsplash impacts and reduced hydraulic roughness causing increased rates and volumes of overland flow; (ii) addition of a highly erodible ash layer that increases the volume of fine, mobile material exported from the hillslope; (iii) increased erodibility of the mineral soil layer due to desiccation and destruction of agents of soil aggregation resulting from heat damage from the fire; and (iv) development of a sub-surface hydrophobic (water-repellent) layer caused by the downward heat-driven vaporization, condensation and concentration of a range of organic substances that adhere to individual soil particles of, in particular, sandy soils (DeBano, 1981; DeBano, 2000; Doerr et

al., 2007; Leighton-Boyce et al., 2007; Letey, 2001; Tessler et al., 2012) that limit the water-holding capacity of soil profiles and cause rapid development of saturated overland flow, thin, unstable layers of saturated topsoil characterized by strong interflow and the increased likelihood of debris flows (Gabet, 2003; Gabet and Sternberg, 2008). Interactions between the outcomes of these changes further enhance the erosional susceptibility of hillslopes. For instance, structural and depositional sealing due to rainfall impact and ash clogging of soil pores in the surface topsoil layers further enhance the generation and erosional impacts of overland flow (Larsen et al., 2009).

Despite the broad agreement on heightened high post-fire erosion rates occurring in many parts of the world, field observations have found divergent outcomes between different landscapes which may have experienced similarly severe vegetation destruction by fire (Shakesby, 2013), indicating that one or more key mediating factors could control the actualization of high potential erosion vulnerability typical of severe post-fire conditions. For example, Martin et al. (2011) reported how the remaining duff layer was the primary cause of limiting soil erosion rates despite severe fire in the closed-canopy sub-alpine forests in the Canadian Rockies. In California, much further south, Knapp et al. (2005) also pointed to the importance of duff in mitigating soil erosion rates after fire in the old-growth mixed conifer forest in Sierra Nevada, Sequoia National Park. It was interesting to note in the two studies mentioned above, little attention had been given to the specific characteristics of the various rainfall events that may or may not have led to erosion activation thresholds being exceeded. Furthermore, there is a need to incorporate the changing conditions of post-fire ground surfaces through time as various erosive forces work through vulnerable ash or burnt topsoil layers and encounter lower A2 and even B horizons of the soil profile which would influence the likely hillslope erosion rates via soil characteristics (e.g. texture) and erodibility, as demonstrated by Nyman et al. (2013). Hence, although a large body of literature has been

accumulated from the past few decades, it is important that workers be sceptical of "established truths" (Shakesby, 2013) about post-fire processes and work to further uncover new knowledge, or question previous assumptions for this area of research to progress.

2.1. Post-fire erosion in the western United States

Compared to other wildfire-prone regions in the world, the United States has accumulated the largest body of knowledge about post-fire erosion and vegetation recovery in the past century of research (Moody and Martin, 2009). Research into the various environmental effects of fires was pioneered in the United States and only in the recent decades has similar work been done in other fire-prone regions around the world such as the Mediterranean and Australia (Moody et al., 2013). Many parts of the western United States such as southern California are prone to wildfire and severe post-fire erosion because of its Mediterranean-like climate (Moody et al., 2013). In most years, this region experiences substantial periods of dry weather rendering many areas susceptible to ignition and spread of fires, coupled with episodes of intense rainfall occurring as convective thunderstorms, particularly during summer (Moody and Martin, 2001a). In this region, the Ponderosa pine (*Pinus ponderosa*) dominated forests of the cooler northern regions, and the chaparral scrub in the southwest are considered to be amongst the most fire-prone (Keeley, 2009; Keeley et al., 2008; Keeley et al., 2009; Yufang et al., 2015).

Much work has been done in the description and categorization of fire-intensity according to the characteristics of the fire itself (e.g. fireline intensity), the visible changes to vegetation (e.g. the extent and strata consumed by fire) and soil (e.g. ash characteristics, aggregate stability, hydrophobicity) (Brown and Smith, 2000; Neary et al., 2005). These United States derived categorizations have been variably applied in the Mediterranean as well as Australia, and therefore provide important frameworks for the study of post-fire erosion and ecosystem transitions beyond the region and at the global scale. In the United States, fire

regimes are classified into four main types, according to the locations and extent of damage to plants wrought by the forest fires (Brown, 2000): (i) Understory fire regimes where there is approximately 20% or less above-ground plant mortality; (ii) Stand-replacement fire regimes where 20% or less of above-ground vegetation survives, resulting in major changes in the floristic composition of a large contiguous area; (iii) Mixed-severity fire regimes occupy the variety of possible extents of fire impacts that may see differences in vegetation damage by extent, spatial patterns, species selectivity and strata affected; and (iv) Non-fire regime where there is very rare or nil occurrence of fire naturally (although human-attributed ignitions are still quite possible).

There is also the distinction between pre and post-settlement fire regimes; the significance of deliberate ignition by Native Americans in the last 20,000 years and earlier has been recognized (Brown, 2000), but not yet fully examined. The fire regimes associated with indigenous practices are in clear distinction from the significant landscape changes caused by widespread clearance of native vegetation for broadacre monoculture agriculture and settlements commencing from the turn of the 19th Century – similar to the Australian experience of pre and post European settlement and clearing of native bushland (Lunt et al., 2006). According to Youberg (2013), Ponderosa pine and mixed conifer forests used to experience low to moderate severity fires, but have recently seen a shift towards a fire regime characterized by large, extensive patches of mixed severity burns or high severity crown fires; this has been ascribed to the combined outcomes of climate change, widespread livestock grazing, fire suppression and consequent fuel buildup. This means that the impacts of fire are complex and past patterns of ignition and burning are imprinted onto current vegetation patterns and landscape processes. The lack of physiological adaptations of most forest species to extensive, high-severity fires in the landscape has meant that many forested

areas in western United States may not recover fully within the human timescale and therefore remain hydrologically and erosionally vulnerable for long time periods.

Since the 1900s, there has been an increase in mixed-severity and stand-replacement "lethal fires" compared to understorey "non-lethal fires" in the western United States. This has been due to the sharp reduction in traditional burning because of the re-location and spatial concentration of indigenous Native Americans into reservations (Grissino Mayer and Swetnam, 2000), accumulation of fuel loads due to extensive attempts at fire exclusion, and overstocking and growth-stagnation of dense stands of trees (Arno, 2000). Notably, the fire-prone ponderosa pine forests have been significantly affected and have become vulnerable to large-scale epidemics due to attacks by bark beetles and other defoliating insects, in addition to infections from a range of other diseases. The associated die-backs and increased fuel loads have therefore heightened the risk and extent of stand-replacement fires. For instance, severe wildfires burnt through close to 400,000 ha of ponderosa pine forest in the decade of 1986 to 1996 (Arno, 2000). Recently in Aug-Sep 2015, 12 large wildfires in California burnt through large tracts of scrub and forest, with the Valley Fire in Lake County having burnt 67,000 acres (approx. 27,000 ha) and the Butte Fire in Amador & Calaveras Counties having burnt 71,660 acres (approx. 29,000 ha) (State of California, 2015).

Lodgepole pine (*Pinus contorta*) forests can be particularly vulnerable to mass attacks by mountain pine beetles and this can cause severe and widespread mortality and weakening of large stands (Safranyik et al., 2007), rendering them particularly susceptible to stand-replacement fires and therefore heightened rates of erosion over long time periods. Hence, very long "windows of disturbance" (Prosser and Williams, 1998; Shakesby and Doerr, 2006; Shakesby et al., 2016; Swanson, 1981), possibly in the range of decades would be expected as forest regeneration would only progress from successful seed germination, and much time would be taken for the trees to reach maturity, even without any further major

disturbances. As noted by George et al. (2004), 'long-term erosion rates in fire-prone landscapes may be higher than often believed', and the environmental impacts of the sediment pulses when activated by significant rainfall events can thus be substantial.

Most studies of post-fire erosion are focused on the first year, or at most the first *few* years after fire. This is the period of sudden increase in the availability and erodibility of soil, ash and other organic detritus in this exposed and vulnerable condition, creating major flood and sedimentation hazards. However, this means a general paucity of knowledge about post-fire erosion dynamics after these early years. In a survey of recent works on post-fire runoff and erosion at the 2013 AGU Chapman Conference by Moody and Martin (2013), there was similar emphases. Nevertheless, there have been some studies that have examined longer-term changes of ground and soil conditions, and their responses to erosive hillslope processes. For example, Benavides-Solorio and MacDonald (2001) conducted rainfall simulation experiments on 6-year old burnt plots on lodgepole pine in the Colorado Front Range burnt in the 1994 Hourglass Fire and found that ground cover percentage accounted for a large percentage of the measured sediment yield. Larsen et al. (2009) have also conducted longer-term studies (>5 years) and raised doubts about the primacy of the contribution of soil water repellency on post-fire erosion rates, instead attributing ground cover as the principal factor controlling rates of overland flow and runoff on burnt hillslopes of the Colorado Front Range.

Recent regional-scale modelling work using the Disturbed Water Erosion Prediction Project (Disturbed WEPP) and GeoWEPP by Miller et al. (2011) predicted mean annual erosion rates of 50 to 155 Mg ha^{-1} for the forests of north-western California, western Oregon and western Washington, but much lower rates of 5 Mg ha^{-1} for the Rocky Mountains and inter-montane west. Their sensitivity analyses found greater sensitivity of erosion rates to mean annual precipitation than to bare soil percentage. More recently, Orem and Pelletier

(2016) reported that at least 90% of denudation at the geologic time scales (~10^3 to 10^6 years) in the Valles Caldera, New Mexico, could be attributed to wildfire-affected erosion. Short-term (up to 2 years post-fire) mean watershed (area-averaged) erosion rates were greater than 1 mm yr^{-1}, 103 to 105 times more than comparable unburnt areas. Long-term denudational rates (all causes including wildfire) were estimated at 0.01 to 0.1 mm yr^{-1}.

Moody and Martin (2009) provided an excellent synthesis of annual post-fire sediment yields (up to 2 years post-fire) in the western United States from a total of 70 published references (comprising 135 measurements) from 1927 to 2007. They found that the average annual sediment yield was 82 t ha^{-1} for hillslopes, three times lower when compared to 240 t ha^{-1} for channels. However, the runoff responsible for sediment generation from channels came mainly from the hillslopes. The lower hillslope sediment yield values would have been due to sediment mass values diffused over larger areal values of all the hillslope surfaces, compared to the limited "channel areas". This highlights the centrality of hillslope processes in influencing sediment processes in catchments and drainage basins. The results also indicated that sediment availability, rather than topographic slope or soil erodibility, was more important in predicting post-fire sediment yields; an essential point relevant to the present research. Based on results from the synthesis, Moody and Martin (2009) concluded that fire was an important geomorphic agent of landscape change when coupled with sufficient rainfall, and that increased post-fire erosion could be expected with increases in wildfire frequency, intensity and extent in the western United States.

In their review and projections of climate change induced shifts in Rocky Mountains ecosystems, Rocca et al. (2014) found that in the short-term (up to 50 years from present), fire frequencies were likely to increase due to higher temperatures and increased length and severity of the fire season. More winter precipitation would also occur as rain rather than snow/ice, and spring snowmelt would occur earlier, increasing the risks of intensified erosion

by splash and surface runoff. In the long-term (more than 50 years, over several fire cycles), reductions in primary production in water-limited regimes would result in reduced fuel accumulations and lower fire frequencies. These changes were projected to significantly affect the water-limited pinyon-juniper and lower montane (Ponderosa-pine dominated) forests. Similar projections were also reported with climate-wildfire-erosion ensemble modelling work by Sankey et al. (2017). With these projections, it is likely that post-fire erosion in the western United States in the next 50 years will continue to be more active and will require sustained efforts in understanding and managing post-fire erosion, and investigating rehabilitation techniques in a background shifting hydro-climatic and ecological conditions. At the time of writing, 17 large wildfires had broken out in the state of California, across the Sonoma, Mendocino, Napa and Yuba counties, burnt 115,000 acres and were yet to be controlled (CAL FIRE, 2017); and were described as 'unprecedented' in simultaneity, severity and extent (Wong and Gee, 2017), further highlighting the geomorphic significance of wildfires in the western United States in the past and present (Orem and Pelletier, 2016), as well as the future, which has been projected to see increased sedimentation in burnt watersheds, leading to heightened risks to water supply quantity and quality, stream channel stability and aquatic ecosystems (Sankey et al., 2017).

2.2. Post-fire erosion in the Mediterranean

The Mediterranean region's susceptibility to frequent wildfires arises from the distinctive hot, long and dry summers of this hydro-climatic region - type *Cs* in the Köppen–Geiger classification system (Chen and Chen, 2013). These typically lead to low fuel moisture and ease of ignition, and rapid spread of wildfire especially where regional convection in the Northern Hemisphere summer promotes high wind speeds. Proximity of natural and post-agricultural shrublands and forests to human settlements leads to both higher ignition occurrences and risks to infrastructure, property and lives. The harsh dry summers are typically followed by substantial rainfall throughout the autumn, winter and early spring seasons that provide ample amounts of fluvial to rapidly erode soil, ash and litter in the immediate to early post-fire period (Shakesby, 2011). The hazards to human lives and property due to fire, post-fire flooding and sedimentation are thus of greater imminent concern compared to most fire-prone areas in the western United States and southeast Australia.

Some of the distinctiveness of wildfire occurrence and post-fire erosion in this region is related to the long history of anthropological interference and disruption to natural ecosystems; substantial, extensive long-term clearance of natural Mediterranean forests and shrublands over many centuries (Kaplan et al., 2009), followed by more recent abandonment of agricultural lands triggering vegetation re-colonization (Kutiel, 1994; Shakesby, 2011). The contemporary introduction and expansion of fast-growing but fire-prone tree plantation species such as pine and eucalypts (in particular, *Pinus pinaster* and *Eucalyptus globulus*) into many parts of the Mediterranean such as the Iberian Peninsula for paper pulp, timber and firewood (Cerasoli et al., 2016) has exacerbated wildfire risks and occurrences, and heightened the post-fire erosion and hydrological hazards (Shakesby, 2011). Recent work by Campos et al. (2015) on post-fire erosion from monoculture plantations reported high

mercury mobilization (30% of Hg content in pre-fire soils) that add to the range of possible negative environmental impacts. Therefore, it can be surmised that post-fire erosion in the Mediterranean occurs over landscapes that have been substantially modified by humans; clearly different from many fire-prone forests, shrublands and rangelands of western United States and southeast Australia.

Post-fire erosion research in the Mediterranean has a relatively short history compared with the western United States, with peer-reviewed publications in this domain reported from the 1980s (Shakesby, 2011) even though human experiences of wildfires in this region would have been extensive throughout history. Nevertheless, various aspects of the phenomena have been investigated using a range of approaches, including soil hydrophobicity and infiltration studies (Cerdà et al., 2013; Tessler et al., 2012), catchment-scale monitoring of water, sediment and nutrients (Machado et al., 2015; Mayor et al., 2007; Moussoulis et al., 2015; Stoof et al., 2011), erosion modelling (de Vente et al., 2009; Diodato and Bellocchi, 2010), rainfall simulation studies (Rulli et al., 2006) and scaling issues (Cammeraat, 2004; Ferreira et al., 2008). Generally, Mediterranean post-fire erosion rates are lower compared to the western United States and southeast Australia, and these are mainly due to sediment-supply limited conditions on the thin and stony soils in many parts of the region, although protracted recovery periods are common due to significant post-fire soil fertility limitations (Rulli et al., 2006; Shakesby, 2011).

Notably, post-fire erosion research in the Mediterranean has seen many studies sustaining measurements over several years, giving useful insights into the transitions and complexities of post-fire processes, with contrasting results and opinions as to which are the key factors influencing post-fire erosion in their respective study areas. The reader is referred to the compilation of hillslope erosion rates by Rulli et al. (2006) and the review by Shakesby (2011) for details. Cerdà et al. (2013) advocated the long-term monitoring of soil properties

beyond the first post-fire year because of the fundamental influences of infiltration rates on the hillslope hydrological cycle, controlling runoff, water availability to plant growth and rates of post-fire vegetation regeneration. Úbeda et al. (2005) tested the soil parameters of various samples obtained 7 years after fire, from the Mediterranean region of Llagostara in Catalonia, northeast Spain which was burnt at different fire severities in 1994. Amongst several results, they found that many of the soil parameters had not reverted to the original values; soil pH of soil burnt at high intensity was significantly higher at 6.49 compared to the control forest soil at 5.94; organic carbon and N levels were significantly lower for the high-intensity burnt soil than the control. Úbeda et al. (2005) showed that post-fire recovery of soil parameters such as cation concentration, soil organic carbon and total soil nitrogen was slow after high-intensity fires, and this affected the rates and characteristics of vegetation regeneration (conifers) and their distribution. Mayor et al. (2007) analyzed the catchment-scale post-fire sediment dynamics in the dry-Mediterranean region of eastern Spain over 7 years and found prolonged periods of heightened sediment generation from burnt catchments. Rates of runoff and sediment yield increased and peaked at 3 years post-fire, and continued to remain heightened up to 5 years post-fire. These were attributed primarily to droughts that delayed plant recovery and diminished soil fertility resulting from post-fire erosion. Cerdà and Doerr (2005), in their 11-year study of post-fire erosion following severe fires in the Serra Grossa Range in eastern Spain, showed that under trees and small shrubs, substantial erosion was still occurring, whereas under herbs and shrubs, erosion was practically insignificant. This highlights the complexities of hydrological and erosional processes when examining post-fire plant canopy effects at the detailed scale. Long-term work done by Cerdà et al. (2013) on post-fire infiltration rates in the Serra Grossa, Spain over 23 years found that fire effects on reduced infiltration only applied 2 to 4 years post-fire. Steady-state infiltration decreased from 53.54 mm h^{-1} to 34.43 mm h^{-1} in the first post-fire winter with greatest

reduction of 35.45 % at 2 years post-fire, and rates recovered close to pre-fire rates after 4 years. This indicated the transience of post-fire hydrophobicity as a contributing factor to post-fire erosion rates.

Vieira et al. (2016) monitored annual runoff and sediment generation rates from microplots in three eucalypt plantations which were either ploughed or unploughed during their pre-fire history and found that unploughed sites had consistently lower sediment losses (0.11 Mg ha^{-1} y^{-1}) which were four to eight times lower than two ploughed sites (0.47 and 0.83 Mg ha^{-1} y^{-1}). Runoff volumes and coefficients were also higher for ploughed sites (slope parallel ploughed: 1257 mm, 26%; contour ploughed: 1915 mm, 40%) than for unploughed sites (865 mm, 14%) with increasing trends for runoff coefficients observed with time after fire, contradicting the general "window of disturbance" model and common expectations. Therefore, it is highly likely that post-fire runoff and erosion rates in the Mediterranean region are significantly influenced by a persistent imprint of historical human-related disturbances that influence hillslope hydrology and soil erosion.

Shakesby (2011) reviewed the state of knowledge of post-fire erosion in Mediterranean ecosystems. Important features of this region included (i) supply-limited conditions (thin soils and high stone content) leading to low post-fire sediment generation despite high hydrologic vulnerability, (ii) preferential removal of nutrient-rich and aggregative fine sediments and organic matter being as important as total soil volume eroded, (iii) aspect as a particularly important landscape factor at the macro-scale, accounting for differential erosion rates, with drier south-facing slopes more vulnerable than north-facing slopes. Key research gaps requiring attention included (i) quantitative study of post-fire soil nutrient depletion to better understand the impacts of post-fire erosion on soil fertility; (ii) the impacts of prescribed fire, increasingly being considered and used as a "dirty" fire suppression solution, on air pollution, carbon losses and soil nutrient depletion; (iii) clarifying

the scaling impacts of post-fire hydrophobicity on hydrological and erosional processes operating at the hillslope and catchment scales; (iv) wind erosion effects on post-fire soil loss and nutrient depletion. These research gaps are underscored by reports of both intensification and areal expansion of aridity in the Mediterranean region in the past century (Chen and Chen, 2013).

Climate change is also expected to lead to shifts in fire regimes and ecosystem functions and patterns in the Mediterranean region due to increased aridity (Gao and Giorgi, 2008); similar to the western United States and southeast Australia (Shakesby, 2011). Ecosystem modelling by Guiot and Cramer (2016) predicts that the Mediterranean region will see rapid ecosystem changes outside the Holocene envelope in response to a possible global warming scenario of 2°C or above because of increased radiative input and reduced precipitation. The risk of wildfires would be heightened, and changes in vegetation structures and floristics towards more aridity-adapted, xerophytic forms are likely. Indeed, where fire effects are severe and frequencies are high, populations of common species such as *Pinus sylvestris* (Scots Pine) could fail to re-establish post-fire due to limited seed availability and dispersal, competition from herbs and sprouters, and high soil aridity, signalling substantial floristic composition shifts as a strong possibility (Vacchiano et al., 2014). Furthermore, the combined effects of climate change and increased fire frequency and extent are likely to result in increased occurrence of flash floods and heightened sediment generation from burnt catchments (Versini et al., 2013).

This brief review of post-fire erosion in the Mediterranean region illustrates the complexity of the phenomenon and the importance of further work to ultimately distil the key factors influencing the rates of soil erosion, their fate and the concomitant impacts on the source and destination sites especially on soil fertility, the rates and characteristics of post-fire recovery, and the response to higher-order shifts in environmental parameters due to

climate change. Fire-induced soil hydrophobicity, frequently cited as a major contributor to accelerated erosion (Doerr et al., 2006; Doerr et al., 1996; Letey, 2001; Shakesby et al., 2000; Tessler et al., 2012), is likely to be only one of the many factors such as inherent soil and landscape attributes, rainfall characteristics and vegetation re-growth to collectively control post-fire erosion rates (Shakesby, 2011; Shakesby, 2013). Landscape patches covered by *Eucalyptus* and Pine plantations may play distinctive roles in post-fire Mediterranean sediment dynamics, and work done on regions containing comparable tree species, such as Eucalypt forests of southeast Australia or Pine forests of western United States could provide some useful insights. The relatively longer-term studies in the Mediterranean have also shown how protracted "windows of disturbance" with heightened hydrologic and erosional vulnerability can be created because of retarded vegetation regrowth arising from a combination of prolonged drought conditions, diminished soil fertility due to post-fire erosion itself removing fine sediments and organic matter from top layers, and inherently skeletal soils to begin with. It is these complex moderate to longer-term patterns of change in vegetation and erosion that need to be examined in the hydro-climatic and eco-geomorphological context of southeast Australia, the subject of the following section.

2.3. The distinctive southeast Australian context

In this section, I examine in some detail, aspects of southeast Australian eucalypt forests as they relate to fire occurrence, post-fire vegetation regeneration, hillslope hydrology and hillslope erosion. Shakesby et al. (2007) opined that deeper and more comprehensive understanding of post-fire erosion and associated hazards could only be attained by 'adopting a concept of global regional variants and endemic factors that distinguish some regions in terms of post-fire erosion characteristics' (p. 347); the eucalypt forests of southeast Australia, one of the most wildfire prone regions in the world, are seen to be distinct from other comparable fire-prone regions of the western United States and the Mediterranean. Recent reviews by Moody et al. (2013) and Shakesby (2011) provide detailed analyses and commentary on the state of knowledge in these two latter regions in addition to the overview provided in the previous two sections. Some of the distinctiveness of post-fire hydrology and erosion in southeast Australian forests stems from unique biological features of many eucalypt species, such as rapid post-fire vegetation re-growth, fine root mats, abundant development of litter-dam microterrace complexes (Shakesby et al., 2007) and high levels of bioturbation activity especially by ants (Wilkinson et al., 2009) which lead to distinctive geomorphological impacts manifested as seemingly short periods of erosion vulnerability and high density of plant and microtopographic sinks for overland flow and hillslope sediments, when compared to similarly fire-prone landscapes in the western United States and the Mediterranean. Adding to the specificity of the southeast Australian context is how the hydro-climatic regime and accompanying meteorological features are strongly influenced by the El Niño-Southern Oscillation (ENSO) (see Chapter Three).

<u>2.3.1. Flammability</u>

The eucalypt forests of southeast Australia are highly flammable (Gill and Zylstra, 2005). This is due to the combination of hydro-climatic (Sturman and Tapper, 2006) (see also Chapter Three) and plant physical and biochemical characteristics (Williams and Woinarski, 1997). While many parts of the region are classified under temperate climate regimes: types *Cfb* or *Cfa* (Chen and Chen, 2013), the region typically experiences long hot summers that dry-out the litter increasing ignitability and fuel loads in the background of increased leaf-fall from plants due to heat and water stress, after some vigorous growth during the preceding wet and temperate spring season. Live plant parts and foliage also become dehydrated and above-ground fuels are also rendered vulnerable to being ignited and combusted. The sclerophyllous foliage with low water, high natural oil and lignin contents can ignite easily and fuel wildfires of high severity and intensity (Orians and Milewski, 2007). Hence, southeast Australia experiences large fire events even though high precipitation amounts (i.e. ≥ 550 mm annual rainfall) are received (Hantson et al., 2017).

Post-fire field assessment of burn severity in southeast Australia is usually done using a visual, qualitative approach categorizing areas of interest by the strata (ground/shrub/crown) consumed by fire, and whether stems ≥ 10 mm diameter were consumed by the fire, into six levels: (i) unburnt; (ii) low; (iii) moderate; (iv) high; (v) very high; and (vi) extreme (Chafer, 2008; Chafer et al., 2004; Hammill and Bradstock, 2006; Heath et al., 2016). These are shown in Figure 2-1.

(i) unburnt (no visible damage)	(ii) low severity (grasses/herbs burnt)
(iii) moderate severity (shrubs consumed)	(iv) high severity (lower canopy scorched)
(v) very high severity (stems < 10 mm diameter consumed)	(vi) extreme severity (stems ≥ 10 mm diameter consumed)
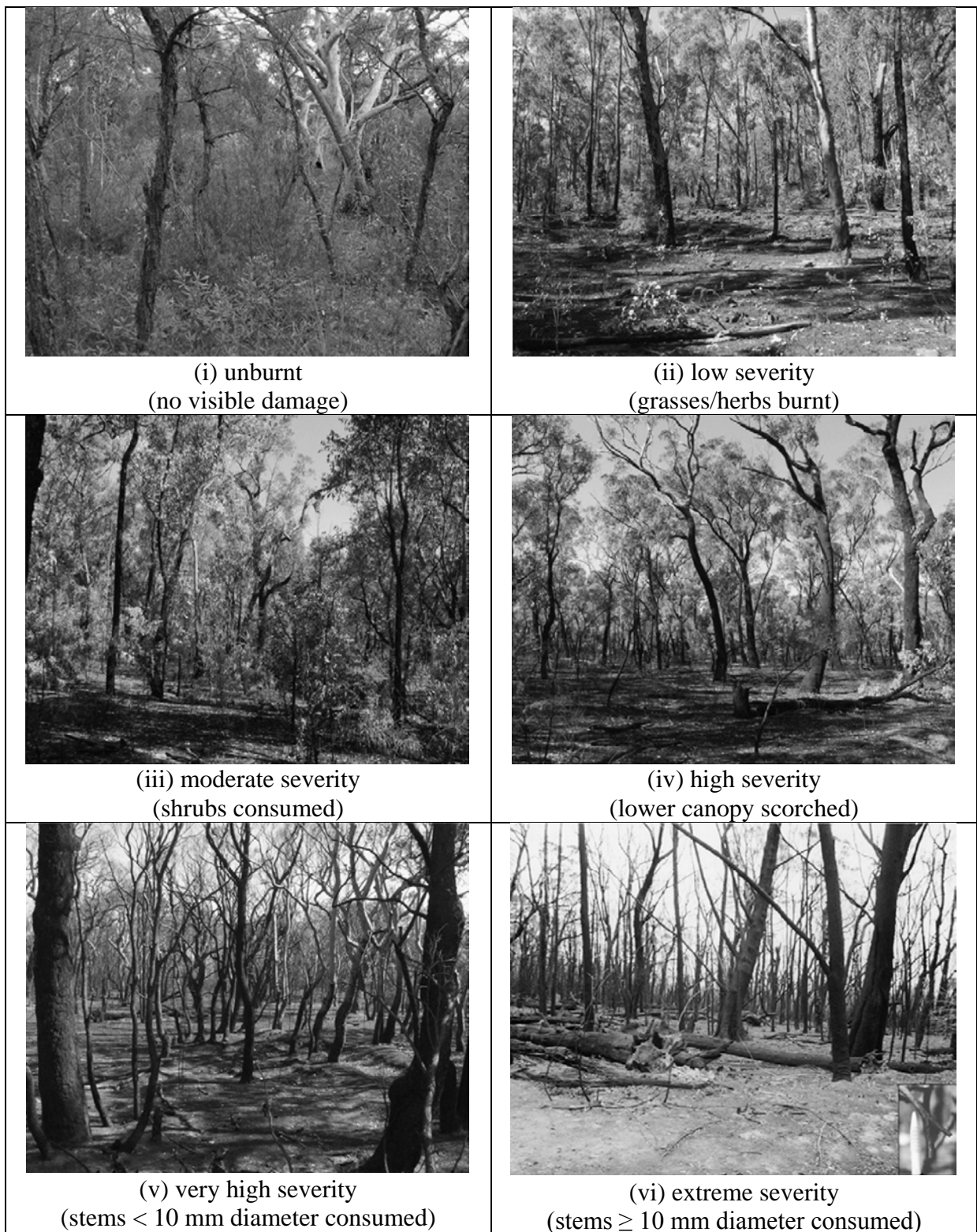
Figure 2-1. (i) to (vi). Fire-severity classes based on visual assessment of vegetation damage by burning. For (vi) note the bottom-right inset showing a nominal scale comparison between a pen and a sample burnt twig of diameter ≥ 10 mm. Source: Chafer (2008).

High to extreme severity wildfires have the potential to cause widespread tree mortality as well as weaken surviving individuals at the landscape scale, rendering them vulnerable to toppling by strong wind gusts on what are usually shallow, poorly aggregated and desiccated burnt soils. Post-fire tree throw has been reported in different regions (Bohlin et al., 2017; Brown and Smith, 2000; Hancock et al., 2012; Miller, 2000; Phillips and Marion, 2004) and is broadly recognized as playing a role in soil development and landscape evolution by creating 'pit-mound' topographies on hillslope, although this has been poorly studied (Gabet et al., 2003; Hancock et al., 2012). For *Eucalyptus* species, lignotubers, prominent nutrient-rich swellings of the root crown (also called "burls") are commonly observed just above or below the soil surface, and can bud and extend shoots very soon, sometimes in weeks, after disturbances such as fire. (Carr et al., 1982; Chattaway, 1958; Jacobs, 1955; Penfold and Willis, 1961; Pryor, 1976). While lignotubers are by no means exclusive to the Eucalyptus genus (Paula et al., 2016; Susanne, 1984), this means that compared with the fire-prone forest or woodland formations in regions such as the USA and Mediterranean, many eucalypt forests (especially dry types) have greater volumes of the hillslope occupied by larger total root mass that includes lignotubers. Therefore, where tree-throw were to occur, the pit-mound topography could be quite pronounced, and the consequent pedological changes rather distinct (Amundson et al., 2015; Phillips and Marion, 2004). As discussed by Phillips (2017), the long-term pedological changes from such disturbances could lead to convergent or divergent development of soilscapes; or a complex combination of both.

Fire regimes in Australia have shifted in the past, and can be broadly divided into the following phases: (i) naturally-caused, possibly low-frequency pre-Aboriginal influence more than 60,000 years ago; (ii) the Aboriginal-influenced, pre-European phase, from approximately 60,000 years ago to the 1800s during which there would have been increased

but probably spatially-dispersed fire frequency; and (iii) the European (colonization) phase from *circa* 1800 to present times, which has seen early extensive land clearance for agriculture using fire, and increased fire frequency and extent particularly in recent times, along with more recent attempts to suppress fire hazards through low-intensity prescribed burning to reduce fuel loads (Bowman et al., 2011; Bradshaw, 2012; Eamus et al., 2006). With the rapid expansion of human activities and settlements, human-initiated as well as naturally-attributed (lightning strikes) ignitions are likely to have contributed to increased ignition frequency. Although located in the temperate climatic zone where rainfall is adequate and well-distributed across seasons, supporting year-round growth and large tracts of dry to wet sclerophyll forests, there can be significant variability in rainfall depth and distribution on an inter-annual and inter-decadal basis because of regional climatic controls through the El-Nino Southern Oscillation (ENSO), the Indian Ocean Dipole (IOD) and the mid-latitude ridges and troughs (Sturman and Tapper, 2006); more details in Chapter Three. The plant species making up much of the fire-prone dry-sclerophyll forest, such as the *Eucalypt* and *Acacia* genera (Eamus et al., 2006), in this region are adapted to survive drought conditions that recur on an approximately decadal basis, and can extend for several years. Of particular relevance is the Millennium Drought that affected most parts of Australia from 2001 to 2009 (van Dijk et al., 2013), and was associated with the occurrence of the extensive fires of 2006/7 (Great Divide Fires) which affected the study area in the present research (Flinn et al., 2008a), and the 2009 Black Saturday Bushfires (Cruz et al., 2012). The abundant organic litter - leaves and twigs of the *Eucalypt* and *Acacia* genera are recalcitrant, resisting rapid decomposition even when moist, due to their sclerophylly and high tannin contents. Therefore, they accumulate and remain readily available as potential fine fuels for long periods of time on the forest floors while offering significant protection by attenuating rainfall and throughfall splash effects and disrupting overland flow.

During summers, and enhanced by droughts (some multi-year), rapid curing occurs and dry litter accumulates on forest floors. Elevated fine fuels in the form of shrubs and saplings and shallow-rooted ground-strata plants (e.g. grasses) also become susceptible. Upon ignition, these fine fuel sources would burn strongly and spread rapidly upon ignition vertically and horizontally, especially when strong regional winds accelerate the spread of fire (Clarke et al., 2011). The results of such extensive burning with high severity over very large areas - mega-fires (Bradstock, 2008; Fairman et al., 2015) create extensive areas of bare and dry hillslopes with minimal canopy or ground cover, burnt large diameter litter (trunks and branches), ash layers of variable thickness, and highly erodible, poorly aggregated soil depleted of moisture and organic matter that are highly vulnerable to erosion by post-fire rainfall events, with the possibility of this vulnerability remaining heightened for prolonged time periods.

2.3.2. Post-fire regeneration

In contrast to many of the forests and woodlands of the western United States, *Eucalyptus* and *Acacia* genera which dominate forests of southeast Australia are well-adapted to the effects of wildfire (Fairman et al., 2015) and therefore regenerate rapidly after being burnt during severe wildfire. Many eucalypt species are facultative re-sprouters and are able to regenerate after fire through new growth from their undamaged epicormic tissues (Meier et al., 2012a) or from lignotubers ("burls"); new individuals will also readily germinate from seed should the seedbank still be available and not depleted through erosion or destroyed by the fire; many *Acacia* species are prolific seeders and germination is stimulated by heat and smoke generated by fires (Whelan, 1995).

In contrast, it is uncommon for conifers in the United States to resprout epicormically from the root collar or root crown after fire (Miller, 2000). Hence, there is little post-fire resprouting ability of this plant group; similarly, for the broad-leaf evergreen trees.
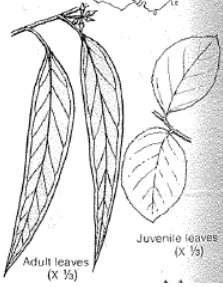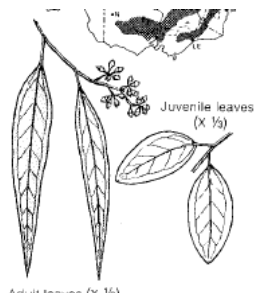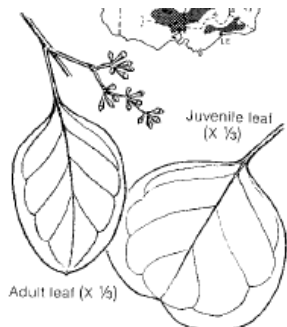
Deciduous trees and shrubs would commonly sprout from root collar, root crown or roots, with some shrubs re-sprouting from rhizomes but these may be severely damaged where severe fires on the forest floor have caused significant damage to plant organs; most forest trees in the western USA rely strongly on seedling establishment in severe, stand-replacement fires because it is likely that most of the above-ground and surface/near surface litter and mineral horizons and plant parts could be damaged irreparably during fire (Miller, 2000). Where the fire has been particularly severe and intense and/or severe erosion of the topsoil has occurred during large post-fire events, the substantial depletion of the seed bank through heat damage and/or removal would see large tracts of forests populated by dead trees and slowly recovering ground and shrub cover as long as decades, as recruitment of new individuals may occur by importation for unaffected areas at the edges of the burnt region, or from faunal action. Rapid vegetation regeneration due to fire-adapted physiological features of eucalypts and establishment of ground litter layer have frequently been invoked as reasons for quick recovery of erosion rates to close to "background" levels from very high values in the immediate post-fire period (Shakesby et al., 2007). Indeed, Vivian and Cary (2012) highlight how the specific environmental conditions of mountainous southeast Australia create limits across all the studied shrub species in terms of post-fire ecological responses (e.g. leaf traits with respect to nutrient accumulation)

2.3.3. Leaf characteristics

One of the interesting aspects of southeast Australian eucalypt forests that has not been examined in much detail is the unique leaf characteristics of plant species in this region compared to those in other fire-prone regions in the world, and how these might influence forest hydrological and erosional processes. Many *Eucalyptus* and *Acacia* species in Australian dry sclerophyll forests exhibit heterophylly - having different leaf forms (shape and size) between the juvenile and adult stages (Penfold and Willis, 1961), with both leaf

forms co-existing near or at maturity (Brooker and Kleinig, 2006; Jacobs, 1955). For instance, typical dry sclerophyll forest species such as *Eucalyptus macrorhyncha* (Red Stringybark) have juvenile leaves that are sessile or shortly petiolate, and are ovate in shape with dimensions 12 x 5 cm (length x breadth) while the adult leaves are petiolate and lanceolate, with leaf dimensions up to 15 x 2.5 cm; *Eucalyptus polyanthemos* (Red Box) have juvenile leaves that are petiolate, orbicular, emarginated with dimensions 6.5 x 8 cm while the adult leaves are petiolate, arranged in alternating fashion, are ovate to broad lanceolate to 9 x 3 cm or lanceolate to 14 x 3 cm (depending on subspecies) (see Table 2-1).

Table 2-1. Juvenile and adult leaf characteristics of 3 common *Eucalyptus* species found in dry sclerophyll forest in southeast Australia – the Licola study area investigated in this research (Brooker and Kleinig, 2006).

Species (Common name)	Leaf characteristics	Pictorial illustration (Costermans, 2009)
Eucalyptus macrorhyncha (Red Stringybark)	Juvenile: • Sessile or shortly petiolate • Ovate, to 12 x 5 cm Adult: • Petiolate • Lanceolate, to 15 x 2.5 cm	
Eucalyptus melliodora (Yellow Box)	Juvenile • Petiolate • Elliptic, to 11 x 5 cm Adult • Petiolate • Narrow-lanceolate to lanceolate, to 15 x 1.8 cm	
Eucalyptus polyanthemos (Red Box)	Juvenile • Petiolate, orbicular, emarginate • 6.5 x 8 cm Adult • Petiolate; Alternating • Ovate to broad-lanceolate to 9 x 3cm (subspp. Polyanthemos and vestita); or Lanceolate to 14 x 3 cm (subsp. Longior)	

Most eucalypts have a pendulous, steep hanging habit that presents a small vertically-facing leaf area; steep leaf angles (i.e. vertical foliage) are widely believed to reduce mid-day heat stresses, increase water efficiency and carbon gain by focusing photosynthetic activity towards the early and late daylight hours of the day, especially during summer (Williams and Woinarski, 1997). With this adaptation, light is also intercepted more efficiently when low solar elevation angles occur during winter and at the mid and high latitudes; radiative heat loss during cold, clear nights in late autumn, winter or early spring months can also be minimized (Anderson, 1981; Brooker and Kleinig, 2006; Falster and Westoby, 2003; Jacobs, 1955; James and Bell, 2000). Furthermore, the leaves of most *Eucalyptus* species are strongly sclerophyllous in texture, rendering them quite hydrophobic, and are flat with minimal curvature of leaf surfaces, meaning that little water is typically retained on the leaves.

In relation to hillslope hydrology and erosion, the interception and canopy storage capacity of eucalypt leaves and open canopy in dry sclerophyll forests (Eamus et al., 2006) are likely to be lower than other tree genera and species such as pine, fir or oak that are widespread in western United States and the Mediterranean (although it should be noted that *Eucalyptus* plantations are increasingly popular in this region). The sparse canopy could also enable higher rates of evapo-transpirative losses from the forest floor, contributing to the dryness and fire-risk of these vegetation formations. However, the *Eucalyptus'* unique leaf and branching habits may lead to increased interception of rainfall arriving with a strong wind-induced horizontal component. Also, dense and rapid post-fire regrowth of wider and larger juvenile leaves are likely to cause higher interception rates and rainfall modulation effects compared to unburnt individuals and stands with narrower and smaller mature leaves. The possible throughfall effects are discussed in Section 2.4.5. In the present study, the focus

61

is on the foliage characteristics of *Eucalyptus polyanthemos*, the dominant species at the study site, described in Chapter Three.

2.3.4. Crown architecture

Crown characteristics (e.g. overall shape, branching habit, leaf density and orientation) are primarily the outcome of inherent genetically-determined physiological factors, the prevailing patterns of solar radiation (direction, intensity) and interaction with other competing individuals (Pearcy et al., 2005; Penridge and Walker, 1988; Walker et al., 1988). At higher latitudes, aspect is also a key factor where structural and foliar growth may be oriented towards the predominant direction of the sun (viz. south-facing in the northern hemisphere and vice–versa). In many cases, the branches of mature-crowned eucalypts have no specific growth habit but tend to spread to a typical "mushroom" fashion as clumps of twigs and leaves; some branches angle downwards at the ends while others reach upwards. This is in contrast to other tree species like hazel, radiata pine and Douglas fir in North American coniferous forests, which have branches that slope downwards *towards* the stem and facilitate comparatively higher stemflow production (Langford and O'Shaughnessy, 1978). The density of leaves in the crowns of eucalypts, measured through the Leaf Area Index (LAI) are also very low compared to other forests; Anderson's (1981) study of Leaf Area Index (LAI) of 16 locations in southeastern New South Wales mostly covered by eucalypt forest, found that values were consistently low at the average of 1.5 to 1.9. While leaf characteristics are inconsequential in the immediate post-fire period, they become increasingly important as the typically rapid post-fire re-growth by eucalypts take effect in the ensuing years, as the ecosystem enters the intermediate canopy recovery phase.

The hanging habit, leaf shapes and branching habits contribute to the development of an open crown, even for fully developed crowns of mature eucalypts (Specht, 1970). This results in significantly weak overhead shade, even where total leaf areas can be as high as

those of European hardwoods; the Forestry and Timber Bureau found that leaf area of an alpine ash (*Eucalyptus gigantea*) was six times the vertical crown projection on the ground. The Ponderosa pine, common in the Colorado Ranges of the western United States, has the typical narrow triangular "Christmas tree", or pointed top/teardrop crown shapes with dense foliage for canopy trees younger than 150 years old (Huckaby et al., 2003). Eucalypts provide substantial side shade but poor overhead shade (Jacobs, 1955). Eucalypt foliage also tends to "clump", making it likely to produce distinct rainfall interception and modulation characteristics, and under-canopy microclimates. Moisture levels of the 'O' and 'A' horizons under these open-canopy conditions are therefore likely to be low with the high exposure to solar radiation increasing ground-level evapotranspiration rates. Crockford and Richardson (1990d) reported consistently lower rainfall interception rates for dry eucalypt forests compared to pine plantations for continuous and discontinuous rainfall events; eucalypt forest intercepted approximately 7% while pine plantation intercepted approximately 12% of a discontinuous 25 mm rainfall event. This would also contribute to low canopy storage capacity, interception, distinct throughfall spectra through crown-architecture and foliage-determined modulation of precipitation, affecting the volume, rates and characteristics of the water reaching the ground surface affecting hydrology, splash effects and overland flow generation.

2.3.5. Canopy modulation and throughfall in intermediate post-fire conditions

When the different factors of crown architecture, foliage habits and post-fire regrowth characteristics combine, it is highly likely that *throughfall spectra*, the distribution and range of drop sizes, their number and rates of arrival at the forest floor during and after rainfall events, vary considerably between different vegetation formations and species of different regions at the global scale (Anderson et al., 2005). Different species, subspecies and floristic compositions would also occur across different forests in the same broad region; for example southeast Australian dry vs. wet eucalypt forest, and the attendant variations with aspect and topography. Therefore, one would expect to find varying states and rates of post-fire vegetation regrowth at different spatial and temporal scales. A selection of studies serves to illustrate this point. Zhou et al. (2002) reported increased kinetic energy of throughfall drops and accelerated soil erosion for rainfall intensities between 5 mm h^{-1} and 20 mm h^{-1} for single-layer canopy *Eucalyptus exserta* plantations in southern China. Brauman et al. (2010) demonstrated how increased canopy density and height contributed to levels of throughfall that were double those found in another similar forest with lower canopy density and height, primarily because of the differential rate of cloud interception in native forests on the leeward side of Hawaii island. Mululo Sato et al. (2011) described the spatial heterogeneity and temporal stability of throughfall in plantations of hybrid *Eucalyptus grandis* and *Eucalyptus urophylla* in southeast Brazil, highlighting the distinctive 'funnel effect' of the tree canopy architecture as a key factor in the observed patterns. One of the sampling arrangements in this study saw throughfall/precipitation ratio of 146% at positions close to the tree trunks, while between-trunk locations had ratio of 86%. Looking at non-eucalypt throughfall, Geißler et al. (2012a) used sand-filled cups to compare erosivity under old and young growth stands of *Schima superba* and *Castanopsis eyrei* with open-field rainfall in Gutianshan National Nature Reserve (GNNR) in humid subtropical southeast China and found that under-canopy

erosivity was 2.59 times that of open-field rainfall. They also found that medium and old growth forests had throughfall erosivity 1.53 times that of young forest, and that significant differences in throughfall heterogeneity were found between the two tree species.

The literature on the influences of vegetation differences on hydrological and geomorphological processes; in particular throughfall and under-canopy hydrology and erosion, across southeast Australia, is rather limited. For intermediate post-fire vegetation, it is virtually non-existent; most post-fire erosion studies in this area have been concerned primarily with hydrological partitioning and water resources, rather than hydrology and erosion at the hillslope and plot scales. Indeed, work by Onda et al. (2008) demonstrated the dynamic evolution of soil surface and hydrological characteristics over very short timescales. Hence, even though hydrologic vulnerability in dry eucalypt forests can remain high (see Chapter One), even when under intermediate recovery conditions, there is little formal knowledge in this area, and this gap needs to be addressed. Langford and O'Shaughnessy (1978) found that mixed species of mature dry sclerophyll forest intercepted approximately 23.3% of gross rainfall, with throughfall percentage of approximately 75.4%. In combination with the leaf characteristics and branching habits of eucalypt trees mentioned above, it is possible that raindrops encountering a mature or substantially regenerated eucalypt canopy may be substantially modified by coalescence of smaller droplets into larger ones, and consequently have greater erosivity than open-field raindrops. No previous work on this has been found.

Using a rainfall simulator on six *Eucalypt* tree species, one *Acacia* species and one *Pinus* species, Aston (1979) showed that the proportion of rainfall passing through the canopy was a function of the leaf area index. Crockford and Richardson (1990a) characterized the hydrological partitioning of *Eucalyptus mannifera* and *Pinus radiata* trees and found substantially high spatial heterogeneity of throughfall for *Eucalyptus* compared to

Pinus due to the development of numerous drip points associated with the clumping of leaves and pendulous leaf habit of the *Eucalyptus* canopy. At the catchment scale, Kuczera (1987) developed a two-parameter model of long-term water yield for the *Eucalyptus* regnans (Mountain Ash) catchments following disturbance by bushfires, and suggested that water yields would recover only after the forest reached maturity, 100 to 150 years after commencing regeneration. In the intervening years, complex changes in canopy composition and cover contributed by various strata and plant species would combine to influence forest hydrological and erosional processes. More recent work on the association between canopy cover and characteristics of *Eucalyptus* forests and catchment water balance that explicitly incorporate considerations of hydrological partitioning include studies by Mitchell et al. (2012), Webb et al. (2012) and Brookhouse et al. (2013).

Past post-fire erosion studies in Australia have   given minimal in-depth treatment of the vegetation factor. There is usually description of the original vegetation types and cover, observations of vegetation condition as indicators of fire severity, and the percentage of ground or canopy cover recovered after several years with little further detail. This at best represents the key vegetation factor as a grey-box. Although Shakesby et al. (2007) developed their review based on a noticeable number of studies conducted on post-fire erosion in southeast Australia, the distribution of studies and the range of methods and scales adopted in the various work also enabled some gaps in the current research landscape in this region to be identified. I observed the strong emphasis on sclerophyll forests on sandstone terrain in New South Wales and more specifically the Sydney Basin, with a smaller number of studies scattered across Victoria and the Australia Capital Territory. This means that many of the reported soil erosion rates were based largely on yields from areas with coarse soil textures. In eastern and southeastern Victoria, many catchments are underlain by Palaeozoic mudstone and siltstone, as well as sandstone (Birch et al., 2003). Together, these parent

geologies contribute to the development of fine-textured soils (CSIRO, 2011) that have lower infiltration rates than coarse-textured sandy soils from sandstone, and are more erodible (Bryan, 2000; Lal and Elliot, 1994; Song et al., 2005).

At present, the specific effects of vegetation characteristics on hydrological partitioning and hillslope erosion are treated rather simplistically. Along with the reporting on the background of the study site in terms of geology, soil characteristics and general rainfall inputs, there are few clear links made to the operation of the hydrological and geomorphological processes being investigated. Table 2-2 summarizes the studies conducted in southeast Australia relevant to this work; with the selection developed initially from the review by Shakesby et al. (2007), and then updated by searching for relevant articles conducted on the region of interest - southeast Australia, citing the review. It was observed that most of the studies focus on the immediate post-fire period, where high erosion rates and the occurrence of corresponding hazards are reported. These usually halt when the study areas are seen to have reverted to "background" levels of catchment, hillslope or plot erosion rates. Furthermore, many studies in the region have been conducted at the catchment scale, which do not enable detailed insights into vegetation-erosion interactions at the hillslope and plot scale, the importance and complexity of which are emphasized in this chapter. Furthermore, the reduction of erosion rates is generally attributed to the regeneration of vegetation in particular of ground cover without further detailed quantitative treatment or incorporation of the role of canopy cover. Recently, the review on relationships between soil burn severity and post-fire runoff and interrill erosion response by Vieira et al. (2015) noted that only one out of the twenty studies cited was conducted in southeast Australia; the study by Sheridan et al. (2007). Hence, for this region, there is currently little insight into the complex influences exerted by recovering canopy cover *and* other sub-strata on hydrological and erosional processes that are likely to be of scientific interest and applicability.

Table 2-2. Survey of selected studies on post-fire erosion in southeast Australia (with focus on Victoria). (Earlier studies in Appendix A)

Authors	Location(s) and fire(s)	Focus of study	Vegetation type(s)	Treatment of vegetation factor	Experiment/ observation timeframe	Geology and soils	Selected findings
Nyman et al. (2019)	Various large-scale fires in southeast Australia; Grampians 2006, Wilson's Promontory 2005 and 2009, Beechworth and Kilmore 2009.	Investigation of post-fire debris-flow occurrences in relation to ENSO-related climatic extremes; 21 debris-flow clusters identified in the study area, which occurred in 11 periods from 2003 to 2013.	Grassy or shrubby dry sclerophyll forests, floristics varying with study location	Background factor; rapid post-fire recovery of eucalyptus forests indicated.	2003 to 2013	Beechworth and Kilmore-Murrundindi: mostly Silurian mudstones (marine); clay-rich loams. Wilson's Promontory (granite) and Grampians (sandstone), loamy sands.	Two distinct debris-flow mechanisms. Runoff-generated type on clay-rich soils after extreme rainfall events after/during drought (El Niño related). Landslide-generated type on sandy soils independent from fire history from extreme rainfall (La Niña related).
Yang et al. (2018)	Warrumbungle National Park in New South Wales; Jan 2013 severe fires.	Near real-time prediction of erosion risk using revised universal soil loss equation (RUSLE) and event/daily-based rainfall data. Twelve closed erosion plots at various locations used for 'ground-truthing'.	Grassy and shrubby dry-sclerophyll forest according to Hunter (2015); similar vegetation structure to Victorian dry-sclerophyll forests.	RUSLE Cover and management (C-factor) determined using MODIS, Landsat 8 and RapidEye satellite imagery combined with ground survey and on-ground hyperspectral soil-vegetation data.	2013–17	Geology: Warrambungle Volcanics (basalt) overlying Jurassic sandstones. Soils: Brown to red Dermosols; Red and yellow Chromosols; Rudosols on recent exposures	For all erosive events (> 12.7 mm depth), modelled average hillslope erosion was 1.35 Mg ha-1 yr-1 from 2013-17, with declining trend. Minimum 0.10 Mg ha-1 yr-1 , maximum 50.56 Mg ha-1 yr-1 ; standard deviation 9.36 Mg ha-1 yr-1. Significant
Zhou et al. (2015)	Yarra River, La Trobe River and Starvation Creek catchments. Ash Wednesday fires, 1983 Moderate to severe burns affecting 19 to 84% of catchments.	Quantifying impacts of bushfire occurrences and climate variability on post-fire streamflow in three burnt catchments, using (AWRA-L, Xinanjiang and GR4J hydrological models.	Mostly wet sclerophyll forests dominated by E. *regnans*, and including E. *obliqua*, E. *cypellocarpa* and E. *sieberi*.	Post-fire vegetation recovery extent affects modelled interception storage, evapotranspiration losses, soil moisture storage, infiltration-excess/saturation-excess runoff, and groundwater storage/drainage.	1983-1999	Victorian Central Uplands composed of Devonian granites fringed by hornfels. Soils mostly deep, well-structured Ferrosols and Dermosols with high moisture storage capacity and good hydraulic conductivity.	Results show that for the first 15 years post-fire, vegetation losses (retarded evapotranspiration) and soil surface changes (reduced infiltration rates) account for streamflow increases. Climate effects observed after this period, with continued effects from vegetation and soil recovery.
Nyman et al. (2015)	Eastern Victorian Uplands (various research stations). 2007 Great Dividing Range Fires and 2009 Black Saturday Fires	Field-surveys of post-fire debris flows to quantify erosion magnitude, identify sources and causal storm characteristics. Evaluate topographic factors and model/identify risk areas.	Dry sclerophyll forests at lower elevations and rain-shadows to wet sclerophyll (Alpine or Mountain Ash) at higher / sheltered areas.	Forest types and extent of post-fire recovery key factors affecting the triggering and magnitude of debris flows with respect to rainfall event intensity-duration.	2007-2009	Palaeozoic marine mudstone, shales and sandstone with sporadic granitic intrusions and volcanics	315 debris flows; 1st two years sediment yields: 113–294 t ha⁻¹ (2–3 orders magnitude > undisturbed forests). Volumes 539 to 33,040 m³; hillslopes contributed 18–62% of total.

Authors	Location(s) and fire(s)	Focus of study	Vegetation type(s)	Treatment of vegetation factor	Experiment/ observation timeframe	Geology and soils	Selected findings
Nyman et al. (2011)	16 locations distributed across the Great Dividing Range in Victoria	Identification and description of post-fire debris flows at various locations	15 sites with grassy, heathy or shrubby dry sclerophyll forest & 1 wet montane forest	Observed 'rapid recovery of the overstorey vegetation… within the first year of after wildfire'. No specific quantitative description	Variable, ranging from 0 to 8 years after fire	Mostly Palaeozoic marine sedimentary with distinct areas of fluvial sedimentary, metamorphic (schists and gneisses) and patches of granitic formations	All debris flows occurred within 12 months after fire; triggered by intense short-duration events of I_{30} (35-59 mm h^{-1}); runoff generated debris flows important post-fire process in dry eucalypt forests.
Sheridan et al. (2011)	Slippery Rock Creek and Springs Creek, East Kiewa Research Catchments, NE Victoria	Catchment-scale discharge and sediment concentration using weir/flume at catchment outlets; turbidity probes; flow stage water auto-sampler	Wet eucalypt forest; *E. delegatansis* (lower slopes), *E. regnans* (upper slopes)	Vegetation cover measured using 900 cm^2 frames along transect Vegetation recovery phase was the main cause of irregular patterns in sediment rating exponent "*b*"; no details provided on vegetation recovery and not utilized quantitatively as factor affecting sediment exports	3 years post-fire	Quartz diorite and gneiss; friable brown gradational clay-loams and sandy clay-loams generally not extending 1.5 m depth; Acidic Eutrophic Red Dermosols.	Maximum non-linearity between discharge and sediment delivery in immediate post-fire period; reducing hillslope and increasing channel contributions of sediment through time; recovered state achieved 24 to 38 months after fire.
Nyman et al. (2010)	Slippery Rock Catchment, East Kiewa Research Catchments, NE Victoria; 2007 high-intensity fires	Combined effects of soil water repellency and macropore flow on hydraulic conductivity on burnt forest soil using tension (mini-disk) and ponded infiltrometers	Wet sclerophyll forest of mainly Alpine Ash (*Eucalyptus delegatiensis*) with scattered Mountain Gum (*Eucalyptus darlympeana*)	Rapid vegetation recovery invoked as key reason for rapid recovery of infiltration and runoff to "pre-fire conditions" Fire-induced water repellency is widespread	2nd and 8th month of the first year following fire in 2007.	Gneiss and schist from regionally metamorphosed sedimentary rocks; Acidic Eutrophic Red Dermosol with friable and highly structured clay-loam A-horizon.	70% and 60% of plot areas were water repellent in summer and winter respectively. Macropore flow helped to negate water repellency effects; occurrence of ponding important for infiltration
Smith et al. (2010)	Northeast Victoria -Flat Creek and Steep Creek; 2005 prescribed burns; 2006 prescribed burn to riparian areas	The effect of the prescribed fires on stream exports of suspended Sediment using weirs and automatic water samplers at catchment outlets	Mature dry to damp open Eucalyptus forest with dominant species including narrow-leaved peppermint (*E. radiata*), broad-leaved peppermint (*E. dives*), red stringybark (*E. macrorhyncha*) and manna gum (*E. viminalis*).	Burnt areas were mapped Ground cover for riparian areas surveyed along 25 m transects using visual comparison of 0.2 by 0.2-m quadrats. Rapid riparian area ground cover recovery was quantified (2006: 47%; 2007:86%) and invoked as a causal factor for reducing catchment exports.	0 – 18 months after fire	Ordivician sandstones, siltstones and mudstones; silty loam to heavy clay at depth with variable gravel content	Significant difference between pre and post-fire with peak suspended sediment of 11.5 kg ha^{-1} yr^{-1} and total P of 0.016 kg ha^{-1} yr^{-1}. Strong correspondence of catchment exports with rainfall input volume. Period of erosion vulnerability up to 18 months.

Authors	Location(s) and fire(s)	Focus of study	Vegetation type(s)	Treatment of vegetation factor	Experiment/ observation timeframe	Geology and soils	Selected findings
Noske et al. (2010)	East Kiewa, northeast Victoria Slippery Rock Creek and Springs Creek; 2003 moderate-severe intensity fire with almost 100% crown scorch	Stream exports of coarse matter and phosphorus after wildfire at the catchment scale using weir/flume, bedload samples and turbidity probes catchment outlets	*Eucalyptus delegatensis* plus other Mixed eucalypt (no specifics)	Vegetation species as background description of study area; no further description, exploration or integration quantitatively as a causal factor.	0 to 3 yrs	Gneiss and quartz diorite, some granodiorite; clay loams and sandy clay loams with strong aggregation	Coarse matter exports approached pre-fire levels after 3 to 4 years; Strong decreases for winter/spring; most P exports with suspended sediments.
Sheridan et al. (2007)	East Kiewa, northeast Victoria 2003 moderate-severe intensity fire with almost 100% crown scorch	Pre and post-fire runoff and erosion rates at the plot and hillslope scale using rainfall simulation experiments (100 mm/h for 30 mins)	Mature Alpine Ash (*Eucalyptus delegatensis* RT Baker)	Focus of the rainfall simulations were on the percentage of ground contact cover; no discussion of canopy cover	0 to 3 yrs	Quartz diorite and gneiss; Sandy clay loams and clay loams (Acidic Eutrophic Red Dermosols)	Ten-fold increase with exponential decrease in 2 years with ground cover increase to 90%. Seasonal water repellency reported.
Smith and Dragovich (2008)	Thredbo, Snowy Mountains, southeast Australia 2003 moderate severity fire with widespread loss of ground cover and partial crown scorch	Estimation of post-fire hillslope erosion and deposition rates using erosion pins	Sub-alpine woodland (*Eucalyptus pauciflora*) and wet sclerophyll forest (*Eucalyptus delegatensis–E. dalrympleana* alliance) dominating lower parts of the slopes	Focus on ground-level vegetation recovery which remained low; Qualitative observations of the variable extent and recovery of canopy but not quantified as a causal factor	0 to 2.3 yrs	Granites, gneisses, porphyries, Tertiary basalts and metamorphosed sediments; Chernic Tenosols – alpine humus (upper/mid-slope) and Brown Dermosols (lower slopes)	Estimated erosion rates: 2.7 to 94.3 t ha^{-1}; differing process dominance for burnt and unburnt hillslopes; "exhaustion" of sediment supply likely on some burnt hillslopes.

2.3.6. Climate change impacts and fire regimes in SE Australia

Global climate change is expected to cause shifts in Australian fire regimes, as also projected for the western United States and the Mediterranean. Southeast Australia's climate is likely to shift with increased global CO_2 concentrations and concomitant climatic circulation adjustments; for instance the poleward expansion of the Hadley Cell in the Southern Hemisphere (CSIRO, 2012) which may result in the greater persistence of sub-tropical high-pressure systems causing drier and warmer conditions favourable to wildfire ignition and spread. On the other hand, in regions where rainfall depth or event intensities are projected to increase, accelerated soil erosion and nutrient leaching are also likely to cause ecological problems such as eutrophication of aquatic environments (Sinha et al., 2017). Modelling projections of future regional climate and wildfire risk by Kelley and Harrison (2014) showed that the extent of burnt areas would likely increase in southern Australia, but decrease in northern Australia, and drive an increased dominance of fire-adapted species in wooded areas. Furthermore, Clarke et al. (2011) predicted longer fire seasons for eastern Australia with higher Forest Fire Danger Index (FFDI) (Dowdy and Mills, 2012b; Noble et al., 1980) values in the late spring/early summer seasons.

Fairman et al. (2015) have emphasized that 'alternative stable states' would be very likely this century, even for fire-adapted eucalypt forests in southeast Australia which can experience very high fire recurrence intervals of 11 years or less. As these alternative stable states become increasingly widespread over the southeastern Australian region, the relative contribution and activity of hillslope hydrologic and erosional processes associated with intermediate vegetation structures could increase in comparison to the "original" stable structures. Fairman et al. (2015) commented that both fire-sensitive and fire-tolerant vegetation species can undergo substantial shifts in floristic composition through the effects of recurrent fires that prevent the often assumed "recovery" to the original climax vegetation

71

composition and structure, especially when the regenerating species have not yet reached sexual maturity but the repeat disturbance is imposed on the area. This "double-burning" phenomenon occurred in the 2006/7 Great Divide Fires when part of the burnt area overlapped with that of the 2003 Eastern Victorian Alpine Fires (details in Chapter Three). Hence, changes in vegetation floristics, structure, fuel accumulation and microclimate could already be in motion over many areas in southeast Australia. Therefore, workers in post-fire hydrologic and geomorphic sciences need to be able to understand and represent a wide range of new alternative stable (albeit dynamically changing) states brought about by such ecological alterations, what Bowman et al. (2013) have termed 'fire-driven state shifts'. Indeed, in the present era where the human influence on global systems is indubitable, the combination of both natural and human activities is likely to have created innumerous 'landscape traps' at the global scale (Lindenmayer et al., 2011). In this regard, Fairman et al. (2015) commented on the 'surprising paucity' of work investigating the effects of recurrent wildfires on tree mortality and regeneration in Victoria's forests.

If not much is currently known about the alterations in post-fire vegetation composition and structure under fire regimes of higher frequency of occurrence and likely higher severity over very large areas – 'mega-fires' (Attiwill and Binkley, 2013), there would be even less knowledge about the complex and variable operation of hillslope hydrologic and geomorphic processes under these "new normals". Thus, post-fire erosion scientists need to look further into the "window of recovery" (Prosser and Williams, 1998) (see Chapter One), and incorporate detailed observations of the range of vegetation characteristics and their dynamic changes through space and time into current knowledge of how hillslope erosional and hydrologic processes operate. This detailed work studying the intermediate post-fire phase could be enabled by applying and extending the 'zones of influence' concept (Dunkerley, 2000) to the post-fire erosion context, as presented in the following section.

2.4. Zones of influence of plants in post-fire conditions

2.4.1. Existing studies

Studies of specific vegetation effects on hydrology and erosion at the detailed plot scale may appear to be unimportant, operating at the lower-order scale and having only minor impacts on the processes and outcomes of interest at the catchment and drainage-basin scales. However, from the ecohydrological perspective (Eamus et al., 2006) their cumulative impacts should not be discounted when scaling-up or down models of erosion and runoff (Parsons et al., 2006). For arid landscapes where dryland shrubs dominate, Dunkerley (2000) demonstrated the paramount importance of plant position and physical characteristics in determining the attributes of 'zones of influence' of each individual's water balance and throughfall characteristics. This was because these factors controlled the consequent splash and overland flow processes. Therefore, these phenomena need to be examined carefully in the light of the different physical attributes of different plant species, including those found in dry eucalypt forests under intermediate post-fire conditions.

Wainwright et al. (2000) highlighted how individual shrubs in semi-arid regions, through the preferential accumulation of fine particles by attenuating splash erosion forces under their canopies in a positive feedback loop, generate localized 'islands of fertility' that enable the retention of nutrients and water in an otherwise meagre environment. Interesting intra-canopy variations in throughfall erosivity according to canopy architecture of different plant species with different leaf characteristics, have also been demonstrated by Foot and Morgan (2005) through laboratory experiments. The result of these 'patches of fertility' is increasing land surface and soil *heterogeneity* favouring the dominance of desert shrubs, and subsequent rapid desertification of Southern New Mexico and the Sahel (Schlesinger et al., 1990).

Ludwig et al. (2005) showed the importance of vegetation patches in exerting clear but complex effects on the spatio-temporal distribution soil moisture, plant growth and runoff/erosion at the broader landscape scale for semi-arid regions in Australia, Europe and North America. Most recently, Kidron (2015) highlighted the instrumental influence of under-canopy biocrusts in *increasing* runoff and sediment yields in arid dunefield shrublands of the wester Negev Desert in Israel. While much potential insight can be gained by adopting these eco-hydrological and eco-geomorphological approaches in post-fire erosion studies in southeast Australia, their application is at present quite limited. This is discussed in the following section where I propose the Dynamic Zones of Influence (DZI) framework.

2.4.2. Dynamic zones of influence (DZI) in post-fire eucalypt forests

In view of the various knowledge gaps highlighted in the previous sections, some questions should be addressed when considering post-fire erosion applied to dry eucalypt forests in southeast Australia. If these forests have such distinctive characteristics, what are the higher-order controls and influences over hillslope erosion processes under intermediate post-fire conditions where substantial vegetation regrowth has occurred? How can the dynamic changes to the vegetation canopy be described? What are the ways in which rainfall events are modulated by the changing canopy structure and extent? What are the possible changes to the soil surface and subsurface horizons?

Building on the earlier ecohydrological work by Wainwright et al. (2000) and Dunkerley (2000), I propose a Dynamic Zone of Influence (DZI) framework that can be applied to post-fire landscapes, as well as other environments where significant perturbations have resulted in extensive vegetation loss (e.g. clearfell logging). This is illustrated using a model sequence of post-fire vegetation regeneration of tree canopy species in dry sclerophyll forests (see Figure 2-2). Firstly, I consider the zone of influence of an individual tree, for instance *Eucalyptus polyanthemos* (as described earlier) that exhibits distinctive leaf

characteristics including heterophylly, regenerates post-fire readily from lignotubers and/or epicormically (Eamus et al., 2006), and has a generally "bullet-shaped" crown shape. Active outward and upward expansion of the canopy is led by new leaf buds at the outer edges of branches and twigs. Inwards from the canopy edge, larger, fully-developed leaves with their typical pendulous hanging habit occur in clumps. As older leaves on the inside of the canopy senesce, they fall off the twigs and are deposited on the ground.

As highlighted by Dunkerley (2000), the arbitrary binary division between patch (vegetated) and inter-patch (unvegetated, exposed) areas obscures important variations within plants' zones of influence, especially when the growth-correlated dynamic spatial colonization by the plant (Christophe et al., 2003) is considered. Therefore, three component sub-zones under the eucalypt canopy are suggested: (i) the inner zone which has the highest volume of leaf litter but less foliage above it, except for new foliage growing at the apex of the growing crown; this zone would also be the primary recipient of stemflow (Dunkerley, 2014a); (ii) the middle zone which has the highest volume of overhanging foliage with numerous vertical overlaps of branches, twigs and leaves; and (iii) the outer zone which is where active lateral expansion of the plant is occurring, and is importantly a transitional zone between the under-canopy and open, exposed non-canopy areas.

Having established the structure of the individual zone of influence (Figure 2-2), I consider the dynamic changes of this zone by commencing with the near-term post-fire situation where noticeable active re-growth has commenced (Figure 2-3a). The zones of influence of individual plants on the hillslope therefore, through spatial colonization, expand laterally and extend vertically through time as post-fire regrowth proceeds further, exerting their effects at the expense of the contracting open areas (Figure 2-3b). Ground cover would concomitantly increase as the regeneration proceeds but may be variable depending on micro-scale conditions (see Figures 1-6 c-d).

75
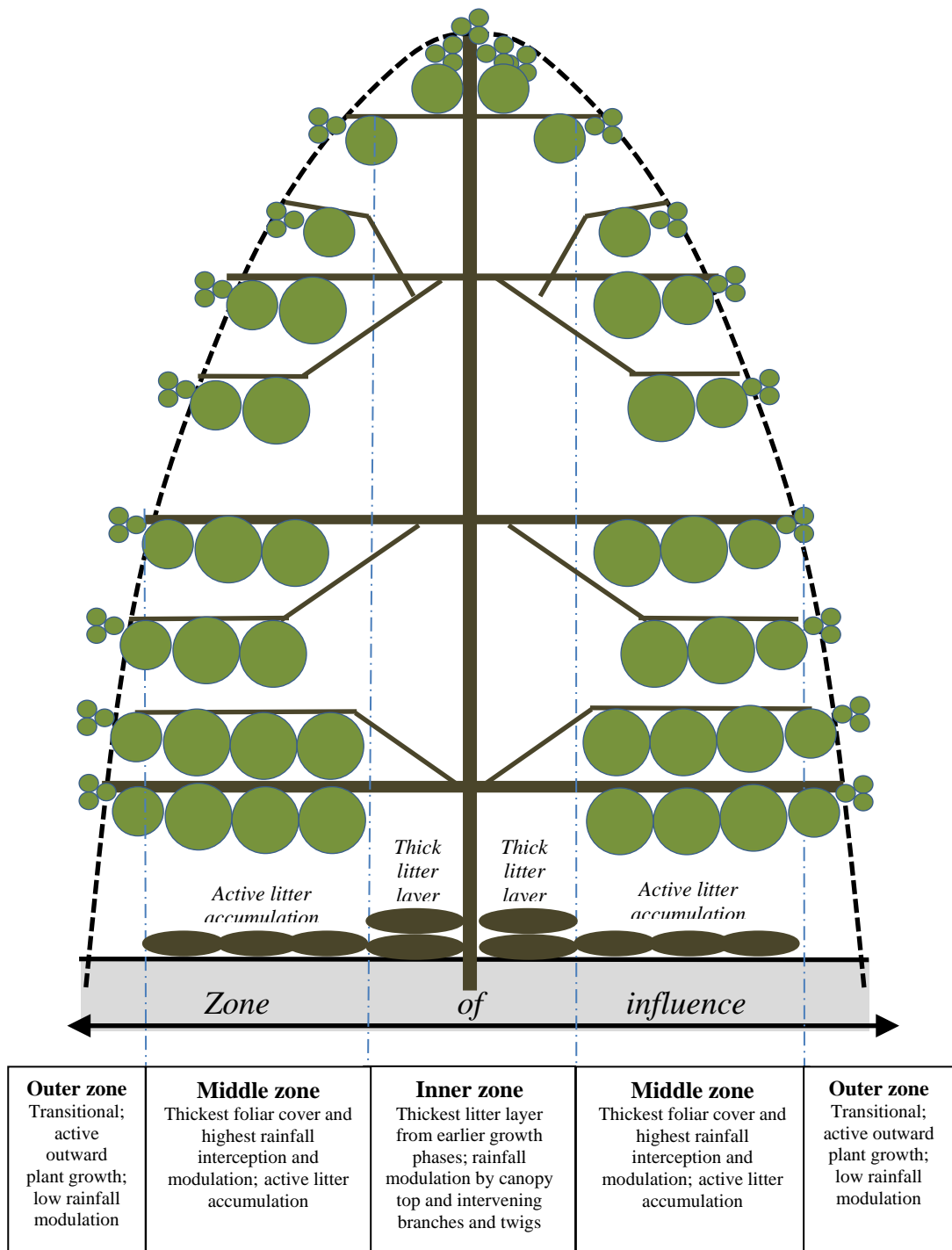
Figure 2-2. Proposed Dynamic Zone of Influence (DZI) model composed of 3 sub-zones: (i) inner, (ii) middle and (iii) outer. Each zone has differing ground, canopy and hydrological/erosional process responses to rainfall input.
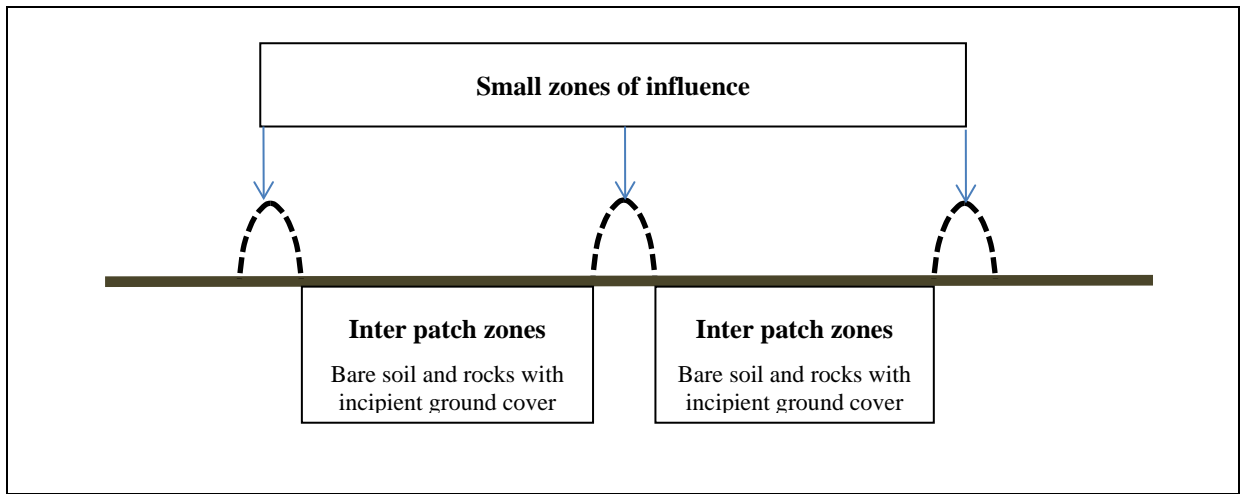
(a)
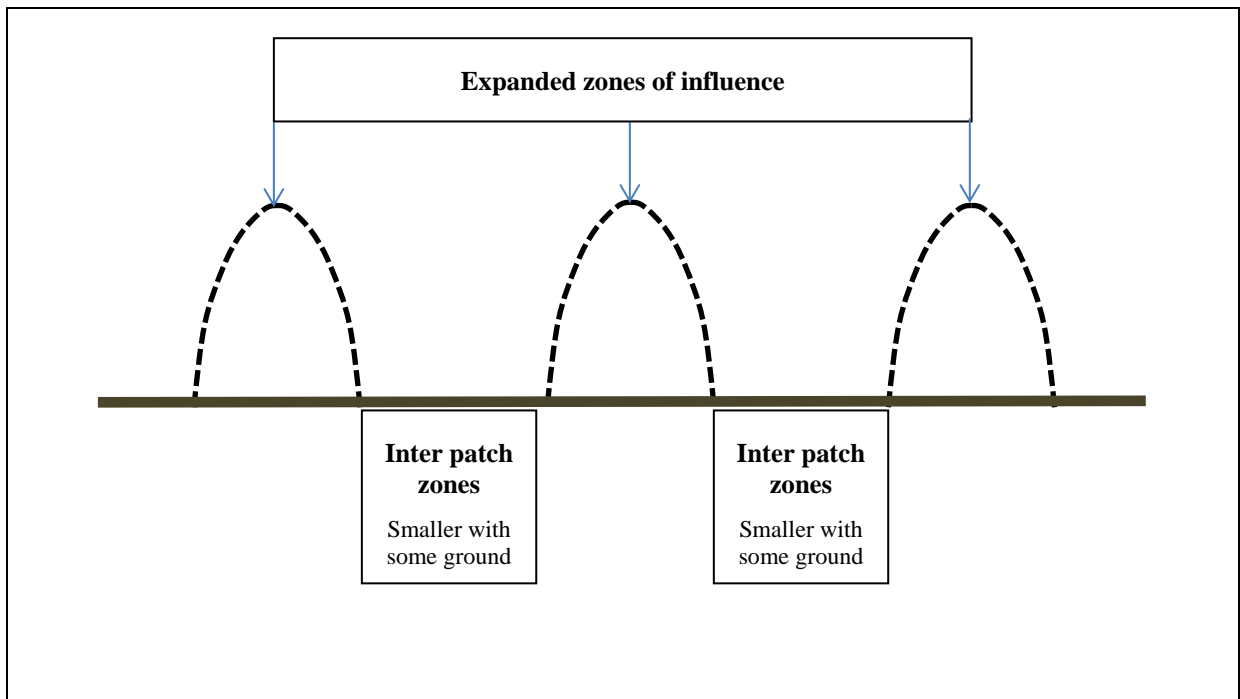
(b)

Figure 2-3. Hillslope-scale DZI model. (a) Near-term post-fire conditions. Small zones of influence with large inter patch zones. The zones of influence would be expected to grow dynamically laterally and vertically as post-fire recovery proceeds. (b) Intermediate post-fire conditions. Substantial but incomplete vegetation regeneration has occurred. Zones of influence have expanded substantially while inter-patch zones concomitantly contract; extent of ground cover recovery may be spatially variable depending on micro-scale differences in water availability, soil conditions and availability of grass/forb/shrub seedbank.

Vegetation-erosion interactions are presently under-examined even though they are fundamentally important and are complex and variable through time and space. The Dynamic Zone of Influence (DZI) framework could be applied at the scale of the individual plant, and should also be applied at the broader hillslope scale, to better synthesize knowledge of plant ecology and physiology with the geomorphological interests of hillslope erosion and hydrology in post-fire erosion science for southeast Australian eucalypt forests. With the increased extent and complexity of responses of vegetation assemblages to regional and global climate changes, and heightened probabilities of major perturbations to vegetation at the landscape scale due to the likely increased occurrence of large wildfires in this region, the DZI framework has good potential for application in the fields of ecogeomorphology and ecohydrology.

The preceding discussion has delved into the various aspects of regionally-specific vegetation characteristics, the general hydro-climatic contexts and the likely impacts of climate change within the next century. However, one key factor still needs to be incorporated into the discussion – that of detailed rainfall characteristics that has been largely missing from many post-fire erosion studies.

2.5. The importance of detailed rainfall event characteristics

Thus far, much focus in this thesis has on establishing the need for increased study of post-fire hydrology and erosion in intermediate vegetation conditions, and these transitions can be framed in the aforementioned DZI model and the associated transitions in hydrologic vulnerability. However, being the main driver of post-fire erosion, rainfall event characteristics such as intra-event intensity variations, peak intensity-durations and rainfall erosivity, also need to be carefully investigated in terms of their complex interactions with vegetation canopies and strata, ground-level litter layer and soil surfaces as to how erosional processes operate on burnt hillslopes – particularly in intermediate vegetation conditions. Even though these rainfall characteristics have a key role to play in controlling the operation of splash impact and runoff generation (and run-on losses) on hillslopes (Dunkerley, 2012) that are essential for understanding post-fire erosion dynamics, minimal work has been done in either the immediate or intermediate post-fire conditions. Indeed, plants' DZIs would operate differently according to the characteristics of rainfall events arriving at the canopy, for example depths and intensities, duration, event stage (early, middle, or late), time of day (e.g. day or night), micro-meteorological conditions during the event, and antecedent conditions. By extension, throughfall processes and patterns resulting from variable canopy interception and modulation effects on rainfall events of varying characteristics, also play an integral role in hillslope hydrological and erosional processes under intermediate post-fire vegetation conditions.

In their modelling of post-fire rainfall-runoff responses using the Kinematic Runoff and Erosion Model (KINEROS2) and Automated Geospatial Watershed Assessment Tool (AGWA), Sidman et al. (2016) demonstrated that varying the temporal and spatial characteristics of a range of post-fire rainfall events led to large changes to the modelled peak flow, with events synthetically represented at uniform intensity giving the least accuracy in

model output by underestimating peak flows. Therefore, post-fire erosion rates derived from commonly conducted constant-intensity rainfall simulations, e.g. Rulli et al. (2006); Sheridan et al. (2008); Leighton-Boyce et al. (2007), could have resulted from incomplete characterizations of hydrological and erosional behaviour under natural rainfall conditions (Dunkerley, 2008b), although these well-controlled studies have provided useful knowledge on key hydrological and erosional processes. Mohamadi and Kavian (2015), working on moderately steeply sloping rangelands in Iran reported positive linear relationships between soil loss and rainfall intensity at lower intensities. However, non-linear, logarithmic and exponential relationships were found at higher rainfall intensities, therefore demonstrating the operation of processes-response thresholds - often overlooked complexities when trying to understand post-fire hydrological and erosional responses to natural rainfall events (Larsen and MacDonald, 2007).

The temporal scale at which rainfall is represented and utilized as a causal factor or correlate, is of fundamental importance because vast differences can be found in the derived erosional energy (Dunkerley, 2010b). Most workers would agree in-principle that rainfall depths integrated over yearly, monthly, weekly or even daily timescales provide rather coarse approximations of the actual events, and would therefore be insufficient to enable the determination of sediment yields with much confidence. Despite this, rainfall events have generally been treated rather simplistically in many previous post-fire erosion studies, possibly out of convenience or limited data resolution.

Rainfall events need to be of sufficient albeit variable combinations of depth, intensity and duration for any discernible operation of splash erosion or surface runoff; for an *activation threshold* to be crossed (Larsen and MacDonald, 2007; Römkens et al., 2002). The acquisition of these detailed metrics is now increasingly feasible with modern rainfall measurement equipment and processing techniques. Various levels and extents of structural

80

and functional (dis)connectivity on the hillslope could then be examined (Fryirs et al., 2007; Reaney, 2013; Wester et al., 2014; Williams et al., 2016). Furthermore, the treatment of the rainfall data and the partitioning of rainfall events, and the subsequent statistics derived from them, also require detailed examination (Dunkerley, 2008a). Barros et al. (2013) demonstrated how the space-time structure of rainfall, modulated by terrain and regional climatic patterns, was fundamental in influencing surface and subsurface flows, with interflow being one of the key processes involved in the triggering of debris flows in the southern Appalachian mountains. Youberg (2013) described how the hydro-geomorphic response of burnt catchments could be categorized according to the different *rainfall* regimes that they experienced across the southwestern United States. When examining post-fire rainfall-runoff processes related to 5 fires over 40 years in the eucalypt forests of the Nattai catchment in southeast Australia, Tomkins et al. (2008) found that rainfall characteristics exerted higher-order influence on surface runoff. They reported that moderate-high intensity falls of around one-year average recurrence interval (ARI) produced substantial surface runoff, indicating threshold rainfall characteristics for sufficient erosive energy to be present. While these events were not exceedingly rare, they were nevertheless found to be quite unreliable in their occurrence in the several ensuing post-fire years, possibly due to these fire and post-fire rainfall events occurring during drought years. Hence, quite high levels of uncertainty are inherent in predicting post-fire erosion and vegetation recovery rates. For inter-regional comparisons to inform post-fire erosion science at the global scale, more work needs to be done with a certain degree of parity, in establishing rainfall energy thresholds, their impacts and outcomes on post-fire hillslopes of varying soil and vegetation conditions.

Illuminatingly, more than half-century ago, Horton (1945) discussed the causes and effects of "rain-wave trains" associated with intra-event intensity peaks that drove surface runoff and soil erosion as accelerated, non-linear pulses down hillslopes, rather than as single,

continuous overland flow events which may be commonly visualized and conceptualized. Hence, intra-event high-intensity "bursts" of rainfall over very short time periods (possibly over a few seconds) are likely to have strong accelerative impacts on post-fire hillslope erosion processes (Moody and Martin, 2001a; Moody and Martin, 2001b). Therefore, commonly-used rainfall intensity values across 30-minute or even 15-minute time periods could significantly mask the effects of these "bursts" that impart strong erosional forces through the abrupt increase in mass of water and the momentum provided for erosional "pulses" of splash and overland flow to work above their averaged competence levels, and account for non-linear outcomes (Römkens et al., 2002). Indeed, Moody and Martin (2015) found that *rainfall acceleration*, the rate of change in rainfall intensity within the event, strongly affected the time to ponding and the generation of overland flow which accounted for a large proportion of post-fire eroded sediments on hillslopes in the Fourmile Canyon, Colorado. The actions of these intra-event high-intensity rainfall pulses, over heterogeneous post-fire hillslope surfaces, exert considerable influence over the spatial and temporal patterns of hydrological and sediment connectivity (Reaney, 2013) but have not been studied sufficiently to be understood comprehensively.

As demonstrated by Angulo-Martínez and Barros (2015), numerous uncertainties exist in current understanding and representation of relationships between rainfall kinetic energy and intensity that can seriously confound attempts to link specific rainfall-intensity thresholds to the initiation of the important hillslope erosional processes of splash, overland flow, or debris flows, and therefore to predict with much accuracy soil erosion rates through computer modelling. Further complicating this problem would be the rainfall modulating effects of different plant covers and canopy architectures that would increase or decrease any under-canopy drop erosivity and overland flow generation rates, as discussed earlier for post-fire intermediate conditions.

Brogan et al. (2013) reported that spatial variability in rainfall from thunderstorms exerted key primary controls over the operation of erosional and depositional processes in the streams of Hill Gulch and Skin Gulch watersheds in Colorado that had been burnt at moderate to high severities. Although this study did not specifically examine hillslope sediment dynamics, the importance of detailed rainfall event characteristics on channel processes at the watershed scale, and by implication hillslope-scale processes, was demonstrated. Moody et al. (2013) argued that, as part of the range of research gaps to be addressed in post-fire erosion science, more work was needed to investigate the spatial and temporal variability of precipitation events at the meso-scale in the post-fire erosion and hydrology contexts. This was because of the possibilities of better representation of rainfall events at the sub-daily scale with improved monitoring equipment, the sophistication of current numerical models in being able to process high temporal resolution data over long time periods, and the inherent problems of time-averaging on simplifying the hydrological and erosional impacts of intra-event intensity variations that lead to losses in the ability to identify the timings and relationships of intensity peaks, acceleration/deceleration and troughs or interludes. Even though rainfall metrics such as AI_{15} (rainfall amount multiplied by maximum 15-min intensity) (Mayor et al., 2007), varied-duration intra-event rainfall intensities (Dunkerley, 2012; Dunkerley, 2015a; Dunkerley, 2016) and geomorphically effective events (Huang, 2006) have been occasionally examined, more consistent attention is needed to draw clear links between their physical bases and the theorized or observed post-fire erosion processes (Moody et al., 2013).

2.6. Synthesis

In this chapter, I have reviewed existing studies on post-fire erosion and their key controlling factors for the eucalypt forests in southeast Australia. While the distinctiveness of post-fire vegetation and recovery in this biogeographic region has been generally established vis-à-vis the western United States and the Mediterranean, more work needs to be done to establish deeper understanding of the specific and dynamic controls and interactions post-fire vegetation, particularly tree canopy species, have over hillslope erosional and hydrological processes under intermediate post-fire recovery conditions. For the dry eucalypt forests of southeast Australia, this entails examining the influences of key factors such as distinctive leaf shapes and sizes of juvenile eucalypt leaves, branching habits, the resultant canopy architecture, rates of growth, leaf litter deposition and the consequent impacts of rainfall modulation by the regenerating post-fire canopy which control throughfall fraction, erosivity and overland flow processes that drive hillslope material (soil and litter) fluxes. This means that workers need to pay more attention to the time periods deeper into the post-fire "window of disturbance" (Prosser and Williams, 1998) even though impressive hillslope erosion rates may not necessarily be observed.

The DZI framework has been proposed to describe and analyze vegetation-erosion relationships, particularly canopy modulation of rainfall events, across a landscape. Climate change is expected to bring important shifts to rainfall, temperature and humidity patterns that are quite likely to result in altered fire regimes in terms of higher fire frequency, and longer durations and larger extents of vegetated areas remaining in "recovery" phases. This also means that vegetation structures and distribution of fire-prone regions such as southeast Australia are likely to shift in response to these changes. Accompanying the projected changes in climate will also be changes in rainfall patterns and the normal rainfall event characteristics. With the ongoing scarcity of knowledge of how post-fire erosion varies with

rainfall event characteristics, the need to understand this in the shifting background of changing rainfall patterns associated with climate change in southeast Australia makes this even more important.

This research has been developed to address the various research gaps and needs reviewed in this chapter. I now proceed to Chapter Three where the geophysical and ecological context of the study site are presented. This will set the groundwork for Chapter Four where the materials and methods for this study are described.

CHAPTER THREE: SITE DESCRIPTION

In this chapter, the key attributes of the study site and region are described to provide an integrative view of the key systems controlling intermediate post-fire hydrological and erosional processes and outcomes in the area. Firstly, the location of the study site is identified. Secondly, the 2006/7 Victorian Great Divide megafire that affected extensive areas in the state of Victoria, southeast Australia is described to frame the discussion that follows of the key factors and processes operating in this landscape. Thirdly, the geology and topography of the study area are presented to account for the general landscape attributes such as slope, aspect and soils along with the attendant geomorphic processes, and to also relate the terrain attributes to the climatic patterns experienced by the study area.

Fourthly, the climate and rainfall regime of the region and study site are described to provide a regional, meso-scale understanding of the range of meteorological mechanisms that determine rainfall event occurrences and characteristics, including their temporal and spatial distribution which are illustrated through an examination of selected synoptic charts and rainfall radar images during major precipitation events in summer and winter. The patterns of diurnal-nocturnal rainfall occurrence are also explored to drive a discussion on the implications of this poorly-examined factor on intermediate post-fire hydrological and geomorphological processes with respect to soil and vegetation canopy hydrology. Lastly, I discuss the pre-and post-fire vegetation and soils to provide a clear idea of the intermediate conditions five years after the fires; the focus of this research. The abovementioned components of this chapter will help to establish the relevance of the study site as a useful exemplar of intermediate post-fire hillslopes in the broader region, develop sufficient understanding of the study site, and support the discussion on materials and methods in Chapter Four.

3.1. Location

The study site (Coordinates: UTM 55H 465990E 5845220S; Elevation: 330 m a.s.l.) was located 15 km north of the town of Licola (refer to Figure 3-1). Situated in the foothills of the southern flank of the Great Dividing Range in the Alpine National Park in Victoria, southeast Australia (Parks Victoria, 2016), the steep upland topography represented well the terrain of many catchments in the region, where the extensive loss of vegetative cover and soil degradation caused by the 2006/7 Great Divide Fire and subsequent severe erosion episodes, had significant downslope and downstream impacts (Shakesby et al., 2007; Smith et al., 2011).
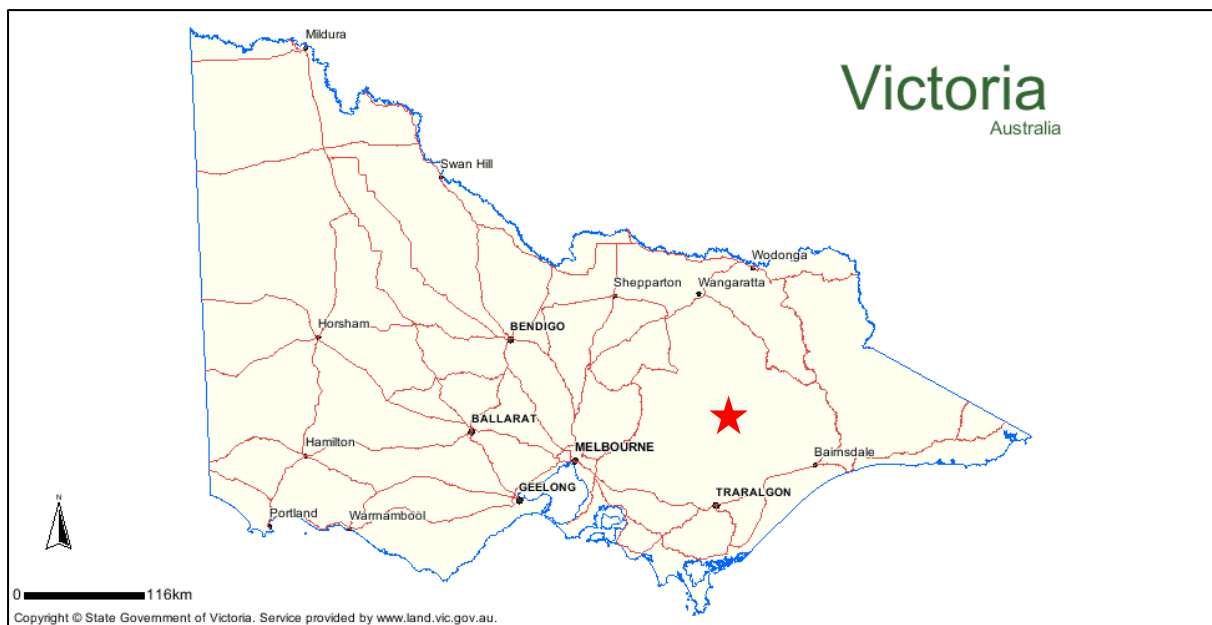
Figure 3-1. Location of study area. Source: State Government of Victoria (2015).

The study area was selected also because it was representative of the broader geology, soils and vegetation of this substantial physiographic and ecological sub-region of southeast Australia. The general hydroclimatic conditions driving rainfall and runoff experienced in the area were also broadly similar across the region. Therefore, findings from this field area could provide some insights into intermediate post-fire hillslope erosion processes operating in other similar locations and catchments. The site was located within the Alpine National

Park which was declared in 1989 and spans 646,000 ha. Prior to 1989, major modern-era anthropogenic disturbances in the region were grazing and logging. Logging in the area ended in 1981 (Lloyd et al., 2005) and grazing licences were terminated in 2005 (Williamson et al., 2014). Presently, the range of activities in the area include recreational camping, fishing, hiking and off-road (4WD car and motorcycle) trail driving, representing potential causes of ignition or accelerated soil erosion in specific locations. Compared to the predominantly agricultural land use outside the park boundaries, most parts of the Park therefore would not have experienced very major recent anthropogenic disturbances to the forests to artificially affect wildfire occurrence, vegetation recovery and soil erosion processes - the focus of this study. Nevertheless, it should be acknowledged that traditional Aboriginal burning practices over many millenia would have already left their imprints on the landscape and ecology in post-European settlement times (Gammage, 2011).

The earliest known relevant scientific survey of the region was the reconnaissance study of the ecology and land-use of the region comprising the catchments of the Glenmaggie Reservoir conducted by Rowe and Downes (1960) of the then Soil Conservation Authority (SCA), Victoria. This report provided useful descriptions of the terrain, soils, climate and hydrology and vegetation of the Snowy Plains, Barkly, Yangoura, Glenmaggie, Macalister and Wellington land systems. The present study area was part of the Wellington land system and where relevant, information from Rowe and Downes (1960) has been included to help establish a clear picture of the study area in its "original" conditions.

3.2. Geology

In this section, we briefly examine the geology of the region to provide an understanding of the landscape, soils and vegetation of the study area. This region is mainly underlain by poorly-bedded middle to late Devonian mudstone, with minor occurrences of sandstone and conglomerate. These are part of the Snowy Plains Formation in the upper region of the Avon

River Group (State Government of Victoria, 2015). This region of the Great Dividing Range, an intraplate highland belt (Bishop, 1988), was formed as part of the Lachlan Orogeny during the Paleozoic era that involved widespread folding, thrust faulting and wedge accretion associated with plate convergence and subduction (Gray and Foster, 2004). Indeed, the southeastern Australian highlands have been identified as having one of the highest bedrock erosion rates, estimated at 20 to 50 m Ma^{-1} (McPherson et al., 2014). It has been widely assumed that subsequent tectonic stability during the Cainozoic (Sandiford, 2003), and subaerial denudation of the uplifted landmass led to the present steep, dissected landscape of the study area. However, it is likely that broad-scale tectonic activity would have caused general uplift of the highlands resulting in the rejuvenation of fluvial erosion causing the pronounced topography and seemingly entrenched drainage patterns; these have been variably attributed to passive isostatic uplift in response to erosional unloading, dynamic isostatic rebound, and intermittent, short periods of volcanically-associated uplift (Bishop, 1988).

Neotectonic activity further helps to explain recent and contemporaneous geomorphological processes and forms of the region. Sandiford (2003) highlighted the high spatial intensity of seismic activity in a narrow belt including the southern and eastern highlands of Victoria. These have helped to provide good evidence for the high level of *in-situ*, intra-plate stresses causing 'active deformation' characterized by Quaternary reverse faulting that, in our area of interest specifically are thrust-strike slip with maximum stress oriented in the southeast-northwest direction (Sandiford, 2003), and are probably responsible for driving the ongoing denudational activity, although broad-scale regional variations and spatial occurrence of the mechanics and outcomes of such neotectonic uplift across southeast Australian highlands exist (McPherson et al., 2014).

The physiography of the area is dominated by north-south oriented ridges determined by the folding of sedimentary beds of the Lachlan Orogen (Rowe and Downes, 1960), and these have therefore determined directions of river flow and led to aspect-associated spatial distributions of vegetation and soil types elaborated upon later in this chapter. The parent material – mudstone and siltstone, have contributed to the development of highly erodible silt sandy loam and loamy sand soils in many parts of the region, facilitating active, ongoing hillslope erosion by fluvial activity and maintaining the steep terrain over time.

3.3. Topography

The topography of the study area is presented in Figures 3-2 and 3-3. This area is part of the Wellington land system of the Glenmaggie catchment which Rowe and Downes (1960) described as 'narrow and gorge-like' (p. 13) 'low montane land', steep to very steep topography and with 'fairly high' erosion hazard (p. 42). The Wellington River (see Figures 3-2 and 3-3) flows generally from north to south towards the town of Licola where it meets the Macalister River flowing through the Barkly land system which covers higher elevations to the west and north of the Wellington land system. Williamson et al. (2014) described the Wellington River as a 'stony upland river' in 'pristine condition' with riverbed geology of Quaternary alluvium and Silurian siltstone and mudstone, with the catchment 'well forested with native vegetation… …'[mostly] native open [dry eucalypt] forest' (p. 376-377).

Rowe and Downes (1960) reasoned that the Barkly land system situated to the west of the Wellington, was likely to be causing a rain-shadow effect over the study area with respect to the westerly frontal systems dominating over the region, therefore causing higher aridity and influencing vegetation structure and distribution (see Section 3.5). The local-scale rainfall regime and event characteristics would also be influenced and consequently affect the study site's ecological, hydrological and erosional processes and outcomes.

Following the classification scheme of the National Committee on Soil and Terrain Australia (2009), the landform patterns were Rolling hills (RH) to Steep hills (SH) with high relief at 140 m. Across the landscape, elevation above sea level ranged from 280 m in the valley of the Wellington River to around 1000 m at the tops of the dissected plateau (see Figure 3-2). Slope profiles were generally concave at the lower slopes to convex at the upper slopes. Gradients of the lower slopes ranged between 18° and 30°, while those of the upper slopes ranged between 32° and 50° with the latter dominant towards the summit.
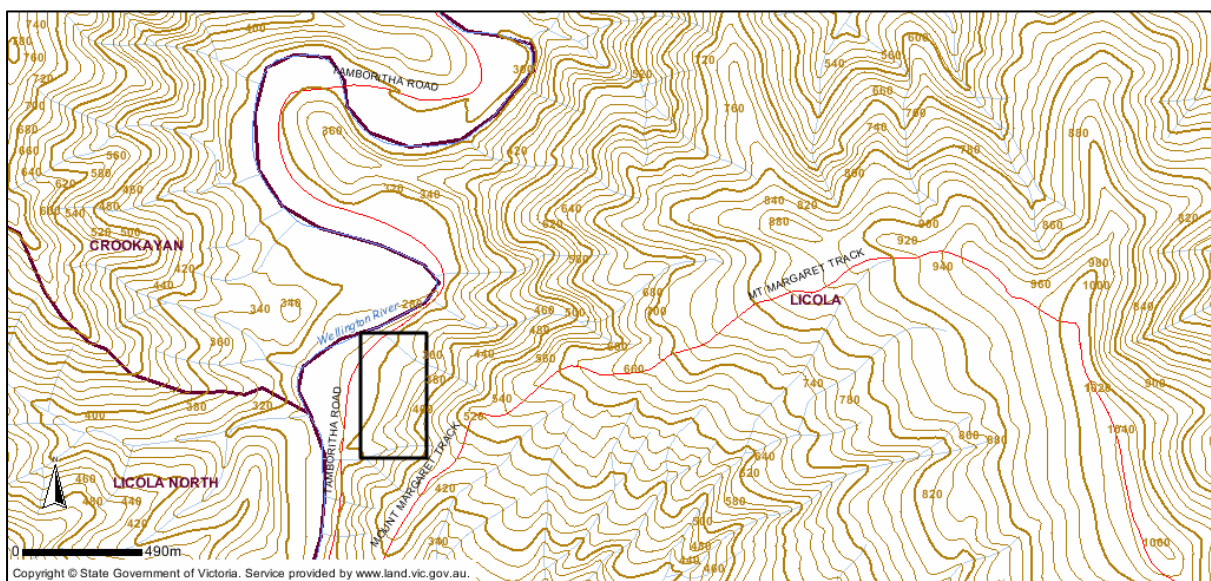
Figure 3-2. General topography of the study area 15 km north of the town of Licola (study site indicated by the black rectangle). Source: State Government of Victoria (2015).

Aspect of the study site slopes was westerly to northwesterly (see Figure 3-2). These slopes were also distinctly steeper than the southwest-facing slopes in the neighbouring area just southeast of the study site across the watershed marked by the Mount Margaret Track. Plate 3-1 provides the aerial view of the study area. Detailed descriptions and photographs of post-fire erosion conditions are presented in section 3.7.2 This would be related to the active fluvial erosion of slopes directly adjacent to the Wellington River. Hillslope hydrological and erosional processes were likely to be active and rapid on these steep slopes. In such hilly and mountainous terrain, aspect and topographic position exert higher-order controls on vegetation distribution in dry eucalypt forests due to differences in temperature, water

balance and soil development with xeric species dominating on the northwest-facing upper slopes. These are due to the growth-limiting high heat and poor soil water conditions of exposed aspects and topographic positions, that impact particularly strongly during late-afternoon evapotranspirative peaks, (Kirkpatrick and Nunez, 1980).

For the study site, it was likely that these microclimatic factors exacerbated the associated differences in post-fire vegetation recovery rates, structure and floristics, and therefore soil erosion, deposition and recovery patterns as discussed by Leitch et al. (1983). For example, exposed north, northwest and west-facing upper-slopes were more likely to have sparser and retarded post-fire recovery of tree canopy and ground cover, with more active erosion. In contrast, more well-sheltered south, southeast and east-facing lower slopes would have more rapid post-fire vegetation recovery and lower soil erosion rates.
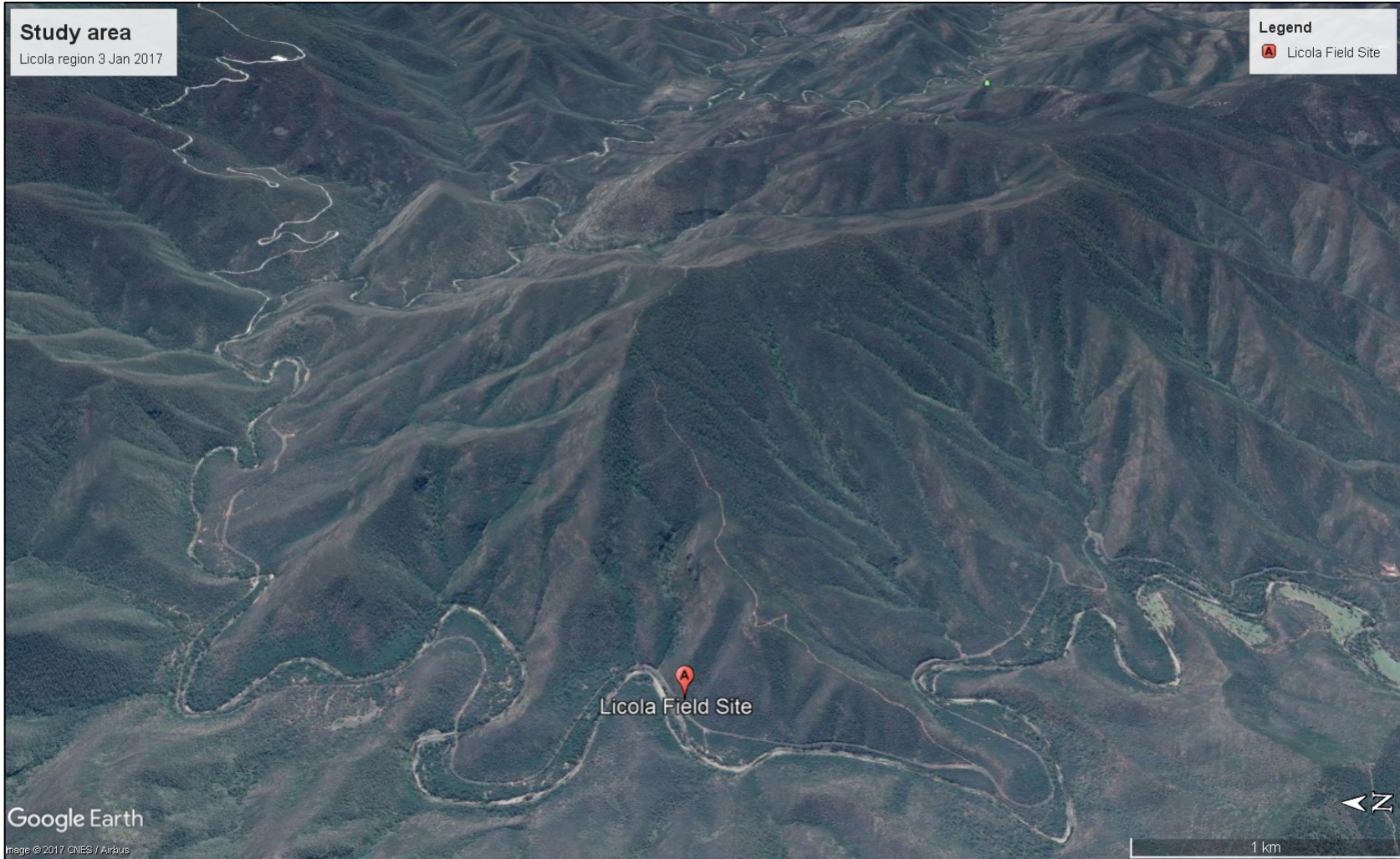
Plate 3-1. Aerial (oblique) view of study area looking east, 3 Jan 2017. The Wellington River flows in an east-west direction (left-side of image) before entering the study area to flow in a north-south (image foreground); note the asymmetry in slope steepness and vegetation density discernable via brown and green shades between north and south-facing slopes respectively. Source: Google Earth (2017). Imagery: CNES/Airbus. Region surrounding the study site location: UTM 55H 465990E 5845220S.

3.4. The 2006/7 Great Divide Fires

Leading up to the major series of ignitions on 1 Dec 2006, the region was already deep in the grip of the Millennium Drought (van Dijk et al., 2013), with the large 2003 Alpine wildfires having occurred just 3 years prior. El Niño conditions had persisted prior to, and through 2006, which would have led to regional-scale accumulation and curing of fuels as large tracts of forests, shrublands and grasslands would have responded to the drought conditions with extensive leaf drop. Furthermore, die-off of many plants would have added to the total dry fuel available, contributing to warmer and drier forest microclimates, increasing likely fire-intensities and rates of spread (Ruthrof et al., 2016) which eventually occurred. Rainfall totals for Victoria in Sep – Nov 2006 were in the lowest decile for the entire record for the state. Streamflows for October 2006 were lower than 10% of the long-term average. Air temperatures across Victoria were also at very high levels, exacerbating fire risks (Flinn et al., 2008a). With reference to Figure 3-3 illustrating the locations of the main weather stations in Victoria, Figure 3-4 presents the maximum air temperatures for Mt. Moornapa weather station (Lat: 37.7481 S, Long: 147.1428 E; Elevation: 480 m) the nearest to the study site at similar elevation, from Nov 2006 to Feb 2007.
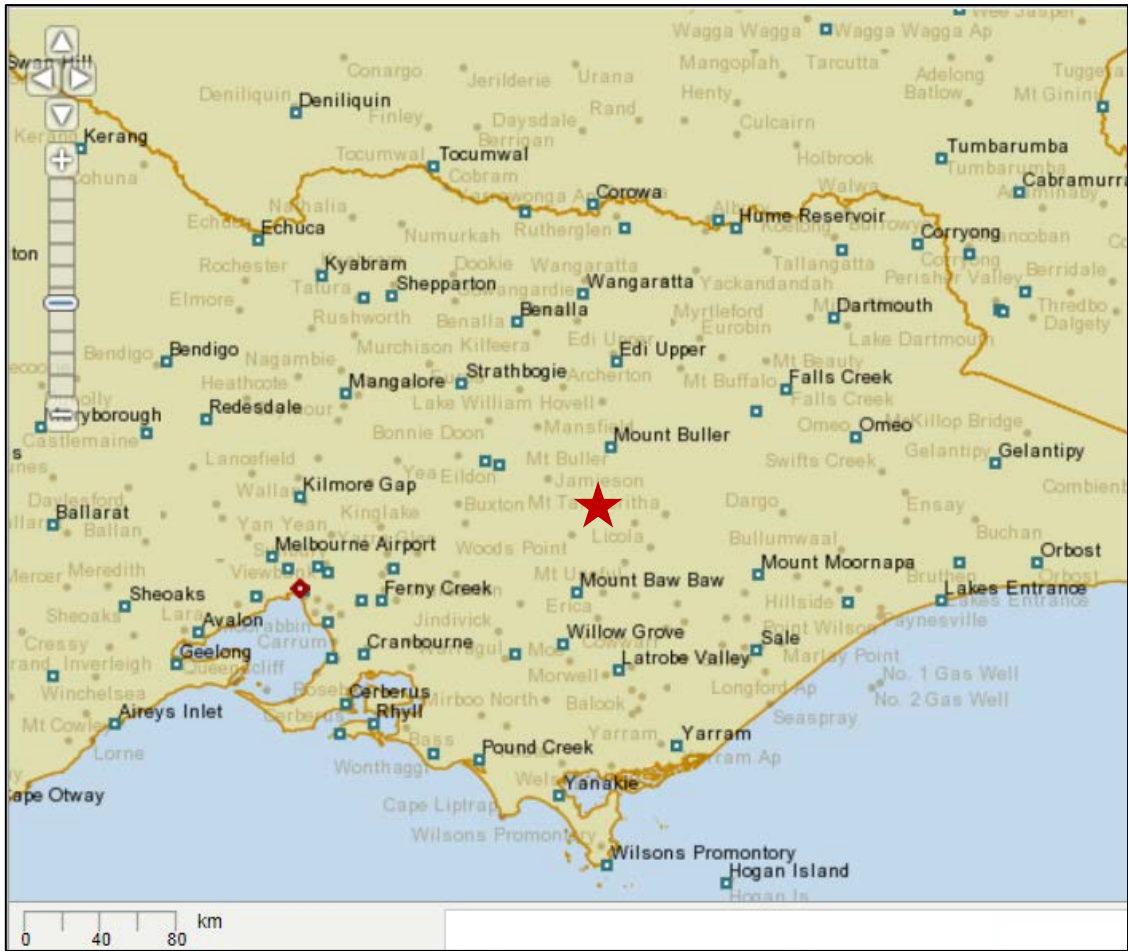
Figure 3-3. Weather station locations in Victoria. Red star indicates study area.
Source: Bureau of Meteorology (2017c).
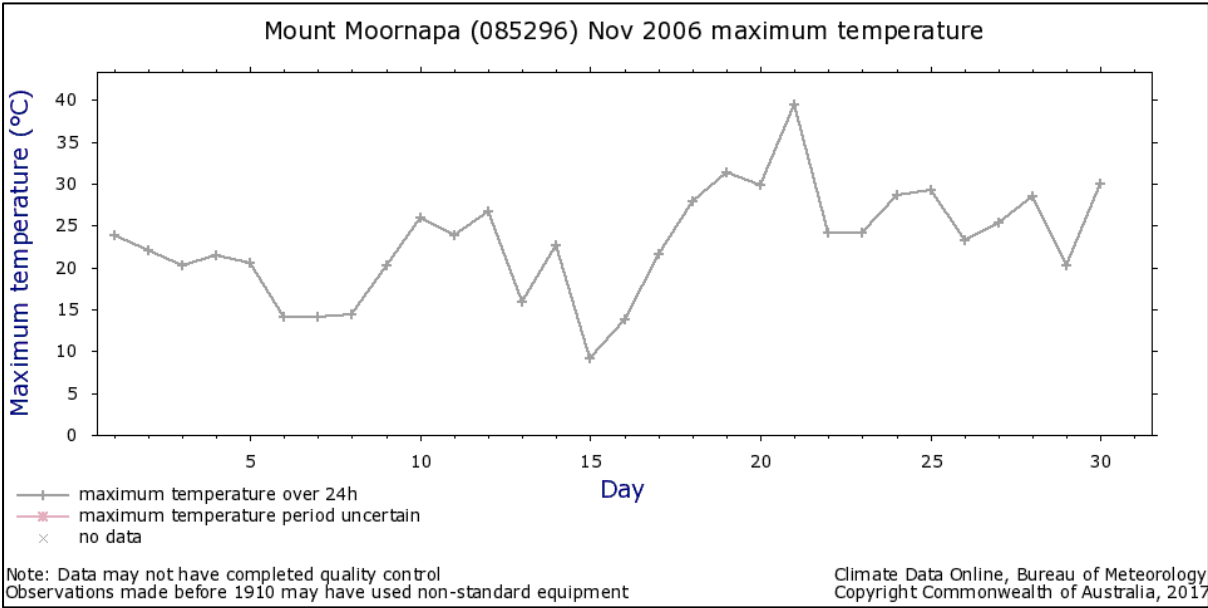
(a)
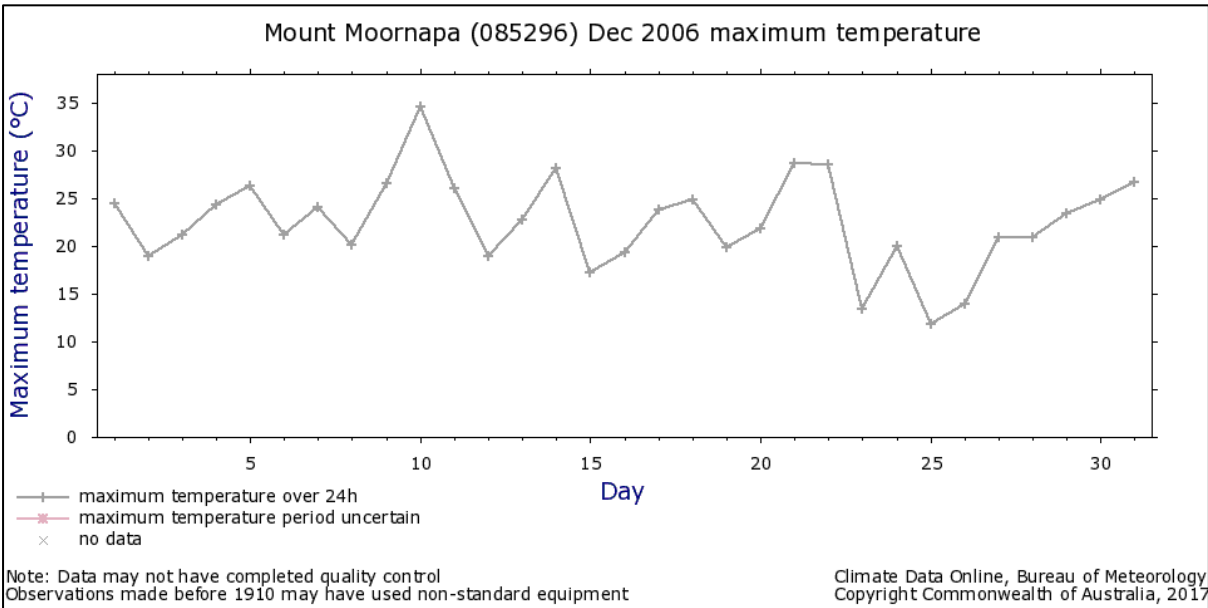
(b)
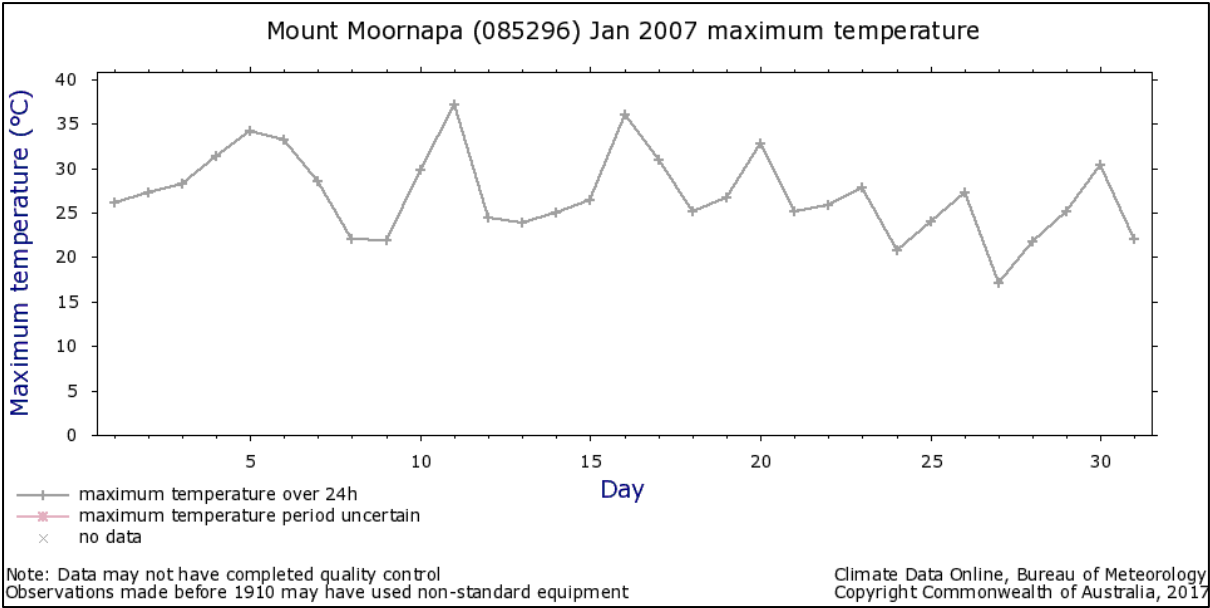
(c)
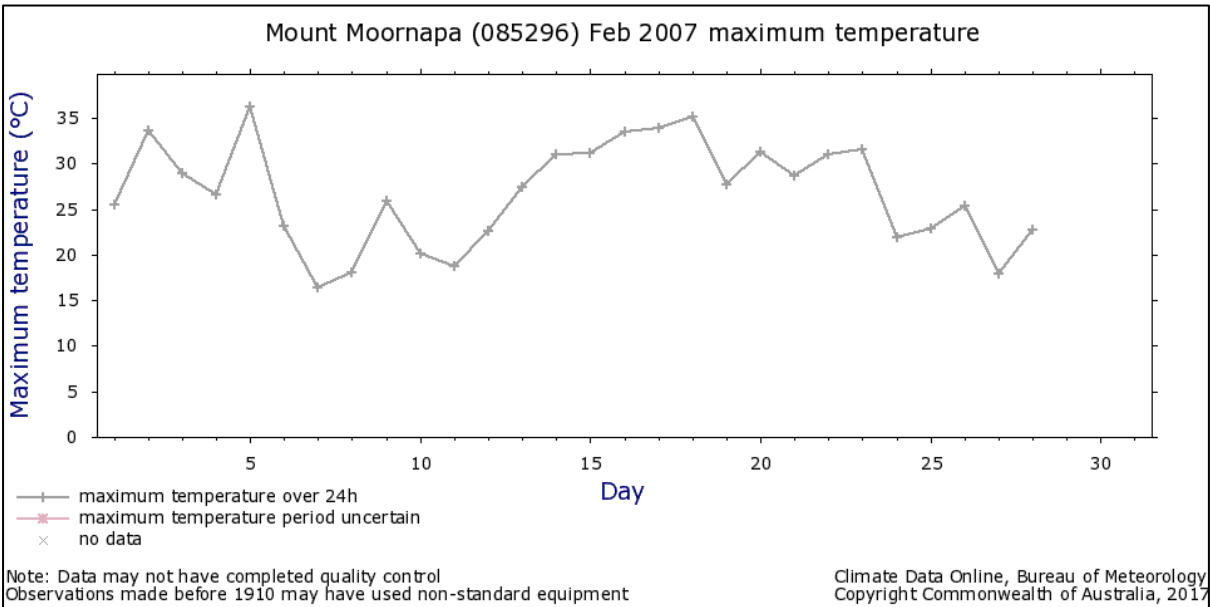
(d)

Figure 3-4. Maximum air temperatures for Mount Moornapa in (a) November, (b) December 2006; (c) January and (d) February 2007. Source: Bureau of Meteorology (2017c).

The Keetch-Byram Drought Index (KBDI) (Heim, 2002; Keetch and Byram, 1968) anomaly for Victoria ranged from 25% to 100% drier than average, with the study region in the 50 to 75% drier range (Flinn et al., 2008a). Within the latter ranges, any ignited fires were likely to sustain overnight, especially if warm (and dry) conditions persisted. Most live/green and dead/dry fuels would be consumed by fire and towards the higher end of the KBDI range, heavy fuels such as logs and stumps would also ignite and burn. The Macarthur's Forest Fire Danger Index FFDI (Mark V) (Noble et al., 1980) for the study area on 30 Nov 2006 (1600 hrs) was in the 15.0 to 25.0 range ("high") with much of western Victoria above 35 ("very high" to "extreme") (Flinn et al., 2008a). Figures 3-5 and 3-6 present the calculated FFDI and KBDI values respectively for three most relevant stations (Lucas, 2010): Omeo (Lat: 37.1017 S, Long: 147.6008 E; Elevation: 690 m), Sale (Lat: 38.1156 S, Long: 147.1322 E; Elevation: 5 m) and Melbourne Airport (Lat: 37.6655 S, Long: 144.8321 E; Elevation: 113 m) stations for the entire month of November 2006, the period leading up to the major fire outbreaks on 1 Dec 2006.
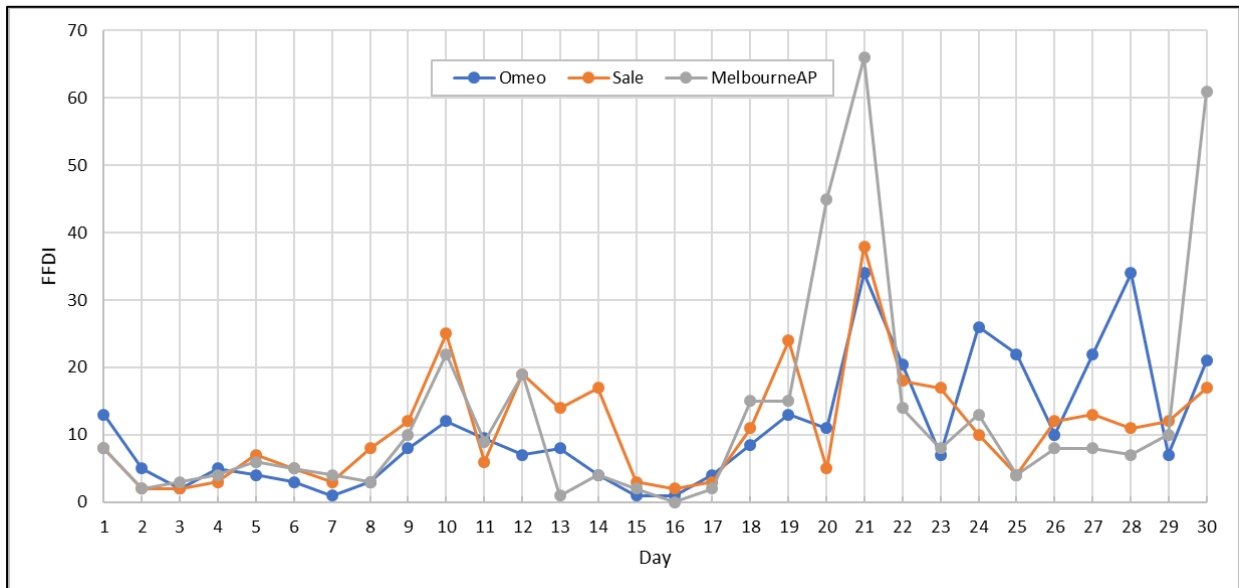
Figure 3-5. MacArthur's Forest Fire Danger Index (FFDI) for Omeo, Sale and Melbourne Airport (AP) stations from 1 to 30 Nov 2006. Data source: Lucas (2010).
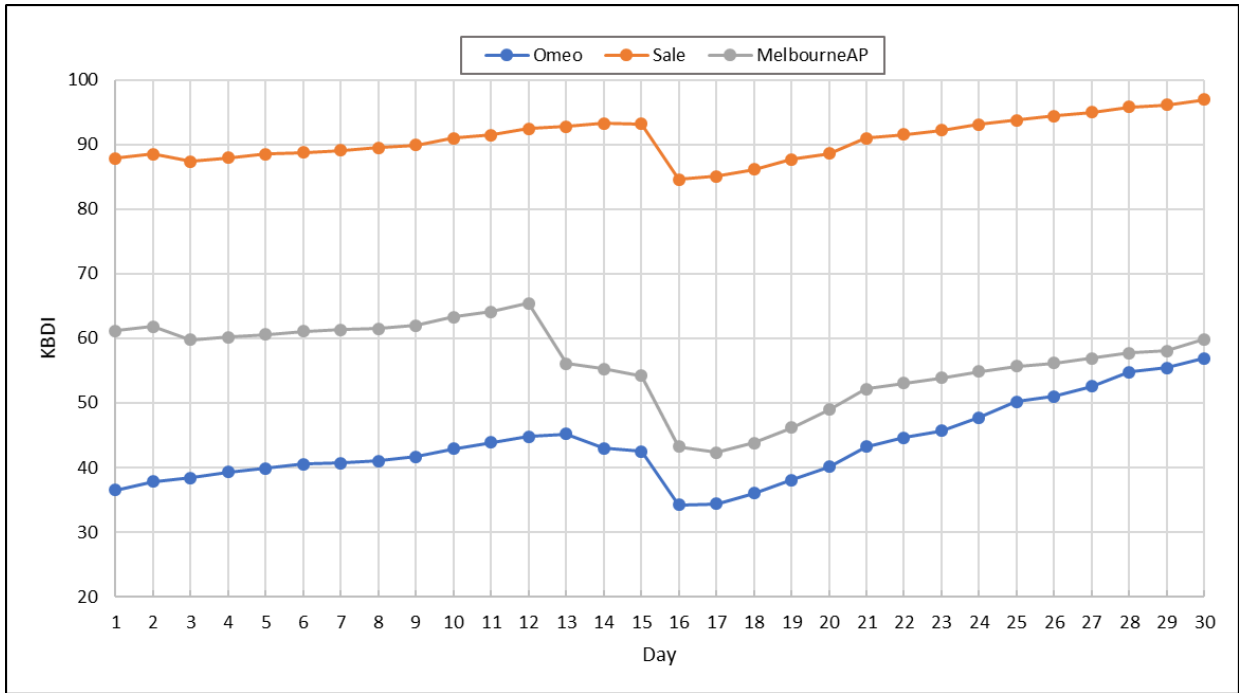
Figure 3-6. Keetch-Byram Drought Index (KBDI) for for Omeo, Sale and Melbourne Airport (AP) stations from 1 to 30 Nov 2006. Data source: Lucas (2010).

In the spring of 2006, the Bushfire Co-operative Research Centre (CRC) had already predicted, based on increased fuel loads, drought and climatic outlooks, an earlier start than average "above normal fire potential" for the Victorian fire season (Bushfire Cooperative Research Centre, 2006). By 1 Dec 2006, the then Department of Sustainability and Environment (DSE) had already attended to 312 fires from 1 Jul 2006, compared to the 30 year average of 127 (Flinn et al., 2008a).

This major wildfire episode began with multiple ignitions across the forests, shrub and grasslands of the Great Dividing Range due to intense lightning activity on 1 Dec 2006 (Flinn et al., 2008a). Over the following weeks, the multiple fire areas merged to form a large megafire complex which consequently became very difficult to suppress and contain because of the extreme fire weather, large areal extent, and steep, difficult terrain in most parts of the Eastern Highlands of the Range. The fire was finally controlled on 6 Feb 2007 and by then huge tracts of forests (including the study area), approximately 1.048 Million ha had been

burnt at moderate to high severity (Smith, 2007). Figure 3-7 illustrates the extent and distribution of this megafire; refer to Section 2.4.1 (Figure 2-1) for field-based fire-severity classifications by Chafer (2008).

These 'exceptionally intense forest fires' affected atmospheric conditions at the global scale due to the massive smoke aerosol plume (Dirksen et al., 2009). As will be described later in this chapter, in addition to the extensive vegetation damage and defoliation, and loss of property and infrastructure to the fire (Smith, 2007), widespread damage was also caused due to the severe post-fire erosion and floods triggered by the rainfall events in the following months. The extent of the 2003 East Victoria Alpine Bushfires is also indicated in Figure 3-7; just adjacent to the east and northeast of the 2006/7 fires. There was substantial overlap of 130,000 hectares in burnt area between these two fires, meaning that large tracts of forest were also "double-burnt" (Sinclair Knight Merz, 2009). The very frequent occurrence of extensive fires in this region indicated its high susceptibility to 'megafires' that cover millions of hectares (Attiwill and Binkley, 2013). These could mean possible state shifts of massive areas of dry eucalypt forests towards alternative vegetation floristic compositions and structures (Fairman et al., 2015) and under intermediate vegetation recovery conditions.
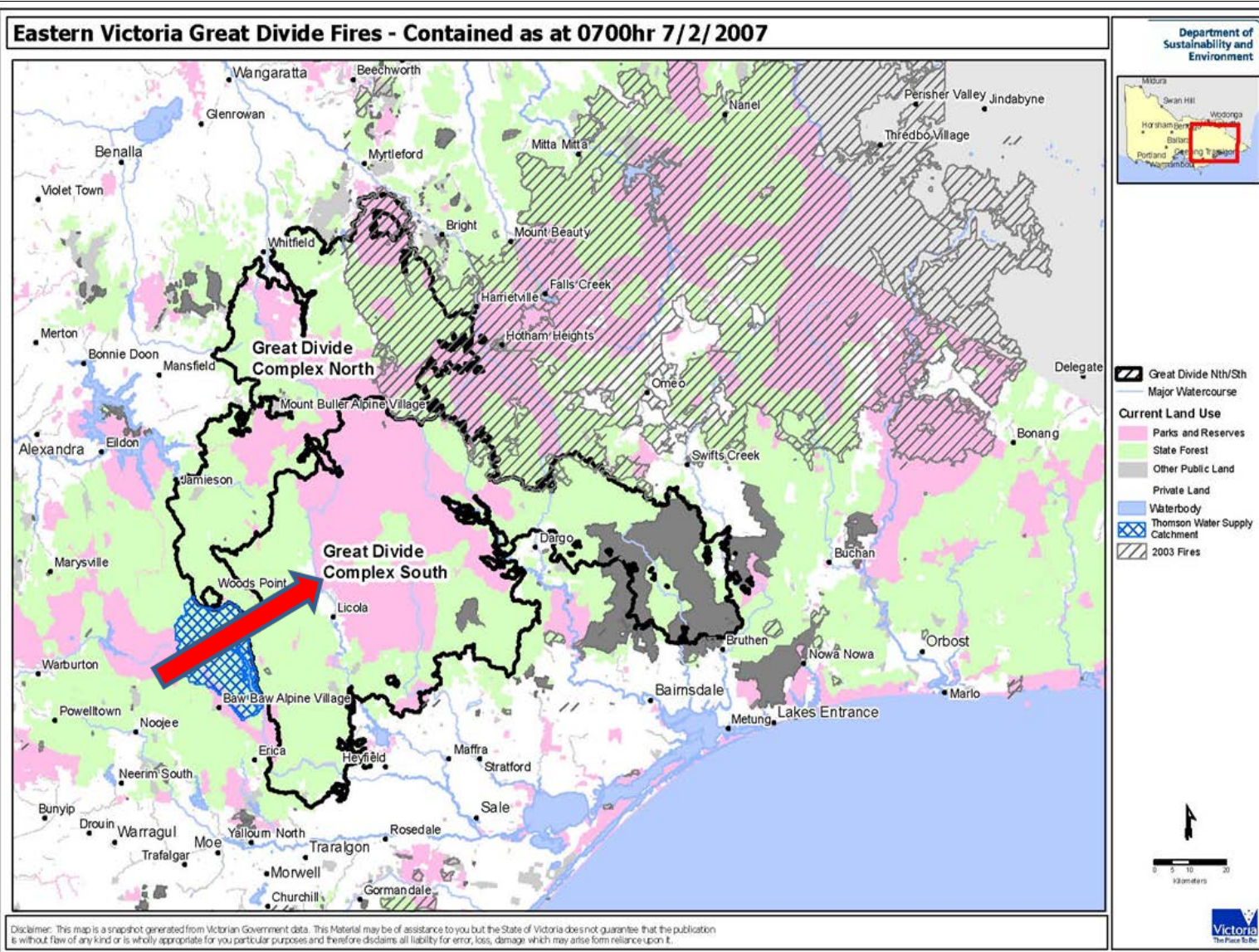
Figure 3-7. Map of the extent of the 2006/7 Eastern Victoria Great Divide Fires on 7 Feb 2007. Bold black line indicates boundaries and extent of the fire complex. Red arrow indicates location of study site. (Source: Department of Sustainability and Environment, State of Victoria (2007).

101

The study area, amidst the main fire complex, was also extensively burnt and at high-intensity, as shown in Figure 3-8.
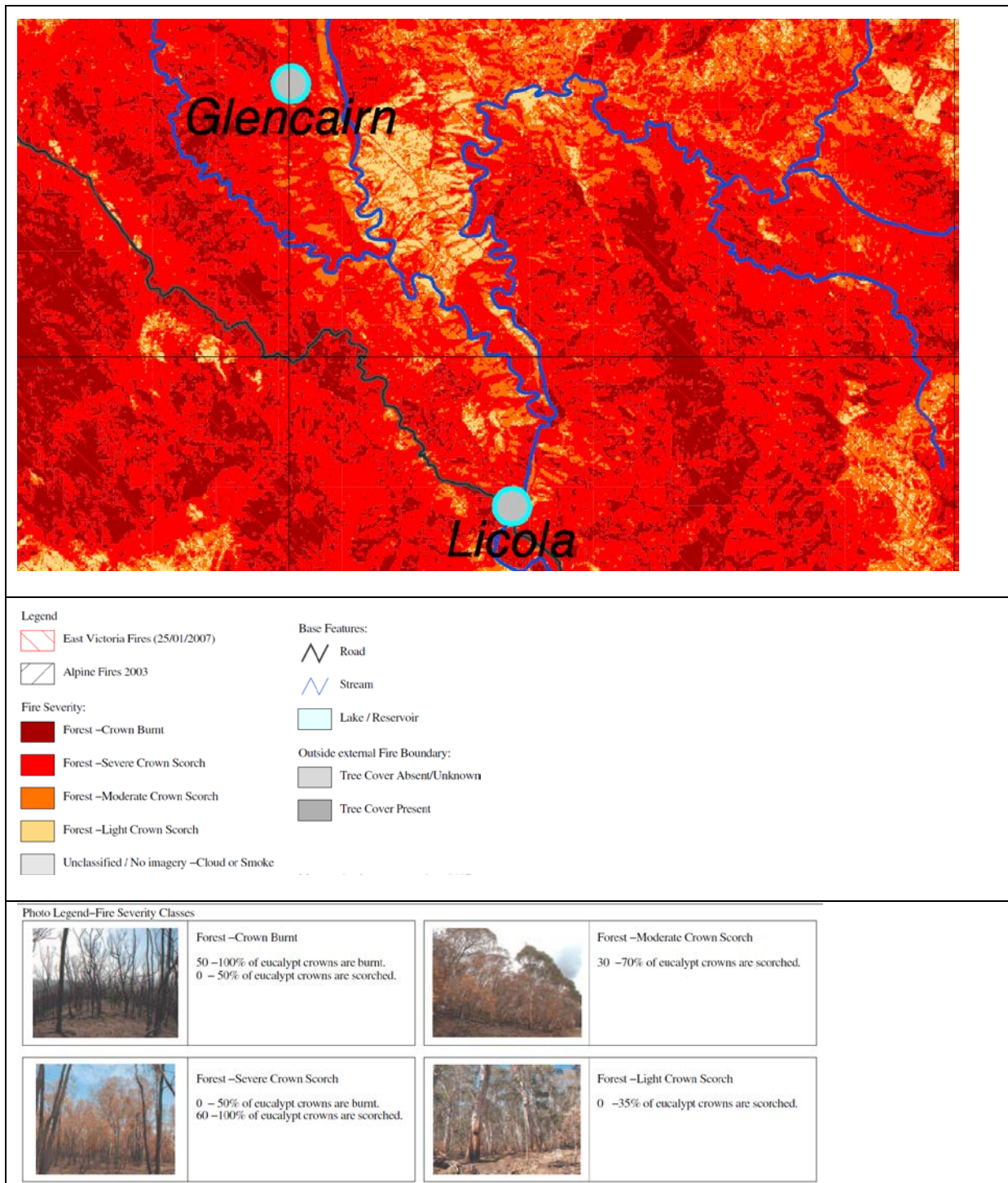
Figure 3-8. Fire severity map of the study area. Black arrow indicates study site location in relation to the towns of Licola (UTM 55H 466782 E, 5835405 S) Glencairn (UTM 55H 460240 E, 5846235 S). Source: Flinn et al. (2008b).

The satellite images of the study presented in Figures 3-9a (before fires) and 3-9b (after fires) illustrate the widespread, near-complete loss of foliage cover from all live vegetation strata, ground cover, litter layers and the exposure of the underlying soils and rocks, making them extremely vulnerable to erosional processes. Details of the deleterious erosion outcomes in the post-fire period are discussed in Section 3.7.

On 17 January 2013, the Aberfeldy-Donnelly's Creek bushfires ignited, spread rapidly and 'unexpectedly' to become yet another 'extreme fire' (Quill and Sharples, 2015), this time affecting forests in the Mt. Useful and Macalister Gorge Natural Features and Scenic Reserves, and agricultural lands approximately 15 km south of Licola town (Evans, 2013) and burning close to 86,000 ha (Victoria Country Fire Authority, 2013b) (see Figure 3-10). From on-ground observations, these fires were, like the preceding ones, very severe and at high-intensities, burning out large tracts of dry sclerophyll forests. This prevented access to the study site via Licola Road from Heyfield (the nearest large town) for further data collection in 2013, and also underscored the continued susceptibility of the region to wildfires and post-fire hydrological and erosional hazards, and the need for better understanding of the factors and processes involved.

Most recently in February 2019, another large bushfire broke out in the Licola region and by mid-March had burnt through more than 80,000 ha (Gippsland Times and Maffra Spectator, 2019; VicEmergency, 2019).

Figure 3-9a. Aerial view of the study region before the 2006/7 fires, *circa* 2003. Source: Google (2012). Imagery: TerraMetrics; Map data: Google, Whereis(R), Sensis Pty Ltd.
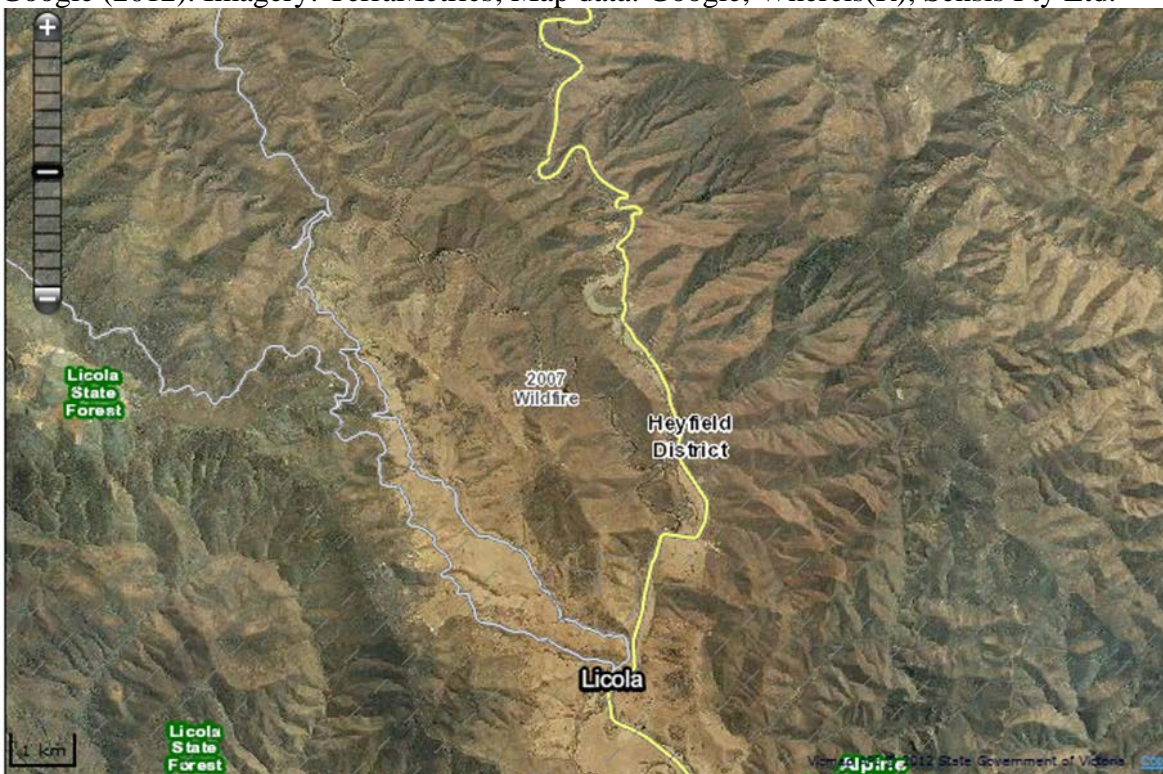
Figure 3-9b. Aerial view of the study region in the near-immediate post-fire period in 2007. Source: State Government of Victoria (2012).
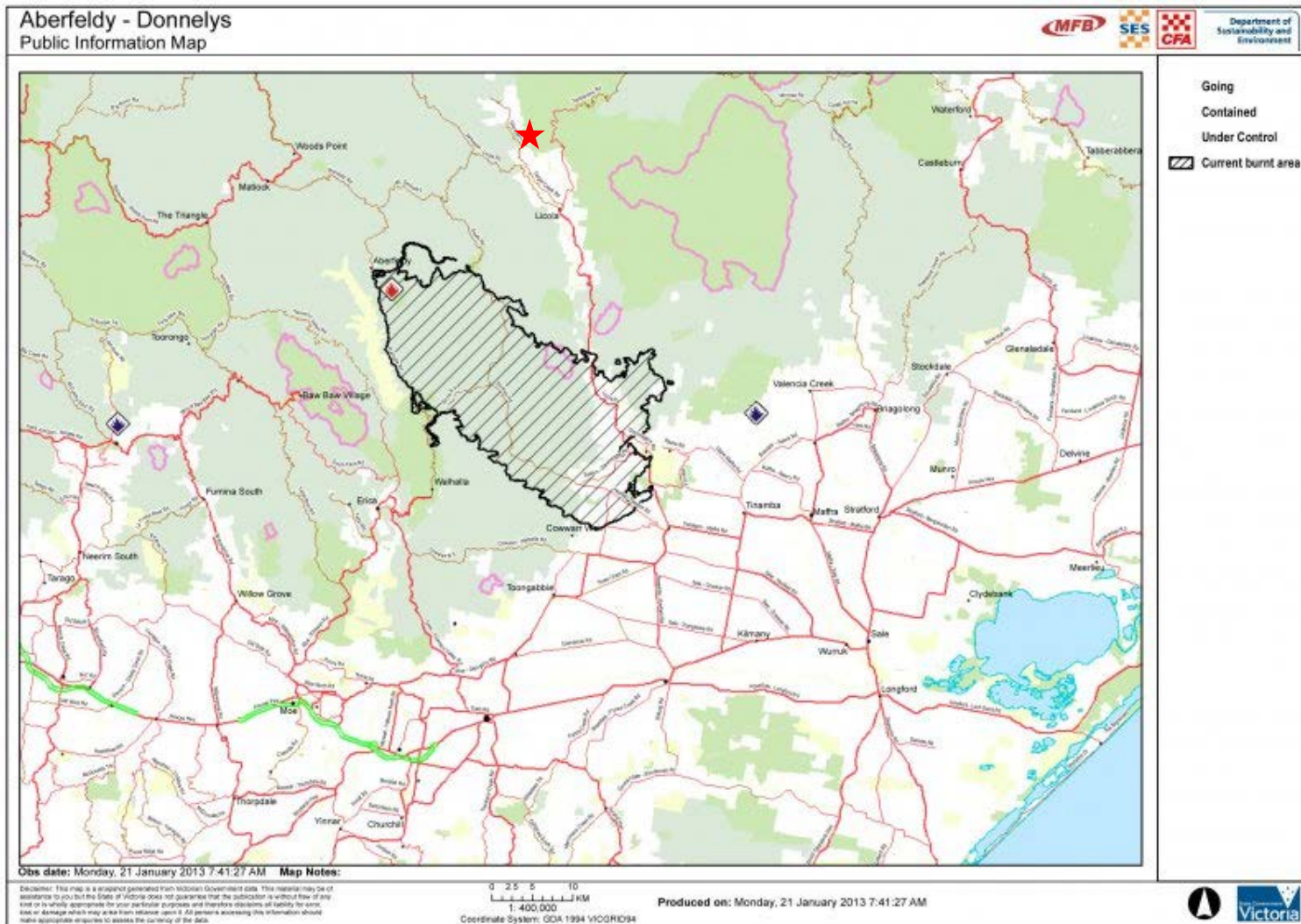
Figure 3-10. Area and extent of the 2013 Aberfeldy-Donnellys fire. Red star indicates study site location.
Source: Victoria Country Fire Authority (2013a).

Thus far, I have described the geology and topography of the study area, and broadly described the causes, characteristics and impacts of the Great Divide Fires of 2006/7. The occurrence, extent and severity of this megafire, and indeed many others in the past, have been and will continue to result from the multi-scale interactions of climatic and meteorological systems with ecosystems, associated vegetation formations and their distributions, at the continental, regional and local scales. Indeed, climate remains the primary determinant of fire regimes in different regions of the world, even where human efforts in "fire suppression" are active at the various local areas (Khabarov et al., 2016; Marlon et al., 2008). In the next section, we turn to examining the regional and continental-scale climate systems that exert higher-order controls of rainfall, temperature and vegetation re-growth, in relation to pre and post-fire weather, for our region of interest. It is also important to be cognizant that these broad-scale natural systems and patterns drive the hydrological and geomorphological processes operating on hillslopes and in catchments, the key focus of this thesis.

3.5. Climate and weather

3.5.1. Continental and regional scale systems

3.5.1.1 General description

Situated at 37.54 °S, 146.61 °E, the climate of the study site and the wider region in southeast Australia is classified as *Cfb* in the Köppen-Geiger climate classification: warm temperate climate with sufficient precipitation throughout the year with warmest month > 22°C; ≥ 4 months with temp > 22°C (Crosbie et al., 2012). Broadly, the climate is composed of the typical four seasons: summer from December to February (DJF); autumn from March to May (MAM); winter from June to August (JJA); and spring from September to November (SON) (Sturman and Tapper, 2006). Based information from the Bureau of Meteorology (2017b), southeast Australian climate and weather is influenced by an assemblage of regional and continental-scale systems that vary in their spatial extent and influence through the seasons. These include the mid-latitude frontal systems; East Coast Lows (ECLs); Southern Annular Mode (SAM); Sub-tropical Ridge (STR); easterly troughs, and northwest cloud bands. At the broader temporal scale, the El Niño-Southern Oscillation (ENSO) (NOAA, 2017) exerts higher-order controls over conditions at the continental and regional scales by influencing the activity, strength and positions of the various systems mentioned above (see Figure 3-11).
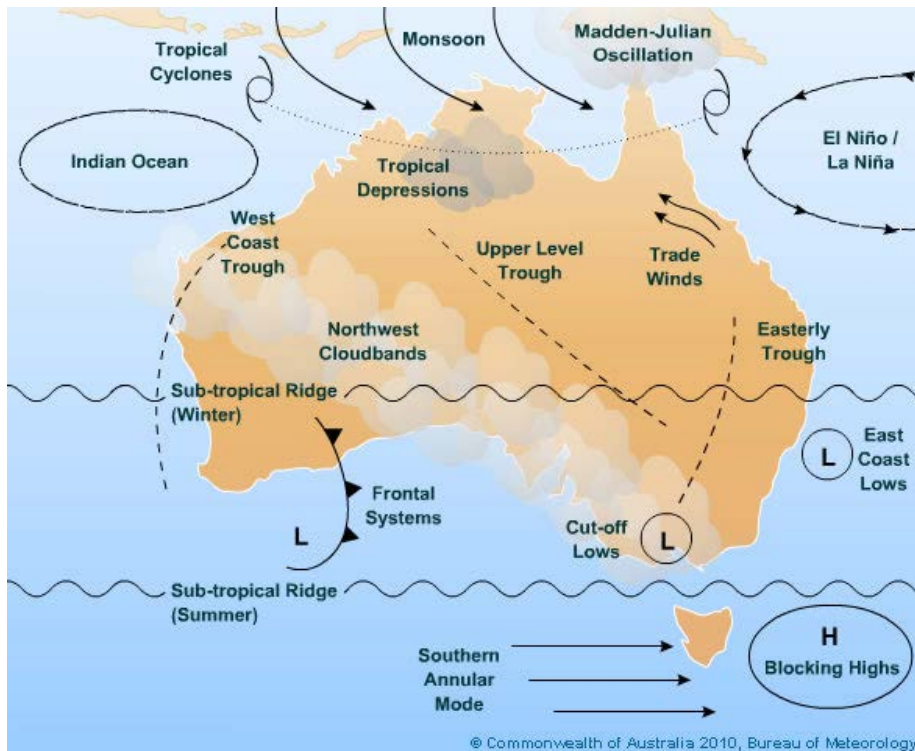
Figure 3-11. Illustration of the key climate drivers on Australian climate.
Source: (Bureau of Meteorology, 2017b)

Because of variations in the mean positions and activities of these systems, winter (JJA) precipitation tends to be driven by west-east moving frontal systems and East-Coast Lows. Summer (DJF) precipitation tends to be characterized by convection-related easterlies and sometimes, southerlies (Aldrick et al., 1984). The pronounced terrain of the Great Dividing Range with the general north-south orientation of highlands in the study area (see section 3.3) interacts with the major weather systems, causing orographic and aspect-related influences on rainfall, although the results can vary over different seasons (Pepler et al., 2014). For instance, the rain-shadow effect of the Barkly Land System on the Wellington Land System (Rowe and Downes, 1960) would be more pronounced during winter (westerly systems) compared to summer (southerly/easterly systems).

The weather of southeast Australia has been found to be distinct from those in similar temperate latitude locations in the Northern Hemisphere, because of distinct frontogenesis

patterns compared to North America or Europe. While the latter two regions have their land masses orientated in a general north-south manner adjacent to the Pacific and Atlantic oceans respectively, the Australian continent has a long east-west coastline delineating the hot dry continental interior equatorward, and large uninterrupted cool ocean expanse (the Southern Ocean) on the poleward side (Sturman and Tapper, 2006). We now examine these systems with some general consideration of the higher-order influences on rainfall and consequent hillslope erosion in southeast Australia where the study site is located.

3.5.1.2 Mid-latitude frontal systems

Mid-latitude frontal systems account for much of the rainfall in southeast Australia, and tend to dominate rainfall events during winter months (JJA) (Bureau of Meteorology, 2017b). Generally, these systems are driven by the continental-scale interaction between the cold, moist maritime air masses with origins in the Antarctic and Southern Ocean, and the warm, dry continental air from the interior of the Australian mainland. Frontal systems generally move from west to east, affecting weather conditions from durations spanning days to one week. These are central in bringing important "cool season" rainfall to southern Australia that typically recharges surface, soil and groundwater storages (CSIRO, 2012). However, regional climate change projections point towards generally lowered average cool season rainfall in autumn and winter (Timbal and Jones, 2008). In terms of hydrological and geomorphic processes, rainfall events from frontally-induced stratiform clouds tend to be of lower-intensity and longer duration, as compared to shorter, higher-intensity rainfall events from convection-induced cumuliform clouds (Dunkerley, 2010b).

3.5.1.2 East Coast Lows

East Coast Lows (ECLs) are intense regional-scale low-pressure systems that develop off the eastern coast of the Australian continent, usually extending towards the southeastern corner

(Bureau of Meteorology, 2007a). Their occurrences have been shown to be consistently independent from the Indian Ocean Dipole and ENSO systems (Pepler et al., 2014). With higher frequency of occurrence in autumn and winter, and highest in June, ECL development in winter is usually attributed to the deepening of low pressures from pre-existing troughs or in the wake of cold fronts moving eastwards from southeast Australia to the Tasman Sea. ECLs tend to bring very heavy and widespread rainfall with strong winds south of the low centre, lasting a few days (Bureau of Meteorology, 2007a). ECLs contribute strongly to the meteorological conditions that bring high amounts of rainfall and erosive energy to the study region during winter, and tend to be overlain onto the pattern of westerly rain-bearing frontal systems; they have also been cited as a main contributor of heavy rainfall on coastal regions of Australia's Eastern Seaboard that includes the present study area (Pepler et al., 2014).

3.5.1.3 Prefrontal troughs

Prefrontal troughs (PFTs) are particularly important during the Australian summer months (DJF) in terms of fire weather; these regional-scale, linear (north-south oriented) low pressure zones develop and precede the arrival of the main front itself (Sturman and Tapper, 2006). They generate strong northwesterly flows of warm and dry air from the Australian continental interior and extend any existing fire fronts. Fire risks are heightened and existing conditions exacerbated because the further drying-out of existing vegetation, ground and litter cover increases fuel ignitability. As the main front arrives over the region, the abrupt shift to westerly winds that signal the impending cool change expand the existing fire front and cause even larger areas to be burnt (Sturman and Tapper, 2006). This sequence of meteorological conditions helps to account for the regular occurrence of megafires in southeast Australia (Boer et al., 2008; Bradstock et al., 2010).

3.5.1.4 Southern Annular Mode (SAM) / Antarctic Oscillation (AAO)

The Southern Annular Mode (SAM) / Antarctic Oscillation (AAO) largely controls the strength and mean latitude of westerly winds in relation to the Australian mainland (southern Australia) and the Southern Ocean. "Positive" SAM conditions tend to lead to weaker than usual westerlies with the corresponding wind belt contracted towards the South Pole, leading to reduced rainfall from the mid-latitude frontal systems in southeast Australia and hence generally drier weather; and the converse for "Negative" SAM conditions. "Positive" SAM conditions tend to be more frequent during summer (DJF) and autumn (MAM) (Bureau of Meteorology, 2017b; Hendon et al., 2007). During these conditions, thermally-induced convective storms bring short-duration, high-intensity rainfall events of variable spatial extent from storm cells of cumuliform clouds (Dunkerley, 2010b) bringing concentrated bursts of energy that would have stronger erosive impacts on bare, exposed soil surfaces, and greater capacities to "breakthrough" any existing vegetation canopies without necessarily saturating their storage capacities. The biannual/triannual oscillation of SAM/AAO is a likely contributor to "wet" years" giving favourable plant growth conditions increasing biomass that then becomes an accumulated fuel load during the "dry" years when wildfires are more likely to ignite and spread (Russell-Smith et al., 2007).

3.5.1.5 Subtropical ridge (STR)

During the summer months (DJF), the subtropical ridge (STR), associated with large, regional surface high pressures and stable weather on the poleward edge of the Hadley Cell, tends to migrate further south and suppress frontal activity and weakens weather associated with any cold fronts that do break through the ridge (Bureau of Meteorology, 2017b). Present throughout the year, these semi-stationary anticyclonic cells migrate slowly from west to east, usually enabling frontal systems to follow. STR positions and effects are clearly associated with "positive" SAM conditions in summer described above. Thus, rainfall amounts in

southeast Australia and the study site can be on average slightly lower compared to the winter months; this is borne out in the rainfall data for the study site presented in the following section. Rainfall event characteristics and the resultant throughfall would also be different between seasons.

Heightened fire risks and severity tend to be associated with the warm, dry and stable conditions of the STR during summer that lead to increased fuel accumulation (through increased leaf drop due to evapo-transpirative stress) and ignitability (by strong drying and curing) (Bradstock et al., 2010; Bureau of Meteorology, 2010). The risks of fire ignition by lightning are also heightened due to strong surface heating inducing rapid convection and cumuliform cloud development at the local and regional scales (Albrecht et al., 2016). These have the potential to lead to short, intense thunderstorms that will have high erosive impacts. However, these are likely to be of relatively restricted spatial extent compared to frontally-induced stratiform rainfall events. As the STR migrates northwards during winter, more frontal rain events arrive in southeast Australia as the cold fronts extend further onto mainland Australia. Stronger southwesterlies and lower temperatures are associated with the moist and cold maritime air with origins in the Antarctic and Southern Ocean (Bureau of Meteorology, 2017b). In terms of vegetated hillslopes, canopy and soil moisture storages may be more quickly attained and exceeded during winter, and throughfall and overland flow processes may operate with higher frequency (albeit perhaps with lower intensity) compared to summertime.

3.5.1.6 Easterly Trough (EST)

The Easterly Trough (EST) is a linear low-pressure system normally positioned along the western, leeward flank of the Great Dividing Range that is oriented north-south along the eastern Australian coastline and then east-west in the southeast corner in Victoria. The EST exerts major influences on synoptic patterns during summer (Bureau of Meteorology, 2017b).

Driven by terrestrial heating during the Australian summer, the EST can generate convective circulations driving southerly and easterly airflows from the Southern Ocean and Tasman Sea respectively. Combined with orographic effects caused by the Great Dividing Range, widespread and intense rainfall events in areas such as the study region can be generated. When the EST interacts with any low pressure troughs or cold fronts moving through the region from the west, rainfall events may be further enhanced in depth, intensity and duration (Bureau of Meteorology, 2017b), and hence lead to higher water erosion rates.

3.5.1.7 Northwest Australia cloud bands

The continental-scale northwest Australia cloud bands tend to span the autumn, winter and early spring months from March to October, extending from the northwest to the southeast of the Australian continent (Bureau of Meteorology, 2017b). Characterized by heavy stratiform cloud with origins in convective activity in the Indian Ocean they can bring heavy rainfall across south and southeast Australia due to moisture-laden air advected from tropical maritime regions, especially when they combine with the more southerly-situated frontal systems and cut-off lows (Sturman and Tapper, 2006). This seasonally-active system thus contributes to slightly higher rainfall during the cooler seasons over the study area and could also therefore drive higher activity of erosive processes on hillslopes.

3.5.1.8 ENSO cycles

In addition to the systems described above that tend to fluctuate on a seasonal basis, southeast Australian climate and weather patterns are further influenced strongly at broader temporal scales by the multi-year El Niño-Southern Oscillation (ENSO) cycles (NOAA, 2017). Reduced rainfall and streamflow in southeast Australia tend to be closely associated with El Niño conditions, particularly during spring and summer due to enhanced atmospheric stability caused by the STR. On the other hand, La Niña conditions see higher than average

rainfall depths and increased streamflow due to the enhanced regional and continental scale convection due to higher than average sea-surface temperatures in the western Pacific (Chiew and McMahon, 2003; Tomkins et al., 2008).

Thus, post-fire vegetation recovery and erosion processes need to be considered in the context of ENSO cycles; vegetation recovery may be retarded by prolonged periods of El Niño induced drought and the landscape could remain vulnerable to wind and water erosion for longer than expected periods of time (Mayor et al., 2007); erosion rates may not necessarily correspond with the high soil erodibility and availability characteristic of post-fire conditions due to the limited rainfall depth, duration or intensity during these drought years, although even low-moderate sized events could have substantial hydrologic and geomorphic impacts. When there is a shift from El Niño towards wetter neutral or La Niña conditions (NOAA, 2017), rainfall events of sufficient magnitude to deliver significant erosive power would be more likely. Water erosion processes would then be more active and effective as vegetation recovery would lag the increased water and erosive energy in the form of higher rainfall frequency, larger rainfall depth and/or higher-intensity events; these dynamics were reported by Mayor et al. (2007) for the Mediterranean region, and discussed by Tomkins et al. (2008) for the southeast Australian context. The ENSO cycles are themselves influenced by the broader temporal scale Inter-decadal Pacific Oscillation (IPO) (Meehl et al., 2016), and therefore affect the overall fire and rainfall regimes of southeast Australia.

3.5.1.9 Discussion

In this section, I have briefly examined the main systems affecting regional weather and climate. Other than exerting higher-order influences on the occurrence of rainfall events that are the primary drivers of post-fire erosion processes and vegetation recovery, it has also been demonstrated that the frequent occurrence of large-scale fires in southeast Australia can be ascribed to the spatio-temporal extent and distribution these systems and their interactions. At the landscape scale, these systems integrate and further interact with the local physiography to give specific rainfall and temperature patterns that influence vegetation distribution, fire impacts and post-fire erosion and vegetation recovery. Consequently, specific patterns and processes of hillslope material flux under intermediate post-fire conditions would occur in complex, transitory landscapes such as the study area.

In addition to post-fire vegetation recovery rates, between year variations in temperature and rainfall also exert broader-scale influences on *pre-fire* rates of vegetation growth, biomass and fuel accumulation, and thus fire risks. Like many evergreen forests around the world (Liu et al., 2017), *Eucalyptus* species deal with drought conditions by restricting their stomatal conductance reducing transpirative losses. These would be accompanied by reduced foliage growth and increased senescence. However, in favorable non-drought years where more soil moisture is available, their stomatal conductance increases rapidly and results in vigorous flushes of new leaves and extensions of twigs and branches (Zeppel et al., 2008). This would then later result in increased live or dead fuels available for burning if fire breaks out. In this way, the ENSO cycles discussed above strongly influence the pulses and ebbs of vegetation growth and fuel accumulations, and also fire regimes at the inter-annual and decadal timescales.

Having provided the context of major climatic systems and meteorological conditions affecting southeast Australian dry eucalypt forest ecology, hydrology and erosion, I now

provide, in the next section, a brief but important study of lightning in relation to the occurrence of wildfires applicable to the present study region.

3.5.2. Lightning

Lightning is the most important natural cause of wildfire ignition (Krause et al., 2014), accounting for 26% of all ignitions in Victoria, Australia, second only to human-caused ignitions (Flinn et al., 2008a). Lightning has been defined as 'an energetic electrical discharge caused by the separation of positive and negative charge in clouds leading to voltage differences of order 10 – 100 MV' (Latham and Williams, 2001, p. 376). This charge separation is primarily caused by turbulent cloud microphysical processes that concentrate negative charges at the lower-altitude regions of clouds and vice-versa. The resultant positive dipole causes two main types of lightning (i) intracloud (IC); and (ii) cloud-to-ground (CG) lightning - the main agent for natural wildfire ignitions (Latham and Williams, 2001). CG lightning is initiated when, within a region of high electric field, an ionized path is forged toward the ground as a 'stepped leader' carrying a large negative potential. As the stepped leader comes into close proximity with the ground surface, an intense electric field is developed between them. Electric streamers are then propagated upwards from high points on the ground (e.g. tree crowns) to the downward-moving leader within the intense electric field. Upon connection, a bright, high-current 10-100 kA return stroke occurs and spreads upwards approximately $1\text{-}2 \times 10^8$ m s^{-1}. This entire process is called the leader-return stroke sequence (Latham and Williams, 2001). However, the duration of the return stroke (a few microseconds) generally limits its ability to ignite fuels and light fires because of the inadequate fuel temperature reached. Instead, actual ignition is frequently enabled by the occurrence of a continuing current (CC) which is a sustained current of low amplitude that flows within the channel to the ground lasting from milliseconds to hundreds of milliseconds (Fuquay et al., 1972). CC occurrences are also variable; 90% of CG lightning transfer negative charge to the ground and almost 50% of these contain CC. The other 10% of CG

lightning transfer positive charge to the ground and almost all of them contain CC (Latham and Williams, 2001).

Convective Available Potential Energy (CAPE), the key factor driving convective thunderstorm development, is strongly correlated to lightning frequency (Kuleshov et al., 2006). Notably, "dry lightning" (lightning that occurs without any significant rainfall depth) that tends to occur in association with strong convective conditions has been found to exert a strong positive influence on the probabilities of fire per lightning stroke especially over Victoria in southeast Australia (Dowdy and Mills, 2012a). The significance of "dry lightning" in accounting for wildfire occurrences has also been reported in other fire-prone landscapes such as the western United States (Hall, 2007) and the Mediterranean (García-Ortega et al., 2011). The meteorological mechanisms favouring the development of strong convective systems mean that the late spring, summer and early autumn months are associated with higher lightning occurrence frequencies. Furthermore, these generally coincide with low fuel moisture conditions and hence increase the risks of wildfire ignition and spread. However, it should be noted that in temperate mid-latitude regions of southeast Australia, lightning also occurs during the colder winter months in association with strong frontal storm activity generally associated with steep cold fronts (Kuleshov et al., 2006). Nevertheless, successful wildfire ignition and spread is much less likely in the cold and wet conditions of winter.

Lightning occurrence can, in return, be influenced by large fires. Pyrocumulus and pyrocumulonimbus clouds, driven by the convective heating from the fire, and the massive addition of cloud condensation nuclei from combustion byproducts, have been widely observed in association with southeast Australian wildfires (Cruz et al., 2012; Fromm et al., 2010; Gatebe et al., 2012). These clouds are a prime source of positive CG lightning strikes providing numerous CCs for further ignitions to occur (Latham and Williams, 2001). From data by Kuleshov et al. (2006), southeast Australia nominally experiences average lightning

ground flash densities ranging from 0.70 km^{-2} y^{-1} (Mt. Burnett) to 0.87 km^{-2} y^{-1} (Melbourne); at the continental scale, lower latitudes experience higher lightning occurences (e.g. Brisbane 1.43 km^{-2} y^{-1}, Darwin 6.67 km^{-2} y^{-1}). In their study of wildland fire ignitions on public land by lightning over 9 years (2000-2009) in southeast Australia, Dowdy and Mills (2012b) found that lightning occurrence was not significantly related to the time of day. Instead, time of the year was significant, with heightened ignition risks seen in October (late spring) (~0.45%), peaking in January at around 0.72% and then declining to around 0.42% in February (late summer). Dowdy and Mills (2012a) also examined lightning occurrence, ignitions and fires on public lands in southeast Australia, and found a seasonal summer bias, with 96% of lightning fires occurring between November and March with modal occurrences in January, albeit with large inter-annual variability from 60 in the year 2000, to 380 in the year 2007. On a diurnal basis, lightning fires were usually firstly observed in the afternoon, after 1300 hrs to 1900 hrs Australian Eastern Standard Time. These results indicate the importance of factors such as fuel moisture, humidity and wind speeds in successful lightning ignitions of wildfires, their sustenance and spread (Dowdy and Mills, 2012a).

Collins et al. (2015) examined the spatial patterns of wildfire ignitions in south-eastern Australia and found some positive spatial correlations of lightning ground flash density with natural vegetation cover percentage ($R^2 = 0.12$), mean elevation ($R^2 = 0.28$), terrain (elevation standard deviation) ($R^2 = 0.47$). These provide some indications that forested, mountainous terrain have a higher incidence of lightning-ignited wildfires. In their study of 12 months of lightning data for the Mediterranean region, Kotroni and Lagouvardos (2008) found that lightning was positively correlated with elevation only during spring and summer; positive correlation between lighting and elevation slope through spring, summer and autumn but not winter, and high lightning yield for woodland areas and low lightning yield for bare-ground areas. They explained that the forest and woodland canopies helped to

mitigate soil moisture losses which then led to the increased lightning "yield". Furthermore, the tree-tops formed natural high points at which leader-return stroke sequences and CCs were more likely to occur. The existence of these conditions and processes are also plausible when applied to Australian dry eucalypt forests across the Great Dividing Range, corroborating with the findings reported by Dowdy and Mills (2012a); Dowdy and Mills (2012b).

However, vegetation canopies also intercept rainfall, reducing, smoothing-out or even eliminating the proportion of canopy-incident rainfall that eventually reaches the ground-level litter and vegetation, and before any infiltration occurs (Sidle and Ziegler, 2017). This could therefore contribute to curing of fine fuels and heightened ignitability, particularly during dry summer conditions, and exacerbated in extended drought periods where effective rainfall events would be less likely; and also in general because of the strong positive skew in rainfall event magnitudes towards low event depths (Brown et al., 1985). On the other hand, more arid forest micrometeorological conditions can lead to greater fuel ignitability where lightning might strike, due to increased soil and fuel moisture losses giving dry fine fuels resulting from canopy "opening", and increased fuel load with disturbances such as logging (Lindenmayer et al., 2009) or widespread die-offs, defoliation and canopy cover decline due to landscape-scale drought stress (Flinn et al., 2008a).

At the broader spatial and temporal scales, the patterns and frequency of lightning activity leading to wildfires are projected to shift as global climate changes. Modelling projections by Krause et al. (2014) showed that CG lightning occurrences over land could increase by up to 21.3% by the end of the century under RCP85 conditions. However, the spatial distribution of these increases leading to fire activity was variable. While decreases were projected for Europe (-10.80%) and South America (-10.71%), there could be increases in Australia (+7.42%) (where southeast Australia was well-represented), Southeast Asia

(+32.88%), continental Asia (+18.03%), North America (+10.77%) and most parts of Africa (+2.79%) where the estimated extent of burnt areas was influenced by fuel load availability as well as the projected CG lightning frequencies and locations.

This section has briefly examined the processes of lightning occurrence and their association with wildfire ignition to build some basic understanding of the occurrence of the 2006/7 Great Divide Fires, as well as other major fires in Victoria in the past, as well as in the future. This should be understood in the context of the main climatic patterns of southeast Australia outlined in section 3.5.1. While human-caused ignitions may continue to be the most significant cause of fire ignitions, the projected increases in lightning occurrence in southeast Australia in the near to medium-term are likely to contribute to some increases in the frequency of wildfire occurrence by natural causes in this region.

Having sketched out the macro-scale systems influencing the broader region within which the study area is situated, I now narrow the focus to describe and analyze the specific climatic and meteorological conditions of the study site in the next section, using data synthesized from various sources.

3.5.3. Study area climate

3.5.3.1. General rainfall patterns

According to Bureau of Meteorology (2017c), the mean annual rainfall of the study site is 802 mm (median 845 mm); see Figure 3-12. The probabilities of occurrence of various rainfall depth and duration for the study site are presented using the Intensity-Duration-Frequency curves in Figure 3-13. The distribution of rainfall, while generally evenly distributed through the year, is slightly biased with higher average rainfall during the winter (JJA) and spring (SON) months, compared to summer (DJF) and autumn (MAM). Rowe and Downes (1960) had earlier observed that rainfall minima for Licola and Licola North occurred from February to April (late summer to autumn). It was also suggested that rainfall of the central parts of the Glenmaggie catchment (within which the study area was located) was likely to be influenced by the rain shadow caused by high mountains at the western boundary of the catchment (Rowe and Downes, 1960) where west-east moving frontal systems over the Dividing Range would bias rainfall contributions towards the western portion of the catchment and reduce average rainfall receipt over the more centrally located study area. Thus, such rainfall variability over the study area also contributes to the uncertainty of erosion activity under post-fire intermediate vegetation conditions.
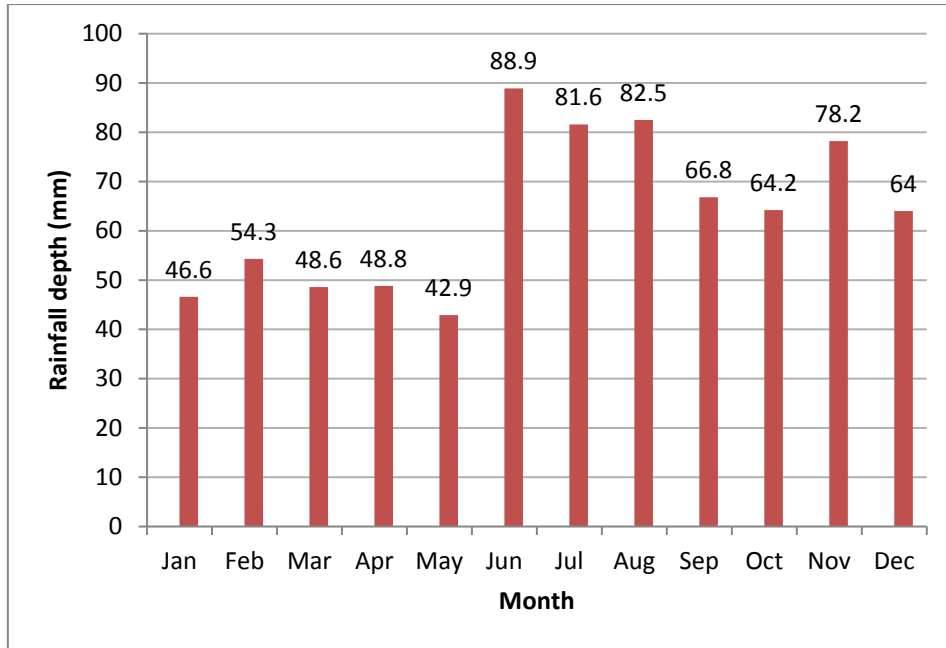
Figure 3-12. Mean monthly rainfall for study region. Data source: Bureau of Meteorology (2017c).
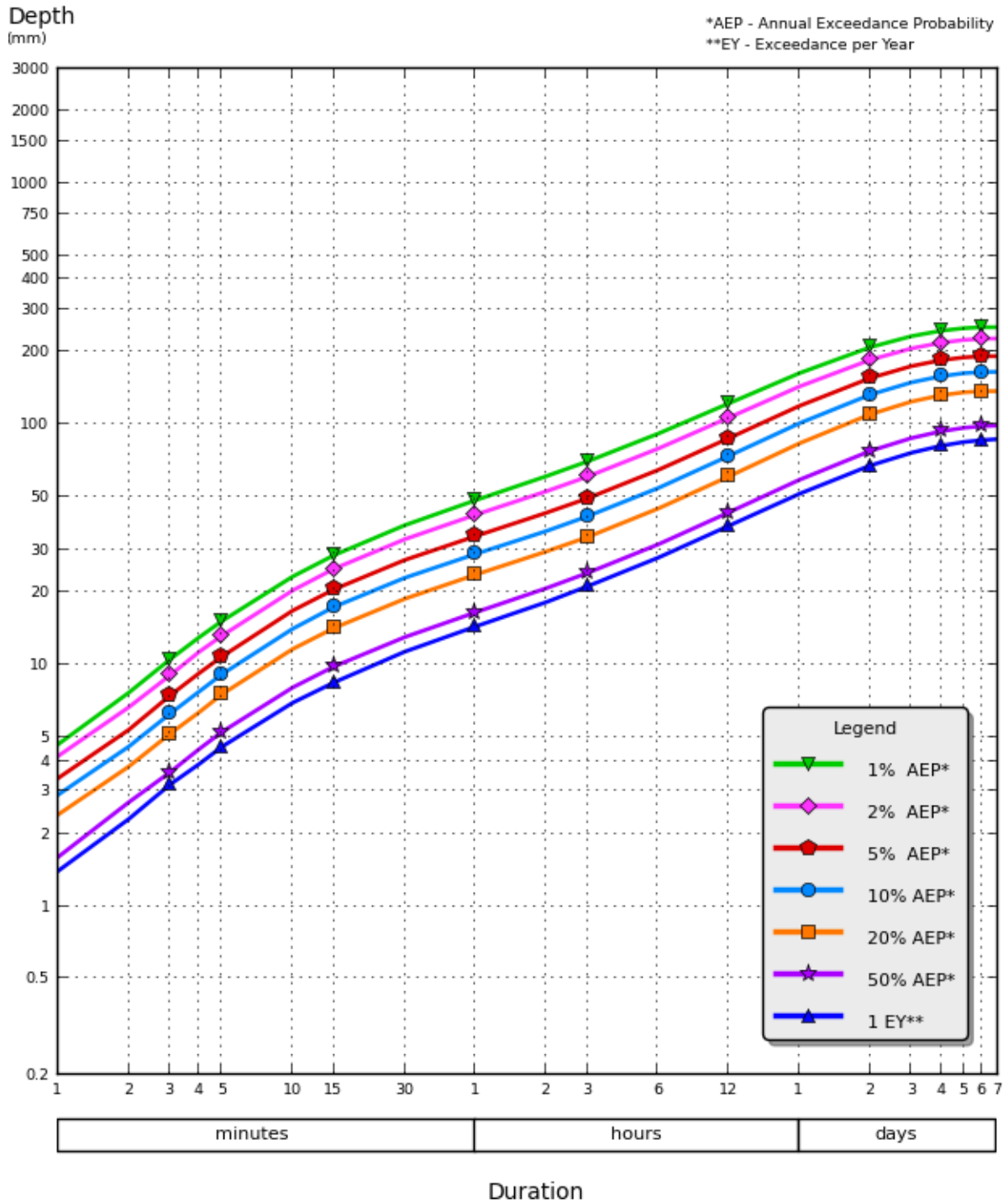
Figure 3-13. Intensity-Duration-Frequency curves for the study site. Source: (Bureau of Meteorology, 2014). Note: The 1 EY curve indicates the event intensity-duration metric that will be exceeded in any given year.

Seasonal variations in the dominant rainfall-generating meteorological mechanisms over the region are also likely to generate rainfall events of differing character, contrasting interactions with vegetation canopies and soils, and varying hillslope erosion responses between summer-autumn and winter-spring periods, at the study area. As noted in section 3.5.1., the summer-autumn convection-related rainfall events are more likely to generate high-intensity rainfall events of limited spatial extent that could penetrate the intermediate post-fire canopies and exceed erosion thresholds as high-intensity and energy "pulses", generating substantial hillslope material flux even where actual event depths and seasonal totals may not be high. However, during winter-spring, frontally-generated rainfall events normally associated with broad-scale stratiform clouds generating long-duration, low (< 2 mm hr^{-1}) to moderate (> 2 mm hr^{-1}; < 5 mm hr^{-1}) intensity rainfall events (Tokay and Short, 1996), would likely cause more gentle wetting-up of vegetation canopy storages, higher interception and intra-storm canopy moisture losses (Dunkerley, 2014b; Dunkerley, 2008c). Released throughfall drip points be activated gradually and possibly sustained over long durations to cause splash erosion. Soil moisture would slowly increase to reach saturation to generate overland flow erosion processes, depending on antecedent conditions. However, ECLs occur with higher frequency during winter (JJA) and contribute long-duration, large-depth and widespread rainfall with strong erosive impacts, adding on to the impacts of the gentle to moderate-intensity frontal events. In terms of the geomorphological outcomes, main seasonal differences between rainfall event characteristics and interactions with the ground (i.e. vegetation cover, litter and soil) conditions may not just cause differential erosion rates and volumes, but also the selectivity/non-selectivity of sediment size ranges transported with the varying strengths and durations of erosive energies exerted.

3.5.3.2. Temperature, relative humidity, solar radiation and potential evapotranspiration

Detailed and comprehensive climatological data was not available for the study area. As an alternative, interpolated daily rainfall data from 1889 to 2016 (total 128 years) from the SILO climate database "Data Drill" (Queensland Government, 2017) covering the study area region (Latitude 37.6 °S, Longitude 146.6 °E) was acquired and processed to describe the temperature, relative humidity, solar radiation and potential evapotranspiration parameters for the study area and their expected annual seasonal variations.

Figure 3-14 shows the derived mean maximum and minimum temperatures for the Licola region. The temperature variations and transitions are typical of a mid-latitude temperate climate. Maximum temperatures range from highest of 25.9 °C in February to lowest of 11.0 °C in July. Minimum temperatures range from highest of 11.6 in February to lowest of 2.9 °C in July.
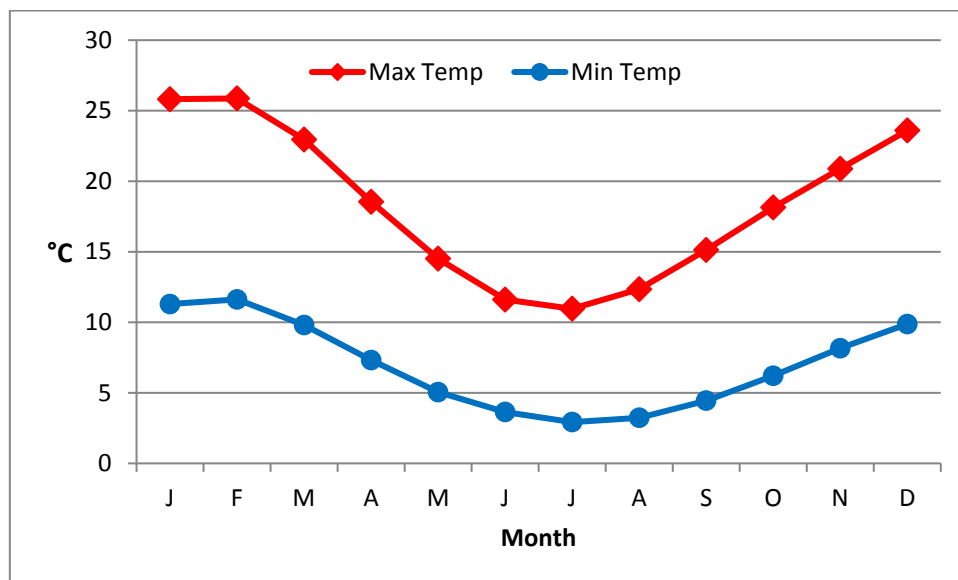
Figure 3-14. Mean monthly maximum and minimum temperatures for the Licola region. Data source: Queensland Government (2017).

The mean daily solar radiation received for the Licola region through the months of the year is presented in Figure 3-15. Maximum mean solar radiation received was 23.8 MJ m^{-2} in January. Minimum mean solar radiation received was 6.8 MJ m^{-2} in June.
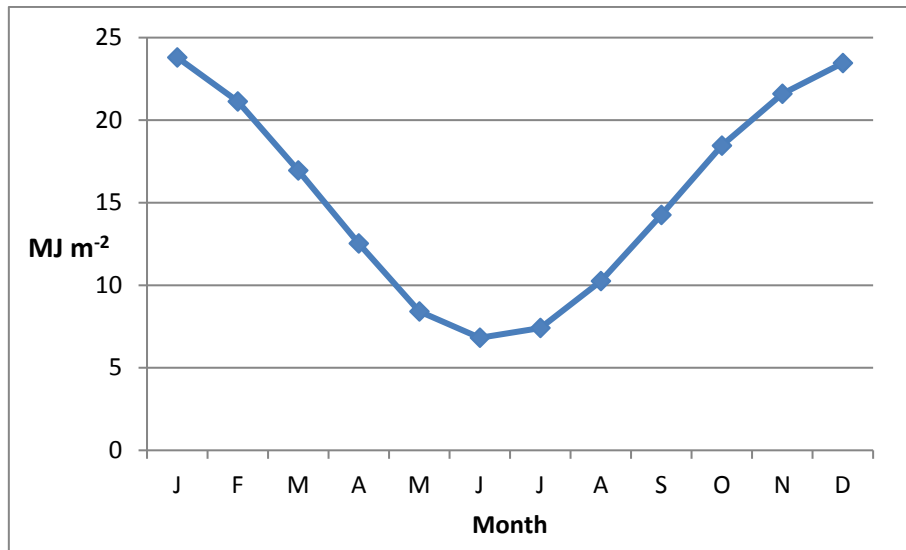
Figure 3-15. Mean daily solar radiation (MJ m^{-2}) (by month) received for the Licola region. Data source: Queensland Government (2017).

Figure 3-16 shows the mean monthly maximum relative humidity (%) for the Licola region. Peak mean maximum relative humidity occurred in June at 63.2% with a gradual decrease in the following months. Lowest mean maximum relative humidity was in January at 42.7%, followed by a moderately rapid increase over the following months to the June peak.
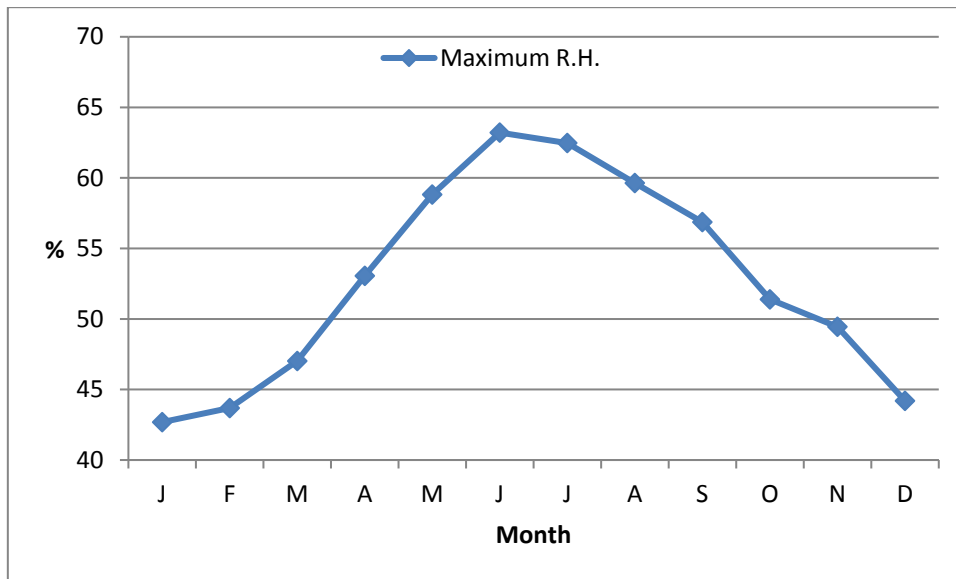
Figure 3-16. Mean daily relative humidity (%) by month for the Licola region. Data source: Queensland Government (2017).

Figure 3-17 presents the estimated daily potential evapotranspiration (PET) using the FAO Penman-Monteith equation (FAO56) (Allen et al., 1998). Highest mean daily PET is found in January at 4.8 mm d^{-1}, while lowest mean daily PET is found in June at 0.8 mm d^{-1}. PET patterns closely reflect temperature (Figure 3-14) and solar radiation (Figure 3-15) patterns which are prime controls over evaporation and transpiration rates, and therefore also indicate plant photosynthetic activities. These affect soil moisture conditions which influence the operation of splash and runoff erosion processes, as well as canopy storage and evaporation losses during and between rainfall events, influencing throughfall processes.
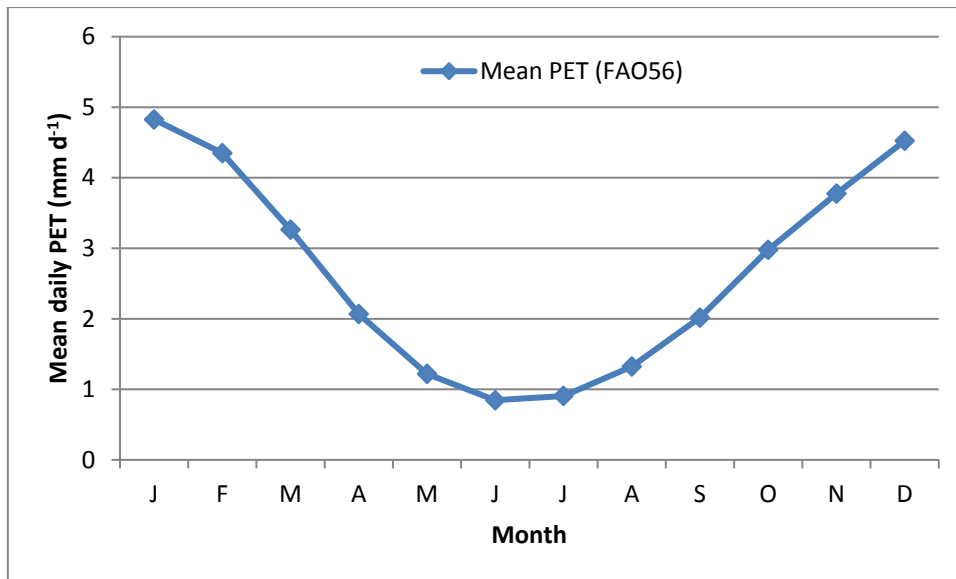
Figure 3-17. Mean Daily Potential Evapotranspiration (PET) by month for the Licola region. Data source: Queensland Government (2017).

In the following section, I examine the diurnal-nocturnal occurrence of rainfall over the study area. This aspect of rainfall is presently underexplored in the context of hillslope hydrology and geomorphology, and not been applied so far to our study area and region of interest, the time-of-day of rainfall occurrence can have important influences on processes such as soil moisture content, litter content, plant canopy wetness and evaporation rates.

3.5.3.3. Diurnal-nocturnal rainfall distribution

3.5.3.3.1. Background

Rainfall has high spatio-temporal variability which manifests at the sub-daily timescale, other than at the monthly and seasonal timeframes. Key factors affecting these patterns include general land surface characteristics such as terrestrial or oceanic locations, aspect, vegetation, land-use and terrain, all of which affect local and regional convection and mobility as well as the location of temperate-climate frontal systems. Global and continental-scale climatic systems and their oscillations, such as monsoonal systems and global atmospheric circulatory cells are also important. At the global scale, Chiu (2001) reported the dominance of peaks in land rainfall in the afternoon hours (1500 to 1800 hrs) with these patterns particularly pronounced in the equatorial regions of Africa and Amazonia. In the mountainous western US and central America, evening to nocturnal (2100 to 0300 hrs) maxima were found. Similarly, the southern slopes of the Himalayan ranges were dominated by rainfall occurring in the late-night hours. Land rainfall tends to have more pronounced diurnal rainfall differences. In contrast, oceanic rainfall tends to peak in the afternoon and early evening (1200 to 2100 hrs), although the diurnal differences are much less pronounced (Chiu, 2001). For lowland equatorial rainforests in Indonesia, Vernimmen et al. (2007) found that while three-quarters of all rain fell at night, higher mean event intensities were found for afternoon events (8.3 mm hr^{-1}) compared to mean night-time (6.0 mm hr^{-1}) and mean morning (5.9 mm hr^{-1}) event intensities.

Yang and Smith (2006) offer a range of explanations for the range of diurnal variability of *tropical* rainfall at the global scale. It is generally agreed that mid to late afternoon rainfall maxima over continental surfaces can be attributed to land surface heating by solar radiation which is diurnally regulated and differs seasonally in the tropics and mid-high latitudes, for instance over the Australian continent (Rauniyar and Walsh, 2010). Dai et

al. (2007) presented strong global-scale evidence of the control of the daily (24-hour) cycle over sub-daily precipitation variations. Over land areas, summer months clearly had afternoon-evening dominant rainfall and mean to peak amplitude of 30% to 100% of daily mean precipitation amount. Nevertheless, nocturnal summer precipitation maxima can also be found in regions where nocturnal environments exert only minor controls over broader-scale convective processes, for example over the central United States and southeast China where continental-scale pressure patterns dominate. Over maritime areas, peak rainfall times were midnight to early morning. On the other hand, the cold seasons during and around winter correlate with weaker diurnal-nocturnal rainfall differences with morning maxima observed over most land areas (Dai et al., 2007).

Although it may seem trivial in passing, the time-of-day of rainfall occurrence can be both interesting and significant in relation to hydrological and geomorphological processes. Diurnal-nocturnal rainfall occurrence can, in many cases, be intimately linked to their meteorological formation mechanisms, interactions with terrain, and resultant cumuliform or stratiform rainclouds that can differ substantially in terms of rainfall intensity and spatial extent (Kendon et al., 2012). Therefore, the actual impact of a rainfall event or series of events on a catchment and its landscape can vary substantially. Intra-event evaporative losses can be significant, especially during high-temperature, low-humidity conditions that prevail during summer in the mid-latitude regions, other than areas in the Australian arid and semi-arid interior (Dunkerley, 2008c) and Mediterranean-climate regions in Western Australia. At the daily timescale, peak intra-event and near-event (pre and post) evapo-transpirative losses would occur during the late afternoon to early-evening hours (Kirkpatrick and Bridle, 1998; Kirkpatrick and Nunez, 1980). These will determine the net amount of water that reaches the plant canopy and saturates it, infiltrates into the soil for plant uptake and growth processes, and also erosive energy (Dunkerley, 2008c). On the other hand, where rain falls during the

cooler night-time hours, intra-event evaporative losses from plant canopy, soil surfaces and from the hydrometeors themselves, together with minimal plant water uptake, will be lower compared to warm and dry daytime rainfall conditions. This will then lead to higher rates of water arrival at the plant canopy and soil surfaces, volumes of water available for infiltration into soil and runoff generation, and therefore also greater splash and overland flow erosion activity. The long-term impacts on vegetation distribution in the landscape can be substantial (Kirkpatrick and Bridle, 1998; Kirkpatrick and Nunez, 1980) and so would be the consequent feedback loops for hillslope hydrological and geomorphological processes.

The research examining diurnal-nocturnal rainfall occurrences around the world is presently quite sparse, with the exception of the continental United States (Dai et al., 2007). In Australia, not much work has been done to comprehensively characterize and explain the diurnal-nocturnal rainfall occurrences at the regional or local scales. Rauniyar and Walsh (2010) studied the effects of the Madden-Julian Oscillation (MJO) categories (active, suppressed and weak) on diurnal rainfall rates over monsoonal northern Australia (Darwin and adjacent regions). They found that suppressed/weak MJO led to higher evening rainfall, while active MJO days saw greater occurrence of rather unusual nocturnal (past midnight) rainfall maxima; active MJO days also saw 1.5 times more morning rainfall than during other MJO phases.

For southeast Australia, our area of interest, Verdon-Kidd and Kiem (2009) examined the regional (synoptic) and large-scale climate drivers of rainfall, and identified 20 key regional synoptic patterns using monthly records from nine rainfall stations distributed across Victoria, and Mean Sea Level Pressure (MSLP) charts from 1948 to 2007. These were then categorised into 8 "wet", 8 "dry" types and 4 wet-dry types being spatially-variable across Victoria. Notably, the station for the Macalister catchment, of which the present study area is a part, was also included. The broad-scale, albeit seasonally variable, influence of ENSO,

IOD and SAM systems on Victorian rainfall (and its spatial variability) was demonstrated (cf. section 3.5.3.1.). However, while the various multi-scale meteorological mechanisms of rainfall occurrence over Victoria are quite well-described (Keim and Verdon-Kidd, 2009) minimal work has been done to examine time-of-day rainfall occurrence in hilly and mountainous parts of central and eastern Victoria where these various factors and processes can combine to influence the spatio-temporal distribution of rainfall events and their characteristics, that then affect hydrological and geomorphological processes.

Furthermore, Australia's large continental area, combined with the large maritime areas adjacent to it, present prime conditions where continental-scale, rather than regional-scale conditions, can dominate meteorological conditions and rainfall occurrence to give diurnal alongside nocturnal rainfall peaks in the mid-latitudes (Dai et al., 2007). Indeed, the strong diurnal rainfall variations in southeast Australia being identified by Dai et al. (2007) deserve some detailed study.

This section aimed to systematically examine the diurnal-nocturnal occurrence of rainfall over the study location in region of Licola town, situated on the southern fall of the Great Dividing Range where wildfire occurrence and post-fire erosion vulnerability can be heightened. This was done using 14 years of hourly rainfall records selected from the years between 1992 and 2012.

3.5.3.3.2. Materials and methods

i. Data processing and filtering

Hourly rainfall records from 1993 to 2012 were extracted from DELWP (2016) (http://data.water.vic.gov.au/monitoring.htm) for Licola town (Station no. 225209; rainfall records for Licola weather station commenced only in 9 Oct 1992). This station was selected because, being just 15 km south, it was most proximal to the study site and also had a sufficiently long, good-quality rainfall record to enable the study of diurnal-nocturnal rainfall occurrences. Hourly rainfall rates integrate depths over a substantial time period, and can considerably mask intra-event rain rate variations (Dunkerley, 2008b). Nevertheless, the 60-minute integration time was used for this exploratory work as it was the most consistent sub-daily dataset available for examination, and had also been used by several other workers such as Dai et al. (2007).

The records were then examined in Microsoft Excel™ for completeness and accuracy with reference to Quality Codes (QC) indicated by DELWP (2016), as shown in Table 3-1. Firstly, year-long records for 1993, 1994, 2002, 2004, 2007 and 2009 were excluded from the analysis because they contained unacceptably high proportions (more than one month of rainfall records) with $QC \geq 100$. This gave 14 years of rainfall records, very close to the nationwide average of 15 years for availability of detailed pluviometric data (Jennings et al., 2010). Secondly, records with $QC < 100$ were examined for their veracity and accuracy. For records with $QC = 76$ and $QC = 80$, checks against other nearby weather station records and radar images (The Weather Chaser, 2017) to corroborate the occurrences of rainfall and the likely depths and intensities on a nominal basis.

Table 3-1. Quality Code (QC) and Descriptions of rainfall records. Source: (DELWP, 2016)

Quality Code	Description
2	Good quality data - minimal editing required. Drift correction
11	Raw data used for operational purposes. (Not validated)
76	Reliable non-linear interpolation using other data sources, not a correlation.
80	Accumulated (Rainfall or Flow totals only).
100	Irregular data, Use with caution. Beyond QC=50 or unexplained
151	Data lost due to natural causes / vandalism
180	Data not recorded, equipment malfunction.
255	No data exists

ii. Rain rate classification

Classification of rainfall intensity was applied following the scheme by Tokay and Short (1996); also see (Dunkerley, 2008b) which was based on the derived boundaries between different raindrop spectra corresponding with different rain rate ranges associated with stratiform and convective rainfall types (see Table 3-2). Following this, classification could also enable direct inference of rainfall erosivity with respect to the drop-size distributions reported by Tokay and Short (1996).

Table 3-2. Rainfall rate categories of Tokay and Short (1996). From Dunkerley (2008b).

Rain rate category	Rain rate R (mm h^{-1})
Very light	$R < 1$
Light	$1 \leq R < 2$
Moderate	$2 \leq R < 5$
Heavy	$5 \leq R < 10$
Very heavy	$10 \leq R < 20$
Extreme	$R \geq 20$

iii. Diurnal-nocturnal rainfall classification

To explore possible seasonal patterns of diurnal rainfall occurrence, the records were collated into individual months. These were then sorted by hour of occurrence in a 24-hour format. The data was segregated into months, because day-night hours for the region in the latitude 38 °S vary through the year. Specific sunrise-sunset times were obtained from Geoscience Australia (2015). Generalised monthly sunrise-sunset times, correct to the nearest hour, were generated (see Table 3-3). Rainfall records were firstly categorized into nocturnal and diurnal rainfall occurrence times-of-day (hours). Nocturnal (evening, night or early morning) rainfall as regarded as all rainfall recorded in the hour after sunset, up to and inclusive of the sunrise hour. Diurnal rainfall (morning and afternoon) was regarded as all rainfall recorded in the hours after the sunrise hour, up to and including the sunset hours.

Table 3-3. Generalised sunrise-sunset times (to the nearest hour-of-day) to categorize rainfall occurrence as either diurnal or nocturnal. Adapted from Geoscience Australia (2015).

Month	J	F	M	A	M	J	J	A	S	O	N	D
Sunrise	0500	0500	0600	0600	0700	0700	0700	0700	0600	0600	0500	0500
Sunset	1900	1900	1800	1800	1700	1700	1700	1700	1800	1800	1900	1900

The grouping of rainfall data by months was adopted because the specific climatic conditions and rainfall-generating mechanisms (and concomitantly spatial distribution of rainfall) can vary significantly by seasons (see section 3.5.). I could also ensure that rainfall occurrences in similar climatic conditions were compared without any *a priori* assumption of rainfall variations by seasons.

To determine how "wet" a particular hour of the day was throughout the 14-year record, three key variables were calculated for each month. Rainfall hours were obtained by

counting the number of hours a specified hour of the day (0000 hrs – midnight, to 2300 hrs – 11 p.m.) that any rainfall was recorded; minimally 0.2 mm (the value of a single pluviometer tip). Rainfall hour-depth was calculated by summing the rainfall depths for each rainfall hour. Total rainfall percentage was calculated by expressing the rainfall hour-depth as a proportion of all recorded rainfall for the month, to account for the quantitative contribution of each hour to the total rainfall depth. Using this approach, I was also able to determine and examine the distribution of rainfall depth values and their averages (mean and median), across the diurnal and nocturnal hours for each month.

Using SPSS, One-way ANOVA was conducted on the summed rainfall hour depth for each month to discern any differences in the distribution of rainfall values between months (between group differences), and Post-hoc Tukey HSD to identify groups of months with similar rainfall hour depth value distributions. Non-parametric Kruskal-Wallis Test was used to analyze skewed and non-normal distributions of wet-hour rainfall depth values, being highly skewed towards low values of 0.2 mm in an hour.

3.5.3.3.3. Results

i. General findings

The diurnal-nocturnal occurrence of rainfall varied through the year. Figure 3-18 presents the percentage occurrence of total rainfall depth occurring during the day or night. Daytime rainfall tended to dominate, beginning in November (58.3%) through to a peak in February (70.9%). In contrast, nocturnal rainfall dominated from April (55.7%) through to the peak in August (64.9%). Almost equal rainfall percentages between day and night were found in March, September and October.
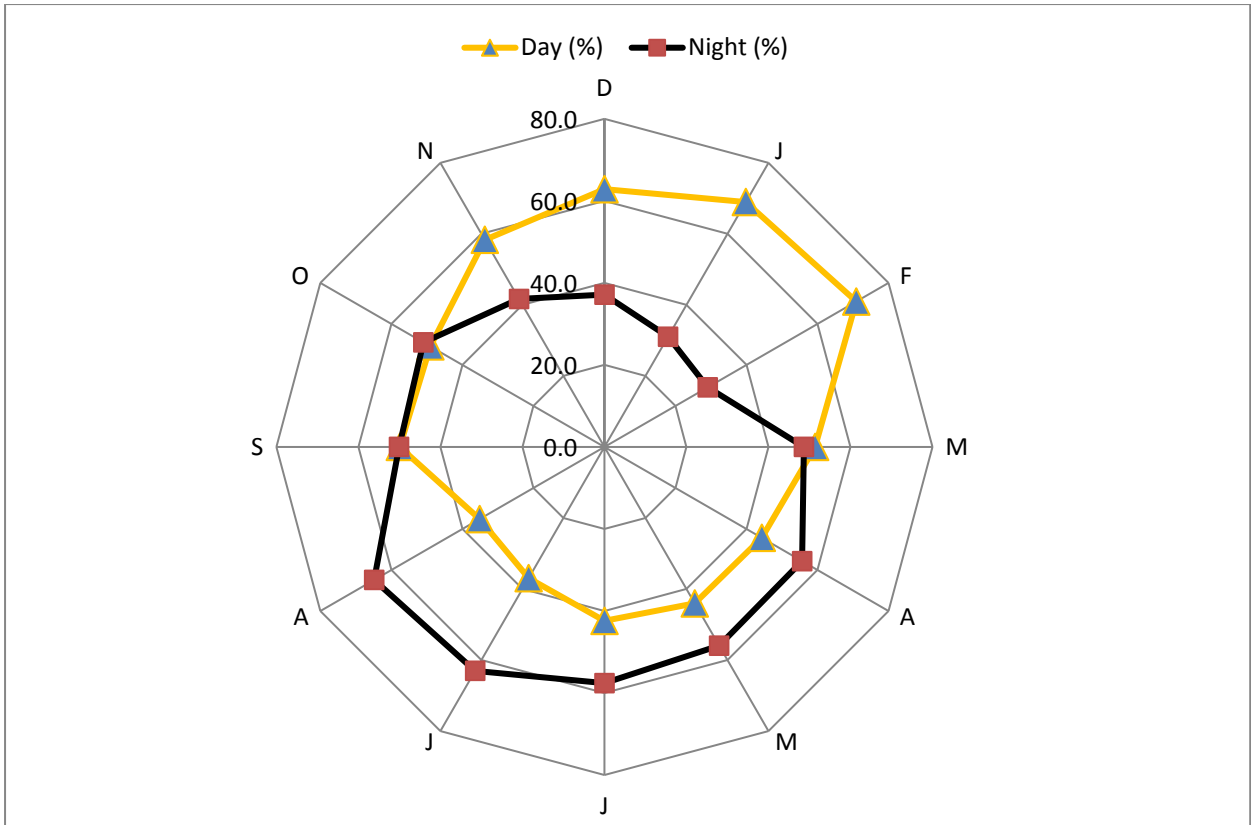
Figure 3-18. Day-night rainfall percentage as a proportion of total recorded rainfall depth for each month from January (J) through to December (D) (read clockwise).

Table 3-4 presents the mean and median rainfall intensities for all identified "wet" hours during day and night times identified in Table 3-3. Mean diurnal intensities were clearly higher than nocturnal intensities for the summer months of December, January and February, and also in May (late autumn). March, June, September and October had rather similar mean diurnal and nocturnal rainfall intensities. April, July and August saw higher nocturnal than diurnal rainfall intensities, with somewhat marginal figures for November. For median rainfall intensity values, statistically significant differences between diurnal and nocturnal rainfall intensities were only found for January and April using the non-parametric Kruskal-Wallis Test ($p < 0.05$).

Table 3-4. Mean and median hourly rainfall intensities (in mm h^{-1}) for Day or Night hours of each month (cf. Table 3-3). Superscripts *a* and *b* for median values indicate statistically significant different medians and distributions from non-parametric Kruskal-Wallis Test (p < 0.05).

	D	J	F	M	A	M	J	J	A	S	O	N
Mean Daytime	1.10	1.57	1.96	1.00	0.70	0.94	1.01	0.68	0.79	0.75	0.95	1.20
Mean Nighttime	0.96	1.12	1.35	0.96	0.89	0.82	1.02	0.74	0.92	0.69	0.91	1.27
Median Daytime	0.40	0.60[a]	0.60	0.60	0.30[a]	0.40	0.40	0.40	0.40	0.40	0.40	0.60
Median Nighttime	0.40	0.40[b]	0.60	0.40	0.40[b]	0.40	0.40	0.40	0.40	0.40	0.40	0.60

Table 3-5. Modal and minimum rainfall occurrence hours of the day. Mean rainfall hours and standard deviation (s.d.) of rainfall hours calculated are included for more complete description of the distributions.

	D	J	F	M	A	M	J	J	A	S	O	N
Total Rf hours	646	432	526	473	601	751	982	953	1152	1200	985	851
Modal Rf time of day (Total hrs)	1200 (34)	1600 (29)	1700 (32)	1900 (28)	1300 (33)	0000 (39)	0600; 1600 (48)	1700 (48)	2000 (71)	1300 (59)	2100 (58)	1000 (44)
Min Rf time of day (Total hrs)	0800 (17)	0400 (11)	1000 (15)	2300 (12)	0800 (16)	1100 (20)	0300 (33)	1200 (30)	2100 (35)	0400 (36)	0700 (30)	1400 (14)
Mean rainfall hours mth^{-1}	26.9	18.0	21.9	19.7	25.0	31.3	40.9	39.7	48.0	50.0	41.0	35.5
s.d. (rainfall hours)	4.0	4.3	4.5	4.0	4.1	4.0	4.0	5.0	7.6	5.3	7.8	4.9

Table 3-5 presents the modal, minimum, mean and standard deviation of rainfall hours for each month. Generally, 7 out of the 12 months (Dec -Feb; Apr; Jul, Sep and Nov) had high rainfall occurrence during daylight hours. November and December appeared to be dominated by rainfall occurring at late morning (1000 hrs) and mid-day (1200 hrs) respectively. However, mid-day rainfall (1300 hrs) also occurred frequently in April and September. In contrast, January and February were dominated by late afternoon rainfall (1600 hrs and 1700 hrs respectively). However, this was also seen in July (1700 hrs). Late evening to night-time rainfall frequencies were highest for May (1900 hrs), August (2000 hrs) and October (2100 hrs). Only May had the modal rainfall hour at midnight, and only June had modal rainfall hour in the early morning (0600 hrs). The highest modal value of 71 hours was found for August (2000 hrs); interestingly, the following hour at 2100 hrs had the lowest rainfall occurrence. June had two rainfall hour peaks, each at 48 hours – pre-dawn at 0600 hrs and late afternoon at 1600 hrs. September had the highest mean monthly rainfall hours at 50.0 hours, while January had the lowest mean rainfall hours at 18.0 hours, showing that mid-spring was generally the wettest while mid-summer was the driest (in terms of rainfall occurrence).

The standard deviation (s.d.) in rainfall hours was used to determine the variation for each month over the 14 years of records. The highest variability in the number of rainfall hours per month was in October (7.8), with August in a close second at 7.6. Lowest variability, showing most consistency in the number of rainfall hours in any year, was seen in December, March, May and June (all at 4.0); April also was similarly low at 4.1.

ii. Seasonal and monthly variations

In this section, I examine in detail the times of occurrence and contribution of rainfall according to seasons and months. Figure 3-19 summarizes the total rainfall hours and total rainfall depth for each month. While there was a general positive correspondence between total rainfall hours and total rainfall depth, some contrasts occurred, for example in February and November where there were low rainfall hours but high rainfall depth, indicating possible dominance of short-duration, high-intensity events; and contrastingly in July where high rainfall hours were accompanied by low total depth, indicating possible dominance long-duration, low-intensity events.
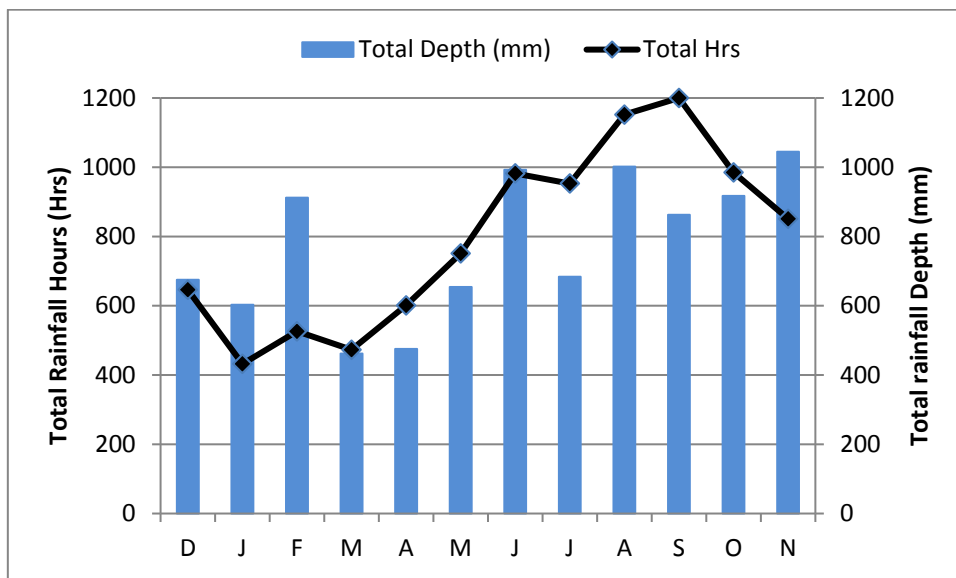
Figure 3-19. Total rainfall hours and depths for the Licola 14-year record.

iii. Between-month differences in hourly rainfall depth values

One-way ANOVA was conducted on the distribution of total rainfall depth values across individual hours of the day for all the 12 months. Significant between group differences were found (F = 10.462, p < 0.001). Post-hoc Tukey HSD found 4 groups of months that had similar mean rainfall depths at the 0.05 significance level, as shown in Table 3-6.

Table 3-6. Results of Tukey HSD post-hoc test on mean rainfall depth values in mm (N = 24 for individual hours of any day for each month). Notes: Months 1 = Jan and 12 = Dec. Groups 1 to 4 were homogeneous subsets and their arithmetic means (no. of hours) displayed.

Month	Group 1	Group 2	Group 3	Group 4
3	19.2500			
4	19.8167			
1	25.1292	25.1292		
5	27.2542	27.2542	27.2542	
12	28.1250	28.1250	28.1250	
7	28.5000	28.5000	28.5000	
9		35.9417	35.9417	35.9417
2			38.0167	38.0167
10			38.2292	38.2292
6				41.3667
8				41.7417
11				43.5417
Within-group significant differences	0.370	0.156	0.140	0.679

From the ANOVA test, at least two distinct groups of months could be discerned: (a) Lower mean rainfall range in December, January, March, April, May and July; (b) Higher mean rainfall range in February, June, August, September, October and November.

iv. Intra-day variability in rainfall depth – 3 main categories

Standard deviation of rainfall depth hours, providing a measure of intra-day variation in rainfall across the different hours of the day were also examined (see Figure 3-20). Three groups could be discerned: (i) High variability (> 15 mm) in January (17.5 mm) and February (28.7 mm); (ii) Medium variability (> 10, ≤ 15 mm) in December (13.6 mm), August (12.8 mm), September (11.0 mm) and October (11.9 mm); (iii) Low variability (< 10 mm), in March (7.1 mm), April (4.7 mm), May (8.3 mm), June (6.5 mm), July (5.9 mm) and November (8.8 mm).
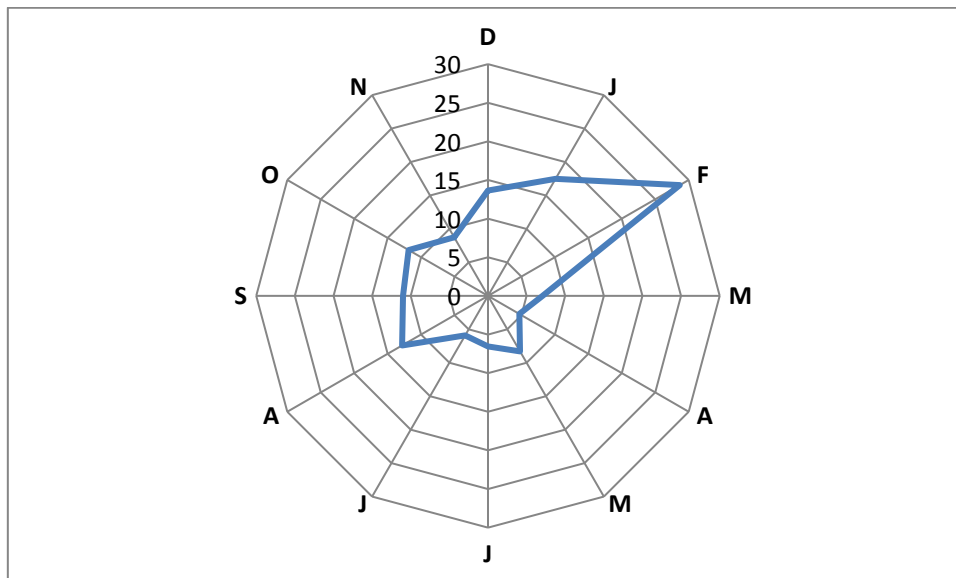
Figure 3-20. Standard deviation of rainfall hour-depth values for all months at Licola.

Detailed examination of rainfall hours and percentages to discern patterns of rainfall occurrences at different times of the day was also conducted. This information is available in Appendix B.

v. Heavy rainfall

For the dataset, a nominal rain rate threshold for "heavy rainfall" was adopted by selecting the top 52 hourly rainfall depths from the total 14-year rainfall record. This constituted 0.005% of the entire record. Hourly rainfall depths in this subset ranged from minimum of 9.2 mm to maximum of 60.8 mm, placing them in the upper-end of the "heavy" to "extreme" ranges of rain rates described by Tokay and Short (1996) (see Table 3-2). Intense rainfall events are particularly important in causing post-fire soil transformations (Francos et al., 2016).

a. Monthly distribution

Occurrence of heavy rainfall events was quite unevenly distributed through the year, with primary dominance in late-spring and summer; and secondarily in late autumn-early winter (see Figure 3-21). Summer (DJF) had 57.7% (30 hours) of all large depths, dominating the record. Preceding this, November (late spring) also made a significant contribution of 5 hours (9.6%). These appeared to coincide closely with the daytime rainfall occurrences during these months described above. There was a secondary cluster of high hourly rainfall occurring during early winter in June (15.4%, 8 hours), and preceding it in May (late spring) (4 hours, 7.7%) which coincided with the dominantly nocturnal rainfall occurrence in May and pre-dawn occurrence in June. Only August and October each recorded 2 hours (3.8%) of high hourly rainfall; No top 52 hourly rainfall rates occurred in March-April (early-mid autumn), July (mid-winter) and September (early spring).
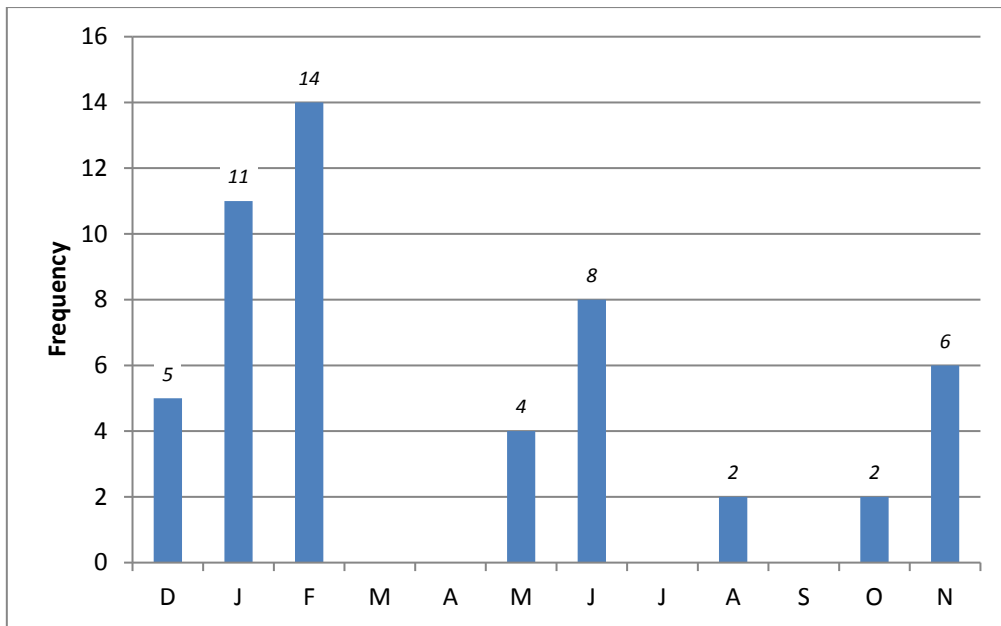
Figure 3-21. Temporal distribution (by month) of "heavy" rainfall events ≥ 9.2 mm^{-1} using one-hour time-resolution.

The occurrence of heavy rainfall events is therefore highly temporally selective, concentrating in the period November to February, and then a minor cluster during May to June.

Figure 3-22 shows the occurrence frequency of heavy rainfall according to time-of-day. Peak occurrences of heavy rainfall were in the mid-afternoon (1500 hrs) and early evening (1900 hrs). Furthermore, the afternoon hours (1400 hrs to 1800 hrs) dominated heavy rainfall occurrence, with 4 or more events during these times. In contrast, there was a distinct lack of heavy rainfall events; 2 or less events, from night-time (2200 hrs) to mid-morning (1000 hrs).
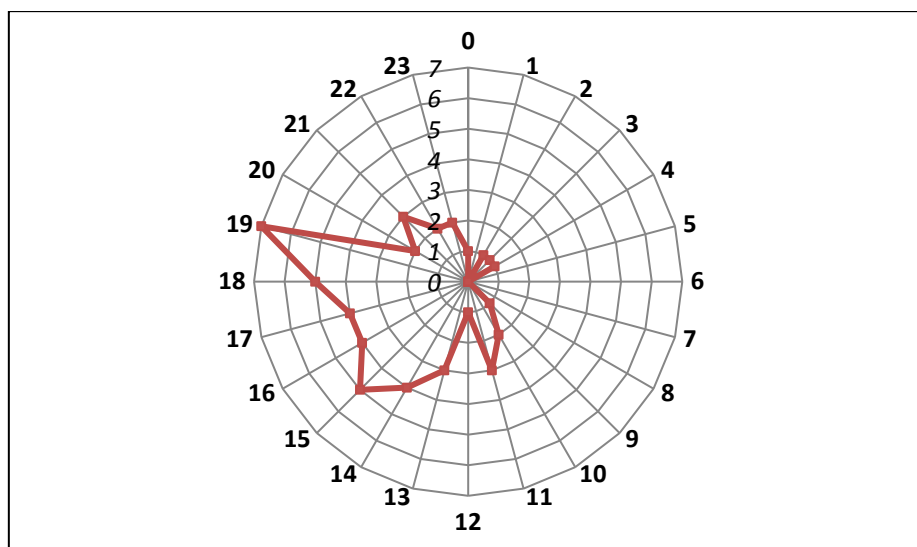
Figure 3-22. Occurrence of top 52 heavy rainfall events according to time-of-day. The perimeter indicates times with 0 indicating 0000 hrs (midnight) and 23 indicating 2300 hrs (11 p.m.).

3.5.3.3.4. Discussion

Daytime dominant rainfall occurrence was found in November through to February (Figure 3-18); this is corroborated by modal rainfall occurrences during daylight hours for these months, as seen in Table 3-5, although specific times of the day at which these peaks occurred, varied from late morning to late afternoon. As seen in Table 3-4, mean wet-hour intensities were clearly higher for the diurnal than nocturnal rainfall hours with median intensities for February showing statistical significance for the abovementioned patterns. The concentration of heavy rainfall events in these months, as shown in Figure 3-24, was also evident. Therefore, there must have been a set of regularly occurring meteorological conditions over the region of the study area that accounts for these rainfall event characteristics. It was likely that warm "summery" conditions exerted some controls over the weather during these months, with strong regional (associated with the Australian continental interior) and local convection, along with topographical forcing (Kendon et al., 2012) being particularly dominant during these months. Specifically, strong updrafts in the late afternoon hours were very likely to occur due to high thermal gain from intense solar insolation, resulting in local and regional convection flows being activated. In addition to uplift of air from local surfaces, there would also have been active advection of moister air from adjacent near-coastal and coastal areas in the region south, west and east of Licola. Enhanced by regional orographic effects of the Great Dividing Range (see Section 3.3), this would cause higher-intensity rainfall to be generated from cumuliform clouds. While November is conventionally treated as the "late-spring" period in the southern hemisphere, the rainfall characteristics appear to be more like summer, rather than spring conditions. Hence, it could be deduced that summer-type local-regional scale convection driven rainfall events have a strong influence on the rainfall patterns during November for the study region.

It could be argued that one of the confounding factors to these findings, is that the variable times of day and night determine the classification and resultant amount of rainfall hours and depth (cf. Table 3-3). However, it should be noted that the diurnal-nocturnal rainfall peaks did not correspond to the months in which the summer and winter solstices occurred (Figure 3-18). Although the summer solstice for this location fell on 22nd December, peak diurnal rainfall occurred in the month of February; while the winter solstice falls on 21st June, peak nocturnal rainfall occurred in the month of August.

The highest variability in rainfall hour-depths was found during the summer months of December to February. These were likely to be related to the spatially-limited extent of many convective storm cells (Kendon et al., 2012) that occurred over this area resulting in a "hit-or-miss" occurrence of rainfall being recorded for the locality of Licola itself (while other adjacent areas may have been "missed-or hit". However, where the convective rainfall events prevalent in summer "hit" over Licola, large rainfall depths and intensities were recorded during the mid to late diurnal hours, as shown in Figures 3-18 and 3-21. Secondary peaks in the evening to night hours could represent lags in time from which moisture advection from distant coastal areas to the southwest and southeast occur (nominally 150 km and 100 km respectively) while the land surface continues to remain warm, encouraging ongoing convection into the evening, and for rainfall-generating mechanisms in clouds to operate fully and finally result in rainfall occurring.

During the "warmer" months, the STR would exert a strong influence on regional pressure patterns, pushing rain-bearing frontal systems further south from their median position and thus reducing frontally-induced stratiform cloud rainfall. Furthermore, low-humidity air emanating from the arid Australian continental interior would have reduced the chance of cloud formation. However, natural variations in the shape and extent of the STR would have still enabled some fronts to break through and provide rainfall over locations in

and around the present study area. Also, strong summer regional and continental-scale heating, generating broad-scale convection and moisture advection from the maritime areas to the west and south would have caused higher-intensity but temporally and spatially-limited cumuliform cloud rainfall.

Nocturnal rainfall was dominant from April through to August, and could be explained by the STR retreating north and allowing a higher frequency of the passage of fronts over the study area. With lower solar insolation, cool land surfaces, lower temperatures and higher relative humidity, soils and plant canopies remaining moist for longer time periods compared to summer conditions, convection processes were thus muted and therefore contributed little to diurnal occurrence of rainfall. Concomitantly, East Coast Lows (ECLs) were likely to have been more frequent in late autumn to winter because of large gradients in sea surface temperatures, and were also more likely to develop in the evening because of the highest likelihood of instability in the maritime boundary layer (Bryant, 1997), therefore helping to account for the greater dominance of nocturnal rainfall hours and depths during this season of the year.

In the following section, to illustrate the seasonal variation that is an important part of rainfall regime affecting the study area, we examine the contrasting synoptic and meteorological conditions between summer-autumn and winter-spring dominant systems during the immediate post-fire period in 2007. These will support some initial discussions on how different rainfall events may drive hillslope erosion in the study area at different times of the year. The following sections also help to illustrate the rapidity and scale of post-fire hillslope and catchment responses to rainfall inputs to explain the severe and extensive erosion and flooding that occurred in the study region during first post-fire year.

3.5.4.1. Summer 2007 post-fire storms

In late February 2007, the study region had been rendered highly vulnerable to water erosion in this immediate post-fire period due to the very large areas of steep hillslopes that were bare and exposed after the extensive and severe vegetation damage by the 2006/7 Great Divide Fires (see section 3.4). The rainfall events and ensuing hillslope erosion and floods that occurred on 23-24 Feb 2007 caused major damage to Licola town (Houghton, 2007). As reported by the Australian Associated Press (2007), a near-stationary trough over the region in southeast Australia brought substantial, sustained rainfall to the broader region with localized intensive convective cells causing spatially variable rainfall in the study area. Figure 3-23 shows the location of precipitation gauges relevant to the study area: Mt Useful (Lat: 37.7000 S, Long: 146.5167 E; Elevation: 1440 m), Glencairn (Lat: 37.5277 S, Long: 146.5458 E; Elevation: 380 m) and Mt. Tamboritha (Lat: 37.4667 S, Long: 146.6883 E; Elevation: 1446 m). Table 3-7 shows the corresponding daily rainfall depth for the three stations from 21 to 24 Feb 2007. Because of the localized, spatially heterogeneous nature of these summer storms, the sparse distribution of gauges may have failed to capture the true rainfall intensities and depths received at many other ungauged locations, with the radar images provide only nominal, approximate indications of the rainfall parameters.

Figure 3-23. Locations of precipitation gauges at study region. Red star indicates study site location. Source: State Government of Victoria (2016).

Table 3-7. Daily rainfall (mm) for Glencairn, Mt. Tamboritha and Mt. Useful precipitation gauges 21 to 24 Feb 2007. Source: Bureau of Meteorology (2017c).

Date	Glencairn (380 m)	Mt. Tamboritha (1446 m)	Mt. Useful (1440 m)
21/02/2007	0.0	0.0	0.0
22/02/2007	4.2	30.4	14.4
23/02/2007	1.0	0.2	12.8
24/02/2007	5.8	3.4	16.2

*Note: No data available for Licola station between 2003 and 2009 either from DELWP (2016) or Bureau of Meteorology (2017c).

The development of the relevant weather system is shown in the synoptic charts in Figures 3-24 a-d. On 21 Feb 2007, 1800 hrs (Figure 3-24a), a trough extended from the continental interior of Australia, and across and beyond southeast Australia into the Tasman Sea; this was likely to have been caused by the intense regional terrestrial heating in summer. This trough was wedged between two high pressure cells; one just west of the study area over the Southern Ocean and the other due east over the Tasman Sea. As a result, the near-

stationary trough generated convective air flows over the region that drew-in southerly and easterly moist maritime air (from the aforementioned high-pressure cells) that were then further modified with orographic uplift caused by the high relief of the Great Dividing Range. By 22 Feb 2007, 1800 hrs (Figure 3-24b), this had caused some rainfall over the study region in southeast Australia including the study area, with the eastward movement of the trough restricted by the twin high pressure cells dominating over the Tasman Sea. This led to rainfall depths of 4.2 mm 30.4 mm and 14.4 mm recorded at Glencairn, Mt. Useful and Mt. Tamboritha respectively (Table 3-7).

By 23 Feb 2017, 1800 hrs (Figure 3-24c), the high pressure cell positioned over the Southern Ocean had moved further east over New Zealand and therefore enabled the trough to shift slightly eastwards. Nevertheless, rainfall in the region continued. Very modest depths of 1 mm and 0.2 mm were recorded at Glencairn and Mt. Useful respectively. However, 12.8 mm rainfall was recorded at Mt. Tamboritha (see Table 3-7). By 24 Feb 2017, 1800 hrs (Figure 3-24d), the trough had dissipated over the Tasman Sea but the convective clouds that had developed over the Range contributed rainfall depths of 5.8 mm, 3.4 mm and 16.2 mm for Glencairn, Mt. Useful and Mt. Tamboritha respectively (see Table 3-7).
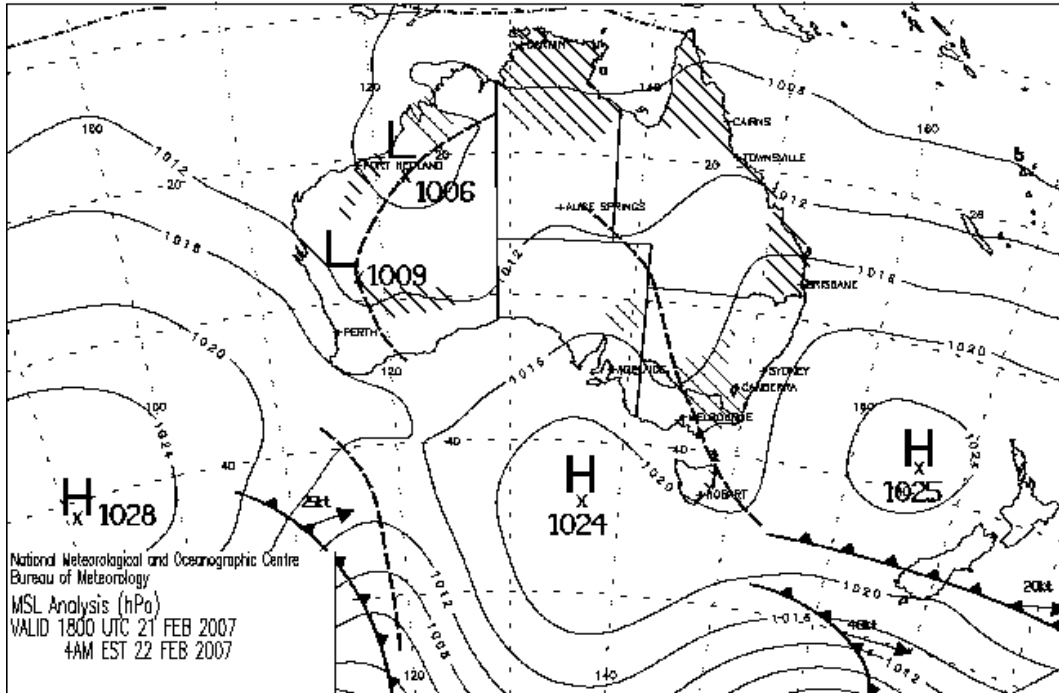
a.   Mean Sea Level Pressure (MSLP) Analyses for 21 Feb 2007, 1800 hrs
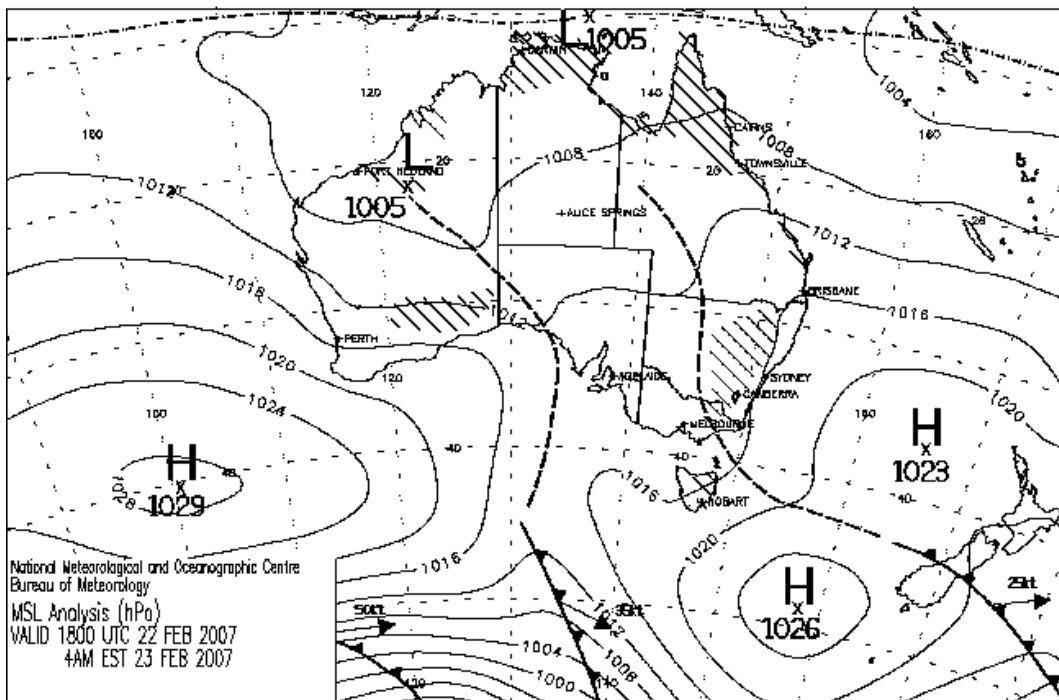
b.   Mean Sea Level Pressure (MSLP) Analysis for 22 Feb 2007, 1800 hrs
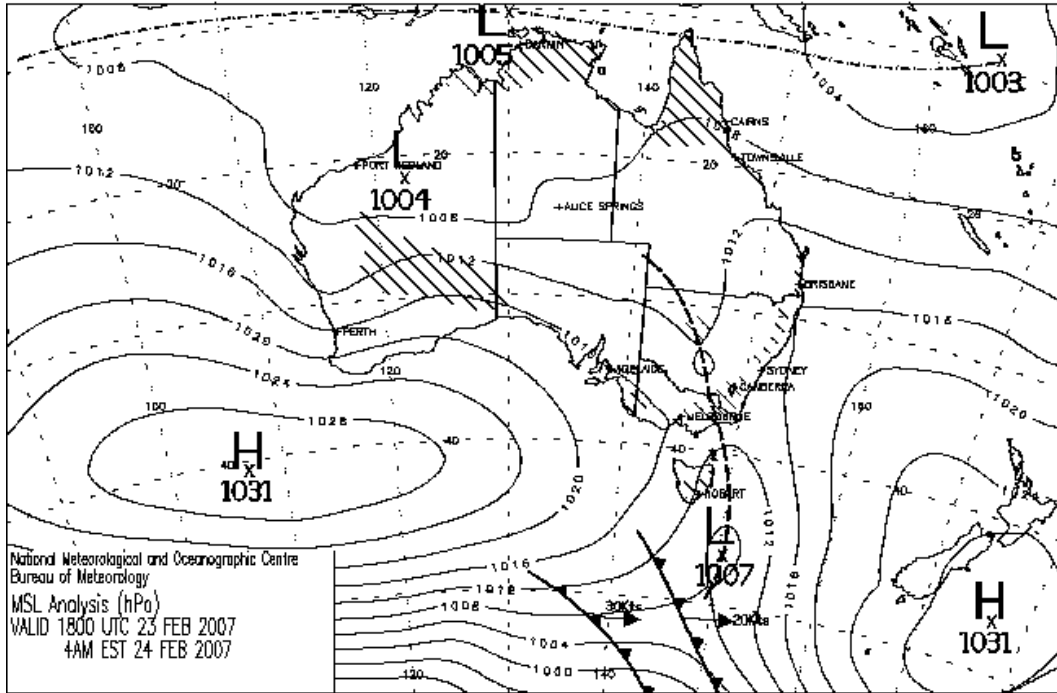
c. Mean Sea Level Pressure (MSLP) Analysis for 23 Feb 2007, 1800 hrs
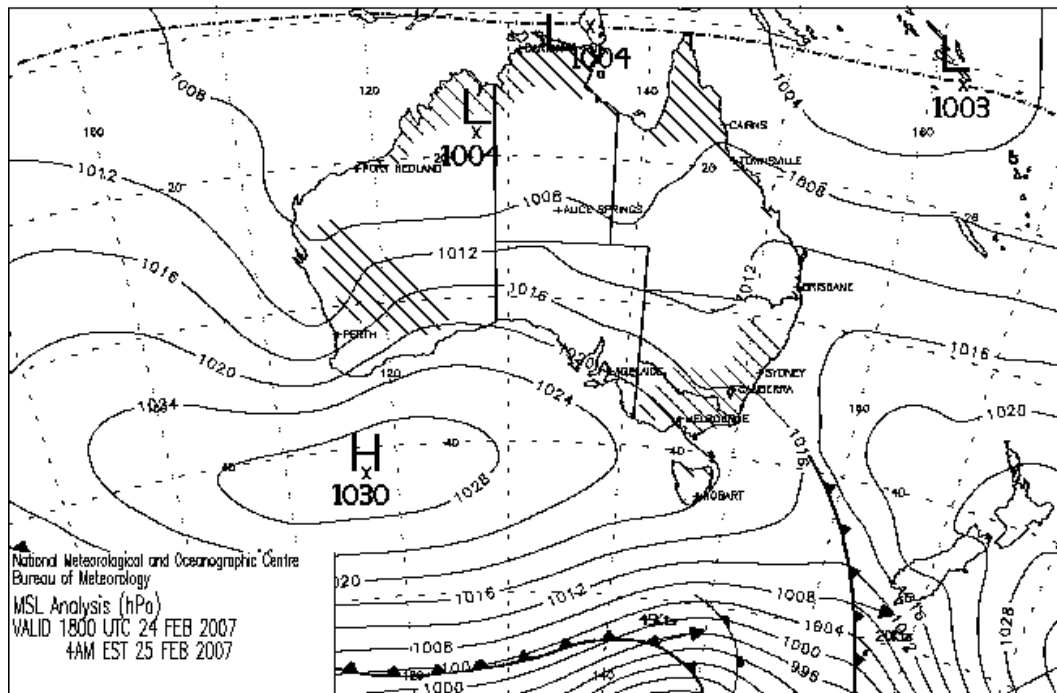
d. Mean Sea Level Pressure (MSLP) Analysis for 24 Feb 2007, 1800 hrs

Figure 3-24. Mean Sea Level Pressure (MSLP) Analyses charts at 1800 hrs for 21 to 24 Feb 2007. Source: (Bureau of Meteorology, 2017a).

The storm cells generated from summer convective processes are also well-illustrated with a snapshot view of the rainfall radar on 22 Feb 2007, 5.40 p.m. (Figure 3-25), where thunderstorm cells with localized high-intensity rainfall and lower-intensity fringes occurring over parts of the Great Dividing Range in Victoria, can be observed.
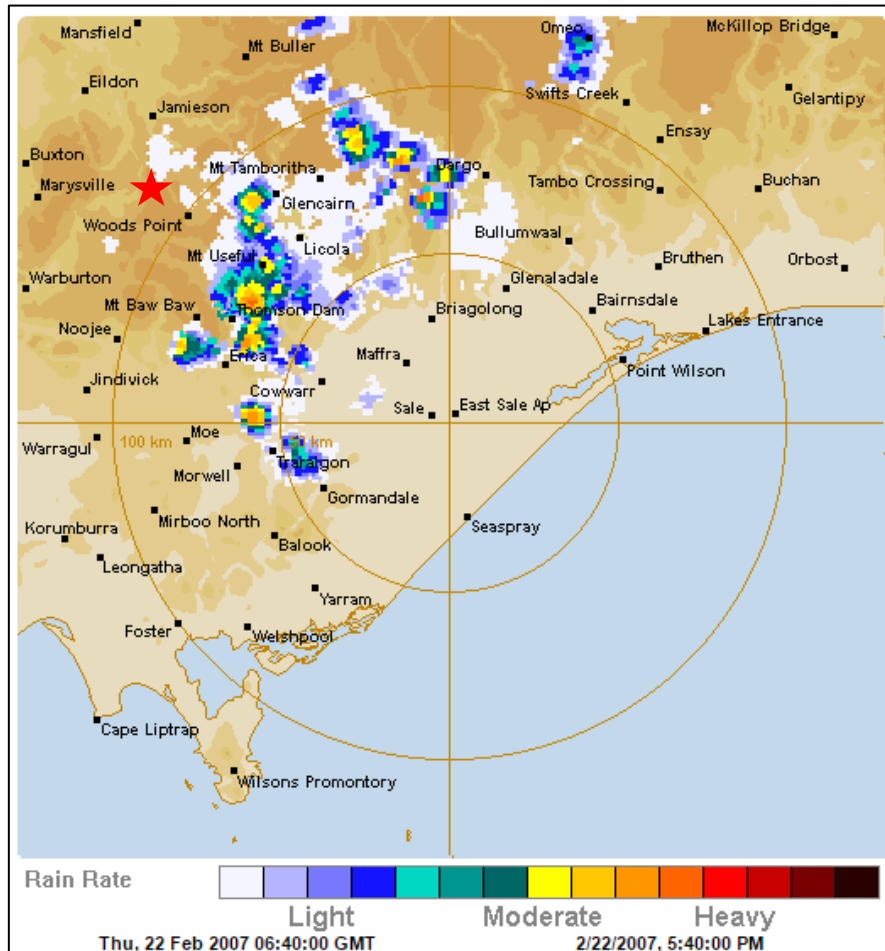
Level	Colour		Approx. Rainfall Intensity (mm/hr)
0	clear	Not visible	Under 0.2
1		Off-white	0.5
2		Sky-blue	1.5
3		Light Blue	2.5
4		Blue	4
5		Light Cyan	6
6		Cyan	10
7		Dark Cyan	15
8		Yellow	20
9		Yellow-orange	35
10		Orange	50
11		Orange-red	80
12		Red	120
13		Dark Red	200
14		Maroon	300
15		Dark Brown	over 360

Figure 3-25. Rainfall intensity distribution over Victoria on 22/2/2007, 5.40 p.m. as shown from the Bureau of Meteorology Radar (128 km radius) at Sale (IDR573). Each pixel represents an area 0.25 km^2. Star indicates study site location. Radar image source: The Weather Chaser (2017). Legend source: Bureau of Meteorology (2017d). Image copyright of Bureau of Meteorology, Australia.

As discussed earlier in section 3.5.3, the development of extensive troughs and interactions with the mid-latitude high and low-pressure cells can lead to the greater occurrence of convective rainfall from cumuliform clouds giving localized, high-intensity thunderstorm cells during summer that generate sudden bursts of erosive energy on selected hillslopes within the catchment. This could be further exacerbated with wet antecedent conditions caused by previous rainfall events. The rain gauge network in the region was probably too sparse to record the rainfall supplied by many of the quite localized convective cells. This can be seen through the considerable variability in catchment-scale rainfall recorded by the three gauges (Table 3-7). The main convection-related rainfall generating systems during summer would therefore lead to different hydrological and geomorphological outcomes compared to the rainfall from frontal-related systems during winter. As seen in Figures 3-24 a-d, the positions of the mid-latitude high pressure cells and fronts are further south than what is experienced during winter.

The steepness and large catchment area of the upper Macalister, where the study site was located, frequently causes 'rapid, fast-flowing and turbulent floods' (Wellington Shire Council, 2016). As a result of the rainfall events described above, major flash flooding (river gauge height more than 3.6 m) (Bureau of Meteorology, 2017e) occurred on 23-24 Feb 2007 (Australian Associated Press, 2007; Goulburn Broken CMA, 2009) during which the river gauge at Licola was damaged. Indeed, the rainfall event depths experienced (Table 3-7) were quite modest. However, it was likely that the burnt-out, exposed and vulnerable hillslopes had high hydrologic connectivity, low infiltration rates and high rainfall-runoff ratios and steep topography all conspired to cause rapid erosion and swift increases in stream discharge. This scenario was repeated in November 2007 during which more late spring/early summer storms occurred, with the consequent flooding causing extensive damage, including the loss of infrastructural repair works that had already commenced.

Flash floods are a frequent and major post-fire hazard due to highly localized (and difficult to detect in sparsely distributed gauge network) thunderstorms that supply 'pulse wet microbursts' that recur with stationary/semi-stationary cell regeneration, and cause enhanced runoff generation due to fire-induced soil hydrophobicity, and heightened soil erodibility and availability (Gallucci et al., 2011). Rain-wave trains (Horton, 1945) are likely to be instrumental to the spikes in the volumes of material eroded from hillslopes. Peak flood levels at Licola gauging station on 4, 5 and 6 November were: 3.28 m, 3.24 m (ARI: 12 years approx.) and 2.83 m (ARI: 6 years approx.) (2.7 m being the minimum flood level) (State Emergency Services Victoria, 2013; State Government of Victoria, 2016). These events certainly underscore the importance of being able to understand and predict post-fire hydrological and geomorphological processes that operate in response to complex rainfall inputs in the region.

3.5.4.2. Winter 2007 post-fire storms

This section describes the winter rainfall resulting from meteorological conditions that are more active during this season – ECLs and frontal systems. With the ground surface of the region remaining highly vulnerable to erosion, winter storms during 26 to 28 Jun 2007 caused major floods and damage in the Macalister catchment. Notably, the gauging station at Licola was washed away (Wellington Shire Council, 2016) and Cheynes Bridge further downstream on the Macalister River was destroyed (State Emergency Services Victoria, 2013). There were also reports of losses of livestock and damage to other property and infrastructure (Miletic, 2007). The Department of Sustainability and Environment and Parks Victoria (2010) observed that areas that had been burnt extensively, had particularly exposed and vulnerable soils and suffered noticeably greater flood damage than other areas less or unaffected by the 2006/7 fires. These events and observations served to emphasize the importance of vegetative cover in mitigating hillslope erosion and runoff rates, and being able to understand post-fire hydrological and geomorphological processes driven by the rainfall events generated by meteorological mechanisms described in this section.

Figure 3-26 a-d illustrate the meteorological conditions leading to an East Coast Low (ECL) (see section 3.5.2) and subsequent passage of a cold front over the south and southeast of Australia during winter from 28 Jun to 1 Jul 2007 that contributed large total rainfall depths and widespread flooding in the Glenmaggie catchments (see also Table 3-8) (Bureau of Meteorology, 2007b). State Emergency Services Victoria (2013) would later report 24-hour rainfall totals at Murderers Hill, Mt. Wellington, Callignee North and Koornalla to be greater than 1 in 100-year ARI; 24-hour rainfall depths for Mt. Tassie and Reeves Knob were estimated at between 50 and 100 years ARI.

Table 3-8. Daily rainfall (mm) for Glencairn and Mt. Useful precipitation gauges 27 Jun to 1 Jul 2007. Source: Bureau of Meteorology (2017c).

Date	Glencairn (380 m)	Mt. Useful (1440 m)
27/06/2007	24.6	6.6
28/06/2007	92.6	136.0
29/06/2007	4.6	5.0
30/06/2007	1.6	0
01/07/2007	2.2	1.2

*Notes: No data for Mt. Tamboritha 28 Jun to 12 Jul 2007, likely due to storm damage to equipment.
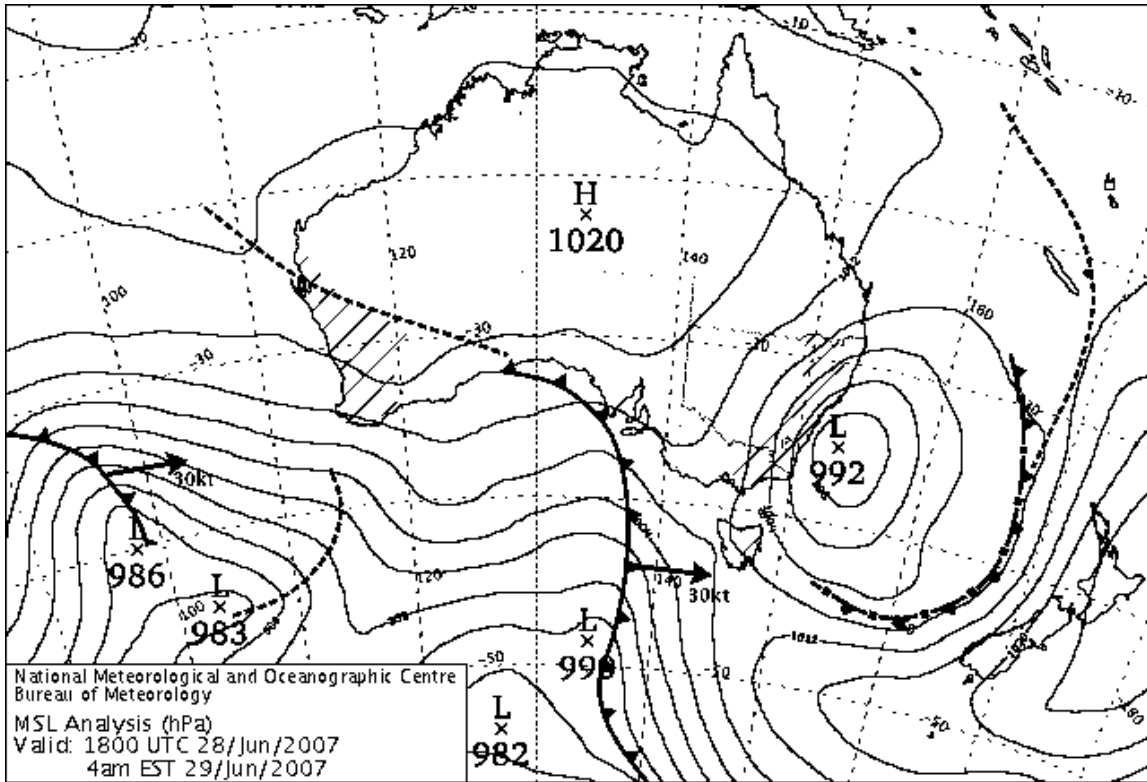
a. Mean Sea Level Pressure (MSLP) Analysis for 28 Jun 2007, 1800 hrs.
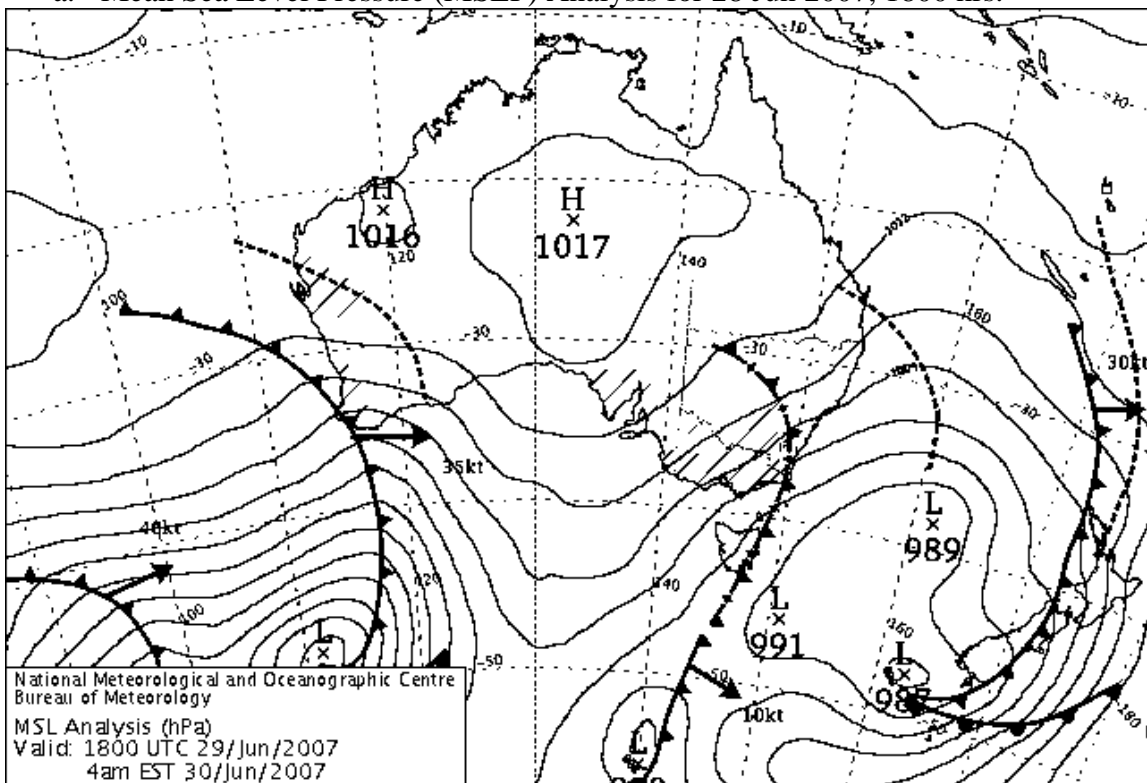
b. Mean Sea Level Pressure (MSLP) Analysis for 29 Jun 2007, 1800 hrs.
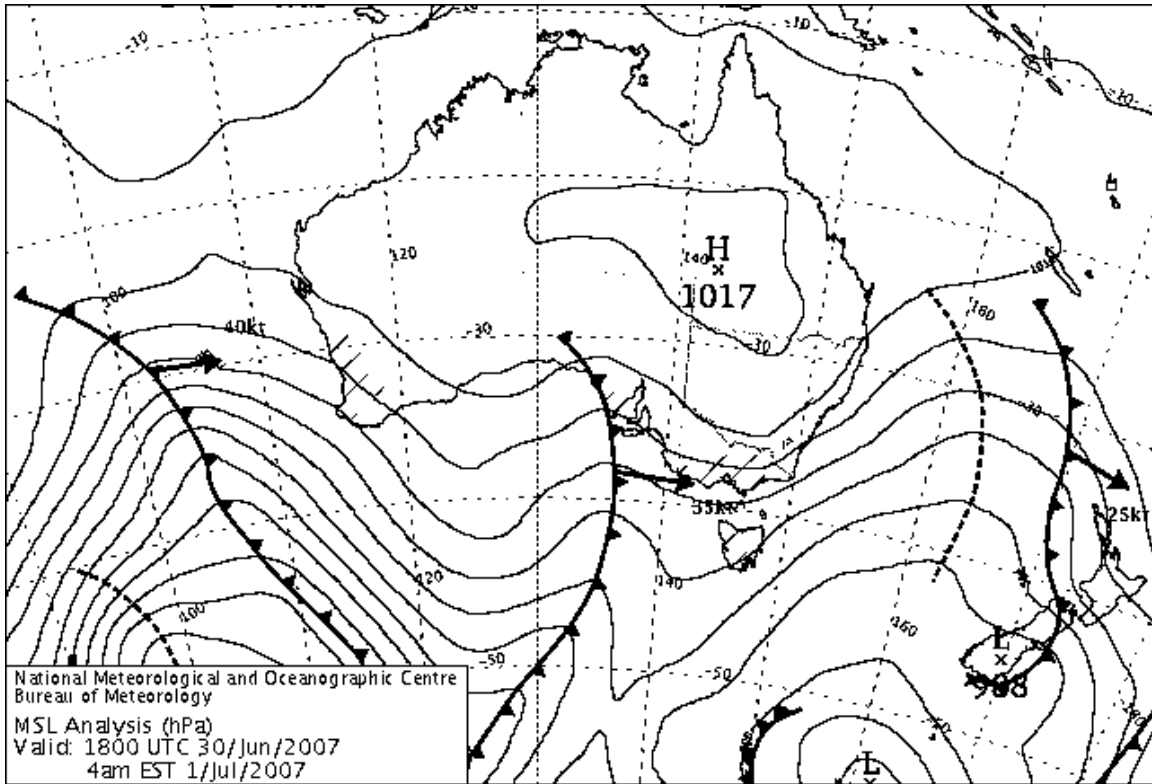
c. Mean Sea Level Pressure (MSLP) Analysis for 30 Jun 2007, 1800 hrs.
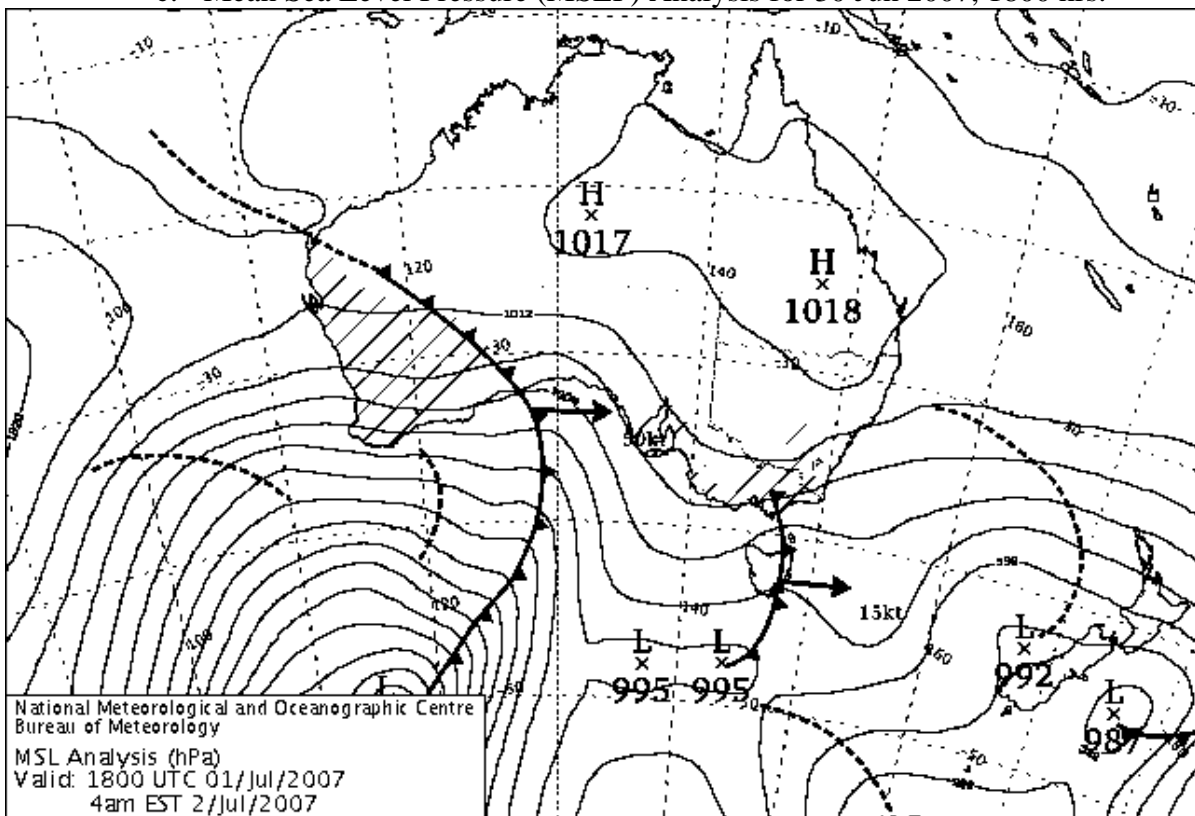
d. Mean Sea Level Pressure (MSLP) Analysis for 1 Jul 2007, 1800 hrs.

Figure 3-26. Mean Sea Level Pressure (MSLP) Analyses charts at 1800 hrs for (a) 28 Jun to (d) 2 Jul 2007. Source: (Bureau of Meteorology, 2017a).

As shown in Figure 3-26a, the ECL (seen as a deep low-pressure over southeastern Australia) on 26 to 28 June brought heavy rainfall of extended durations and widespread flooding to many parts of east and southeast Australia, including the study area (Bureau of Meteorology, 2007d; State Emergency Services Victoria, 2013); no high-resolution rainfall data was available from any sources to discern specific intensities. Very high daily rainfall depths of 24.6 mm and 92.6 mm on 27 and 28 Jun 2007 respectively at Glencairn, and at Mt. Useful, 6.6 mm and 136 mm on 27 and 28 Jun 2007 respectively, were recorded (Table 3-8). The extent of the meteorological impact of the ECL is illustrated through the rainfall radar snapshot for 27 Jun 2007, 2200 hrs in Figure 3-30.

By 29 June 1800 hrs (Figure 3-26b), as the ECL shifted further east across the Tasman Sea, a cold front moved in from the west towards southeast Australia. By 30 June 1800 hrs (Figure 3-26c) the cold front had arrived at Victoria and moved quickly past southeast Australia, bringing light, widespread rains across the region. However, the catchment would have been saturated from the preceding rains and much runoff would have been generated on the hillslopes and erosion would have occurred. At this point of time, a second cold front had reached the southwest corner of the Australian continent. By 1 Jul 2007 (Figure 3-26d), this second front was already over the Gippsland region and even more rainfall was received. At this time, yet another strong cold front was approaching South Australia and Victoria from Western Australia, moving quickly westwards across the Great Australian Bight.
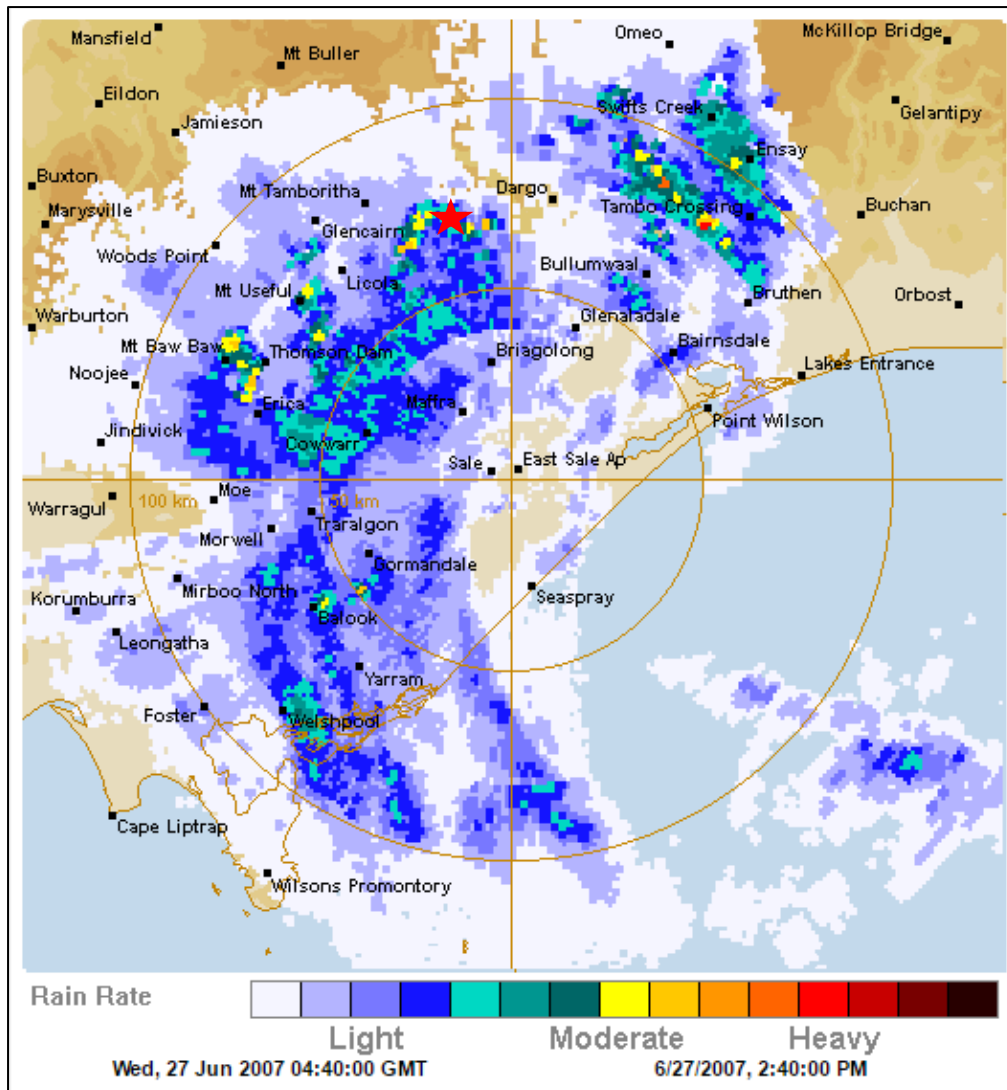
Figure 3-27. Rainfall intensity distribution over Victoria on 27/6/2007, 1440 hrs as detected by the Bureau of Meteorology Radar (128 km radius) at Sale (IDR573). Each pixel represents an area 0.25 km^2. Red star indicates study site location. Source: The Weather Chaser (2017). Image owner: Bureau of Meteorology, Australia.

Figure 3-28 presents the rainfall radar image snapshot for our region of interest at 29 Jun 2007, 1800 hrs which provides good insights into the cloud formations and precipitation associated with the mid-latitude frontal systems that are more active during winter than summer. Note the long, broad cloud band associated with the cold front, moving from west to east, bringing light rain over broad areas in the region. These are quite distinct from the localized convection-generated storm cells bringing high-intensity rainfall, as shown in Figure 3-25.
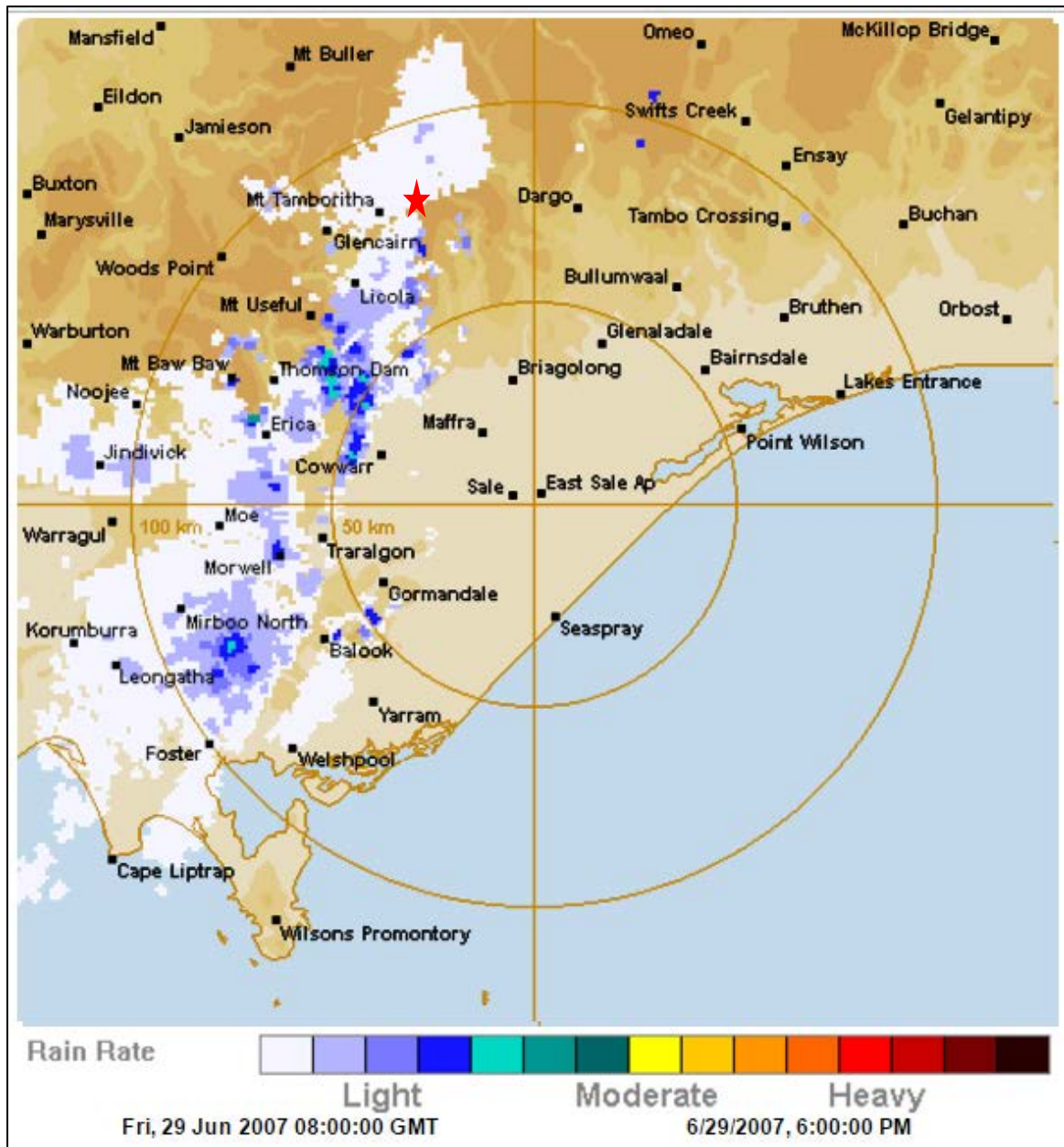
Figure 3-28. Rainfall intensity distribution over Victoria on 29/6/2007, 6.00 p.m. as detected by the Bureau of Meteorology Radar at Sale (IDR573). Red star indicates study site location. Source: The Weather Chaser (2017). Image copyright of Bureau of Meteorology, Australia.

The description of ECL and frontal systems in this section helps to explain why slightly more rainfall is usually received at the study site during winter, as well as specifically accounting for the massive post-fire floods and sedimentation experienced in the Licola region in late June/early July (Environment and Natural Resources Committee, 2008; Miletic, 2007; Wellington Shire Council, 2016). During this near-immediate post-fire period, the

weekly rainfall totals for the region far exceeded the long-term averages (see Figure 3-29 and

Table 3-9).
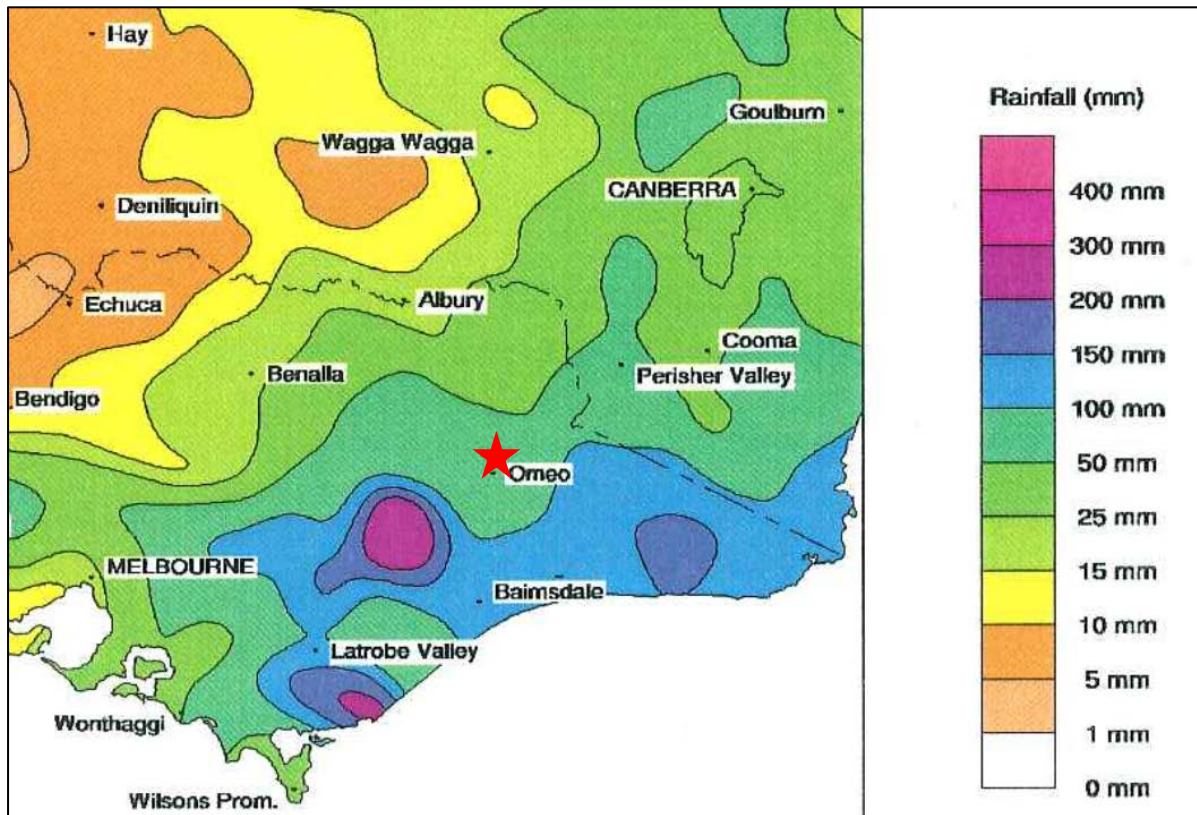
Figure 3-29. Rainfall distribution for the week ending 3 July 2007. Source: Victorian Government (2007) using data from the Bureau of Meteorology, Australia. Red star indicates approximate study site location.

Table 3-9. 4-day rainfall totals, 12 hr and 24 hr maximum rainfall for selected locations. Source: Victorian Government (2007) using data from the Bureau of Meteorology, Australia.

Location*	4-day total (mm)	12 hr max rainfall		24 hr hr max rainfall	
		Amount (mm)	ARI** (Years)	Amount (mm)	ARI** (Years)
Briagolong	150.6	86.0	10-20	131.0	20-50
Callignee North	*-na-*	124.0	> 100	180.0	> 100
Mt. Useful	147.6	92.0	2-5	135.0	5-10
Mitchell River at Rosehill	*-na-*	68.0	2-5	113.0	10-20
Mt. Tassie	212.6	124.0	20-50	198.0	50-100
Mt. Moornapa	210.2	131.0	50-100	157.0	20-50
Mt. Wellington	377.0	205.0	> 100	318.0	> 100
Murderers Hill	226.0	141.0	50-100	215.0	> 100
Reeves Knob	321.2	141.0	20-50	228.0	50-100
The Channel	123.8	72.0	2-5	118.0	10-20
u/s Cowwarr Weir	*-na-*	44.0	1-2	68.0	2-5

*Refer to Fig. 3-31 for map of locations. **ARI: Annual Recurrence Interval.

The river heights of the Macalister at Licola could not be presented accurately here due to the loss of equipment from the flood, but an unprecedented 5.15 m gauge height, and flood ARI of 1 in 200 years were estimated, which made it the largest flood on record for the Macalister River (Goulburn Broken CMA, 2009; State Emergency Services Victoria, 2013). There was thus a large data gap between 22 Jun and 11 Jul 2007 (State Government of Victoria, 2016), but Forest Fire Victoria Inc. (2007), Environment and Natural Resources Committee (2008) and Gippsland Emergency Recovery Committee (2007) provided detailed qualitative insights into the dramatic processes and impacts of post-fire rainfall, flooding and

erosion in the burnt hillslopes in the Glenmaggie catchment, as well as the downstream damage to infrastructure such as the Glenmaggie Reservoir weir and regional water supplies, and environmental impacts including sedimentation of the Thomson River and Gippsland Lakes. A similar set of rainfall and flood events also occurred in early June 2012 (State Emergency Services Victoria, 2013), within the measurement period of the present study.

The rapid passage of fronts over our region of interest, at higher frequencies compared to summertime conditions, tends to bring successive "waves" of rainfall events of light to moderate intensity over a broad area, moving from west to east, where "rain shadow" impacts (Rowe and Downes, 1960) on the Wellington River catchment might occur. When the ECLs, which also tend to develop more frequently in winter, extend into the study region, large and long-duration rainfall is likely to occur, and the prolonged heavy rain strongly drive throughfall, overland flow and hillslope erosion processes. Furthermore, the higher humidity and lower temperatures during winter are likely to contribute to lower intra-event evaporative losses (Dunkerley, 2008c) and higher percentage mass of water reaching the ground surfaces to drive overland flow and erosion processes. Instantaneous plant water uptake and transpiration rates are also likely to be much lower during winter compared to summer (Dawson and Pate, 1996) and these would contribute to quicker saturation of upper soil horizons and rapid generation of overland flow.

With a clear understanding of the rainfall regime driving hydrology and erosion in the study region, we now turn to examining the "targets" of rainfall - the vegetation strata that modulate rainfall, and the soil that ultimately gets eroded, transported and deposited, as they occurred in the pre and post-fire time periods.

3.6. Vegetation

The key features of southeast Australian dry sclerophyll forests in general, and main structural and physiological features relevant to the present study area were described in section 2.4. In this section, detailed features of the pre and post-fire vegetation discerned from field observations and information from existing databases are presented.

3.6.1. Pre-fire vegetation

The original vegetation in the study area was classified by Rowe and Downes (1960) as *Short Dry Sclerophyll Forest* composed of the *E. melliodora - E. macrorhyncha - E. polyanthemos* alliance approaching woodland-type distribution and structures in these rain-shadow parts of the catchment (see Plate 3-2).

Plate 3-2. Dry sclerophyll forest vegetation typical of the study area in long unburnt condition. *Eucalyptus spp.* comprise the canopy layer with tussock grass *(Poa spp.)* ground cover and substantial litter layer. Note the discontinuous and open canopy. Image source: Gupta et al. (2015).

Associated with this formation was patchy ground cover comprising kangaroo grass *(Themeda australis)* and tussock grass *(Poa spp.)*. Situated within the Highlands – Southern Fall bioregion, the Ecological Vegetation Class (EVC) groups (Parkes et al., 2003; Woodgate et al., 1996) of this area were *Grassy Dry Forest* on the exposed west and north-facing lower slopes (the study site location). Neighbouring slopes with more sheltered south and east-facing aspects, and riparian areas were covered by *Valley Grassy Forest*. *Shrubby Dry Forest* was found on the middle and upper slopes (DEPI, 2013); see Figure 3-30.
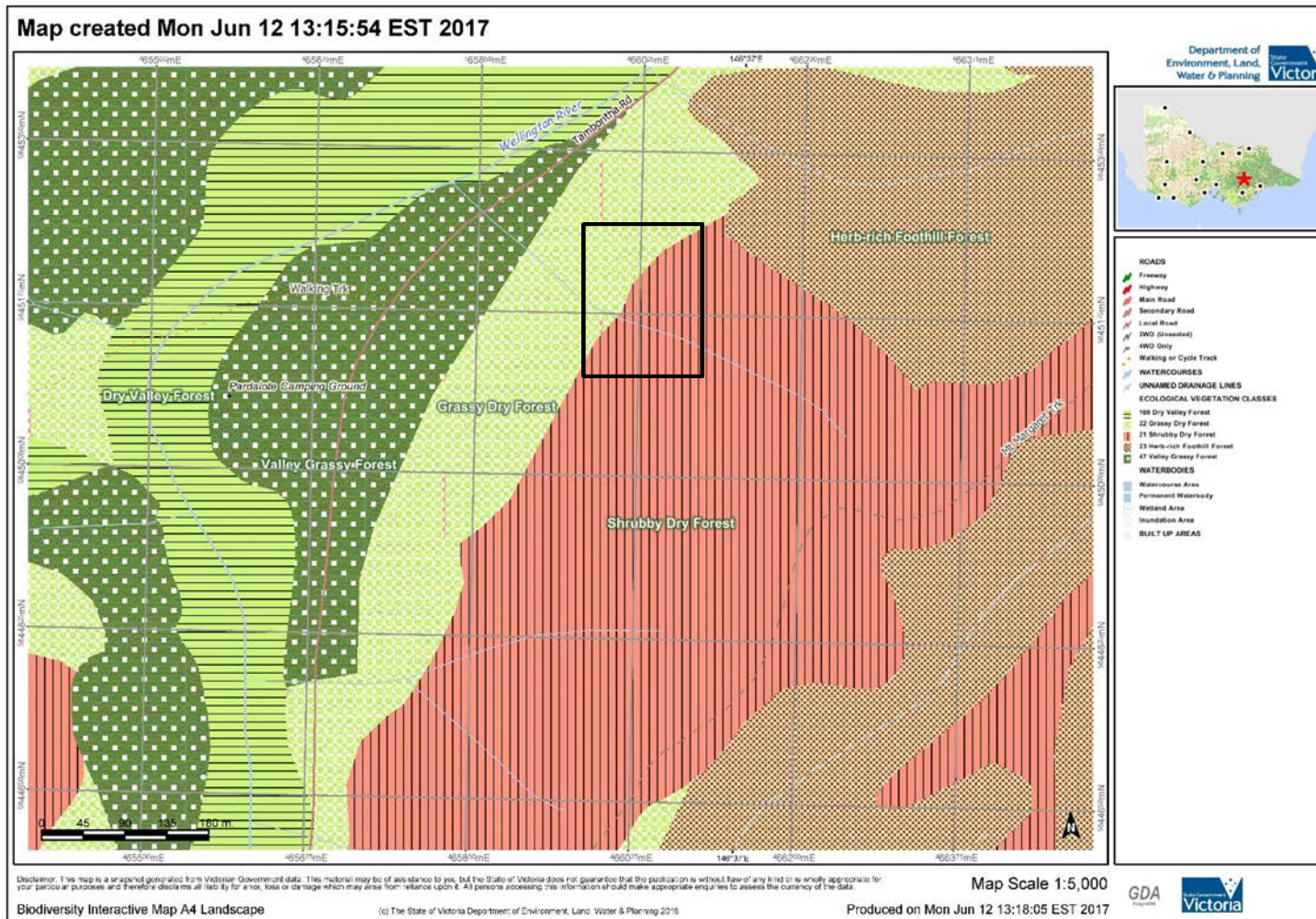
Figure 3-30. Ecological Vegetation Class (EVC) map of study area and surrounds. The black rectangle indicates the study area location. Source: Department of Environment Land Water and Planning (2016).

These were taken to be the pre-fire climax vegetation, while keeping in mind the high fire frequency in the region. It was therefore assumed that mature foliage dominated the area during the pre-fire period. Adult leaves of *Eucalyptus polyanthemos* (the species of interest in this study) are petiolate and vary from ovate to broad-lanceolate with dimensions up to 9 (length) x 3 (width) cm (Brooker and Kleinig, 2006; Costermans, 2009), and are quite distinct from juvenile leaf forms typical of post-fire regrowth, as discussed below.

Dry sclerophyll forests, even when unburnt, have an open canopy with crown cover ranging between 20 and 50% and foliage cover ranging between 10 and 30% (National Committee on Soil and Terrain Australia, 2009). The vertically-hanging foliage of the *Eucalyptus* tree species (King, 1997) enable strong sunlight penetration through the canopy at high solar zenith angles. Along with the sparse woodland-like distribution of trees at the study site, this leads to relatively exposed sub-canopy and forest floor microclimates where the litter of dry sclerophyll forests can accumulate as fine fuels and dry-off rapidly during summer, increasing fire risks over a broad region (Price and Gordon, 2016).

Equilibrium surface fuel loads in dry sclerophyll eucalypt forests of southeast Australia, usually reached 5 to 8 years after fire, have been estimated to range from 15 t ha^{-1} (Brooks et al., 2004; Gilroy and Tran, 2009) to 19 t ha^{-1} (Clarke et al., 2016); it is likely that these fuel loads were reached in the study area (and the wider region) leading up to the megafire of Dec 2006 to Feb 2007 (Flinn et al., 2008a). In comparison, for dry open "jarrah" *Eucalyptus marginata* forests in Western Australia, Gould et al. (2008) reported lower surface fuel loads of 10 to 11 t ha^{-1} 10 years after fire which then slowly increased to reach a steady 13 to 14 t ha^{-1} at 25 years after fire. Under the fuel load classification system by Luke and McArthur (1978), pre-fire fuel load conditions for the study area were very likely to have been in the 'Severe' to 'Catastrophic' ranges (Chen et al., 2017).

As described in Section 3.4, large contiguous areas of the dry sclerophyll forests in the Great Dividing Range in Victoria were burnt at moderate to high severity (see Section 2.4 and Figure 3-8) in the 2006/7 megafires. Therefore most trees in the affected region either had severe crown scorch or had their crowns burnt, causing the removal of the protective canopy cover over very large areas. Attiwill et al. (2014) reported that close to 90% of the *Eucalypt* mixed species forests in Victoria burnt in the 2006/7 fire were classified as moderate or severely burnt or had crown-scorch. Post-fire storm events caused damaging floods, erosion and sedimentation in the affected catchments (Forest Fire Victoria Inc., 2007) (see also section 3.5.2). Field observations of near-immediate post-fire conditions, of areas close to the study site by Nyman et al. (2011) noted almost complete defoliation of the existing vegetation with ample evidence of crown burn. Nevertheless, because of the fire-adapted nature of the plant species in these forests (Clarke et al., 2015) there was successful and ample regeneration that occurred over the ensuing years.

In line with the focus of this research on intermediate-stage post-fire erosion a ground survey of the study hillslopes over an approximately 0.5 ha area (see section 3.1) was undertaken five years after the fire in Nov/Dec 2011 in preparation for the fieldwork campaign in 2012 (see Chapter Four). With reference to Costermans (2009) for plant identification, the main tree canopy species identified were regenerating *Eucalyptus polyanthemos* (Red Box) (most dominant), *E. macrorhyncha* (Red Stringybark), *E. melliodora* (Yellow Box). Shrub-level species were mostly *Acacia implexa* (Lightwood) *Acacia verniciflua* (Varnish Wattle), and *Acacia melanoxylon* (Blackwood). Live ground cover was characterized by fragmented, isolated patches of what appeared to be *Themeda triandra* (kangaroo grass) and *Poa labillardierei* (tussock grass). Some of the ground was bare, especially the inter-spaces between patches of regenerating trees, shrubs and grass

patches. Organic litter, mostly in the form of dead leaves and small twigs, could be found sparsely distributed over the mostly bare inter-spaces, but accumulated behind barriers such as the stems of regenerating *Eucalyptus* trees, fallen logs and large rocks.

Stem-density of all *Eucalyptus* trees was estimated at 181 stems ha^{-1}. In comparison, Stewart et al. (1979) reported stem density at 123 stems ha^{-1} and biomass at 344 Mg ha^{-1} for mixed-species eucalypt forests containing *E. agglomerata, E. muellerana and E. sieberi* in Genoa, Eastern Victoria where there was higher annual rainfall (927 mm) than the present study site. By the time of initial site visits in 2011, post-fire regrowth and spatial re-colonization of the *Eucalyptus spp.* was already substantial with dominance of basal sprouting from near surface lignotubers and some examples of epicormic growth from the trunks of the few trees that had survived the fire damage (see Plate 3-3).

Plate 3-3. Regenerating *Eucalyptus polyanthemos* individual at the study site. Yellow tape measure at 1 m length provides scale. Note mostly bare ground outside the edges of the regenerating plant. (Photograph by author)

I observed some substantial re-growth of the *Acacia spp.* (wattles) at slope bases where slope gradients were gentler (see Plate 3-4a) and, presumably, much of the seed bank had accumulated due to transportation from upslope sources, caused by hillslope erosion and deposition processes. Occurrence of the juvenile wattles was much sparser on the bare inter-spaces (Plate 3-4b).

(a)   (b)

Plate 3-4. Vegetation conditions of study site. (a) Dense post-fire regrowth of *Acacia* (wattles) at the slope bases of the study site (photo taken from side of Tamboritha Road); and (b) Bare inter-spaces with sparse re-growth of *Acacia spp.* individuals. (Photographs by author)

Of particular interest was *Eucalyptus polyanthemos*, because of its very distinct heterophylly. Juvenile leaves of *E. polyanthemos* are petiolate, orbicular, emarginate with dimensions approximately 6.5 cm (length) x 8 cm (width), which are quite different from mature leaf forms. Hanging habits of eucalypt leaves are also unique with steep leaf inclination (60 - 70°). These were verified with the use of a handheld clinometer at the study site. With their sclerophylly and hydrophobicity, it was hypothesized that the open forest canopy still in recovery would have limited canopy storage capacity, and there would be distinctive interception and throughfall characteristics compared to other plant species with different leaf habits and characteristics. Field observations of post-fire vegetation regeneration found a dominance of juvenile leaf growth of *E. polyanthemos* in the study area

(see Plate 3-5). The pendulous hanging habit of the E. polyanthemos leaves can be observed in the upward-looking photo of the plant canopy in Plate 3-6.

Plate 3-5. Post-fire foliage of *Eucalyptus polyanthemos* dominated by orbicular, juvenile leaf forms. It was postulated that distinct throughfall fractions and rates, and drop-size spectra could be the outcome of modulation of rainfall on this regenerating canopy. There would thus be interesting and important controls by canopy characteristics on ground-level splash erosion, infiltration and runoff generation. (Photograph by author)

Plate 3-6. Pendulous hanging habit of *E. polyanthemos* leaves observed at field site. Part of the plant stem can be seen in the left foreground. (Photograph by author)

3.7. Soils

3.7.1. Pre-fire soils

According to Rowe and Downes (1960), soils of the study area ranged from solodic soils at the gentle to moderate gradient footslopes, to leptopodsols with some lithosols on moderate to steep upper slopes. Solodic soils were found at or near the crests of the high ridges. These soils were likely to have developed due to the combination of the steep terrain, the dominant climatic conditions and associated meteorological occurrences, vegetation characteristics and the underlying geology - nutrient-poor Devonian sedimentaries (mudstone, sandstone and conglomerates) described in section 3.2. These soils were mainly composed of thin 'A' horizons with medium to coarse sandy loam textures with weak or non-existent structure, with gravelly to sandy-clayey 'B' horizons.

More recent data from CSIRO (2011) for the study area prior to the 2006/7 fires classified soils in the study area as texture-contrast Chromosols (Isbell, 2002). Soil pH (1:5 $CaCl_2$) was 4.6 to 4.8 with loamy sand/sandy loam textures (< 10% clay) and shallow profile depths of 0.3 to 0.5 m (CSIRO, 2011) (Australian Soil Resource Information System Level 4 data). Just adjacent to the study area, the neighbouring hillslopes with more sheltered south and easterly aspects had Dermosols (Isbell, 2002). From the classification and descriptions of soils in the study area, the fire-induced defoliation reducing protective vegetation cover, and the likely loss of soil organic material and aggregate stability, post-fire erodibility of the topsoil would have been very high. In combination with the steep topography and the lack of barriers to impeded sediment movements, the volume of hillslope sediment and organic material lost in post-fire erosion would have been very high. The outcomes of the severe soil erosion on the study site are described in the following section.

With the extensive fires and numerous reports of post-fire erosion and floods in the region (Australian Associated Press, 2007; Department of Sustainability and Environment and Parks Victoria, 2010; Gippsland Emergency Recovery Committee, 2007; Houghton, 2007), many changes to the soil, in addition to the vegetation, occurred. Post-fire ground survey of the soils at the study site by the author in Nov 2011 found rather depleted, skeletal soil conditions. Much of the original topsoil had been stripped away by severe post-fire erosion and debris flows, and voluminous amounts had been exported from the hillslopes to the stream system (Nyman et al., 2011). This can be observed in Plate 3-7 which shows how the existing gullies had been widened and deepened, and acted as concentrated pathways for large volumes of sediment and water as debris flows to be evacuated downslope to the bases of the steep hillslopes and into the stream network. Plate 3-8 provides an impression of the voluminous post-fire debris flow deposits in the study region reported by Nyman et al. (2011). Much of the eroded material entered the adjacent Wellington River (Plate 3-9) and contributed to the major floods and damage to Licola town, Glenmaggie Reservoir and Cowarr Weir (ABC News, 2010; Department of Sustainability and Environment and Parks Victoria, 2010; East Gippsland Catchment Management Authority, 2007; Gippsland Emergency Recovery Committee, 2007; Goulburn Broken CMA, 2009; Tryhorn et al., 2008).

Plate 3-7. Large gully in the study area. Note the large boulders deposited in the gully and the bark stripped-off bark on the upslope portion of the trees, indicating the likely height, volume and impacts of the post-fire debris-flows. Photo credit: Bushfire and Natural Hazards CRC (2017).

Plate 3-8. Debris-flow deposits hindering access along Tamboritha Road near Licola in late February 2007. Source: Flinn et al. (2008a). Photo credit: Department of Sustainability and Environment (DSE).

Plate 3-9. Post-fire sediment washout to Wellington River at the base of study site slopes circa 2012. Flow direction indicated by blue arrow - south towards the confluence with the Macalister River at Licola town. (Photograph by author)

Evidence of the severe erosion that had already occurred at the study site included very thin, unstructured stony topsoil containing high percentages of gravel and rock, and the occurrence of fine sedimentary bedrock (mudstone, siltstone and sandstone) within 10 cm of the soil surface; the average soil depth. There were also large mounds of unconsolidated and unsorted sediment, including large rocks, at slope bases, with intermittent evidence of the original soil horizons protected under the occasional fallen, burnt out logs. The original topsoil of the Chromosol profile would have been stripped away by the erosive processes prior to the commencement of the study period triggered by storms in the immediate and short-term post-fire period, leaving behind what would have been the original 'B' and 'C' horizons. The state of the depleted, skeletal post-fire soils at the site is illustrated in Plate 3-10.

(a)	(b)	(c)
Site soil profile as observed from a gully wall. Profile depth indicated by the measuring tape was 1.5 m. Observed topsoil depth was variable; 10 to 30 cm and very stony.	Thin topsoil at the study site. Fallen log provided some protection of the original soil surface (~6 cm higher than current) from erosion.	Foreground: Patchy ground cover at the study site with scattered regeneration by *Acacia spp.* Post-fire eucalyptus regrowth in background.
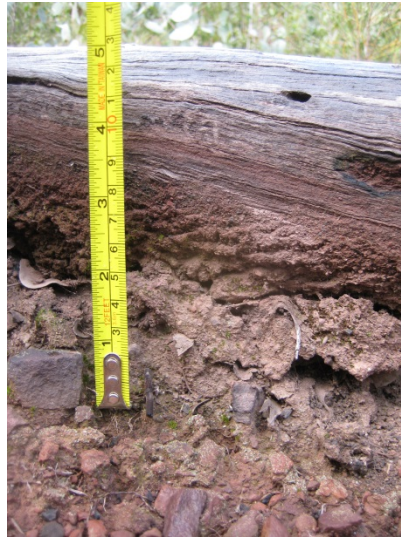
Plate 3-10. Post-fire soil conditions in 2011, approximately 5 years after fire occurrence; (a) soil profile from gully wall; (b) thin, gravelly soils; (c) bare, patchy soil surface. (Photographs by author)

Six topsoil samples were obtained from lower slope positions about 20 m from one another roughly along the 340 m contour in the study area and then bulked for particle size analysis using laser diffraction (Eshel et al., 2004), pH (H_2O) using 1:5 soil:water ratio (Rayment and Lyons, 2010) and organic material using the Loss-On-Ignition method (Rayment and Lyons, 2010). The soil profile was extremely shallow, ranging from 7 to 15 cm, with large rocks deterring any deeper sampling (cf. Plate 3-8). The topsoil texture was gravelly-sandy silt loam with moderate to high stoniness and would have been of moderate to high erodibility (Bryan, 2000; Lal and Elliot, 1994; Song et al., 2005). The soil was extremely acidic with pH (H_2O) of 4.0. Such acidic forest soils are widely distributed across southeast Australia and usually have high, toxic levels of exchangeable Aluminum to which many native plants (e.g. *Eucalyptus* and *Acacia spp.*) are well-adapted (Khanna et al., 1994).

Field measurements found that topsoil depth was limited to around 7 cm in most positions, below which large stones (mudstone and siltstone) were encountered (see Plate 3-8 a-b). There was no textural or colour differentiation between these thin upper layers, except for certain locations where a thin layer of organic material (about 5 mm) had accumulated. The topsoil was generally poorly aggregated and had minimal structure with minimal visual evidence of soil organic matter. The soils were thus classified as Leptic Lithic Rudosols, where minimal pedological development had occurred (Isbell, 2002). This substantial contrast with the pre-fire soil classifications (see 3.7.1.) also underscores the importance of post-fire erosion processes in pedological development and classification, particularly where there is redistribution of large volumes of soil across the landscape (Shakesby et al., 2007).

Ground cover by live plants was patchy and limited (see Plate 3-8c) with many large, bare interspaces. Litter cover was heterogeneous across the study site, with much more litter found directly under the recovering trees and shrubs, especially upslope of the stems where there was likely to have been some accumulation of litter transported and detained from upslope sources. This was quite similar to the Faulconbridge site, 70 km west of Sydney in the Blue Mountains, studied by Dragovich and Morris (2002) where it was noted that ground cover recovery was patchy and limited even though the trees and shrubs had recovered relatively rapidly.

The plant-soil interactions at the study site appeared to reflect the "Nutrient-Poverty/Intense-Fire Theory" (Orians and Milewski, 2007). Because of the low macro (e.g. phosphorus) and micronutrient (e.g. zinc) availability in the thin gravelly soils, plants such as the *Eucalyptus spp.* channel excess energy to the rapid production of high-lignin, nutrient poor biomass that limits herbivory and organic litter decomposition. This results in the rapid accumulation of fuel loads particularly in dry sclerophyll forests in the present study area.

This recalcitrant, spatially heterogeneous and relatively mobile litter load influences hillslope processes in a variety of ways.

Firstly, and the most obviously, would be a rapid rise in fire risk accompanying the quick recovery of the plant canopy. At the microscale, the copious fuels at the base of stems will increase the likelihood of crown fire due to the vertical "laddering" of fuel. If fire were to break out again in the area, conditions would revert to the high vulnerability of the immediate post-fire period. Secondly, the presence of litter would provide a protective layer to mitigate rainsplash impact (Geddes and Dunkerley, 1999), disrupt overland flow paths, increase infiltration rates and mitigate soil moisture losses. Under these "intermediate" conditions (see Chapter Two) they are, however, mostly situated under individual regenerating plants. Thirdly, their sclerophylly and hydrophobic surfaces could, somewhat counter-intuitively, transform free and released throughfall drops to surface runoff because of their low infiltrability and protective mulching effects of maintaining soil moisture levels. Fourthly, the litter can be highly mobile in the steep terrain being of low density, they can be easily transported by flowing water and/or wind down or across hillslopes. Depending on their location and concentrations, hillslope processes could be accordingly influenced.

3.8. Prolonged post-fire erosion vulnerability

Despite reports of rapid post-fire re-establishment of vegetation in dry eucalypt forests (Heath et al., 2016; Shakesby et al., 2007) with substantial regrowth observed within a year after fire, it seems that the region has displayed prolonged vulnerability to erosion even into the "intermediate" recovery period where resistance to erosion is meant to be relatively high (Prosser and Williams, 1998). Frequent bouts of erosion and flooding have continued to occur in the Licola region even though the upstream areas have seen substantial vegetation recovery. One notable event reported in the media in Feb 2010 was the damage caused by the significant flooding and sedimentation to the town of Licola (ABC News, 2010). This was

followed moderate floods, three years after the fire, in Sep 2010 (3.53 m) and Dec 2010 (3.33 m) (Wellington Shire Council, 2016). In Aug 2011, winter storms caused major flooding at 3.62 m. In 2012, flooding at Licola was again reported, with river gauge heights of 4.27 m on 5 Jun 2012 (major flooding) and 2.90 m (minor flooding) on 7 Jun 2012 (Bureau of Meteorology, 2017e; DELWP, 2016).

Hence, post-fire erosion vulnerability does not necessarily have a simple negative, monotonic relationship with the number of years after fire, or even with the extent of vegetation recovery. Indeed, while the stochastic interplay between rainfall regime, fire regime, catchment "priming" and the occurrence of extreme erosion events is important for modelling and prediction (Jones et al., 2014), there is still a need to investigate the complex post-fire erosion and hydrological factors and responses deeper into the "window of disturbance" (Prosser and Williams, 1998; Shakesby, 2013) in this geomorphic and hydroclimatic region, because these are of both practical and scientific significance.

Having established a good understanding of the landscape, fire regime, hydro-climatic conditions, vegetation and soils of the study region which continues to manifest extended erosion vulnerabilities even in the intermediate post-fire period, we now turn to the methods used to investigate the rainfall, vegetation, throughfall and hillslope material fluxes of the study area in Chapter Four.

CHAPTER FOUR: METHODOLOGY

4.1. Introduction

In this chapter, the methods adopted in this research will be presented. Firstly, I describe the layout of the measuring apparatus for a good picture of the site setup within the partially-vegetated hillslope in intermediate post-fire conditions. Following this, the specific methods will be described in the following order: (i) rainfall measurements and analysis, (ii) canopy cover measurements of intermediate post-fire vegetation, (iii) throughfall fraction (iv) erosivity of throughfall and rainfall, (v) laboratory-based throughfall drop-size measurements; and (vi) measurement of hillslope material fluxes using sediment fences. The adoption of the suite of methods in the field enabled the concurrent measurement and subsequent investigations of possible relationships between the various factors, processes and outcomes of hillslope erosion in intermediate post-fire vegetation conditions, important research gaps discussed in Chapters One and Two.

The laboratory experiments were conducted to develop essential insights into how intermediate post-fire vegetation canopies of dry sclerophyll forests dominated by juvenile leaf forms might modulate rainfall distinctly from long unburnt canopies with mostly mature leaf forms. The field experiments were conducted over 6 time periods across 10 months in 2012. While this was a relatively small number of measurement periods, this was thought to be sufficient to capture the wide range of rainfall types and event characteristics that would elicit a range of responses from the plant canopies in rainfall modulation and hillslope erosional processes.

Higher temporal data resolution was hindered by the long distance of the study site from the university, the need to select non-rain days for field data collection and limited manpower resources available. Furthermore, several site visits within each of the 6 measurement periods found that, in some cases, minimal or no sediments had been

transported across the hillslope surface to be deposited at the sediment fences because there had been insufficient erosive energy from small rainfall events during the intervening time. In view of these reasons, the workload for this research was thought to be suitably scoped for insights to be gleaned into the intermediate post-fire hillslope hydrological and erosional processes, the focus of this research.

4.2. Site selection and instrument layout

Informed by reconnaissance visits of the study area in 2011 (see Chapter Three; Figure 3-4), a suitable study site with intermediate post-fire vegetation conditions was selected (Lat: 37.54° S, Long: 146.61°; UTM: 55H 465948 E, 5845213 S). The selection criteria included: (i) similarity of soil and intermediate vegetation conditions to the broader region that had been burnt in the 2006/7 fires; (ii) low likelihood of recent human disturbance in the area (e.g. dirt-bike riding, bush-walking or camping) since Feb 2007; (iii) accessibility from a sealed road that would not hinder transport, installation and maintenance of equipment and apparatus, and sample collection; (iv) reasonably safe in terms of slope stability and movement across the terrain; (v) well-hidden from public view to minimize the chances of vandalism, equipment theft or tampering by passers-by. Figure 4-1 shows the layout of the various instruments for simultaneous measurement of rainfall, throughfall and hillslope material fluxes were deployed at the study site. The local topography, geology, soils and climate were described in Chapter Three. Details of the methods and instruments adopted are provided in the following subsections.
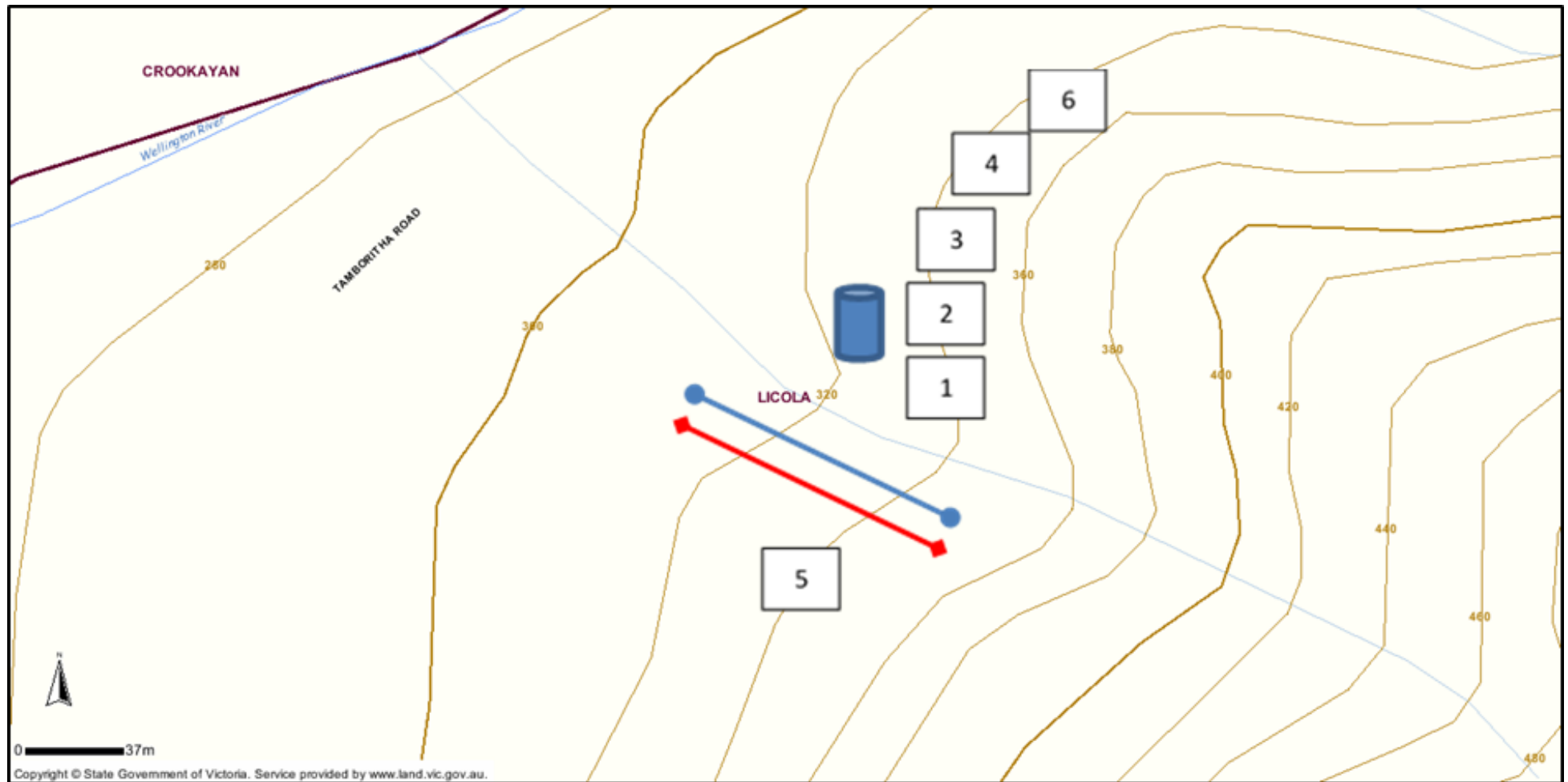
Figure 4-1. Detailed topography and instrument layout of study site. Notes: (i) Blue cylinder symbol denotes position of pluviometer in a natural clearing; (ii) Blue line with round ends indicates transect layout of TIF funnels and (iii) Red line with square ends indicates transect layout of splash cups, perpendicular to contours. (iv) Open-field TIFs and splash cups were installed in a circular pattern surrounding the pluviometer. (v) Numbered boxes 1-6 indicate positions of sediment fences. Map source: (State Government of Victoria, 2014).

190

4.3. Rainfall

Study area rainfall was measured using a Hydrological Services Tipping Bucket rain gauge (TB3) (0.5 mm resolution, 200 mm diameter) equipped with a Hobo® event logger (Onset Computer Corp.) which recorded the date and timestamp for each recorded tip of 0.5 mm rainfall depth. Similar to the study by Stoof et al. (2012), the pluviometer was located in a circular naturally-occurring treeless clearing approximately 10 m in diameter. It was installed on a 30 x 30 cm square concrete slab on the ground surface and levelled with the aid of a bubble level (see Plate 4-1). An earlier attempt to install the pluviometer on a steel pole driven into the ground was thwarted by the shallow profile and underlying rocks that prevented any firm footings to be gained. After installation, initial attempts at rainfall measurement were foiled because rainsplash had caused substantial amounts of fine clay and silt-sized particles to be detached from the adjacent bare soil surfaces and then deposited at the orifice of the pluviometer funnel, clogging it. While this delayed the progress of the project, the high rates and volumes of splash erosion from the soil surface were shown to be very significant. To mitigate against this, around 4 m^2 of HDPE UV-stabilized shadecloth were lain on the ground surface bordering the pluviometer to attenuate any rainsplash energy and enable it to operate much more reliably without the funnel clogging. Rainfall records from Glencairn weather station (DELWP, 2016) approximately 4 km west of the study site (elevation 380 m) were used as reference and backup data for the study site.

Plate 4-1. Pluviometer installed at study site. Photo was taken prior to installation of shadecloth border to attenuate splash erosion from adjacent bare soil surfaces. Note the evidence of rainsplash erosion and deposition on the outside walls of the instrument. Regrowing seedlings seen in the background of photo were trimmed regularly to prevent any interference with accurate rainfall measurement.

Boxcar Pro 4.0 software (Onset Corp.) was used to download the readings from the datalogger. It was then imported into Microsoft Excel for data preparation and processing. Following Haile et al. (2010), 'primitive' rainfall events of 1 mm minimum depth, and 60 minute minimum inter-event time were identified. Primitive events at this initially high temporal and quantitative resolution allow the examination of the various factors influencing resultant erosional impacts such as antecedent soil moisture (affecting soil infiltration rates and runoff generation) and can be aggregated to form "composite" events where necessary or desired, especially for studies of processes leading to soil erosion (Brown et al., 1985).

The prepared rainfall dataset was processed using the Rainfall Intensity Summarization Tool (RIST) (version 3.88) (Agricultural Research Service, 2013) to develop a range of statistics for all the recorded storms, in particular the $I_{1\,min}$, $I_{5\,min}$, $I_{10\,min}$, $I_{15\,min}$, $I_{20\,min}$, $I_{30\,min}$ and $I_{60\,min}$ intra-event rainfall rate values. The $I_{1\,min}$ values were used for detailed analysis of threshold intensity-duration effects on overall hillslope material eroded, and also

for studying threshold erosional relationships with the different sediment size components. The equation by McGregor et al. (1995) was used to derive event energy and erosivity in RIST, based on rainfall erosivity parameters developed for the Revised Universal Soil Loss Equation (RUSLE) (Renard et al., 1997):

$$e = 0.29 \ [1 - 0.72^{e\ (-0.08i)}],$$ where e is kinetic energy expressed in MJ ha^{-1} mm^{-1}

and i = rainfall intensity expressed in mm hr^{-1}.

Event kinetic energy was expressed in MJ ha^{-1}; and

Erosivity of rainfall was $\dfrac{MJ.mm}{ha.hr}$ (presented in this document as MJ*mm ha^{-1} h^{-1}).

All descriptive and inferential statistical analysis was performed using IBM SPSS Statistics Version 22.

4.4. Canopy cover

Canopy cover measurements were taken at the start of each measurement period. I used the vertical photography method described by Dunkerley (2010a) who examined throughfall fractions under sub-alpine snowgum woodland and closed shrub heath canopies in Victoria, Australia, with good results. To determine the canopy cover as foliage projective cover (FPC), vertical photographs recording the branch, twig and foliar cover directly overhead of each sampling point (TIF and splash cup) were taken using a Panasonic Lumix FZ5 digital camera (5MP) in the widest possible lens angle. Canopy photographs included branches and twigs together with foliage because of the inherent difficulty in separating foliage and non-foliage portions of each image. Furthermore, these woody plant parts were also interception surfaces for vertically-falling raindrops, and would also contribute to canopy hydrological partitioning and rainfall modulation. The photographs of leaves, branches and twigs with the sky as background were captured in overcast conditions or during dusk to mitigate any image over-exposure to direct sunlight while the sun was at a high zenith angle in the sky, or from

reflection of sunlight off leaf surfaces even at low solar zenith angles. This was important to enable accurate derivation of canopy cover data by subsequent image conversion and thresholding.

The images were imported into the Java-based Image J software (National Institutes of Health, USA, v.1.46, downloadable from http://rsb.info.nih.gov/ij/), and converted by thresholding of greyscale images into binary (black and white) format to obtain the closest possible representation of vertical canopy cover in black (foliage, branches and twigs) and white (open sky). The canopy cover percentage was determined by calculating the proportion of total pixels (4,915,200) occupied by black (i.e. canopy cover) pixels. Figures 4-2a and 4-2b show the original vertical photo and thresholded image used to derive canopy cover percentage, respectively.

(a)   (b)

Figure 4-2. Sample image used to obtain canopy cover percentages: (a) Original photograph (note small patch of blue sky in background amidst generally overcast conditions); and then (b) Thresholded 8-bit binary black and white image processed in Image J software.

4.5. Throughfall fraction

Throughfall volume and fraction were determined using a chemical time-integration approach using Throughfall Integrating Funnels (TIFs) and Plaster of Paris (calcium sulfate hemihydrate) tablets following the design by Dunkerley (2010a), as shown in Figure 4-3.
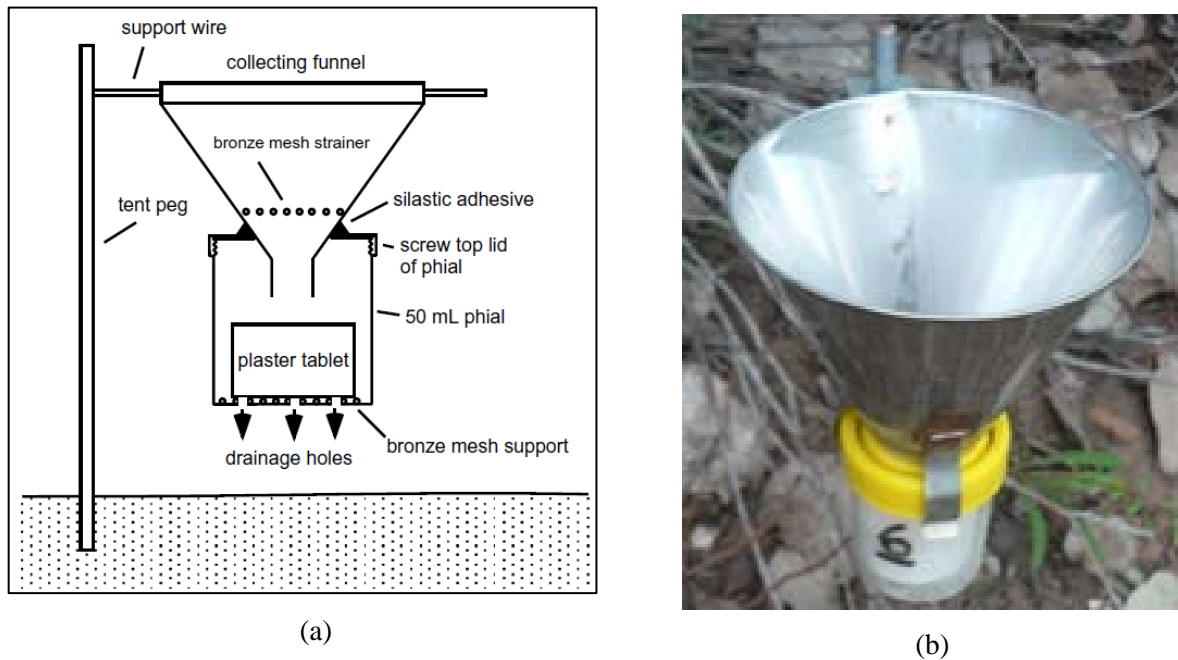
Figure 4-3. Throughfall Integrating Funnel (TIF). (a) Schematic; Source: Dunkerley (2010a) and (b) TIF (#6) installed at the field site (Photo by author).

Each TIF assembly comprised of a stainless-steel collecting funnel attached to a steel tent peg driven into the soil to hold it in place. A circular mesh strainer was installed inside the funnel orifice to trap any large litter fragments that might clog the funnel, but still allow water to freely drain through. The funnel was itself attached to the screw top phial lid in which a hole was drilled to fit the funnel neck through to converge water flow directly onto the calcium sulfate hemihydrate (Plaster of Paris) tablets (detailed in the following paragraph), which were themselves held in the phial body resting on another mesh strainer at the base. Drainage holes were drilled at the base of the phial to allow free evacuation of water after it had passed over the tablet surface. The measure of tablet weight loss from their original weights resulting from dissolution provided an indication of the rainfall or

195

throughfall depth volumes that had occurred. This method was demonstrated by Dunkerley (2010a) to have high correspondence to traditional measurement methods using throughfall troughs. Over eight integration time periods (251 days, 871.1 mm total rainfall depth) for low-lying *Eucalyptus pauciflora* (snowgum) canopy in the Bogong High Plains in Victoria, Australia, the TIF method (14 TIFs were deployed) gave throughfall fraction of 0.82 (s.d. = 0.23) which was extremely close to independently derived figures of 0.84 (s.d. = 0.06) from the "normal" throughfall trough method (4 were deployed). Compared to troughs, TIFs have the advantages of flexibility in spatial distribution of sampling points and ease of installation especially under low plant canopies, such as that encountered in post-fire vegetation regeneration conditions of the study site, or alpine snowgum-closed heath vegetation studied by Dunkerley (2010a).

Individual tablets were prepared by slicing Plaster of Paris cylinders formed in tubular moulds created from standard polyvinyl chloride (PVC) drainage pipes. I used a commonly available Uni-Pro brand (www.unipro.com.au) Plaster of Paris obtained from a local hardware shop. Each circular plaster tablet was approximately 36 mm in diameter and 20 mm in thickness. Tablets were oven-dried at 105 °C, left to cool to room temperature and then weighed to the nearest 10 mg using a precision laboratory balance to determine the uneroded mass. Subsequently, the tablets were carefully placed in 50 mL plastic phials padded with cotton wool and bubble wrap to minimize plaster loss by vibrations or knocks, for transport to the study site; this had been identified by Dunkerley (2010a) as a source of error to be mitigated. The fresh tablets were then deployed by carefully unwrapping them and transferring to the 50 mL phials as part of the TIF assembly (Figure 4-3b). At the end of each measurement period, the eroded tablets were carefully removed from the phial-funnel assembly and transported in the same padded phials back to the Monash University Soils Research Laboratory. Eroded plaster tablets from the TIFs were returned to the lab and oven-

dried for 24 hrs. They were then cleaned by extracting any visible fragments of organic litter using pincers and a soft paintbrush. Figure 4-4 shows the tablets' appearance after field deployment and in the laboratory environment for cleaning prior to weighing.

(a)	(b)
TIF tablets post field deployment. Tablets (#16-20) in front row (foreground) were exposed to open-field rainfall. (Photo by author)	TIF #10 post-field deployment. Cleaning was done using soft brush and tweezers (Photo by author)

Figure 4-4. TIF tablets after field deployment ready for drying and cleaning.

Open-field TIFs, receiving rainfall directly without any canopy interception, would experience greater weight loss compared to under-canopy TIFs which would have had some of the rainfall intercepted by the plant canopy and detained on leaves and twigs, lost through evaporation, or diverted to stemflow prior to their arrival at the TIF's orifice. Throughfall fraction for this intermediate post-fire canopy cover was determined by calculating the mean weight loss of plaster tablets #1 to #15, as a fraction of the mean weight loss of the 5 open-field TIFs (#16 to #20) (Dunkerley, 2010a).

A total of 20 TIFs were installed on the field site to determine relative throughfall volumes in open-field rainfall (5 TIFs) and under-canopy conditions (15 TIFs) (see Figure 4-1). The 5 open-field TIFs were positioned in the clearing (see section 4.3.), surrounding the pluviometer in a roughly circular manner, each about 30 cm from one another and the

pluviometer. Only 5 open-field, compared to 15 under-canopy, TIFs were deployed as it was expected that un-intercepted rainfall would have much lower variability in rainfall depth received over a small area of the clearing, compared to the heterogeneous under-canopy conditions (Nanko et al., 2016a). These were borne out in the TIF throughfall data reported in Chapter Six. The 15 under-canopy TIFs were arranged in an uphill transect on average 5 m from one another (Figure 4-1). Each TIF was positioned about 30 cm from the main stem of a regenerating *E. polyanthemos* tree. In their paired-catchment study of post-fire runoff and erosion, Stoof et al. (2012) similarly installed a total of 15 throughfall collectors fabricated from 5L jugs, divided equally under 3 shrubs, for the 9.7 ha Valtorto burnt catchment and the 4.9 ha Espinho catchment. This method was similar to that described by Dunkerley (2010a) in his study of throughfall under sub-alpine snowgum woodland and closed shrub heath in Victoria, Australia which yielded good results when compared to the "traditional" throughfall trough method that, having a large-linear collection area, integrated measurements over a substantial area giving poor spatial resolution and could not be flexible in spatial distribution of sampling points. Because this study necessitated the measurement of throughfall beneath the low branches from *E. polyanthemos* individuals due to the substantial post-fire epicormic growth and lignotuber sprouting that had already occurred since the fire five years prior, the TIF method was thus very suitable.

4.6. Throughfall erosivity

To measure splash erosion by throughfall and rainfall drops, sand-filled splash cups following the Tübingen splash cup (T splash cup) design by Scholten et al. (2011) were used with slight modifications based on locally available materials. As shown in Figure 4-5, the assembly consisted of: (i) sand-filled cylindrical splash cups (height: 50 mm, diameter: 43 mm; sampling area 14.5 cm^2) fabricated from PVC drainage pipes. Each cup had a permeable polyester fabric "base" which enabled constant hydraulic connection with the water reservoir while preventing any sediment losses from the bottom of the cup; (ii) cup holder using PVC pipe coupling with cotton facial pads at the base to enable good hydraulic contact with the cups; (iii) 500 mL LDPE bottle acting as water reservoir with a hydraulic connection maintained with the splash cup via the cup holder using a cotton wick threaded through a drilled hole in the bottle's polypropylene screwcap. It was important that the sand cups were kept at close to saturation, and that any changes to sand moisture content due to rain/throughfall or evaporation would be rapidly adjusted to nominally near-saturation or field capacity levels, as splash erosion processes and impacts are critically dependent on this factor (Poesen and Savat, 1981; Truman and Bradford, 1990). The PVC cup holder was securely attached to the screwcap using silastic adhesive. The screwcap-cupholder assembly could be easily unscrewed to allow the water reservoir to be refilled with stream water collected from the nearby Wellington River. A small aperture was drilled on the top of the main body of the bottle to allow air to freely enter and displace any water being wicked up to the sand cup, and also to allow excess water contributed by rainfall or throughfall to be evacuated without the splash cup assembly being inundated. As demonstrated by Scholten et al. (2011), the constructions were robust and reliable, making them suitable for measuring throughfall and rainfall splash energy in remote areas, harsh environments and on steep terrain.

Each cup was filled with dry-sieved oven-dried medium sand of 212-500 µm particle size range, up to ~2 mm from the rim of the cup. Medium sand, rather than fine sand (125–200 µm particle size range) used by Scholten et al. (2011), was used because of its higher availability, acquired by sieving sand purchased from a local gardening shop. It was also less vulnerable to aeolian erosion that could have caused sediment losses that could not be attributed to rainfall and throughfall splash effects, leading to erroneous results. As found from initial trials, the use of medium sand also saw minimal losses by displacement during preparation, packing, transport, field deployment and retrieval of the sand cups. This was especially important because of the long distance of 240 km between the University and the study site, and the rough terrain to, and at the study site. In the laboratory, each cup was weighed to the nearest 10 mg using a precision laboratory balance to determine the uneroded "initial" mass. They were then sealed using LDPE food packaging clingfilm and securely transported in polyethylene boxes padded with bubble wrap and cotton wool pads to minimize sand loss from jolts and vibrations during transport. The same method was used for retrieving and transporting the eroded sand cups from the study site. The 15 under-canopy splash cups (#1 to #15) were arranged in a transect in a similar manner as the TIFs (see Figure 4-1). The 5 open-field splash cups (#16 to #20) were also arranged in the similar manner as the open-field TIFs while ensuring that they were placed far enough to not affect the accuracy of the TIFs, other splash cups or the pluviometer by having sand particles deposited into their funnels. Under-canopy splash cups were positioned approximately 30 cm from the main stem of each tree, as was done by Geißler et al. (2012b). All splash cup assemblies were secured using nylon cable ties to a stainless-steel tent peg driven firmly into the ground (see Plate 4-2). Similar to the TIFs, the splash cups had a low vertical profile (~230 mm height) and could be flexibly deployed under low vegetation canopies and provided for good spatial distribution of sampling points.
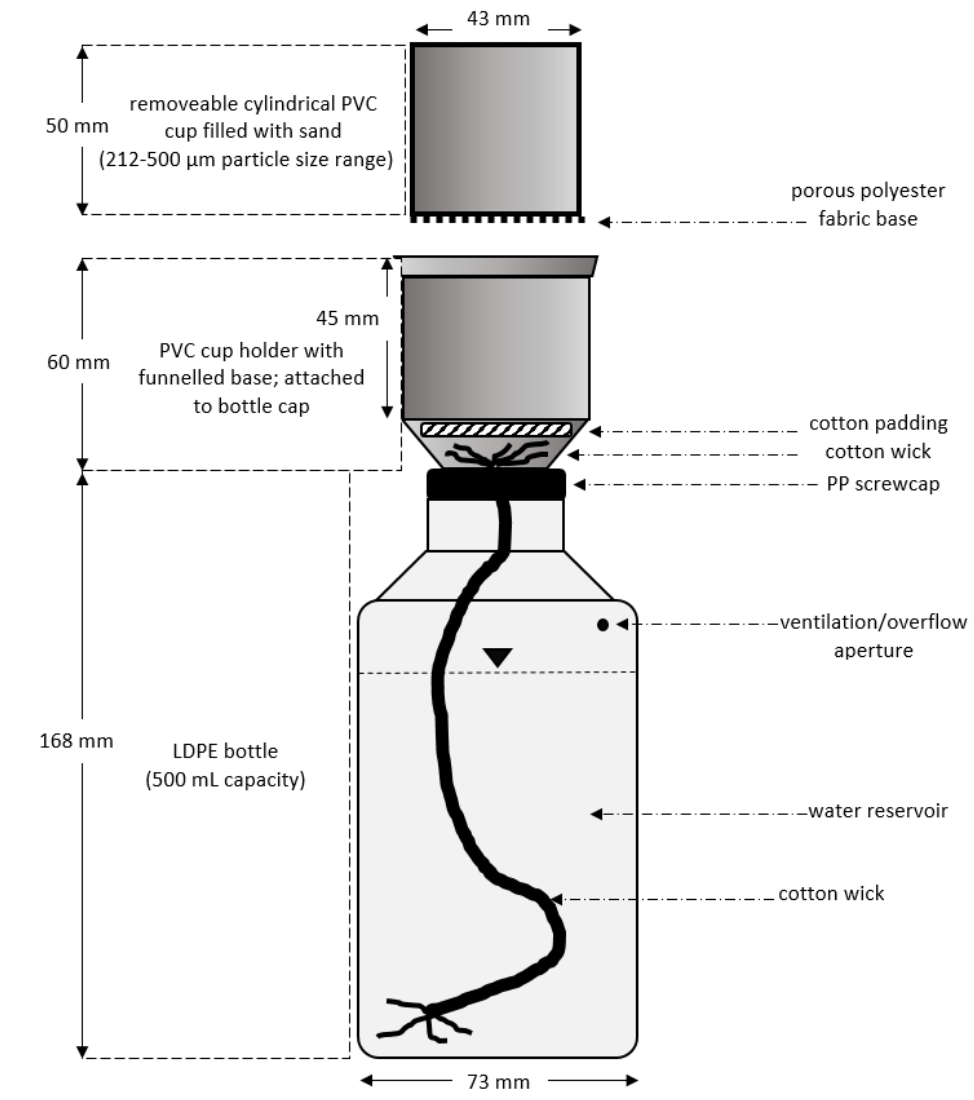
Figure 4-5. Schematic of splash cup assembly.

Plate 4-2. Splash cup assembly deployed in the field.

At each site visit, eroded sand cups were collected from their individual positions and replaced with fresh sand-filled cups, with the water reservoir replenished each time if water levels were low. The eroded sand cups were carefully re-packaged and returned to the laboratory and oven-dried for 24 hrs.

As can be discerned from Plate 4-3, the sand cup surfaces for (a) open rainfall were quite distinct from those that had been exposed to (b) under-canopy throughfall. (a) had small, evenly-distributed and shallow pits; in contrast, (b) had large, unevenly-distributed and deep pits. Together, they provided clear, qualitative indications of the small water drop sizes and low splash impacts of open-rainfall conditions, and the opposite for under-canopy throughfall conditions. Prior to any weighing, it was quite apparent that for most cups the sand surfaces for under-canopy throughfall were distinctly lower than those for the open-rainfall conditions, providing initial indications of the higher erosivity of the throughfall drops.

(a)	(b)

Plate 4-3. Sand cup surface conditions for (a) open-rainfall conditions and (b) under-canopy throughfall conditions.

Upon return to the laboratory, the cups were cleaned by extracting any visible fragments of organic litter (see for example Plate 4-3) using a pair of stainless-steel pincers. Following that, a soft brush was used to gently remove any sand grains deposited on the narrow rim of the cup and on its external surface, because these were deemed to have been removed by the splash impacts of rain and throughfall drops. Each sand cup was weighed to the nearest 10 mg. Sand weight loss was determined by subtracting the post-exposure dry weight from the original pre-exposure dry weight. Following this, an **erosivity ratio** representing the extent of under-canopy splash erosion against open-rainfall splash was determined by dividing the mean weight loss of plaster tablets #1 to #15, by the mean weight loss of the 5 open-field splash cups (#16 to #20).

4.7. Throughfall drop-sizes (Laboratory experiments)

The quantification of drop sizes was a key aspect of this research to shed light on how intermediate juvenile leaf-form dominant *Eucalyptus polyanthemos* foliage modulated rainfall, and examine if there were discernable differences with mature leaf forms. However, this project did not have access to advanced equipment such as a laser (Angulo-Martínez and Barros, 2015), or optical disdrometer (Fernández-Raga et al., 2010). Hence, I decided to employ an improved low-cost method using dyed filter papers after reviewing various options examined by Kathiravelu et al. (2016).

4.7.1. Low-cost dyed filter-paper method

The initial step for this method was to trial and evaluate the use of the dyed filter-paper method for indirectly measuring water-drops of varied sizes and masses using readily-available, low-cost materials such as hypodermic needles, syringes, water-soluble food dye and laboratory-grade filter paper. This was performed in the laboratory environment.

Whatman^{TM} No.3 (Grade 3) standard qualitative cellulose filter papers (185 mm diameter) were stained using a solution of standard tap water and water-soluble blue food dye (Queens^{TM}), mixed in a 1:10 dye:water ratio. The filter papers were fully saturated with the food dye mixture in a shallow tray and then removed and left to air-dry on stainless-steel wire racks at room temperature (~20°C) for 48 hours in the laboratory. Whatman^{TM} No.3 filter papers were used because they were strongly hydrophilic, preventing any beading-up of water drops arriving on the surface and at 390 µm thickness, were more than double that of the No. 1 (Grade 1) filter papers (190 µm) used in earlier reported studies such as Hall and Calder (1993), and gave excellent wet strength mitigating any tearing, which was particularly important during the wet dyeing (and subsequent drying) process during the experiments. These thick filter papers also proved to be robust and easy to handle before, during and after any water drop experiments were conducted. The 185 mm diameter size was selected because

it was large enough for sufficient numbers of drops to be collected at any one time (compared to smaller-area filter papers) while still small enough to be easily handled with one hand.

Using standard tap water from the metropolitan reticulated water supply network (Melbourne Water), a range of drop sizes was generated using seven hypodermic needles of different gauges (Largest: 16G, 1.19 mm inner diameter; Smallest: 27G, 0.21 mm inner diameter) (Sigma-Aldrich, 2017); hypodermic needles have frequently been used to generate target drop sizes, with strong positive correspondences between needle gauge and drop diameters (Zhao et al., 2014a) indicating high precision and reliability in drop-size generation. 50 drops from each needle gauge size were generated to fall on the filter paper targets positioned 10 cm below the tip of each needle. Each drop created a stain of a lighter shade of blue compared to the original dyed colour, and had a thin dark-blue border that delineated the perimeter of each drop stain. This occurred because the water from each drop would dissolve some of the dye and spread outwards from the area of initial drop incidence with the filter paper; and the dissolved dye that had been transported would then be concentrated at the edge of the drop stain, forming a distinct circular perimeter containing a lighter-coloured interior (see Figure 4-6). The shape of each stain was not fully circular but slightly elliptical (see Table 4-1). During the process of dripping on the filter papers, care was taken to constantly reposition the filter paper by hand to ensure minimal merging between stains created by individual drops; any merged stains were excluded from the data set. As the experiment was conducted, it could be seen that the stain areas created by drops from the same needle gauge were quite consistent, and that stain areas of water drops from different needle gauges were distinct, with coarse needle gauges creating larger water drops and vice-versa (see Figures 4-6a and b).
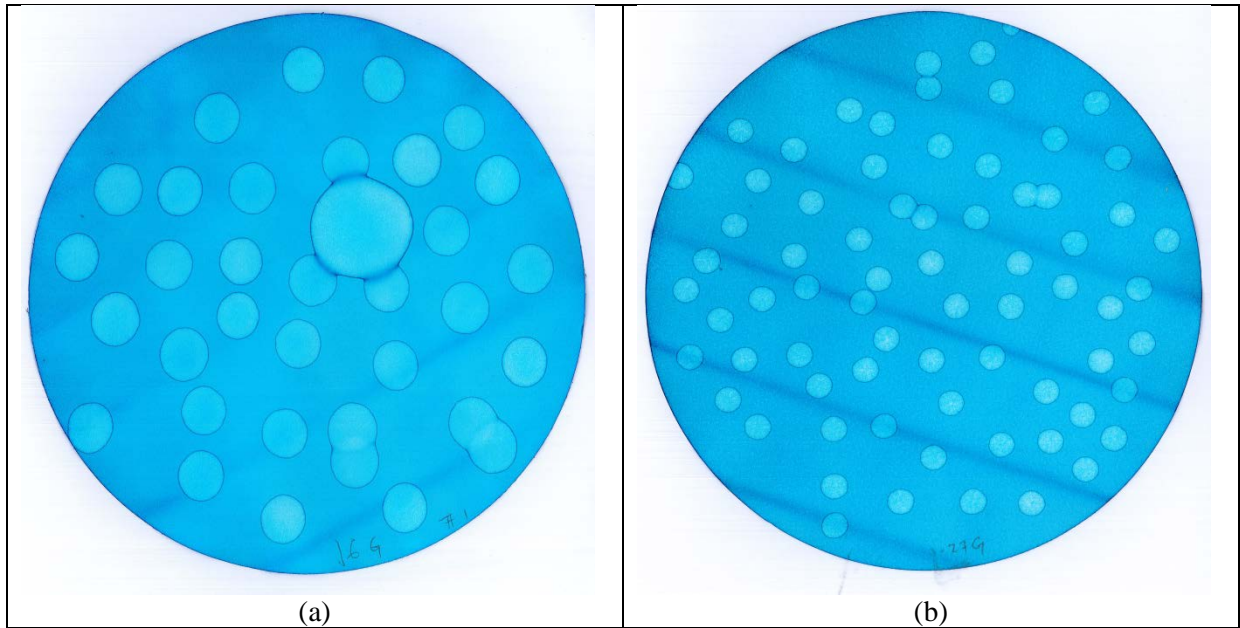
Figure 4-6. Drop stains on dyed filter paper for (a) 16G (largest) and (b) 27G (smallest) needle gauge. Filter papers were 185 mm in diameter. Note that large stains created by overlapping water drops were excluded from the analyses.

To determine the *volumes* of water drops from the needles, 15 mL polypropylene centrifuge tubes (Centristar^{TM}) were initially weighed dry (with cap) using a precision laboratory analytical balance (0.0001 g resolution). The tubes were then positioned 10 cm vertically beneath the needle tip and were each used to collect 25 water drops generated from each needle gauge. After recapping, they re-weighed to ascertain the mass of the 25 water drops collected. After subtracting the dry weight of the centrifuge tube, the difference in mass (giving the mass of water in the tube) was divided by 25 to determine the mass of an individual water drop. The count of 25 drops was used because of the increasing likelihood of experimental error after this number (e.g. pushing too hard on the syringe to generate a stream of water rather than drops or miscounting of total drop numbers) and to minimize evaporative losses from the tubes. For each needle gauge, 4 replicates of this experiment were conducted for a total of 100 water drops.

The water drop stained filter papers were scanned at 400 dpi (colour) using a Toshiba EStudio 555 multi-function machine (Toshiba Corp.). The acquired colour images in Tagged

Image Format (.tif) were prepared and analyzed using Image J software (National Institutes of Health, 2017). TIF format was used to maximize the retention of the original image details, being a lossless image compression format compared to the JPEG lossy image format. The *wand* (tracing) tool was used to identify the perimeter of the individual stains (using threshold setting of 30; 4-connected mode). The identified area for each stain was then flood-filled with black pixels to facilitate accurate image thresholding. The original colour images were converted to 8-bit black and white images, and then thresholded again so that the stains appeared as distinctive individual black silhouettes against a white background.

The *Analyze Particles* function was used to determine the area and circularity of individual stains; stain area would increase with drop size reflecting volumetric differences (Best, 1950; Hall, 1970; Kathiravelu et al., 2016). The measurements generated by Image J on the individual drop stains were transferred to Microsoft Excel for data processing. Statistical analyses of the data were performed using IBM SPSS Version 22. Independent sample t-tests were conducted to compare the means of drop stain area, circularity and roundness between different groups (needle gauges and later, leaf sizes and mature/juvenile *E. polyanthemos* leaf types).

Area of each stain was calculated automatically using the scale information in the Tagged Image Format (.tif) files. Image scale in pixels per unit area was determined using the Set Scale function in Image J.

Roundness of stain was expressed as a ratio between 0 (straight line) to 1 (perfect circle) determined by:

$4 \times [Area] / (\pi \times [Major\ axis]^2)$ where Major axis was the length of the primary axis (longest line) of the best fitting ellipse of the stain shape.

Following this, all data on drop stain areas (generated in Image J – *Analyze Particles* function) and drop masses were prepared in Microsoft Excel and then analyzed for standard descriptive statistics with linear regression analysis applied to quantify and evaluate the relationships between drop stain size and drop mass. Table 4-1 presents the summary statistics of the drop size areas and drop size mass experiments.

Table 4-1. Summary statistics of drop stains and drop mass experiments.

Parameter	Needle gauge sizes						
	27G	25G	23G	22G	21G	19G	16G
Mean mass per drop (mg) (n = 100)	5.368	6.407	9.064	11.408	12.535	16.903	22.309
Mean stain area in cm² (n = 50)	0.552	0.602	0.883	0.998	1.165	1.510	1.858
Standard deviation stain area	0.011	0.015	0.021	0.040	0.034	0.076	0.132
Mean roundness index of stain (0-1)	0.943	0.908	0.920	0.907	0.916	0.908	0.919
Standard deviation roundness index	0.018	0.018	0.013	0.021	0.020	0.016	0.020
Inferred mean individual drop diameter (mm)	2.172	2.304	2.587	2.797	2.882	3.184	3.492

Linear regression analysis between drop size area on the filter papers and measured drop mass showed a very strong linear relationship as seen in Figure 4-7.
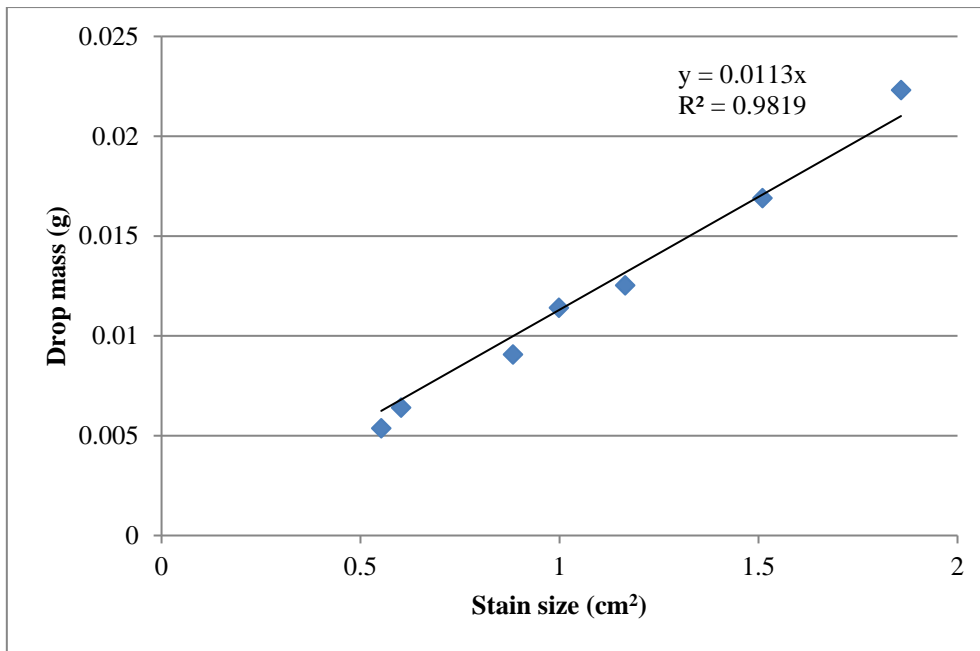
Figure 4-7. Scatterplot and linear regression between mean stain size and mean drop mass from different needle gauges.

Hence, drop mass could be predicted with a high degree of confidence from drop stain size on dyed filter paper using **Equation 1** with the regression equation with x and y intercepts set at zero:

$$y = 0.01131x$$

Where x is stain size in cm^2 and y is the drop mass, with $R^2 = 0.982$.

Drop diameter in millimetres was calculated using **Equation 2** (assuming water density at 1 g cm^{-3}):

$$D = 20 \ [3V.(4\pi)^{-1}]^{1/3}$$

Where D is the drop diameter, and V is the volume of individual water drop in cm^3; assumed to be equivalent to drop mass in grams.

The results of Experiment 1, from which Equations 1 and 2 were derived, provided sufficient confidence in the evaluated dyed filter-paper method to discern, through Experiment 2, drop size distributions from *Eucalyptus polyanthemos* juvenile and mature foliage, and open rainfall, the subject of the following section. The results of Experiment 1 showed that a reliable linear relationship could be derived between drop mass (and by inference, drop diameter), and stain sizes on standard Whatman No. 3 filter paper (185 mm diameter) impregnated with standard food dye. This technique used relatively low-cost and commonly available materials. While the dyed filter paper technique does not eliminate the problem of accurately measuring drop sizes during very heavy rainfall (Kathiravelu et al., 2016), it is amenable to executing many replicate attempts to measure drop sizes in such "difficult" conditions that could then eventuate in a small number of successful attempts to capture individual drop stains. For reference, Tokay and Short (1996) classified light intensity rain rates at < 2 mm hr^{-1}, moderate intensity from 2 to < 5 mm hr^{-1}, and high intensities (heavy) $\geq$ 5 mm hr^{-1}. Nevertheless, this method would yield more success for rainfall events at light to moderate intensities. Also, this method can be readily used to determine how well the drop size distributions of rainfall simulators represent those of natural rainfall events at varying rainfall intensities; where possible, drop arrival rates, another important pluviometric parameter, could also be reliably measured where the corresponding exposure duration are measured as well (Dunkerley, 2008b).

4.7.2. Drop size distributions from foliage and open-rainfall

With good confidence in results from the first experiment, I then proceeded to examine the drop sizes released from juvenile and mature leaves of *Eucalyptus polyanthemos* (Red Box); comparing drop spectra between these two types of leaves and then also comparing them with open-field rainfall.

4.7.2.1. Leaf samples

100 juvenile leaf samples were obtained at eye to chest level from *Eucalyptus polyanthemos* individuals in a patch of dry sclerophyll forest in Victoria, southeast Australia, north of the town of Licola, that was in the process of recovering from the Great Divide Wildfires in 2007 (Flinn et al., 2008a). 100 mature leaf samples in a similar way from unburnt *E. polyanthemos* individuals close to Licola town. From each pool of 100 samples, four leaves, representing the entire range (large to small) of the encountered leaf sizes were selected. Areas of juvenile leaves ranged from 9.8 to 35.6 cm^2, while for mature leaves the range was from 9.5 to 43.6 cm^2. Figure 4-8 presents images of the leaves used in the experiment. The leaves were used fresh with no applications to preserve them. Experiments were conducted within 48 hours of harvesting and no visible deterioration of leaf surfaces or edges were observed.
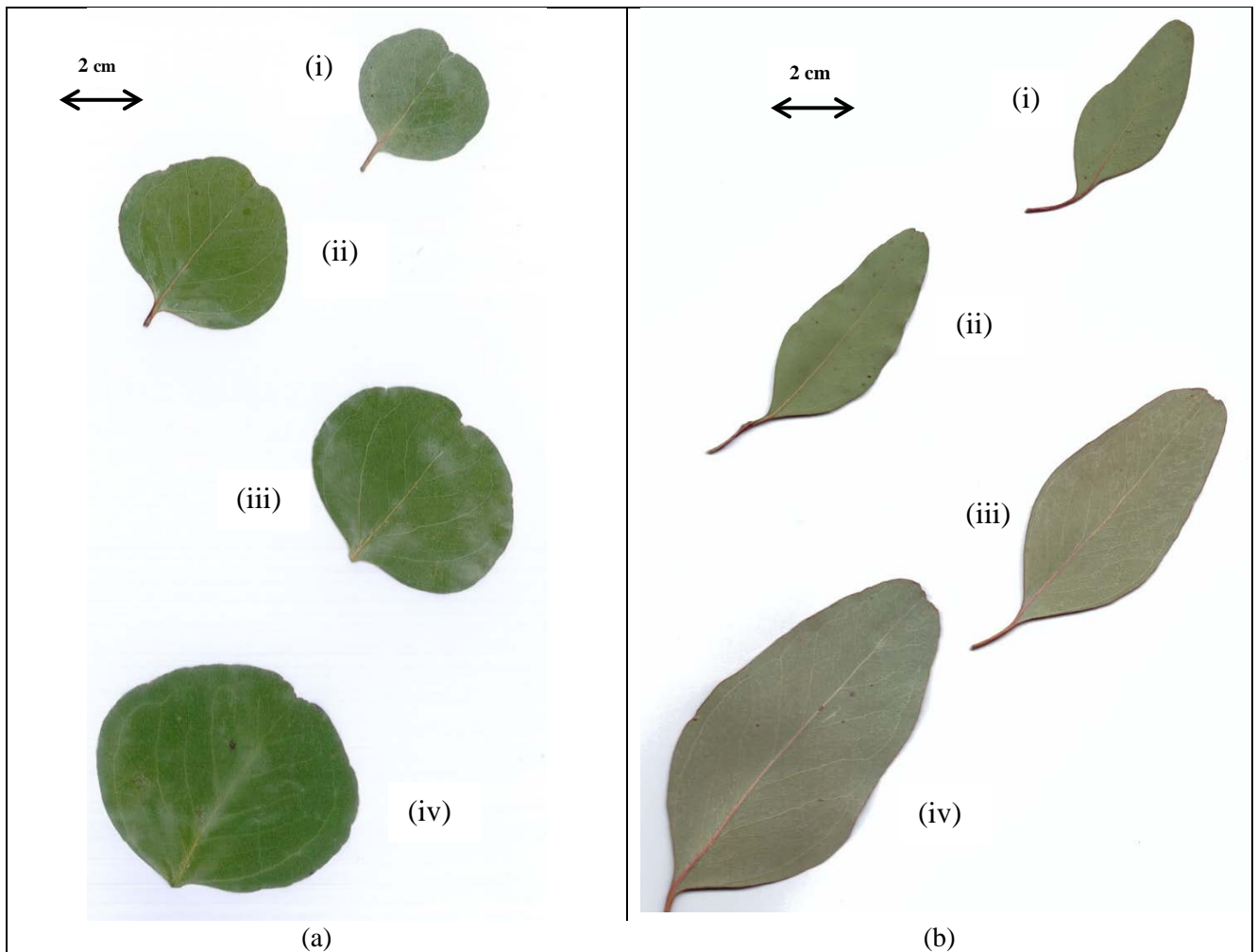
Figure 4-8. (a) Orbicular shaped **juvenile** leaves of *E. polyanthemos* used in the experiment. Leaf areas were: (i) 9.8, (ii) 17.0, (iii) 23.8 and (iv) 35.6 cm^2; (b) Broad ovate-lanceolate shaped **mature** leaves of *E. polyanthemos*. Leaf areas were (i) 9.5, (ii) 13.2, (iii) 23.4 and (iv) 43.6 cm^2. (Scale: Arrows are 2 cm across). Note the characteristic notched tips for this species, for both juvenile and mature specimens.

4.7.2.2. Foliage drop-generation and rainfall drops

Individual juvenile and mature leaves were positioned at a steep 70° hanging angle to replicate natural conditions of pendulous hanging habits of leaves observed in the field and reported in the literature (Bell and Williams, 1997; Brooker and Kleinig, 2006; Cerasoli et al., 2016; Crockford and Richardson, 1990a; Jacobs, 1955; King, 1997). Hanging angles were verified using a small hand-held clinometer prior to and after each experimentation run. No noticeable changes were found in leaf hanging angles after each experiment.

For each experimental run, mist spray was gently applied using a hand-spray bottle to a twig of either mature or juvenile leaves to saturate them and then allow drops to be released naturally from their surfaces. The dyed filter papers were positioned approximately 10 cm beneath the leaves and observed drip points to intercept drops that naturally detached from the foliage. A rigid plastic shield was used to minimize the direct deposition of mist spray onto the filter paper. To minimize overlapping of drop stains created, the filter paper was re-positioned constantly. Because of the diffuse nature of the mist spray, drops also developed on the apparatus. To avoid these erroneous drops, the appendages of the apparatus, e.g. clip and stalk holding the leaf, were tilted downwards and away from the leaf so that water drops would travel downwards and away from the filter paper. Care was also taken to ensure that the filter paper was positioned beneath the leaf to collect drops developed from it. Drop stains made in error were immediately marked with an "X" using a ballpoint pen and a fresh area selected for the remainder of the experiment.

For comparison with a nominal rainfall event drop size spectrum, open rainfall drop sizes were measured during a storm event on 16 Jun 2015 occurring over the Monash University Clayton Campus car park C11 open area (no obstructions from nearby buildings) using a standard passenger sedan car as a rain-shelter. Drop stains from a burst of heavy rainfall during the storm were also obtained opportunistically; this enabled the collection of

some stains from larger drop sizes associated with higher than average intensity rainfall. The dyed filter papers were exposed to falling rainfall drops for approximately 5 seconds at a time.

After exposure, the drop-stained filter papers were transferred indoors and air-dried lying flat on a wire rack for 48 hours. These were then scanned and digitally analysed using Image J software by the same method as described in section 4.7.1. Drop masses were inferred from drop stain area (in cm^2) using Equation 1, and equivalent drop diameters calculated using Equation 2 (cf. section 4.7.1.). It was noted that free-falling raindrops were encountered at a much higher velocity than those from syringes in the laboratory condition, and some splatter from larger raindrops creating minute stains on the filter paper occurred. The main drop stains from raindrops also created slightly scalloped boundaries. Nevertheless, in the absence of any perfect solution, these issues were mitigated by the high absorptive capacity of the filter paper (minimizing most splatter), and careful, minute adjustments to the calculated stain area were made to nominally account for areal loss due to splatter, enabling the same equations to be used for both laboratory experiments and free-falling raindrops. IBM SPSS™ Statistics 22 was used to describe and analyse the data using One-way ANOVA and related post-hoc tests where significant between-group (mature/juvenile leaves; leaf sizes) were found.

4.8. Hillslope material flux measurements

4.8.1. Sediment fence (SF) design and installations

To measure hillslope material fluxes caused by the erosional processes in these post-fire intermediate vegetation conditions, six 1.5 m wide sediment fences (SFs), adapted from the design of Robichaud and Brown (2002) (see Figure 4-9) were installed perpendicular to the main slope direction, approximately along the 340 m contour to trap downward moving hillslope sediment and organic litter. Two differences from the original design were made. Firstly, instead of using geotextile fabrics with a choice of different Apparent Opening Sizes (AOS) to allow water to flow through, acting as a sieve, I used Polyethylene builder's film (Grunt[TM]; extra heavy-duty; 200 µm thickness) to create a non-permeable surface for the deposition of eroded sediments. The main reason for this alternative was the dominance of fine silt-sized sediments in the study area's soil texture derived from the mud and siltstone parent material composing much of the local and regional geology (see section 3.2). Most of these fine sediments would have escaped through the comparatively large opening sizes described by (Robichaud and Brown, 2002) of which the finest aperture diameter was 0.177 mm.

The builder's film was then reinforced by a layer of porous HDPE UV stabilized shadecloth behind and below it. Secondly, iron pickets rather than wooden stakes were used as installation posts. These were driven through the shallow soil and into the underlying rocks to create a firm upright structure to support the film, shadecloth and the deposited sediments. Nylon UV-resistant cable ties were used to secure the film and shadecloth to the iron pickets. Earlier attempts using wooden stakes had failed to establish any proper foothold in the shallow soil and rocks.

Plate 4-4 shows one of the SFs installed at the study site. While six SFs may appear to be a rather small sample size, because of the rugged terrain preventing proper installation at

many positions, and the intensity of resources needed for the fieldwork, six was considered to be an appropriate number of installations to be managed by a single field worker, alongside the other measurements of rainfall, throughfall and canopy cover described above. Similarly, Vieira et al. (2016) installed four microplots per condition to monitor runoff and sediment losses when comparing long-term post-fire erosion processes of ploughed and unploughed sites in eucalypt plantations.
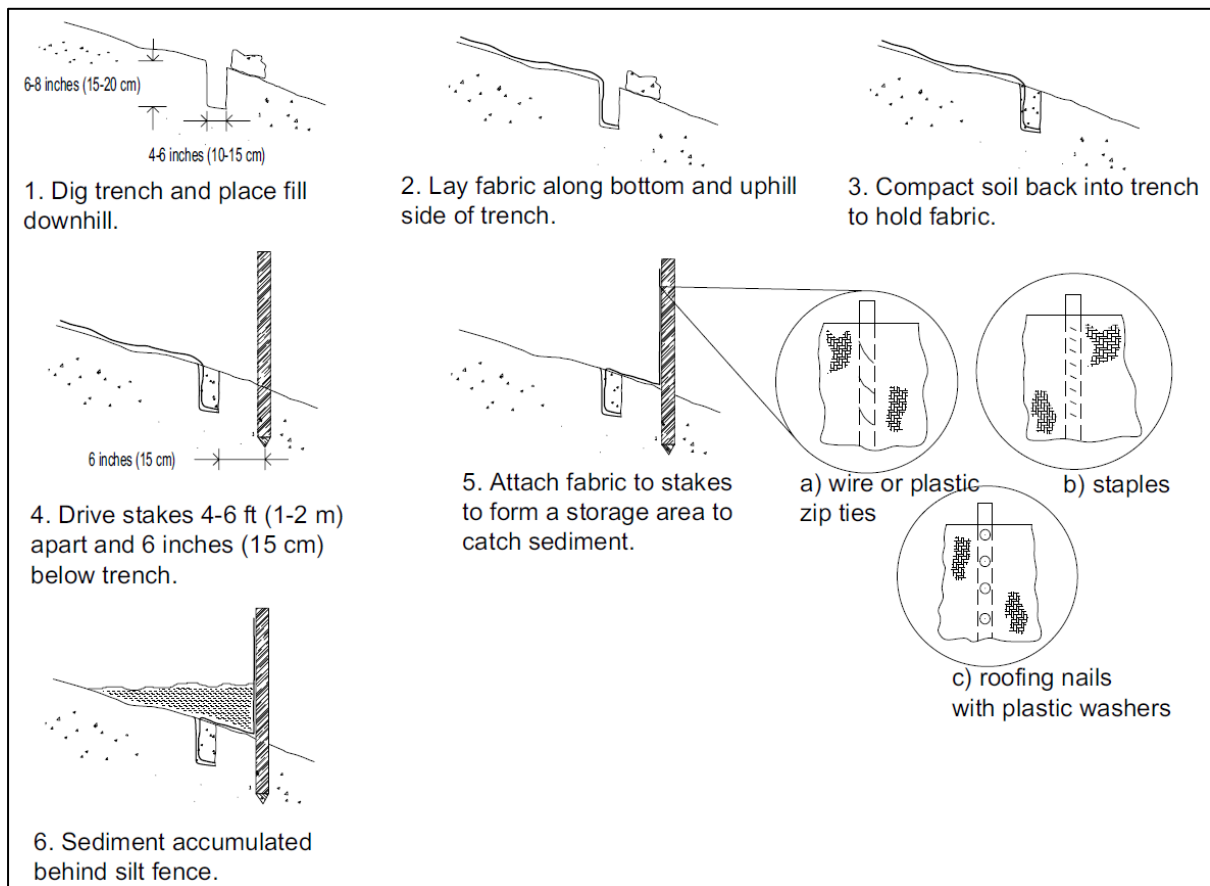
Figure 4-9. Steps for installing silt fence (termed 'sediment fence' – SF in the present work). Source: Robichaud and Brown (2002).

Plate 4-4. Sediment fence (#1) installed at the study site. Width of collecting area was 1.5 m. The large rocks seen on the left of the image were used to weigh-down the black impermeable sheet to maintain a relatively flat and smooth surface flush with the thin, rocky soil surface.

Earlier initial attempts to install 3 m width fences in Nov-Dec 2011 were unsuccessful because of the rugged terrain and thin, rocky soils that hindered the establishment of sufficiently smooth collection surfaces acceptably flush with the existing soil surface. Under intermediate post-fire recovery, there was significant growth of canopy cover but it was incomplete and variable, creating a high-degree of heterogeneity. Ground-level soil surface conditions were also heterogeneous, with distinct patches (of variable area) of bare and exposed soil, sometimes rocky areas with variable amounts of litter and post-fire debris scattered around. The six sediment fences were installed in positions that represented the range of different ground cover, vegetation and slope angles observed at the study area that were likely to exhibit different factors, hydrological and erosional process operations, and soil erosion outcomes (Table 4-2). The layout of the SFs was presented in Figure 4-1.

Table 4-2. Sediment Fence (SF) descriptions

SF No.	Gradient	Distance from tree (m)	% exposed soil surface	Description
1	16.1°	4.9	85	Minimal ground contact cover; small amounts of twigs and leaf litter; fallen log upslope; Small regrowth of *Acacia verniciflua* of 15-30 cm tall. Large substantial regrowth of *Eucalyptus polyanthemos* approx. 5 m upslope of fence.
2	18.2°	2.5	70	Rill observed upslope of fence; noticeable leaf litter and regrowth *Acacia verniciflua* up to 60 cm tall.
3	25.3°	1.5	80	On open, steep, and bare (~75%) site with minimal ground plant re-growth or litter cover within 3m of fence except for recovering *Eucalyptus polyanthemos* tree 1.5 m upslope.
4	30.7°	15.5	95	On very open, steep, stony and bare site (~90%) with minimal plant re-growth or litter cover within 5 m of the fence.
5	16.6°	3.0	30	Dense canopy, sheltered area with mix of *Eucalyptus polyanthemos*, *Acacia verniciflua and Eucalyptus macrorhyncha*. Substantial amounts of plant litter, gravel and charcoal on ground surface (~70%) – rough ground surface to fence with minimal live ground cover.
6	20.1°	1.5	40	On steep, moderately bare patch with some *Acacia verniciflua* up to 60cm tall. Substantial postfire regrowth of *Eucalyptus polyanthemos* tree just 1.5 m upslope of fence.

At the end of each measurement period, all the trapped sediment and organic litter were collected from the 6 sediment fences using a Nyglass trowel and stored in resealable plastic bags for secure transport back to the Monash University Soils Research Laboratory. The collected material from each sediment fence were transferred to aluminum foil pans and allowed to air-dry at ambient room conditions or, where required in cases where excessive water had been collected together with the fine sediments, dried at elevated air temperature of 40 °C until sufficient moisture had evaporated. The material was first dry-sieved using a two mm Endecotts™ stainless steel woven wire laboratory test sieve (Endecotts, n.d.) to separate the soil (fine earth fraction) from gravel and larger-sized organic litter such as leaves, twigs and large organic fragments. The organic litter was then carefully separated from both the gravel and soil components by hand, and for finer fragments, using tweezers. The soil component was then oven-dried to remove any remaining water. Soil, gravel and litter components were weighed separately using a precision laboratory balance to the nearest 10 mg.

The soil component of eroded sediment collected from each sediment fence was subsampled for particle size analysis (PSA). A 10 g subsample was obtained from the sieved and oven-dried primary sample and placed in a 250 mL capacity glass beaker. 100 mL of sodium hexametaphosphate (*Calgon*™) was added to the sample. The soil-dispersant mixture was heated to and maintained at 95 °C and stirred regularly for 45 minutes before removing from heat and left to cool overnight. The mixture was then poured out and sieved through a 1000 μm laboratory sieve. De-ionised water was used for the wet sieving. Particles >1000 μm and <2000 μm were retained and oven-dried on small aluminum foil trays for weighing of the coarse sand fraction. The sieved mixture containing particles ≤1000 μm was then agitated for re-suspension in a glass beaker using a magnetic stirrer. A small pipette was used to obtain a

subsample of the suspension for PSA using the Beckman-Coulter LS 200™ laser particle size analyzer (http://www.beckmancoulter.com). The system provided data on particle size distribution of the subsample of all particles ≤1000 μm based on laser diffraction (Eshel et al., 2004). This data was used to build the particle size distribution characteristics of each individual soil sample from each SF between 0 and 2000 μm (i.e. fine earth fraction). Sediment size limits for sand, silt and clay followed the World Reference Base (WRB) system (IUSS Working Group WRB, 2015).

4.9. Measurement periods

Data was collected between 8 Feb to 5 Dec 2012. There were 6 periods within this period where hillslope sediment and organic material flux (section 4.8.) were measured simultaneously with rainfall (section 4.3.), canopy cover (section 4.4.), throughfall fraction (section 4.5.) and erosivity (section 4.6.). This was done to enable the exploration of possible relationships between the various factors (canopy cover, rainfall event characteristics, SF characteristics) with the outcomes (throughfall fraction, throughfall erosivity, erosion of hillslope sediment and litter). The dates of data collection were primarily determined by the likely occurrence of significant rainfall events in the preceding time since the last data collection to ensure that substantial rainfall, throughfall, splash and downslope erosion transport could be clearly detected and measured by the various instruments. These also had to be non-rain days so as not to interfere with the operation of the processes of interest (rainfall, throughfall, hillslope erosion processes), and for safety reasons in the remote location and rugged terrain. The measurement periods were (Table 4-3):

Table 4-3. Measurement periods for simultaneous measurement of rainfall, throughfall (fraction and erosivity) and hillslope material flux.

Period	From	To	Days	Season(s)
A	8-Feb	2-Mar	22	Summer
B	3-Mar	27-Apr	55	Autumn
C	28-Apr	27-Jun	60	Late autumn to winter
D	28-Jun	7-Aug	40	Winter
E	8-Aug	5-Oct	58	Late winter to spring
F	6-Oct	5-Dec	60	Late spring to early summer

In the following chapters, the results and analyses of rainfall, throughfall fraction, throughfall erosivity and hillslope material flux will be presented.

CHAPTER FIVE: RAINFALL

In this chapter, I present the results and analyses of the rainfall received at the study site. Firstly, I describe the main aspects of rainfall for the 10-month measurement period in the context of the entire year (2012). Based on the *primitive event* definition of 1 mm minimum depth, and 60 minute minimum inter-event time (Haile et al., 2010) (see also Chapter 4), I present statistics for the 106 primitive rainfall events identified for the measurement period in the forms of event depth, duration, intra-event intensities at various integration durations (e.g. 5, 10, 15 minutes), as well as event energy. Secondly, I examine the rainfall statistics for the individual measurement periods, labelled A to F. Because of the differences between periods in the rainfall event characteristics (depth, duration, intensity, erosivity) and the inter-event temporal distribution, each period served as specific, distinct "treatments" applied to the study site.

Thirdly, I present the results of the exploratory analysis of one-minute intra-event rainfall-intensities in each of the periods. Here, the one-minute intensities are also examined in the context of individual primitive events, specifically focusing on the 5 mm h^{-1} intensity as the threshold rain rate between light rain from stratiform clouds and moderate to heavy rain from cumuliform clouds. As demonstrated by Tokay and Short (1996), high-temporal resolution of one-minute integration times enable physically-relevant proxy insights into the cloud microphysical processes that result in the stratiform/cumuliform sources, their accompanying drop-size distributions (DSDs) and drop arrival rates; all of which would strongly influence canopy processes (e.g. interception, evaporation and throughfall), as well as hillslope hydrologic and erosional processes (Dunkerley, 2008b). Furthermore, modern optical disdrometers measure raindrop diameters in single 'raining minute[s]' (Carollo et al., 2018) and so one-minute intensities present congruent temporal bases for comparison of "traditional" rainfall metrics with data derived from more high-precision, technologically-

advanced techniques. These analyses have been done to develop insights into the rainfall features that could help to explain possible non-linear throughfall and hillslope erosional responses presented in Chapters 6 and 7.

Lastly, I discuss the results of the rainfall analyses, casting them as the key, albeit complex factor driving post-fire hydrology and erosion under intermediate conditions. The stage is then set for examining the processes and outcomes of interest: throughfall and hillslope erosion, in Chapters 6 and 7 respectively.

5.1. General patterns

The total annual rainfall depth for the study area in 2012 was 916.2 mm. This was significantly "wetter" than the mean annual rainfall of 802 mm (median 845 mm) for the years 2003 to 2013 (Bureau of Meteorology, 2017c; Queensland Government, 2017). For the field study period (8 Feb to 5 Dec 2012), onsite rainfall data was collected using a tipping-bucket pluviometer (details in Chapter 4). The entire field measurement duration was subdivided into six measurement time periods (A to F) during which throughfall and hillslope erosion data were simultaneously obtained. The total rainfall depth during these ten months was 738.9 mm, with primitive events (Haile et al., 2010) contributing 683.3 mm (92.5% of total study period rainfall). Figure 5-1 shows the mean monthly rainfall for the study area. The data was from Bureau of Meteorology (2017c) and DELWP (2016) for Licola station, and would not completely correspond with the study site's rainfall records. On average, slight higher rainfall is received in the winter months (Jun – Aug) compared to spring (Sep – Nov) the second-wettest season, and distinctly higher than summer (Dec – Feb) and autumn (Mar – Apr). It is worthwhile to highlight that the decade leading up to the occurrence of the 2006/7 bushfires that affected the area extensively, was during the Millennium Drought period of 1997 to 2009 (van Dijk et al., 2013) which saw 512 mm average annual rainfall (CSIRO, 2010; CSIRO, 2012); far below the long-term average of 802 mm. However, above-average rainfall occurred from 2010 to 2012, and this was attributed to La Niña conditions which brought eastern and southeast Australia out of the El Niño conditions and broke the drought (Bureau of Meteorology, 2015).

Figure 5-2 compares monthly rainfall distribution for 2006 (drought and bushfire year) (Flinn et al., 2008a), 2012 (data collection year) and the average monthly rainfall calculated from the 2003 to 2013 data. The significant departures of monthly and annual rainfall depths from the ten-year mean demonstrate how this region is subjected to significant variations in

rainfall amounts and distribution on a year to year basis, to give high frequencies of high wildfire risks and occurrences in drier years, interspersed with wetter years that encourage rapid plant growth, biomass increases and consequently accumulation of fuels that enhances fire risks when the climate swings to warmer and drier conditions. This observed oscillation between multiple wet and dry years is a likely contributor to the region's high susceptibility to wildfires, as well as to inter-annual variations in hydrologic and erosional responses to the total rainfall depth and accompanying rainfall event characteristics.
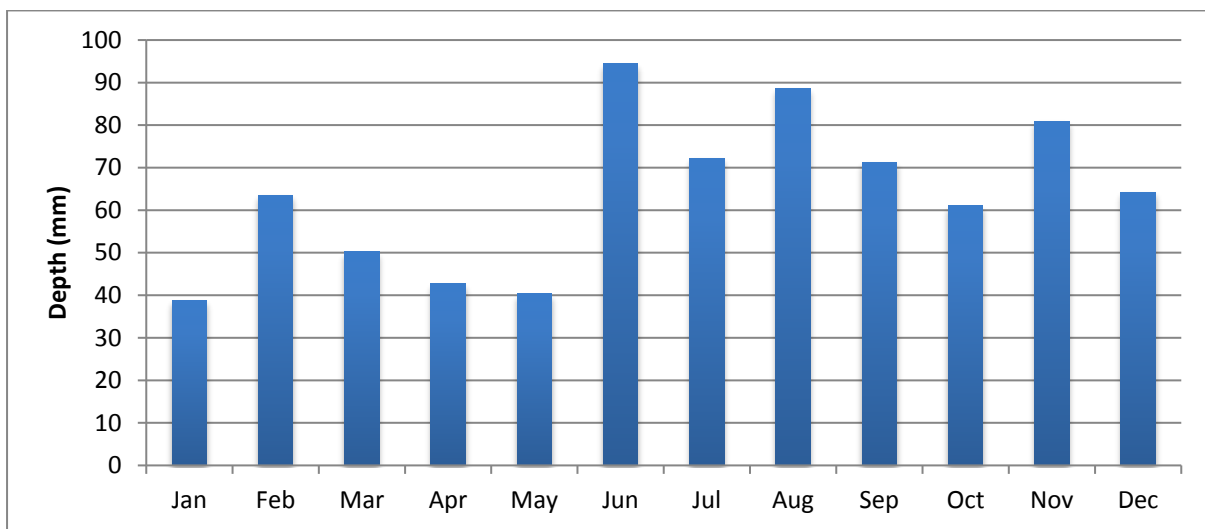
Figure 5-1. Mean monthly rainfall for the study area for the years 2003 to 2013. Data sources: Bureau of Meteorology (2017c) and DELWP (2016).
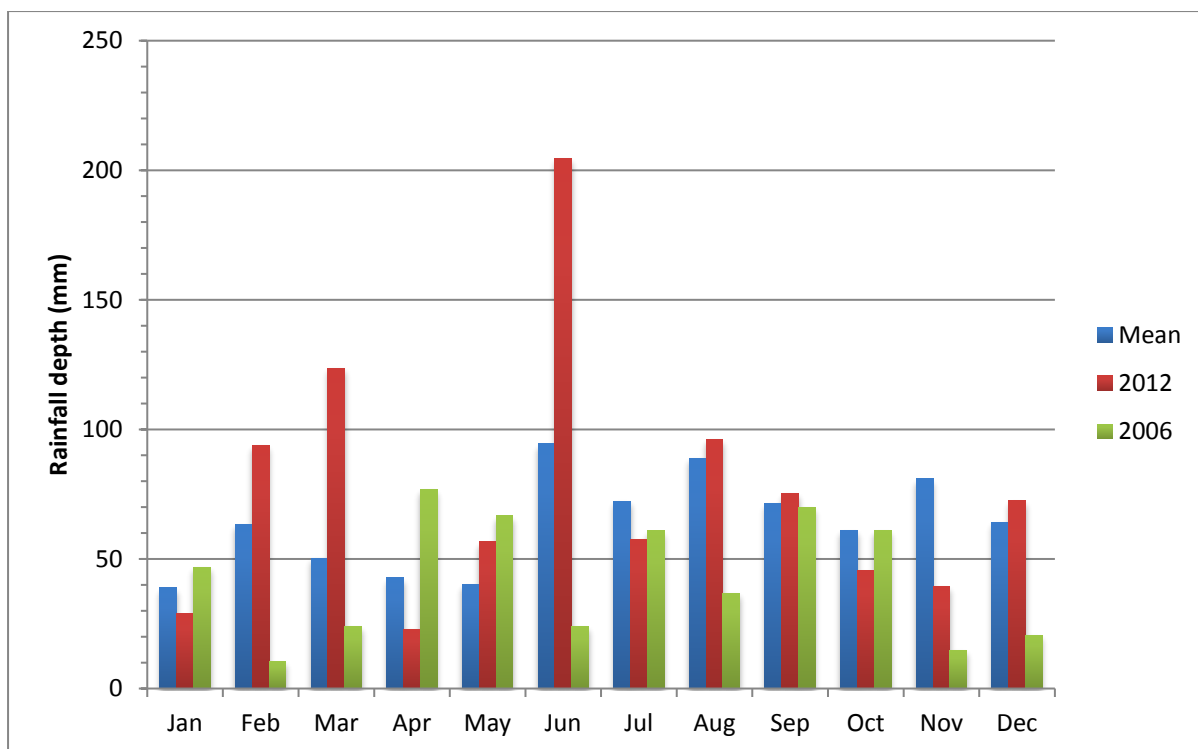
Figure 5-2. Comparison of mean monthly rainfall for 2006 (green; wildfire year), 2012 (red; study year; intermediate conditions) and mean (blue) for the decade 2003 to 2013. Data sources: Bureau of Meteorology (2017c) and DELWP (2016).

The below-average rainfall in 2006, preceded by multiple years of drought would have exacerbated the significant water deficiency stress on the vegetation in the study region, and also contributed to extensive curing and accumulation of litter and other above-ground fuel for the severe bushfires that eventually burnt through the area in Dec 2006 to Jan 2007 (Flinn et al., 2008a). With higher than average rainfall received in 2007 by a bare, burnt-out landscape, massive rates of erosion and multiple debris flows occurred (see Chapter 3), extensively altering soil conditions with intense stripping away of upper soil horizons and their translocation to the bases of hillslopes, or loss to the riverine system (Wellington River and downstream). 2012 was a particularly wet year with 900.8 mm total rainfall depth. In contrast, 2008 and 2009 saw 601.2 mm (lowest annual depth of station records excluding 2006) and 664.4 mm respectively. Although less rain is likely to fall during an extended drought period, the hydrologic and erosional significance of rather moderate rainfall depths

226

could be amplified due to the high post-fire vulnerability of the bare, exposed soils to rapid runoff generation and erosion (Prosser and Williams, 1998), and would have led to the significant erosion events across large parts of the catchment as reported by Australian Associated Press (2007), Houghton (2007) and (Department of Sustainability and Environment and Parks Victoria, 2010), and described in Chapter 3. With depleted soil moisture storage capacity and fertility of the now skeletal soils, these conditions would also have delayed vegetation recovery and extended the "window of disturbance" (Chapter 1; Figure 1-5c) even though more water may have been supplied to the system in the ensuing years. However, 2010 and 2011 were wetter with 887.0 mm and 894.4 mm total rainfall depths respectively and would have had significantly higher hydrologic and erosional impacts than in the previous years.

In total, 106 primitive events were recorded for the study period. Table 5-1 shows the main rainfall statistics for all the primitive events, together with intra-event rainfall intensity values at different integration-time resolutions (I_{5-60}). Note that event energy was derived from RUSLE-based calculations and presented as an area-specific unit (MJ ha^{-1}). Rainfall erosivity (R) (as shown in Table 5-2) is a compound factor presented as a rainfall depth-intensity and area-specific unit (MJ*mm ha^{-1} hr^{-1}) (Gonzalez-Bonorino and Osterkamp, 2004; McGregor et al., 1995; Renard et al., 1997; Risal, 2016; Salles et al., 2000; Wischmeier and Smith, 1978).

Table 5-1. Rainfall event statistics for all primitive events (N = 106) and intra-event intensities ($I_{5\,min}$, $I_{10\,min}$, $I_{15\,min}$, $I_{20\,min}$, $I_{30\,min}$ and $I_{60\,min}$).

	Depth (mm)	Duration (hr)	I_5	I_{10}	I_{15}	I_{20}	I_{30}	I_{60}	Event Energy (MJ ha^{-1})
					(mm hr^{-1})				
Mean	6.3	3.4	8.4	6.2	5.2	4.5	3.7	2.6	0.9
Median	2.6	1.9	5.4	4.5	3.8	3.4	3.0	1.8	0.3
Max	109.0	31.9	98.4	69.6	56.8	46.8	35.6	21.8	17.3
Min	1.0	0.3	2.4	1.2	0.8	0.6	0.4	0.4	0.1
s.d.	12.5	4.5	11.0	7.7	6.2	5.2	4.0	2.7	2.0

There were wide variations in rainfall event depth, duration and energy values. However, the distributions of these values were strongly positively skewed as indicated by the median compared to the mean values. These show the dominance of "small" rainfall depth events; for instance, the mean rainfall event depth was 6.3 mm while the median was 2.6 mm. As integration durations of rainfall intensity increased from 5 through to 60 minutes, the mean, median, maximum, minimum and standard deviation values decreased. These were likely to be due to the averaging effect on higher-intensity "pulses" within the event by the more abundant lower rainfall intensity episodes.

5.2. Individual measurement periods (A to F)

Figure 5-3 presents the depth-duration values for all rainfall events for periods A to F. Period C, followed by Period A looked to have the greatest and second-greatest significance in terms of erosional impacts. Period C had the largest event depth (109.0 mm) and longest duration (31.94 hrs). Period C also recorded the second-longest event at 23.04 hrs with a rather large 23.4 mm depth. Two large events during Period A were notable; one with 42.6 mm depth and 21.73 hrs duration; the other with 36.4 mm depth and 6.66 hrs duration. Numerically, small short-duration events dominated the dataset, shown in the clustering of values on the lower ranges of both axes, indicating how the strong positive skew in the distribution of rainfall values were present in all the individual periods.

The key rainfall statistics for the six measurement periods A to F (refer to Table 4-3 for start/end dates and durations) are shown in Table 5-2. Rainfall statistics for each period differed substantially from one another, and thus constituted a range of distinct "treatments" that caused the varying outcomes for throughfall fraction, throughfall erosivity and sediment fence results presented in the following chapters. Notably, Kampf et al. (2016) demonstrated and emphasized the importance of rainfall intensities in driving erosion and geomorphic change across scales within a catchment, and this research has worked to examine the

impacts of widely varying natural rainfall events rather than using highly-controlled simulated rainfall experiments.
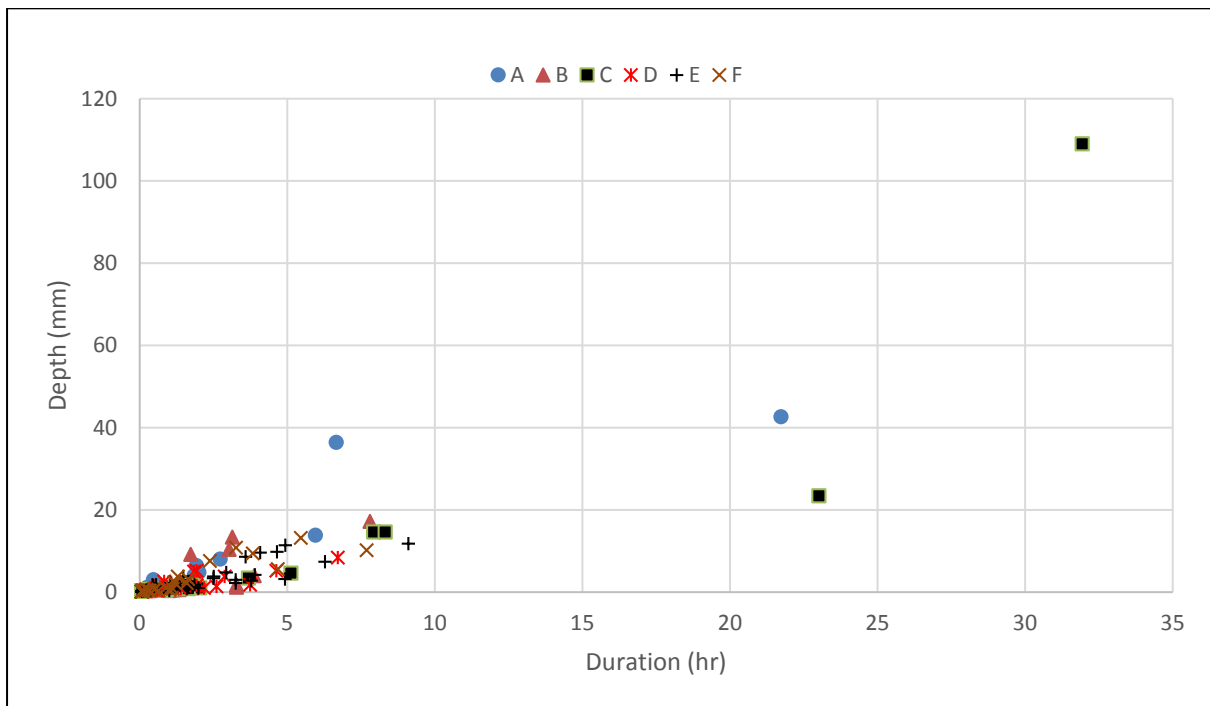
Figure 5-3. Scatterplot of Depth-duration values for all events, categorized by Periods A to F.

Table 5-2. Rainfall statistics for the measurement periods A to F in 2012.

Period	Total Depth (mm)	No. Primitive Events	Total Primitive Event Depth (mm) (% of total depth)	Max. Event Depth (mm)	Mean Event Depth (mm)	s.d. Event Depth	Mean Event Duration (hr)	Mean Event Intensity (mm hr^{-1})	Mean Event Energy (MJ ha^{-1})	Total Event Energy (MJ ha^{-1})	Mean Erosivity (MJ*mm ha^{-1} hr^{-1})	Total Erosivity (MJ*mm ha^{-1} hr^{-1})	Mean Inter-Event Time (hr)
A	128.2	11	123.6 (96.4)	42.6	11.2	14.5	4.2	3.1	1.8	19.7	31.2	343.7	44.4
B	89.5	23	76.5 (85.5)	18.0	3.3	4.7	1.5	2.7	0.5	10.8	5.6	128.5	54.2
C	218.0	17	206.0 (94.5)	109.0	12.1	26.8	5.1	2.6	2.3	38.6	24.2	411.0	77.4
D	80.8	13	79.4 (98.2)	8.5	3.3	2.5	1.5	3.3	0.4	5.2	10.2	132.8	80.2
E	125.4	28	110.8 (88.4)	11.8	4.0	3.3	2.7	1.7	0.5	13.3	1.8	50.0	44.5
F	97.0	14	87.0 (89.7)	18.0	6.2	5.9	1.9	4.2	0.9	12.7	8.2	114.6	105.0

Total rainfall depth for each period varied markedly from one another, and so did other key statistics such as total energy, mean erosivity and total erosivity. For mean inter-event time (IET), values for Periods A, B and E were markedly lower than those for Periods C, D and F, indicating higher event occurrence frequency of the former group compared to the latter. Nominally, Periods A, B and E could be classified as high event frequency periods, Period C and D as moderate event frequency periods, and F as low event frequency periods. The dominance of primitive events increased as total depth increased. The periods with high dominance of primitive events were A (96.4%), C (94.5% and D (98.2%). On the other hand, periods with relatively lower dominance of primitive events were B (85.5%), E (88.4%) and F (89.7%) – indicating more rain from smaller "sub-primitive" events.

Periods A and C saw the highest total rainfall depth of 123.6 mm and 206.0 mm from primitive events respectively. They also stood out with highest mean event erosivity of 31.2 and 24.2 MJ*mm ha^{-1} hr^{-1} respectively. Associated with these were significantly higher total erosivity values of 343.7 and 411.0 MJ*mm ha^{-1} hr^{-1}. However, mean IET differed substantially between Periods A and C at 44.4 and 77.4 hrs respectively. Period E, in contrast, had the lowest mean erosivity (1.8 MJ*mm ha^{-1} hr^{-1}) and total erosivity (50 MJ*mm ha^{-1} hr^{-1}). Mean inter-event time was 44.5 hrs and almost the same as that for Period A.

Period D, with only 13 primitive events recorded, had the second lowest total primitive rainfall depth (79.4 mm) with joint-lowest mean event depth (3.3 mm) and associated with this were the lowest mean event energy (0.4 MJ ha^{-1}) and total energy (5.2 MJ ha^{-1}). However, Period D also had the third-highest total erosivity (132.8 MJ*mm ha^{-1} hr^{-1}) and mean erosivity (10.2 MJ*mm ha^{-1} hr^{-1}). While having the lowest mean event energy (0.4 MJ ha^{-1}), it had the second-highest mean event intensity (3.3 mm/hr^{-1}).

Period E had 28 primitive events, the highest amongst the other periods with a moderately high total depth of 110.8 mm, but had the lowest average mean event intensity

(1.7 mm h^{-1}), mean erosivity (1.8 MJ*mm ha^{-1} hr^{-1}) and total erosivity (50 MJ*mm ha^{-1} hr^{-1}) even though it showed moderate mean event duration of 2.7 mm and total energy of 13.3 MJ ha^{-1}).

Period F had the longest mean IET of 105 hrs and relatively low total rainfall depth from primitive events of 87.0 mm. Mean event erosivity was moderately high at 8.2 MJ*mm ha^{-1} hr^{-1} compared to Periods D and E, indicating the high erosive energy of many of the individual rainfall events during this relatively dry period. Total erosivity was therefore high at 114.6 MJ*mm ha^{-1} hr^{-1}.

5.3. One-minute rainfall intensity thresholds

To enable the examination of rainfall events at high temporal resolution, all the identified primitive events in each period (A to F) were disaggregated into one-minute rainfall intensities, also called *intra-event rain rates* (Dunkerley, 2008b; Dunkerley, 2010b). The number of minutes at or above a particular set threshold rainfall intensities were then summed. The 5 mm hr^{-1} intensity was selected as the threshold because of its relevance as a proxy for the cloudforms (convective or stratiform) responsible for the rainfall, and the consequent implications for the interception of rainfall by vegetation cover, hydrologic processes and erosional impacts. As discussed in Chapters 3 and 4, the meteorological mechanisms for rainfall associated with different seasons and periods of the year over southeast Australia can be quite distinct, resulting in rainfall events (and sequences) of certain characteristics, and thus varying hydrologic and erosional impacts on intermediate post-fire hillslopes. Tokay and Short (1996) demonstrated that stratiform-regime type rainfall was mostly light to moderate with rain rates up to 5 mm hr^{-1}; whereas convective-regime type rainfall was heavy to extreme with rain rates of more than 5 mm hr^{-1}. Although this approach effectively filtered-out many low rain rate components of the rainfall events, this importantly enabled the distillation of specific intra-event episodes during which relatively higher

intensities, with the potential ability to exert higher-order hydrologic and erosional impacts. Their possible impacts could then be further explored. The statistics for one-minute rainfall intensity thresholds of 5, 10, 15, 20, 30 and 40 mm hr^{-1} are presented in Table 5-3.

Table 5-3. Number of minutes (N) above threshold intra-event intensities of 5, 10, 15, 20, 30 and 40 mm hr^{-1} .

Period	N ≥ 5 mm hr^{-1}	N ≥ 10 mm hr^{-1}	N ≥ 15 mm hr^{-1}	N ≥ 20 mm hr^{-1}	N ≥ 30 mm hr^{-1}	N ≥ 40 mm hr^{-1}
A	329	122	47	22	16	10
B	186	78	39	20	10	2
C	520	140	34	3	0	0
D	65	24	6	2	1	1
E	183	56	8	3	1	0
F	177	54	20	9	4	1

Each of the periods had varying numbers of minutes at the different threshold intensities. Period A had the highest number of very high-intensity minutes, with 22, 16 and 10 minutes at and beyond 20, 30 and 40 mm hr^{-1} respectively. Period B, although having lowest total rainfall depth (76.5 mm from primitive events; Table 5-2), had more high-intensity minutes; 20, 10 and 2 minutes at 20, 30 and 40 mm hr^{-1} levels. Period C, on the other hand, had the highest rainfall depth (206 mm total from primitive events) and 520, 140 and 34 minutes at 5, 10 and 15 mm hr^{-1} threshold rainfall intensities but zero minutes at the 30 and 40 mm hr^{-1} levels. Period D was largely characterized by low-intensity rainfall (only 65 minutes at or above 5 mm/hr) but had only one minute above 40 mm hr^{-1} rainfall intensity. Period E tended towards low-moderate values with only 8 and 3 minutes of rainfall at or above 15 and 20 mm hr^{-1} intensities respectively. Period F, in comparison, had moderate rainfall intensity distributions with 20, 9 and 4 minutes at or above 15, 20 and 30 mm hr^{-1} rainfall intensities. These threshold rainfall intensity-durations will be examined later in terms of their influences on hillslope material flux.

The one-minute rainfall intensity dataset was also examined for intra-event rainfall intensities of ≥ 5 mm hr^{-1}, for all primitive events. The number of minutes that met this

threshold criterion were counted, and then expressed as a percentage of the entire duration of each primitive event to gauge the extent of their occurrence and influence. Overall, it was found that 62.3% (66 events) of the 106 primitive events had at least one minute of rainfall intensity at ≥ 5 mm hr^{-1}. The mean percentage composition of event occupied by ≥ 5 mm hr^{-1} was 10.0% while the median percentage was 5.8%. Minimum percentage was 0.5% while maximum percentage was 50%. Standard deviation of the values was 10.0. In terms of the numbers of events that had at least one-minute of rainfall intensity ≥ 5 mm hr^{-1}, the count by Periods was: **A**: 9; **B:** 16; **C**: 6; **D**: 7; **E**: 17 and **F**: 11.

In addition to the selected primitive events that contained one-minute rainfall intensities of ≥ 5 mm hr^{-1}, the analysis also found 8 sub-primitive events (rainfall events that failed to meet the 1 mm depth and 60 minute minimum inter-event duration criteria) that nonetheless contained at least one-minute of rainfall intensities ≥ 5 mm hr^{-1}. The details of the individual events are presented in Table 5-4.

Table 5-4. List of sub-primitive events that had at least one-minute of rainfall with intensity $\geq$ 5 mm hr^{-1}.

Event date in 2012 (Period A to F)	Depth (mm)	Duration (minutes)	One-minute intensity value(s) (mm hr^{-1})	Comments
3 Mar (B)	0.4	5	14.4	
6 Apr (B)	0.8	7	14.4, 6 and 18	In consecutive minutes
26 Jul (D)	0.4	5	14.4	
18 Aug (E)	0.4	5	14.4	
22 Aug (E)	0.6	5	14.4	
13 Sep (E)	0.8	13	14.4	
8 Nov (F)	0.6	7	6, 6	In consecutive minutes
19 Nov (F)	0.4	5	14.4	

It was notable that these high-intensity sub-primitive events occurred only in Periods B, D, E and F. While most of these "bursts" were recorded in single minutes, two of the sub-

primitive events (Period B, 6 Apr and Period F, 8 Nov) showed consecutive minutes of high-intensity rainfall with the former displaying notably high intensities.

5.4. Temporal distribution

5.4.1. Multiple intra-day occurrences

The temporal distribution of events and event depths for Periods A to F is presented in Figure 5-4 (A-F) with the individual primitive events occurring within the same day distinguished from one another. Some rain days recorded up to four primitive events. Wilks (2006) explained that the occurrence of precipitation events display 'persistence' or 'positive serial dependence' (p. 15) to a particular limit; a key feature of the nature of episodic atmospheric events. In the present case of precipitation, the passage of fronts over a specific region on the ground over two to three days bring a series of discrete but causally-connected rainfall events. Alternatively, during summer months, several discrete "showers" could occur within a day with the development of convection-related thunderstorms that usually occur in the late-afternoon and early evening hours, although these may be quite spatially-limited and not register accurately on pluviometer records. This indicates that attributing hydrologic and erosional outcomes to a single coarse measurement such as daily rainfall depth may not necessarily be sufficiently meaningful because the hydrologic and erosional processes (and intermediate plant canopy rainfall interception, partitioning and modulation processes) set into operation by a series of short-duration bursts of rainfall compared to an extended session of lower-intensity rainfall for a similar depth of rainfall, are likely to differ substantially (Kampf et al., 2016).

Periods A and D did not have more than two primitive events occurring on the same day. However, Periods B and E had greater occurrences of three or more primitive events in the same day. Period C mostly single or double event occurrences in any one day, but

interestingly also had four small primitive events occurring on Day 96. Period D had mostly

single-event days, with double-events only on Days 143 and 162. Notably, the observed event

depths were quite modest, with the largest events at 9.6 mm (Day 181), 8.5 mm (Day 157)

and 7.5 mm (Day 170). In contrast, Period E had 3 days of four distinct primitive rainfall

events; Days 205, 234 and 235, with 8.4 mm, 18.8 mm and 6.6 mm total daily depths

respectively. At longer time-integration periods, days 234 and 235 could be considered as one

single long event with some rainfall "interludes" across one hour or more. It was also notable

that day 205 was also bookended by single-event wet days 204 (2.6 mm) and 205 (4.2 mm).

For Period F, only Day 294 was a triple-event day with total 20.0 mm total rainfall depth with

double-events on Days 252 and 274 with total daily rainfall depths of 11.0 and 8.5 mm

respectively.

A

B

C

237
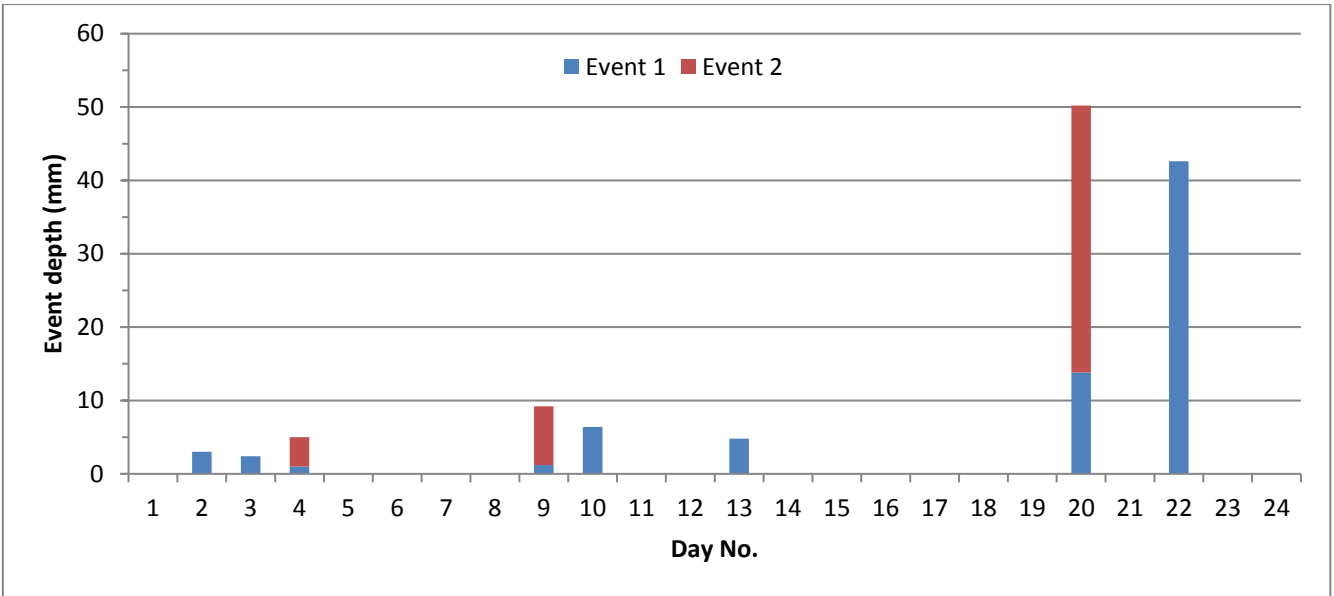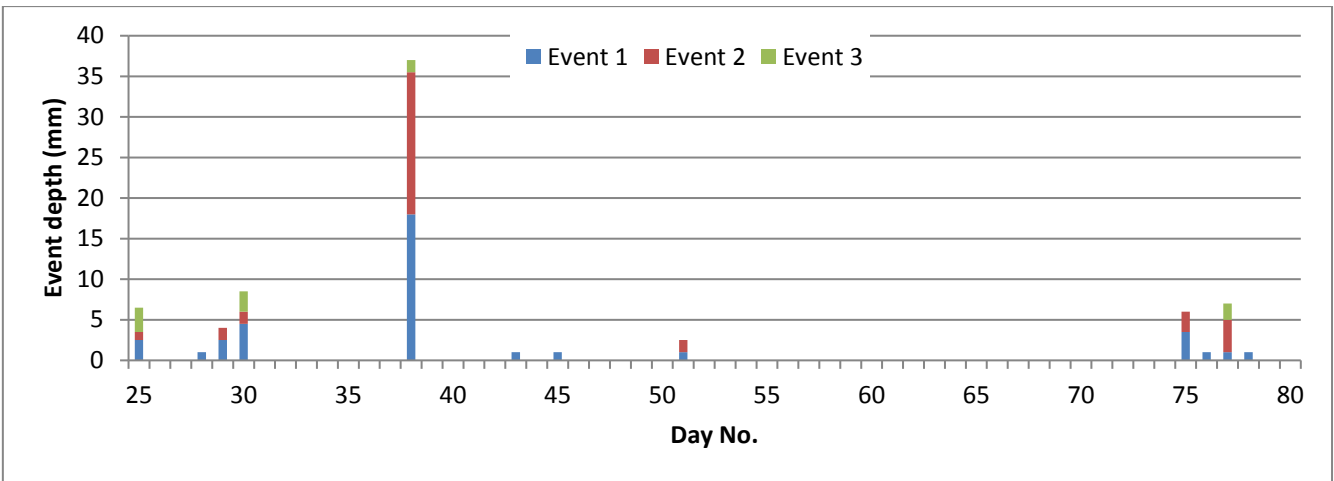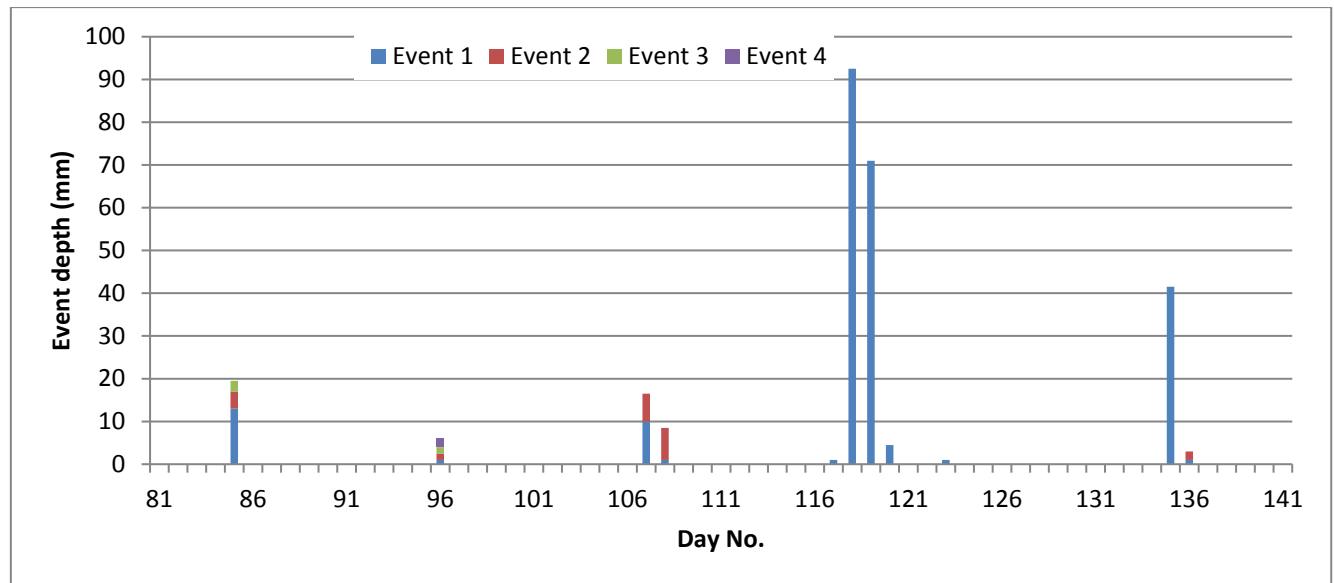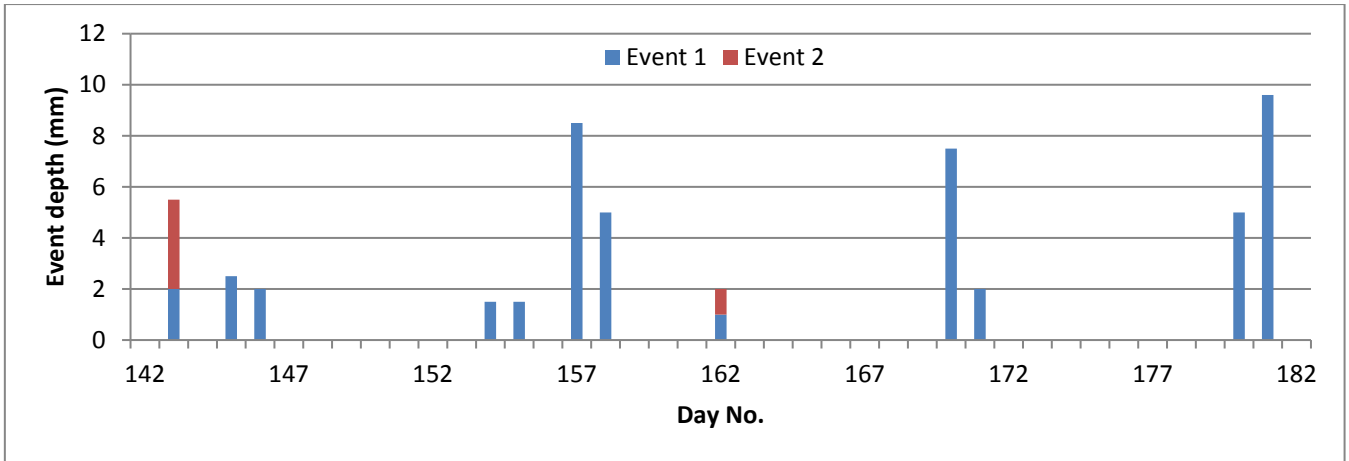
D
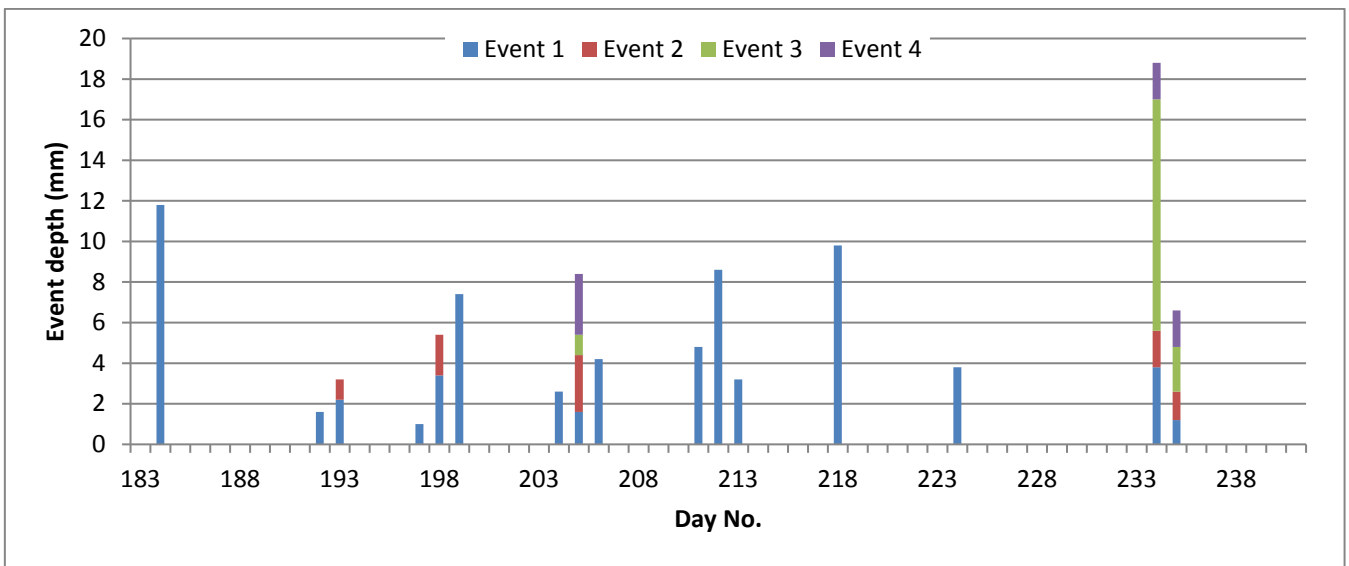
E
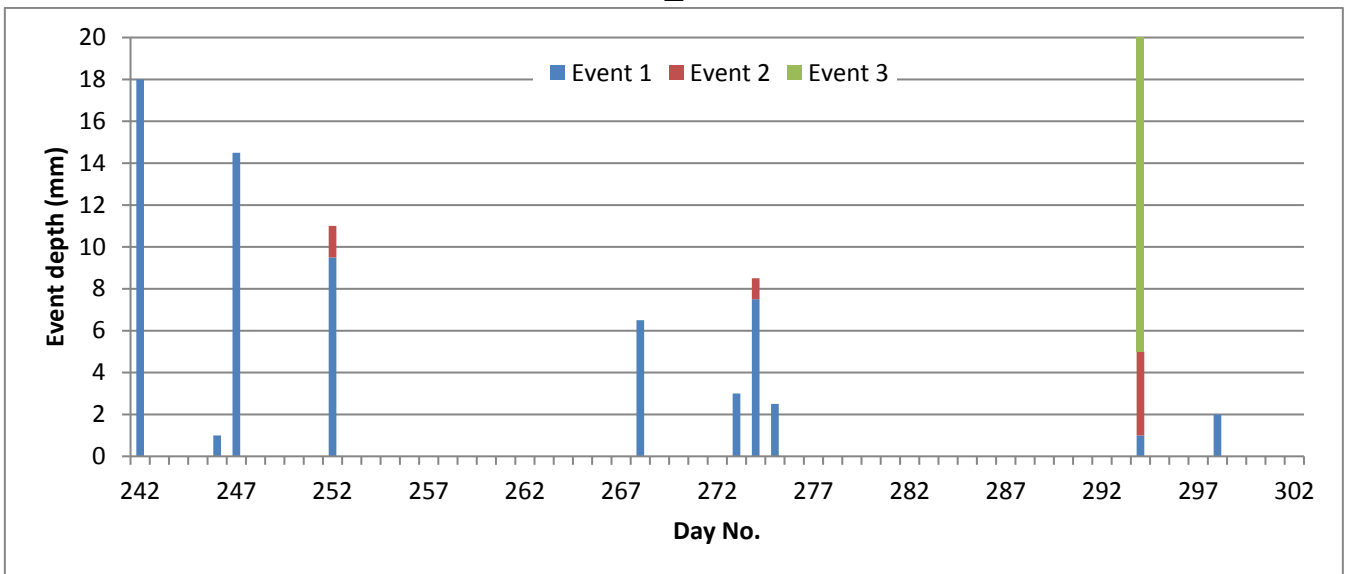
F

Figure 5-4. Rainfall event occurrence for individual days in Periods A to F. Discrete, individual primitive events within a single day are displayed in blue, red, green and purple sequentially. Note different y-axis (depth) scales to accommodate the wide range of event depths.

238

5.4.2. Clustered and single wet days

At the slightly coarser timescale, rainfall event occurrences could be examined whether they occurred as single or consecutive "wet days" ($\geq$ 1.0 mm daily rainfall depth; see (Bureau of Meteorology, 2007c)) from Figure 5-4. Period A showed two clusters, the first from days 2-4, and the second from days 9-10; interestingly, days 4 and 9 were themselves double-event days. In Period B, consecutive wet days occurred from days 28-30 with days 29 and 30 being double and triple-event days respectively, and increasing total daily depth over these three days. A four-day long cluster could also be observed for days 75-78. with double-event day 75 followed by single-event day 76; then triple event day 77 followed by single-event day 78. For Period C, clusters were seen for days 107-108 with both days themselves being "double-event" days, and days 117-120, all four of those days single-event days. Within this cluster, days 118 and 119 had the largest recorded total daily depths for the entire measurement period, of 92.5 mm and 71 mm respectively. Days 135-136 also constituted a small cluster, with day 136 being a very small double-event day (total 3 mm depth). Notably, the single-day occurrences on days 85 and 96 were both multiple-event days.

Period D had five 2-day clusters on days 145-146, 154-155, 157-158, 170-171 and 180-181. All of these clusters were single-event days. All event depths remained below 10 mm. Period E had five clusters in total, on days 192-193, 197-199, 204-206, 211-213 and 234-235. These were a heterogeneous mix of single-event day clusters (211-213) and multiple-event day clusters (e.g. 234-235), giving a wide range of hydrologic impacts and erosional energies during this period. Period F only had 2 clusters, on days 246-247 and 273-275. All the other events were single-day events, albeit with a triple-event day on day 294 (total 18 mm).

5.4.3. Diurnal-nocturnal occurrences

I also examined the rainfall event start-times for all events (primitive and non-primitive events) for each period (Figure 5-5). The number of daytime and nighttime event starts were summed for each period, and a day:night (D:N) ratio was calculated (see Table 5-5).
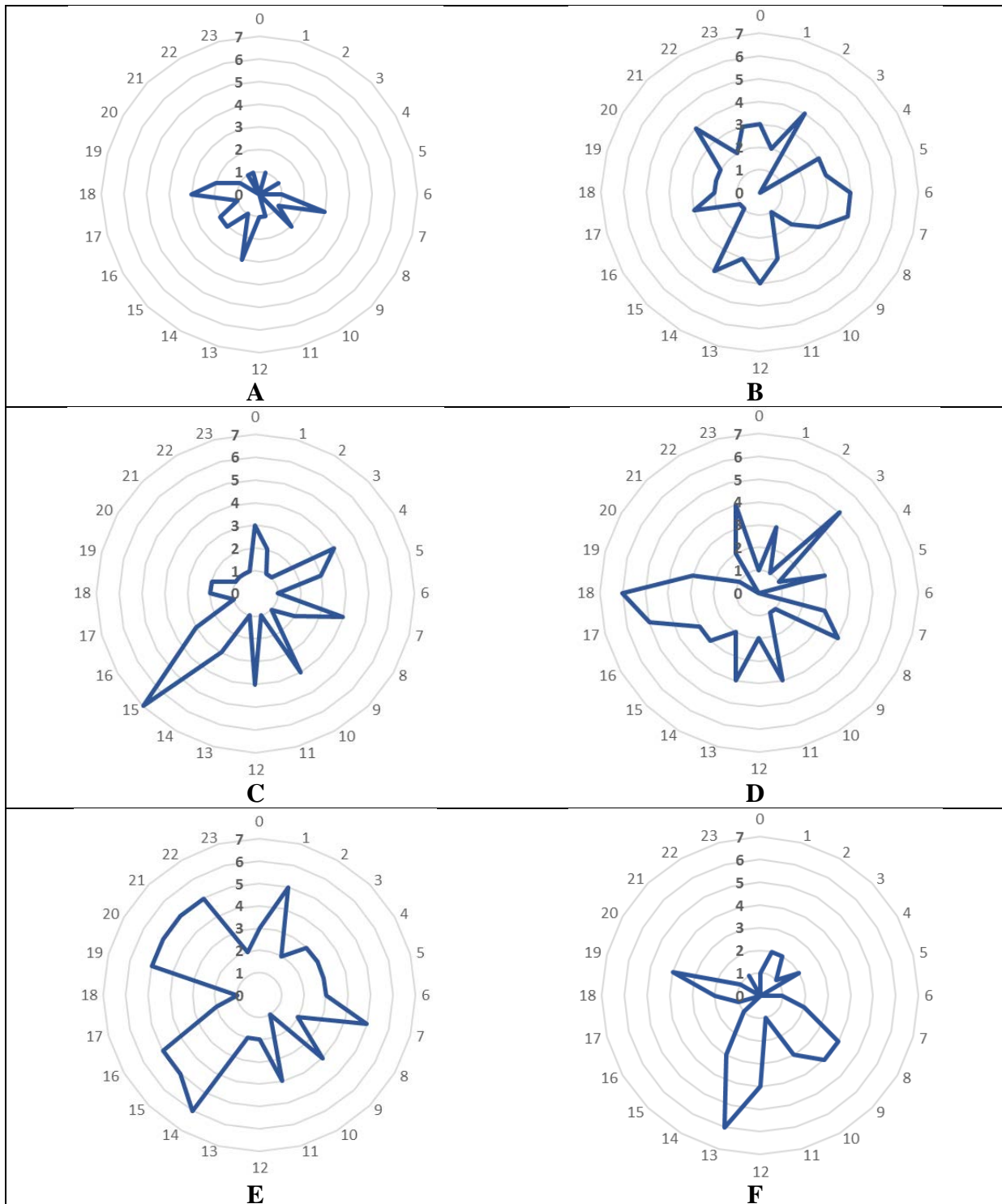
Figure 5-5. Rainfall event start times for Periods A to F.

As seen in Figure 5-5, Period A saw only single rainfall events starting at the hours around midnight. On the other hand, 0700 hrs, 1300 hrs and 1800 hrs had 3 rainfall events starting at those specific daytime hours. There were also 2 rainfall events occurring for each of the hours of 0900 hrs, 1500 hrs and 1600 hrs. Period F had a similar pattern, albeit with more rainfall events in total; for example 6 rainfall event start times at 1300 hrs, and 4 at 0800 hrs, 0900 hrs and 1900 hrs. These have played out to give the highest D:N ratios for event start times shown in Table 5-5, with Period A at 4.60 and Period F at 2.83; distinctively higher than the other Periods. Period B (see Figure 5-5) appeared to have a rather even spread of rainfall start times. For instance, 4 rainfall event start times were each recorded at 0200 hrs, 0600 hrs, 0700 hrs, 1200 hrs and 2100 hours; as seen in Table 5-5, Period B had a low D:N ratio of 1.25. Period C was rather distinctive in that 7 rainfall start events occurred around 1500 hrs, dominating the daytime rainfall. Therefore, there could be some specific mechanisms leading to the observed concentration. However, this was somewhat balanced by 3 rainfall start times each at midnight, 4 at 0400 hrs and 4 at 0700 hrs. These played out to give a D:N ratio of 1.35 as seen in Table 5-5.

Table 5-5. Summary of rainfall event start times and day:night start ratios.

Period	Total	Day	Night	D:N Ratio
A	28	23	5	4.60
B	63	35	28	1.25
C	54	31	23	1.35
D	62	32	30	1.07
E	83	39	44	0.89
F	46	34	12	2.83

As seen in Table 5-5, Periods D and E had the most balanced D:N ratios of 1.07 and 0.89 respectively, indeed with only Period E having more night-time event starts than the other periods. The rainfall start occurrence patterns for Periods D and E seemed quite different, as observed in Figure 5-5. Period D had more night-time rainfall start times in the

2300 hrs to 0500 hrs in a "spiky" pattern of occurrences, with 4 rainfall event starts at 2300 hrs and 0300 hrs. Daytime start-time was dominated by 6 events at 1800 hrs. On the other hand, Period E had night event start-times occurring largely (although not exclusively) across 1900 hrs to 0100 hrs with less unevenness. 5 event start times were recorded for each of the hours from 1900 hrs to 2200 hrs, after which there was a "dip" to 2 event starts at 2300 hrs and then increasing up to 5 event starts at 0100 hrs. Daytime event starts for Period E appeared to be more frequent in the 1400 hrs (6 events) to 1600 hrs (5 events) period.

5.5. Discussion

At the broad temporal scale, large inter-annual variability in rainfall depths was observed. These also manifested as significant variations in average rainfall received in the individual months of each year. The wide rainfall variations are the result of oscillations in regional and continental-scale systems such as the ENSO, IOD and SOI (see Chapter Three). Furthermore, projected global and regional-scale climate shifts are likely to be further overlain onto these existing systems at the decadal timescale, strongly affecting temperature and rainfall at and around the study site. Rainfall, as well as temperature and humidity patterns determined by these large systems therefore exert higher-order influences on the hydrogical and erosional processes on post-fire hillslopes; these also interact with the complex vegetation responses to increased or decreased temperature and water availability in any year, season or month. Depending on the particular favourable or unfavourable growth conditions, these manifest their impacts in the form of rapid or retarded leaf, branch and stem growth and drop/loss, root growth patterns (which would be largely unmeasurable), and evapo-transpiration rates, that can impact soil moisture changes and patterns.

In the pre-fire period the region would naturally oscillate between wet and cooler favourable "growth" periods characterized by pulses of rapid biomass accumulation. Drier, particularly drought conditions would see much of that biomass being transformed into abundant fuels that are recalcitrant to decomposition, ripe for fire ignition and spread with high potential for the development of megafires. During the post-fire period, these climatic oscillations would variably combine to direct the regional systems through one or combination of the various post-fire recovery trajectories discussed in Chapter One.

The examination of one-minute rainfall intensities, in particular the "search" for high-intensity occurrence have helped to show the distinctiveness of each period's rainfall "treatment" applied to the site. These also help to explain the site's responses of throughfall

fraction and erosivity and hillslope material fluxes (as will be presented and discussed in the chapters that follow). While rainfall depths, the most frequently reported metric, are very important as they have a positive correlation with erosivity, they do not reveal important details of the rainfall-runoff-erosion parameters and processes. By examining whether intra-event "pulses" occur, and their intensity, we could better understand and explain the observed hydrologic and erosional outcomes. Higher-intensity pulses have greater likelihoods of "breaking through" vegetation canopies, whether as free throughfall drops or by momentarily saturating and exceeding canopy storages which, in dry eucalypt forests can be limited and unevenly distributed under intermediate post-fire conditions. The sudden input of energy could also cause physical perturbations in the canopy, causing more water drops to be released from the foliage as well as activating, connecting and accelerating canopy flow pathways to create a cascading, as well as a "funnelling" effect (Mululo Sato et al., 2011) with higher erosional impacts in a very concentrated, short (sub-minute) time period.

As proxy, albeit on-ground indicators of attribution of rainfall to particular meteorological mechanisms and conditions (Tokay and Short, 1996), high-intensity pulses may help to indicate the presence cumuliform supplying precipitation at high-intensities. Alternatively, where high-intensity pulses have been enclosed within lower intensity rainfall, these may indicate the presence of cumuliform clouds embedded within larger, mobile frontal systems, or agglomeration of stratiform clouds in a quasi-stationary system (Catto and Pfahl, 2013).

In terms of the activation and operation of hillslope hydrologic and erosional processes, one-minute rainfall integration durations are considerable and physically meaningful when thinking about the speeds and rates at which rain drops arrive at plant canopies or ground litter/soil surfaces, and the near-instantaneous hydrologic and erosional responses. As soon as a rain drop falling through the air encounters the surface of a leaf or

twig, the physical conditions of the surface (e.g. hydrophobic/non-hydrophobic; occurrence of existing water; rigidity), as well as the prevailing environmental conditions (e.g. temperature, humidity, wind) (Nanko et al., 2006), and the size of the drop (and concomitantly its kinetic energy) would together determine the percentage of the raindrop mass that will adsorb to the leaf/twig surface, deflect off it, impart its momentum to other water droplets on the surface, or be lost to evaporation. Similarly, as soon as rainfall or throughfall arrives at the soil surface, the fate of the raindrop and its associated energy will interact instantaneously with the physical conditions of the soil, for example, extent of surface crusting, matric suction determined by soil texture, soil moisture content and dynamics (Hillel, 2004), extent and type of biological soil crusts (Dunkerley, 2011; Kidron, 2015) and soil erodibility (Bryan, 2000), to determine the proportion of water that will infiltrate into the soil, develop as surface runoff, and deflect off the soil surface while also dislodging and entraining any soil particles or organic material. Dunkerley (2008b) highlighted how important it was to consider drop arrival rates for rain event properties; citing, for example, 56 impacts m^{-2} s^{-1} at the simulated constant rainfall rate of 10 mm h^{-1}; at a one-minute integration time, this equated to quite a numerous and physically significant 3360 drop impacts over one square meter. Furthermore, drop arrival rates for natural rainfall events have been found to vary widely, from < 100 to > 5000 m^{-2} s^{-1} (Dunkerley, 2008b) adding to the complexity of processes that could occur within the space of a single minute. In view of how rainfall rates can vary drastically within individual events, even at sub-minute timescales albeit with significant hydrologic and erosional impacts, examining rainfall at one-minute integration intervals could yield significant insights into the processes and factors of interest in many studies.

Period A (see Table 5-3), having the highest number of very high one-minute intensity rainfall rates N ≥ 15 mm hr^{-1}, were likely to have resulted from the dominance of

summer thunderstorm systems typically experienced during this time of the year, typically attributed to continental-scale processes (the SAM/AAO and EST) regional and local convection patterns, as well as orographic effects on the moist maritime air being drawn from the coastal regions (see Section 3.5). These high-intensity episodes also occurred with high-frequency – within the short space of 22 days. These also corresponded with the long-term average rainfall patterns for the study which indicate highest summer rainfall hours and high depth for the month of February, as shown in Figure 3-19 (section 3.5). With such high-intensity rainfall pulses occurring at high frequencies within the period, substantial erosive energies and impacts were expected to be observed in terms of both throughfall erosivity and hillslope material movements. Despite the high frequency of occurrence, there were only a few "wet day" clusters (section 5.4.2.). The high D:N ratio of 4.60 for this period (similarly for Period F detailed below) can largely be attributed to the strong positive feedback between soil moisture, evapotranspiration and precipitation, particularly during summer, to cause daytime (in particular, afternoon) bias in rainfall occurrences (Findell et al., 2011).

Period B likely reflected the combination of late summer conditions and the transition towards autumn-type climatic and meteorological systems. While having a lower total number of one-minute intensities ≥ 5 mm hr^{-1} than Periods A and C, Period B still had the second-highest number of one-minute intensities ≥ 15 mm hr^{-1}, and likewise for the higher intensity values. However, these rainfall events and high-intensity episodes occurred over a longer duration and occurred with lower frequency compared to Period A (Table 5-2; mean IET of 54.2 hrs), as well as being composed of a larger number (23; Table 5-2) of smaller primitive events (mean event depth: 3.3 mm; Table 5-2). This pattern of rainfall event characteristics and occurrence is also possibly indicated by the presence of two isolated sub-primitive event, high-intensity rainfall spurts as seen in Table 5-2. The rather even ratio of day:night rainfall event start times (Table 5-5) in Period B indicate the diminished operation

of the convective soil-atmosphere-precipitation mechanisms so prominent in Period A and F; giving way to the increased dominance of frontally-dominated, stratiform cloudforms that would have caused the high number of double/triple event days as well as wet-day clusters (section 5.4.2.) with mainly gentler (i.e. lower rainfall-intensity) rainfall events.

Period C covered late-autumn to early-winter, during which the site's weather would have been strongly dominated by the mid-latitude frontal systems, as well as the impacts of any ECLs that might have extended south and inland over the study area, alongside the concomitant northwards contraction of the STR (section 3.5.1.). The meteorological conditions led to the highest number (520) of one-minute intensities ≥ 5 mm hr^{-1} , albeit restricted to zero occurrences of recorded rainfall at ≥ 30 mm hr^{-1}; in contrast with the observed one-minute intensities for Periods A, B and F (see Table 5-3). The developed rainfall events appeared to give rise to a moderate number of 17 primitive events of largest mean event depths and event energy, and moderate frequency (mean IET of 77.4 hrs; Table 5-2). An examination of Figure 5-3C shows this, as well as the two large events on Days 118 and 119. Notably, no isolated high-intensity sub-primitive events were detected for Period C (see Table 5-4). These indicate that stratiform clouds supplied much of the rainfall during this period that at times led to rather large and long-duration rainfall events that enclosed numerous higher intra-event intensity episodes of ≥ 5 mm hr^{-1} but below 30 mm hr^{-1} which would be expected from particularly strong and steep cold fronts. The day:night event start time ratio of 1.35 for Period C might have indicated similar meteorological mechanisms influencing cloud and precipitation development as Period B; the concentration of rainfall event start times at 1500 hrs appeared to be quite similar to peak rainfall intensities clustered around 1500 to 1700 hrs reported by Buytaert et al. (2006) for the Páramos region of the south Ecuadorean Andes where the large diurnal temperature differences in the mountainous landscape cause a "day-summer", "night-winter" convective-orographic mechanisms for mid-

late afternoon precipitation. It may be that an analogue of these mechanisms operate in this study region, but more focused meteorological examination is needed for any firm parallels to be drawn. Nonetheless, it was clear that the rainfall event characteristics for Period C were therefore likely to be quite different from those of Periods A and B.

Period D rainfall would have resulted largely from winter-dominant systems; the mid-latitude frontal systems and the ECLs (section 3.5.1.). Displaying the lowest number of one-minute intensities ≥ 5 mm hr^{-1} and the lowest number of events with at least single one-minute intensities ≥ 5 mm hr^{-1} indicate the strong dominance of stratiform cloudforms during this period. Because of the dominance of west-east movements of frontal systems in the study region, the rain-shadow effect of the higher-elevation Wellington Land System could have led to the smaller number of rainfall events, depressed rainfall depths and erosivity, as well as the second-highest mean IET (see Table 5-2) although it should be noted that Period D was a shorter 40 days compared to Periods B (55 days) and C (60 days). Nevertheless, significant rainfall intensities probably associated with large frontal systems or ECLs, occurred with 4 minutes ≥ 5 mm hr^{-1} and a single subprimitive high-intensity event at 14.4 mm hr^{-1} (Table 5-4). The day:night ratio of rainfall event start times was second-lowest and indicated the lack of day-processes (convection-related) bias shown in Periods A and F (Table 5-5) with the dominance of stratiform clouds giving long-duration, low-intensity rainfall, sometimes in duple "wet days" (Figure 5-3D).

Period E rainfall reflected the impacts of the climatic and meteorological systems of late-winter and spring conditions. While there would have been some effects of the mid-latitude frontal systems and ECLs in the early part of Period E, the impacts of regional and continental-scale warming and convection, as well as more localized convection systems developing with the shift to longer daylight hours and land-surface heating would have started to take effect, moving into September. This translated into a higher $N \geq 5$ mm hr^{-1} of

183 compared to 65 for Period D (Table 5-3), as well as three high-intensity sub-primitive events (Table 5-4). These indicate the increase in occurrence of cumuliform clouds bringing higher-intensity rainfall episodes, either embedded within larger frontal systems or falling as small, isolated events. Correspondingly, there were also the largest number of primitive events and shortest mean IET. However, the event mean and total erosivity for Period E were the lowest in the record (Table 5-2) and the dominance of numerous small events can be observed in Figure 5-3E. However, the events occurred as clusters that might have, together exerted stronger hydrologic and erosional impacts than expected with high antecedent soil moisture more likely to generate runoff. Interestingly, Period E had the highest nocturnal rainfall occurrence, although these were concentrated in the evening hours of 1900 to 2200 hrs (Figure 5-5E), perhaps because the slower development of convection-attributed clouds from regional and local daytime insolation that supplied rain only in the evening, rather than in the afternoon.

Period F, spanning mid-spring to early-summer would have seen the significant return to the broad-scale impacts of regional and continental-scale convection with some contribution of rainfall from the mid-latitude frontal systems to bring the typical wet conditions for the study area (see section 3.5.3. and Figure 3-21). The outcomes were that Period F saw a moderate number of $N \geq 5$ mm hr^{-1}, but with a notably high $N \geq 15$ mm hr^{-1} of 20 as well as relatively high figures for the other threshold intensities presented in Table 5-3. The conditions gave the longest mean IET (105 hrs) (see Figure 5-3F), but interestingly also led to the highest mean event intensity (Table 5-2), as well as two sub-primitive high-intensity events (Table 5-4). The more isolated occurrence of rainfall events was also borne out in the limited multiple-event days (Figure 5-3F). Furthermore, the strong D:N rainfall event ratio of 2.83 (Table 5-5) hints at the likely meteorological mechanisms responsible for the rainfall received in Period F for the study site. Together the findings indicate the strong

dominance of convection-attributed cumuliform clouds causing high-intensity rainfall occurrences, largely unaffected by the rain-shadow effects on the mid-latitude frontal systems likely exerted during Period D.

The examination of rainfall event occurrences and very detailed analysis of short interval rainfall data has shown that each time period, composed of a spectrum of differing individual events, constitute a specific and distinct composite rainfall treatment applied to the study site progressing through the study duration. The huge variation in individual rainfall event characteristics underscore the range and complexity of mass and energy inputs into the intermediate post-fire soil-vegetation system, that have to be grappled with in order to develop in-depth understanding of hydrologic and erosional responses. Much remains to be examined in the realm of climatic, meteorological and land surface-atmosphere interactions to explain many of the observed patterns which are mostly beyond the scope of this work. However, in terms of the hydrologic and erosional responses of the intermediate post-fire canopy, ground cover and soils, a range of distinct processes and outcomes corresponding to each time period would also be expected. Hence, we now turn to examining the patterns of intermediate plant canopy response to these varying rainfall inputs in the form of throughfall fraction and erosivity in Chapter Six.

CHAPTER SIX: THROUGHFALL

Throughfall results from the interaction of open-field rainfall with a plant canopy and is an important process both hydrologically and geomorphologically (Calder, 2001). In any rainfall event occurring over a vegetated area, raindrops may pass through gaps in the vegetation canopy without encountering any plant parts (free throughfall) while others would be intercepted as they come into contact, and the form and flow of water is modified; a proportion of the intercepted water is stored in the canopy (canopy storage) and may then be lost through evaporation back to the atmosphere (Valente et al., 1997) or redirected as stemflow (Dunkerley, 2014b). Importantly, some of that water proceeds to drip or even flow from the foliage, branches or twigs (released throughfall or 'gravity drops') when the canopy storage capacity is exceeded or momentum is imparted to the plant surfaces to dislodge the detained water drops (Geddes and Dunkerley, 1999; Hall and Calder, 1993). Throughfall has three components: (i) free throughfall, (ii) drips and (iii) splash droplets (Nanko et al., 2006; Nanko et al., 2011). In forested environments, one of the key effects of the vegetation canopy is therefore to result in reduced proportion of total water reaching the lower vegetation strata or the ground surface – the throughfall fraction (Crockford and Richardson, 1990a) and is an essential component of canopy interception models (Valente et al., 1997).

Currently, canopy interception and storage, and associated throughfall fraction, have been widely examined, as these are important factors determining the quantification and prediction of soil moisture changes, water availability to plants for uptake, catchment water supplies and various hydrological processes (Brauman et al., 2010; Calder et al., 1993; Crockford and Richardson, 1990d; Crockford and Richardson, 2000; Germer et al., 2006; Levia and Frost, 2006; McJannet et al., 2007; Mululo Sato et al., 2011). These have the potential to shift with projected temperature increases in most parts of the globe (Klamerus-

Iwan and Błońska, 2018). These would be mediated by shifts in leaf area indexes (LAIs) as plants respond to elevated atmospheric CO_2 that will vary according to specific biomes (Norby et al., 2016), which will also influence feedback pathways via changes in microclimate (Hardwick et al., 2015). Despite much work done in this domain, numerous knowledge gaps remain in current understanding of canopy interception and rainfall interactions with workers moving towards detailed process-based monitoring (Li et al., 2016). For instance, the spatial patterns of throughfall input have been found to exert, minimally, secondary influence over the estimation of overall storm precipitation inputs at the hillslope scale (Hopp and McDonnell, 2011).

Throughfall spectra, the range and distribution of water drop sizes arriving at the ground surface after partial modification by the plant canopy due to interception and release of water drops from plant surfaces, is an aspect that has not been as thoroughly researched as throughfall fractions (Levia et al., 2017). However, their impacts on hydrological and geomorphological processes such as infiltration and splash detachment respectively, are equally important (Armstrong and Mitchell, 1988). The kinetic energy of raindrops and released throughfall drops have been studied for humid subtropical forest species in China (Geißler et al., 2012a; Geißler et al., 2012b), open tropical forest in Brazil (Amazonia) (Germer et al., 2006), Japanese beech forest (Ghahramani et al., 2011), Japanese cypress plantation (Nanko et al., 2008; Nanko et al., 2011; Nanko et al., 2016b; Wakiyama et al., 2010), temperate deciduous forest species in northeast USA (Nanko et al., 2016a), various tropical forests in Columbia (Vis, 1986) and tropical plantation tree species (Hall and Calder, 1993). Previous throughfall work on *Eucalyptus* species has focused largely commercially important species such as *E. globulus* in Portugal (Valente et al., 1997), *E. exserta* in southern China (Zhou et al., 2002) and hybrid *E. grandis-urophylla* in southeastern Brazil (Mululo Sato et al., 2011), and streetscape trees such as *E. nicholii and*

E. saligna (Livesley et al., 2014). So far, no work has been done to evaluate drop size spectra of intermediate post-fire regrowth canopy of dry sclerophyll eucalypt forests dominated by post-disturbance juvenile leaf forms, particularly those of *Eucalyptus polyanthemos* (Red Box), a commonly occurring species that exhibits strong heterophylly between juvenile/regrowth and mature stages (Bell and Williams, 1997; Brooker and Kleinig, 2006; Teulières et al., 2007). This heterophylly sees contrasting shapes between juvenile (orbicular) and mature (ovate-lanceolate) leaves (Costermans, 2009; Jacobs, 1955; King, 1997) (see also Section 2.4.3. and Table 2-1). Furthermore, the persistent and pendulous hanging habit of both mature and juvenile leaves (steep leaf angles of around 70° from the horizontal plane) of *Eucalyptus polyanthemos* are a distinctive (although not completely unique) characteristic of leaves of plants of the *Eucalyptus* genus (Anderson, 1981; Falster and Westoby, 2003; King, 1997), and are likely to exert particular hydrological and geomorphological impacts via their signature drop-size spectra (Calder et al., 1993; Hall and Calder, 1993) although little work has been done to examine this. Indeed, Levia et al. (2017) highlighted the need to close knowledge gaps in understanding how different canopy phenophases affect throughfall drop sizes as a key to accurately characterizing water balances, soil erosion processes and biogeochemical cycling in forests.

Drop size is an important parameter relevant to many hydrological and geomorphological applications. Different rainfall intensities and different plant species have varying drop-size spectra, the range and distribution of drop sizes typically produced from a particular type of rainfall, or throughfall produced via the canopy of a particular plant species (Jones, 1992; Mason and Andrews, 1960; Vis, 1986). The implications of drop size variations are many. Large throughfall drops can have a much higher erosive competence than small drops because their greater mass contributes to higher kinetic energy, even where they would not normally fall at the high terminal velocities smaller free-falling raindrops.

Hence, drop size spectra are important because these determine the specific physical impacts individual drops, and in combination, have on the soil particles and aggregates they encounter. Large drops have higher competence to dislodge and transport larger sediment sizes and bigger aggregates. They are also much more able than small drops to disrupt or destroy soil aggregate structure (Geißler et al., 2012a; Nanko et al., 2016a; Nanko et al., 2008; Wakiyama et al., 2010). Concomitantly, large drop sizes in contrast with smaller drop sizes, can be several orders of magnitude more effective in the creation or destruction of soil surface seals through the intense 'hammering' and compacting effect. This could be exacerbated where canopy modulation of rainfall concentrates water at specific released throughfall drip points repeatedly impacting the same area of soil or litter layer. Resulting higher rates of overland flow generation would then lead to higher rates of soil erosion (Armstrong and Mitchell, 1988). On the other hand, if the drop sizes lie in the lower range, less aggressive processes would operate. Indeed, in circumstances one could easily imagine where low-intensity, long-duration rainfall events generated by frontally-induced stratiform clouds typically experienced in many temperate, mid-latitude regions, large released throughfall drops from gently saturated forest canopies would inherently generate greater erosive energies than the "original" un-erosive drizzle, on hillslope surfaces. Adopting a more comprehensive view of hillslope erosion by rainsplash and overland flow, the timing of drop arrival, number of drops and drop spacing also exert important influences on the multi-scale operation of hydrological and erosive processes on hillslopes and in catchments (Dunkerley, 2008b).

The purpose of this component of the research was to determine the characteristics and effects of throughfall resulting from the modulation of rainfall by the regenerating canopy of a dry sclerophyll forest in southeast Australia at the patch scale, across different various phenophases approximated by Periods A to E and accompanying rainfall

characteristics (Chapters Four and Five). Specifically, the questions posed for this intermediate post-fire canopy were: (i) what is the throughfall fraction; (ii) what is the under-canopy erosivity of throughfall; (iii) how do throughfall fraction and erosivity vary spatially and temporally; and (iv) what are the plausible causes for any observed variability? Addressing these questions would help to fill some of the knowledge gaps in post-fire erosion science applicable to southeast Australia's eucalypt forests, as outlined in Chapter Two.

6.1. Field measurements of canopy cover, throughfall fraction and erosivity

6.1.1. TIF canopy cover and throughfall fraction

Figure 6-1 presents the changes in canopy cover percentage directly over the 15 under-canopy TIFs over the study period. Generally, canopy cover remained at around 75% through Periods A, B and C, and then declined gradually to 69% in Period F.
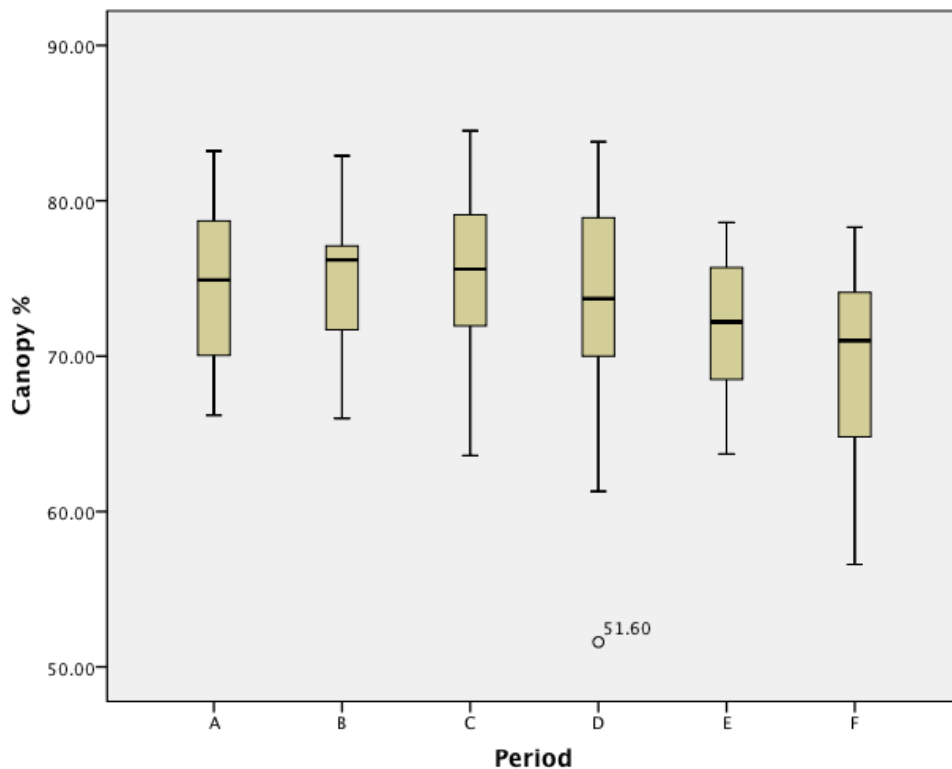
Figure 6-1. Changes in canopy cover percentage above TIFs under regenerating *E. polyanthemos* canopy for Periods A to F.

However, some distinct changes in mean canopy cover and the spread of canopy cover percentages between the time periods could be discerned. An anomalously low value was recorded in Period D (51.6%) and could be explained by the loss of one clump of overhanging twigs and leaves over TIF #4 which cleared some of the canopy cover in that specific position. However, the regrowth after this loss was quite rapid and canopy cover percentage had recovered by Period E.

Table 6-1 presents the throughfall fraction calculated using the TIF method (see

section 4.6). Distinct and interesting variations in throughfall fraction were observed. Overall, average throughfall fraction declined from 0.73 in Period A to 0.63 in Period B. It then increased to 0.75 in Period C and then to a high 0.91 in Period D. After that, it dropped to 0.60 in Period E. In Period F, throughfall fraction unexpectedly increased drastically to 1.17 in Period F, meaning that more water was actually collected at under canopy than in open-field positions.

Table 6-1. Throughfall fraction for Periods A to F determined using the TIF method.

Period	Mean under-canopy weight loss(g) (n = 15)	s.d.	Mean open field weight loss (g) (n = 5)	s.d.	Throughfall fraction
A	1.365	0.232	1.866	0.108	0.73
B	0.843	0.176	1.338	0.059	0.63
C	2.032	0.342	2.698	0.190	0.75
D	2.501	0.150	2.749	0.165	0.91
E	0.798	0.208	1.329	0.065	0.60
F	0.922	0.708	0.787	0.007	1.17*

Examination of the standard deviation of under-canopy weight loss compared to that for open field weight loss found that much variation of values occurred for throughfall compared to open field rainfall. A notable exception was Period D where the standard deviation for open-field rainfall (0.165) was higher than throughfall (0.150); this occurred where the highest weight losses and throughfall fraction (other than Period F) were recorded.

It was also useful to explore the results from individual data points for any discernible patterns. Figure 6-2 presents the TIF tablet weight loss for individual funnels (#1 to #15 in an uphill transect) and their corresponding canopy cover percentage. Large fluctuations in weight loss were found. For instance, TIF #8 in Period B had the highest weight loss at 1.81 g, but in Period E had one of the lowest at 0.57 g. However, in Period F, TIF #8 again had the highest weight loss off 2.82 g; together with TIF #7 (2.00 g) and

#14 (1.70 g) they appeared to contribute significantly to the positive throughfall fraction recorded in Period F.

There did not appear to be any clear patterns of change in canopy cover along the transects for all time periods. However, phenological transitions were likely; canopy cover decreased from Period E to F. This was likely associated with increased litterfall by the plants to manage transpirative stresses as the region entered the hotter and drier late spring/early summer conditions in Nov/Dec 2012.
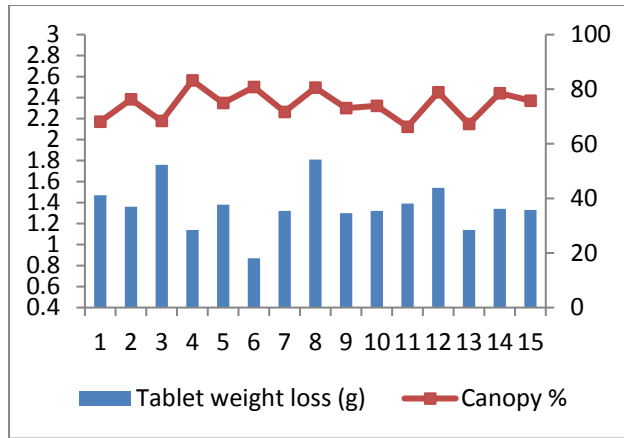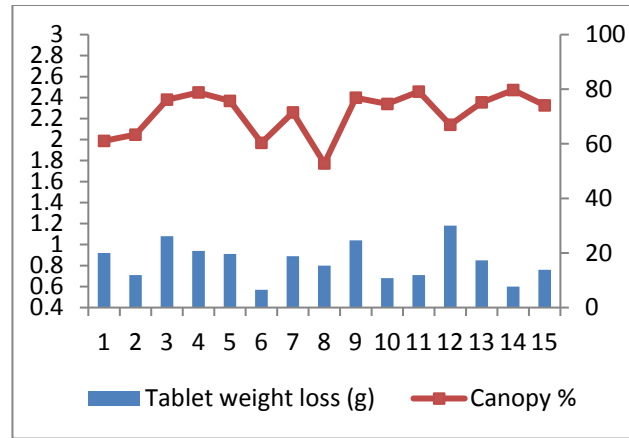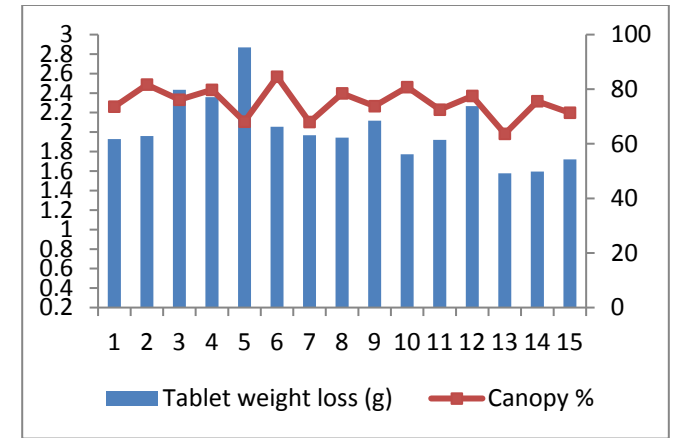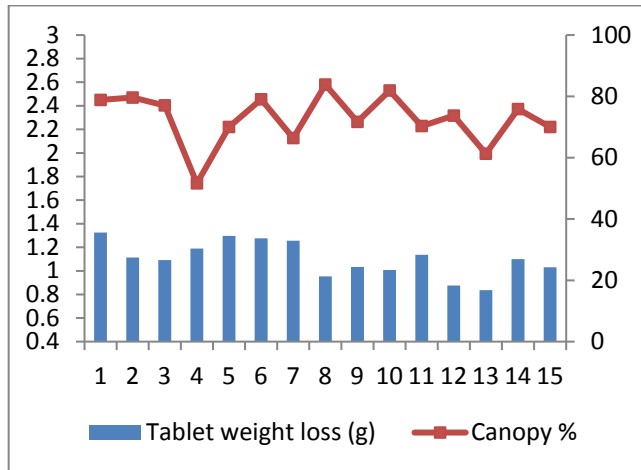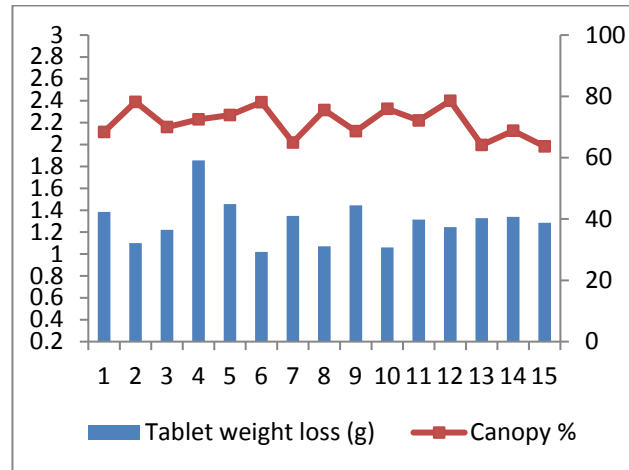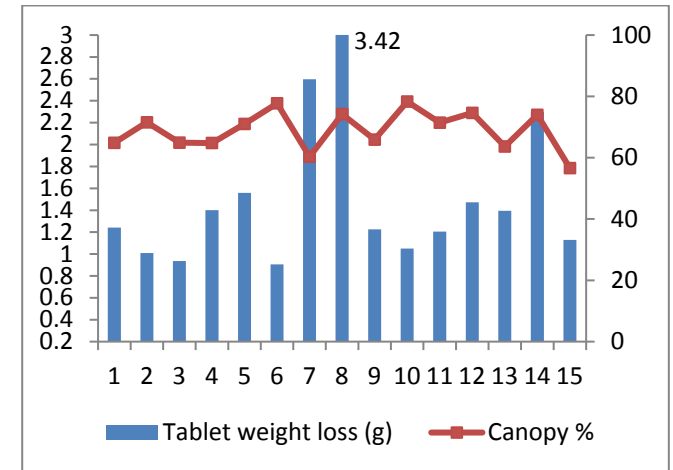
Figure 6-2. Individual TIF (#1 to #15, arranged in a generally uphill transect) tablet weight loss (g) (left-side y-axis; blue vertical bars) with corresponding canopy cover percentage (%) (right-side y-axis; red lines). Rainfall depths include only events qualifying as primitive events (≥1 mm; 60 min inter-event time).

Figure 6-3 presents the changes in mean canopy cover percentage over the 15 under-canopy splash cups during the study period. A distinctly low value of 58.5% was recorded for splash cup #2 in Period A, with a similar "dip" in canopy cover for splash cup #8 in Period B.
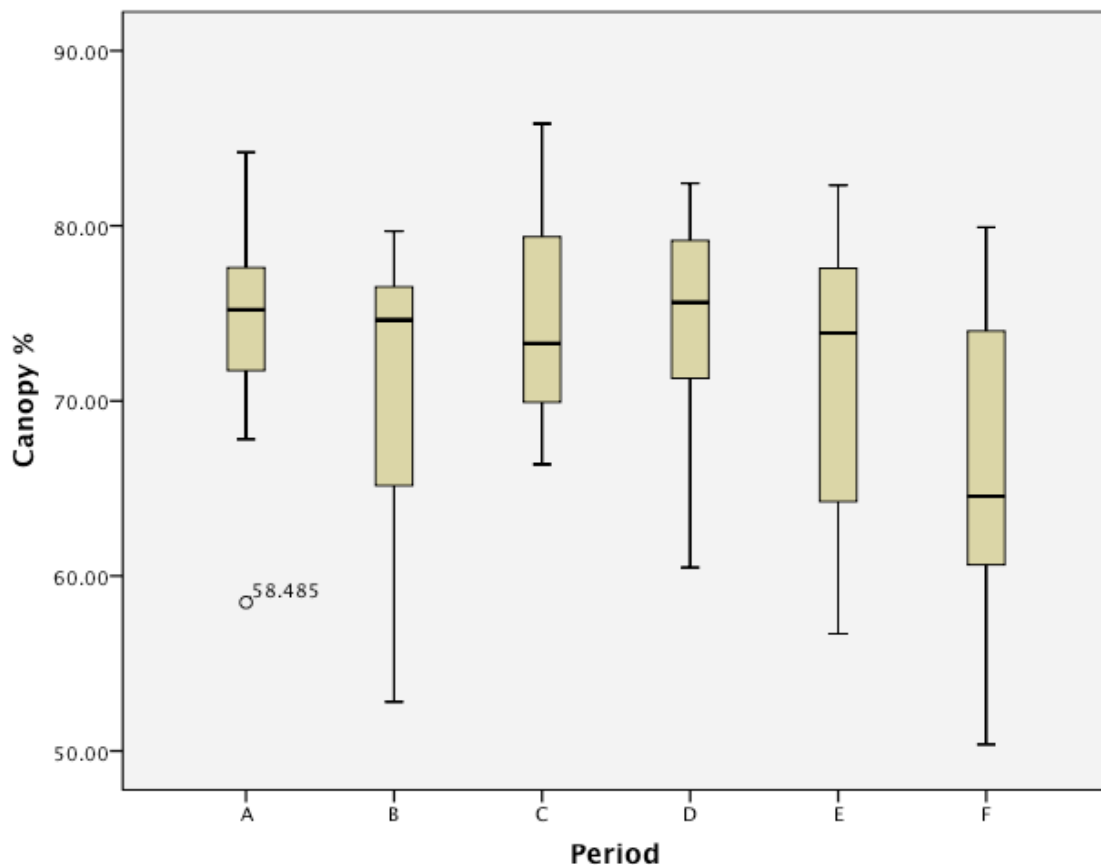
Figure 6-3. Changes in canopy cover percentage above splash cups under regenerating *E. polyanthemos* canopy for the measurement Periods A to F.

In addition to canopy cover measurements, drip heights (Figure 6-4a) were ascertained by using a standard tape measure to measure the distance between the exposed surface of each cup and the bottom edge of the leaves directly above it. Because up to five "levels" of possible drip points were identified, the heights of these preceding layers of foliage were also measured (Figure 6-4b); heights beyond arm's reach were estimated using a timber pole or clinometer-based trigonometrical calculations. Particularly high numbers of levels and drip heights were found for splash cup #3 (5 levels, highest drip height 1242 cm)

and #10 (4 levels, highest drip height 615 cm), in part reflecting the heterogeneous nature of these intermediate post-fire canopies.
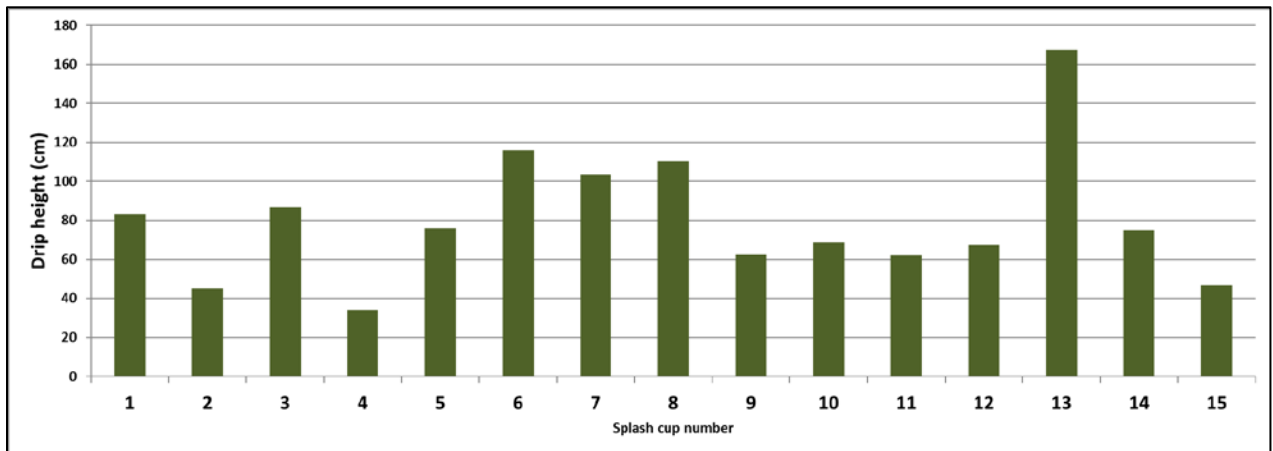
(a)
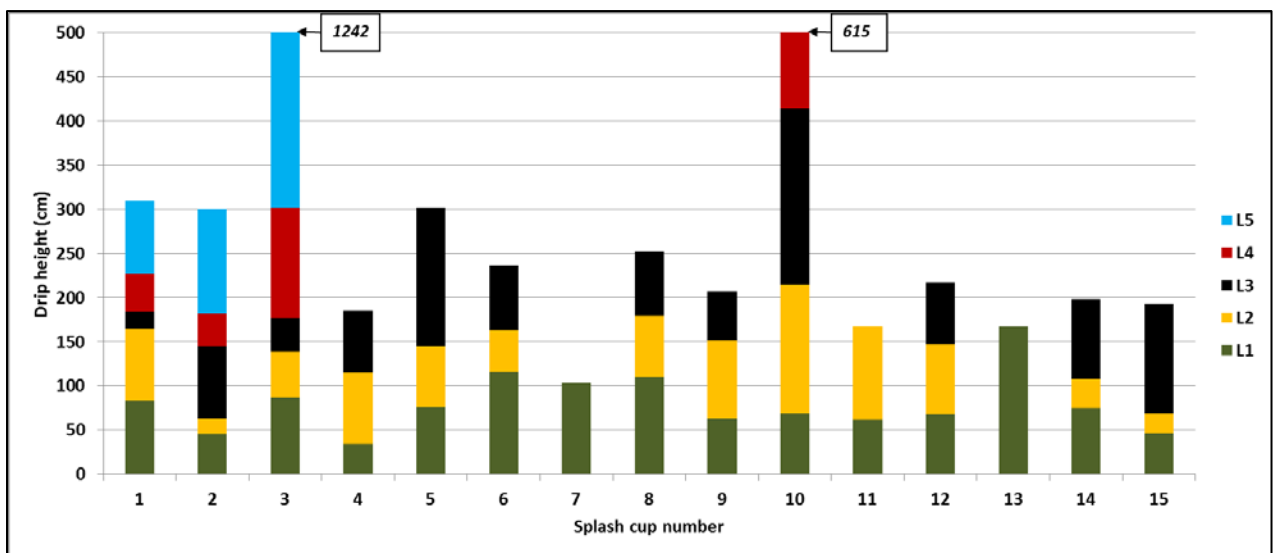
(b)

Figure 6-4. (a) Drip heights of foliage directly above splash cups #1 to #15; and (b) Drip heights at various observed levels (L1 to L5) in the plant canopy. The tops of each coloured bar indicate the height (above cup) of each drop point. Note: Highest drip point above cup #3 was 1242 cm and cup #10 was 615 cm; the y-axis was truncated to enable clear observation of values across all cup positions.
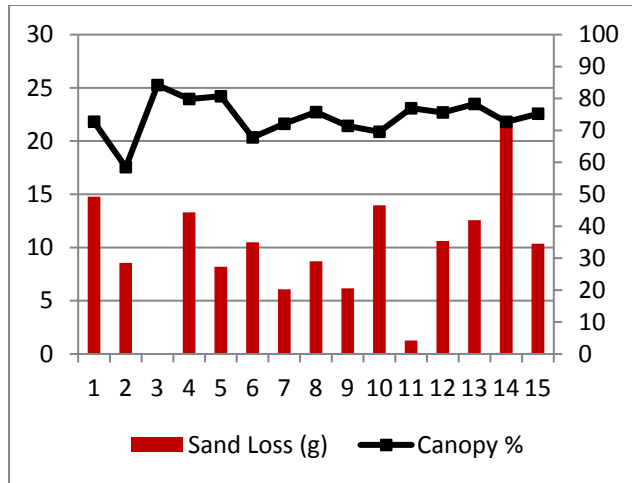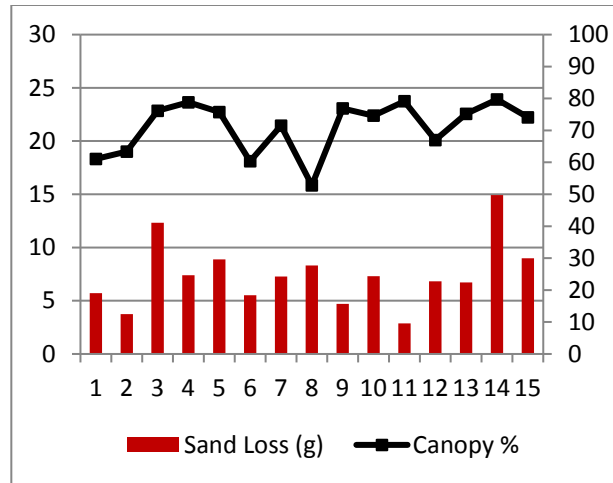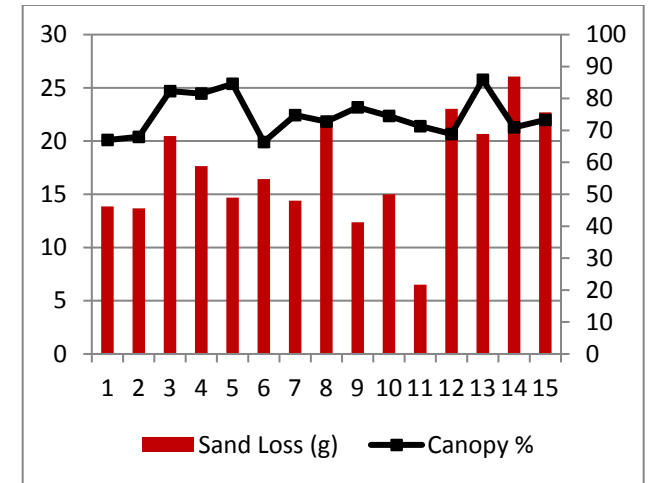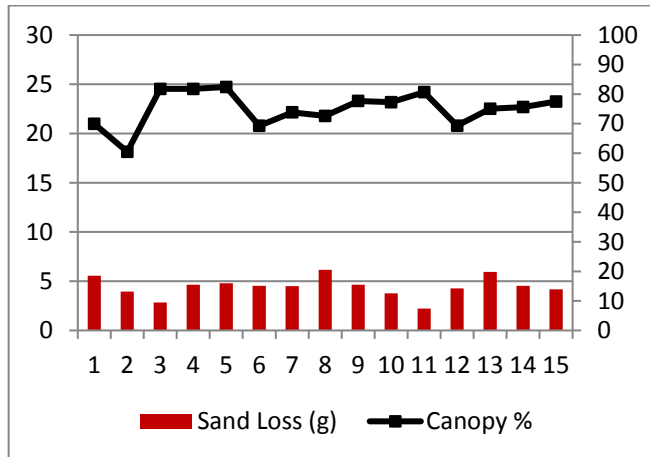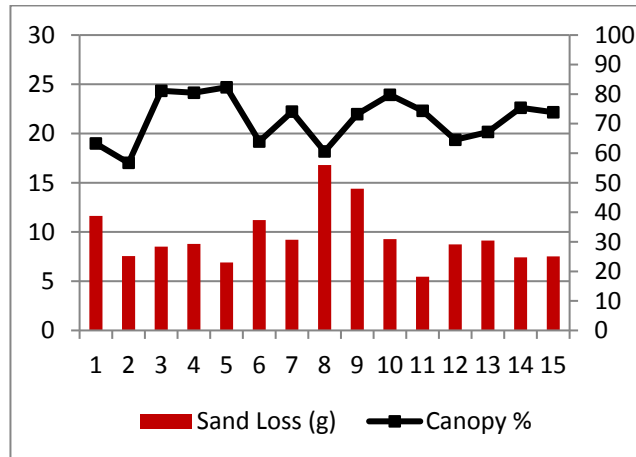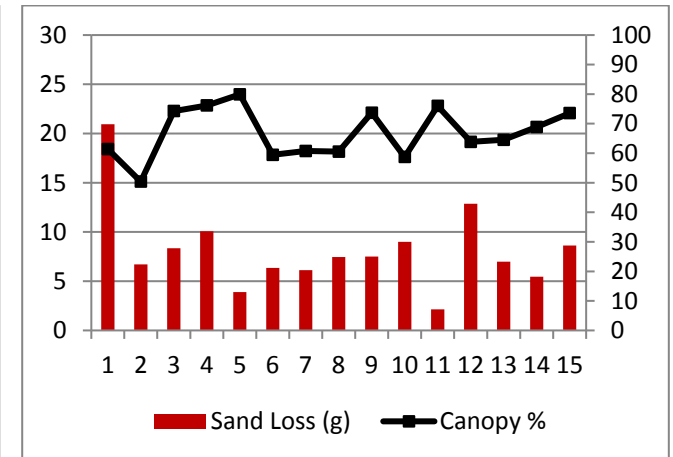
Figure 6-5. Individual splash cups (#1 to #15, arranged in a generally uphill transect) sand weight loss (g) (left-side y-axis; red vertical bars) with corresponding canopy cover percentage (%) (right-side y-axis; black lines). Rainfall depths include only events qualifying as primitive events (≥1 mm; 60 min inter-event time) **Note:** No data for Period A, splash cup #3 due to equipment damage.

Figure 6-5 presents the splash cup sand weight loss for individual funnels (#1 to #15 in an uphill transect) and their corresponding canopy cover percentage. Large fluctuations in weight loss were found between individual cups, and the ways in which the values varied differed across the periods. High canopy cover percentage also did not correspond with low sand loss values. For instance, in Period A cup #14 had the highest sand weight loss of 22.3 g, indicating highest throughfall erosivity, but with a moderately high canopy cover percentage of 72.7%. On the other hand, for cup #11, only 1.26 g of sand loss was recorded for a canopy cover percentage of 77%. Inter-cup variations sand losses were quite muted when low total rainfall was recorded (Period D, 43 mm) in contrast to the other periods. Cup #14 showed highest sand weight loss in Periods A to C, but the responses became muted in Periods D to F. Cup #11 was consistently the lowest yielding position through all the periods.

Table 6-2 presents the corresponding erosivity ratio between under-canopy throughfall and open-field rainfall over the measurement period. Erosivity ratio increased over Periods A to C from 1.84 to 2.02 (the highest value in the measurement period), but dropped suddenly to 1.34 in Period D, and then increased to 1.79 in Period F.

Table 6-2. Erosivity ratio as calculated from weight loss of sand from splash cups between under-canopy and open-field positions.

Period	Under-canopy (n= 15)		Open field (n = 5)		Erosivity ratio
	Mean weight loss (g)	s.d.	Mean weight loss (g)	s.d.	
A	10.522	4.943	5.704	0.882	1.84
B	7.431	3.102	3.934	0.475	1.89
C	17.300	5.140	8.469	0.963	2.04
D	4.433	1.033	3.317	0.401	1.34
E	9.502	3.051	6.830	1.020	1.39
F	8.163	4.506	4.563	0.662	1.79

6.1.3. Discussion

6.1.3.1 Canopy cover changes

Post-fire canopy regeneration is dynamic and heterogeneous over time and space. As seen from the results presented, there was little evidence of any clear trend of increase in canopy cover percentage through time, usually implied in most models of monotonic post-fire "recovery" (Prosser and Williams, 1998). Rather, the results point to fluctuations dominated by seasonal variations in temperature and water availability. This indicates that a quasi-equilibrium in terms of average annual canopy cover has been reached where there is fluctuation around a mean value, although this may only be confirmed through longer-term studies. Phenological changes such as late spring/summer leaf drop in response to high evapotranspirative stresses in hotter and drier conditions were clearly reflected in the lower mean canopy cover percentages for Period F for both the TIFs and splash cups, as well as sudden decreases at selected data points. These can lead to throughfall process transitions resembling to some extent those of deciduous vegetation (*Liriodendron tulipifera L.*) in Maryland, USA examined by Nanko et al. (2016a).

Furthermore, in these conditions, the regenerating plants in this post-fire condition are in competition with other individuals to maximize water availability and photosynthetic gain. Hence, there is also the need to account for the spatial colonization (lateral and vertical) expansion of the plants making up the canopy layer. These are in turn strongly affected by the different individuals' "starting points" arising from different impacts and extents of fire damage, and recovery "strategies" of lignotuber and/or epicormic sprouting. As these occur, the density and characteristics of foliage above each individual TIF or splash cup change; young leaves actively at the outward and upward edges of the plant canopy, while older "inner" branches and twigs defoliate. The combined effect of these

264

growth processes would be to change the ways in which rainfall is modulated by the plant canopy over the same position. This implies that we need to adopt a dynamic view of change in individual plants' 'zones of influence' (Dunkerley 2000) in the post-fire regeneration context. Indeed, the DZI framework (Section 2.5) is particularly relevant in this respect.

6.1.3.2. Throughfall fraction

Generally, it is expected that increased canopy cover would lead to reduced proportions of rainfall penetrating the forest canopy (lower throughfall ratio value). However, this did not appear to be the case. There were no clear correlations found between throughfall fraction with canopy cover percentage ($R^2 = 0.18$), rainfall erosivity nor rainfall depth. For the standard deviation of tablet weight loss for under-canopy vs. open field conditions, there was clear indication of much spatial heterogeneity in the proportion of rainfall that was diverted by the regenerating canopy. By comparison, much lower variations were seen for the open-field TIFs. The results therefore help to quantify the extent to which water drops passing through the regenerating post-fire canopy are modified and describe the increased spatial variability of the characteristics of water arriving at the ground. This heterogeneity was also found for the throughfall erosivity measurements.

The throughfall fractions for this intermediate post-fire dry-sclerophyll *Eucalyptus* canopy, ranging from 0.60 to 0.91 (other than the 1.17 figure) were for most Periods lower than those reported for long unburnt *Eucalpytus* formations in Australia. Data collated by Feller (1981) showed that throughfall fractions for the wet sclerophyll *Eucalyptus regnans* ranged from 0.73 (mature forest in Corandderrk) to 0.80 (23 years old forest at Wallaby Creek); for dry-sclerophyll *Eucalyptus obliqua*-dominant formations: 0.73 (51 years old forest at Mt. Disappointment) to 0.95 (45-60 years old forest at Stewarts Creek). Measurements by Feller (1981) on *E. obliqua* forest found distinct year-to-year differences in throughfall fraction: 0.75 in the first year but 0.90 in the second year, even though any variation in total incident precipitation between both years was negligible (Year 1: 1150 mm; Year 2: 1147 mm). However, the results from this study have revealed how throughfall fractions can vary quite significantly over shorter timescales.

266

6.1.3.3. Throughfall erosivity

It is generally assumed that under-canopy erosivity from throughfall is lower than open field rainfall erosivity (erosivity ratio of < 1). This is because the plant canopy intercepts the rainfall and partitions it to branch flows and stemflows, canopy storage and therefore facilitates canopy losses, effectively reducing the total amount of water arriving at the ground. In addition, the kinetic energy of falling raindrops, likely arriving at terminal velocity, would be attenuated by the canopy, reducing the erosivity of water drops arriving at the ground surface. However, the erosivity ratios indicate quite the opposite – that under-canopy splash effects can be more than double that of open-field rainfall situations. This is, furthermore, in the context of substantially low throughfall fraction values. This therefore demonstrates the high erosivity of gravity drops from plants described earlier by Moss and Green (1987). To estimate this process quantitatively, nominal throughfall and rainfall depth and erosivity were calculated and are presented in Table 6-3. These were based on the rainfall erosivity statistics in Table 5-2, throughfall fraction in Table 6-1 and erosivity ratios in Table 6-2. Derived Tf erosivity was calculated by multiplying the rainfall erosivity by the erosivity ratio. Nominal Tf depth was calculated by multiplying Primitive Rf event depth by Tf fraction, and erosivity per mm rainfall/throughfall depth was calculated by dividing the total erosivity by the total primitive event depth for each period.

267

Table 6-3. Comparison of rainfall and (derived) throughfall depth and erosivity.

Period	Primitive Event Depth (mm)	Rainfall Erosivity (MJ*mm ha⁻¹ hr⁻¹)	Erosivity Ratio	Tf fraction	Derived Tf Erosivity (MJ*mm ha⁻¹ hr⁻¹)	Tf Depth (mm)	Per mm Tf Erosivity (MJ ha⁻¹ hr⁻¹)	Per mm Rf Erosivity (MJ ha⁻¹ hr⁻¹)
A	123.6	343.7	1.84	0.73	632.4	90.2	7.0	2.8
B	76.5	128.5	1.89	0.63	242.9	48.2	5.0	1.7
C	206	411.0	2.04	0.75	838.4	154.5	5.4	2.0
D	79.4	132.8	1.34	0.91	178.0	72.3	2.5	1.7
E	110.8	50.0	1.39	0.60	70.0	66.5	1.0	0.5
F	87	114.6	1.79	0.72*	205.1	90.2	3.3	1.3

Nominal throughfall fraction of 0.72 for Period F used (calculated as the mean throughfall fraction for Periods A to E). Original "measured" throughfall fraction value of 1.17 for Period F was not possible and likely resulted from canopy funneling processes for selected measuring positions, discussed in the following paragraphs.

Correlation analysis between canopy cover percentage with erosivity ratio found no clear relationships. On the other hand, good correlation between total erosivity of events for each period and erosivity ratio ($R^2 = 0.712$) were found (see Figure 6-6). This is quite close to the relationship reported by Nanko et al. (2008) between soil splash detachment rates and rainfall erosivity indices ($R^2 = 0.632$) for unmanaged Japanese cypress (*Chamaecyparis obtusa*) plantations in Japan. The highest erosivity ratio was also associated with the highest rainfall depth amongst all the periods (206 mm in Period C). However, the total erosivity was found be a better parameter for predicting erosivity ratio because it incorporated storm event intensity, which is important in the processes of overcoming canopy storage capacities, "breaking through" the protective effects of the plant foliage and activating the distinctive "funnelling effect" of eucalypt canopies discussed below.
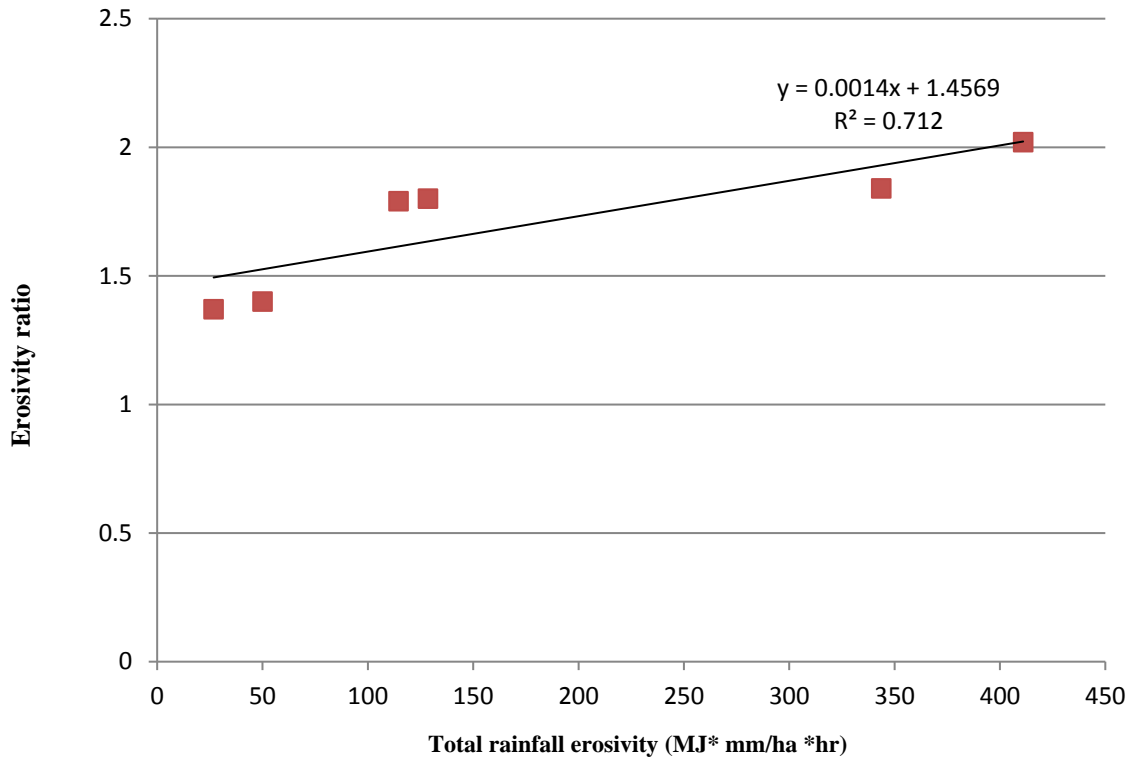
Figure 6-6. Results of correlation analysis between total erosivity in each period and the corresponding erosivity ratio.

Thus, for the measured range of canopy cover percentage for post-fire regenerating vegetation, throughfall erosivity was not strongly influenced by the extent of canopy cover. Rather, it was the erosivity of the rainfall arriving at the regenerating eucalypt canopy that accounted for the erosivity ratio variations. The positive relationship also indicated that the regenerating canopy enhanced under-canopy splash erosion energy vis-à-vis open-field splash erosion, rather than providing protective cover. This is consistent with the results from field experiments reported by Geißler et al. (2012a) who reported an average erosivity ratio of 2.59 for humid subtropical forests of *Schima superba* and *Castanopsis eyrie*. Geißler et al. (2012a) also reported medium and old growth forest having higher throughfall erosivity than young forest. The findings in this section have shown the throughfall characteristics of "young" post-fire dry eucalypt forests. Whether throughfall erosivity would be higher, lower or similar in more mature growth stages for dry eucalypt forests, will be discussed in the next section which examines the differing corresponding leaf-forms and their influences on drop-

269

size distributions.

These findings yield interesting insights into the 'zones of influence' of post-fire regenerating *E. polyanthemos* of the area, and possibly more broadly to other similar dry sclerophyll forests in post- fire recovery phase. It is likely that canopy structure of such post-fire regenerating vegetation actually concentrates water over a number of drip points or "hot spots" (Nanko et al., 2016a) which are also likely to create water drops that are larger than most of the drop sizes occurring in the rainfall arriving at the canopy layer (and at the ground level for open-field non-canopy locations).

This process has been described as the distinctive 'funnel effect' of the *Eucalypt* tree canopy architecture (Mululo Sato et al., 2011) that cause the spatial heterogeneity and temporal stability of throughfall in plantations of hybrid *Eucalyptus grandis* and *Eucalyptus urophylla* in southeast Brazil. This process is attributed to the way in which eucalypt leaves tend to hang downwards at steep angles (usually at 60° or more to the horizontal) and grow in clumps. Hence, the full canopy storage capacity that attributed to all the available foliage area may not be reached in reality. Instead of rainfall being detained on leaf surfaces or redirected to stemflow, water is more likely to be deflected downwards by or drain quickly from the steeply-inclined leaves; water could also be concentrated at specific drip points and might even flow as mini-rivulets of water, especially with long and large rainfall events.

Released throughfall, with larger median drop sizes but not achieving terminal velocity, would have been more erosive than raindrops with smaller median drop sizes but arriving at higher velocities. The distribution of under-canopy splash erosion values and their mean effects indicate that the drip points were widely distributed enough to be captured by most of the splash cups to record erosivity ratios of >1. This funneling effect could also be responsible for the positive throughfall value obtained from the TIFs. Further work needs

270

to be done to quantify the under-canopy drop-size distributions for different leaf forms, and to compare them with open rainfall drops.

However high under-canopy splash energy may not be uniformly realized as high splash erosion rates. Leaf litter accumulation on the ground is usually greater directly under plant canopies and can be very effective in attenuating the energy of water drops (Geddes and Dunkerley 1999). On the other hand, the higher energy levels also increase the likelihood leaf litter, other organic detritus and soil being impacted and transported downslope, especially in steeply sloping conditions such as the study site. Asymmetrical upslope/downslope patterns and processes of muted/enhanced erosion could be created (see Section 1.3.3; Figure 1-6d). Furthermore, surface runoff may develop rapidly due to the hydrophobic nature of undecayed leaves at the top of the organic litter layer, and consequently contribute to higher rates of erosion downslope in the more exposed inter-patch areas with lower levels of ground cover.

There are also important albeit unforeseen hydrological and erosional implications where the removal of ground-level fuels is targeted using prescribed fire to reduce the risks of widespread and severe fires (Cawson, Sheridan et al. 2012, Cawson, Sheridan et al. 2013). Such burning would not only reduce the total volume of coarse organic material providing physical protection to the mineral soil horizon, but also increase the erodibility of the remaining ash and charred material. Hence, increased rates of soil erosion caused by strong under-canopy splash may occur within these plants' 'zones of influence' when prescribed fire is applied.

Many past studies on post-fire hillslope erosion have not investigated the detailed characteristics of throughfall under intermediate vegetation regeneration conditions. This research aimed to address this gap by measuring, over 10 months, the throughfall fraction

and throughfall erosivity of post-fire regenerating canopy five years after severe fire swept through the region. By applying simple methods that enabled us to measure throughfall volumes and erosivity in a distributed manner, at low height clearances characteristic of post-fire vegetative regrowth, we found that throughfall fraction was variable through time and that throughfall erosivity ranged from 1.39 to 2.04 times higher than open field rainfall. In addition to the importance of rainfall erosivity, specific canopy structure and foliage characteristics have contributed to the observed outcomes (Armstrong and Mitchell, 1988; Langford and O'Shaughnessy, 1978; Levia et al., 2017; Nanko et al., 2016a).

This section has contributed to further understanding about the distinctive 'zones of influence' of canopy trees of dry sclerophyll forest such as the *E. polyanthemos*, characterized by processes not normally discussed in the more broadly described "recovery" of post-fire erosion rates. A more complex and dynamic view of throughfall under post-fire vegetation conditions, compared to many other studies, is needed. Consequently, it is suggested that the concept of gradually changing 'zones of influence' should also be applied to the investigation and modelling of post-fire hydrological and erosional processes, particularly where vegetation recovery is substantial but incomplete (see Chapter Two).

Because of the heightened erosivity under these types of forest canopies, fuel reduction burns in dry sclerophyll forests may contribute to increased soil erosion rates at the local scale especially where pedological and topographic conditions such as that seen in the study site, contribute to high soil vulnerability to hillslope rill and inter-rill processes. Under-canopy erosivity is also an important consideration for the selection of tree species for plantations on areas with soil and topography (e.g. the present study area with poorly structured sandy loam on steep slopes) that result in increased vulnerability to erosive processes. Indeed, there is some evidence that high-temperature burning, typical of severe

bushfires, can maintain or even enhance soil water repellency (Cawson et al., 2016), and this may contribute to high fluvial erosion rates being maintained while suppressing vegetation recolonization after fire due to limited soil moisture.

Rainfall characteristics such as erosive energy are important factors that influence how and how much rainfall is modulated by a regenerating canopy. These are determined by broader-scale, higher-order meteorological and climatological factors that are both deterministic and stochastic in nature, for a specific location in the landscape. Differences in rainfall event characteristics, integrated over a specific period, can contribute to varying outcomes in throughfall fraction and erosivity. These require more detailed investigation particularly in their complex modulation by dynamically changing plant canopies. Some insights are provided through the laboratory experiments discussed in the following section.

6.2. Laboratory experiments on drop-size distributions

6.2.1. Introduction

While there have been many techniques in the past and present to determine water drop sizes, there still exists a need for simple, reliable, inexpensive and easily replicable methods of measuring water drop sizes from rainfall and throughfall that could be implemented both in the laboratory and field environments. This is particularly important for regions and institutions where financial constraints hinder access to expensive, sophisticated equipment for generating valuable research data. For example, the requirement of sufficient spatial distribution and replication necessitated the use of hand-assembled rain-gauges in (Mululo Sato et al., 2011). Recently, Kathiravelu et al. (2016) reviewed the range of rain drop measurement techniques through the past decades across diverse levels of technological sophistication and found that while laser disdrometers are enjoying increasing popularity, e.g. Angulo-Martínez and Barros (2015), they can be limited in rates of deployment because of high costs, small sampling area, limited numbers of sampling points, and reliability issues in instances of very heavy and intense rainfall giving very high drop arrival rates. Kathiravelu et al. (2016) also noted that the dye-stain technique is still is use in current times and the present study sought to re-evaluate its potential as a low-cost approach for determining drop-size spectra by a wide range of researchers. In Chapter Four, I described how I developed and evaluated the low-cost dyed filter-paper method for determining the size of water drops by measuring the stain areas (section 4.7) corresponding to their masses, from hypodermic syringe-generated drops. In this section, with the aid of mist-spray experiments, I compare and contrast the drop size distribution (DSD) of released throughfall from individual juvenile and mature leaves of *Eucalyptus polyanthemos* (Red Box) and with drop sizes from open-field rainfall to glean insights into how intermediate post-fire vegetation canopies modulate

rainfall and discuss how these might affect hillslope hydrology and geomorphological processes.

6.2.2. Observations of processes

As mist spray was applied to each leaf, the processes of adhesion, accumulation (via cohesion), saturation and release of water drops from the leaf surfaces were observed. Each leaf functioned as mini catchment that accumulated water. Because of the hydrophobic and sclerophyllous nature of the leaves, there was minimal absorption of water by the leaf surfaces. Due to cohesion and surface tension forces, the water drops tended to bead up and expand as more water was added. As soon as any one of the water drops grew too large for stable adhesion to the leaf surface, it would start to deform, detach, then move and accelerate downwards by gravitational force (Nanko et al., 2011). During this passage across the leaf surface, it would collide into other smaller drops, collecting them and the coalesced mass of water would exit at an accelerated speed at the bottom area of the leaf as a single or series of large drops (see Plate 6-1).
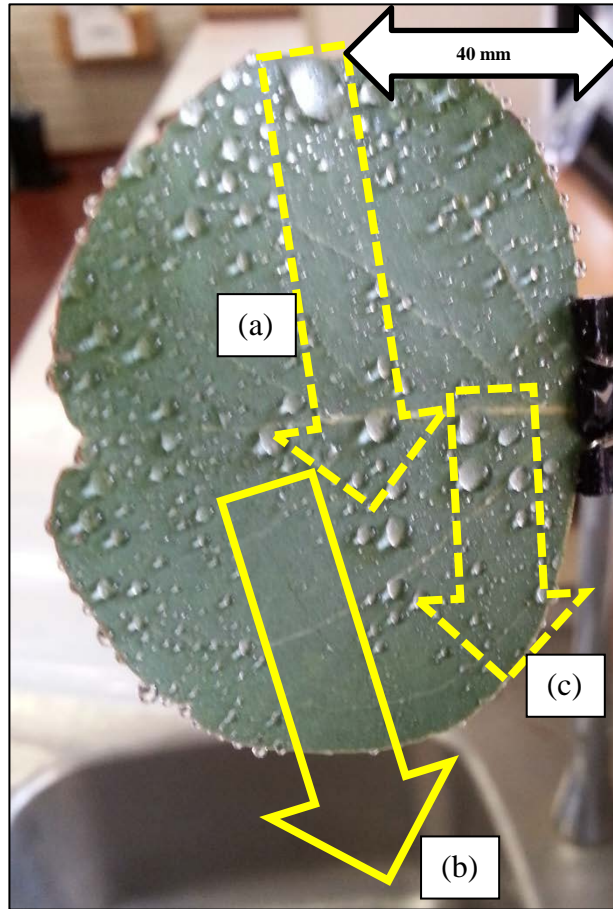
Plate 6-1. Photo of a juvenile leaf during mist-spray experiment and observed on-leaf processes. The dashed arrow at (a): likely pathway of large water drop when it grows large enough to exceed the adhesion forces to the leaf surface, deforms and move downwards due to gravity collecting smaller water drops along the way. Arrow (b): linear "dry" zone due to the recent exit of water drops. Arrow (c): two large water drops in the middle of leaf that may coalesce should the upper drop be dislodged first.

Note also from Plate 6-1 the small droplets at the edges of the leaf; these tended to move along this margin, similarly coalescing along the way to exit either at the bottom of the leaf, or from one of the points along the downward-facing edges of the leaf when the water drops were too heavy to be held by the leaf edge or adhere to the other drops proximal to the leaf surface itself. It was also found that small leaves tended to exhibit single drop exit points, while larger leaves tended to have two exit points that exited the leaf surfaces in close temporal correlation.

6.2.3. Drop sizes and distributions

The summary statistics comparing calculated drop sizes from open rainfall, juvenile leaves and mature leaves are presented in Table 6-4.

Table 6-4. Summary statistics comparing drop size distributions of open rainfall, juvenile leaves and mature leaves of *E. polyanthemos*. (**N = number of drops measured**)

Drop diameter (mm)	Open rainfall (N = 246)	Juvenile leaves (N = 246)	Mature leaves (N = 269)
Mean	1.45	3.89	4.24
Median	1.28	3.81	4.16
Min	0.89	1.41	2.72
Max	2.98	6.35	6.02
s.d.	0.48	0.99	0.66

The mean drop-sizes from juvenile leaves (3.89 mm) and mature leaves (4.24 mm) were close to 2.9 times larger than open rainfall drops (1.45 mm). Mature leaf generated mean, median and minimum drop diameters (4.24 mm, 4.16 mm and 2.72 mm respectively) were higher than those for juvenile leaves (3.89 mm, 3.81 mm and 1.41 mm respectively). However, maximum drop diameter for juvenile leaves (6.35 mm) was higher than for mature leaves (6.02 mm); juvenile leaf drop-size standard deviation (0.99) was higher than mature leaf (0.66). The boxplots of the DSDs for each group illustrate the differences (Figure 6-7).
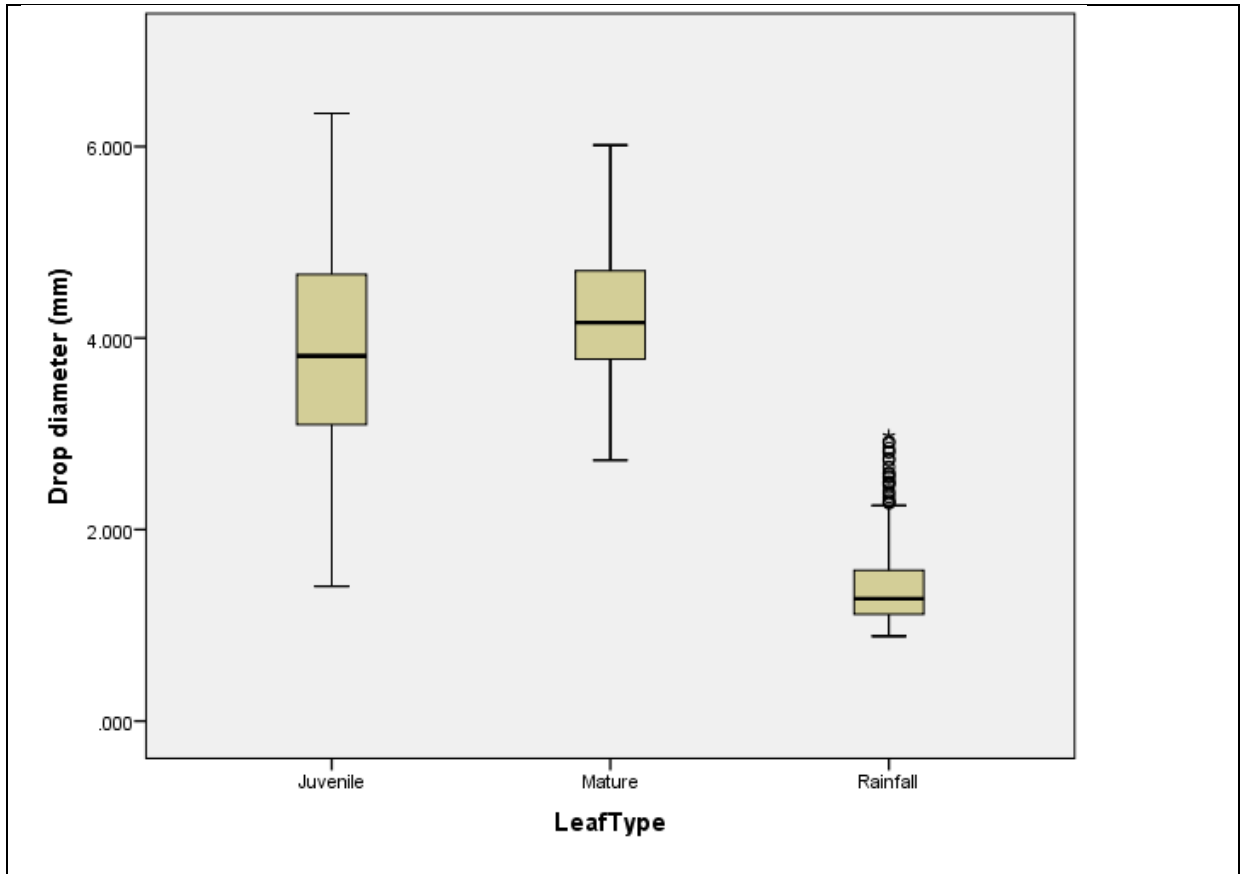
Figure 6-7. Boxplots of Drop-size distributions of (i) Juvenile leaves (ii) Mature leaves of *Eucalyptus polyanthemos* and (iii) open rainfall.

Examination of the histograms of drop-size distributions (Figure 6-8) found that the juvenile and mature leaf drop sizes (released throughfall) were more normally distributed compared to the strongly positively skewed distribution of open rainfall drops (Joss and Gori, 1978; Ulbrich, 1983; Wang et al., 2016a). The average open-field raindrop diameter was 1.42 mm, well within the expected range of 1 to 2 mm, with much fewer occurrences of larger drop sizes (American Meteorological Society, 2012; Nanko et al., 2008).
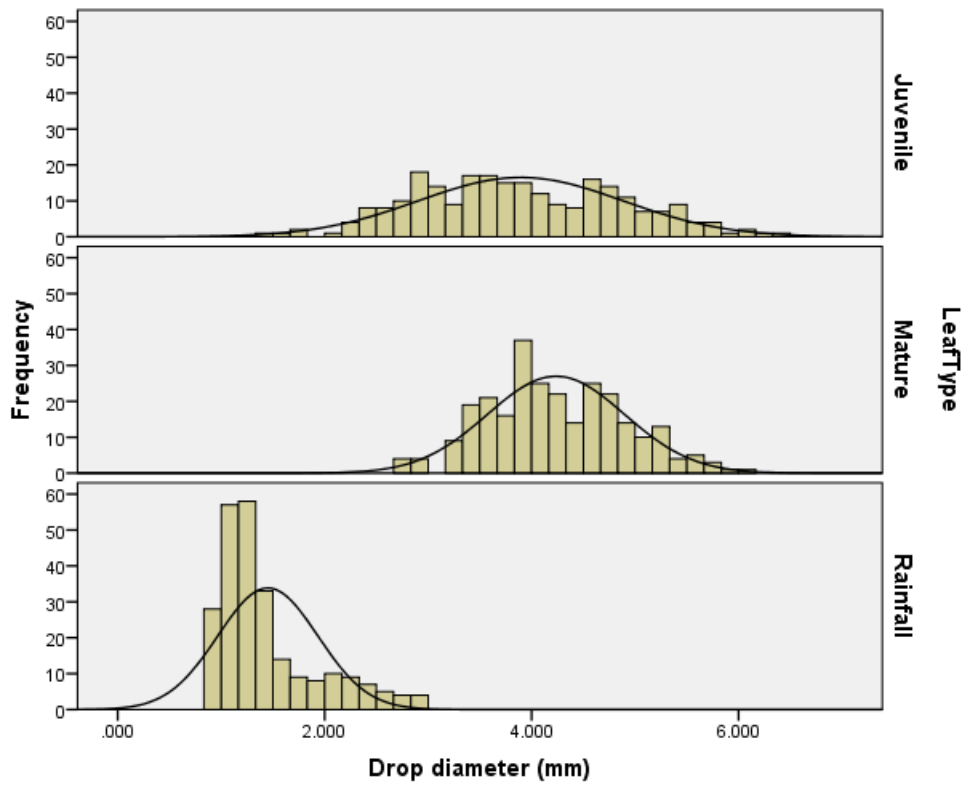
Figure 6-8. Histograms of Drop-size distributions of: (i) Juvenile leaves (ii) Mature leaves of *Eucalyptus polyanthemos* and (iii) open rainfall (hypothetical normal curves overlain for visual reference).

6.2.4. DSD differences between juvenile leaves, mature leaves and open rainfall

One-way ANOVA was conducted to examine differences in drop-size distribution between juvenile and mature leaves, and between the two leaf types with open rainfall. Statistically significant differences were found between all groups from One-way ANOVA: $F_{(2, 758)} = 1.059$, $p < 0.001$. The Tukey post-hoc test found that drop sizes from juvenile leaves were statistically significantly lower than those from mature leaves. This was further supported by results of the non-parametric Mann-Whitney U-Test which found statistically significant differences ($p < 0.001$) between drop diameters from all three groups (juvenile leaves, mature leaves and open rainfall).

From the statistical analysis, and by visual inspection of the histograms shown in Figure 6-9, the drop-size distributions from juvenile and mature leaves were quite distinctive.
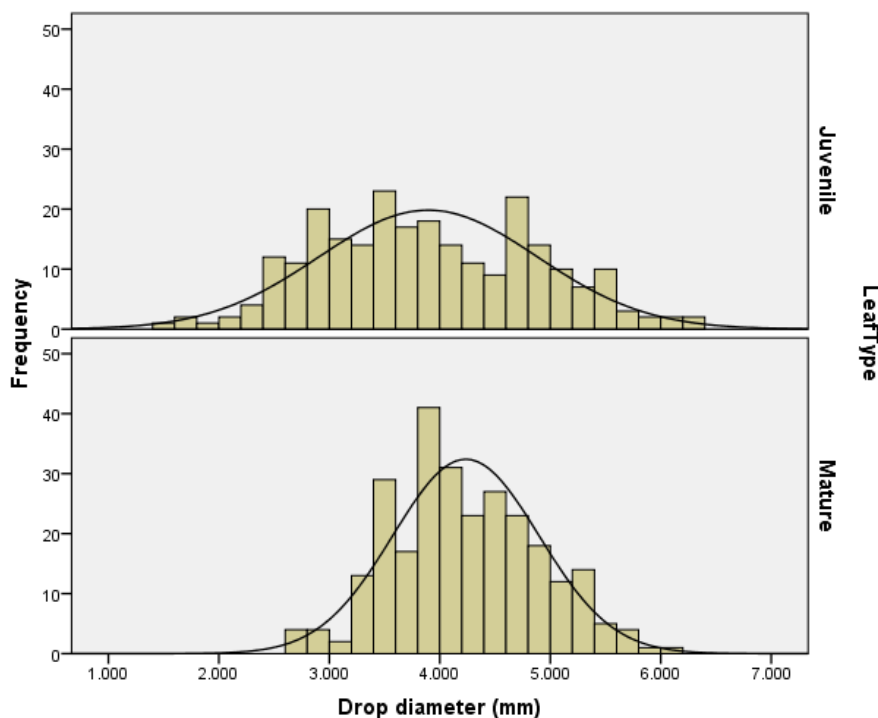
Figure 6-9. Histogram of Drop-size distributions of: (i) Juvenile leaves and (ii) Mature leaves of *Eucalyptus polyanthemos* (hypothetical normal curves overlain for reference).

Mature leaves generated a narrow, concentrated range of drop sizes (min-max), whereas juvenile leaves generated a wider range of larger and smaller drops (min-max). Open rainfall drops were very distinctly smaller than the drops generated from leaves.

6.2.5. Does leaf size matter?

Further examination of drop size distribution within each group of juvenile and mature leaves was conducted to study if any trends according to leaf sizes within juvenile/mature leaf groups could be detected. This would be useful in furthering understanding of factors affecting throughfall drop sizes that may be similar or contrasting, across juvenile and mature leaves.

6.2.5.1. Juvenile leaves – drop size variations with leaf sizes

The summary statistics for drop sizes generated from mist spray on juvenile leaves are presented in Table 6-5. Note that the leaves were labelled 1 (smallest) to 4 (largest) (cf. Plate 2a).

Table 6-5. Summary statistics of drop sizes generated from mist spray on juvenile leaves of *E. polyanthemos*.

Size class	Area (cm^2)	N (drops)	Mean drop diameter (mm)	Min	Max	s.d.
1	9.8	45	4.71	3.06	6.35	0.94
2	17.0	82	3.37	1.41	6.13	0.91
3	23.8	64	3.91	2.59	5.54	0.75
4	35.6	55	3.98	1.63	5.44	0.92

Observation of the distribution of drop size values found interesting contrasts between leaf sizes, particularly for the smaller leaves (see Figure 6-9). The smallest leaf (size class 1) gave the highest mean drop diameter (4.71 mm), the highest minimum drop size (3.06 mm) and highest maximum drop size (6.35 mm) and marginally highest drop size diameter s.d. (0.94). However, the mean drop diameter gradually increased as the size classes increased

from class 2 (3.37 mm) to class 4 (3.98 mm). Size class 2 leaf (see Figure 6-9) generated five

large drop size outliers that were not observed for the other size classes. For size class 3, the

minimum drop size of 2.59 mm was much larger than the other size classes, with a distinctly

lower drop diameter s.d. (0.75).
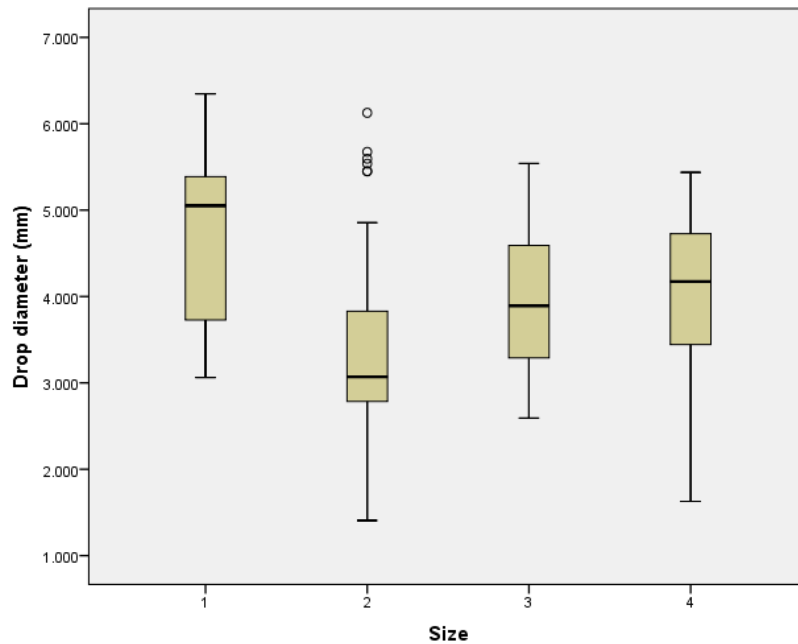
Figure 6-9. Boxplots of Drop-size distributions of different *Eucalyptus polyanthemos* juvenile
leaf sizes (1 the smallest and 4 largest).

From one-way ANOVA, statistically significant between-group differences were found:

$F(3, 242) = 22.845$, $p < 0.001$. Tukey HSD post-hoc test found significant differences

between all leaf size classes ($p < 0.001$) except for the larger leaf sizes 3 and 4 whereby no

significant difference was found ($p = 0.976$). The latter was further verified with Bonferroni

correction post-hoc test with $p = 1.0$ when mean drop diameter values for leaves 3 and 4 were

compared.

6.2.5.2. Mature leaves – variations in drop size distributions

Table 6-6 shows the summary statistics for drop sizes generated from mist spray on different sized mature leaves, with size classes 1 (smallest) to 4 (largest) (cf. Plate 2b). Figure 6-10 presents boxplots of the distribution of drop sizes. The smaller leaf size classes 1 and 2 had slightly higher average drop sizes (4.36 mm and 4.39 mm respectively) compared to the larger leaf size classes 3 and 4 (4.08 mm and 4.14 mm respectively). However, there were generally no clear differences across the drop sizes generated by different leaf sizes for the mature leaf group.

Table 6-6. Summary statistics of drop sizes generated from mist spray on mature leaves of *E. polyanthemos*.

Size class	Area (cm^2)	N (drops)	Mean drop diameter (mm)	Min	Max	s.d.
1	9.5	70	4.36	3.47	5.60	0.54
2	13.2	59	4.39	2.72	5.73	0.70
3	23.4	66	4.08	2.88	5.31	0.56
4	43.6	74	4.14	2.75	6.02	0.77
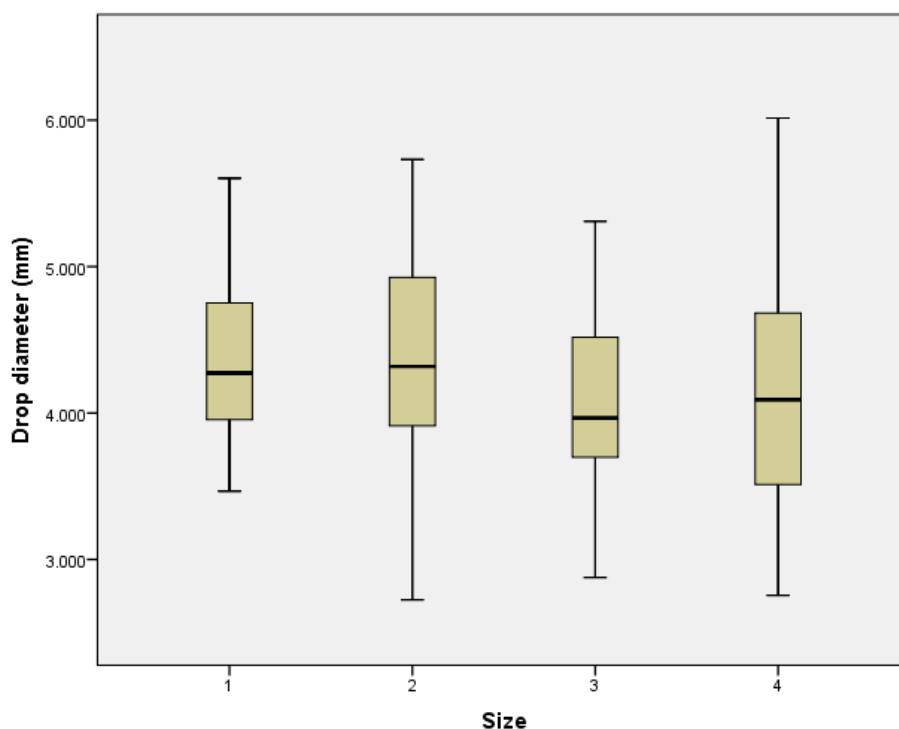
Figure 6-10. Boxplots of Drop-size distributions of different *Eucalyptus polyanthemos* mature leaf sizes (1 the smallest and 4 largest).

One-way ANOVA found statistically significant between group differences: $F(3, 265)$ = 3.637, $p < 0.05$, but Tukey HSD post-hoc test found significant differences only between the intermediate mature leaf sizes 2 and 3 ($p = 0.047$). Bonferroni correction post-hoc test found no significant drop-size differences between any leaf size groups, including drops from leaf sizes 2 and 3 with $p = 0.058$.

The distribution of drop sizes for mature leaves tended to a normal distribution, albeit of significantly larger size than open field rainfall, or unmodified (free) throughfall. This was very similar to the throughfall characteristics reported by Brandt (1989) for differing foliage of plants from three different genera. However, the drop size distribution of *E. polyanthemos* juvenile leaves was distinctly different from that of mature leaves by having a much wider variation in drop sizes, even though the average drop size was slightly lower. Juvenile foliage also showed general increase in mean drop size with leaf sizes from size class 2 to 4 albeit large drop sizes from size class 1 leaves (this is discussed in detail in the following paragraph); mature foliage did not appear to show this trend with mean drop sizes generated remaining relatively uniform. This indicates a unique drop-size spectrum between juvenile and mature *E. polyanthemos* foliage. One of the possible explanations for the distinct drop-size spectra between juvenile and mature leaves is the different leaf shapes (orbicular vs. ovate-lanceolate respectively) combined with the pendulous hanging habits. The orbicular shaped juvenile leaves formed broad "catchments" upon which beads of water drops grew. This provided a wider range of positions from which water drops could move downwards and exit the leaf surface – multiple drip points; but the curvature of the orbicular-shaped juvenile leaf also caused the "rundown" length to differ substantially and therefore lead to wide variations in the resultant volumes of the exiting drops because of differential extents of water drop coalescence. On the other hand, mature leaves, being ovate-lanceolate in shape, did not result in as much variations in "(sub)-catchment" areas and "rundown" lengths, even though variations in drop sizes were still observed; this explanation is illustrated in Figure 6-11.
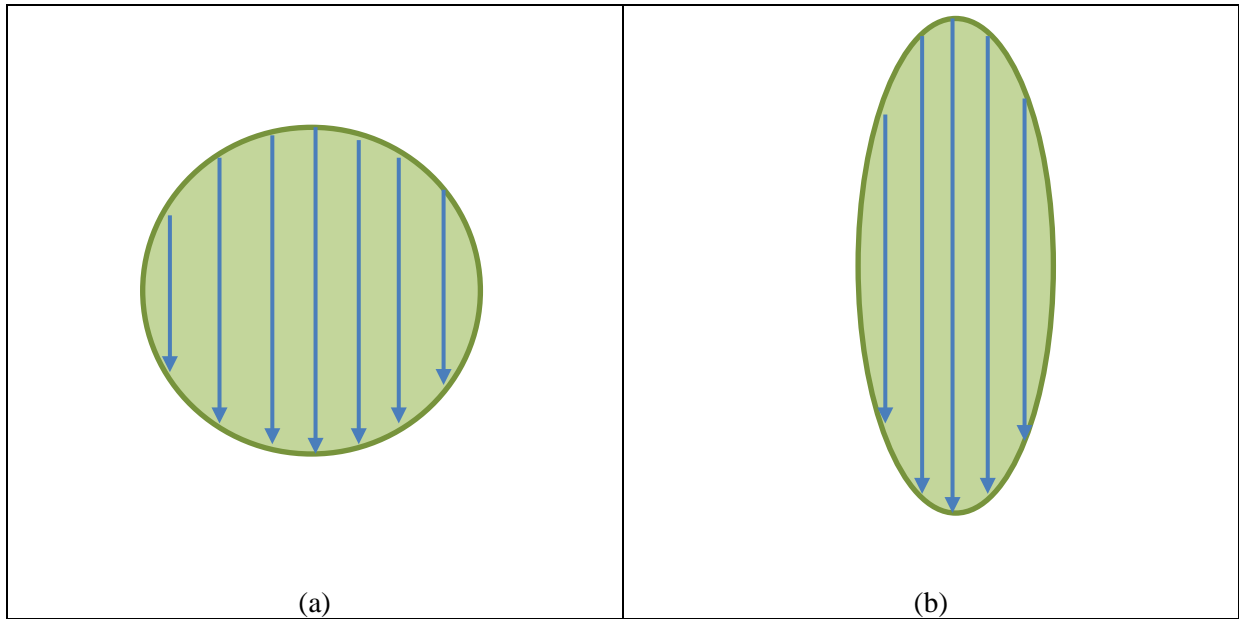
Figure 6-11. Schematic of water "catchments" and "pathways" for (a) juvenile and (b) mature leaves of *E. polyanthemos* (Red Box).

Another interesting observation was also how the mean drop sizes were large and largest from the smallest leaves from both mature and juvenile foliage respectively (see Tables 6-5 and 6-6). This was contrary to normal expectations as one would expect larger leaves to provide larger "catchments", enable greater coalescence of smaller drops to compose larger ones that ultimately exit the leaves as large drops. However, what occurred instead was the natural separation of the leaf's catchments into smaller sub-catchments from which combinations of small and large drops were formed over the larger leaf area and exit as primary and secondary drips from two or more points. For the smallest leaves, only single foliar "catchments" developed where the applied water quickly coalesced as a single mass of water and exited the bottom of the leaf as a large drop. These processes related to the planar, uncurved hydrophobic surface of the *E. polyanthemos* leaves, and was also attributed to the pendulous hanging habit of the *Eucalyptus* leaves which were not conducive for the accumulation of large volumes of water before flow and drip processes were set into motion. This was in contrast with the morphology of many tropical plant species that have inward-inclining leaf curvatures adapted to managing regular heavy tropical rainfall by directing

water towards their midrib of the lamina and then evacuated via drip tips (Dean and Smith, 1978; Holder, 2016; Ivey and DeSilva, 2001).

In comparison with a selection of throughfall drop size studies, the drops generated from *E. polyanthemos* are larger than those reported by Hall and Calder (1993) for Caribbean pine and River Red Gums, but smaller than Paperplant and Umbrella tree reported by Brandt (1989) (see Table 6-7):

Table 6-7. Comparison of drop diameters for *Eucalyptus polyanthemos (Red Box)* mature and juvenile leaves in the present study with other selected species and studies.

Species	*Schefflera* sp. (Umbrella tree)	*Fatsia japonica* (Paperplant)	*Pelargonium* sp. (Geranium)	*Pinus caribaea* (Caribbean pine)	*Tectona grandis* (Teak)	*Eucalyptus camuldensis* (River Red Gum)	*Eucalyptus polyanthamos* (Red Box)	*Eucalyptus polyanthemos* (Red Box)
Foliage type	Mature; large	Mature; large	Mature; medium sized	Mature	Mature	Mature	Mature	Juvenile
Median drop diameter (D_{50}) (mm)	5.28	4.96	5.22	2.3	4.2	2.8	4.24	3.89
Source	(Brandt, 1989)	(Brandt, 1989)	(Brandt, 1989)	(Hall and Calder, 1993)	(Hall and Calder, 1993)	(Hall and Calder, 1993)	Present study	Present study

Extrapolation of the above-mentioned dynamics to the patch scale, and their hydrologic and erosional impacts, can be considered in the context of the 'zones of influence' framework, as well as longer-timeframes where the vegetation formation achieves its climax stage where *Eucalyptus* foliage is dominated by mature leaf forms.

Figure 6-12 illustrates the possible drop spectra, and by implication their hydrologic and erosional impacts under   differing canopy and open non-canopy conditions.

(a) open-field rainfall   (b) juvenile leaf-form dominant   (c) mature leaf-form dominant
                                              (intermediate post-fire)   ("full") post-fire recovery and
                                                                                                         long unburnt)
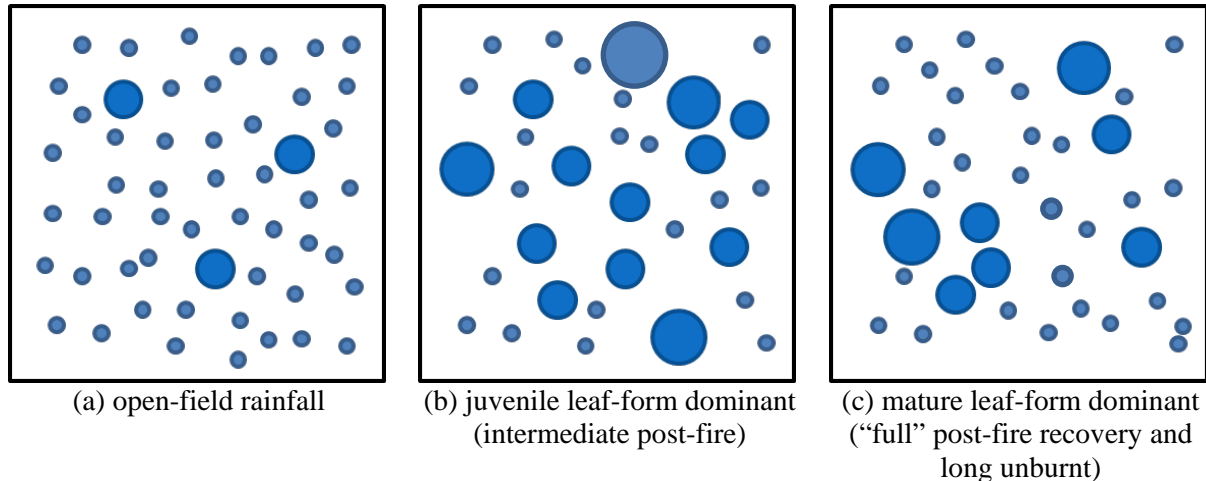
Figure 6-12. Possible drop-size spectra for (a) open-field rainfall; (b) juvenile leaf-form dominant and (c) mature leaf-form dominant dry-eucalypt forests.

For open-field rainfall, (Figure 6-12a), most of the raindrops would be in the smaller size-range and therefore individually have lower capacities to dislodge and entrain soil particles via splash effects, although there would still be a small number of large drops having high kinetic energy on impact. Furthermore, an increased number of larger drops would be expected to occur with high-intensity rain 'pulses' within larger (and longer) events, or in high-intensity thunderstorms (see Chapter Five). While splash erosion in open-field conditions may be limited in one way due to drop-sizes, there would be minimal abstraction of total water mass, albeit as numerous small drops, compared to an under-canopy situation (Figures 6-1a and b). This would lead to higher likelihoods of soil infiltration and moisture storage capacities being exceeded, overland flow being generated and consequently amplification of splash energy even with smaller drops (Farres, 1987; Kinnell, 2005; Salles and Poesen, 2000; Terry, 1998) on bare interspaces. Indeed, the hillslope erosion processes and dynamics in this condition would be quite distinct from the two (intermediate and full post-fire recovery) under-canopy conditions considered below.

For intermediate post-fire canopy conditions dominated by juvenile leaf-forms, throughfall is likely to be dominated by numerous large water drops with potentially higher erosive power than open-field rainfall (Figure 6-12b). Due to the rather dense post-fire canopy regrowth, there would be low proportion of small, free throughfall drops of similar drop-sizes to open-field rainfall. However, the range of released throughfall drop sizes would be rather wide (Figure 6-8). The spatial distribution of these large drops would also be much more heterogeneous than that for open-field rainfall and result in the concentration of splash energy at specific positions below drip points, and minima at areas below the canopy where water is diverted away from. This would have the potential to create pronounced microtopography through cratering effects (e.g. Plate 4-3), as well as hyper-localised positions of overland flow generation.

For mature re-growth (long unburnt) conditions, large drops would also be generated but their abundance rather constrained as the openness of the mature *Eucalyptus* canopy would lead to higher proportion of incoming rainfall of free throughfall instead of released throughfall, although the spatial heterogeneity of drop impacts would still be greater than the open-field rainfall condition (Figure 6-12c). Furthermore, the size range of the large released throughfall drops would be narrower (Figure 6-8). The larger average drop-size for released throughfall from mature leaves compared to juvenile leaves would see higher erosive energy per drop; and this may be enhanced by the higher drip height due to the substantial vertical extension of the canopy after substantial growth "back" to climax vegetation conditions.

For intermediate post-fire under-canopy conditions examined in this research, possible relationships between drip heights (Figure 6-4) and splash energy need to be considered. Table 6-8 presents the 100-drop s^{-1} and one-minute kinetic energies derived from the likely drip-height for each splash-cup, median drop diameter of 3.81 mm (Table 6-3), and

the free-fall velocities of individual water drops corresponding to each drip height, including the effects of air-resistance following Newtonian physics (Kirkby, 2011):

$$K.E. = 0.5\, mv^2$$

where *K.E.* was kinetic energy in Joules; *m* the mass of water drop and *v* the velocity of water drop in free-fall varying with drip height.

Applicable parameters were (a) acceleration due to gravity: 9.80665 m s^{-2}; (b) mass of spherical water drop of diameter 3.81 mm): 2.897 x 10^{-5} kg where density of H_2O was taken to be 1000 kg m^{-3}; (c) drag coefficient of spherical water drop: 0.5; and (d) density of air (falling medium): 1.225 kg m^{-3}.

Table 6-8. Derived drop velocity (m s^{-1}) and kinetic energy (in mJ) for drip heights for splash cups #1 to #15 for median drop diameter of 3.81 mm from juvenile leaves of *Eucalyptus polyanthemos*.

Cup	1	2	3	4	5	6	7	8	9	10	11	12	13	14	15
Ht (cm)	83.0	45.0	87.0	34.0	76.0	116.0	103.5	110.5	62.5	68.5	62.0	67.5	167.5	75.0	46.5
Vel (m/s)	3.5	2.7	3.5	2.3	3.3	4.0	3.8	3.9	3.0	3.1	3.1	3.1	4.6	3.3	2.6
100-drop s^{-1} K.E. (mJ)	17.3	10.3	18.1	8.0	16.2	23.0	20.9	22.1	13.1	14.2	13.6	14.0	30.5	15.4	10.0
1-min K.E. (mJ)	1040.9	615.3	1087.2	479.3	969.2	1378.5	1251.3	1324.6	784.4	852.8	814.7	841.7	1830.2	924.1	600.7

While terminal velocities would not normally be achieved with the rather low drip heights, substantial erosive energy could still be imparted due to the large drop-sizes. Furthermore, the consistency in generating large drop sizes would be high, and the spatial concentration of drop impacts would also be very high due to the static position of each drip point. Exploratory analysis did not find a simple positive relationship between drip height and sand loss or erosivity ratios. Although cup #13 had the highest kinetic energy potential (1830.2 mJ min^{-1}) due to it having the highest drip height (167.5 cm) that was unhindered (only one layer; Figure 6-4b), it did not correspondingly register the highest sand loss (Figure 6-5). Conversely, cup #4 had the lowest drip height and lowest kinetic energy potential

(479.3 mJ min^{-1}) and three layers of foliage but this did not translate into the lowest sand loss mass either (Figure 6-5). Cup #14 had a moderate drip height of 75 cm and 3 layers, but had the highest sand loss mass in Periods A, B and C. These results mean that the throughfall processes are influenced by a complex set of interacting factors that would include not only drip heights, but the configuration and layering of foliage, in interaction with variable rainfall inputs and possibly wind, that determine the rate and nature of throughfall drops arriving at the soil surface and their ensuing hydrological and erosional effects. These should be the subjects of further investigations through controlled experiments using, for example, rainfall simulations and foliage samples.

For researchers' understanding of throughfall processes to advance (Levia et al., 2017), detailed on-leaf dynamics of water flow offer useful insights into how and why some plant canopies generate signature drop-size spectra (Brandt, 1989; Hall and Calder, 1993; Vis, 1986). Furthermore, where significant differences in foliage shape or density are expected to differ temporally seasonally and phenologically, the leaf-scale hydrological processes will be important. Indeed, valuable headway has been made in the examination of released throughfall (Geißler et al., 2012a), stemflow (Dunkerley, 2014a; Dunkerley, 2014b), intra-storm evaporation (Dunkerley, 2008c), intra-storm intensity variations (Dunkerley, 2014b; Nel et al., 2016; Parsons and Stone, 2006) and the consequent soil-water dynamics (Liang et al., 2011).

While the experiments discussed in the present section were conducted under controlled conditions using mist-spray that might approximate light drizzle conditions but would differ substantially from heavier natural rainfall events, detailed insights have been found at the individual leaf scale. This complements findings by workers such as Nanko et al. (2011) who have found systematic under-canopy spatial variations in throughfall kinetic energy with distance from the trunk, and does not preclude future studies capitalizing on the advantages

(low-cost, replicable) of this method to accumulate more empirical data from various regions, vegetation formations and species. With increasing focus on understanding multi-scale inter-relationships in hydrology and geomorphology from the plot, catchment and river basin scales (Bergström and Graham, 1998; Blöschl and Sivapalan, 1995; Merz et al., 2009; Parsons et al., 2006; Verstraeten, 2006; Wainwright et al., 2000), multi-scale examination of canopy hydrology from the leaf, twig, branch to individual tree scale will also be valuable.

6.3. Conclusion

This component of the research developed and evaluated the low-cost dyed filter paper technique for the determination of water drop masses and sizes and found it to be sufficiently reliable for further application (see Section 4.7.1.). The use of thicker media in the form of Whatman No. 3 filter papers (instead of the thinner No. 1 type) was preferred due to the higher robustness and ease of handling in the lab and field; for preparation, experimentation and drying. This approach can also be implemented with relative ease for determining and reporting drop-size spectra from rainfall simulators which can differ markedly from one another (Dunkerley, 2008b).

As described in Section 4.7.2., this technique was then applied to determine and contrast drop-size distributions of released throughfall drops from juvenile and mature leaves of *Eucalyptus polyanthemos*, a common species found in dry sclerophyll forests in southeast Australia (Brooker and Kleinig, 2006), with juvenile leaf forms dominating post-fire regrowth. It was found that juvenile and mature leaves generated distinctly different drop-size spectra that could be attributed to the detailed water drop growth and movement processes on the differently-shaped foliage. Contrary to initial expectations, larger leaves tended to generate primary and secondary drops leading to a lower average drop size due to the increased presence of secondary dripping from multiple points. These findings contribute unique empirical knowledge about drop-size distributions of *Eucalyptus polyanthemos* tree species commonly found in dry sclerophyll forests at juvenile and mature growth stages, that have various applications in representing and predicting hillslope hydrology and geomorphology, particularly for dry sclerophyll *Eucalypt*us forests at various stages of recovering from wildfires.

In addition to the findings presented in this study, new factors must be considered, particularly in the context of projected climate change that will see increased temperature

293

fluctuations with warming trends, as well as shifts in the rainfall regimes towards high-intensity rainfall events. A recent study by Klamerus-Iwan and Błońska (2018) found that increased temperatures led to increased foliage wettability and canopy storage capacity of English oak (*Quercus robur* L.), common beech (*Fagus sylvatica* L.), small-leaved lime (*Tilia cordata* Mill.), silver fir (*Abies alba*), Scots pine (*Pinus sylvestris* L.) and Norway spruce (*Picea abies* L.). These imply possible shifts in detailed canopy hydrology dynamics across different seasons, as well as in the next few decades as the climate warms, and concomitant changes in the splash and runoff erosional processes under the intermediate post-fire plant canopies. These are unexplored aspects for dry eucalypt forests and foliage and deserve some attention from researchers in the near future.

With the close examination of throughfall processes resulting from their modulation of incident rainfall resulting in the revealing of interesting and important intra-foliar dynamics, we now turn to hillslope material fluxes resulting from the rainfall and throughfall inputs on the study area, the subject of Chapter Seven.

Acknowledgement

CHAPTER SEVEN: HILLSLOPE MATERIAL FLUX

Hillslope erosion processes and rates in the aftermath of forest fires are of great concern in many parts of the world (Moody et al., 2013; Shakesby and Doerr, 2006; Shakesby et al., 2016; Tomkins et al., 2008) (see also Chapter One). In the southeast Australian context, the regular occurrences and increasing risks of megafires and higher intensity rainfall in the foreseeable future climate (Kendon et al., 2014) motivate the need to better understand the key processes that determine the "recovery" rates and trajectories during the intermediate, in addition to the immediate post-fire windows (Shakesby, 2013) (see Chapter One). This is even more important when considering the distinctive climate, topography, vegetation and soil characteristics of this region (Shakesby, 2013; Shakesby et al., 2007) (see also Chapters Two and Three), of which the present study area is a small but representative component.

In the intermediate phase of post-fire vegetation recovery, a timeframe that has at present experienced a paucity of detailed research, hillslope erosion is governed by a complex and dynamic set of interacting processes characterized by heterogeneity of ground and vegetation canopy cover. These result in variable extents of rainfall modulation and consequent splash and overland flow erosion rates on postfire hillslopes which can be understood in the context of the DZI framework (Chapter Two).

The specific characteristics of individual rainfall events determine the timing, rate, volume and caliber of sediment transported, including whether thresholds for sediment transport are exceeded; short bursts of high-intensity rainfall are likely to lead to different rates and operations of splash impacts and runoff generation to cause sediment transport on hillslopes, compared to longer and low-intensity events (Spigel and Robichaud, 2007).

There is thus a need for further investigations on the effects of these event characteristics that are frequently not reported in sufficient detail, nor accessible from many weather station records (Martin et al., 2011). Indeed, Dunkerley (2010b) noted that because

Intra-event Rain Rates (IERRs) values varied widely with the duration of the enclosing event and the event delineation technique, wider exploration was needed because of the various important implications on the interpretation of hydrological and geomorphological findings in the published literature. In intermediate post-fire vegetation conditions, where ground and canopy cover conditions are complex and heterogeneous, the rainfall-canopy-ground interactions controlling hillslope erosion, transport and deposition are even more interesting. Indeed, the dynamic variations in throughfall processes and impacts examined in Chapter Six have illustrated some of this complexity that remain to be properly disentangled vis-à-vis hillslope erosion processes and outcomes, the focus of concern for many workers in this area of research.

While the EI_{30} compound variable is widely used in erosion studies in different regions with distinct rainfall regimes, for instance by de Santos Loureiro and de Azevedo Coutinho (2001) in Portugal, Sheridan et al. (2008) in Victoria, Australia, and Wang et al. (2016b) in Beijing, northern China, it actually integrates, smooths-out and obscures substantial and important IERR variations. On the other hand, I_{1min}, one-minute rainfall intensity helps to capture some of these variations through the finer temporal resolution for integrating rainfall depths and thus more closely reflecting the actual event characteristics; this has not been widely explored.

Thus far, we have examined in some detail, rainfall and throughfall characteristics for the study site over the 10-month measurement period and considered their hydrological and erosional outcomes in Chapters Five and Six. In this chapter, I discuss the resultant hillslope erosion rates on this steeply sloping, partially-vegetated post-fire landscape determined from trapped material (gravel, soil and plant litter) collected from six sediment fences (SFs) over Periods A to F (see Chapter Four). Firstly, I describe the general patterns of sediment and litter fluxes across all the sediment fences through Periods A to F, including particle size

distributions of the eroded soil. This is particularly important because the grades of sediment eroded would be a useful indication of the splash and flow energies responsible for their detachment, entrainment and transport. This was done to explore any possible relationships with key rainfall characteristics of each Period reported in Chapter Five. Organic litter trapped in the SFs were also collected, weighed and analyzed. Because of their low densities, the organic litter contributed only a small component of the total mass of eroded hillslope material. I will then proceed to examine the detailed patterns of hillslope material fluxes individual SFs. Following that, I present several analyses that explore the range of possible relationships to selected rainfall metrics. In line with the focus on high-temporal resolution rainfall energy and its hydrological and erosional impacts, I delve into analyzing the eroded soil masses for the various SFs with respect to the one-minute threshold rainfall intensity durations through regression analysis. Finally, I discuss the results and analyses of the hillslope material fluxes by considering how the hydrological and erosional processes occur at each of the SFs, and on the hillslope generally.

7.1. Hillslope sediment and organic litter fluxes

As described in Chapter Three, the study site's soils at the commencement of the fieldwork were classified as Leptic Lithic Rudosols (Isbell, 2002) which were structureless (single grain), except for the top few millimetres of soil where weak aggregation and very slight darkening of soil particles from organic matter were observed. Gravel and pebbles were embedded in a matrix of mostly sand and silt particles with very little clay. It had been deduced from preceding events (massive post-fire erosion and floods), past reports and on-ground evidence that much of the original topsoil had been stripped away, leaving a gravelly, skeletal soil with a very shallow depth to the Silurian-age sedimentary bedrock of mud, silt and sandstones. These composed the source material that were being actively eroded on the study hillslopes under intermediate post-fire conditions. With such a depleted, infertile substrate, rates of post-fire vegetation regrowth may have been significantly retarded, extending the window of recovery. The sediment fences trapped material of all types and size ranges. These were comprised of soil (sediments < 2 mm grain size), gravel (sediments ≥ 2 mm grain size) and organic litter (twigs and leaves including fragments). Plates 7-1 a-c present the soil, gravel and litter components of the hillslope material.
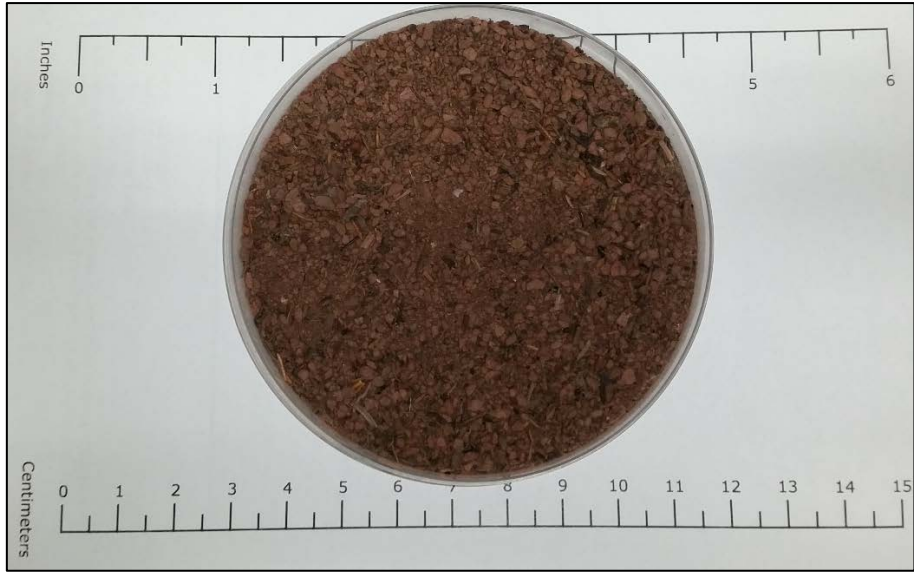
(a)
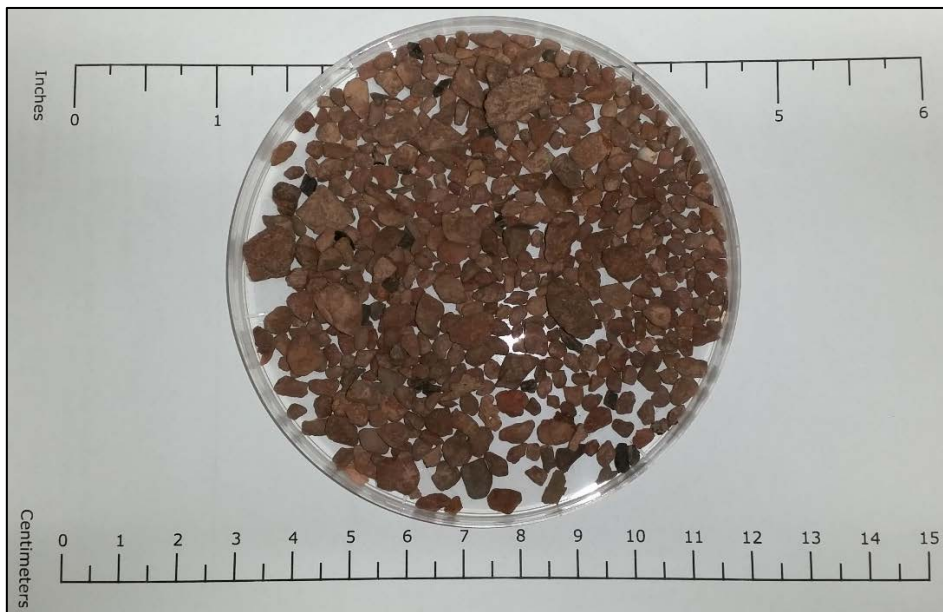
(b)

(c)

Plate 7-1. Hillslope material: (a) soil (fine earth fraction sediments < 2 mm diameter); (b) gravel (sediments ≥ 2 mm diameter); and (c) organic litter.

Upon visual and tactile examination of eroded soil texture in the field, it was found that the trapped sediments were comprised mostly of coarse to fine sand, made up of mostly chemically-unaltered fragments derived from the brown, pinkish sedimentary parent rock. The pebbles and gravel sediments were also very similar in appearances to the parent material. Other than the abundant coarse sediments, the eroded soil was also quite silt-rich, with only a small proportion of clay. In addition to the sediments, organic litter in the form of whole, parts and fragments of twigs and leaves were also trapped in the SFs. It was presumed

300

that this litter had mostly been transported from upslope positions via fluvial as well as dry aeolian processes.

The gravel component of the eroded sediments was observed to be angular, with the occasional inclusion of pebbles alongside more the numerous but smaller calibre gravels. Plate 7-2a shows the largest 50 pebbles and gravels, and Plate 7-2b shows the size range of the smaller gravels.

(a)   (b)
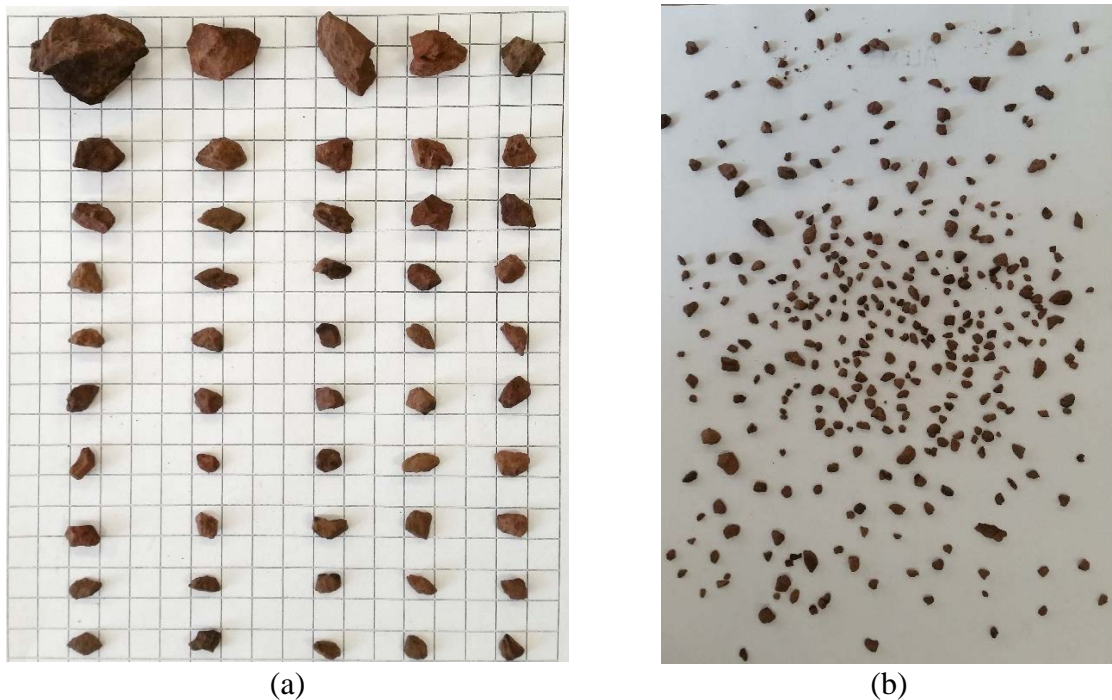
Plate 7-2. Gravel component of eroded sediments: (a) 50 largest gravels (note one cm^2 grid for scale); (b) majority of gravel component (note dimensions of background A4-size paper are 297 mm by 210 mm).

The largest gravel as shown in Plate 7-2a had the following Feret diameters (Merkus, 2009): 36.7 mm (major axis) and 29.2 mm (minor axis). The Aspect Ratio was 1.26; Circularity: 0.63. For all 50 gravels, mean Circularity was 0.76 (standard deviation: 0.05) and mean aspect ratio was 1.49 (standard deviation: 0.3). Feret diameters for the mean sediment size for the top 50 pebbles and gravels were: 11.9 mm (major axis) and 9.5 mm (minor axis). With a strong positive skew in the particle size distribution, median Feret diameters were 9.74 mm (major axis) and 7.8 mm (minor axis). For the small gravels shown in Plate 7-2b (N

= 338), Feret diameters for mean sediment size were: 5.56 mm (major axis) and 3.79 mm (minor axis). For median sediment size which was smaller than the mean due to positive skew in the particle size distribution, Feret diameters were: 3.51 mm (major axis) and 4.89 (minor axis). Mean and median Aspect Ratio were 1.47 and 1.39 respectively. Mean and median Circularity were 0.76 and 0.78 respectively. This description of the pebble and gravel component of the eroded material shows how unrounded they were, giving them high coefficients of drag that may have rendered them more prone to entrainment in overland flow than if they were circular in dimensions. The occasional inclusion of pebble-sized material hinted at the possible operation of strong but infrequent erosive forces, or alternative modes of transport.

Figure 7-1 presents the mass of eroded sediment (soil and gravel) over the 6 integration time periods (A to F).
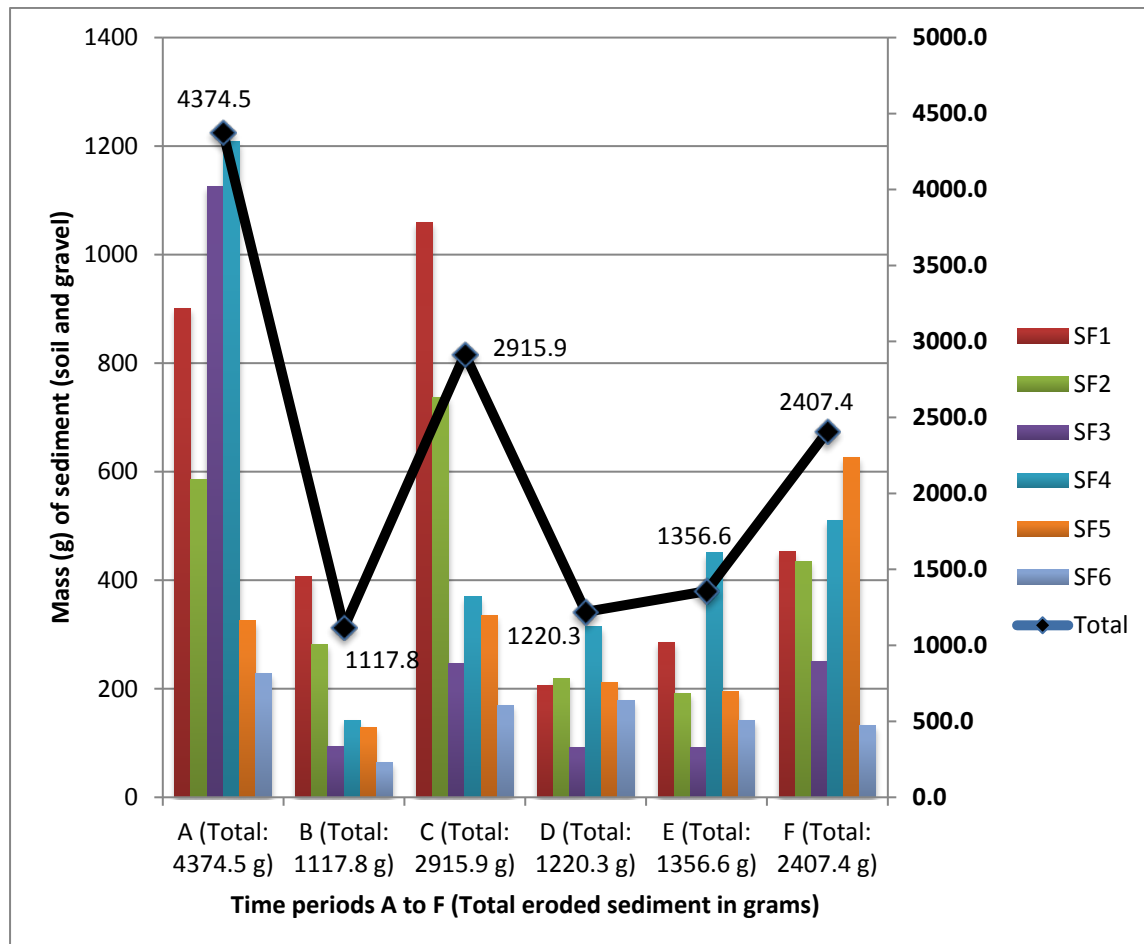
Figure 7-1. Mass of eroded sediment across all time periods (A to F) for SFs 1 to 6.

During this period, a total of 13,392.5 g of sediment (gravel + soil) was collected from the 6 sediment fences (each 1.5 m) totalling 9 m length. Nominally, the study hillslope was generating a gross sediment flux rate of 1488 g per contour metre over the 295 days. With total primitive rainfall depth recorded for the measurement period at 683.3 mm, general sediment flux rates per metre contour per mm of rainfall worked out to be 2.2 g soil m^{-1} mm^{-1} rainfall. Overall rainfall erosion rate (mass of soil eroded in grams per mm of primitive rainfall) was 19.6 g mm^{-1}. From Figure 7-1, it seemed that sediment yield fluctuated quite wildly between Periods A to C, followed by an increasing trend from Periods D to F.

However, the rainfall depth, as well as other parameters were different between individual periods. Hence, we proceed to examine how erosion rates varied between each periods as presented in Table 7-1.

Table 7-1. Erosion rates for Periods A to F integrated across all SFs expressed as mass of eroded soil (g) per mm primitive rainfall depth.

Period	A	B	C	D	E	F
Total sediment yield	4374.5	1117.8	2915.9	1220.3	1356.6	2407.4
Primitive rainfall (mm)	123.6	76.5	206.0	79.4	110.8	87.0
Mass of eroded soil (g) mm^{-1} rainfall	35.4	14.6	14.3	15.4	12.2	27.7

Periods A and F had the highest erosion rates (35.4 and 27.7 g mm^{-1} respectively). On the other hand, Period E had the most muted erosion rates at 12.2 g mm^{-1}. Low, below-average rainfall erosion rates were observed for Periods B, C and D at 14.6, 14.3 and 15.4 g mm^{-1} respectively. There appeared to be a generally declining trend from Period A to E, followed by a return to high, above-average rainfall erosion rates in Period F.

Examination of Figure 7-1 also found that the different SFs varied in their responses to rainfall input to total sediment yield in each Period. For instance, while SF1 had the highest sediment yield in Periods B and C (406.2 g and 1059.6 g respectively), it was third-highest in Periods A (901.1 g), D (205.8 g) and F (453.3 g); while SF4 had the highest sediment yield in Period A (1209.1 g), D (313.8 g) and E (450.3 g), and ranking second in Period F (511.0 g) and third in Periods B and C (141.5 g and 369.2 g respectively).

To further examine this variability, the rainfall erosion rates for individual SFs in each Period, as well as their percentage composition of total sediment yield were calculated and presented in Figure 7-2. While Period A had the highest rainfall erosion rate, the contribution

from various SFs were quite uneven. While SF4 and SF3 yielded high values of 9.8 and 9.1 g mm^{-1} rainfall respectively, SF6 had the minimal contribution at 1.6 g mm^{-1}. As shown in Figure 7-2 A (ii), SFs 3 and 4 together contributed more than half (54%) of the total sediment yield.

In parallel with the distinct overall rainfall erosion rates between Periods A and B seen in Table 7-1, quite different patterns of sediment yield from the various SFs were found in Period B as shown in Figure 7-2 (b), compared with Period A. SFs 1 and 2 were the most sensitive to the rainfall input with 5.3 and 3.7 g mm^{-1} respectively, contributing 36% and 25% of total sediment yield. In contrast, SF3 and 4 were minor contributors (8% and 13% respectively) with SF6 continuing to be the lowest with 0.8 g mm^{-1} rainfall erosion rate and 6% of total sediment yield for Period B.
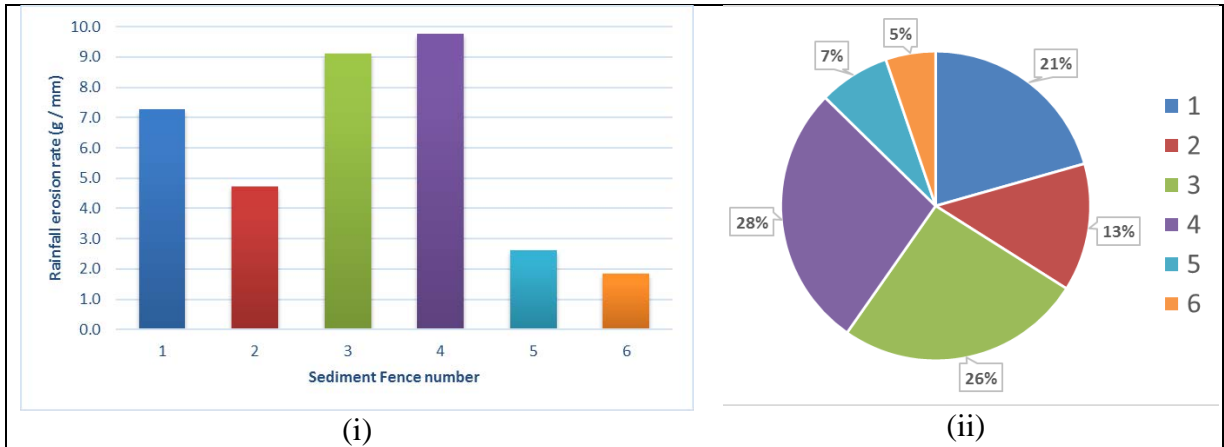
(a) Period A
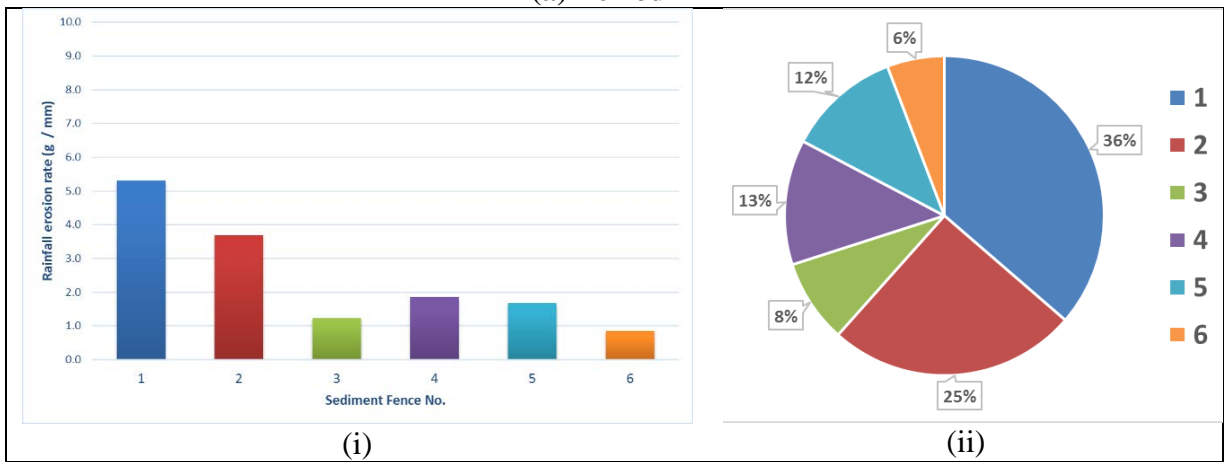
(b) Period B
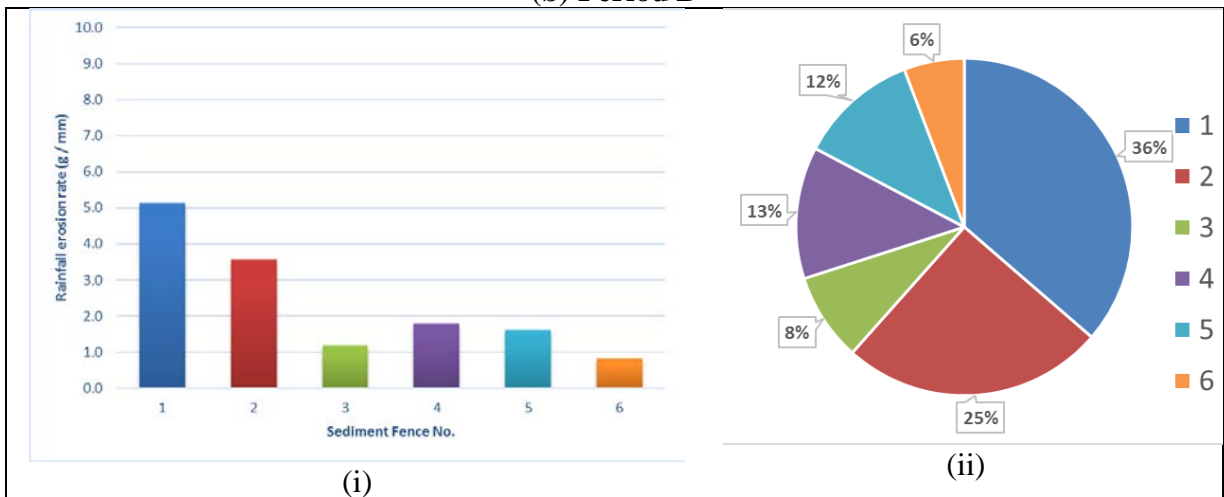
(c) Period C
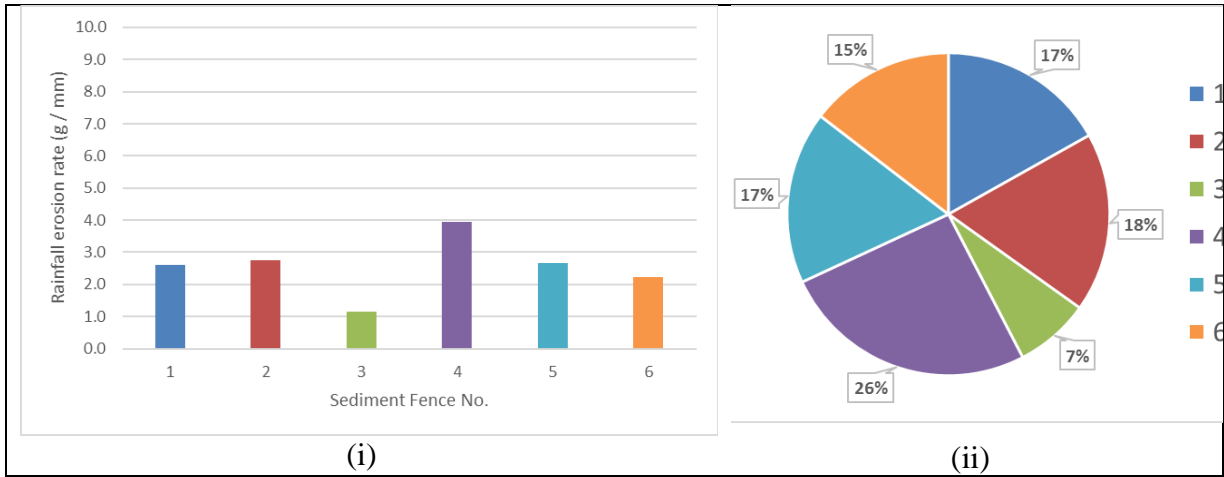
(d) Period D
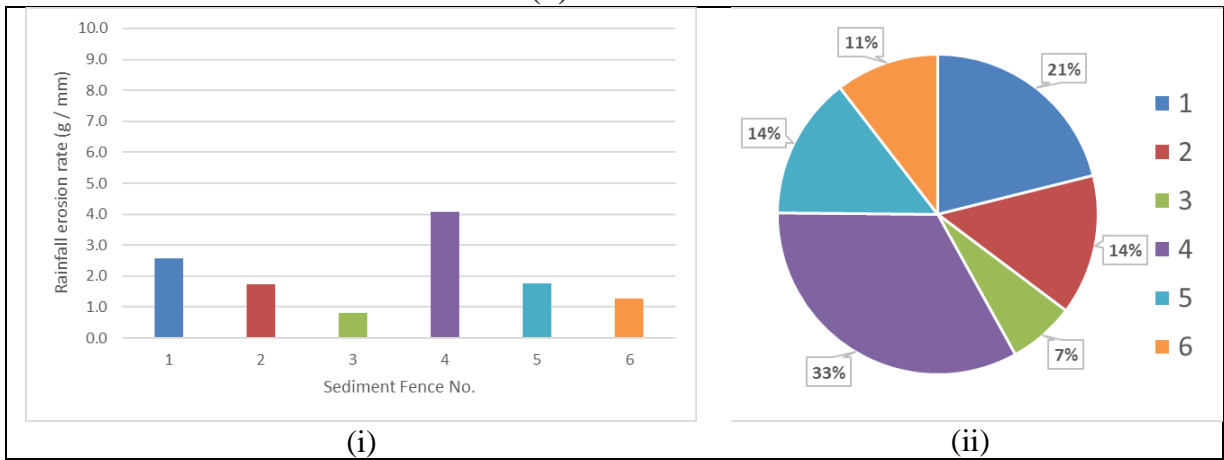
(e) Period E
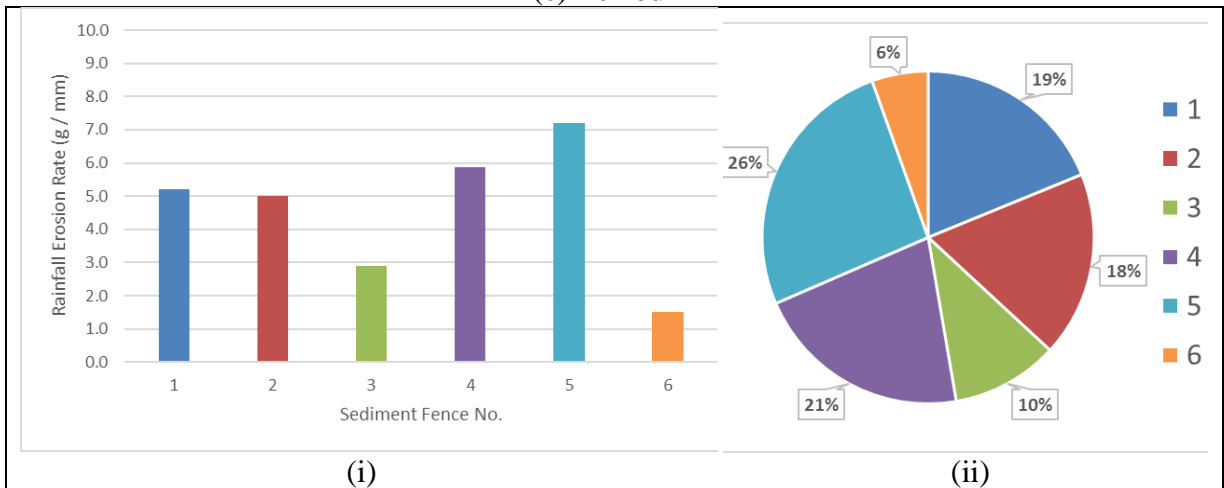
(f) Period F

Figure 7-2. Rainfall erosion rates for individual SFs as (i) eroded soil in g mm^{-1} primitive rainfall depth; and (ii) percentage of total eroded sediment mass for Periods A to F.

From Figure 7-2 (c), Period C had very similar sediment contributions from individual SFs as Period B. This accorded with the overall rainfall erosion rates in Table 7-1 albeit large difference in primitive rainfall depths of 76.5 mm and 206.0 mm for Periods B and C respectively. Only slight differences in rainfall erosion rates were found in Period C. For instance, rainfall erosion rate for SF1 was 5.1 g mm^{-1} (Period B: 5.3 g mm^{-1}); SF2 was 3.6 mm^{-1} (Period B: 3.7 g mm^{-1}) and SF5 was 1.6 g mm^{-1} (Period B: 1.7 mm^{-1}).

Although overall rainfall erosion rate for Period D (15.4 g mm^{-1}; Table 7-1) was similarly muted as the previous two periods, a distinct shift from the previous three Periods in SF contribution patterns was observed (Figure 7-2 (d)). During this peiod, SF4 resurged to give the highest rainfall erosion rate at 4.0 g mm^{-1}. However, this figure was less than 50% of the erosion rate seen for SF4 in Period A (9.8 g mm^{-1}). In contrast to the previous periods, SF6 had higher rainfall erosion rate (2.2 g mm^{-1}) and percentage contribution to total sediment yield (15%) than SF3 (1.2 g mm^{-1} and 7%). Moderate within-period rainfall erosion rates and percenrage contribution were found for SF1 (2.6 g mm^{-1}; 17%), SF2 (2.8 g mm^{-1}; 18%) and SF5 (2.7 g mm^{-1}; 17%), a clear shift from Period C where there were very dominant sediment contributions from SF1 and SF2.

It was found from Figure 7-2 (e) that Period E had rainfall erosion rates and patterns of varied sediment contribution from the SFs that were quite similar to Period D, although this period had the lowest overall rainfall erosion rate of 12.24 g mm^{-1}. Nevertheless, SF4 continued to give the highest rainfall erosion rate of 4.1 g mm^{-1} and the highest percentage sediment contribution at 33%. SF3 also continued to have the lowest rainfall erosion rates (0.8 g mm^{-1}) and sediment contribution percentage (7%), below SF6 (1.3 g mm^{-1}; 11%).

As seen from Figure 7-2 (f), Period F saw a return to high overall rainfall erosion rates (27.67 g mm^{-1}), with SF5 unexpectedly surging to give the highest value of 7.2 g mm^{-1} and contributing 26% of total eroded sediment. These values surpassed the rainfall erosion

rates and sediment contributions for SF4 (5.9 g mm^{-1} and 21% respectively) SF6 reverted to having the lowest rainfall erosion rate (1.5 g mm^{-1}) and sediment contribution (6%) with SF3 the second-lowest with 2.9 g mm^{-1} and 10%.

Table 7-2 enables us to observe how rainfall erosion rates and sediment contributions varied across all the Periods. SF3 and SF4 had the highest standard deviations in rainfall erosion rate values. In contrast, SF6 had the lowest standard deviation, which also saw the lowest variation for percentage sediment contribution. On the other hand, while SF3 and SF4 had high standard deviation in percentage sediment contribution (7.2 and 8.3 respectively), highest standard deviation was found for SF1.

Table 7-2. Mean and standard deviations of rainfall erosion rates and percentage sediment contributions for SFs 1 to 6 through Periods A to F.

Sediment Fence No.	1	2	3	4	5	6
Mean rainfall erosion rate (g mm^{-1})	4.7	3.6	2.7	4.6	2.9	1.4
s.d.	*1.8*	*1.2*	*3.2*	*3.0*	*2.1*	*0.6*
Mean percentage sediment contribution (%)	25.0	19.0	11.2	22.2	14.7	7.9
s.d.	*8.9*	*5.2*	*7.2*	*8.3*	*6.5*	*3.8*

7.1.2. Organic litter

Figure 7-3 shows the mass of plant litter collecting at the SFs for each period. The highest litter masses were found in Periods E (389.8 g) and F (387.9 g). In contrast, the least litter mass was found in Period A (68.3 g). Moderate values were found in Periods B (205.1 g), C (286.9 g) and D (176.3 g). SF5 consistently had the highest litter mass throughout all the periods. In contrast, SF1 was consistently the lowest in litter mass yield except in Period F where is was the second-lowest. While SF2 had the second-highest litter mass trapped in

Periods A to C, it was clearly relegated in periods D to F. Although SF4 had moderate to low litter masses collected in Periods A to C, it surged to register the second-highest litter mass trapped in Periods D to F. Hence, there was considerable variability between SFs in litter mass collected in each of the periods.

While the sediment fluxes discussed in the previous section could be attributed primarily to fluvial processes driven by energy from rainfall (and throughfall) inputs in each period, litter accumulation in the SFs may not be so directly driven, being much more susceptible to aeolian and gravity-driven transport. Nonetheless, fluvial processes would still play a significant role in hillslope litter erosion, transport and deposition. Hence, the daily litter mass accumulation, as well as the rainfall erosion rate for mass of litter were calculated and presented in Table 7-3. While a general increase for daily litter accumulation was seen from 3.11 g in Period A to 6.47 g in Period F, there was a distinct low of 2 g in Period B before a recovery to 4.78 g in Period C. The general increase in rainfall erosion rate (g mm^{-1}) seemed to be clearer, progressing from 0.55 (g mm^{-1}) in Period A to 4.46 (g mm^{-1}) in Period F.
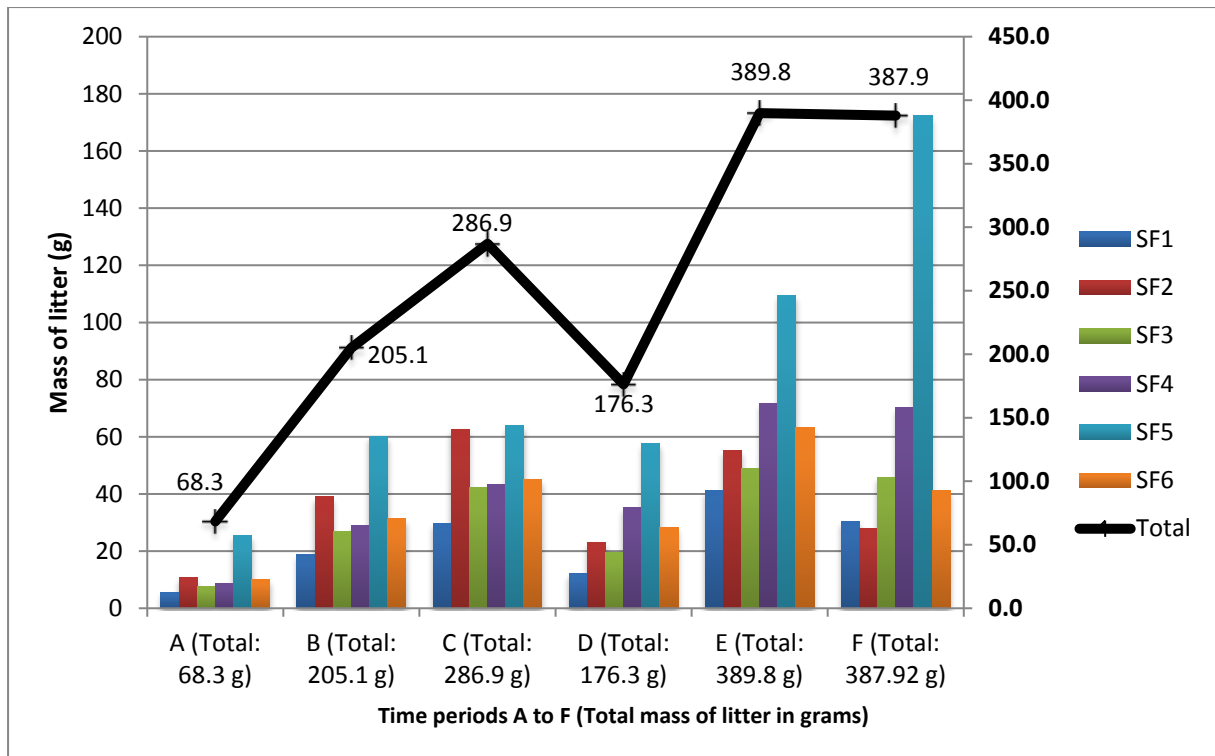
Figure 7-3. Mass of organic litter across all time periods A to F, for SFs 1 to 6.

Table 7-3. Nominal daily litter accumulation (g) and rainfall erosion rate (g mm^{-1}) for Periods A to F.

Period	A	B	C	D	E	F
Total litter mass (g)	68.3	205.1	286.9	176.3	389.8	387.9
No. of days	22	55	60	40	58	60
Primitive rainfall (mm)	123.6	76.5	206.0	79.4	110.8	87.0
Daily litter accumulation (g)	3.11	2.00	4.78	4.41	6.72	6.47
Rainfall erosion rate (g mm^{-1})	0.55	1.44	1.39	2.22	3.52	4.46

7.1.3. Composition of total hillslope material (soil + gravel + organic litter)

The percentage composition of the total mass of hillslope material (gravel, soil and organic litter) eroded downslope is presented in Figure 7-4.
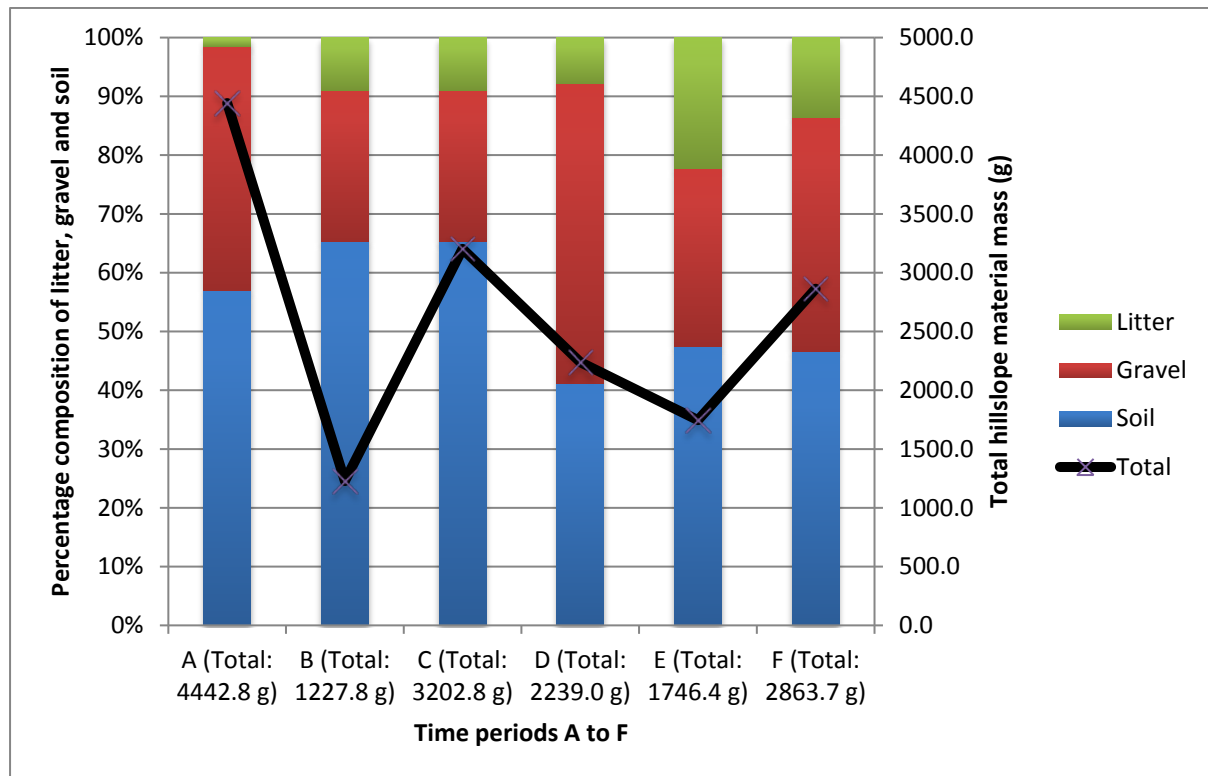
Figure 7-4. Percentage composition by litter, gravel and soil of total hillslope materials moving downslope integrated over SFs 1 to 6.

One of the distinctive patterns found in Figure 7-4 was for Periods D, E and F, where there seemed to be some association of lower total sediment yields with higher percentage composition of litter collected in the sediment fences. This is particularly clear for Period E where total eroded sediment was low at 1746.4 g while litter collected was at the peak percentage composition (22.3%). Gravel comprised 30.2% of total material in Period E, contrasting with 51% in Period D. The converse was seen for Periods A, B and C. There was also, correspondingly, a lower percentage of soil (i.e. fine-earth fraction) eroded in Periods D, E and F. This hinted at possible negative correlation between mass of litter and soil erosion rates. This could have been due to abundant leaf fall due to extended dry periods in the

312

preceding weeks. With reference to Table 5-2, Periods C and D had relatively long mean Inter-Event Times of 77.4 hrs and 80.2 hrs respectively. From Figure 5-4, Period C had ten no-rain days from Days 86 to 95 followed by four very small rainfall events giving a modest 6 mm total on Day 96, and then another ten-day dry period from Days 97 to 106. Another stretch of eight dry days was also seen from Days 109 to 116, as well as eleven dry days from 124 to 134. Period D had two seven-day dry stretches from Days 147 to 153 and Days 163 to 169 as well as an eight-day dry period from Days 172 to 179. These could have enabled soil moisture and canopy storages to be depleted. Furthermore, Periods C and D, being in the late autumn and winter periods with low solar insolation and temperatures, may have contributed to the enhanced leaf fall in response to the lack of photosynthetic gain in these conditions, even though the *Eucalyptus* are not deciduous. Nevertheless, the pulse of leaf litter accumulating below the plant canopies and variably transported onto the barer inter-spaces, would have formed a protective "blanket" muting the impacts of erosive throughflow and rainfall drops, as well as impeding overland flow generation and dissipating erosive flow energy where they were present.

7.1.4. Texture of eroded soil

We examined the textures of the eroded soil collected from the sediment fences, through the Periods A to F, vis-à-vis the total mass eroded to establish if there have been any differences that would have resulted from differences in rainfall event characteristics within each time period; analyses that will be presented in the later sections.

Figure 7-5 shows the soil texture by sand-silt-clay percentages, averaged across the sediment fences, weighted according to each sediment fences' contribution to the total sediment yield each period.
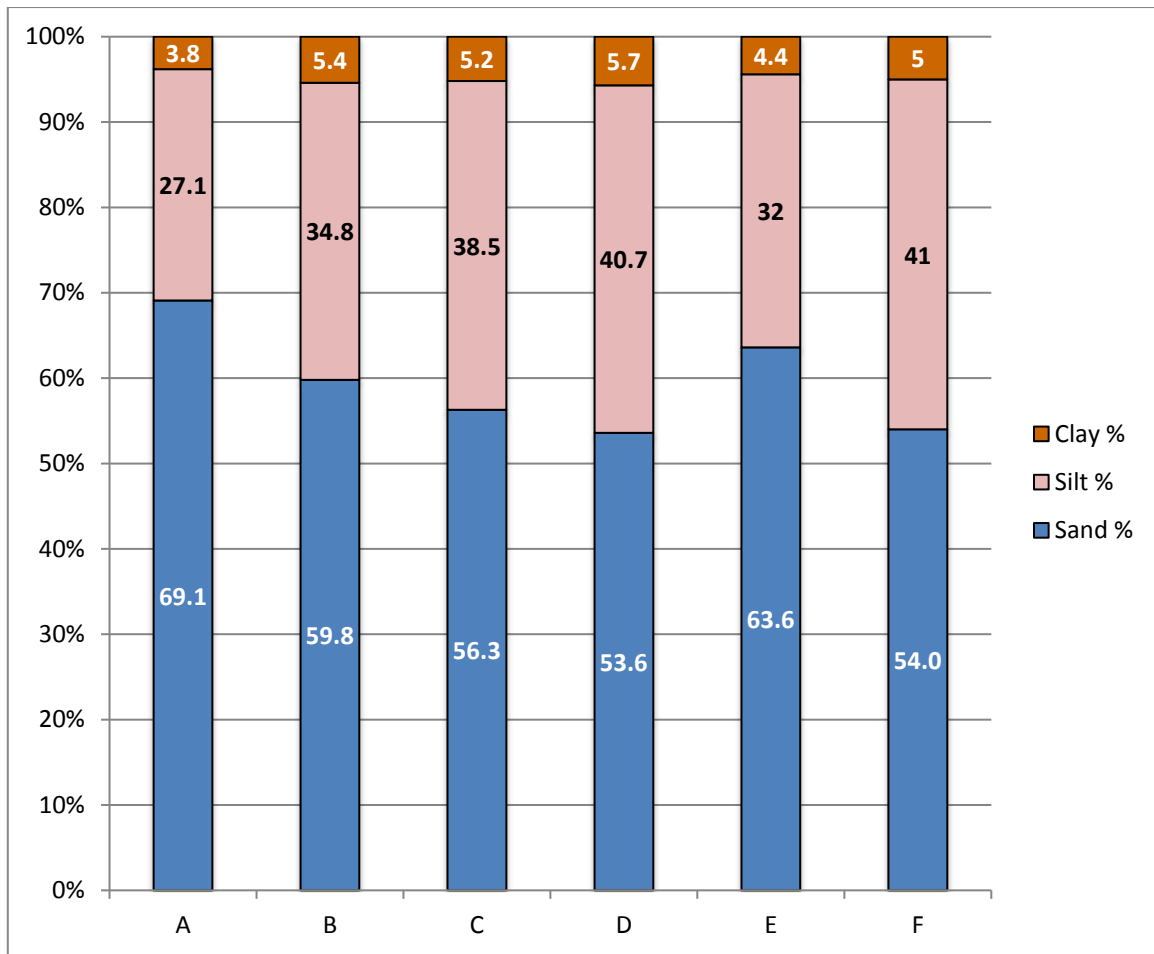
Figure 7-5. Texture of eroded soil by time period (A to F) represented as weighted average (by contribution from individual SF) percentage composition of eroded soil.

Based on the percentage composition of sand, silt and clay for eroded soils from all the sediment fences, the textures were all classified as (coarse) sandy loam (KSL). However, there were some distinct textural variations with each period. As seen from Figure 7-4, there was a general trend through time towards finer sediment sizes as evidenced by the generally decreasing trend of sand percentages, with Period A erosion delivering soil of 69.1% sand, to sand proportion of 54% in Period F which saw silt proportion at the maximum 41%. There appeared to be rather distinct changes in the overall percentage of the sand and silt fractions compared to the rather stable percentage clay fraction through all the time periods (Period A: 3.8% (minimum); Period D: 5.7% (maximum). In Period E, there was a clear shift to increased sand and decreased silt and clay fraction, followed by a clear decrease in sand percentage again in Period F.

314

Figure 7-6 (a-f) presents the textures of the eroded soil accumulating at individual SFs in each period, enabling us to discern any inter-SF differences. For Period A, Figure 7-6 (a) shows how SF1 and SF5 were biased towards finer textures with higher percentages of clay (SF1: 5.7%, SF5: 6.3%) and silt (SF1: 32.6%, SF5: 37.0%). In contrast, SFs 2-4 and SF6 all had high percentages of coarse sand (more than 32%) and fine sand (more than 33%).

From Figure 7-6 (b), it could be seen that Period B had different patterns of textural variations than was found for Period A. SFs 1 to 4 and SF6 had higher clay percentages in Period B than Period A, while SF5 was the only one that recorded a lower clay percentage (B: 4.9%, A: 6.3%). Apart from SF3 (B: 25%, A: 26%), all the other SFs also had higher silt percentages in this period compared to the previous period.

In Period C, shown in Figure 7-6 (c), the erosional processes yielded lower percentages of coarse sand for all SFs except SF5 (C: 21.3%, B: 11.5%). This indicated a general shift towards finer particle sizes being transported albeit with variable responses from individual SFs and contrasting response for SF5 towards coarse sand. Fine sand component increased for SF2 to 4 and decreased for SFs 1, 5 and 6. SF2 showed a substantial increase in fine sand percentage from the previous period (B: 32.4%, C: 43.5%), while SF5 had a sharp decrease (B: 43.8%, C: 33.4%). However, SF5 had minimal shifts in silt and clay percentages. The other SFs showed quite clear changes in silt percentages. For example, in the silt component, SF1 increased 5.4%, SF2 decreased 7.1% and SF6 increased 6.8%. For clay percentages, SF2 also had a decrease of 1.5% in clay component while the other SFs did not register much changes.

As seen in Figure 7-6 (d), Period D saw decreases across all SFs for coarse sand percentage. For fine sand, SFs 1 to 3 showed decreased proportion (in favour of the finer silt and clay fractions), only a slight 1% decrease was seen for SF4 while substantial increases of 8.8% and 10.4% were found for SFs 5 and 6 respectively. Silt percentages increased for SFs

1 to 4 while decreases were seen for SFs 5 and 6. Increases in clay percentages were recorded for SFs 1 to 4 while SFs 5 and 6 had slight decreases.

From Figure 7-6 (e), it was obvious that Period E saw a reversion to coarse textures of eroded soils. All the SFs recorded increases in coarse sand with sudden surge for SF6 to 57.3% in Period E compared to 22.4% in Period D. This was accompanied by decreases in silt and clay contents for all SFs 1-4 and 6. SF5 was the only position that bucked the trend with higher silt percentage (E: 37.8%, D: 34.5%) and similar clay percentage at 4.3%. SF5 also recorded a decrease in fine sand percentage (E: 38.4%, D: 42.2%). Fine sand percentages also decreased for SF6 (although this was in favour of coarse sand) as well as SFs 3 and 4. SFs 1 and 2 had fine sand percentage increases accompanying the increases in coarse sand percentage described earlier.

Period F saw rather mixed responses from the various SFs; see Figure 7-6 (f). SF1 had an increase in coarse sand component from the previous period (E: 8.7%, F: 12.5%) accompanied by a reduced fine sand percentage (30.9% compared to 43.6% in Period E); and SF2 's coarse sand percentage remained the same with a reduction in fine sand percentage to 33.1% (from 45.8% in Period E). However, SFs 3 to 6 all saw a reduced coarse sand percentage together with increased fine sand percentages albeit to varying extents; SF3 had a sharp rise of 8.6% in fine sand percentage while SF4 and SF5 had slight increases of 3% and 1.3% respectively. The most drastic change in eroded soil texture towards finer sediments in this Period was seen in SF6 where coarse sand percentage dropped to 12.6% from 57.3% in the Period E with a jump in fine sand percentage to 49.4 % from 23.3% in Period E; a similar rise in silt percentage to 33.8% compared to 17.3% in Period E and virtual doubling of clay proportion at 4.3% compared to 2.2% in Period E.

With a detailed examination of the eroded soil textures for the various SFs in the different Periods, we can see that individual SFs have varied responses to the same rainfall

input. SF6, for example, appeared to have soil textures that varied quite wildly from one period to another and this manifested quite strongly in the coarse sand component. While Period C and D saw moderately homogeneous responses amongst the SFs, quite major differences in SF responses could be seen, especially in Periods A, B and E.
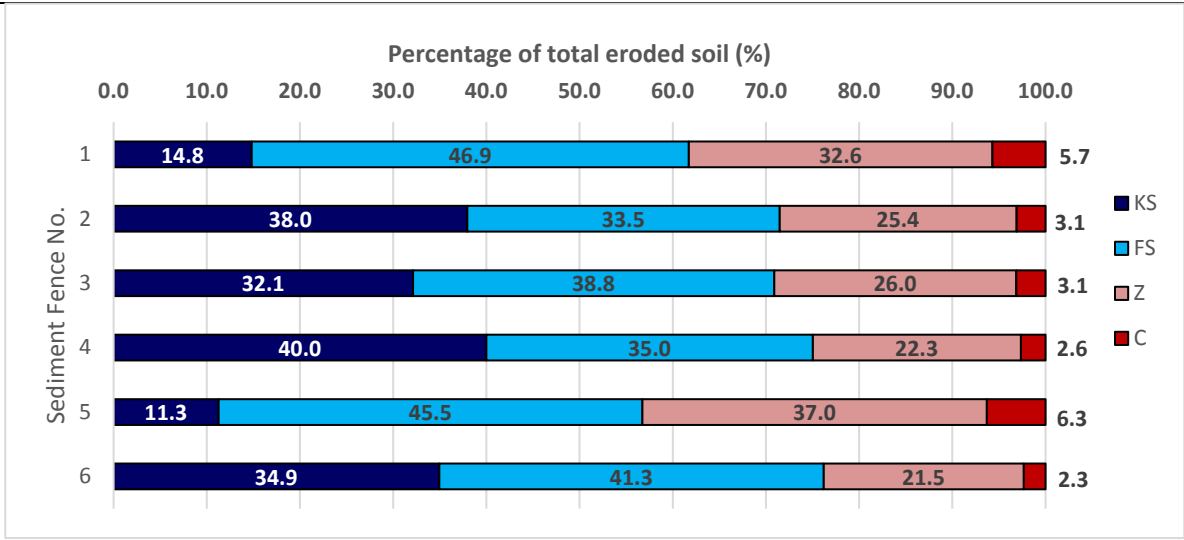
(a) Period A
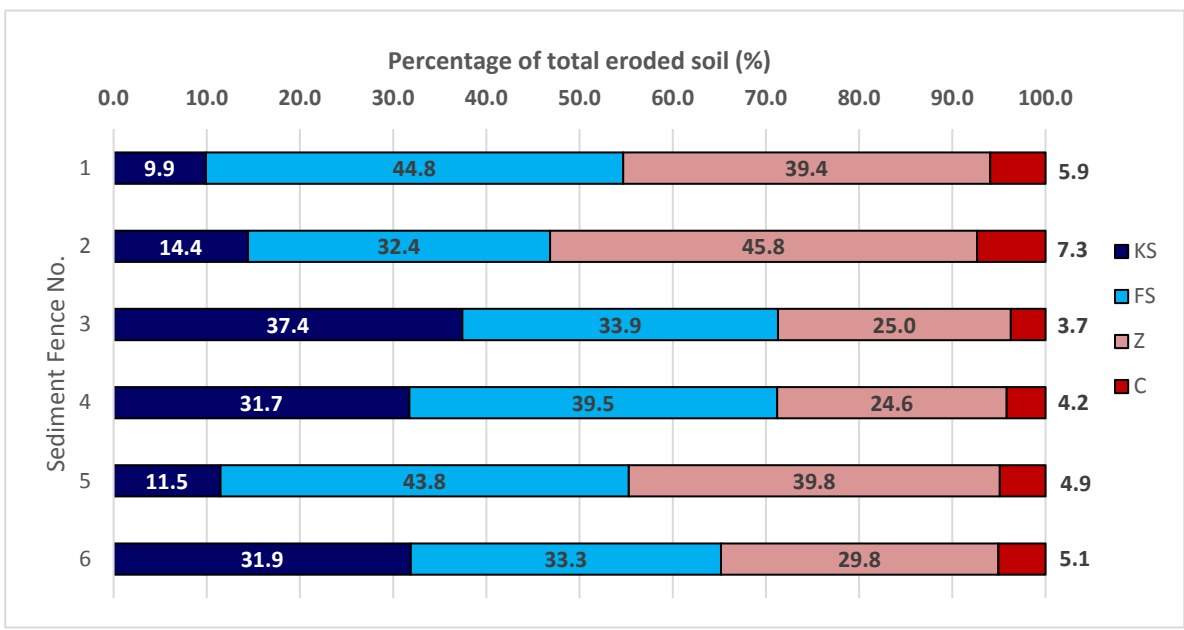
(ii) Period B

(iii) Period C

318
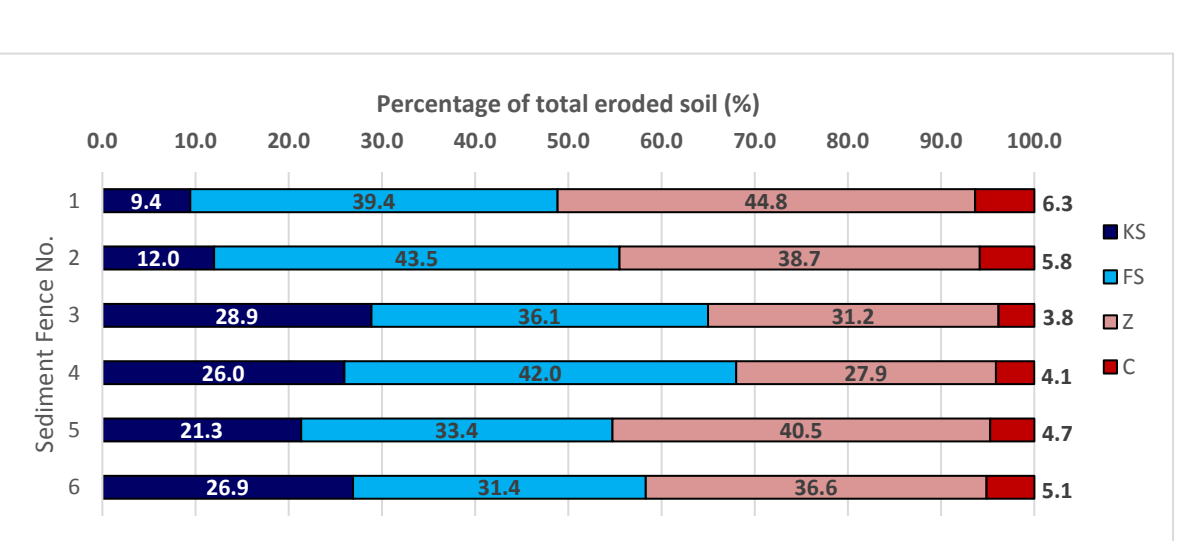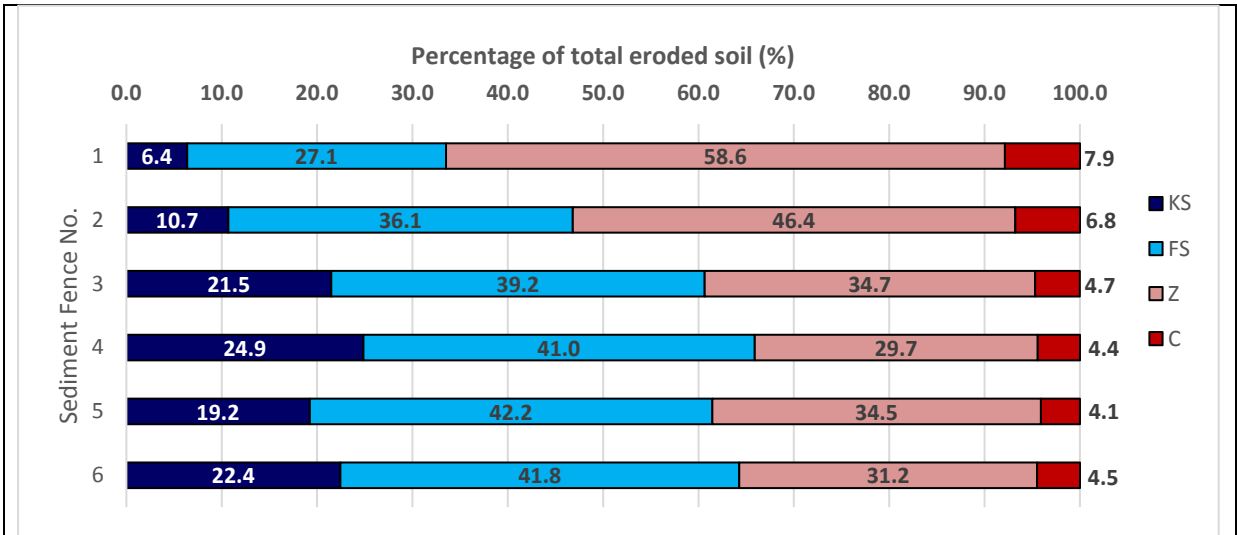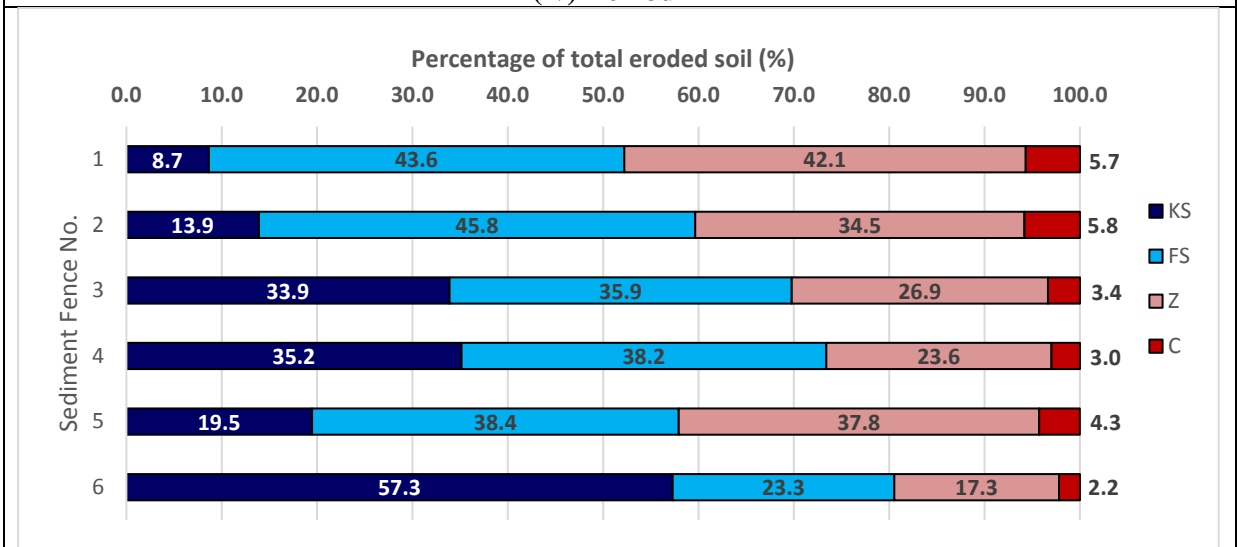
(iv) Period D

(v) Period E
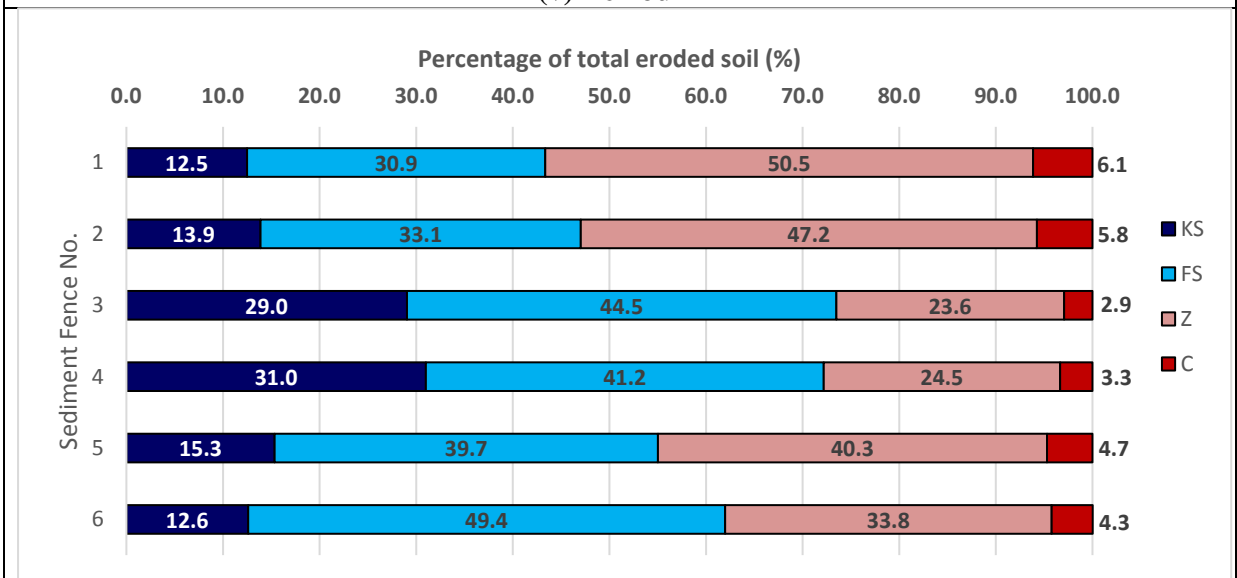
(vi) Period F

Figure 7-6. Soil texture for SFs 1 to 6 for Periods A to F.
Note: KS = Coarse Sand; FS = Fine Sand; Z = Silt; C = Clay.

319

Looking at individual SFs, **SF1** had modal sediment size range in the fine sand component in Periods A, B, E but silt component was more dominant in Periods C, D and F. For **SF2**, modal sediment size range varied more. While fine sand was dominant in Periods C and E, coarse sand was more dominant in Period A and silt component most dominant in Periods B, D and F. **SF3** had fine sand dominating the eroded soil texture in almost all Periods: A, C to F. It was only in Period B that coarse sand dominated.

SF4 had eroded soil textures mainly fine sand range. Coarse sand dominated in Period A, but fine sand was the modal sediment size range for all the other Periods B to F. For **SF5**, fine sand dominated in Periods A and B, shifted to a finer silt-dominated texture in Period C and then reverted to fine sand dominance in Periods D to F. It should be noted that there were very slight difference between fine sand and silt proportions in Periods E (FS: 38.4%, Z: 37.8%) and F (FS: 39.7%, Z: 40.3%). In contrast, **SF6** was dominated by fine sand in Periods A, B, D and F but saw a shift to finer silt-dominant texture in Period C (Z: 36.6%) and a swing to dominance of coarse sand in Period E (KS: 57.3%).

7.2. Analysis of relationships

7.2.1. Overall sediment mass vs total rainfall depth

There was only a weak or unclear relationship between total rainfall depth and total sediment mass eroded (Figure 7-7 (a); $R^2 = 0.19$). Using total rainfall from all primitive events (1 mm depth or more) also did not produce clear relationships (Figure 7-7 (b); $R^2 = 0.23$). For example, sediment yield was high for Period A at 4374.5 g with total 128.2 mm rainfall depth, but a similar total rainfall depth at 125.4 mm for Period E saw a much lower 1356.6 g of sediment yield.
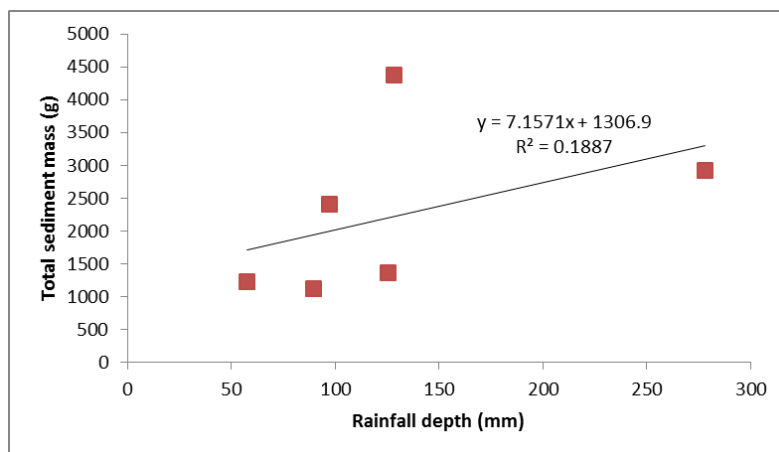
(a)
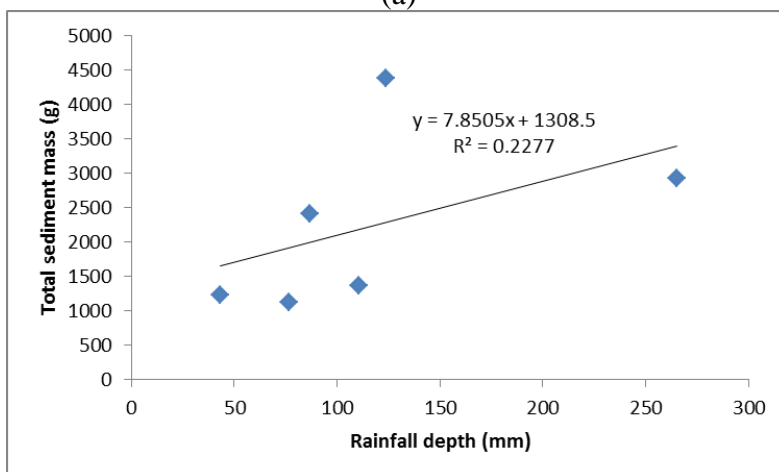
(b)

Figure 7-7. Plot of total eroded sediment (soil + gravel) mass (g) with (a) total rainfall depth (mm) and (b) total rainfall depth only including all primitive events (1 mm or greater).

These results indicate that the relationship between rainfall depths and total mass of sediment eroded is not a simple one, especially for intermediate-recovery vegetation and ground conditions of the study area.

7.2.2. Overall sediment mass vs Largest rainfall event depths

Linear regression analysis of the relationship between the largest event depth for each period and the corresponding total mass of sediment eroded found a high R^2 value of 0.70 (see Figure 7-8a), but the derived relationship could not be conclusive because of the single high-end value for event depth and total sediment mass, and clustering of the other values towards low rainfall event depth values (Brown et al., 1985), and the small number of just six data points. Furthermore, when the plotted regression line was set to intersect at zero, a weaker R^2 value of 0.28 was found (Figure 7-8a). As seen in Figure 7-8b, logarithmic regression yielded a good R^2 value of 0.67 and seemed to provide a reasonable albeit nominal representation of a general relationship between rainfall depth (not necessarily accurately representing rainfall energy) and total eroded sediment as earlier developed by workers such as McGregor et al. (1995).
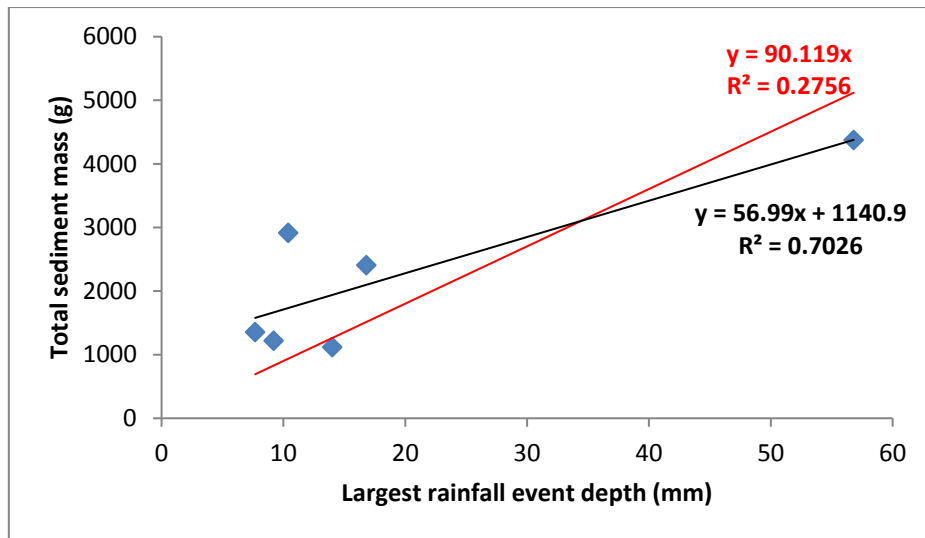
(a)
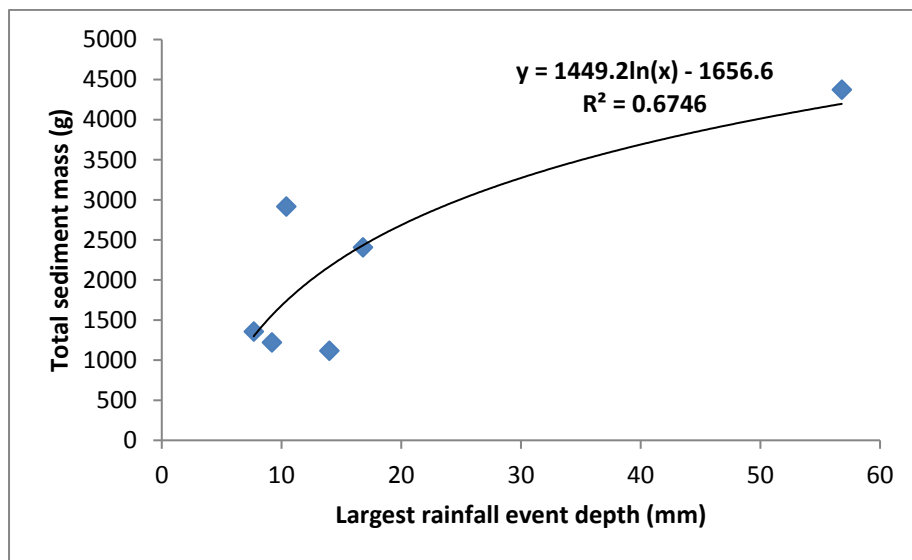
(b)

Figure 7-8. Plot of total eroded sediment (soil + gravel) mass (g) with largest rainfall depth (mm) for each period with (a) linear regression and (b) logarithmic regression.

Regression analysis was also conducted between Total Erosivity (EI$_{30}$) of all primitive events and mass of sediment eroded (g) (i.e. both soil and gravel components). As shown in Figure 7-9, a strong linear relationship was found for the soil component ($R^2 = 0.86$). For gravel, a weak-moderate relationship was found ($R^2 = 0.42$). Hence, while EI$_{30}$ was useful in predicting total (gross) mass of eroded soil across the sediment fences, it was less useful when predicting mass of eroded *gravel*. This hinted at the possibility of different mechanics, threshold energies and rainfall metrics involved in gravel erosion in this landscape. Similar analyses were also conducted between EI$_5$ with eroded soil and gravel. However, no relationship was found between mass of eroded soil and EI$_5$, and a weak negative relationship ($R^2 = 0.34$) between eroded gravel with EI$_5$.
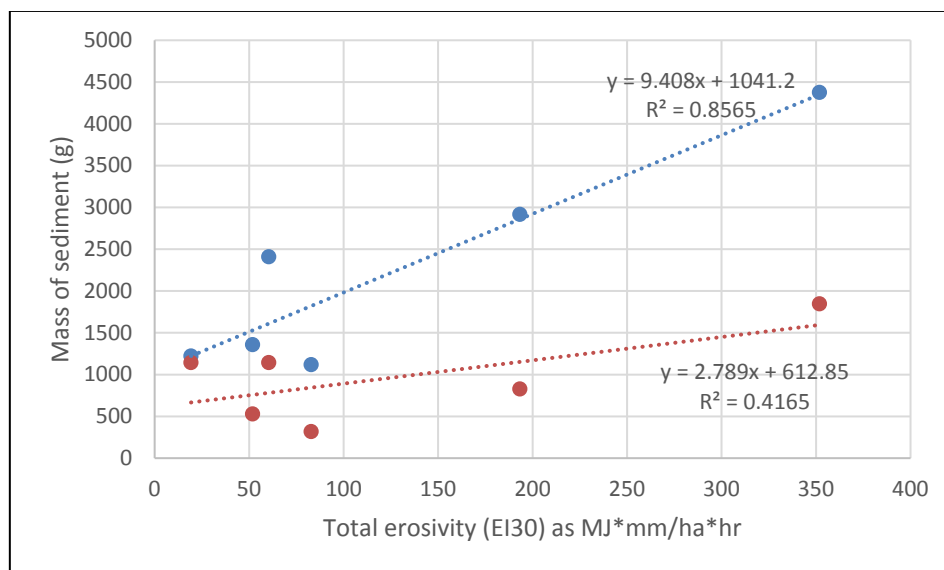
Figure 7-9. Variation of soil (blue, top line) and gravel (red, bottom line) with total EI$_{30}$ across time periods A to F.

Regression analysis between EI$_{60}$ and masses of eroded soil and gravel found a strong positive correlation for soil ($R^2 = 0.80$) and weak, largely inconclusive positive correlation for gravel ($R^2 = 0.27$) (see Figure 7-10).
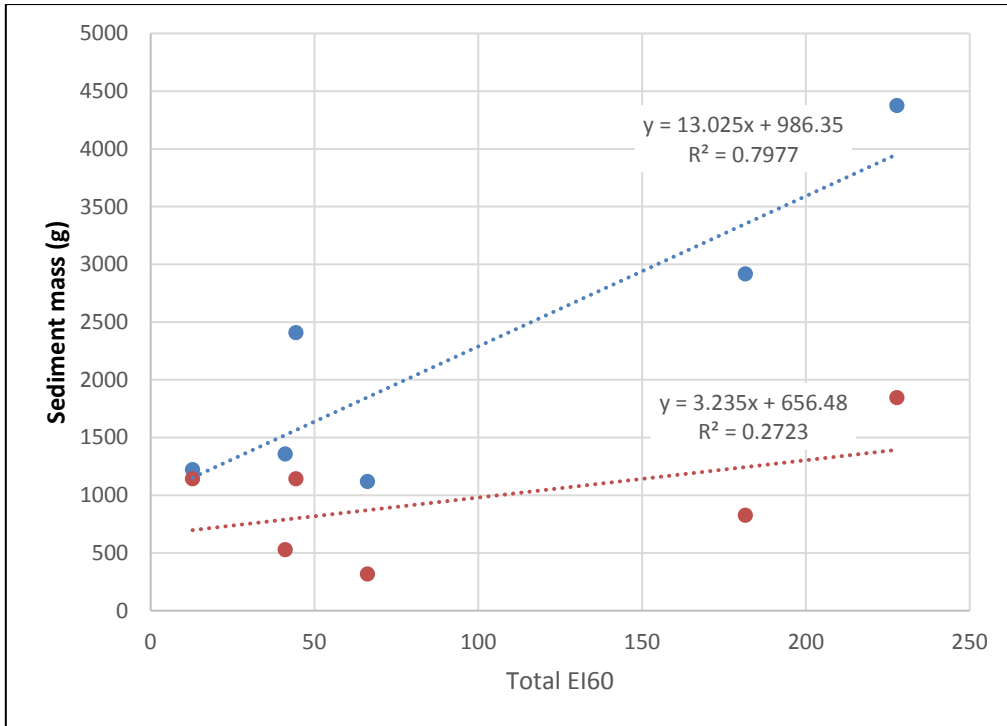
Figure 7-10. Variation of soil (blue, top line) and gravel (red, bottom line) with total EI_{60} across time periods A to F.

7.2.3. Individual sediment fence responses

Regression analyses were also conducted to examine individual sediment fence erosion responses to the integrated inputs from rainfall events of each period, and possible response variations amongst SFs, as described in section 7.1.

As seen from Figure 7-11, strong positive relationships were found between total rainfall erosivity and eroded sediment mass for SF1 and SF2.
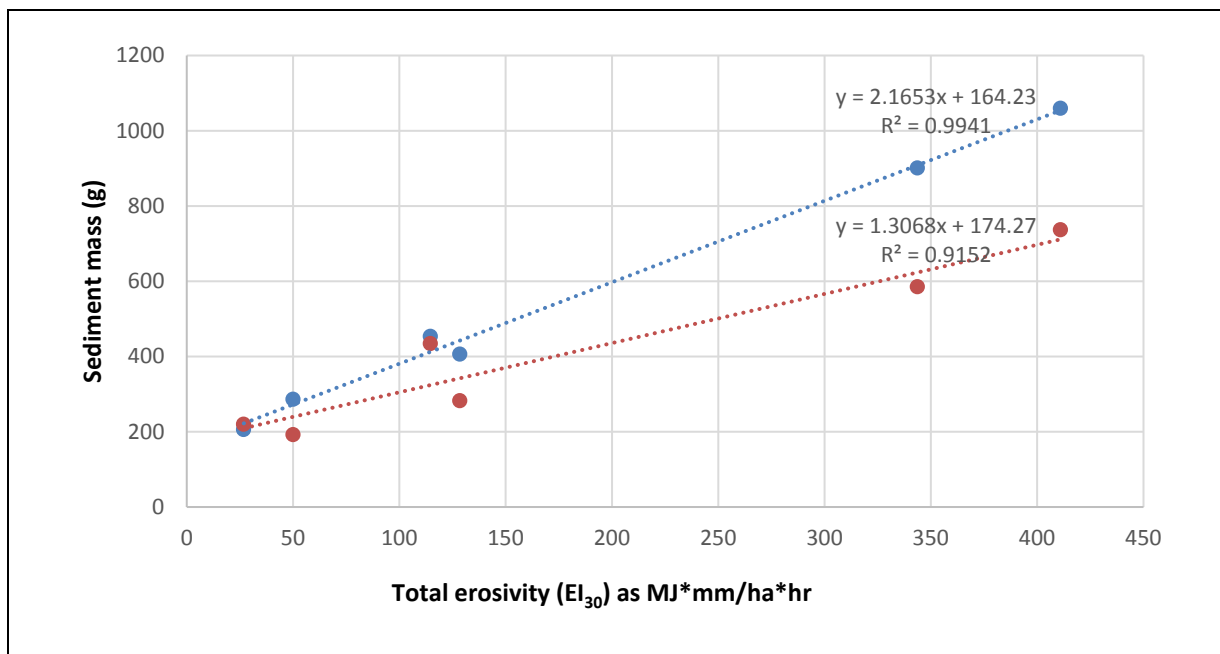
Figure 7-11. SF1 (blue, top line) and SF2 (red, bottom line) variation of eroded sediment mass (g) (gravel + soil) with rainfall erosivity (total EI_{30}) across time periods A to F.

However, the relationship appeared to be more complex for SF3 to SF6 (see Figures 7-12 and 7-13), with diverging responses of mass of eroded soil at different total rainfall erosivity levels. Furthermore, there were no clear relationships found for SF3 to SF6 between total rainfall erosivity and total eroded sediment mass. SF3 and SF4 appeared to have some similarity in responses at higher rainfall erosivities (Figure 7-12). However, it was interesting that the highest total rainfall erosivity (411 MJ*mm/ha*hr) did not lead to high eroded sediment mass (SF3: 246.3 g, SF4: 369.2 g).
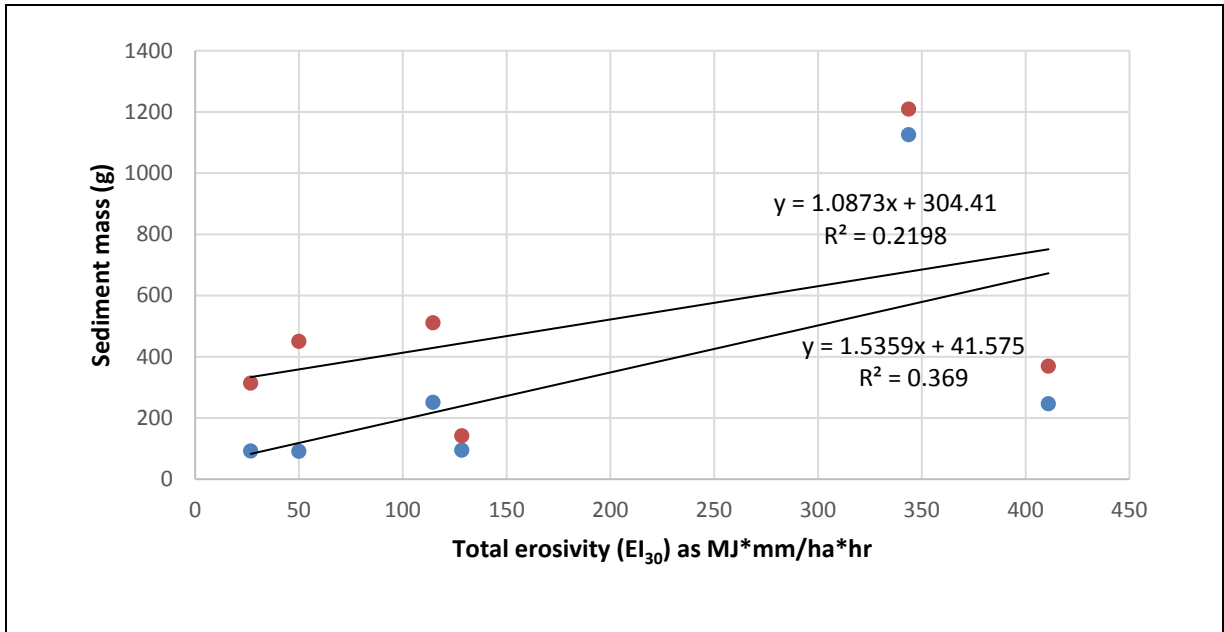
Figure 7-12. SF3 (blue, top line) and SF4 (red, bottom line) variation of eroded sediment mass (g) (gravel + soil) with rainfall erosivity (total EI_{30}) across time periods A to F.
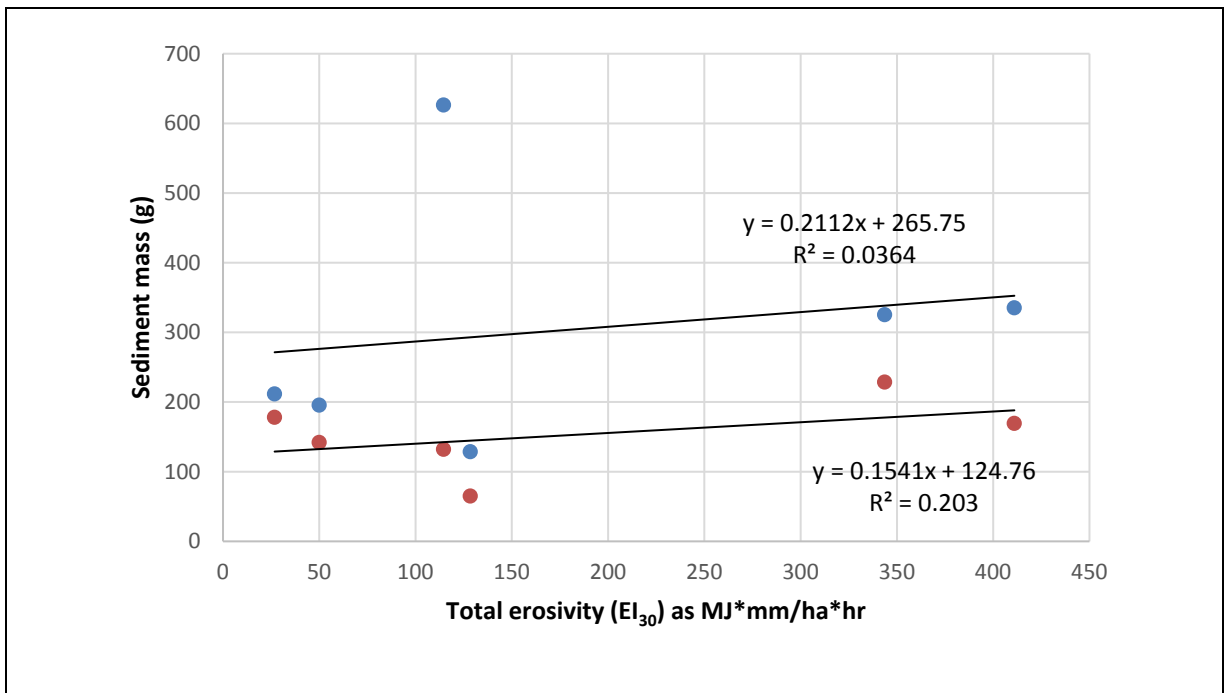
Figure 7-13. SF5 (blue, top line) and SF6 (red, bottom line) variation of eroded sediment mass (g) (gravel + soil) with rainfall erosivity (total EI_{30}) across time periods A to F.

The sediment responses at SF5 and SF6 (Figure 7-13) also displayed minimal relationships with total rainfall erosivity. Except for SF5 which saw a high eroded sediment mass of 626.09 g for a moderate erosivity input of 114.6 MJ*mm/ha*hr in Period F, similar and low eroded sediment masses were recorded across the entire range of low to high rainfall erosivity values.

To further investigate the observed variations in sediment responses to key rainfall input variables in each period, I employed the use of high temporal resolution one-minute intra-event rainfall intensity values (I_{1min}) to test for any relationships to eroded sediment masses for all SFs together, as well as for individual SFs. Possible relationships to individual sediment size ranges (viz. gravel, coarse sand, fine sand and silt) were also examined. The clay component was excluded from this analysis because of its small proportion of total eroded soil mass and inherent difficulties in relating erosion of clay particles to flow and splash energies. As discussed in detail in Chapter 5, all primitive rainfall events were disaggregated into one-minute intensity values and categorized into their respective time periods of occurrence (Periods A to F). Using a range of intensity thresholds: 5, 10, 15, 20, 30 and 40 mm hr^{-1}, the total number of minutes where the specified intra-event intensity threshold was met or exceeded, were summed for each period. The purpose was to find out the key rainfall intensity (and thus rainfall erosivity) thresholds affecting the six sediment fences as a group, and individual sediment fences.

7.2.4.1. Soil and gravel – overall sediment yield

Figure 7-14 (a-f) shows the linear regression results between total sediment yield (soil + gravel) and the number of minutes above 5, 10, 15, 20, 30 and 40 mm hr^{-1} for each measurement period, for all sediment fences. Total eroded sediment appeared to be moderately well-predicted using 10 mm hr^{-1} as the base I_{1min} rainfall intensity at the one-minute interval basis (Figure 7-13b), with the equation:

$$y = 21.164x + 560.1, R^2 = 0.54,$$

where y is sediment yield (g) and x is the number of minutes at or above 10 mm hr^{-1}

In contrast, as seen in Figure 7-14d, the higher 20 mm hr^{-1} intensity did not appear to be a useful I_{1min} baseline. From Figures 7-13(a) and 7-13(c), 5 mm hr^{-1} and 15 mm hr^{-1} seemed to be reasonably good I_{1min} thresholds, with the respective equations:

$$y = 5.183x + 971.02, R^2 = 0.42, \text{ for minimum } I_{1min} \text{ of 5 mm hr}^{-1}$$

$$y = 49.48x + 962.17, R^2 = 0.43, \text{ for minimum } I_{1min} \text{ of 15 mm hr}^{-1}$$

where y is sediment yield (g) and x is the number of minutes at or above the specified I_{1min} value.
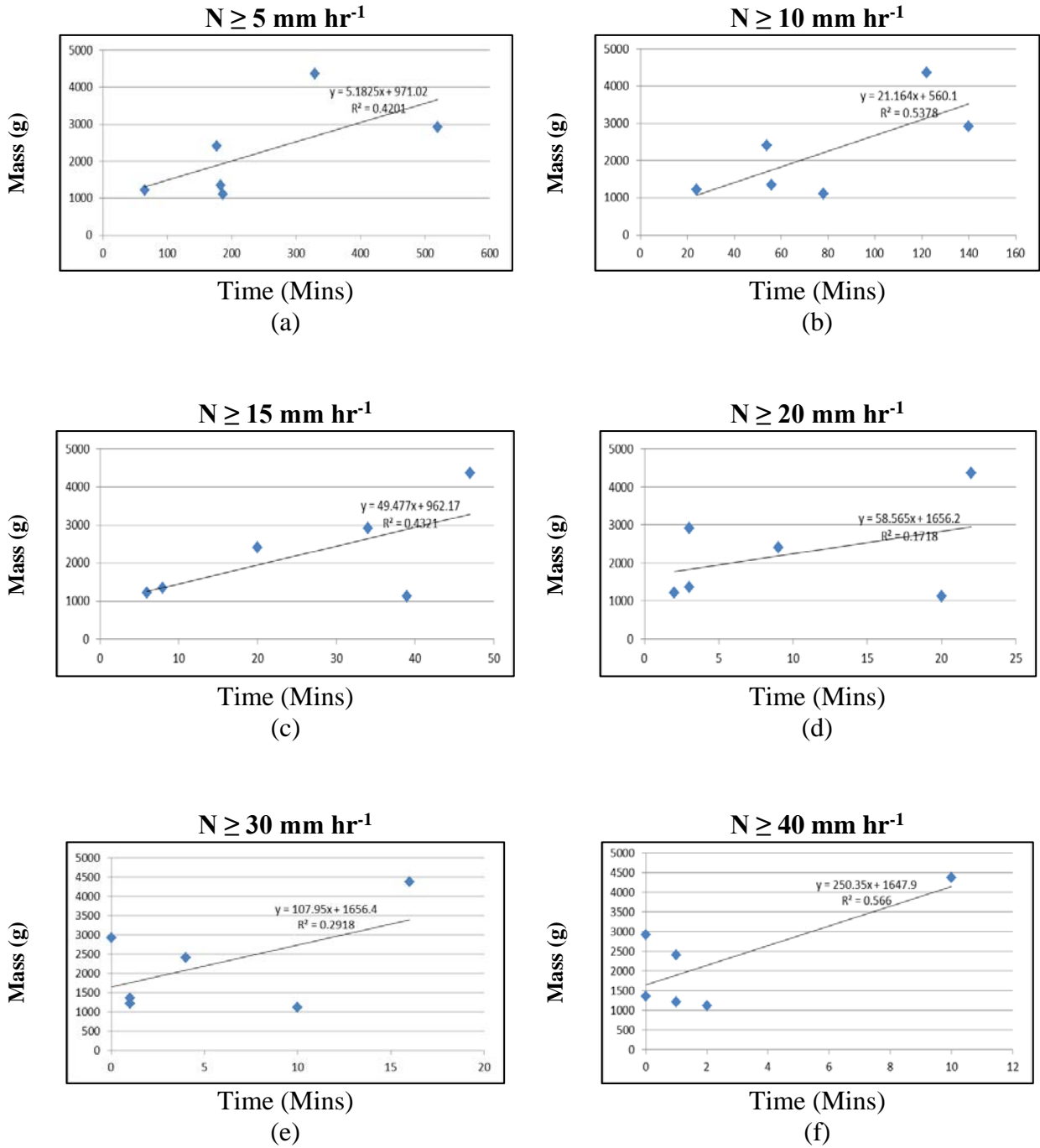
Figure 7-14. Total sediment (soil + gravel) mass eroded (g) of SF1 to 6 with number of minutes in each measurement period where I_{1min} was: (a) $\geq$ 5 mm hr^{-1}; (b) $\geq$ 10 mm hr^{-1}; (c) $\geq$ 15 mm hr^{-1} (d) $\geq$ 20 mm hr^{-1}; (e) $\geq$ 30 mm hr^{-1}; (f) $\geq$ 40 mm hr^{-1}.

From Figures 7-14 (a – f), it was found that the 10 mm hr^{-1} and 40 mm hr^{-1} rainfall intensity duration threshold had the strongest relationships (moderate) with the sediment erosion rates with R^2 values of 0.54 and 0.56 respectively, indicating that these would be

good predictors of gross sediment erosion, although the distribution of data points for the latter would still cast some doubt on the veracity of the modelled relationship, particularly for the 40 mm h^{-1} intensity threshold. Examination of the distribution of data points in Figure 7-14c found an interesting outlying data point (39 min $\geq$ 15 mm hr^{-1}, y = 1117.78 g) that warranted further investigation because this was a relatively low eroded sediment mass value despite the many minutes having $I_1 \geq$ 15 mm hr^{-1}. Without this data point in Period B, a strong regression relationship between N (mins) $I_1 \geq$ 15 mm hr^{-1} and eroded sediment mass, as shown in Figure 7-15.
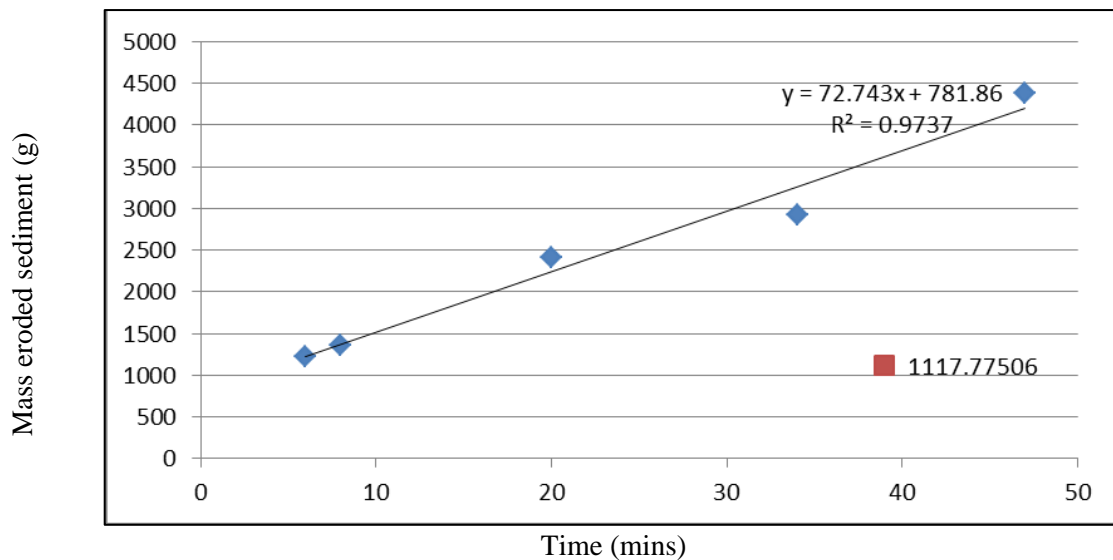
Figure 7-15. Total sediment (soil + gravel) mass eroded (g) of all 6 sediment fences with number of minutes in each measurement period where I_{1min} was $\geq$ 15 mm hr^{-1} and exclusion of Period B data point (red square).

The linear regression for sediment yield with number of minutes I_{1min} was $\geq$ 15 mm hr^{-1}, where the data point for Period B was omitted, could be described by the equation:

$$y = 72.74x + 781.86, R^2 = 0.97$$

where y is sediment yield (g) and x is the number of minutes at or above the specified I_{1min} value.

In view of this analysis, the threshold event one-minute intensity was estimated at 15 mm hr^{-1} with more investigation warranted for Period B rainfall characteristics.

7.2.4.2. Gravel erosion responses – individual SFs

The mass of eroded gravel was also analysed for possible relationships to rainfall intensity metrics of one-minute intensities for 5, 10, 15, 20, 30 and 40 mm hr^{-1}. Linear regression was applied between the number of minutes at or above the specified one-minute intensity and the resultant mass of eroded gravel. The results of the analyses are summarized in Table 7-4.

Table 7-4. Linear regression coefficients for eroded **gravel** mass (g) with duration (mins) above threshold I$_{1min}$ rainfall intensity for each period. The highest coefficient values across the threshold intensity values have been indicated in **bold**.

	Threshold one-minute rainfall intensity levels (mm hr^{-1})					
	5	**10**	**15**	**20**	**30**	**40**
SF1	0.35	0.56	0.57	0.35	0.51	**0.77**
SF2	**0.29**	0.28	0.23	0.02	0.08	0.16
SF3	0.14	0.32	0.45	0.42	0.62	**0.91**
SF4	0.09	0.18	0.19	0.21	0.39	**0.69**
SF5	**0.14**	0.07	0.02	< 0.01	0.01	< 0.01
SF6	0.20	0.23	0.17	0.08	0.15	**0.35**
All fences	0.20	0.33	0.34	0.25	0.39	**0.65**

Analysis at the 40 mm hr^{-1} one-minute rainfall intensity yielded the strongest relationships between rainfall intensity and mass of eroded gravel ($R^2 = 0.65$) when sediment from *all fences* were included. It appeared that the higher the rainfall intensity threshold, the greater the regression coefficient (see Table 7-4).

Individual SF gravel erosion responses to the same rainfall one-minute intensity thresholds were far from uniform. At the 40 mm hr^{-1} threshold, SF3 displayed the strongest response with $R^2 = 0.91$, followed by SF1 ($R^2 = 0.77$) and SF4 ($R^2 = 0.69$). SF2 and SF6 and showed weak to very weak responses at $R^2 = 0.35$ and $R^2 = 0.16$ respect**i**vely. SF5 showed no discernible response at this level. For SF2, slightly better, but still weak, relationships were found at lower intensity values, with $R^2 = 0.29$ for 5 mm hr^{-1} threshold and 0.28 for 10 mm hr^{-1} threshold levels. For SF5, a very weak R^2 value of 0.14 was found only at the 5 mm hr^{-1} threshold which would be disregarded.

During the analysis of gravel yield, one of the most consistent patterns observed was the occurrence of a single outlier gravel yield value for the given causal rainfall input for Period B. SF4 yielded low gravel mass at 74.7 g even though 20 minutes of rainfall with intensity $\geq$ 20 mm hr^{-1} occurred (see Figure 7-16a). Omitting the outlier led to a very strong relationship (see Figure 7-16b) being modelled between N (minutes $\geq$ 20 mm hr^{-1}) with gravel yield using the equation:

$$y = 21.948x + 125.72, R^2 = 0.96$$

where y is the gravel yield (g) and x is N (minutes $\geq$ 20 mm hr^{-1}).
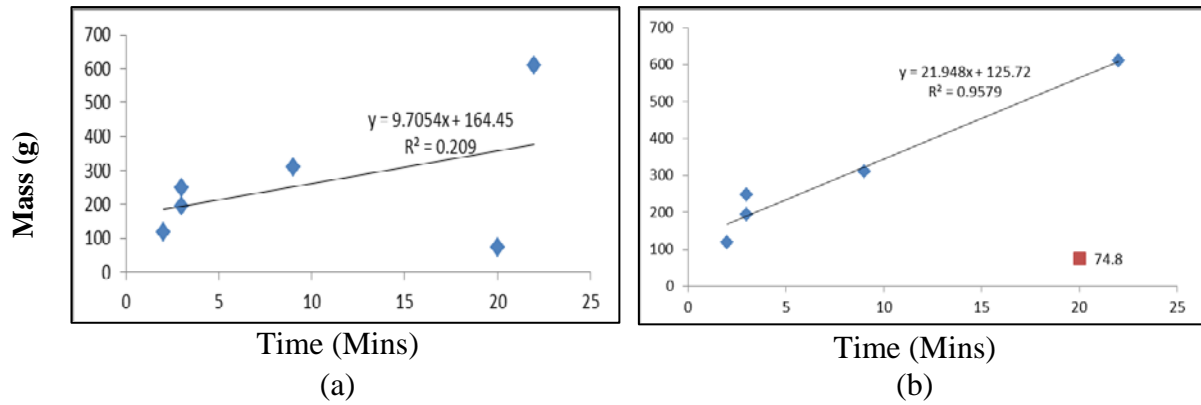
Figure 7-16. SF4 variations in eroded gravel mass at 20 mm hr^{-1} threshold intensity minutes, with (a) all data points from Periods A to F; (b) Period B (red square) omitted.

Hence, there was similarity in response of SF4 to Period B rainfall input to the overall patterns examined in Figure 7-15.

7.2.4.3. Soil erosion responses – individual SFs

The mass of total eroded soil was also analysed for possible relationships to rainfall intensity metrics of one-minute intensities for 5, 10, 15, 20, 30 and 40 mm hr^{-1}. Linear regression was applied between the number of minutes at or above the specified one-minute intensity and the resultant mass of eroded soil. The results of the analyses are summarized in Table 7-5.

Table 7-5. Linear regression coefficients for total soil mass eroded (g) with duration (mins) above threshold I$_{1min}$ rainfall intensity for each period. The highest coefficient values across the threshold intensity values have been indicated in **bold**.

	Threshold one-minute rainfall intensity levels (mm hr^{-1})					
	5	**10**	**15**	**20**	**30**	**40**
SF1	**0.95**	0.89	0.46	0.02	0.02	0.06
SF2	**0.87**	0.82	0.44	0.02	0.02	0.09
SF3	0.14	0.30	0.41	0.36	0.58	**0.90**
SF4	0.06	0.16	0.18	0.20	0.42	**0.81**
SF5	**0.05**	0.07	0.04	< 0.01	< 0.01	0.02
SF6	< 0.01	< 0.01	0.04	**0.09**	< 0.01	0.08
All fences	0.59	**0.67**	0.46	0.10	0.19	0.44

For gross soil erosion mass across all sediment fences, the 10 mm hr^{-1} rainfall-intensity threshold duration gave the best regression coefficient value with R^2 = 0.67. However, as seen in Table 7-5, there was significant variation in examined relationships across the six individual sediment fences. SF1 and SF2 displayed strong relationships at the lowest threshold intensity. At the 5 mm hr^{-1} threshold, the correlation coefficients for SF1 and SF2 were R^2 = 0.95 and R^2 = 0.87 respectively. In contrast, SF3 and SF4 displayed strongest relationships at the highest 40 mm hr^{-1} threshold rainfall intensity at R^2 = 0.90 and R^2 = 0.81 respectively. No discernible regression coefficients were detected for SF5 and SF6 at all threshold rainfall intensity levels.

SF3 displayed interesting deviation of measured values from the modelled trend. In Period C, although 20 mins of rainfall occurred at the 20 mm hr^{-1}, only a low mass of soil was eroded: 48.9 g (see Figure 7-17a). This contrasted with the good correspondence found for Period A which saw 22 mins at or above 20 mm hr^{-1} intensity and 510.5 g of soil being eroded. A similar pattern was observed for SF4, as shown in Figure 7-17b.
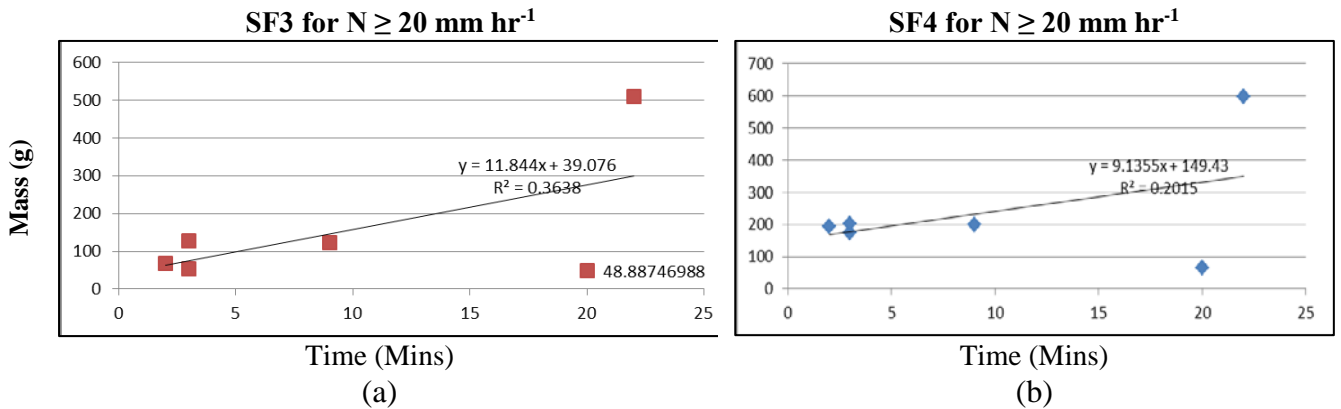
Figure 7-17. Variation of total eroded soil mass (g) for (a) SF3 and (b) SF4 at the **20 mm hr^{-1}** threshold one-minute rainfall intensity (I_{1min}).

A similar pattern was also seen at the 30 mm hr^{-1} threshold rainfall-intensity level for SF3 and SF4 (see Figures 7-18a and b).
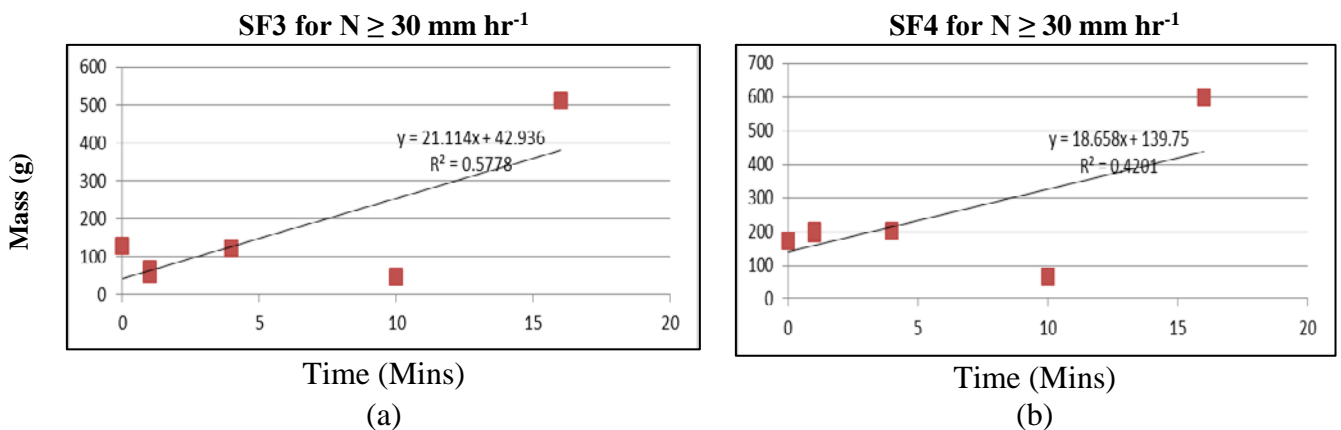
Figure 7-18. Variation of total eroded soil mass (g) for (a) SF3 and (b) SF4 at the **30 mm hr^{-1}** threshold one-minute rainfall intensity (I_{1min}).

The associated diverging data point was also from Period B that saw 10 minutes at or above 30 mm hr^{-1} threshold rainfall intensity.

7.2.4.4. Analysis of Silt component

The mass of the silt component of the total eroded soil was also analysed for possible relationships to rainfall intensity metrics of one-minute intensities for 5, 10, 15, 20, 30 and 40 mm hr^{-1}, also using linear regression. The results of the analyses are summarized in Table 7-6.

Table 7-6. Linear regression coefficients for total eroded mass of silt (g) with duration (mins) above threshold I_{1min} rainfall intensity for each time period. The highest coefficient values across the threshold intensity values are indicated in **bold**.

	Threshold one-minute rainfall intensity levels (mm hr^{-1})					
	5	**10**	**15**	**20**	**30**	**40**
SF1	**0.87**	0.69	0.26	0.006	0.01	< 0.01
SF2	**0.85**	0.68	0.41	0.02	0.01	0.04
SF3	0.02	0.33	0.41	0.34	0.55	**0.89**
SF4	0.02	0.15	0.17	0.19	0.41	**0.81**
SF5	0.02	0.06	0.04	0.01	0.003	0.01
SF6	0.04	0.01	0.07	**0.27**	0.12	< 0.01
All fences	**0.66**	**0.66**	0.39	0.04	0.08	0.26

For eroded silt mass across all fences, good relationships were found at the 5 mm hr^{-1} and 10 mm hr^{-1} threshold rainfall intensities with $R^2 = 0.66$ for both levels. Across the SFs, there were strong, significant relationships found for SF1 ($R^2 = 0.87$) and SF2 ($R^2 = 0.85$) at the 5 mm hr^{-1} threshold. SF3, SF4, SF5 and SF6 did not display strong relationships at the 5 mm hr^{-1} and 10 mm hr^{-1} levels. SF3 and SF4, however, displayed stronger relationships at the higher rainfall intensity threshold levels, with $R^2 = 0.55$ and 0.41 respectively at 30 mm hr^{-1} level, and $R^2 = 0.89$ and 0.81 at the 40 mm hr^{-1} level. SF5 and SF6 did not show any clear relationships for all rainfall intensity levels.

With reference to Figure 7-19a, SF3 displayed a higher than proportionate eroded silt mass response of 195.4 g to 329 mins at or above 5 mm hr^{-1} rainfall intensity threshold; this was also seen for the 10 mm hr^{-1} rainfall intensity. Both these occurrences were during Period A and were likely due to the longest duration at or above higher rainfall intensity threshold levels during summer; of 16 mins for 30 mm hr^{-1} rainfall intensity, and 10 mins for the 40 mm hr^{-1} threshold rainfall intensity. This hints at the importance of short-duration high-intensity "bursts" in explaining silt mass erosion for sediment fence conditions similar to that for SF3. This was further borne out in the high sensitivity shown in the regression analysis for SF3 at the 40 mm hr^{-1} rainfall intensity threshold level. Interestingly, SF3 showed lower than expected eroded silt mass at the highest observed duration values as seen in Figures 7-19 a-b.
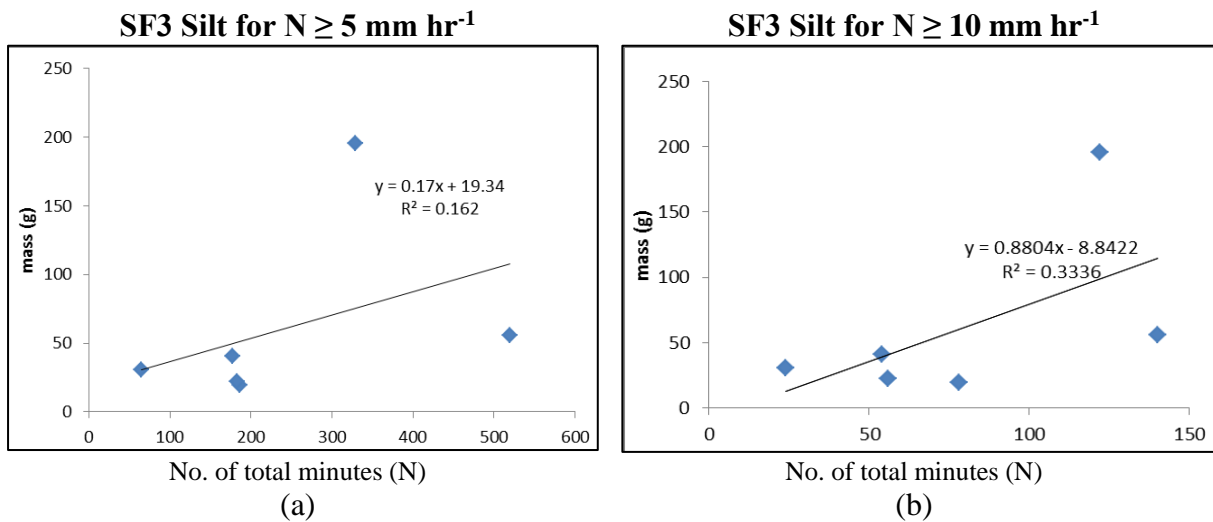
Figure 7-19. Variation of eroded silt mass (g) for SF3 at (a) 5 mm hr^{-1} and (b) 10 mm hr^{-1} threshold one-minute rainfall intensities (I_{1min}).

7.2.4.5. Analysis of Coarse Sand component

Linear regression analysis found a range of responses from the various SFs for coarse sand component to the different rainfall inputs and corresponding threshold one-minute rainfall intensities (Table 7-7). Across all the fences, the highest R^2 value of 0.85 was found for the 40 mm hr^{-1} threshold intensity. However, variation in the possible relationship was observed across the individual fences. SF1 had the highest R^2 value (0.85) at the 10 mm hr^{-1} threshold intensity, with relatively high R2 values of 0.74 and 0.65 for 5 and 15 mm hr^{-1} intensities respectively, and rather low R^2 values for the higher 20, 30 and 40 mm hr^{-1} threshold intensities. In contrast, SF2, SF3 and SF4 had the highest R^2 values of 0.82, 0.91 and 0.86 respectively at the highest 40 mm hr^{-1} threshold intensity. SF5 did not have any clear relationship between coarse sand mass and threshold rainfall intensities with R^2 value of only 0.20 for 15 mm hr^{-1} threshold intensity. No clear relationship was found for SF6 across all examined threshold rainfall intensities.

Table 7-7. Linear regression coefficients for total mass of eroded **coarse sand** (g) with duration (mins) at or above threshold I_{1min} rainfall intensity for each time period. The highest coefficient values across the threshold intensity values are indicated in **bold**.

	Threshold one-minute rainfall intensity levels (mm hr^{-1})					
	5	**10**	**15**	**20**	**30**	**40**
SF1	0.74	**0.85**	0.65	0.17	0.21	0.34
SF2	0.30	0.51	0.57	0.38	0.55	**0.82**
SF3	0.14	0.32	0.44	0.41	0.62	**0.91**
SF4	0.06	0.17	0.23	0.28	0.51	**0.86**
SF5	0.06	0.15	0.20	0.15	0.10	0.02
SF6	0.01	0.01	0.04	0.04	< 0.01	0.06
All fences	0.20	0.37	0.39	0.29	0.49	**0.85**

7.2.4.6. Analysis of Fine Sand component

Applying linear regression analysis for the fine sand component (Table 7-8), a strong R^2 value of 0.72 was found for eroded mass integrated across SFs 1 to 6. However, a wide range of responses was again found amongst the SFs, although these differed somewhat from the patterns found for the coarse sand component. For SF1, very strong R^2 values were found at the two lower threshold rainfall intensities, with the highest at 0.98 for 10 mm hr^{-1}. SF2 had the strongest relationship to the 5 mm hr^{-1} threshold with the highest R^2 value at 0.93. In contrast, SF3 and 4 had the highest R^2 values of 0.89 and 0.77 respectively, albeit at the 40 mm hr^{-1} threshold. No clear relationship was found for SF5. For SF6, only a weak R^2 value of 0.19 was found at the 40 mm hr^{-1} rainfall intensity threshold.

Table 7-8. Linear regression coefficients for total mass of eroded **fine sand** (g) with duration (mins) at or above threshold I_{1min} rainfall intensity for each period. The highest coefficient values across the threshold intensity values are indicated in **bold**.

	Threshold one-minute rainfall intensity levels (mm hr⁻¹)					
	5	**10**	**15**	**20**	**30**	**40**
SF1	0.93	**0.98**	0.60	0.08	0.09	0.16
SF2	**0.93**	0.77	0.27	0.00	0.00	0.01
SF3	0.12	0.28	0.39	0.36	0.57	**0.89**
SF4	0.06	0.15	0.15	0.16	0.36	**0.77**
SF5	0.06	0.07	0.02	< 0.01	0.01	0.07
SF6	< 0.01	< 0.01	0.01	0.01	0.01	**0.19**
All fences	0.63	**0.72**	0.47	0.10	0.01	0.43

In this section, I examine the strongest relationships found between I_{1min} thresholds and sediment size ranges, across all the individual SFs. This is presented in Table 7-9.

Table 7-9. Threshold I_{1min}, $T(I_{1min})$ for highest R^2 values for coarsest (gravel), soil (integrated sand-silt-clay) to fine (silt) sediment ranges examined, for SFs 1 to 6. (As indicated earlier, the clay component was not included in the analysis due to its minor composition of total eroded soil masses.)

	Gravel		Soil		Coarse Sand		Fine Sand		Silt	
	$T(I_{1min})$ mm hr^{-1}	R^2	$T(I_{1min})$ mm hr^{-1}	R^2	$T(I_{1min})$ mm hr^{-1}	R^2	$T(I_{1min})$ mm hr^{-1}	R^2	$T(I_{1min})$ mm hr^{-1}	R^2
SF1	40	0.77	5	0.95	10	0.85	10	0.98	5	0.87
SF2	5	0.29	5	0.87	40	0.82	5	0.93	5	0.85
SF3	40	0.91	40	0.90	40	0.91	40	0.89	40	0.89
SF4	40	0.69	40	0.81	40	0.86	40	0.77	40	0.81
SF5	5	0.14	10	0.07	15	0.20	10	0.07	10	0.06
SF6	40	0.35	20	0.09	40	0.06	40	0.19	20	0.27
All fences	40	0.65	10	0.67	40	0.85	10	0.72	10	0.66

SF1 displayed strong relationships with the lower range of threshold I_{1min} intensities across all sediment ranges, except for the gravel component where $R^2 = 0.77$ for 40 mm hr^{-1}. However, it should also be noted that 10 mm hr^{-1} and 15 mm hr^{-1} thresholds had some moderate correlations at $R^2 = 0.56$ and $R^2 = 0.57$ respectively (see Table 7-4).

SF2 had good relationships at 5 mm hr^{-1} for soil, silt and fine sand with the highest $R^2 = 0.93$ for fine sand. However, $R^2 = 0.82$ was found for coarse sand at the 40 mm hr^{-1} threshold. For the gravel component for SF2, a tenuous $R^2 = 0.29$ was found at the 5 mm hr^{-1} threshold.

SF3 had strong relationships at the highest, 40 mm hr^{-1} threshold across all sediment ranges. This was quite different from the variable rainfall intensity threshold responses from

SF1 and SF2. Like SF3, **SF4** had moderately good relationships with various I_{1min} intensities across all sediment ranges but these were only borne out at the high 40 mm hr^{-1} threshold intensity. The R^2 values found for SF4 were not as high as those found for SF3.

SF5 had very inconclusive relationships with all the examined I_{1min} intensities across all the sediment ranges. **SF6** also had inconclusive relationships with various I_{1min} intensities across all sediment ranges including gravel, although a tenuous relationship was indicated for gravel (40 mm hr^{-1}, $R^2 = 0.35$) and silt (20 mm hr^{-1}, $R^2 = 0.27$).

Across all fences, the most possibly useful I_{1min} threshold values for each of the sediment size categories were: *(i) Gravel: 40 mm hr^{-1} ($R^2 = 0.65$); (ii) Soil: 10 mm hr^{-1} ($R^2 = 0.67$); (iii) Coarse sand: 40 mm hr^{-1} ($R^2 = 0.85$); (iv) Fine sand: 10 mm hr^{-1} ($R^2 = 0.72$); and (v) Silt: 10 mm hr^{-1} ($R^2 = 0.66$).* These provide some indication of the varying factors and processes operating in relation to the terrain, vegetation, soil and ground cover characteristics specific to each SF, and the distinctive rainfall input for each period. This is discussed in the following section.

7.3. Discussion

Generally, the results have shown that substantial variations in the volume and composition of eroded hillslope material occur between each period characterised by distinct rainfall input characteristics, as well as between SFs – each being characterised by different ground and vegetation factors. These interesting and crucial differences will be obscured if predictions are made of hillslope erosion on an annual basis. Indeed, erroneous predictions may result, confounding landscape and catchment managers as to mitigation measures to be taken.

Furthermore, we have found that total rainfall depth may not necessarily be useful for predicting hillslope erosion rates. Specific characteristics of individual rainfall events such as the occurrence of short intra-event high-intensity "bursts" of rainfall need to be considered

for their likely erosional impacts. Indeed, the occurrence of specific rainfall events over particular "target" post-fire landscapes are inherently stochastically independent (Jones et al., 2014), although broad, regional-scale patterns can be discerned (see Chapter 3).

Overlain onto these processes were the dynamically changing vegetation canopy that would have been gradually recovering in terms of extent and strata over time, but also exerting variable effects by seasons associated with flushes of new growth in spring and autumn. Increased litterfall, associated with evapotranspirative stresses in mid/late summer and insufficient solar radiation and/or warmth during winter, would provide additional protective effects on the soil surfaces. Dynamic changes in canopy and litter layers are likely to have an impact on microclimatic conditions. With higher canopy density and extent developing every succeeding year, canopy storage capacity and humidity are likely to drift higher. Canopy shading and litter cover of soil surfaces, where effective, lead to higher average soil moisture levels. Other key controls on erosion in these heterogeneous, intermediate conditions would include slope length, slope angle, bareness of soil surface and distance from nearest significantly dense vegetation regrowth. The complex combination of these factors leads to the observed hillslope sediment flux and shifts in characteristics such as calibre of sediments being eroded.

In terms of general textural shifts of the eroded soil, the largely stable contribution of clay particles to the total eroded soil may be reflective of their mobility across a wide range of event erosivities. Furthermore, being skeletal soils, the source areas would likely to have limited clay percentage composition. On the other hand, the silt and sand fractions displayed a wider range of responses to diverse levels of erosive inputs and process dominance, being of larger calibre compared to clay.

The low sediment yields for Period B were interesting and warranted further investigation. Period B appeared to have a set of distinct rainfall event characteristics

344

compared to the other periods. The total rainfall appeared to be spread out amongst several events of modest depths, as well as being made up of numerous small events. Looking back at Table 5-2, the total 76.5 mm primitive rainfall depth arrived as 23 separate primitive events with the joint second-lowest mean event energy (0.5 MJ ha^{-1}), second-lowest mean erosivity (5.6 MJ*mm ha^{-1} hr^{-1}) and lowest percentage of total rainfall depth falling as primitive events (85.5%). While some of these small primitive events occurred within the same day for Period B (Section 5.4.1.; Figure 5-4) as well as sub-primitive high-intensity "bursts" of $\geq$ 15 mm hr^{-1} occurring in Period B (Section 5.3.), their contribution to total sediment flux were probably subdued by the lack of erosive energy imparted by the numerous other small, weak events. The rather even D:N ratio for rainfall start times could also have contributed (Section 5.4.3.). 23 rainfall events, more than one-third of all rainfall events in Period B commenced between 1100 hrs and 1900 hrs, times of the day which would have seen more intra-event evaporative losses from plant canopies and soil surfaces than for night-commencing events which could have further abstracted effective erosive energies of the numerous small events in Period B.

Although in Period B, N (I$_1$ $\geq$ 15 mm hr^{-1}) = 39 min, the three largest events in this period were of depth 17.2 mm (3 Mar 2012), 13.4 mm (15 Mar 2012) and 10.4 mm. This distribution of modest event depths was also seen in Periods D and E and to some extent, Period F. These were in contrast to Period A with N (I$_1$ $\geq$ 15 mm hr^{-1}) = 47, but had much larger event depths of 42.6 mm (29 Feb 2012; 21.7 hrs) and 36.4 mm (27 Feb; 6.7 hrs) and Period C that saw N (I$_1$ $\geq$ 15 mm hr^{-1}) = 37, and had an extremely large event depth of 109 mm (4 to 5 Jun 2012; 31.9 hrs) and then another substantial event of depth 23.4 mm (21 Jun 2012; 23.0 hrs). Therefore, the occurrence of a minimum event size threshold is likely to be present and important for the generation of significant erosion according to rainfall intensity. The importance of detailed incorporation of rainfall event intensity and duration are also demonstrated by Kleinman et al. (2006).

The variable sediment yield responses to rainfall event inputs amongst the different sediment fences are most likely a result of the differing ground and vegetation conditions in addition to rainfall intensity variations, reflecting the heterogeneity of the area across a small area that translate into different soil availability, erodibility, splash effects under canopy and open-field conditions, and runoff generation (see Table 4-2). SF1 and SF2 were found to be highly responsive directly to rainfall inputs in each period. This was likely to be closely related to the bareness of the slope segment leading down to the fence rendering the patch vulnerable to direct rainfall splash impact and runoff generation and largely unimpeded flows over their relatively smooth surfaces. Even though SF1 had a low slope gradient (16.1°), it had a large exposed soil surface (4.9 m distance to tree upslope) providing for substantial runoff generation from the areas upslope of the SF, as well as for the under-canopy throughfall to translate into overland flow. SF2 had a steeper gradient (18.2°) than SF1 and was also likely to have had greater sediment supply facilitated by the rill erosion, as well as possible intense throughfall splash and under-canopy overland flow generation from the regrowing *E. polyanthemos* tree just 2.5 m upslope. Associated with this would have been the relative availability of soil to be eroded – this appeared to be high for both SF1 and SF2. The centrality of raindrop-induced processes for hillslope sediment transport over bare post-fire surfaces was demonstrated by McGuire et al. (2016). In this respect, work by Kinnell (2005) is instructive. He explained how rainsplash interacted with existing overland flows to enhance erosional effects via two of the four mechanisms discussed: (i) raindrop detachment with transport by raindrop-induced flow transport (RD-RIFT) and (ii) raindrop detachment with transport by flow (RD-FT). In addition to the energy imparted by the falling drops, the temporary thickening of flow depth with these high-intensity rainfall bursts could further enhance the erosive forces (Dunkerley, 2018, *personal communication*). Moss and Green (1983) showed how the kinetic synergy between rainsplash and ponding depth reached

maxima transportation rate of 200 µm sand at depths of 2 to 3 drop diameters. On the other hand, Torri et al. (1987), working with four different soil textures, demonstrated a generally negative relationship between splash detachment and runoff depth. Nevertheless, the existence of a critical depth below which there is a positive relationship between total energy for detachment and transport, and above which there is a negative relationship, have been supported by more recent studies (An et al., 2012; Gao et al., 2003; Hairsine et al., 1999; Rose et al., 1994; Tian et al., 2017). This type of work needs to be furthered in the context of throughfall; the ways in which large throughfall drops arising from canopy modulation of rainfall by *Eucalyptus polyanthemos* foliage (Chapter Six) would interact with any generated overland flow to determine sediment detachment and transport in under-canopy and adjacent positions, remain to be uncovered.

The sediment responses of SF1 and SF2 contrasted starkly with the conditions of SF4 which was very steep (30.7°), bare and rocky with very thin topsoil. The local upslope "source" of soil would have been exhausted, and possibly the sediment pulses trapped by SF4 may have been largely from small slugs of sediment from further upslope, proceeding irregularly downslope with the energy imparted from the various rainfall events as well as via shallow landslides, creep or dry ravel (Gabet and Dunne, 2003; Roering et al., 2001). SF3 also had similarly steep (25.3°) and bare conditions except for having the nearest recovering *E. polyanthemos* tree just 1.5 m upslope that would have exerted close control over throughfall energies, under-canopy overland flow generation, litter generation and sediment fluxes for this position.

SF5 contrasted markedly from the other SFs by having a gentle gradient (16.6°) as well as having very rough gravel and charcoal-strewn surface that would protect the topsoil from direct drop impacts and disrupt runoff flow and having a denser canopy cover and extensive litter cover in a sheltered position; in contrast with the rather exposed nature of

SF1. This patch would therefore have had a milder microclimate which in the preceding of the present study, promoted post-fire regrowth, soil moisture retention and aggregation. Integrating these factors, SF5 would have developed greater resistance to erosive forces by the time of the field campaign. This could also be observed in the silt fraction erosion (see Table 7-9 and Figure 7-5), where the more exposed and erodible SF1, SF2 and SF6 were more sensitive to the lower rainfall intensity threshold of 5 and 10 mm hr^{-1}. Both SF3 and SF4 were insensitive at the lower rainfall intensity thresholds and only showing strong responses to the number of minutes at or above high intensity threshold of 40 mm hr^{-1}. SF5 appeared to be insensitive to all rainfall intensity threshold levels and could have indicated, with its more advanced soil and vegetation "recovery", a distinct set of factors and thresholds controlling erosion processes and rates on this patch of postfire hillslope.

SF6 responses were found to be somewhat similar to those for SF5, having rather inconclusive relationships between various rainfall intensity thresholds and sediment yield for various size ranges, especially for coarse sand. However, possible relationships were found for gravel, fine sand and silt portions of eroded sediment. SF6 had the second-lowest exposed soil surface (40%), close to the 30% exposure of SF5. This level of attenuation of splash energy and disruption of overland flow energy by substantial ground cover as well as the nearby (1.5 m upslope) regenerating canopy could have led to high rainfall intensity thresholds being setup for most erosion to occur. However, there would have been instances where, due to canopy saturation during long events in winter and/or high-intensity bursts, enhanced under-canopy splash and overland flow generation would have caused erosional processes to be active. These help to explain the 40 mm hr^{-1} rainfall intensity threshold R^2 values of 0.35 for gravel and 0.29 for fine sand, and R^2 value of 0.27 for silt at the 20 mm hr^{-1} threshold. The ground surface conditions for SF6 were rather different from those of SF5 even though they had similar levels of ground cover. SF6 had rather smooth surfaces with

some protection afforded by mostly by the litter generated from the tree upslope and sprouting *Acacia* seedlings in contrast with the high surface roughness of SF5 plot. The steeper slope angle of SF6 (20.1°) compared to that of SF5 helped to ensure that where an erosive "breakthrough" occurred, the expected splash and overland flow processes would operate effectively.

Most conceptualizations of hillslope sediment transport assume a positive relationship between erosive energies and erosion rates as well as sediment sizes that can be transported, as reflected in the classic models by Hjulström and Shields (Paphitis, 2001; Simões, 2014). Therefore, as implied in much of the preceding discussion, higher eroded sediment masses and coarser textures of eroded sediments would indicate higher erosive energies stemming from rainfall depth and intensity, and consequent splash and overland flow. However, in the studied context of steep terrain, thin soils with abundant coarse sediments including large pebble and gravel fragments embedded in finer silt and sand material, another possible process of sediment transport can be considered – "winnowing". Refer to Section 7.1 where some descriptions of the coarse fraction (pebbles and gravels) of the eroded sediment were given. In the present soil conditions, fine sand, silt and clay sediments with minimal aggregation are gradually or episodically removed by splash and overland flow erosion and deposited further downslope. This hillslope 'sediment sorting' (Hairsine et al., 1999) is in many ways parallel to what are termed 'downstream fining' processes in the stream geomorphology context (Blom et al., 2016; Chatanantavet et al., 2010). On these hillslopes, this leads to larger pebbles, gravel and coarse sand to be gradually exposed and de-stabilized even under relatively low erosive energy conditions. When these coarse particles are no longer adequately supported by the remaining fine earth material, these sediments would be dislodged and fall, even roll downslope in the steep terrain under colluvial and/or fluvial energies. Hence, the winnowing erosion process can help to explain why coarse sediments,

even the largest pebble size eroded (Feret diameters: 36.7 mm (major axis) and 29.2 mm (minor axis); mass 14.78 g) might be eroded and transported (according to the Hjulström curve, a flow velocity of more than 200 cm s^{-1} would be needed for erosion to effectively operate on the aforementioned pebble) even when erosive energies applied may not be sufficiently high on their own, or occur frequently enough, to move sediments of that size and mass.

It is important to also briefly discuss the rates of downslope movement of litter inferred from the sediment fence data. Clearly, organic litter, as entire or fragments of leaves and twigs, is a vital component of hillslope material flux that is not widely accounted for, even though it is integral to the understanding of intermediate post-fire hillslope processes. These more complex conditions are in stark contrast to immediate post-fire conditions where burnt-out logs and branches and ash are the prime considerations. While it could be assumed that fluvial action plays a critical role in transporting and depositing organic litter at the sediment fences, litter, especially fallen foliage, is frequently of low density and may also be transported through aeolian processes and therefore not necessarily take straightforward downslope pathways. Hence, litter can be highly mobile along and across hillslopes although they would be preferentially trapped and accumulated in specific locations upslope of barriers from small clumps of grass to tree trunks and rock outcrops. With this spatially-selective disruption of erosive energies, localized "islands" of sediment accumulation, seed bank retention and vegetation colonization would be created with a positive feedback mechanism. This was observed at the study site. Litter, despite their low density and total mass, could exert significant influences on detailed hillslope hydrological and geomorphological processes (Geddes and Dunkerley, 1999; Li et al., 2014; Shakesby et al., 2007). Litter can attenuate raindrop and throughfall drop impacts protecting the mineral soil surface. This can be particularly effective in the study site with the large, flat, orbicular juvenile leaves of

Eucalyptus polyanthemos dominant there where they normally lie parallel to the soil surface at repose. Being sclerophyllous and of high lignin content, the leaves decompose slowly and would be effective over long durations, also contributing to accumulating litter storage capacity. The presence of organic litter may also contribute to increased surface roughness disrupting and reducing the competence of overland flows and reducing the volume and grain size of sediment that can be transported downslope. On the other hand, the sclerophyllous, hydrophobic leaves could act as small, overlapping runoff surfaces for rain/throughfall drops that might have infiltrated into the mineral soil surfaces if they had been allowed to contact them. As surface-level fine fuels, their destruction or reduction, either through prescribed or wildfire, may lead to increased soil vulnerability to hillslope erosion processes.

Temporal considerations also need to be included when understanding hillslope erosion in these intermediate conditions. Soil surfaces may become increasingly crusted over time after repeated exposure to rainfall and throughfall splash, and overland flow effects. Hence, a temporally dynamic view of soil surfaces needs be adopted widely; although predicting and representing these changes is fraught with uncertainty and difficulty. Work done by Römkens et al. (2002) is noteworthy in this respect. Using rainfall simulation experiments on Grenada loess in a tilting flume, they found that sequences of simulated storms of decreasing intensity on an initially dry and smooth surface led to higher rates of soil erosion compared to sequences of storms of increasing intensity. Therefore, the temporal arrangements of storms and their characteristics (e.g. intensity and timing) exert important influences on soil erosion rates. The pre and post event soil surface roughness are also important considerations; Römkens et al. (2002) found that initially rough surfaces could lead to higher erosion rates than initially smooth soil surfaces. Kinnell (2005) argued that rainfall-induced splash and overland flow processes on hillslopes would usually lead to a protective veneer of pre-

detached particles on downslope positions that subsequently buffered erosive forces affecting the underlying layer.

The post-fire sediment yield for the present study area and duration is compared with other similar studies, as presented in Table 7-10.

Table 7-10. Post-fire sediment yield from present study and selected studies/regions in southeast Australia, Mediterranean and Western United States.

Region	Southeast Australia								Mediterranean	Western United States	
Sub-region	Present study – southern foothills Alpine National Park, Victoria						Central Highlands, Victoria	Snowy Mountains, Victoria	Góis region, central Portugal	Colorado Front Range	*Synthesis – various locations*
Sources	SF1	SF2	SF3	SF4	SF5	SF6	Leitch et al. (1983)	Smith and Dragovich (2008)	Vieira et al. (2016)	Benavides-Solorio and MacDonald (2005)	Moody and Martin (2009)
Post-fire stage	5 years						0 to 0.4 years	0 to 2.5 years	0 to 4 years	Various: 0 to 6 years	0 to 2 years
Sediment erosion rates (g m^{-2})	123	156	500	52	72	102	2200	270 to 9430	11 (unplowed) to 83 (plowed)	200 to 1000 (high-severity fires)	8200
Reporting Timeframe	10 mths						3 mths	------------------*Annual erosion rates (i.e. g m^{-2} yr^{-1})* ------------------			

Apart from the clear variation in erosion rates amongst the various SFs in the present study, it can be seen from Table 7-10 that while the latter are clearly lower than the heightened erosion rates recorded in the first few months after fire, e.g. 2200 g m^{-2} in just 3 months reported by Leitch et al. (1983) and 8200 g m^{-2} yr^{-1} reported by Moody and Martin (2009), erosion rates for the present study area, five years after fire were still quite substantial, ranging from 52 g m^{-2} to 500 g m^{-2} in 10 months, when compared to the lowest erosion rates of 270 g m^{-2} yr^{-1} reported by Smith and Dragovich (2008) at 2.5 years post-fire for the Snowy Mountains region. Also, Vieira et al. (2016) reported rates 11 and 83 g m^{-2} yr^{-1} for unplowed and plowed fields respectively in the Góis region of central Portugal up to 4

years post-fire. While the lowest erosion rate of 200 g m^{-2} yr^{-1} at 6 years post-fire showed prolonged erosional vulnerability for the Colorado Front Range region, this was lower than SF4 at 500 g m^{-2} and somewhat comparable with SF1 at 123 g m^{-2} and SF2 at 156 g m^{-2} over 10 months for the present study.

7.4. Conclusion

The present section has contributed useful insights into the rates and volumes of soil and litter material flux for intermediate post-fire condition for a patch of burnt dry sclerophyll forest. By detailed study of the hillslope using six sediment fences installed in differing site conditions, and evaluation of various rainfall parameters, I have illustrated the heterogeneous and complex interactions that drive hillslope erosion in intermediate post-fire conditions of recovering dry sclerophyll forest. Hillslope erosion processes and yields are still active, albeit operating in more complex manners and resulting in modest yields.

The erosional effects of series of different rainfall events, over varying plot conditions, could be examined using one-minute resolution rainfall intensities (I_{1min}) that occur within and across events in a particular time period. The physical basis for this metric is likely to be more useful than coarser overall event intensities where total rainfall depth is averaged over the total event duration. This point is clearly demonstrated by Wainwright and Parsons (2002) who examined rainfall intensity variations at the sub-minute bucket-tip, as well as one-minute temporal resolutions, and found that these variations helped to explain why runoff coefficients tended to decrease with increasing slope length. They also highlighted how one-minute "summaries" were likely to have led to underestimation of peak intensities, and clearly demonstrated how mean event intensities, the rainfall metric commonly used in overland flow models, led to startling underprediction of runoff rates. Indeed, near-instantaneous bucket-tip rainfall intensities of up to 1829 mm h^{-1} were reported (Wainwright and Parsons, 2002). Reaney et al. (2006) showed how fragmentation of high-intensity rainfall

episodes led to the generated runoff infiltrating into the soil after a short distance downslope, while contiguous high-rainfall periods caused longer runoff distances that were subsequently realized as stream discharge. In the post-fire context, Reaney (2013) explained the importance of temporal patterns of (intra-event) high-intensity rainfall and their interactions with spatial patterns of overland flow and soil properties in understanding and determining hydrological and sediment connectivity. More recently, Nishigaki et al. (2016) monitored rainfall event characteristics, runoff generation and soil erosion rates at four sites in the Uluguru Mountains of Tanzania, and found that at the highest elevation (1600 m a.s.l.) and steepest slope gradient (20 degrees) site NY, average I_{10min} values, instead of rainfall depths, were significantly correlated with sediment concentration and soil loss. While the temporal resolution adopted by the latter was substantially coarser than sub and one-minute rainfall intensities, the findings indicate that temporally finer resolutions (compared to 30-min or one-hour integration times) enable higher accuracy in representing the hydrological and erosional dynamics operating in reality. Mizugaki et al. (2010) found that maximum I_{10min} values had the strongest relationships with soil detachment on gentle slopes (9° to 16°), but weakest relationships on steep slopes (35° to 39°) and I_{60min} provided the best modelled relationships on average slopes (~26°). Using erosion plots in the Khamsan basin of Iran, Mohamadi and Kavian (2015) found the strongest relationship between maximum I_{20min} values and eroded soil ($R^2 = 0.64$) while the weakest relationship was found with I_{90min} values. In view of the results from the present study alongside work by various other researchers, the importance of incorporating or re-examining rainfall intensity variations into studies of hillslope hydrological and erosion in various regions and contexts should continue to be emphasized.

Nevertheless, it is acknowledged that the availability of high temporal resolution rainfall data would be limited in circumstances where depth readings are only obtained daily

with a non-recording rain-gauge, or especially in remote areas, where equipment or datalogger failure may have occurred, or where fixed temporal resolutions (e.g. 5, 10 or 15-minute intervals) are used. Furthermore, rainfall has inherently high spatial variability over a region (Kampf et al., 2016) which compounds the problem of acquiring accurate records for a local area of interest. However, wherever such data is available, maximizing the temporal resolution could enable workers to glean interesting insights for explaining the operation of geomorphic processes and outcomes observed in the field. One key point from the results of the field experiment discussed in this section is that different sites in the same post-fire area can have differing rainfall intensity thresholds and some consideration of this heterogeneity in hydrological and erosional responses should be included in the assessment and prediction of post-fire erosion processes and rates. In the examination of post-fire hillslope erosion, researchers should move beyond simply event depth or daily rainfall, towards more detailed consideration of the specific event characteristics for better understanding of the physical processes in operation; this is especially so for complex and heterogeneous intermediate post-fire hillslope conditions. Furthermore, in these contexts, the effects of plant litter is an often under-estimated and under-investigated factor that can have impacts beyond their mass contribution to overall hillslope material flux.

Having examined and discussed the complexities of hillslope material movements for the study area in this chapter, I now proceed to the closing chapter where I attempt to synergize the findings from this study and draw some linkages to the concepts developed as part of this study as well as more broadly to the fields of post-fire erosion science, ecohydrology and ecogeomorphology.

CHAPTER EIGHT: CONCLUSION

8.1. Overview

In this closing chapter, I firstly attempt to synthesize the findings from Chapters Five (Rainfall), Six (Throughfall) and Seven (Hillslope materials) to develop a coherent discussion around key hydrological and erosional processes and the factors that affect them, in the context of post-fire erosion under intermediate recovery conditions of dry sclerophyll eucalypt forest represented by the site in the Licola region of southeast Australia. Secondly, I will try to draw linkages to salient conceptual frameworks such as connectivity, alternative post-fire recovery trajectories (Chapter One), anisotropic patterns of post-fire vegetation recovery, hydrology and erosion on steeply sloping terrain (Section 1.3) and the Dynamic Zones of Influence (DZI) framework (Section 2.5.). Thirdly, I highlight the key contributions that have been made by conducting the present research. Fourthly, I will discuss the limitations of the research and further work that should be undertaken for progress in post-fire erosion science to be achieved. Lastly, I will conclude with some final remarks on this research project and area of study.

8.2. Synthesis

In Chapter Five, I provided an overview of the rainfall received during the entire study period and elucidated several rainfall metrics corresponding to each of the six periods. Focusing on the 'primitive event' definition, these included total and mean event depths, event erosivities and energies as well as inter-event times. The diurnal-nocturnal occurrence of rainfall and high temporal resolution one-minute rainfall intensities were also explored to some detail. These analyses showed that each rainfall period was quite distinct and constituted a specific field-experimental 'treatment' on the study area and plots. It was also important to highlight that daily rainfall depth was not a sufficient indicator of erosive power to explain the complex hillslope material responses described in Chapter Seven. Notably, the assemblage of rainfall

events arriving to and affecting the study site was primarily controlled by higher-order systems and cycles interacting with the regional topography and land-surface characteristics to give seasonally-distinct rainfall and climatic parameters (see Chapter Three) that would ultimately impact upon hillslope hydrology and erosional processes and outcomes.

Chapter Six examined the processes and impacts of throughfall in the intermediate post-fire vegetation context. This was done by applying knowledge from the earlier works by Dunkerley (2010a) for throughfall fraction measurements and Scholten et al. (2011) for throughfall splash erosivity. Assessment of the canopy cover through the fieldwork period did not find a simple increasing trend through time as might be normally expected for a "recovering" vegetation formation. Instead, seasonal variations in canopy cover, captured in part by progressing through Periods A to F were quite clear and would have been integral to the interception and modulation of rainfall. Furthermore, canopy cover for individual TIFs and splash cups displayed both the heterogeneity of the recovering vegetation canopy at any one point of time, as well as non-linear changes through time – differences at this detailed spatial resolution that would not normally be well-captured by landscape and regional-scale approaches such as remote-sensing (Hammill and Bradstock, 2006; Sever et al., 2012), that were also observed at individual TIFs and splash cups.

Aggregating over individual TIFs, throughfall fraction ranged from 0.60 to 0.91 and in Period F recorded a seeming anomalous "positive" throughfall fraction. While the throughfall fractions of less than one showed seasonal, non-linear variations through the different rainfall Periods, the "positive" throughfall at 1.17 indicated preliminary evidence of the distinct Eucalyptus funnelling effect (Mululo Sato et al., 2011) of rainfall of particular characteristics in Period F and this is particularly interesting data for juvenile dominant post-fire foliage in southeast Australian dry eucalypt forests. This gave additional explanatory strength to the observed splash cup data which gave erosivity ratios ranging from 1.34 to 2.04

357

varying by Period, supporting and complementing the body of work from other regions reported by workers such as Nanko et al. (2016a), Geißler et al. (2012b), Scholten et al. (2011) and Levia et al. (2017).

The results of the laboratory work showed how throughfall spectra differed from, and were more erosive than rainfall spectra, accounting for the reported throughfall erosivity ratios. It was also found that for the species of interest which was dominant at the study site – *Eucalyptus polyanthemos*, throughfall spectra from juvenile foliage was distinct from that from mature foliage, with the latter giving a narrower range of drop sizes, albeit with slightly higher average drop diameter. These could be explained through detailed observations of distinct leaf-catchment dynamics of water drop adhesion, growth, movement, aggregation and release associated with the orbicular shape of juvenile leaves, as opposed to the ovate-lanceolate shape of mature leaves.

The implications for throughfall-ground surface interactions, and subsequent hillslope hydrology and erosion are that intermediate-stage post-fire eucalypt canopies can generate quite erosive drops and can significantly impact under-canopy soil and litter layers; however, this is subject to factors such as drip height, interception storage and loss. As the vegetation canopy progresses to being dominated by mature foliage over the long-term (e.g. 15 to 20 years post-fire), the canopy is likely to be more open, allowing a higher fraction of less-erosive free throughfall to impact the ground although this might be partially countered by more erosive released throughfall from higher drip-heights and large drops ensuing from mature foliage, that may in some positions be enhanced by the above-mentioned funnelling effects. Despite the clear modulation effects and erosivity potential of the intermediate vegetation canopy from the present study, throughfall spectra would still exhibit a delayed response because time is taken for on-foliage dynamics to work and canopy storages to be

exceeded; in contrast to the direct impacts of rainfall on the ground-level soil and litter layers (if any).

In Chapter Seven, I quantified hillslope material flux rates at two temporal scales: (i) over 10 months, and (ii) at the monthly/bi-monthly scales (periods), and at two spatial scales: (i) the hillslope scale (integrating the six SFs) and (ii) plot scale of individual SFs. This followed naturally from the causal processes of rainfall and throughfall examined in Chapters Five and Six respectively. I showed that overall hillslope sediment flux was lower than immediate post-fire rates, but these were higher than standard 'background' (long-undisturbed) rates and could be regarded as heightened in this 'intermediate' (five-years) post-fire stage, and comparable with other reported rates in Victoria as well as in the Mediterranean (Shakesby, 2011) and western United States (Moody and Martin, 2009; Shakesby et al., 2016). I found that soil erosion rates did not always correspond directly with rainfall depth; higher rates of erosion seemed to occur in the "warmer" months in Periods A (summer) and F (late spring/early summer), and these were likely to relate to the specific character of more erosive rainfall events occurring during these seasons compared to those of other seasons.

Other contributory aspects of the rainfall factor also include the diurnal-nocturnal occurrence, depth of largest event as well as the occurrence of high-intensity (one-minute) "bursts" of erosive energy that can have significant hydrological and erosional effects on the study hillslopes. The times of day during which rainfall occurs vis-à-vis season of the year can be quite important. Active solar radiation receipt during the day translates into sensible heat at both the ground and canopy layers, enabling higher rates of intra and inter-event evaporative losses of canopy and soil moisture storages. Furthermore, active soil moisture uptake by plants for photosynthesis can quickly deplete soil moisture. Hence, when rainfall events occur during the day, canopy and soil moisture storages would take longer to saturate,

overland flow and consequent erosion is less likely; splash erosion is more likely to occur on drier soil surfaces. These storage-depressing processes are quite dormant during the night. Therefore, saturated, erosive conditions are more likely to be reached in nocturnal conditions compared to diurnal conditions, *ceteris paribus*.

Rainfall event characteristics should therefore be examined in more detail than is currently done in most post-fire science, by moving beyond simply daily rainfall depth as causal metrics towards descriptions of event erosivity and intra-event intensity variations, including 'no-rain' pauses (Dunkerley, 2015a; Dunkerley, 2016; Dunkerley, 2018; Shakesby et al., 2016). While rainfall event characteristics exert higher-order influences on hillslope sediment and litter responses, response heterogeneity, corresponding to the large variability in the "target" surfaces manifested as the variable erosion rates for SFs 1 to 6, also need to be recognized. Textures of the eroded sediments can also vary between SFs as well as between rainfall events and periods. On-ground rainfall/throughfall effects would be mediated by any intervening vegetation and litter as well as broader environmental factors such as season, microclimate and time-of-day of rainfall occurrences. Indeed, the complexities of the scale issue in hydrological and geomorphological processes (Braun et al., 1997; de Boer, 1992; Kabat et al., 1997; Liu and Pei, 2003; Phillips, 2016) are multiplied in the intermediate post-fire condition.

In Chapter Seven, I also examined hillslope litter flux, as aspect that is rather important for post-fire erosion science under intermediate vegetation recovery conditions albeit quite under-examined currently. An example of post-disturbance soil and litter erosion on hillslopes is the work by Larsen et al. (1999) which investigated runoff, soil erosion and fine-litter movements on sub-tropical rainforests and lower-montane forests in Puerto-Rico after the impacts from Hurricane Hugo in 1989. Furthermore, some consideration should be made of the physical and chemical influences of litter on hillslope hydrological and erosional

processes, beyond their assumed single effect in retarding hillslope sediment flux rates (Shakesby, 2013; Shakesby et al., 2016; Shakesby et al., 2007). Indeed, Dunkerley (2015b) showed, for *Eucalyptus* spp. leaf litter under simulated rainfall, how litter percolate flux was strongly influenced by differing rainfall profiles (i.e. varying intra-event rain rates) with the same mean event intensity (10 mm h^{-1}). This gave insights into the complex rainfall/throughfall modulation effects of typical *Eucalyptus* forest floor litter that manifest as lagged but variably attenuated or amplified percolation peaks, with significant hydrological and erosional implications.

The results for, and discussion around the post-fire erosion responses presented in Chapters Six and Seven, caused by the rainfall characteristics discussed in Chapter Five can be further examined in the light of existing concepts and frameworks; the focus of the next section.

8.3. Conceptual linkages

8.3.1. The DZI framework

The findings from the present study can be positioned within the DZI framework discussed in section 2.5. Hillslope erosion fluxes reflect the outcomes of the complex interplay between rainfall event erosive energies and their intra-event variations, vegetation canopy extent and characteristics modulating the incident rainfall spectra into throughfall spectra, as well as the surface conditions of the under-canopy zones of influence and the inter-patch zones. The largely-bare inter-patch zones, which are likely to contract as vegetation recovery advances, will likely exhibit direct and immediate responses to the rainfall inputs. Erosion thresholds in the conspicuous absence of vegetation canopy and ground cover, save for any litter cover, would be largely dependent on the soil characteristics such as texture and their inherent erodibility, aggregation and sealing, as well as key factors such as slope steepness and microtopography (see Figure 1-3).

The erosion threshold of undercanopy patches would, apart from the division into the intra-patch inner, middle and outer zones, be a complex composite of the soil and topographical factors described above, the litter layer depth, distribution and decomposition; canopy depth, cover, height and architecture in the three DZI sub-zones. Indeed, there are inherent soil moisture, fertility, aggregation and perhaps even textural differences between interspaces and under-canopy patches (Dunkerley, 2000; Wainwright et al., 2000). Ground-level erosional and hydrological responses to rainfall inputs are likely to be delayed and highly modified, especially in situations where the canopy is dense and dry. However, more immediate modulation of rainfall inputs would occur in wet canopies where canopy and leaf storage capacities are easily exceeded (sparse canopy cover or canopy saturation), or momentum is imparted by falling rainfall or throughfall to detained water droplets; these may

also occur in dry conditions where abrupt, high-intensity rainfall bursts (see Chapter Five) temporarily overcome the limited storage capacities typical of this Eucalypt vegetation.

The anisotropic process connections between inter-patch and patches must also be incorporated (see Figure 1-6). Patches can play a dual-role on steep, intermediate post-fire hillslopes. Firstly, as is commonly construed, upslope of the plant stem, the patch functions as a barrier that helps to trap allochthonous litter and sediment arriving from inter-patches and patches further upslope. Autochthonous litter from the plant itself is also accumulated in this position. These express themselves as the litter-dam complexes that reduce overall hillslope sediment yields as well as the supply of material to the stream system (Shakesby et al., 2007), and also form 'islands of fertility' (Abrahams et al., 1995; Dunkerley, 2008c; Kidron, 2015; Wainwright et al., 2000) that develop a positive feedback mechanism (e.g. by providing a viable moist, fertile and stable soil microenvironment for seed germination and growth). Nevertheless, the capacity of this upslope portion of the patch can be exceeded, with sediment and/or litter "overflowing" to the downslope portion.

In contrast, the functions of the downslope portion of the patch are probably much less studied or conceptualized. As with the upslope, downslope plant canopies areas are similar under the DZI conceptualization if ignoring any asymmetries in plant growth and spatial colonization (Christophe et al., 2003). However, the downslope dynamics would be quite different. While autochthonous litter would dominate on the downslope aspect, litter depths are likely to be shallow, being cut-off from upslope sources. Because there is usually minimal obstruction on the downslope aspect, any accumulating litter would be more likely to be transported away downslope onto the adjacent inter-patch. As shown from Chapter Six, there can be appreciable throughfall drop energy available for litter transport; runoff development may also be enhanced due to the sclerophyllous nature of eucalypt leaves, as well as repeated positions where released throughfall arrive and create localized points of soil

moisture saturation and runoff generation. The integrated effect of these downslope patch dynamics would also be enhanced soil as well as litter erosion and transport onto the downslope inter-patches.

The mostly-bare inter-patches will have a distinct set of hydrological and erosional dynamics from the patches described above. They are likely to function as transient receiving areas for the soil and litter generated from upslope patch areas, where these hillslope materials would be 'smeared' as a thin veneer across the already thin, rocky ground surface but ultimately be deposited and accumulated at the next upslope patch area. The transport mechanisms on the inter-patch would be a combination of overland flow generated from under-canopy downslope aspect patches and short-distance under-canopy splash effects, overland flow generated on the inter-patch itself (Hortonian or saturation-excess flow), interacting with milder rainsplash effects. During dry periods between rainfall events, litter could also be blown around by wind, albeit with a net downslope movement. Because inter-patches are more exposed, soil moisture levels would vary much more compared to patch areas. As inter-patches are likely to be drier, they would function as run-on areas where overland flow and their erosive energy could dissipate leading to sediment and litter deposition, especially in the early stages of storms after a long dry spell. On the other hand, because of the receipt of rainfall without the mitigating and modulating effects of a plant canopy, these areas could reach saturation in the middle and later stages of a storm event and generate runoff.

Variable combination of these patch-interpatch dynamics would be dependent on the status of post-fire regeneration affecting the arrangements and extents of patch vis-à-vis interpatch areas, canopy architecture and foliage types (density, juvenile/mature dominant) as well as the intra and inter- rainfall event variations. From the plan view at the hillslope scale, spatial distribution of patches would affect the lengths of inter-patches, depending on the

364

preferential flows of water on the hillslope surface. Where continuity exists between inter-patches, narrow "avenues" could be created where runoff is able to accumulate erosive energy to transport higher sediment masses as well as larger calibre material such as gravel.

It is essential to highlight that the various strata of concern (canopy, shrub, ground cover and litter layers) recover at different rates and this is likely to be quite salient at the intermediate post-fire recovery stage (see Figure 1-2), and their variable combinations mean that complex interactions and dynamics are in operation. In the immediate and near-term post-fire period, rainsplash, together with erosive branch/twig drips and stemflow from the woody parts of the burnt trees (Dunkerley, 2014a) would have led to much dislodgement of soil particles particularly at the base of trees, primed for easy erosion and transport in subsequent events. Further on at the intermediate post-fire stage during which the present study was conducted, this readily erodible supply of soil may have been strongly impacted by the erosive throughfall drops generated by the large, orbicular juvenile leaves, for transport downslope. However, the extent of this process operating would be strongly dependent on the depth and extent of the sub-canopy litter layer, as well as rates of litter removal/accumulation at the downslope and upslope positions of the patches. Hence, the identification of "optimal" conditions for high soil erosion rates in sub-canopy positions would be quite difficult considering these complex conditions and require careful and detailed investigations. Under "full recovery" conditions where mature foliage dominates, the erosivity of throughfall drops generated would be high, especially where the drops ensue from higher dripping points (see Chapter Six). However, the overall erosive effects would be diluted by the greater throughfall fraction (and therefore smaller unmodified raindrops) associated with the sparser mature *Eucalyptus* forest canopy and a substantial under-canopy litter layer that would effectively attenuate much of the erosive energies of large throughfall drops.

Connectivity concepts (Bracken and Croke, 2007; Bracken et al., 2015; Fryirs et al., 2007; Hopp and McDonnell, 2009; Wester et al., 2014; Williams et al., 2015; Williams et al., 2016), in both horizontal and vertical dimensions are also particularly applicable in the present study that has focused on intermediate post-fire hillslopes, vegetation and soils. Hopp and McDonnell (2009) posited that connectivity in the hillslope hydrological (and erosional) context can be described by how 'hillslope architecture' determines the 'filling and spilling' threshold processes – wetting, saturation, expansion and linking of initially hydrologically isolated surface/subsurface hillslope areas towards a 'whole-slope connectedness', and that storm size (i.e. rainfall depth) strongly influences the non-linear threshold (dis)connectivity spatio-temporal responses. The other main factors are bedrock permeability, soil depth and slope angle.

The present study has shown that in the intermediate post-fire context, storm size may not be the only crucial factor for hillslope hydrological connectivity; rainfall intensity at the high (one-minute) temporal resolution also provide important insights into how transient overland flow pulses caused by rainfall "bursts" would lead to corresponding jolts of sediment (and litter) transport. Furthermore, Moody and Ebel (2014) reported that storm profile, in addition to soil moisture deficit, were key factors determining runoff (and by extension, erosion) of more importance than soil hydraulic properties for fire-affected soils. Indeed, the 'average rainfall acceleration' (Moody and Ebel, 2014) is a relatively novel metric that needs to be incorporated alongside other rainfall metrics (Dunkerley, 2008a; Dunkerley, 2014a) into present and future studies of hillslope erosion for greater descriptive and explanatory power. Instances of transient hillslope connectivity and their positive feedback effects can be considered in how, due to rainfall "bursts" concomitantly cause an increase in ponding depth as well as ponding areas on various hillslope positions. Beyond

depression storage thresholds depending on microtopography and geometry, these ponds would "spillover" and generate concentrated flows that clear and carve-out rill-like pathways that interlink ponds, and also transport the litter (that may otherwise have a protective effect) which is much more buoyant than sediments preferentially along these paths. These could then enable overland flow paths that would be, in subsequent events, readily followed than simple Hortonian processes that may be assumed to operate quasi-randomly on the hillslope.

Clearly, the hillslope connectivity framework is useful for application to post-fire erosion science and some important work in this area has been done by Moody et al. (2013), Wester et al. (2014) and Moody and Martin (2015). It is quite obvious that extremely high hydrological connectivity prevails on post-fire hillslopes in the immediate/close post-fire context, explaining the dramatic erosion spikes in sediment, ash and litter yield that then get quickly transferred in abundance to the stream system due to the heightened hillslope-stream connectivity (Shakesby et al., 2007; Tetzlaff et al., 2007; Williams et al., 2016), causing the human and environmental effects of concern. Indeed, post-fire soil hydrophobicity increases surface and/or near-surface hydrological and erosional connectivity in the immediate/near post-fire conditions across various fire-prone regions (Moody et al., 2013; Shakesby and Doerr, 2006; Shakesby et al., 2000).

However, as vegetation strata recover post-fire, various 'buffers' (Fryirs et al., 2007) are either re-activated or created, that impede sediment and litter movements downhill, and their supply to the stream channel system. Interestingly, not much detailed discussion was given by Fryirs et al. (2007) to the complexities of the dynamic roles of vegetation in hillslope-stream (de)coupling. These have been aptly illustrated in Figure 1-6 and highlighted in Shakesby et al. (2007) as litter-dam microterrace complexes. In fact, the DZI framework can be integrated into the connectivity theory to organize future work around post-fire erosion science, as well as hillslope hydrology and geomorphology more broadly.

The present study is also well-positioned to contribute to the domain of biogeomorphology, the interdisciplinary study of the interactions between biota (particularly but not exclusively vegetation) with landscape form and function (Osterkamp et al., 2012). Wildfire has been widely acknowledged as a key disturbance regime that requires focused attention for biogeomorphologically-framed examination of the co-evolution of vegetation distribution and structure, with landforms and soils (Rice et al., 2012). Exemplifying this is the work by Hyde et al. (2015) who conducted a landscape-scale study of the influences of pre-fire vegetation floristics and structure, vegetation disturbance and topography on the extent of post-fire gully rejuvenation in conveying sediments from hillslopes to channels.

Complementing the work by Hyde et al. (2013) and Hyde et al. (2015), the present study has shed further light on this area of research by showing how post-fire vegetation regeneration can, for a significant duration, exert influences on rainfall modulation, throughfall spectra, overland flow and hillslope material fluxes that are quite distinct from "long-unburnt" pre-fire vegetated conditions; these relate not only to canopy and ground-cover, but also importantly to foliage shapes associated with the distinct heterophylly of many Eucalyptus species that populate the dry sclerophyll forests of fire-prone southeast Australia. Furthermore, the DZI framework developed as part of this work enables focus on the interesting interactions between patches and inter-patches, and the anisotropic patterns of interactions where they occur on steeply-sloping terrain.

A closely related field of research is that of ecohydrology, the interdisciplinary study of the reciprocal exchanges between "environmental" stores and movements of water, with vegetation structure and function; the key domains from which ecohydrology draws on are ecophysiology, hydrology, soil science and micro-meteorology (Bowman and Boggs, 2006; Dunkerley, 2012; Eamus et al., 2006). As an area recovers from the depleted, hydrologically

and micro-meteorologically simplified conditions of the immediate and near post-fire condition, the activity of, and interactions between, the various factors of vegetation, soil and soil water, and micrometeorological conditions of patch and inter-patch areas increase and become more complex from the incipient recovery through to the intermediate and "full" recovery stages (see Figure 1-6). These can be studied with the help of the DZI framework (Section 2.5) together with a cognizance of the range of possible post-fire recovery trajectories primarily controlled by climatic and ecological factors (see Section 1.3; Figure 1-5).

8.4. Key contributions

The main objective of this study was to provide insightful vignettes into key aspects of post-fire erosion processes under intermediate recovery conditions for dry eucalypt forests in southeast Australia. The contributions this research has made include:

  i. Review of the global and regional literature on post-fire erosion, and the highlighting of research gaps in process-based understanding of post-fire erosion under intermediate vegetation recovery and the paucity of studies in southeast Australia, the main motivation for this study;

  ii. Development of concepts and frameworks useful for present and future work in post-fire erosion, including the DZI framework, alternative post-fire recovery trajectories and anisotropy on steep post-fire hillslopes;

  iii. Application and development of new and low-cost approaches to field measurements, such the use of TIFs, splash sand cups, sediment fences and dyed filter paper method for drop-size determination;

  iv. Description and analysis of rainfall metrics not normally examined in detail, but which have some physical relevance to hillslope hydrology and erosion, viz. diurnal-

369

nocturnal rainfall occurrence, one-minute rainfall intensity thresholds, multiple-event days and wet-day "clusters";

v. Quantification and analysis of the throughfall spectra differences between juvenile and mature leaves of *Eucalyptus polyanthemos*, a species typical of fire-prone dry sclerophyll forest, as well as description of the on-leaf dynamics influencing drop-size differentials;

vi. Quantification and analysis of post-fire hillslope erosion fluxes with examination of eroded soil textures and causal one-minute rainfall-intensity values across the six SF plots of heterogeneous characteristics.

8.5. Limitations of study and future work

This study only covered 10 months in 2012 and this was a wet year (see Chapter Five) while there have been significant climatic oscillations between years, decades and centuries. At time of writing this chapter, it was reported that ongoing droughts in central NSW (and southeast Australia) were the most severe in terms of duration in the last 800 years (Freund et al., 2017) and that high risks of wildfire and by extension, post-fire erosion vulnerability, were very likely. To account for such variability, multi-year, multi-site monitoring studies would enable workers to track vegetation-hillslope responses to different rainfall-temperature parameters longitudinally. At the same time, this field research integrated hillslope responses and the rainfall inputs as six periods within which much variability would have been masked. Furthermore, being mainly field-based, the attendant complexities of operating in the natural environment where the entire gamut of factors were not well-controlled nor comprehensively measured, even though useful data has been gathered. There are many factors that remain unquantified and interactions that may have been hidden. Having just six SFs may have limited the validity and generalizability of the findings, even though much variability between SFs was characterized. In contrast, Benavides-Solorio and MacDonald (2005)

deployed 48 sediment fences over two summers and one winter at the Colorado Front Range in west-central United States. Hence, for future studies in post-fire erosion in southeast Australia glean richer insights with more well-instrumented, spatially-distributed and replicated, higher temporal resolution event-based monitoring of rainfall, throughfall and erosion on hillslopes located closer to facilities, or indoor laboratory experiments using rainfall simulations (Doerr and Cerdã, 2005).

This study focused on the rainfall modulation and throughfall impacts of *Eucalyptus polyanthemos* canopies. Other Eucalypt tree species typical of the dry forest formations reported in section 3.6 such as the *E. melliodora* and *E. macrorhyncha* were not included in the present study. While these species did not constitute most of the regenerating eucalypt trees at the study area, it was likely that they would have had their own unique influences on and contributions to the overall hillslope hydrology and geomorphology. Furthermore, an abundance of young *Acacia spp.* shrubs was observed at the base of the study slopes, ostensibly positions where a substantial bank of seeds, stimulated by the fires and smoke (Ashton and Chappill, 1989; Auld and O'Connell, 1991; Gordon et al., 2017), had accumulated and germinated at these relatively gentler slope positions. These would constitute an additional vegetation barrier to sediment and litter movements, mitigating much transfers to the Wellington River System.

Only a static consideration of throughfall spectra has been adopted. This has been a limitation of the technology and equipment available for this study. It would have been ideal for several laser disdrometers to have been made available for high-precision, temporally-continuous, direct measurement of rainfall and throughfall drops in the field across vegetation transects. Temporal variations in throughfall spectra have been demonstrated (Levia et al., 2017; Mululo Sato et al., 2011; Nanko et al., 2016a; Nanko et al., 2011; Wakiyama et al., 2010) to result from modifications to canopy-incident rainfall that itself can vary significantly

(Jones, 1992; Tokay and Short, 1996). Indeed, the effects on wind on canopy interception and rainfall modulation need further study. Furthermore, there can be considerable variations between individuals of the same species especially in the highly heterogeneous post-fire intermediate regrowth condition – this leads to considerable spatial heterogeneity as well, at the hillslope scale. This adds to the intra sub-canopy variations discussed in the DZI framework.

The effects of plant roots in general, and how they may vary with genus and species to influence post-fire soils, hydrology and landscape development has not been sufficiently addressed thus far in biogeomorphology. In this study, the protective effects of roots as barriers for litter and sediment on steep post-fire terrain were treated mostly implicitly and simplistically, albeit observed in the field. Notably, Burylo et al. (2012) conducted flume experiments with specimens of *Robinia pseudo acacia*, *Achnatherum calamagrostis* and *Pinus nigra austriaca* and found, somewhat counter-intuitively but illuminatively, that small, fine and flexible roots played more important roles in mitigating overland flow erosion effects than the stiff, larger roots. We presently have minimal scientific understanding of these relationships in the post-fire erosion context, particularly their application to regenerating vegetation and their associated root networks. The geomorphic (for example in creating pit-mound topographies) and pedological impacts of tree throw have also been poorly studied (Gabet et al., 2003; Hancock et al., 2012; Osterkamp et al., 2012; Phillips and Marion, 2004; Schaetzl and Follmer, 1990) and more intensive examination of these dynamics to post-fire contexts are needed (Gonzalez-Bonorino and Osterkamp, 2004). It should be highlighted though that there was minimal evidence of tree throw observed at the study site.

While the study area was clearly in the intermediate post-fire stage (Figure 1-6 (d)), the specific recovery trajectory the region was on, was difficult to determine. It was possible

that the study hillslopes have been in the "prolonged recovery" period (Figure 1-5 (c)) where drought conditions had persisted after the 2007/8 fires. While significant rainfall events in the immediate post-fire period supplied much water to the area that could have supported vegetation recovery, the severe and widespread erosion of these burnt hillslopes would have stripped away much of the fertile topsoil, thinned the soil profiles and reduced water-holding capacities. The consequence of such drastic modification of the land surface would have been to delay vegetation recovery. Whether alternative floristics have resulted, as described in Figure 1-5 (d) remains to be discovered, possibly via an ecological investigation.

Fine sediment being adsorbed to and transported by fine litter (leaf and twig) was a feature that was observed in this study, but an aspect that seems to be quite poorly studied, and many questions exist. For example: what are the processes of sediment-litter adhesion, how much and what grades of sediment can be transported with leaves, and how are these leaves transported; are there differences between leaves of different Eucalyptus species and growth stages and indeed, leaves of plants from other genera, for example the Acacias?

Although southeast Australia is projected to continue to be highly fire-prone in the foreseeable future, there is still a distinct lack of detailed empirical studies across such a large, varied region where generalizations across different landscapes and vegetation formations are difficult. Nevertheless, field experiments and monitoring are expensive and difficult to sustain, especially in remote areas. Study locations thus must be carefully selected to be representative of the vegetation, soils, topography, geology and climate of the wider region in which they are situated. While the present study has provided insights into intermediate-stage post-fire erosion on thin sandy loams from Silurian-Devonian age sand, silt and mudstone geology, the range of vegetation structural formations and floristics, soils and climatic conditions is huge, even within southeast Australia and remain to be studied to good detail.

To enable a critical level of understanding of the key parameters, processes and dynamics relating to post-fire erosional processes, future fieldwork should also be conducted in other hydro-climatic and biogeomorphological contexts. This will build a richer body of knowledge around the mechanisms of post-fire hydrological and erosional dynamics that the present study has elucidated. For a start, a broad synthesis or meta-analysis of existing work done on different environments on the Australian continent could be done. Significant insights could be gleaned from comparing ecological and pedological work done in Western Australian jarrah forests (Bell, 2001; Bell and Koch, 1980) and coastal dune scrub (Shumack and Hesse, 2018) where cool Mediterranean and semi-arid conditions are experienced, with the post-fire processes on tropical savannah grasslands in Northern Australia (Cook, 1994; Edwards et al., 2013; Russell-Smith et al., 2006) which experience warm, seasonally-humid conditions where highly erosive monsoonal rainfall can have significant effects on soil erosion and fertility, and have their own distinct vegetation influences on rainfall interception and throughfall.

Laboratory-based studies will enable workers to evaluate specific factors on their impacts on post-fire erosion processes, and also uncover specific processes and dynamics in controlled environments. While the present study has cast some light on how leaf shape and size variations between juvenile and mature leaves of *E. polyanthemos* cause different on-leaf water dynamics to result in different released throughfall drop spectra, a larger study will be required in this aspect. Also, more work is needed to examine whether, how and why throughfall drop spectra may differ between juvenile and mature foliage for other *Eucalyptus* species comprising many of the dry sclerophyll forests in southeast Australia. Similar work is also needed on the commonly-distributed *Acacia* species that have seeds which germinate vigorously post-fire. Many Acacias have very contrasting leaf forms between juvenile and mature stages. For example in the juvenile leaf stage, *Acacia melanoxylon* (Blackwood) have

small non-sclerophyllous bi-pinnate leaves while mature stages see the same plant bearing large linear-oblong or lanceolate leaves (Costermans, 2009).

Computer modelling approaches are presently under-utilized in our area of research but present novel avenues for efficient and detailed examination of post-fire hydrology and erosion on hillslopes under differing conditions. In modelling and predicting post-fire vegetation recovery, recent sophisticated approaches such as those demonstrated by Paci et al. (2017) at the landscape scale are instructive, and light the way forward for the shift from monotonic-deterministic vegetation recovery models to flexible stochastic-relativistic models that could be used testing of concepts such as the DZIs as well as variable post-fire recovery pathways in the context of climate change forcings. An exemplary work of how sophisticated computer modelling can be integrated with field measurements to provide novel insights was seen in the way Moody and Ebel (2014) used the HYDRUS 1D numerical model as a 'virtual instrument' to calculate soil moisture, infiltration processes saturation and runoff generation in their study of post-fire erosion with rainfall profile as a key factor, on a hillslope in the Fourmile Canyon, west of Boulder, Colorado in the United States. The possible influences of diurnal-nocturnal rainfall occurrence and how they could influence canopy interception, throughfall and soil-moisture dynamics, may also be examined in this way. These types of work could also be applied effectively to the study of various typical post-fire sites in southeast Australia.

The roles of fine litter (leaves and twigs) in post-fire erosion under intermediate regeneration conditions deserves more detailed examination. While there has been much work on determining litter load accumulations in the context of fuel and fire risks (Chen et al., 2016) there remains much uncertainty about their transport via wet-fluvial and dry-aeolian processes on steep, forested terrain or their specific effects on attenuating or enhancing splash or overland flow in relation to their positions and states of decomposition. It

375

is certainly possible that their influences on hillslope hydrological and erosional processes exceed their mass in the total hillslope material flux. Also, minimal work has been done to examine the movement of fine sediments adhered to litter (in particular, leaf) surfaces. This can be termed 'litter-adhered sediment transport' (LAST). When collecting the litter accumulated in the SFs, I noticed some fine clay and silt particles that had adhered to the leaf, as well as twig surfaces. This were ostensibly facilitated by wet deposition of sediments by splash or overland flow on the litter surfaces, which then led to the adhesion of these fine particles facilitated by the residual water molecules as the excess water dried out. While the total sediment mass from LAST may not be particularly high, much soil fertility is associated with fine particles and these should be examined closely via collection of litter samples from field sites and evaluated for their physico-chemical compositions. Indeed, the fine particles associated with LAST could contribute to the development of under-canopy 'islands of fertility' (Kidron, 2015) on the anisotropic upslope-barrier accumulations of soil and litter on steep post-fire terrain (Figure 1-6).

More detailed examinations of erosional processes are needed. Rainfall pulses, as short-lived high-intensity bursts have the potential to set into motion "wave-trains" (Horton, 1945) that give sharp rises in erosive forces to dislodge and transport sediment as well as litter on hillslopes. These are especially likely in the skeletal soils in many parts of the study area. However, empirical verification of their occurrence and dynamics is necessary. Indeed, recent work by Wu et al. (2018) has revealed the importance and complexity of 'pulsed runoff-erosion' events sediment yields from the Zhifanggou Watershed of the highly-erodible Loess Plateau in China. In Chapter Seven, I suggested "winnowing" (alternatively with "wave-trains") as a possible process in addition to direct fluvial erosion, entrainment and transport by flow, and splash erosion, to explain the transport of coarse sediments such as gravels on steep terrain with skeletal, erodible sandy loam soils. However, this requires some

376

empirical verification that can be best achieved through experimentation with the target soils in a flume or erosion tray, a feasible project in the near future. The experimental work on sediment sorting by raindrop impact in the presence of shallow overland flow under non-equilibrium conditions by Hairsine et al. (1999) is insightful, and can be further developed. In-field detailed observations, perhaps aided by high-speed photography or video capture can be considered, especially where such technology together with remote or sensor-based operation is increasingly affordable and available. The video-based disdrometer presented by Chen et al. (2015) is a useful example of possible new techniques for field-based data capture and analyses. The dynamics of aeolian processes in post-fire conditions and the controlling parameters in different vegetation and topographical considerations also deserve detailed study, and the use of Structure-from-Motion (SfM) photogrammetry techniques in conjunction with numerical simulation modelling by Liu et al. (2018) to investigate aeolian erosion processes is instructive.

It is also important to consider complexities incorporated by the DZI model. For example: is the soil surface in the under-canopy zone always protected by the foliage and twigs/branches above it? This needs to be reconsidered in the light of the increased potential erosivity of throughfall drops. Furthermore, the roles of biological and environmental chemistry in mediating vegetation and soil regeneration processes and rates that ultimately control the physical outcomes of post-fire hydrology and erosion have scarcely been explored. Although there is presently some knowledge of the distinct chemical composition of throughfall and stemflow from *Eucalyptus spp.* vis-à-vis other plant genera (Crockford et al., 1996; Laclau et al., 2003; Yang et al., 2011), and can result in quite distinct downstream effects on aquatic chemistry (Zhu et al., 2018). It is widely known that many *Eucalyptus* species exude allelopathic compounds that suppress ground-level plant regrowth (Becerra et al., 2017; Kirkpatrick, 1977; May and Ash, 1990; Ruwanza et al., 2015). However, little is

known about the consequent influences on undercanopy micrometeorology, hydrology and erosion.

The impacts of allelopathic compounds from *Eucalyptus* in suppressing ground cover regrowth, maintaining soil bareness and thus enhancing under-canopy susceptibility to splash and overland flow erosion, need further investigation. Indeed, overland flow is generated quickly on steep terrain and thin soils. This would enable allelopathic chemicals to be quickly distributed downslope to the inter-spaces, enhancing and prolonging their "bareness" by suppressing regrowth in those areas. Beneath the Eucalypt canopy, while leaves and twigs may physically protect the mineral soil surface from erosive forces, allelopathic compounds would be released in a controlled manner from the slowly-decomposing sclerophyllous leaves and continue to suppress areal colonization by ground-level plant species for long durations through and beyond the intermediate post-fire recovery period.

Similarly, another biological factor that has seen insufficient consideration in the post-fire context is the role of biological soil crusts (BSCs) in influencing (increasing or decreasing) infiltration (and consequently erosion) rates, nitrogen fixation and supply to regenerating plants and their possible microclimatic effects (Eldridge and Greene, 1994), both in patch and inter-patch areas. BSCs have been found to play important roles in the ecohydrology of soils in the arid zone (Dunkerley, 2011; Dunkerley, 2012; George et al., 2003) and have been found to provide augmented resistance to splash erosion on the extremely erodible soils of the Loess Plateau in China (Zhao et al., 2014b). Hence, the survival, recovery, development and spatial distribution of BSCs as well as their specific ecohydrological influences (Pueyo et al., 2013) in post-fire conditions, deserve much research attention.

We also need to seriously consider the position of post-fire erosion science in the much broader backdrop of rising atmospheric carbon dioxide concentrations (Ekwurzel et al.,

2017; Jackson et al., 2017) and the spectrum of impacts and interactions with global and regional climates (Millar et al., 2017), vegetation (Tietjen et al., 2017) and soils (Bond-Lamberty et al., 2018), as well as increasing concentrations of non-CO_2 greenhouse gases, primarily methane and nitrous oxide (Fellmann et al., 2018; Tian et al., 2015). Analysing the interactions between global vegetation cover and climate change, Forzieri et al. (2017) showed how 'vegetation greening', detected through higher Leaf Area Index (LAI), has occurred in boreal and arid regions. These were attributed to carbon dioxide fertilisation (Donohue et al., 2013; Zhu et al., 2016) as well as anthropogenically-enhanced nitrogen supply and deposition to ecosystems. The outcomes of these processes in the boreal regions have been warming trends due to reduced surface albedo; in the arid regions this has led to evapotranspiration-driven cooling (Forzieri et al., 2017). In sub-Saharan Africa, many of these shifts have been manifested as woody-plant encroachment (WPE) at the continental scale (Venter et al., 2018). For the arid and semi-arid regions of Australia, moderate greening rates were related to a cooling trend, and agree with earlier work by Donohue et al. (2013). In terms of the dry eucalypt forests in the temperate climates of southeast Australia, it is possible that the 'rapid greening' and concomitant warming of these ecosystems are already in process. The LAI-surface biophysics interactions can be amplified 'up to five times under extreme warm-dry and cold-wet years' (Forzieri et al., 2017), climatic oscillations that are typical of the fire-prone southeast Australian region. Hence, it is likely that consecutive 'greening' years would lead to extended and elaborated plant canopy (and possibly root) architecture and higher juvenile foliage density. These would thus see increased rainfall modulation effects, as well as interception rates by plant canopies while simultaneously increasing litter accumulation that would, in the ensuing dryer years, enhance fire risks as well as lead to altered throughfall and erosion processes with sparser plant canopies. In this context, the specific outcomes in terms of plant architecture, foliage types and spatial

colonization, as well as root architecture and extent are basically unknown. Furthermore, there is no simple positive response of plant growth ('greening') to carbon dioxide fertilisation due to the variable physiological and biochemical characteristics and adaptations to the altered abiotic and biotic conditions (Cramer et al., 2001; Zhu et al., 2017) and the meta-analysis by Wang et al. (2012) emphasizes the complexity of responses. Indeed, Obermeier et al. (2016) demonstrated how the carbon fertilisation effect (CFE) for temperate C3 grasslands greatly diminished or disappeared under abnormal (wetter, drier and/or hotter) environmental conditions. Furthermore, Korner (2006) cautioned against unrealistic overestimates of CFE based on controlled nutrient "unlimited" (e.g. glasshouse pot trials) experiments, when actual plant biomass accumulation depended on natural nutrient cycling processes and their bioavailability that would in reality be quite restricted.

Therefore, it is very difficult to accurately project how rainfall-canopy interactions and hillslope erosion processes will operate in association with climate change. This also means that 'black box', or at most 'grey box' types studies typically at the catchment scale will not be suitable for monitoring the intricate and dynamic interactions between vegetation, rainfall and erosion processes in post-fire conditions under change climatic conditions. The present study may also be construed as a possible approach for simultaneously studying, in detail, rainfall event attributes, vegetation characteristics, in particular leaf forms, and their spatial dominance as patches/inter-patches to better understand hillslope erosion processes. Indeed, the findings from the present study could serve as useful baselines several decades in the future when shifts in vegetation, climate and soil conditions would then be quite apparent and well-studied.

8.6. Concluding remarks

There is mounting scientific evidence that the ongoing shifts in global and regional climates will result in more frequent, severe and extensive megafires (Clarke et al., 2011; Kinoshita et al., 2016; Krause et al., 2014; Stevens-Rumann et al., 2017; Williams and Bowman, 2012). While much public and scientific foci will naturally tend be on the hazards to, and losses of, lives, property, infrastructure and environmental assets and services resulting from the fires themselves, the post-fire hydrological and sedimentation processes, hazards and impacts are equally pertinent (Diakakis et al., 2017). Therefore, it is essential that research in post-fire erosion science continues to be active.

Workers in post-fire erosion need to address a comprehensive set of environmental variables, rather than individual factors such as slope steepness, rainfall depth or burn severity, for accurate prediction of post-fire sediment yields and the associated hazards (Morris et al., 2014). This requires increased investments of manpower as well as equipment. Indeed, more cross-disciplinary work in this complex area of research is essential (Doerr and Cerdã, 2005).

From the geomorphological viewpoint, although the occurrences and impacts of wildfires and post-fire sedimentation are intermittent, episodic and brief over geological timescales, their significance in long-term denudation rates, landform development and landscape evolution cannot be understated (Orem and Pelletier, 2016; Shakesby et al., 2016). Indeed, over decadal and centurial timescales, wildfires and post-fire erosion may be perceived as catastrophic events, but viewed as uniformly impacting landscapes over millennial and longer geological timescales (Allen, 2005). There is also a need to discard commonly-held notions of uniform erosion of land surfaces, as well as implicitly assumed unlimited supplies of sediment. This is particularly important in steep, thinly soil-mantled environments where soil thickness can be quite variable, albeit thin; slugs of sediment

moving over bare, rocky surfaces need to also be considered in these contexts where the rates of soil removal exceed those for soil formation (Montgomery, 2007; Phillips, 2017; Phillips and Marion, 2004) and indeed, supply-limited soil erosion rates are highly likely in many post-fire contexts.

This research has provided some insights into the complex ways in which post-fire erosion operate under intermediate post-fire conditions, a stage that has so far lacked scientific attention (Ebel et al., 2018). This has been achieved through a combination of empirical study in the field and laboratory, together with some conceptual developments particularly relevant to the domain of post-fire erosion science as well more broadly to the fields of biogeomorphology, ecohydrology and geomorphology. Much more work remains to be done in both empirical and theoretical aspects for this area of study, and I hope to be able to contribute more in the future.

REFERENCES

ABC News, 2010. Storm, floods hit near Licola. Accessed 15 Nov 2013 from http://www.abc.net.au/news/stories/2010/02/11/2816360.htm?site=news.

Abrahams, A.D., Parsons, A.J., Wainwright, J., 1995. Effects of vegetation change on interrill runoff and erosion, Walnut Gulch, southern Arizona. Geomorphology, 13(1-4): 37-48. DOI:10.1016/0169-555x(95)00027-3

Agricultural Research Service, 2013. RIST - Rainfall Intensity Summarization Tool. United States Department of Agriculture.

Albrecht, R.I., Goodman, S.J., Buechler, D.E., Blakeslee, R.J., Christian, H.J., 2016. Where Are the Lightning Hotspots on Earth? Bulletin of the American Meteorological Society, 97(11): 2051-2068. DOI:10.1175/BAMS-D-14-00193.1

Aldrick, J.M. et al., 1984. A study of the land in the catchment of the Gippsland Lakes. Vol. 1, Report No. TC-17. Accessed 10 Jun 2016 from http://vro.agriculture.vic.gov.au/dpi/vro/egregn.nsf/pages/eg_landform_Land_systems_gipps_lakes_docs/$FILE/gippsland_lakes_vol1.pdf.

Allen, P., 2005. Striking a chord. Nature, 434: 961. DOI:10.1038/434961a

Allen, R.G., Pereira, L.S., Raes, D., Smith, M., 1998. Crop evapotranspiration - Guidelines for computing crop water requirements - FAO Irrigation and Drainage Paper 56.

American Meteorological Society, 2012. Glossary of meteorology - "Raindrop". Accessed 6 Jun 2016 from http://glossary.ametsoc.org/wiki/Raindrop.

Amundson, R., Heimsath, A., Owen, J., Yoo, K., Dietrich, W.E., 2015. Hillslope soils and vegetation. Geomorphology, 234 (Supplement C): 122-132. DOI:10.1016/j.geomorph.2014.12.031

An, J., Zheng, F., Lu, J., Li, G., 2012. Investigating the role of raindrop impact on hydrodynamic mechanism of soil erosion under simulated rainfall conditions. Soil Science, 177(8): 517-526. DOI:10.1097/SS.0b013e3182639de1

Anderson, M.C., 1981. The geometry of leaf distribution in some south-eastern Australian forests. Agricultural Meteorology, 25: 195-206. DOI:10.1016/0002-1571(81)90072-8

Anderson, M.G., McDonnell, J.J., Thomson, G., Wiley, I., 2005. Encyclopedia of hydrological sciences. Accessed 7 Jun 2017 from http://galenet.galegroup.com/servlet/eBooks?ste=22&docNum=CX2589699999&q=columbiau. John Wiley & Sons, Hoboken, N.J.

Angulo-Martínez, M., Barros, A.P., 2015. Measurement uncertainty in rainfall kinetic energy and intensity relationships for soil erosion studies: An evaluation using PARSIVEL disdrometers in the Southern Appalachian Mountains. Geomorphology, 228: 28-40. DOI:10.1016/j.geomorph.2014.07.036

Armstrong, C.L., Mitchell, J.K., 1988. Plant canopy characteristics and processes which affect transformation of rainfall properties. Transactions of the American Society of Agricultural Engineers (ASAE), 31(5): 1400-1409.

Arno, S.F., 2000. Chapter Five: Fire in Western Forest Ecosystems. In: Brown, J.K., Smith, J.K. (Eds.), Wildland Fire in Ecosystems: Effects of Fire on Flora, pp. 257.

Asadi, H., Ghadiri, H., Rose, C.W., Yu, B., Hussein, J., 2007. An investigation of flow-driven soil erosion processes at low streampowers. Journal of Hydrology, 342(1-2): 134-142. DOI:10.1016/j.jhydrol.2007.05.019

Ashton, D., Chappill, J., 1989. Secondary succession in post-fire scrub dominated by Acacia verticillata (L'hérit) Willd at Wilsons Promontory, Victoria. Australian Journal of Botany, 37(1): 1-18. DOI:10.1071/BT9890001

Ashton, D.H., Chinner, J.H., 1999. Problems of regeneration of the mature Eucalyptus regnans F. Muell, (The Big Ash) forest, in the absence of fire at Wallaby Creek, Victoria, Australia. Australian Forestry, 62(3): 265-280. DOI:10.1080/00049158.1999.10674791

Aston, A.R., 1979. Rainfall interception by eight small trees. Journal of Hydrology, 42: 383-396.

Attiwill, P., Binkley, D., 2013. Exploring the mega-fire reality: A 'Forest Ecology and Management' conference. Forest Ecology and Management, 294: 1-3. DOI:http://dx.doi.org/10.1016/j.foreco.2012.12.025

Attiwill, P.M. et al., 2014. Timber harvesting does not increase fire risk and severity in wet eucalypt forests of southern Australia. Conservation Letters, 7(4): 341-354. DOI:10.1111/conl.12062

Auld, T.D., O'Connell, M.A., 1991. Predicting patterns of post-fire germination in 35 eastern Australian Fabaceae. Australian Journal of Ecology, 16(1): 53-70. DOI:10.1111/j.1442-9993.1991.tb01481.x

Australian Associated Press, 2007. Flood wrecks homes in fire-ravaged township. The Age Company Ltd., Melbourne, Australia. Accessed 10 Jan 2017 from http://www.theage.com.au/news/national/flood-wrecks-homes-in-fireravaged-township/2007/02/24/1171734062395.html.

Barros, A.P., Tao, J., Nogueira, M., Lowman, L., 2013. On the space-time organization of precipitation and hydrologic response in mountainous regions - examining opportunities for improving the predictability of post-wildfire floods and debris flows. In: Moody, J.A., Martin, D.A. (Eds.), AGU Chapman conference on synthesizing empirical results to improve predictions of post-wildfire runoff and erosion responses. U.S. Geological Survey, National Research Program, YMCA Conference Center, Estes Park, Colorado, USA.

Becerra, P. et al., 2017. Inhibitory effects of Eucalyptus globulus on understorey plant growth and species richness are greater in non-native regions. Global Ecology and Biogeography, 27(1): 68-76. DOI:10.1111/geb.12676

Bell, D.T., 2001. Ecological response syndromes in the flora of southwestern Western Australia: Fire resprouters versus reseeders. The Botanical Review, 67(4): 417-440. DOI:10.1007/bf02857891

Bell, D.T., Koch, J.M., 1980. Post-fire succession in the northern jarrah forest of Western Australia. Australian Journal of Ecology, 5(1): 9-14. DOI:10.1111/j.1442-9993.1980.tb01226.x

Bell, D.T., Williams, J.E., 1997. Eucalypt ecophysiology. Eucalypt ecology: individuals to ecosystems. Cambridge University Press, Cambridge: 168-196.

Benavides-Solorio, J., MacDonald, L.H., 2001. Post-fire runoff and erosion from simulated rainfall on small plots, Colorado Front Range. Hydrological Processes, 15(15): 2931-2952. DOI:10.1002/hyp.383

Benavides-Solorio, J.D., MacDonald, L.H., 2005. Measurement and prediction of post-fire erosion at the hillslope scale, Colorado Front Range. International Journal of Wildland Fire, 14(4): 457-474. DOI:10.1071/WF05042

Berg, N.H., Azuma, D.L., 2010. Bare soil and rill formation following wildfires, fuel reduction treatments, and pine plantations in the southern Sierra Nevada, California, USA. International Journal of Wildland Fire, 19(4): 478-489. DOI:10.1071/WF07169

Bergström, S., Graham, L.P., 1998. On the scale problem in hydrological modelling. Journal of Hydrology, 211(1-4): 253-265. DOI:10.1016/S0022-1694(98)00248-0

Best, A.C., 1950. The size distribution of raindrops. Quarterly Journal of the Royal Meteorological Society, 76(327): 16-36. DOI:10.1002/qj.49707632704

Birch, W.D., Ferguson, J.A., Slots, M., 2003. Geology of Victoria (3rd ed.). Special publication (Geological Society of Australia) 23. Melbourne : Geological Society of Australia, Victoria Division, 2003.

Bishop, P., 1988. The eastern highlands of Australia: the evolution of an intraplate highland belt. Progress in Physical Geography, 12(2): 159-182. DOI:10.1177/030913338801200203

Blom, A., Viparelli, E., Chavarrías, V., 2016. The graded alluvial river: profile concavity and downstream fining. Geophysical Research Letters, 43(12): 6285-6293. DOI:10.1002/2016GL068898

Blöschl, G., Sivapalan, M., 1995. Scale issues in hydrological modelling: A review. Hydrological Processes, 9(3-4): 251-290.

Boer, M., Sadler, R., Bradstock, R., Gill, A., Grierson, P., 2008. Spatial scale invariance of southern Australian forest fires mirrors the scaling behaviour of fire-driving weather events. Landscape Ecology, 23(8): 899-913. DOI:10.1007/s10980-008-9260-5

Bohlin, I., Olsson, H., Bohlin, J., Granström, A., 2017. Quantifying post-fire fallen trees using multi-temporal lidar. International Journal of Applied Earth Observation and Geoinformation, 63(Supplement C): 186-195. DOI:10.1016/j.jag.2017.08.004

Bond-Lamberty, B., Bailey, V.L., Chen, M., Gough, C.M., Vargas, R., 2018. Globally rising soil heterotrophic respiration over recent decades. Nature, 560(7716): 80-83. DOI:10.1038/s41586-018-0358-x

Bouten, W., Heimovaara, T.J., Tiktak, A., 1992. Spatial patterns of throughfall and soil water dynamics in a Douglas fir stand. Water Resources Research, 28(12): 3227-3233. DOI:10.1029/92WR01764

Bowman, D.M.J.S. et al., 2011. The human dimension of fire regimes on Earth. Journal of Biogeography, 38(12): 2223-2236. DOI:10.1111/j.1365-2699.2011.02595.x

Bowman, D.M.J.S., Boggs, G.S., 2006. Fire ecology. Progress in Physical Geography, 30(2): 245-257. DOI:10.1191/0309133306pp482pr

Bowman, D.M.J.S. et al., 2013. Forest fire management, climate change, and the risk of catastrophic carbon losses. Frontiers in Ecology and the Environment, 11(2): 66-67. DOI:10.1890/13.WB.005

Bracken, L.J., Croke, J., 2007. The concept of hydrological connectivity and its contribution to understanding runoff-dominated geomorphic systems. Hydrological Processes, 21(13): 1749-1763. DOI:10.1002/hyp.6313

Bracken, L.J., Turnbull, L., Wainwright, J., Bogaart, P., 2015. Sediment connectivity: a framework for understanding sediment transfer at multiple scales. Earth Surface Processes and Landforms, 40(2): 177-188. DOI:10.1002/esp.3635

Bradshaw, C.J.A., 2012. Little left to lose: deforestation and forest degradation in Australia since European colonization. Journal of Plant Ecology, 5(1): 109-120. DOI:10.1093/jpe/rtr038

Bradstock, R., Hammill, K., Collins, L., Price, O., 2010. Effects of weather, fuel and terrain on fire severity in topographically diverse landscapes of south-eastern Australia. Landscape Ecology, 25(4): 607-619. DOI:10.1007/s10980-009-9443-8

Bradstock, R.A., 2008. Effects of large fires on biodiversity in south-eastern Australia: disaster or template for diversity? International Journal of Wildland Fire, 17(6): 809-822. DOI:10.1071/WF07153

Brandt, C.J., 1989. The size distribution of throughfall drops under vegetation canopies. CATENA, 16(4): 507-524. DOI:http://dx.doi.org/10.1016/0341-8162(89)90032-5

Brauman, K.A., Freyberg, D.L., Daily, G.C., 2010. Forest structure influences on rainfall partitioning and cloud interception: A comparison of native forest sites in Kona, Hawai'i. Agricultural and Forest Meteorology, 150(2): 265-275. DOI:10.1016/j.agrformet.2009.11.011

Braun, P., Molnar, T., Kleeberg, H.-B., 1997. The problem of scaling in grid-related hydrological process modelling. Hydrological Processes, 11(9): 1219-1230. DOI:10.1002/(SICI)1099-1085(199707)11:9<1219::AID-HYP553>3.0.CO;2-S

Brogan, D.J., Nelson, P.A., MacDonald, L.H., 2013. Erosion, deposition, and stream channel response after the 2012 High Park Fire. In: Moody, J.A., Martin, D.A. (Eds.), AGU Chapman Conference on Synthesizing Empirical Results to Improve Predictions of Post-wildfire Runoff and Erosion Responses. U.S. Geological Survey, National Research Program, YMCA Conference Center, Estes Park, Colorado, USA.

Brooker, M.I.H., Kleinig, D.A., 2006. Field guide to eucalypts. Bloomings Books Pty Ltd, Melbourne, Australia, 356 pp.

Brookhouse, M.T., Farquhar, G.D., Roderick, M.L., 2013. The impact of bushfires on water yield from south-east Australia's ash forests. Water Resources Research, 49(7): 4493-4505. DOI:10.1002/wrcr.20351

Brooks, M.L. et al., 2004. Effects of invasive alien plants on fire regimes. BioScience, 54(7): 677-688. DOI:10.1641/0006-3568(2004)054[0677:EOIAPO]2.0.CO;2

Brown, B.G., Katz, R.W., Murphy, A.H., 1985. Exploratory analysis of precipitation events with implications for stochastic modeling. Journal of Climate and Applied Meteorology, 24(1): 57-67. DOI:10.1175/1520-0450(1985)024<0057:eaopew>2.0.co;2

Brown, J.K., 2000. Introduction and Fire Regimes (Chapter 1). In: Brown, J.K., Smith, J.K. (Eds.), Wildland Fire in Ecosystems: Effects of Fire on Flora, pp. 257.

Brown, J.K., Smith, J.K., 2000. Wildland fire in ecosystems: effects of fire on flora, General Technical Report RMRS-GTR-42-Volume 2. United States Department of Agriculture, Forest Service General Technical Report RMRS-GTR-42-Volume 2, 257 pp. DOI:10.2737

Bryan, R.B., 2000. Soil erodibility and processes of water erosion on hillslope. Geomorphology, 32(3-4): 385-415.

Bryant, E., 1997. Climate process & change. Melbourne: Cambridge University Press, 209 pp.

Bureau of Meteorology, 2007a. About East Coast Lows. Commonwealth of Australia, Bureau of Meteorology. Accessed 31 Jan 2017 from http://www.bom.gov.au/nsw/sevwx/facts/ecl.shtml.

Bureau of Meteorology, 2007b. Australian Monthly Climate Summary: June 2007. Commonwealth of Australia. Accessed 1 Feb 2017 from http://www.bom.gov.au/climate/current/month/aus/archive/200706.summary.shtml, Melbourne, Victoria, Australia.

Bureau of Meteorology, 2007c. Climate Data Online - definition of rainfall statistics. Commonwealth of Australia, Bureau of Meteorology.

Bureau of Meteorology, 2007d. June 2007 East Coast Lows. Commonwealth of Australia, Bureau of Meteorology. Accessed 31 Jan 2017 from http://www.bom.gov.au/nsw/sevwx/facts/events/june-07-ecl/index.shtml.

Bureau of Meteorology, 2010. Australian climate extremes - fire. Commonwealth of Australia 2010, Bureau of Meteorology. Accessed 31 Jan 2017 from http://www.bom.gov.au/lam/climate/levelthree/c20thc/fire.htm.

Bureau of Meteorology, 2014. Intensity-Frequency-Duration 2013 Data release: Engineers Australia guidance. Commonwealth of Australia. Accessed 6 Jun 2015 from http://www.bom.gov.au/water/designRainfalls/ifd/transition-guidance.shtml.

Bureau of Meteorology, 2015. Recent rainfall, drought and southern Australia's long-term rainfall decline. Commonwealth of Australia. Accessed 1 Mar 2018 from http://www.bom.gov.au/climate/updates/articles/a010-southern-rainfall-decline.shtml.

Bureau of Meteorology, 2017a. Analysis Chart Archive. Commonwealth of Australia. Accessed 6 Feb 2017 from http://www.bom.gov.au/australia/charts/archive/.

Bureau of Meteorology, 2017b. Australian Climate Influences. Commonwealth of Australia. Accessed 20 Jan 2017 from http://www.bom.gov.au/climate/about/?bookmark=introduction.

Bureau of Meteorology, 2017c. Climate Data Online. Bureau of Meteorology, Commonwealth of Australia. Accessed 6 Jun 2017 from http://www.bom.gov.au/climate/data/.

Bureau of Meteorology, 2017d. How to interpret radar images. Commonwealth of Australia. Accessed 14 Dec 2017 from http://www.bom.gov.au/australia/radar/about/using_radar_images.shtml#rate.

Bureau of Meteorology, 2017e. Victorian Flood Class Levels south of Divide. Commonwealth of Australia. Accessed 13 Jan 2017 from http://www.bom.gov.au/vic/flood/floodclass_south.shtml.

Burgess, J.S., Rieger, W.A., Olive, L.J., 1981. Sediment yield change following logging and fire effects in dry sclerophyll forest in southern New South Wales. In: Davies, T.R.H., Pearce, A.J. (Eds.) (Ed.), Erosion and Sediment Transport in Pacific Rim Steeplands. International Association of Hydrological Sciences (IAHS), Christchurch, New Zealand, pp. 375–385.

Burylo, M., Rey, F., Mathys, N., Dutoit, T., 2012. Plant root traits affecting the resistance of soils to concentrated flow erosion. Earth Surface Processes and Landforms, 37(14): 1463-1470. DOI:10.1002/esp.3248

Bushfire and Natural Hazards CRC, 2017. Science-backed tools enhance water catchment management. Accessed 1 Sep 2017 from https://www.bnhcrc.com.au/news/2017/science-backed-tools-enhance-water-catchment-management.

Bushfire Cooperative Research Centre, 2006. Seasonal bushfire assessment 2006-2007, Fire Note Issue 5, September 2006. Accessed 3 Sep 2017 from http://www.bushfirecrc.com/sites/default/files/managed/resource/bcrcfirenoteseasonaloutlook220906.pdf.

Buytaert, W., Celleri, R., Willems, P., Bièvre, B.D., Wyseure, G., 2006. Spatial and temporal rainfall variability in mountainous areas: A case study from the south Ecuadorian Andes. Journal of Hydrology, 329(3): 413-421. DOI:10.1016/j.jhydrol.2006.02.031

CAL FIRE, 2017. California Statewide Fire Summary: Tuesday, October 10, 2017. Accessed 11 October 2017 at http://calfire.ca.gov/communications/communications_StatewideFireSummary. California Department of Forestry and Fire Protection, State of California, USA.

Calder, I.R., 2001. Canopy processes: implications for transpiration, interception and splash induced erosion, ultimately for forest management and water resources. Plant Ecology, 153(1): 203-214. DOI:10.1023/a:1017580311070

Calder, I.R., Hall, R.L., Prasanna, K.T., 1993. Hydrological impact of Eucalyptus plantation in India. Journal of Hydrology, 150(2-4): 635-648. DOI:10.1016/0022-1694(93)90129-w

Cammeraat, E.L.H., 2004. Scale dependent thresholds in hydrological and erosion response of a semi-arid catchment in southeast Spain. Agriculture, Ecosystems & Environment, 104(2): 317-332.

Campos, I., Vale, C., Abrantes, N., Keizer, J.J., Pereira, P., 2015. Effects of wildfire on mercury mobilisation in eucalypt and pine forests. Catena, 131: 149-159. DOI:10.1016/j.catena.2015.02.024

Carollo, F.G., Serio, M.A., Ferro, V., CerdÃ , A., 2018. Characterizing rainfall erosivity by kinetic power - Median volume diameter relationship. Catena, 165: 12-21. DOI:10.1016/j.catena.2018.01.024

Carr, D.J., Carr, S.G.M., Jahnke, R., 1982. The Eucalypt Lignotuber: a Position-dependent Organ. Annals of Botany, 50(4): 481-489. DOI:10.1093/oxfordjournals.aob.a086388

Catry, F.X., Moreira, F., Tujeira, R., Silva, J.S., 2013. Post-fire survival and regeneration of Eucalyptus globulus in forest plantations in Portugal. Forest Ecology and Management, 310(Supplement C): 194-203. DOI:10.1016/j.foreco.2013.08.036

Catto, J.L., Pfahl, S., 2013. The importance of fronts for extreme precipitation. Journal of Geophysical Research: Atmospheres, 118(19): 10,791-10,801. DOI:10.1002/jgrd.50852

Cawson, J.G., Nyman, P., Smith, H.G., Lane, P.N.J., Sheridan, G.J., 2016. How soil temperatures during prescribed burning affect soil water repellency, infiltration and erosion. Geoderma, 278: 12-22. DOI:10.1016/j.geoderma.2016.05.002

Cawson, J.G., Sheridan, G.J., Smith, H.G., Lane, P.N.J., 2012. Surface runoff and erosion after prescribed burning and the effect of different fire regimes in forests and shrublands: a review. International Journal of Wildland Fire, 21(7): 857-872. DOI:http://dx.doi.org/10.1071/WF11160

Cawson, J.G., Sheridan, G.J., Smith, H.G., Lane, P.N.J., 2013. Effects of fire severity and burn patchiness on hillslope-scale surface runoff, erosion and hydrologic connectivity in a prescribed burn. Forest Ecology and Management, 310: 219-233. DOI:10.1016/j.foreco.2013.08.016

Cerasoli, S., Caldeira, M., Pereira, J., Caudullo, G., de Rigo, D., 2016. Eucalyptus globulus and other eucalypts in Europe: distribution, habitat, usage and threats. In: Jesus San-Miguel-Ayanz, D.d.R., Giovanni Caudullo, Tracy Houston Durrant, Achille Mauri (Ed.), European Atlas of Forest Tree Species. Publication Office of the European Union, Luxembourg.

Cerdà, A., Doerr, S.H., 2005. Influence of vegetation recovery on soil hydrology and erodibility following fire: an 11-year investigation. International Journal of Wildland Fire, 14(4): 423-437. DOI:10.1071/WF05044

Cerdà, A., Jordàn, A., Martínez-Murillo, J.F., 2013. Long-Term Monitoring of Infiltration Rates During the Post-wildfire Period in Eastern Spain. In: Moody, J.A., Martin, D.A. (Eds.), AGU Chapman Conference on Synthesizing Empirical Results to Improve Predictions of Post-wildfire Runoff and Erosion Responses. U.S. Geological Survey, National Research Program, Estes Park, Colorado, USA.

Certini, G., 2005. Effects of fire on properties of forest soils: a review. Oecologia, 143(1): 1-10. DOI:10.1007/s00442-004-1788-8

Chafer, C.J., 2008. A comparison of fire severity measures: An Australian example and implications for predicting major areas of soil erosion. CATENA, 74(3): 235-245.

Chafer, C.J., Noonan, M., Macnaught, E., 2004. The post-fire measurement of fire severity and intensity in the Christmas 2001 Sydney wildfires. International Journal of Wildland Fire, 13(2): 227-240. DOI:10.1071/WF03041

Chatanantavet, P., Lajeunesse, E., Parker, G., Malverti, L., Meunier, P., 2010. Physically based model of downstream fining in bedrock streams with lateral input. Water Resources Research, 46(2). DOI:10.1029/2008WR007208

Chattaway, M., 1958. Bud development and lignotuber formation in eucalypts. Australian Journal of Botany, 6(2): 103-115. DOI:https://doi.org/10.1071/BT9580103

Chen, C., Weng, C., Hwang, C., Hsieh, C., Jong, T., 2015. A study of video-based droplet detection, 2015 IEEE International Instrumentation and Measurement Technology Conference (I2MTC) Proceedings, pp. 1014-1018. DOI:10.1109/I2MTC.2015.7151409

Chen, D., Chen, H.W., 2013. Using the Köppen classification to quantify climate variation and change: An example for 1901–2010. Environmental Development, 6: 69-79. DOI:http://dx.doi.org/10.1016/j.envdev.2013.03.007

Chen, Y., Zhu, X., Yebra, M., Harris, S., Tapper, N., 2016. Strata-based forest fuel classification for wild fire hazard assessment using terrestrial LiDAR. Journal of Applied Remote Sensing, 10: 16. DOI:10.1117/1.JRS.10.046025

Chen, Y., Zhu, X., Yebra, M., Harris, S., Tapper, N., 2017. Development of a predictive model for estimating forest surface fuel load in Australian eucalypt forests with LiDAR data. Environmental Modelling & Software, 97: 61-71. DOI:http://dx.doi.org/10.1016/j.envsoft.2017.07.007

Chessman, B., 1986. Impact of the 1983 wildfires on river water quality in East Gippsland, Victoria. Marine and Freshwater Research, 37(3): 399-420. DOI:http://dx.doi.org/10.1071/MF9860399

Chiew, F.H.S., McMahon, T.A., 2003. El Niño/Southern Oscillation and Australian rainfall and streamflow. Australasian Journal of Water Resources, 6(2): 115-129. DOI:10.1080/13241583.2003.11465216

Chiu, L.S., 2001. Diurnal cycle of oceanic precipitation from microwave radiometry. IGARSS 2001. Scanning the Present and Resolving the Future. Proceedings. IEEE 2001 International Geoscience and Remote Sensing Symposium (Cat. No.01CH37217), Geoscience and Remote Sensing Symposium, 2001. IGARSS \'01. IEEE 2001 International, IGARSS 2001. geoscience and remote sensing, 3: 1140.

Christophe, A., Moulia, B., Varlet-Grancher, C., 2003. A Quantitative Analysis of the Three-Dimensional Spatial Colonization by a Plant as Illustrated by White Clover (Trifolium repens L.). International Journal of Plant Sciences, 164(3): 359-370. DOI:10.1086/374194

Clarke, H. et al., 2016. An investigation of future fuel load and fire weather in Australia. Climatic Change, 139(3): 591-605. DOI:10.1007/s10584-016-1808-9

Clarke, H.G., Smith, P.L., Pitman, A.J., 2011. Regional signatures of future fire weather over eastern Australia from global climate models. International Journal of Wildland Fire, 20(4): 550-562. DOI:http://dx.doi.org/10.1071/WF10070

Clarke, P.J. et al., 2015. A synthesis of postfire recovery traits of woody plants in Australian ecosystems. The Science of the total environment, 534: 31-42. DOI:10.1016/j.scitotenv.2015.04.002

Collins, K.M., Price, O.F., Penman, T.D., 2015. Spatial patterns of wildfire ignitions in south-eastern Australia. International Journal of Wildland Fire, 24(8): 1098-1108. DOI:https://doi.org/10.1071/WF15054

Cook, G.D., 1994. The fate of nutrients during fires in a tropical savanna. Australian Journal of Ecology, 19(4): 359-365. DOI:10.1111/j.1442-9993.1994.tb00501.x

Costermans, L.F., 2009. Native trees and shrubs of south-east Australia. Rigby Publishers, Melbourne, 440 pp.

Cramer, W. et al., 2001. Global response of terrestrial ecosystem structure and function to CO2 and climate change: results from six dynamic global vegetation models. Global Change Biology, 7(4): 357-373. DOI:10.1046/j.1365-2486.2001.00383.x

Crockford, R., Richardson, D., Sageman, R., 1996. Chemistry of rainfall, throughfall and stemflow in a Eucalypt and a Pine plantation: 3. Stemflow and total inputs. Hydrological processes, 10: 25-42. DOI:10.1002/(SICI)1099-1085(199601)10:13.0.CO;2-W

Crockford, R.H., Richardson, D.P., 1990a. Partitioning of rainfall in a eucalypt forest and pine plantation in southeastern australia: I throughfall measurement in a eucalypt forest: Effect of method and species composition. Hydrological Processes, 4(2): 131-144. DOI:10.1002/hyp.3360040204

Crockford, R.H., Richardson, D.P., 1990b. Partitioning of rainfall in a eucalypt forest and pine plantation in southeastern australia: II stemflow and factors affecting stemflow in a dry sclerophyll eucalypt forest and a pinus radiata plantation. Hydrological Processes, 4(2): 145-155. DOI:10.1002/hyp.3360040205

Crockford, R.H., Richardson, D.P., 1990c. Partitioning of rainfall in a eucalypt forest and pine plantation in southeastern australia: III determination of the canopy storage capacity of a dry sclerophyll eucalypt forest. Hydrological Processes, 4(2): 157-167. DOI:10.1002/hyp.3360040206

Crockford, R.H., Richardson, D.P., 1990d. Partitioning of rainfall in a eucalypt forest and pine plantation in southeastern australia: IV the relationship of interception and canopy storage capacity, the interception of these forests, and the effect on interception of thinning the pine plantation. Hydrological Processes, 4(2): 169-188. DOI:10.1002/hyp.3360040207

Crockford, R.H., Richardson, D.P., 2000. Partitioning of rainfall into throughfall, stemflow and interception: effect of forest type, ground cover and climate. Hydrological Processes, 14(16-17): 2903-2920. DOI:10.1002/1099-1085(200011/12)14:16/17<2903::AID-HYP126>3.0.CO;2-6

Crosbie, R.S. et al., 2012. Changes in Köppen-Geiger climate types under a future climate for Australia: hydrological implications. Hydrology and Earth System Sciences, 16: 3341-3349. DOI:10.5194/hess-16-3341-2012

Cruz, M.G. et al., 2012. Anatomy of a catastrophic wildfire: The Black Saturday Kilmore East fire in Victoria, Australia. Forest Ecology and Management, 284: 269-285. DOI:http://dx.doi.org/10.1016/j.foreco.2012.02.035

CSIRO, 2010. Climate variability and change in south-eastern Australia: A synthesis of findings from Phase 1 of the South Eastern Australian Climate Initiative (SEACI).

CSIRO, 2011. ASRIS - Australian Soil Resource Information System. Commonwealth Scientific and Industrial Research Organisation. Accessed 10 Sep 2013 from http://www.asris.csiro.au.

CSIRO, 2012. Climate and water availability in south-eastern Australia: A synthesis of findings from Phase 2 of the South Eastern Australian Climate Initiative (SEACI), Commonwealth Scientific and Industrial Research Organisation (CSIRO Australia).

Dai, A., Lin, X., Hsu, K.-L., 2007. The frequency, intensity and diurnal cycle of precipitation in surface and satellite observations over low- and mid-latitudes. Climate Dynamics(7-8): 727. DOI:https://doi.org/10.1007/s00382-007-0260-y

Dawson, T.E., Pate, J.S., 1996. Seasonal water uptake and movement in root systems of Australian phraeatophytic plants of dimorphic root morphology: a stable isotope investigation. Oecologia, 107(1): 13-20. DOI:10.1007/BF00582230

de Boer, D.H., 1992. Hierarchies and spatial scale in process geomorphology: a review. Geomorphology, 4(5): 303-318. DOI:https://doi.org/10.1016/0169-555X(92)90026-K

de Santos Loureiro, N., de Azevedo Coutinho, M., 2001. A new procedure to estimate the RUSLE EI30 index, based on monthly rainfall data and applied to the Algarve region, Portugal. Journal of Hydrology, 250(1–4): 12-18. DOI:http://dx.doi.org/10.1016/S0022-1694(01)00387-0

de Vente, J., Poesen, J., Arabkhedri, M., Verstraeten, G., 2007. The sediment delivery problem revisited. Progress in Physical Geography, 31(2): 155-178. DOI:10.1177/0309133307076485

de Vente, J., Poesen, J., Govers, G., Boix-Fayos, C., 2009. The implications of data selection for regional erosion and sediment yield modelling. Earth Surface Processes and Landforms, 34: 1994-2007. DOI:10.1002/esp.1884

Dean, J.M., Smith, A.P., 1978. Behavioral and Morphological Adaptations of a Tropical Plant to High Rainfall. Biotropica, 10(2): 152-154. DOI:10.2307/2388018

DeBano, L.F., 1981. Water repellent soils: a state of art, Gen. Tech. Rpt. PSW-46. Berkeley, CA, 21 pp.

DeBano, L.F., 2000. The role of fire and soil heating on water repellency in wildland environments: a review. Journal of Hydrology, 231-232: 195-206.

DeBano, L.F., Neary, D.G., Ffolliott, P.F., 1998. Fire: its effect on soil and other ecosystem resources. John Wiley and Sons Inc., New York, USA, 333 pp.

DELWP, 2016. Water Measurement Information System. Department of Environment Land Water and Planning, Victoria.

Department of Environment Land Water and Planning, 2016. Biodiversity Interactive Map. The State of Victoria. Accessed 12 Jun 2017 from http://mapshare2.dse.vic.gov.au/MapShare2EXT/imf.jsp?site=bim., Victoria, Australia.

Department of Sustainability and Environment, 2009. Bushfire history - Major bushfires in Victoria. State of Victoria, Australia, East Melbourne, Victoria, Australia.

Department of Sustainability and Environment, Parks Victoria, 2010. 2007 Gippsland Flood/Storm Recovery Program Final Report. , Melbourne, Australia.

DEPI, 2013. Biodiversity Interactive Map - 3.2 (Extract). The State of Victoria, Department of Environment and Primary Industries.

Diakakis, M., Nikolopoulos, E.I., Mavroulis, S., Vassilakis, E., Korakaki, E., 2017. Observational evidence on the effects of mega-fires on the frequency of hydrogeomorphic hazards. The case of the Peloponnese fires of 2007 in Greece. Science of The Total Environment, 592: 262-276. DOI:https://doi.org/10.1016/j.scitotenv.2017.03.070

Diodato, N., Bellocchi, G., 2010. MedREM, a rainfall erosivity model for the Mediterranean region. Journal of Hydrology, 387(1–2): 119-127. DOI:10.1016/j.jhydrol.2010.04.003

Dirksen, R.J. et al., 2009. An aerosol boomerang: Rapid around-the-world transport of smoke from the December 2006 Australian forest fires observed from space. Journal of Geophysical Research: Atmospheres, 114(D21): 1-15. DOI:10.1029/2009JD012360

Doerr, S. et al., 2004. Heating effects on water repellency in Australian eucalypt forest soils and their value in estimating wildfire soil temperatures. International Journal of Wildland Fire, 13(2): 157-163. DOI:10.1071/WF03051

Doerr, S.H., Cerdã, A., 2005. Fire effects on soil system functioning: new insights and future challenges. International Journal of Wildland Fire, 14(4): 339-342. DOI:10.1071/WF05094

Doerr, S.H., Ritsema, C.J., Dekker, L.W., Scott, D.F., Carter, D., 2007. Water repellence of soils: new insights and emerging research needs. Hydrological Processes, 21(17): 2223-2228. DOI:10.1002/hyp.6762

Doerr, S.H. et al., 2006. Effects of differing wildfire severities on soil wettability and implications for hydrological response. Journal of Hydrology, 319(1-4): 295-311.

Doerr, S.H., Shakesby, R.A., Walsh, R.P.D., 1996. Soil hydrophobicity variations with depth and particle size fraction in burned and unburned Eucalyptus globulus and Pinus pinaster forest terrain in the Águeda Basin, Portugal. CATENA, 27(1): 25-47.

Doerr, S.H., Shakesby, R.A., Walsh, R.P.D., 2000. Soil water repellency: its causes, characteristics and hydro-geomorphological significance. Earth-Science Reviews, 51(1–4): 33-65. DOI:http://dx.doi.org/10.1016/S0012-8252(00)00011-8

Donohue, R.J., Roderick, M.L., McVicar, T.R., Farquhar, G.D., 2013. Impact of CO2 fertilization on maximum foliage cover across the globe's warm, arid environments. Geophysical Research Letters, 40(12): 3031-3035. DOI:10.1002/grl.50563

Dowdy, A.J., Mills, G.A., 2012a. Atmospheric and Fuel Moisture Characteristics Associated with Lightning-Attributed Fires. Journal of Applied Meteorology and Climatology, 51(11): 2025-2037. DOI:10.1175/JAMC-D-11-0219.1

Dowdy, A.J., Mills, G.A., 2012b. Characteristics of lightning-attributed wildland fires in south-east Australia. International Journal of Wildland Fire, 21(5): 521-524. DOI:https://doi.org/10.1071/WF10145

Dragovich, D., Morris, R., 2002. Fire intensity, slopewash and bio-transfer of sediment in eucalypt forest, Australia. Earth Surface Processes and Landforms, 27(12): 1309-1319. DOI:10.1002/esp.413

Dunin, F., Smith, C., Denmead, O., 2007. Hydrological change: Reaping prosperity and pain in Australia, 11. DOI:10.5194/hess-11-77-2007

Dunkerley, D., 2000. Hydrologic effects of dryland shrubs: defining the spatial extent of modified soil water uptake rates at an Australian desert site. Journal of Arid Environments, 45(2): 159-172. DOI:http://dx.doi.org/10.1006/jare.2000.0636

Dunkerley, D., 2008a. Identifying individual rain events from pluviograph records: a review with analysis of data from an Australian dryland site. Hydrological Processes, 22(26): 5024-5036. DOI:10.1002/hyp.7122

Dunkerley, D., 2008b. Rain event properties in nature and in rainfall simulation experiments: a comparative review with recommendations for increasingly systematic study and reporting. Hydrological Processes, 22(22): 4415-4435. DOI:10.1002/hyp.7045

Dunkerley, D., 2010a. A new method for determining the throughfall fraction and throughfall depth in vegetation canopies. Journal of Hydrology, 385(1-4): 65-75.

Dunkerley, D., 2011. Desert Soils. In: Thomas, D.S. (Ed.), Arid Zone Geomorphology. John Wiley & Sons, Ltd. DOI:10.1002/9780470710777.ch7

Dunkerley, D., 2012. Effects of rainfall intensity fluctuations on infiltration and runoff: rainfall simulation on dryland soils, Fowlers Gap, Australia. Hydrological Processes, 26(15): 2211-2224. DOI:10.1002/hyp.8317

Dunkerley, D., 2014a. Stemflow on the woody parts of plants: dependence on rainfall intensity and event profile from laboratory simulations. Hydrological Processes, 28(22): 5469-5482. DOI:10.1002/hyp.10050

Dunkerley, D., 2014b. Stemflow production and intrastorm rainfall intensity variation: an experimental analysis using laboratory rainfall simulation. Earth Surface Processes and Landforms, 39(13): 1741-1752. DOI:10.1002/esp.3555

Dunkerley, D., 2015a. Intra-event intermittency of rainfall: an analysis of the metrics of rain and no-rain periods. Hydrological Processes, 29(15): 3294-3305. DOI:10.1002/hyp.10454

Dunkerley, D., 2015b. Percolation through leaf litter: What happens during rainfall events of varying intensity? Journal of Hydrology, 525: 737-746. DOI:https://doi.org/10.1016/j.jhydrol.2015.04.039

Dunkerley, D., 2016. An approach to analysing plot scale infiltration and runoff responses to rainfall of fluctuating intensity. Hydrological Processes: 191–206. DOI:10.1002/hyp.10990

Dunkerley, D., 2018. How is overland flow produced under intermittent rain? An analysis using plot-scale rainfall simulation on dryland soils. Journal of Hydrology, 556: 119-130. DOI:https://doi.org/10.1016/j.jhydrol.2017.11.003

Dunkerley, D.L., 2008c. Intra-storm evaporation as a component of canopy interception loss in dryland shrubs: observations from Fowlers Gap, Australia. Hydrological Processes, 22(12): 1985-1995.

Dunkerley, D.L., 2010b. How do the rain rates of sub-event intervals such as the maximum 5- and 15-min rates (I5 or I30) relate to the properties of the enclosing rainfall event? Hydrological Processes, 24(17): 2425-2439. DOI:10.1002/hyp.7650

Eamus, D., Hatton, T., Cook, P., Colvin, C., 2006. Ecohydrology : Vegetation Function, Water and Resource Management. [electronic resource]. Melbourne : CSIRO PUBLISHING, 2006.

East Gippsland Catchment Management Authority, 2007. East Gippsland floods - flood recovery works, Floods Week 6_EG News 15 August 2007.

Ebel, B.A., Romero, O.C., Martin, D.A., 2018. Thresholds and relations for soil-hydraulic and soil-physical properties as a function of burn severity 4 years after the 2011 Las Conchas Fire, New Mexico, USA. Hydrological Processes, 32(14): 2263-2278. DOI:10.1002/hyp.13167

Edwards, A.C., Maier, S.W., Hutley, L.B., Williams, R.J., Russell-Smith, J., 2013. Spectral analysis of fire severity in north Australian tropical savannas. Remote Sensing of Environment, 136: 56-65. DOI:https://doi.org/10.1016/j.rse.2013.04.013

Ekwurzel, B. et al., 2017. The rise in global atmospheric CO2, surface temperature, and sea level from emissions traced to major carbon producers. Climatic Change, 144(4): 579-590. DOI:10.1007/s10584-017-1978-0

Eldridge, D., Greene, R., 1994. Microbiotic soil crusts - a review of their roles in soil and ecological processes in the rangelands of Australia. Soil Research, 32(3): 389-415. DOI:https://doi.org/10.1071/SR9940389

Endecotts, n.d. Woven Wire Sieves. Accessed 21 Dec 2017 from https://www.endecotts.com/products/sieves/woven-wire-sieves/product-specifications/.

Environment and Natural Resources Committee, 2008. Inquiry into the Impact of Public Land Management Practices on Bushfires in Victoria. In: Parliament of Victoria, A. (Ed.). Parliamentary Paper. Parliament of Victoria, Melbourne, VIC 3002.

Eshel, G., Levy, G.J., Mingelgrin, U., Singer, M.J., 2004. Critical Evaluation of the Use of Laser Diffraction for Particle-Size Distribution Analysis. Soil Science Society of America Journal, 68(3): 736-743.

Evans, J., 2013. Bushfire threatens Licola township in Victoria's east. The Herald Sun, News Corp.

Evans, J.P., Pitman, A.J., Cruz, F.T., 2010. Coupled atmospheric and land surface dynamics over southeast Australia: a review, analysis and identification of future research priorities. International Journal of Climatology. DOI:10.1002/joc.2206

Fairman, T.A., Nitschke, C.R., Bennett, L.T., 2015. Too much, too soon? A review of the effects of increasing wildfire frequency on tree mortality and regeneration in temperate eucalypt forests. International Journal of Wildland Fire: -. DOI:http://dx.doi.org/10.1071/WF15010

Falster, D.S., Westoby, M., 2003. Leaf size and angle vary widely across species: what consequences for light interception? New Phytologist, 158(3): 509-525. DOI:10.1046/j.1469-8137.2003.00765.x

Farres, P.J., 1987. The dynamics of rainsplash erosion and the role of soil aggregate stability. CATENA, 14(1-3): 119-130. DOI:10.1016/s0341-8162(87)80009-7

Feller, M.C., 1981. Water balances in Eucalyptus regnans, E. obliqua, and Pinus radiata forests in Victoria. Australian Forestry, 44(3): 153-161. DOI:10.1080/00049158.1981.10674308

Fellmann, T. et al., 2018. Major challenges of integrating agriculture into climate change mitigation policy frameworks. Mitigation and Adaptation Strategies for Global Change, 23(3): 451-468. DOI:10.1007/s11027-017-9743-2

Fernández-Raga, M. et al., 2010. The kinetic energy of rain measured with an optical disdrometer: An application to splash erosion. Atmospheric Research, 96(2-3): 225-240. DOI:10.1016/j.atmosres.2009.07.013

Ferreira, A.J.D., Coelho, C.O.A., Ritsema, C.J., Boulet, A.K., Keizer, J.J., 2008. Soil and water degradation processes in burned areas: Lessons learned from a nested approach. CATENA, 74(3): 273-285. DOI:10.1016/j.catena.2008.05.007

Findell, K.L., Gentine, P., Lintner, B.R., Kerr, C., 2011. Probability of afternoon precipitation in eastern United States and Mexico enhanced by high evaporation. Nature Geoscience, 4: 434. DOI:10.1038/ngeo1174

Flinn, D.W., Wareing, K., Wadsley, D., 2008a. The Victorian Great Divide Fires December 2006-February 2007 (Vol. 1). In: Department of Sustainability and Environment (Ed.). The State of Victoria Department of Sustainability and Enviroment, East Melbourne, pp. 137.

Flinn, D.W., Wareing, K., Wadsley, D., 2008b. The Victorian Great Divide Fires December 2006-February 2007 (Vol. 4). In: Department of Sustainability and Environment (Ed.). The State of Victoria Department of Sustainability and Enviroment, East Melbourne, pp. 137.

Florence, R.G., 2004. Ecology and Silviculture of Eucalypt Forests. CSIRO Publishing.

Foot, K., Morgan, R.P.C., 2005. The role of leaf inclination, leaf orientation and plant canopy architecture in soil particle detachment by raindrops. Earth Surface Processes and Landforms, 30(12): 1509-1520. DOI:10.1002/esp.1207

Forest Fire Victoria Inc., 2007. The consequent impact of bushfires on the June/July 2007 Gippsland flood.

Forzieri, G., Alkama, R., Miralles, D.G., Cescatti, A., 2017. Satellites reveal contrasting responses of regional climate to the widespread greening of Earth. Science, 356(6343): 1180.

Francos, M., Pereira, P., Alcañiz, M., Mataix-Solera, J., Úbeda, X., 2016. Impact of an intense rainfall event on soil properties following a wildfire in a Mediterranean environment (North-East Spain). Science of The Total Environment, 572: 1353-1362. DOI:http://dx.doi.org/10.1016/j.scitotenv.2016.01.145

Freund, M., Henley, B.J., Karoly, D.J., Allen, K.J., Baker, P.J., 2017. Multi-century cool- and warm-season rainfall reconstructions for Australia's major climatic regions. Clim. Past, 13(12): 1751-1770. DOI:10.5194/cp-13-1751-2017

Fromm, M. et al., 2010. The Untold Story of Pyrocumulonimbus. Bulletin of the American Meteorological Society, 91(9): 1193-1209. DOI:10.1175/2010BAMS3004.1

Fryirs, K.A., Brierley, G.J., Preston, N.J., Kasai, M., 2007. Buffers, barriers and blankets: The (dis)connectivity of catchment-scale sediment cascades. CATENA, 70(1): 49-67. DOI:10.1016/j.catena.2006.07.007

Fuquay, D.M., Taylor, A.R., Hawe, R.G., Schmid, C.W., 1972. Lightning discharges that caused forest fires. Journal of Geophysical Research, 77(12): 2156-2158. DOI:10.1029/JC077i012p02156

Gabet, E.J., 2003. Post-fire thin debris flows: sediment transport and numerical modelling. Earth Surface Processes and Landforms, 28(12): 1341-1348. DOI:10.1002/esp.590

Gabet, E.J., Dunne, T., 2003. A stochastic sediment delivery model for a steep Mediterranean landscape. Water Resources Research, 39(9). DOI:10.1029/2003WR002341

Gabet, E.J., Reichman, O.J., Seabloom, E.W., 2003. The effects of bioturbation on soil processes and sediment transport. Annual Review of Earth and Planetary Sciences, 31(1): 249-273. DOI:10.1146/annurev.earth.31.100901.141314

Gabet, E.J., Sternberg, P., 2008. The effects of vegetative ash on infiltration capacity, sediment transport, and the generation of progressively bulked debris flows. Geomorphology, 101(4): 666-673. DOI:http://dx.doi.org/10.1016/j.geomorph.2008.03.005

Gallucci, J., Tryhorn, L., Lynch, A., Parkyn, K., 2011. On the meteorological and hydrological mechanisms resulting in the 2003 post-fire flood event in Alpine Shire, Victoria. Australian Meteorological and Oceanographic Journal, 61(1): 31-41.

Gammage, B., 2011. The biggest estate on earth: how Aborigines made Australia.

Gao, B. et al., 2003. Investigating ponding depth and soil detachability for a mechanistic erosion model using a simple experiment. Journal of Hydrology, 277(1): 116-124. DOI:https://doi.org/10.1016/S0022-1694(03)00085-4

Gao, X., Giorgi, F., 2008. Increased aridity in the Mediterranean region under greenhouse gas forcing estimated from high resolution simulations with a regional climate model. Global and Planetary Change, 62(3): 195-209. DOI:http://dx.doi.org/10.1016/j.gloplacha.2008.02.002

García-Ortega, E., Trobajo, M., López, L., Sánchez, J., 2011. Synoptic patterns associated with wildfires caused by lightning in Castile and Leon, Spain. Natural Hazards and Earth System Sciences, 11(3): 851.

Gatebe, C.K., Varnai, T., Poudyal, R., Ichoku, C., King, M.D., 2012. Taking the pulse of pyrocumulus clouds. Atmospheric Environment, 52: 121-130. DOI:http://dx.doi.org/10.1016/j.atmosenv.2012.01.045

Geddes, N., Dunkerley, D., 1999. The influence of organic litter on the erosive effects of raindrops and of gravity drops released from desert shrubs. CATENA, 36(4): 303-313. DOI:10.1016/s0341-8162(99)00050-8

Geißler, C. et al., 2012a. Splash erosion potential under tree canopies in subtropical SE China. CATENA, 91(0): 85-93. DOI:10.1016/j.catena.2010.10.009

Geißler, C. et al., 2012b. Impact of tree saplings on the kinetic energy of rainfall—The importance of stand density, species identity and tree architecture in subtropical forests in China. Agricultural and Forest Meteorology, 156(0): 31-40. DOI:10.1016/j.agrformet.2011.12.005

George, D.B. et al., 2003. The effects of microbiotic soil crusts on soil water loss. Arid Land Research and Management, 17(2): 113-125. DOI:10.1080/15324980301588

George, G.I., Daniel, G.N., Paul, W.A., 2004. Effects of wildfire on soils and watershed processes. Journal of Forestry, 102(6): 16.

Geoscience Australia, 2015. Compute Sunrise, Sunset & Twilight Times. Accessed 5 Jul 2017 from http://www.ga.gov.au/geodesy/astro/sunrise.jsp.

Germer, S., Elsenbeer, H., Moraes, J.M., 2006. Throughfall and temporal trends of rainfall redistribution in an open tropical rainforest, south-western Amazonia (Rondônia, Brazil). Hydrol. Earth Syst. Sci., 10(3): 383-393. DOI:10.5194/hess-10-383-2006

Ghahramani, A., Ishikawa, Y., Gomi, T., Shiraki, K., Miyata, S., 2011. Effect of ground cover on splash and sheetwash erosion over a steep forested hillslope: A plot-scale study. CATENA, 85(1): 34-47. DOI:10.1016/j.catena.2010.11.005

Gill, A.M., Zylstra, P., 2005. Flammability of Australian forests. Australian Forestry, 68(2): 87-93. DOI:10.1080/00049158.2005.10674951

Gilroy, J., Tran, C., 2009. A new fuel load model for eucalypt forests in southeast Queensland. Proceedings of the Royal Society of Queensland, 115: 137.

Gippsland Emergency Recovery Committee, 2007. History - June 2007 floods set records, Gippsland's bushfire recovery program. Accessed 28 Jul 2016 from http://www.gippsrecover.cin/history.html#top.

Gippsland Times and Maffra Spectator, 2019. 11 Mar 2019 Large fires have joined. Accessed 16 Mar 2019 http://www.gippslandtimes.com.au/story/5947140/large-fires-have-joined/.

Gleason, K.E., Nolin, A.W., 2016. Charred forests accelerate snow albedo decay: parameterizing the post-fire radiative forcing on snow for three years following fire. Hydrological Processes, 30(21): 3855-3870. DOI:10.1002/hyp.10897

Gonzalez-Bonorino, G., Osterkamp, W.R., 2004. Applying RUSLE 2.0 on burned-forest lands: An appraisal. Journal of Soil and Water Conservation, 59(1): 36-42.

Gordon, C.E., Price, O.F., Tasker, E.M., Denham, A.J., 2017. Acacia shrubs respond positively to high severity wildfire: Implications for conservation and fuel hazard management. Science of The Total Environment, 575: 858-868. DOI:https://doi.org/10.1016/j.scitotenv.2016.09.129

Goulburn Broken CMA, 2009. Post 2000 Floods. State Government of Victoria.

Gould, J.S. et al., 2008. Project Vesta : Fire in Dry Eucalypt Forest - Fuel Structure, Fuel Dynamics and Fire Behaviour. CSIRO Publishing, Victoria, Australia.

Gray, D.R., Foster, D.A., 2004. Tectonic evolution of the Lachlan Orogen, southeast Australia: Historical review, data synthesis and modern perspectives. Australian Journal of Earth Sciences, 51(6): 773-817. DOI:10.1111/j.1400-0952.2004.01092.x

Grissino Mayer, H.D., Swetnam, T.W., 2000. Century scale climate forcing of fire regimes in the American Southwest. The Holocene, 10(2): 213-220. DOI:10.1191/095968300668451235

Guiot, J., Cramer, W., 2016. Climate change: The 2015 Paris Agreement thresholds and Mediterranean basin ecosystems. Science, 354(6311): 465. DOI:10.1126/science.aah5015

Gupta, V., Reinke, K., Jones, S., Wallace, L., Holden, L., 2015. Assessing metrics for estimating fire induced change in the forest understorey structure using terrestrial laser scanning. Remote Sensing, 7(6): 8180. DOI:10.3390/rs70608180

Haile, A.T., Rientjes, T., Habib, E., Jetten, V., 2010. Rain event properties and dimensionless rain event hyetographs at the source of the Blue Nile River. Hydrol. Earth Syst. Sci. Discuss., 7(4): 5805-5849. DOI:10.5194/hessd-7-5805-2010

Hairsine, P.B. et al., 1999. Unsteady soil erosion due to rainfall impact: a model of sediment sorting on the hillslope. Journal of Hydrology, 220(3): 115-128. DOI:https://doi.org/10.1016/S0022-1694(99)00068-2

Hall, B.L., 2007. Precipitation associated with lightning-ignited wildfires in Arizona and New Mexico. International Journal of Wildland Fire, 16(2): 242-254. DOI:https://doi.org/10.1071/WF06075

Hall, M.J., 1970. Use of the Stain Method in Determining the Drop-Size Distributions of Coarse Liquid Sprays. Transactions of the American Society of Agricultural Engineers (ASAE), 13(1): 33-37.

Hall, R.L., Calder, I.R., 1993. Drop Size Modification by Forest Canopies: Measurements Using a Disdrometer. J. Geophys. Res., 98(D10): 18465-18470. DOI:10.1029/93jd01498

Hammill, K.A., Bradstock, R.A., 2006. Remote sensing of fire severity in the Blue Mountains: influence of vegetation type and inferring fire intensity. International Journal of Wildland Fire, 15(2): 213-226. DOI:10.1071/WF05051

Hancock, G.R., Evans, K.G., McDonnell, J., Hopp, L., 2012. Ecohydrological controls on soil erosion and landscape evolution. Ecohydrology, 5(4): 478-490. DOI:10.1002/eco.241

Hantson, S. et al., 2017. Rare, Intense, Big fires dominate the global tropics under drier conditions. Scientific Reports, 7: 14374. DOI:10.1038/s41598-017-14654-9

Hardwick, S.R. et al., 2015. The relationship between leaf area index and microclimate in tropical forest and oil palm plantation: Forest disturbance drives changes in microclimate. Agricultural and Forest Meteorology, 201: 187-195. DOI:https://doi.org/10.1016/j.agrformet.2014.11.010

Heath, J.T., Chafer, C.J., Bishop, T.F.A., Van Ogtrop, F.F., 2016. Post-fire recovery of Eucalypt-dominated vegetation communities in the Sydney Basin, Australia. The Journal of the Association for Fire Ecology, 12(3): 53-79. DOI:10.4996/fireecology.1203053

Heim, R.R., 2002. A Review of Twentieth-Century Drought Indices Used in the United States. Bulletin of the American Meteorological Society, 83(8): 1149-1165. DOI:10.1175/1520-0477(2002)083<1149:AROTDI>2.3.CO;2

Hendon, H.H., Thompson, D.W.J., Wheeler, M.C., 2007. Australian rainfall and surface temperature variations associated with the Southern Hemisphere Annular Mode. Journal of Climate, 20(11): 2452-2467. DOI:10.1175/JCLI4134.1

Herwitz, S.R., 1987. Raindrop impact and water flow on the vegetative surfaces of trees and the effects on stemflow and throughfall generation. Earth Surface Processes and Landforms, 12(4): 425-432. DOI:10.1002/esp.3290120408

Hillel, D., 2004. Introduction to environmental soil physics. [electronic resource]. Amsterdam ; Boston : Elsevier Academic Press, c2004.

Holder, C.D., 2016. Plant–Water Interactions, International Encyclopedia of Geography: People, the Earth, Environment and Technology. John Wiley & Sons, Ltd. DOI:10.1002/9781118786352.wbieg0120

Hopp, L., McDonnell, J.J., 2009. Connectivity at the hillslope scale: Identifying interactions between storm size, bedrock permeability, slope angle and soil depth. Journal of Hydrology, 376(3-4): 378-391. DOI:10.1016/j.jhydrol.2009.07.047

Hopp, L., McDonnell, J.J., 2011. Examining the role of throughfall patterns on subsurface stormflow generation. Journal of Hydrology, 409: 460-471. DOI:10.1016/j.jhydrol.2011.08.044

Horton, R.E., 1945. Erosional development of streams and their drainage basins; Hydrophysical approach to quantitative morphology. Geological Society of America Bulletin, 56(3): 275-370. DOI:10.1130/0016-7606(1945)56[275:edosat]2.0.co;2

Houghton, J., 2007. Town caught between fire and flood, The Age. The Age Company Ltd. Accessed 15 Jun 2013 from http://www.theage.com.au/news/national/flood-wrecks-homes-in-fireravaged-township/2007/02/24/1171734062395.html.

Huang, X., 2006. An evaluation of the geomorphically effective event for fluvial processes over long periods. Journal of Geophysical Research, 111(F3): F03015. DOI:10.1029/2006JF000477

Huckaby, L.S., Kaufmann, M.R., Fornwalt, P.J., Stoker, J.M., Dennis, C., 2003. Field guide to old ponderosa pines in the Colorado Front Range.

Hunter, J., 2015. Vegetation and flora of Warrumbungle National Park. DOI:10.13140/RG.2.1.1026.9289

Huxel, G.R., McCann, K., Polis, G.A., 2002. Effects of partitioning allochthonous and autochthonous resources on food web stability. Ecological Research, 17(4): 419-432. DOI:10.1046/j.1440-1703.2002.00501.x

Hyde, K., Jensco, K., Riley, K., Wilcox, A., 2013. Vegetation as a First-order Control on Post-wildfire Erosion: A Cross-scale Study Integrating Field and Satellite Data. In: Moody, J.A., Martin, D.A. (Eds.).

Hyde, K.D., Jencso, K., Wilcox, A.C., Woods, S., 2015. Influences of vegetation disturbance on hydrogeomorphic response following wildfire. Hydrological Processes, 30(7): 1131-1148. DOI:10.1002/hyp.10691

Isbell, R.F., 2002. The Australian Soil Classification : Revised Edition. CSIRO Publishing, Collingwood, VIC, Australia.

IUSS Working Group WRB, 2015. World Reference Base for Soil Resources 2014, update 2015 - International soil classification system for naming soils and creating legends for soil maps.

Ivey, C.T., DeSilva, N., 2001. A Test of the Function of Drip Tips. BIOTROPICA, 33(1): 188-191. DOI:10.1646/0006-3606(2001)033[0188:ATOTFO]2.0.CO;2

Jackson, R.B. et al., 2017. Warning signs for stabilizing global CO 2 emissions. Environmental Research Letters, 12(11): 110202.

Jacobs, M.R., 1955. Growth habits of the Eucalypts. Forestry and Timber Bureau, Department of the Interior, Canberra, Australia, 262 pp.

James, S.A., Bell, D.T., 2000. Leaf orientation, light interception and stomatal conductance of Eucalyptus globulus ssp. globulus leaves. Tree Physiology, 20(12): 815-823. DOI:10.1093/treephys/20.12.815

Jennings, S.A., Lambert, M.F., Kuczera, G., 2010. Generating synthetic high resolution rainfall time series at sites with only daily rainfall using a master–target scaling approach. Journal of Hydrology, 393(3): 163-173. DOI:http://dx.doi.org/10.1016/j.jhydrol.2010.08.013

Jones, D.M.A., 1992. Raindrop spectra at the ground. Journal of Applied Meteorology, 31(10): 1219-1225. DOI:10.1175/1520-0450(1992)031<1219:rsatg>2.0.co;2

Jones, O., Nyman, P., Sheridan, G., 2014. Modelling the effects of fire and rainfall regimes on extreme erosion events in forested landscapes. Stochastic Environmental Research & Risk Assessment, 28(8): 2015-2025. DOI:10.1007/s00477-014-0891-6

Joss, J., Gori, E.G., 1978. Shapes of Raindrop Size Distributions. Journal of Applied Meteorology, 17(7): 1054-1061. DOI:10.1175/1520-0450(1978)017<1054:SORSD>2.0.CO;2

Kabat, P., Hutjes, R.W.A., Feddes, R.A., 1997. The scaling characteristics of soil parameters: From plot scale heterogeneity to subgrid parameterization. Journal of Hydrology, 190(3-4): 363-396.

Kampf, S.K., Brogan, D.J., Schmeer, S., MacDonald, L.H., Nelson, P.A., 2016. How do geomorphic effects of rainfall vary with storm type and spatial scale in a post-fire landscape? Geomorphology, 273: 39-51. DOI:http://dx.doi.org/10.1016/j.geomorph.2016.08.001

Kaplan, J.O., Krumhardt, K.M., Zimmermann, N., 2009. The prehistoric and preindustrial deforestation of Europe. Quaternary Science Reviews, 28(27–28): 3016-3034. DOI:http://dx.doi.org/10.1016/j.quascirev.2009.09.028

Kathiravelu, G., Lucke, T., Nichols, P., 2016. Rain Drop Measurement Techniques: A Review. Water, 8(1): 29.

Keeley, J.E., 2009. Fire intensity, fire severity and burn severity: a brief review and suggested usage. International Journal of Wildland Fire, 18(1): 116-126. DOI:10.1071/WF07049

Keeley, J.E., Brennan, T., Pfaff, A.H., 2008. Fire severity and ecosystem responses following crown fires in California shrublands. Ecological Applications, 18(6): 1530-1546. DOI:10.1890/07-0836.1

Keeley, J.E., Safford, H., Fotheringham, C.J., Franklin, J., Moritz, M., 2009. The 2007 Southern California Wildfires: Lessons in Complexity. Journal of Forestry, 107(6): 287-296.

Keetch, J.J., Byram, G.M., 1968. A Drought Index for Forest Fire Control, USDA Forest Service, Asheville, North Carolina.

Keim, A.S., Verdon-Kidd, D.C., 2009. Climatic Drivers of Victorian Streamflow: Is ENSO the Dominant Influence? Australian Journal of Water Resources(1): 17.

Kelley, D.I., Harrison, S.P., 2014. Enhanced Australian carbon sink despite increased wildfire during the 21st century. Environmental Research Letters, 9(10): 104015.

Kendon, E.J. et al., 2014. Heavier summer downpours with climate change revealed by weather forecast resolution model. Nature Climate Change, 4: 570. DOI:10.1038/nclimate2258

Kendon, E.J., Roberts, N.M., Senior, C.A., Roberts, M.J., 2012. Realism of Rainfall in a Very High-Resolution Regional Climate Model. Journal of Climate, 25(17): 5791-5806. DOI:10.1175/JCLI-D-11-00562.1

Khabarov, N. et al., 2016. Forest fires and adaptation options in Europe. Regional Environmental Change, 16(1): 21-30. DOI:10.1007/s10113-014-0621-0

Khaleghpanah, N., Shorafa, M., Asadi, H., Gorji, M., Davari, M., 2016. Modeling soil loss at plot scale with EUROSEM and RUSLE2 at stony soils of Khamesan watershed, Iran. CATENA, 147: 773-788. DOI:http://dx.doi.org/10.1016/j.catena.2016.08.039

Khanna, P.K., Raison, R.J., Falkiner, R.A., 1994. Chemical properties of ash derived from Eucalyptus litter and its effects on forest soils. Forest Ecology and Management, 66(1): 107-125. DOI:http://dx.doi.org/10.1016/0378-1127(94)90151-1

Kidron, G.J., 2015. Runoff and sediment yields from under-canopy shrubs in a biocrusted dunefield. Hydrological Processes: 1665–1675. DOI:10.1002/hyp.10742

King, D.A., 1997. The Functional Significance of Leaf Angle in *Eucalyptus*. Australian Journal of Botany, 45(4): 619-639. DOI:10.1071/BT96063

Kinnell, P.I.A., 2005. Raindrop-impact-induced erosion processes and prediction: A review. Hydrological Processes, 19(14): 2815-2844.

Kinoshita, A.M. et al., 2016. Wildfire, water, and society: Toward integrative research in the "Anthropocene". Anthropocene, 16: 16-27. DOI:http://dx.doi.org/10.1016/j.ancene.2016.09.001

Kirkby, L., 2011. Physics: A Student Companion. Scion Publishing, Banbury, UNITED KINGDOM.

Kirkpatrick, J.B., 1977. Eucalypt invasion in Southern California. Australian Geographer, 13(6): 387-393. DOI:10.1080/00049187708702717

Kirkpatrick, J.B., Bridle, K.L., 1998. Environmental relationships of floristic variation in the alpine vegetation of southeast Australia. Journal of Vegetation Science, 9(2): 251-260. DOI:10.2307/3237124

Kirkpatrick, J.B., Nunez, M., 1980. Vegetation-Radiation Relationships in Mountainous Terrain: Eucalypt-Dominated Vegetation in the Risdon Hills, Tasmania. Journal of Biogeography, 7(2): 197-208.

Klamerus-Iwan, A., Błońska, E., 2018. Canopy storage capacity and wettability of leaves and needles: The effect of water temperature changes. Journal of Hydrology, 559: 534-540. DOI:https://doi.org/10.1016/j.jhydrol.2018.02.032

Kleinman, P.J. et al., 2006. Role of rainfall intensity and hydrology in nutrient transport via surface runoff. Journal of environmental quality, 35(4): 1248-59. DOI:10.2134/jeq2006.0015

Knapp, E.E., Keeley, J.E., Ballenger, E.A., Brennan, T.J., 2005. Fuel reduction and coarse woody debris dynamics with early season and late season prescribed fire in a Sierra Nevada mixed conifer forest. Forest Ecology and Management, 208(1-3): 383-397.

Korner, C., 2006. Plant CO2 responses: an issue of definition, time and resource supply. The New phytologist, 172(3): 393-411. DOI:10.1111/j.1469-8137.2006.01886.x

Kotroni, V., Lagouvardos, K., 2008. Lightning occurrence in relation with elevation, terrain slope, and vegetation cover in the Mediterranean. Journal of Geophysical Research: Atmospheres, 113(D21). DOI:10.1029/2008JD010605

Krause, A., Kloster, S., Wilkenskjeld, S., Paeth, H., 2014. The sensitivity of global wildfires to simulated past, present, and future lightning frequency. Journal of Geophysical Research: Biogeosciences, 119(3): 312-322. DOI:10.1002/2013JG002502

Kuczera, G., 1987. Prediction of water yield reductions following a bushfire in ash-mixed species eucalypt forest. Journal of Hydrology, 94(3): 215-236. DOI:http://dx.doi.org/10.1016/0022-1694(87)90054-0

Kuleshov, Y., Mackerras, D., Darveniza, M., 2006. Spatial distribution and frequency of lightning activity and lightning flash density maps for Australia. Journal of Geophysical Research: Atmospheres, 111(D19). DOI:10.1029/2005JD006982

Kutiel, P., 1994. Fire and ecosystem heterogeneity: A mediterranean case study. Earth Surface Processes and Landforms, 19(2): 187-194. DOI:10.1002/esp.3290190209

Laclau, J.-P., Ranger, J., Bouillet, J.-P., de Dieu Nzila, J., Deleporte, P., 2003. Nutrient cycling in a clonal stand of Eucalyptus and an adjacent savanna ecosystem in Congo: 1. Chemical composition of rainfall, throughfall and stemflow solutions. Forest Ecology and Management, 176(1): 105-119. DOI:https://doi.org/10.1016/S0378-1127(02)00280-3

Lal, R., Elliot, W., 1994. Erodibility and erosivity. In: Lal, R. (Ed.), Soil Erosion Research Methods. Soil and Water Conservation Society and St. Lucie Press, Delray Beach, Florida.

Lane, P.N.J., Feikema, P.M., Sherwin, C.B., Peel, M.C., Freebairn, A., 2007. Physically-Based Prediction of Water Yield from Disturbed Forested Water Supply Catchments. In: Oxley, L., Kulasiri, D. (Eds.), MODSIM 2007 International Congress on Modelling and Simulation. . Modelling and Simulation Society of Australia and New Zealand, December 2007, Modelling and Simulation Society of Australia and New Zealand, December 2007.

Langford, K.J., O'Shaughnessy, P.J., 1978. A study of canopy interception in native forests and conifer plantations, Melbourne and Metropolitan Board of Works, Melbourne.

Larsen, I. et al., 2009. Causes of Post-Fire Runoff and Erosion: Water Repellency, Cover, or Soil Sealing? Soil Science Society of America Journal, 73(4): 1393-1407.

Larsen, I.J., MacDonald, L.H., 2007. Predicting postfire sediment yields at the hillslope scale: Testing RUSLE and Disturbed WEPP. Water Resour. Res., 43(11): W11412. DOI:10.1029/2006wr005560

Larsen, M.C., Torres-Sánchez, A.J., Concepción, I.M., 1999. Slopewash, surface runoff and fine-litter transport in forest and landslide scars in humid-tropical steeplands, luquillo experimental forest, Puerto Rico. Earth Surface Processes and Landforms, 24(6): 481-502. DOI:10.1002/(SICI)1096-9837(199906)24:6<481::AID-ESP967>3.0.CO;2-G

Latham, D., Williams, E., 2001. Lightning and Forest Fires-Chapter 11. In: Johnson, E.A., Miyanishi, K. (Eds.), Forest Fires: Behaviour and Ecological Effects. Academic Press, San Diego, California.

Leighton-Boyce, G., Doerr, S.H., Shakesby, R.A., Walsh, R.P.D., 2007. Quantifying the impact of soil water repellency on overland flow generation and erosion: a new approach using rainfall simulation and wetting agent on in situ soil. Hydrological Processes, 21(17): 2337-2345. DOI:10.1002/hyp.6744

Leitch, C.J., Flinn, D.W., van de Graaff, R.H.M., 1983. Erosion and nutrient loss resulting from Ash Wednesday (February 1983) wildfires a case study. Australian Forestry, 46(3): 173-180. DOI:10.1080/00049158.1983.10674396

Letey, J., 2001. Causes and consequences of fire-induced soil water repellency. Hydrological Processes, 15(15): 2867-2875. DOI:10.1002/hyp.378

Levia, D.F., Frost, E.E., 2006. Variability of throughfall volume and solute inputs in wooded ecosystems. Progress in Physical Geography, 30(5): 605-632. DOI:10.1177/0309133306071145

Levia, D.F., Hudson, S.A., Llorens, P., Nanko, K., 2017. Throughfall drop size distributions: a review and prospectus for future research. Wiley Interdisciplinary Reviews: Water, 4(4): e1225-n/a. DOI:10.1002/wat2.1225

Li, X., Niu, J., Xie, B., 2014. The Effect of Leaf Litter Cover on Surface Runoff and Soil Erosion in Northern China. PLOS ONE, 9(9): e107789. DOI:10.1371/journal.pone.0107789

Li, X. et al., 2016. Process-based rainfall interception by small trees in Northern China: The effect of rainfall traits and crown structure characteristics. Agricultural and Forest Meteorology, 218: 65-73. DOI:http://dx.doi.org/10.1016/j.agrformet.2015.11.017

Liang, W.-L., Kosugi, K.i., Mizuyama, T., 2011. Soil water dynamics around a tree on a hillslope with or without rainwater supplied by stemflow. Water Resour. Res., 47(2): W02541. DOI:10.1029/2010wr009856

Lindenmayer, D.B., Hobbs, R.J., Likens, G.E., Krebs, C.J., Banks, S.C., 2011. Newly discovered landscape traps produce regime shifts in wet forests. Proceedings of the National Academy of Sciences, 108(38): 15887-15891. DOI:10.1073/pnas.1110245108

Lindenmayer, D.B., Hunter, M.L., Burton, P.J., Gibbons, P., 2009. Effects of logging on fire regimes in moist forests. Conservation Letters, 2(6): 271-277. DOI:10.1111/j.1755-263X.2009.00080.x

Liu, B., Qu, J., Ning, D., 2018. Amplification factors to estimate wind erosion of piles of soil with different heights: Numerical simulation and structure-from-motion photogrammetry verification. Journal of Soil and Water Conservation, 73: 377-385.

Liu, C., Sun, G., McNulty, S.G., Noormets, A., Fang, Y., 2017. Environmental controls on seasonal ecosystem evapotranspiration/potential evapotranspiration ratio as determined by the global eddy flux measurements. Hydrol. Earth Syst. Sci., 21(1): 311-322. DOI:10.5194/hess-21-311-2017

Liu, J., Pei, T., 2003. Research progress on hydrological scaling. Chinese Journal of Applied Ecology, 14(12): 2305-2310.

Livesley, S.J., Baudinette, B., Glover, D., 2014. Rainfall interception and stem flow by eucalypt street trees – The impacts of canopy density and bark type. Urban Forestry & Urban Greening, 13(1): 192-197. DOI:http://dx.doi.org/10.1016/j.ufug.2013.09.001

Lloyd, N.J., Nally, R.M., Lake, P.S., 2005. Spatial autocorrelation of assemblages of benthic invertebrates and its relationship to environmental factors in two upland rivers in southeastern Australia. Diversity & Distributions, 11(5): 375-386. DOI:10.1111/j.1366-9516.2005.00166.x

Lucas, C., 2010. On developing a historical fire weather data-set for Australia. Australian Meteorological and Oceanographic Journal, 60: 1-14.

Ludwig, J.A., Wilcox, B.P., Breshears, D.D., Tongway, D.J., Imeson, A.C., 2005. Vegetation patches and runoff-erosion as interacting ecohydrological processes in semi-arid landscapes. Ecology, 86(2): 288-297. DOI:10.1890/03-0569

Luke, R.H., McArthur, A.G., 1978. Bushfires in Australia. Australian Government Publishing Service for CSIRO., Canberra, x + 359 pp. pp.

Lunt, I.D., Jones, N., Spooner, P.G., Petrow, M., 2006. Effects of European colonization on indigenous ecosystems: post-settlement changes in tree stand structures in Eucalyptus–Callitris woodlands in central New South Wales, Australia. Journal of Biogeography, 33(6): 1102-1115. DOI:10.1111/j.1365-2699.2006.01484.x

Machado, A.I. et al., 2015. Cation export by overland flow in a recently burnt forest area in north-central Portugal. Science of the Total Environment, 524-525: 201-212. DOI:10.1016/j.scitotenv.2015.04.026

Marlon, J.R. et al., 2008. Climate and human influences on global biomass burning over the past two millennia. Nature Geosci, 1(10): 697-702. DOI:http://www.nature.com/ngeo/journal/v1/n10/suppinfo/ngeo313_S1.html

Martin, Y.E., Johnson, E.A., Gallaway, J.M., Chaikina, O., 2011. Negligible soil erosion in a burned mountain watershed, Canadian Rockies: field and modelling investigations considering the role of duff. Earth Surface Processes and Landforms, 36(15): 2097-2113. DOI:10.1002/esp.2236

Mason, B.J., Andrews, J.B., 1960. Drop-size distributions from various types of rain. Quarterly Journal of the Royal Meteorological Society, 86(369): 346-353. DOI:10.1002/qj.49708636906

May, F., Ash, J., 1990. An Assessment of the Allelopathic Potential of <I>Eucalyptus</I>. Australian Journal of Botany, 38(3): 245-254. DOI:https://doi.org/10.1071/BT9900245

Mayor, A.G., Bautista, S., Llovet, J., Bellot, J., 2007. Post-fire hydrological and erosional responses of a Mediterranean landscpe: Seven years of catchment-scale dynamics. CATENA, 71(1): 68-75. DOI:http://dx.doi.org/10.1016/j.catena.2006.10.006

McCarthy, M.A., Malcolm Gill, A., Lindenmayer, D.B., 1999. Fire regimes in mountain ash forest: evidence from forest age structure, extinction models and wildlife habitat. Forest Ecology and Management, 124(2): 193-203. DOI:http://dx.doi.org/10.1016/S0378-1127(99)00066-3

McGregor, K.C., Bingner, R.L., Bowie, A.J., Foster, G.R., 1995. Erosivity index values for northern Mississippi. Transactions - American Society of Agricultural Engineers, 38(4): 1039-1047.

McGuire, L.A., Kean, J.W., Staley, D.M., Rengers, F.K., Wasklewicz, T.A., 2016. Constraining the relative importance of raindrop- and flow-driven sediment transport mechanisms in postwildfire environments and implications for recovery time scales. Journal of Geophysical Research: Earth Surface, 121(11): 2211-2237. DOI:10.1002/2016JF003867

McJannet, D., Wallace, J., Reddell, P., 2007. Precipitation interception in Australian tropical rainforests: I. Measurement of stemflow, throughfall and cloud interception. Hydrological Processes, 21(13): 1692-1702. DOI:10.1002/hyp.6347

McPherson, A., Clark, D., Macphail, M., Cupper, M., 2014. Episodic post-rift deformation in the south-eastern Australian passive margin: evidence from the Lapstone Structural Complex. Earth Surface Processes and Landforms, 39(11): 1449-1466. DOI:10.1002/esp.3535

Meehl, G.A., Hu, A., Teng, H., 2016. Initialized decadal prediction for transition to positive phase of the Interdecadal Pacific Oscillation. 7: 11718. DOI:10.1038/ncomms11718

Meier, A.R., Saunders, M.R., Michler, C.H., 2012a. Epicormic buds in trees: a review of bud establishment, development and dormancy release. Tree Physiology, 32(5): 565-584. DOI:10.1093/treephys/tps040

Meier, A.R., Saunders, M.R., Michler, C.H., 2012b. Epicormic buds in trees: a review of bud establishment, development and dormancy release. Tree Physiology. DOI:10.1093/treephys/tps040

Meng, R., Dennison, P.E., Huang, C., Moritz, M.A., D'Antonio, C., 2015. Effects of fire severity and post-fire climate on short-term vegetation recovery of mixed-conifer and red fir forests in the Sierra Nevada Mountains of California. Remote Sensing of Environment, 171 (Supplement C): 311-325. DOI:https://doi.org/10.1016/j.rse.2015.10.024

Merkus, H.G., 2009. Particle size measurements. [electronic resource] : fundamentals, practice, quality. Particle technology series: v. 17. Dordrecht : Springer, c2009.

Merz, R., Parajka, J., Blöschl, G., 2009. Scale effects in conceptual hydrological modeling. Water Resources Research, 45(9).

Miletic, D., 2007. Disasters come in threes as flood decimates farm. Accessed 17 Jun 2016 from http://www.theage.com.au/news/national/disasters-come-in-threes-as-flood-decimates-farm/2007/06/29/1182624171468.html. The Age Company Ltd.

Millar, R.J., Nicholls, Z.R., Friedlingstein, P., Allen, M.R., 2017. A modified impulse-response representation of the global near-surface air temperature and atmospheric concentration response to carbon dioxide emissions. Atmos. Chem. Phys., 17(11): 7213-7228. DOI:10.5194/acp-17-7213-2017

Miller, M., 2000. Fire Autoecology. In: Brown, J.K., Smith, J.K. (Eds.), Wildland Fire in Ecosystems: Effects of Fire on Flora, pp. 257.

Miller, M.E., MacDonald, L.H., Robichaud, P.R., Elliot, W.J., 2011. Predicting post-fire hillslope erosion in forest lands of the western United States. International Journal of Wildland Fire, 20(8): 982-999. DOI:http://dx.doi.org/10.1071/WF09142

Mirra, I.M., Oliveira, T.M., Barros, A.M.G., Fernandes, P.M., 2017. Fuel dynamics following fire hazard reduction treatments in blue gum (Eucalyptus globulus) plantations in Portugal. Forest Ecology and Management, 398 (Supplement C): 185-195. DOI:https://doi.org/10.1016/j.foreco.2017.05.016

Mitchell, P.J., Benyon, R.G., Lane, P.N.J., 2012. Responses of evapotranspiration at different topographic positions and catchment water balance following a pronounced drought in a mixed species eucalypt forest, Australia. Journal of Hydrology, 440–441: 62-74. DOI:http://dx.doi.org/10.1016/j.jhydrol.2012.03.026

Mizugaki, S., Nanko, K., Onda, Y., 2010. The effect of slope angle on splash detachment in an unmanaged Japanese cypress plantation forest. Hydrological Processes, 24(5): 576-587. DOI:10.1002/hyp.7552

Mohamadi, M.A., Kavian, A., 2015. Effects of rainfall patterns on runoff and soil erosion in field plots. International Soil and Water Conservation Research, 3(4): 273-281. DOI:http://dx.doi.org/10.1016/j.iswcr.2015.10.001

Montgomery, D.R., 2007. Soil erosion and agricultural sustainability. Proceedings of the National Academy of Sciences, 104(33): 13268-13272. DOI:10.1073/pnas.0611508104

Moody, J.A., Ebel, B.A., 2014. Infiltration and runoff generation processes in fire-affected soils. Hydrological Processes, 28(9): 3432-3453. DOI:10.1002/hyp.9857

Moody, J.A., Martin, D.A., 2001a. Initial hydrologic and geomorphic response following a wildfire in the Colorado Front Range. Earth Surface Processes and Landforms, 26(10): 1049-1070. DOI:10.1002/esp.253

Moody, J.A., Martin, D.A., 2001b. Post-fire, rainfall intensity–peak discharge relations for three mountainous watersheds in the western USA. Hydrological Processes, 15(15): 2981-2993. DOI:10.1002/hyp.386

Moody, J.A., Martin, D.A., 2009. Synthesis of sediment yields after wildland fire in different rainfall regimes in the western United States. International Journal of Wildland Fire, 18(1): 96-115. DOI:http://dx.doi.org/10.1071/WF07162

Moody, J.A., Martin, D.A. (Eds.), 2013. Synthesizing empirical results to improve predictions of post-wildfire runoff and erosion responses. U.S. Geological Survey, National Research Program, YMCA Conference Center Estes Park, Colorado, USA, 180 pp.

Moody, J.A., Martin, R.G., 2015. Measurements of the initiation of post-wildfire runoff during rainstorms using in situ overland flow detectors. Earth Surface Processes and Landforms, 40(8): 1043-1056. DOI:10.1002/esp.3704

Moody, J.A., Shakesby, R.A., Robichaud, P.R., Cannon, S.H., Martin, D.A., 2013. Current research issues related to post-wildfire runoff and erosion processes. Earth-Science Reviews, 122: 10-37. DOI:10.1016/j.earscirev.2013.03.004

Morris, R.H. et al., 2014. Environmental assessment of erosion following prescribed burning in the Mount Lofty Ranges, Australia. International Journal of Wildland Fire, 23(1): 104-116. DOI:http://dx.doi.org/10.1071/WF13011

Moss, A., Green, P., 1983. Movement of solids in air and water by raindrop impact. effects of drop-size and water-depth variations. Soil Research, 21(3): 257-269. DOI:https://doi.org/10.1071/SR9830257

Moussoulis, E., Mallinis, G., Koutsias, N., Zacharias, I., 2015. Modelling surface runoff to evaluate the effects of wildfires in multiple semi-arid, shrubland-dominated catchments. Hydrological Processes: 4427–4441. DOI:10.1002/hyp.10509

Mululo Sato, A., de Souza Avelar, A., Coelho Netto, A.L., 2011. Spatial variability and temporal stability of throughfall in a eucalyptus plantation in the hilly lowlands of southeastern Brazil. Hydrological Processes, 25(12): 1910-1923. DOI:10.1002/hyp.7947

Nanko, K., Hotta, N., Suzuki, M., 2006. Evaluating the influence of canopy species and meteorological factors on throughfall drop size distribution. Journal of Hydrology, 329(3): 422-431. DOI:http://dx.doi.org/10.1016/j.jhydrol.2006.02.036

Nanko, K., Hudson, S.A., Levia, D.F., 2016a. Differences in throughfall drop size distributions in the presence and absence of foliage. Hydrological Sciences Journal/Journal des Sciences Hydrologiques, 61(3): 620-627. DOI:10.1080/02626667.2015.1052454

Nanko, K., Mizugaki, S., Onda, Y., 2008. Estimation of soil splash detachment rates on the forest floor of an unmanaged Japanese cypress plantation based on field measurements of throughfall drop sizes and velocities. CATENA, 72(3): 348-361. DOI:10.1016/j.catena.2007.07.002

Nanko, K., Onda, Y., Ito, A., Moriwaki, H., 2011. Spatial variability of throughfall under a single tree: Experimental study of rainfall amount, raindrops, and kinetic energy. Agricultural and Forest Meteorology, 151(9): 1173-1182.

Nanko, K., Onda, Y., Kato, H., Gomi, T., 2016b. Immediate change in throughfall spatial distribution and canopy water balance after heavy thinning in a dense mature Japanese cypress plantation. Ecohydrology, 9(2): 300-314. DOI:10.1002/eco.1636

National Committee on Soil and Terrain Australia, 2009. Australian soil and land survey. [electronic resource] : field handbook. Australian soil and land survey handbook handbook series: v. 1. Collingwood, Vic. : CSIRO Pub., c2009. 3rd ed.

National Institutes of Health, 2017. ImageJ: Image Processing and Analysis in Java. U.S. Department of Health and Human Services.

Neary, D.G., Ryan, K.C., DeBano, L.F., 2005. Wildland fire in ecosystems: effects of fire on soils and water, U.S. Department of Agriculture, Forest Service,.

Nel, W. et al., 2016. Intra-event characteristics of extreme erosive rainfall on Mauritius. Physical Geography, 37(3-4): 264-275. DOI:10.1080/02723646.2016.1189756

Nishigaki, T., Sugihara, S., Kilasara, M., Funakawa, S., 2016. Surface Runoff Generation and Soil Loss Under Different Soil and Rainfall Properties in The Uluguru Mountains, Tanzania. Land Degradation & Development, 28(1): 283-293. DOI:10.1002/ldr.2499

NOAA, 2017. El Niño/Southern Oscillation (ENSO) Technical Discussion, Accessed 12 Dec 2017 from https://www.ncdc.noaa.gov/teleconnections/enso/enso-tech.php. National Oceanic and Atmospheric Administration (NOAA), Department of Commerce, United States of America Government.

Noble, I.R., Gill, A.M., Bary, G.A.V., 1980. McArthur's fire-danger meters expressed as equations. Australian Journal of Ecology, 5(2): 201-203. DOI:10.1111/j.1442-9993.1980.tb01243.x

Norby, R.J. et al., 2016. Model–data synthesis for the next generation of forest free-air CO2 enrichment (FACE) experiments. New Phytologist, 209(1): 17-28. DOI:10.1111/nph.13593

Noske, P.J., Lane, P.N.J., Sheridan, G.J., 2010. Stream exports of coarse matter and phosphorus following wildfire in NE Victoria, Australia. Hydrological Processes, 24(11): 1514-1529. DOI:10.1002/hyp.7616

Nyman, P., Rutherfurd, I.D., Lane, P.N.J., Sheridan, G.J., 2019. Debris flows in southeast Australia linked to drought, wildfire, and the El Niño–Southern Oscillation. Geology, 47(5): 491-494. DOI:10.1130/g45939.1

Nyman, P., Sheridan, G., Lane, P.N.J., 2010. Synergistic effects of water repellency and macropore flow on the hydraulic conductivity of a burned forest soil, south-east Australia. Hydrological Processes, 24(20): 2871-2887.

Nyman, P. et al., 2013. Sediment availability on burned hillslopes. Journal of Geophysical Research: Earth Surface, 118(4): 2451-2467. DOI:10.1002/jgrf.20152

Nyman, P., Sheridan, G.J., Smith, H.G., Lane, P.N.J., 2011. Evidence of debris flow occurrence after wildfire in upland catchments of south-east Australia. Geomorphology, 125(3): 383-401. DOI:10.1016/j.geomorph.2010.10.016

Nyman, P. et al., 2015. Predicting sediment delivery from debris flows after wildfire. Geomorphology, 250: 173-186. DOI:https://doi.org/10.1016/j.geomorph.2015.08.023

Obermeier, W.A. et al., 2016. Reduced CO_2 fertilization effect in temperate C3 grasslands under more extreme weather conditions. Nature Climate Change, 7: 137. DOI:10.1038/nclimate3191

Onda, Y., Dietrich, W.E., Booker, F., 2008. Evolution of overland flow after a severe forest fire, Point Reyes, California. CATENA, 72(1): 13-20. DOI:https://doi.org/10.1016/j.catena.2007.02.003

Orem, C.A., Pelletier, J.D., 2016. The predominance of post-wildfire erosion in the long-term denudation of the Valles Caldera, New Mexico. Journal of Geophysical Research: Earth Surface, 121(5): 843-864. DOI:10.1002/2015JF003663

Orians, G.H., Milewski, A.V., 2007. Ecology of Australia: the effects of nutrient-poor soils and intense fires. Biological Reviews, 82(3): 393-423. DOI:10.1111/j.1469-185X.2007.00017.x

Osterkamp, W.R., Hupp, C.R., Stoffel, M., 2012. The interactions between vegetation and erosion: new directions for research at the interface of ecology and geomorphology. Earth Surface Processes and Landforms, 37(1): 23-36. DOI:10.1002/esp.2173

Paci, L., Gelfand, A.E., Beamonte, M.A., Rodrigues, M., Pérez-Cabello, F., 2017. Space-time modeling for post-fire vegetation recovery. Stochastic Environmental Research and Risk Assessment, 31(1): 171-183. DOI:10.1007/s00477-015-1182-6

Paphitis, D., 2001. Sediment movement under unidirectional flows: an assessment of empirical threshold curves. Coastal Engineering, 43(3): 227-245. DOI:https://doi.org/10.1016/S0378-3839(01)00015-1

Parkes, D., Newell, G., Cheal, D., 2003. Assessing the quality of native vegetation: The 'habitat hectares' approach. Ecological Management & Restoration, 4: S29-S38. DOI:10.1046/j.1442-8903.4.s.4.x

Parks Victoria, 2016. Alpine National Park. Parks Victoria, State Government of Victoria.

Parsons, A.J., 2006. Erosion and Sediment Transport by Water on Hillslopes. Encyclopedia of Hydrological Sciences. John Wiley & Sons, Ltd. DOI:10.1002/0470848944.hsa082

Parsons, A.J., Brazier, R.E., Wainwright, J., Powell, D.M., 2006. Scale relationships in hillslope runoff and erosion. Earth Surface Processes and Landforms, 31(11): 1384-1393. DOI:10.1002/esp.1345

Parsons, A.J., Stone, P.M., 2006. Effects of intra-storm variations in rainfall intensity on interrill runoff and erosion. CATENA, 67(1): 68-78. DOI:10.1016/j.catena.2006.03.002

Paula, S., Naulin, P.I., Arce, C., Galaz, C., Pausas, J.G., 2016. Lignotubers in Mediterranean basin plants. Plant Ecology, 217: 661+.

Pausas, J.G., Keeley, J.E., 2014. Evolutionary ecology of resprouting and seeding in fire-prone ecosystems. The New phytologist, 204(1): 55-65.

Pearcy, R.W., Muraoka, H., Valladares, F., 2005. Crown architecture in sun and shade environments: assessing function and trade-offs with a three-dimensional simulation model. New Phytologist, 166(3): 791-800. DOI:10.1111/j.1469-8137.2005.01328.x

Penfold, A.R., Willis, J.L., 1961. The Eucalypts - Botany, Cultivation, Chemistry and Utilization. Leonard Hill [Books] Ltd., London.

Penridge, L.K., Walker, J., 1988. The crown-gap ratio (C) and crown cover: Derivation and simulation study. Australian Journal of Ecology, 13(1): 109-120. DOI:10.1111/j.1442-9993.1988.tb01420.x

Pepler, A., Coutts-Smith, A., Timbal, B., 2014. The role of East Coast Lows on rainfall patterns and inter-annual variability across the East Coast of Australia. International Journal of Climatology, 34(4): 1011-1021. DOI:10.1002/joc.3741

Phillips, J.D., 2016. Vanishing point: Scale independence in geomorphological hierarchies. Geomorphology, 266: 66-74. DOI:https://doi.org/10.1016/j.geomorph.2016.05.012

Phillips, J.D., 2017. Soil Complexity and Pedogenesis. Soil Science, 182(4): 117-127. DOI:10.1097/ss.0000000000000204

Phillips, J.D., Marion, D.A., 2004. Pedological memory in forest soil development. Forest Ecology and Management, 188(1): 363-380. DOI:https://doi.org/10.1016/j.foreco.2003.08.007

Pierson, F.B. et al., 2010. Hydrologic Vulnerability of Sagebrush Steppe Following Pinyon and Juniper Encroachment. Rangeland Ecology & Management, 63(6): 614-629. DOI:http://dx.doi.org/10.2111/REM-D-09-00148.1

Poesen, J., Nachtergaele, J., Verstraeten, G., Valentin, C., 2003. Gully erosion and environmental change: importance and research needs. CATENA, 50(2-4): 91-133.

Poesen, J., Savat, J., 1981. Detachment and transportation of loose sediments by raindrop splash: Part II Detachability and transport ability measurements. CATENA, 8(1): 19-41. DOI:https://doi.org/10.1016/S0341-8162(81)80002-1

Price, O.F., Gordon, C.E., 2016. The potential for LiDAR technology to map fire fuel hazard over large areas of Australian forest. Journal of Environmental Management, 181: 663-673. DOI:http://dx.doi.org/10.1016/j.jenvman.2016.08.042

Prosser, I.P., Williams, L., 1998. The effect of wildfire on runoff and erosion in native Eucalyptus forest. Hydrological Processes, 12(2): 251-265. DOI:10.1002/(sici)1099-1085(199802)12:2<251::aid-hyp574>3.0.co;2-4

Pryor, L.D., 1976. The biology of Eucalypts. Studies in Biology No. 61. Edward Arnold (Publishers) Limited, London, UK, 82 pp.

Pueyo, Y., Moret-Fernández, D., Saiz, H., Bueno, C.G., Alados, C.L., 2013. Relationships Between Plant Spatial Patterns, Water Infiltration Capacity, and Plant Community Composition in Semi-arid Mediterranean Ecosystems Along Stress Gradients. Ecosystems, 16(3): 452-466. DOI:10.1007/s10021-012-9620-5

Purdie, R.W., Slatyer, R.O., 1976. Vegetation succession after fire in sclerophyll woodland communities in south-eastern Australia. Australian Journal of Ecology, 1(4): 223-236. DOI:10.1111/j.1442-9993.1976.tb01111.x

Pypker, T.G., Bond, B.J., Link, T.E., Marks, D., Unsworth, M.H., 2005. The importance of canopy structure in controlling the interception loss of rainfall: Examples from a young and an old-

growth Douglas-fir forest. Agricultural and Forest Meteorology, 130(1–2): 113-129. DOI:10.1016/j.agrformet.2005.03.003

Pypker, T.G., Levia, D.F., Staelens, J., Van Stan, J., II, 2011. Canopy Structure in Relation to Hydrological and Biogeochemical Fluxes. In: Levia, D.F., Carlyle-Moses, D., Tanaka, T. (Eds.), Forest Hydrology and Biogeochemistry. Ecological Studies. Springer Netherlands, pp. 371-388. DOI:10.1007/978-94-007-1363-5_18

Queensland Government, 2017. SILO Climate Data. The State of Queensland. Accessed 1 Jul 2017 from https://data.qld.gov.au/dataset/silo-climate-database.

Quill, R., Sharples, J.J., 2015. Dynamic development of the 2013 Aberfeldy fire. In: Weber, T., McPhee, M.J., Anderssen, R.S. (Eds.), 21st International Congress on Modelling and Simulation. Modelling and Simulation Society of Australia and New Zealand, Gold Coast, Australia, pp. 284-290.

Rauniyar, S.P., Walsh, K.J.E., 2010. Scale Interaction of the Diurnal Cycle of Rainfall over the Maritime Continent and Australia: Influence of the MJO. Journal of Climate, 24(2): 325-348. DOI:10.1175/2010JCLI3673.1

Rayment, G., Lyons, D., 2010. Soil Chemical Methods - Australasia. CSIRO Publishing, Melbourne.

Reaney, S., 2013. Physical causes of rainfall threshold and connectivity for post-wildfire runoff. In: Moody, J.A., Martin, D.A. (Eds.), AGU Chapman Conference on Synthesizing Empirical Results to Improve Predictions of Post-wildfire Runoff and Erosion Response, Estes Park, Colorado, USA, 25 to 31 August 2013, pp. 109.

Reaney, S.M., Bracken, L.J., Kirkby, M.J., 2006. Use of the Connectivity of Runoff Model (CRUM) to investigate the influence of storm characteristics on runoff generation and connectivity in semi-arid areas. Hydrological Processes, 21(7): 894-906. DOI:10.1002/hyp.6281

Renard, K.G., Foster, G.R., Weesies, G.A., McCool, D.K., Yoder, D.C., 1997. Predicting soil erosion by water: A guide to conservation planning with the Revised Universal Soil Loss Equation (RUSLE). Agriculture Handbook Number 703, Agricultural Research Service (ARS).

Rhoades, C.C., Entwistle, D., Butler, D., 2011. The influence of wildfire extent and severity on streamwater chemistry, sediment and temperature following the Hayman Fire, ColoradoA. International Journal of Wildland Fire, 20(3): 430-442. DOI:http://dx.doi.org/10.1071/WF09086

Rice, S., Stoffel, M., Turowski, J.M., Wolf, A., 2012. Disturbance regimes at the interface of geomorphology and ecology. Earth Surface Processes and Landforms, 37(15): 1678-1682. DOI:10.1002/esp.3326

Risal, A., 2016. Application of Web ERosivity Module (WERM) for estimation of annual and monthly R factor in Korea, 147. DOI:10.1016/j.catena.2016.07.017

Robichaud, P.R., Brown, R.E., 2002. Silt fences: an economical technique for measuring hillslope soil erosion. U.S. Department of Agriculture, Forest Service, Rocky Mountain Research Station., Fort Collins, CO. Accessed 10 Sep 2011 from: http://www.treesearch.fs.fed.us/pubs/4543.

Rocca, M.E., Brown, P.M., MacDonald, L.H., Carrico, C.M., 2014. Climate change impacts on fire regimes and key ecosystem services in Rocky Mountain forests. Forest Ecology and Management, 327: 290-305. DOI:http://dx.doi.org/10.1016/j.foreco.2014.04.005

Rodríguez, J. et al., 2017. Wildfire effects on the microbial activity and diversity in a Mediterranean forest soil. CATENA, 158: 82-88. DOI:http://dx.doi.org/10.1016/j.catena.2017.06.018

Roering, J.J., Gerber, M., 2005. Fire and the evolution of steep, soil-mantled landscapes. Geology, 33(5): 349-352. DOI:10.1130/G21260.1

Roering, J.J., Kirchner, J.W., Sklar, L.S., Dietrich, W.E., 2001. Hillslope evolution by nonlinear creep and landsliding: An experimental study. Geology, 29(2): 143-146. DOI:10.1130/0091-7613(2001)029<0143:HEBNCA>2.0.CO;2

Römkens, M.J.M., Helming, K., Prasad, S.N., 2002. Soil erosion under different rainfall intensities, surface roughness, and soil water regimes. CATENA, 46(2–3): 103-123. DOI:http://dx.doi.org/10.1016/S0341-8162(01)00161-8

Rose, C.W. et al., 1994. Modeling processes of soil erosion by water. Trends in Hydrology, 1: 443-451.

Rowe, R.K., Downes, R.G., 1960. Reconnaissance survey of the ecology & land-use in the catchment of the Glenmaggie Reservoir, Soil Conservation Authority, Victoria.

Rulli, M.C., Bozzi, S., Spada, M., Bocchiola, D., Rosso, R., 2006. Rainfall simulations on a fire disturbed mediterranean area. Journal of Hydrology, 327(3–4): 323-338. DOI:http://dx.doi.org/10.1016/j.jhydrol.2005.11.037

Russell-Smith, J., Yates, C., Lynch, B., 2006. Fire regimes and soil erosion in north Australian hilly savannas. International Journal of Wildland Fire, 15(4): 551-556. DOI:https://doi.org/10.1071/WF05112

Russell-Smith, J. et al., 2007. Bushfires down under: patterns and implications of contemporary Australian landscape burning. International Journal of Wildland Fire, 16(4): 361-377. DOI:https://doi.org/10.1071/WF07018

Ruthrof, K.X. et al., 2016. How drought-induced forest die-off alters microclimate and increases fuel loadings and fire potentials. International Journal of Wildland Fire, 25(8): 819-830. DOI:https://doi.org/10.1071/WF15028

Ruwanza, S., Gaertner, M., Esler, K.J., Richardson, D.M., 2015. Allelopathic effects of invasive Eucalyptus camaldulensis on germination and early growth of four native species in the Western Cape, South Africa. Southern Forests: a Journal of Forest Science, 77(2): 91-105. DOI:10.2989/20702620.2014.965985

Safranyik, L., Carroll, A.L., Wilson, B., 2007. Chapter One: The biology and epidemiology of the mountain pine beetle in lodgepole pine forests. In: Safranyik, L., Wilson, B. (Eds.), The mountain pine beetle: a synthesis of biology, management and impacts on lodgepole pine. Natural Resources Canada, Canadian Forest Service, Pacific Forestry Centre, Victoria, BC, Canada, pp. 3-66.

Salles, C., Poesen, J., 2000. Rain properties controlling soil splash detachment. Hydrological Processes, 14(2): 271-282. DOI:10.1002/(sici)1099-1085(20000215)14:2<271::aid-hyp925>3.0.co;2-j

Salles, C., Poesen, J., Govers, G., 2000. Statistical and physical analysis of soil detachment by raindrop impact: Rain erosivity indices and threshold energy. Water Resour. Res., 36(9): 2721-2729. DOI:10.1029/2000wr900024

Sandiford, M., 2003. Neotectonics of southeastern Australia: linking the Quaternary faulting record with seismicity and in situ stress. In: Hillis, R.R., Müller, R.D. (Eds.), Evolution and Dynamics of the Australian Plate. Geological Society of America.

Sankey, J.B. et al., 2017. Climate, wildfire, and erosion ensemble foretells more sediment in western USA watersheds. Geophysical Research Letters, 44(17): 8884-8892. DOI:10.1002/2017GL073979

Santín, C., Doerr, S.H., Otero, X.L., Chafer, C.J., 2015. Quantity, composition and water contamination potential of ash produced under different wildfire severities. Environmental Research, 142: 297-308. DOI:10.1016/j.envres.2015.06.041

Schaetzl, R.J., Follmer, L.R., 1990. Longevity of treethrow microtopography: implications for mass wasting. Geomorphology, 3(2): 113-123. DOI:https://doi.org/10.1016/0169-555X(90)90040-W

Schlesinger, W.H. et al., 1990. Biological feedbacks in global desertification. Science, 247(4946): 1043-1048.

Scholten, T., Geißler, C., Goc, J., Kühn, P., Wiegand, C., 2011. A new splash cup to measure the kinetic energy of rainfall. Journal of Plant Nutrition and Soil Science, 174(4): 596-601. DOI:10.1002/jpln.201000349

Sever, L., Leach, J., Bren, L., 2012. Remote sensing of post-fire vegetation recovery; a study using Landsat 5 TM imagery and NDVI in North-East Victoria. Journal of Spatial Science, 57(2): 175-191. DOI:10.1080/14498596.2012.733618

Shakesby, R.A., 2011. Post-wildfire soil erosion in the Mediterranean: Review and future research directions. Earth-Science Reviews, 105(3-4): 71-100. DOI:10.1016/j.earscirev.2011.01.001

Shakesby, R.A., 2013. Twenty-five Years of Wildfire Experience and 'Established Truths'. In: Moody, J.A., Martin, D.A. (Eds.), AGU Chapman Conference 2013: Synthesizing Empirical Results to Improve Predictions of Post-wildfire Runoff and Erosion Responses. U.S. Geological Survey, National Research Program, Estes Park, Colorado, USA, pp. 125-126.

Shakesby, R.A. et al., 2003. Fire Severity, Water Repellency Characteristics and Hydrogeomorphological Changes Following the Christmas 2001 Sydney Forest Fires. Australian Geographer, 34: 147-175. DOI:https://doi.org/10.1080/00049180301736

Shakesby, R.A., Doerr, S.H., 2006. Wildfire as a hydrological and geomorphological agent. Earth-Science Reviews, 74(3-4): 269-307. DOI:10.1016/j.earscirev.2005.10.006

Shakesby, R.A., Doerr, S.H., Walsh, R.P.D., 2000. The erosional impact of soil hydrophobicity: current problems and future research directions. Journal of Hydrology, 231-232: 178-191. DOI:10.1016/s0022-1694(00)00193-1

Shakesby, R.A., Moody, J.A., Martin, D.A., Robichaud, P.R., 2016. Synthesising empirical results to improve predictions of post-wildfire runoff and erosion response. International Journal of Wildland Fire, 25(3): 257-261. DOI:http://dx.doi.org/10.1071/WF16021

Shakesby, R.A. et al., 2007. Distinctiveness of wildfire effects on soil erosion in south-east Australian eucalypt forests assessed in a global context. Forest Ecology and Management, 238(1-3): 347-364. DOI:10.1016/j.foreco.2006.10.029

Sheridan, G.J., Lane, P.N.J., Noske, P.J., 2007. Quantification of hillslope runoff and erosion processes before and after wildfire in a wet Eucalyptus forest. Journal of Hydrology, 343(1-2): 12-28. DOI:10.1016/j.jhydrol.2007.06.005

Sheridan, G.J., Lane, P.N.J., Sherwin, C.B., Noske, P.J., 2011. Post-fire changes in sediment rating curves in a wet Eucalyptus forest in SE Australia. Journal of Hydrology, 409(1–2): 183-195. DOI:http://dx.doi.org/10.1016/j.jhydrol.2011.08.016

Sheridan, G.J., Noske, P.J., Lane, P.N.J., Sherwin, C.B., 2008. Using rainfall simulation and site measurements to predict annual interrill erodibility and phosphorus generation rates from unsealed forest roads: validation against in-situ erosion measurements. CATENA, 73(1): 49-62. DOI:10.1016/j.catena.2007.08.006

Shumack, S., Hesse, P., 2018. Assessing the geomorphic disturbance from fires on coastal dunes near Esperance, Western Australia: Implications for dune de-stabilisation. Aeolian Research, 31: 29-49. DOI:https://doi.org/10.1016/j.aeolia.2017.08.005

Sidle, R.C., Ziegler, A.D., 2017. The canopy interception–landslide initiation conundrum: insight from a tropical secondary forest in northern Thailand. Hydrol. Earth Syst. Sci., 21(1): 651-667. DOI:10.5194/hess-21-651-2017

Sidman, G., Guertin, D.P., Goodrich, D.C., Unkrich, C.L., Burns, I.S., 2016. Risk assessment of post-wildfire hydrological response in semiarid basins: the effects of varying rainfall representations in the KINEROS2/AGWA model. International Journal of Wildland Fire, 25(3): 268-278. DOI:http://dx.doi.org/10.1071/WF14071

Sigma-Aldrich, 2017. Needle gauge chart. Accessed 27 Jul 2017 from http://www.sigmaaldrich.com/chemistry/stockroom-reagents/learning-center/technical-library/needle-gauge-chart.html.

Simões, F.J.M., 2014. Shear velocity criterion for incipient motion of sediment. Water Science and Engineering, 7(2): 183-193. DOI:https://doi.org/10.3882/j.issn.1674-2370.2014.02.006

Sinclair Knight Merz, 2009. Combined impact of the 2003 and 2006/07 bushfires on streamflow - broadscale assessment, Armadale, Victoria, Australia.

Sinha, E., Michalak, A.M., Balaji, V., 2017. Eutrophication will increase during the 21st century as a result of precipitation changes. Science, 357(6349): 405-408. DOI:10.1126/science.aan2409

Smith, H.G., Dragovich, D., 2008. Post-fire hillslope erosion response in a sub-alpine environment, south-eastern Australia. CATENA, 73(3): 274-285. DOI:10.1016/j.catena.2007.11.003

Smith, H.G., Sheridan, G.J., Lane, P.N.J., Nyman, P., Haydon, S., 2011. Wildfire effects on water quality in forest catchments: A review with implications for water supply. Journal of Hydrology, 396(1-2): 170-192. DOI:10.1016/j.jhydrol.2010.10.043

Smith, H.G., Sheridan, G.J., Lane, P.N.J., Sherwin, C.B., 2010. Paired Eucalyptus forest catchment study of prescribed fire effects on suspended sediment and nutrient exports in south-eastern Australia. International Journal of Wildland Fire, 19(5): 624-636. DOI:10.1071/WF08208

Smith, R., 2007. Key Issues Identified from Operational Reviews of Major Fires in Victoria 2006/07, Department of Sustainability and Environment (DSE), State Government of Victoria.

Song, Y., Liu, L., Yan, P., Cao, T., 2005. A review of soil erodibility in water and wind erosion research. Journal of Geographical Sciences, 15(2): 167-176. DOI:10.1007/bf02872682

Specht, R.L., 1970. Vegetation. In: Leeper, G.W. (Ed.), The Australian environment. [Melbourne] : Commonwealth Scientific and Industrial Research Organization, Australia, in association with Melbourne University Press, 1970. 4th ed.

Spigel, K.M., Robichaud, P.R., 2007. First-year post-fire erosion rates in Bitterroot National Forest, Montana. Hydrological Processes, 21(8): 998-1005. DOI:10.1002/hyp.6295

Spooner, P.G., Smallbone, L., 2009. Effects of road age on the structure of roadside vegetation in south-eastern Australia. Agriculture, Ecosystems & Environment, 129(1): 57-64. DOI:https://doi.org/10.1016/j.agee.2008.07.008

Staelens, J., De Schrijver, A., Verheyen, K., Verhoest, N.E.C., 2006. Spatial variability and temporal stability of throughfall water under a dominant beech (Fagus sylvatica L.) tree in relationship to canopy cover. Journal of Hydrology, 330(3–4): 651-662. DOI:http://dx.doi.org/10.1016/j.jhydrol.2006.04.032

State Emergency Services Victoria, 2013. Wellington Shire Flood Emergency Plan: A Sub-Plan of the Municipal Emergency Management Plan. State Government of Victoria, Wellington Shire Council and Floodsafe.

State Government of Victoria, 2014. Interactive map - Land Channel: Topographical map extract of Licola-Crookayan area. State Government of Victoria. Accessed 30 Oct 2015 from http://services.land.vic.gov.au/maps/interactive.jsp.

State Government of Victoria, 2015. Earth Resources - GeoVic - Explore Victoria Online. State Government of Victoria, Department of Economic Development, Jobs, Transport and Resources, Victoria, Australia.

State Government of Victoria, 2016. Water Measurement Information System. State Government of Victoria. Accessed 12 Jan 2017 from http://data.water.vic.gov.au/monitoring.htm.

State of California, U., 2015. CALFIRE: California Statewide Fire Summary Tuesday, September 15, 2015. Accessed 20 Jun 2017 at http://calfire.ca.gov/communications/communications_statewidefiresummary.php.

Stevens-Rumann, C.S. et al., 2017. Evidence for declining forest resilience to wildfires under climate change. Ecology Letters, 21(2): 243-252. DOI:10.1111/ele.12889

Stewart, H., Flinn, D., Aeberli, B., 1979. Above-Ground Biomass of a Mixed Eucalypt Forest in Eastern Victoria. Australian Journal of Botany, 27(6): 725-740. DOI:https://doi.org/10.1071/BT9790725

Stoof, C.R. et al., 2011. Hydrological response of a small catchment burned by experimental fire. Hydrol. Earth Syst. Sci. Discuss., 8(2): 4053-4098. DOI:10.5194/hessd-8-4053-2011

Stoof, C.R. et al., 2012. Hydrological response of a small catchment burned by experimental fire. Hydrol. Earth Syst. Sci., 16(2): 267-285. DOI:10.5194/hess-16-267-2012

Sturman, A., Tapper, N., 2006. The weather and climate of Australia and New Zealand. Melbourne : Oxford University Press, 2006. 2nd ed., 541 pp.

Susanne, J., 1984. Lignotubers and burls: Their structure, function and ecological significance in Mediterranean ecosystems. Botanical Review, 50(3): 225-266.

Swanson, F.J., 1981. Fire and geomorphic processes. In: Mooney, H., Bonnicksen, T.M., Christensen, N.L., Lotan, J.E., Reiners, W.A. (Eds.), Proceedings of the Conference on Fire Regimes and Ecosystem Properties. USDA Forest Service, Honolulu, Hawaii, pp. 410–420.

Terry, J.P., 1998. A rainsplash component analysis to define mechanisms of soil detachment and transportation. Australian Journal of Soil Research, 36(3): 525-542. DOI:10.1071/S97078

Tessler, N., Wittenberg, L., Greenbaum, N., 2012. Soil water repellency persistence after recurrent forest fires on Mount Carmel, Israel. International Journal of Wildland Fire. DOI:http://dx.doi.org/10.1071/WF12063

Tetzlaff, D. et al., 2007. Connectivity between landscapes and riverscapes—a unifying theme in integrating hydrology and ecology in catchment science? Hydrological Processes, 21(10): 1385-1389. DOI:10.1002/hyp.6701

Teulières, C., Bossinger, G., Moran, G., Marque, C., 2007. Stress studies in Eucalyptus. Plant stress, 1(2): 197-215.

The Weather Chaser, 2017. BoM Weather Radar Loops Archive - Rain Rate & Doppler Wind. Accessed 1 Feb 2017 from http://www.theweatherchaser.com/radar-loop/.

Tian, H. et al., 2015. Global methane and nitrous oxide emissions from terrestrial ecosystems due to multiple environmental changes. Ecosystem Health and Sustainability, 1(1): 1-20. DOI:10.1890/EHS14-0015.1

Tian, P., Xu, X., Pan, C., Hsu, K., Yang, T., 2017. Impacts of rainfall and inflow on rill formation and erosion processes on steep hillslopes. Journal of Hydrology, 548: 24-39. DOI:10.1016/j.jhydrol.2017.02.051

Tietjen, B. et al., 2017. Climate change-induced vegetation shifts lead to more ecological droughts despite projected rainfall increases in many global temperate drylands. Global Change Biology, 23(7): 2743-2754. DOI:10.1111/gcb.13598

Timbal, B., Jones, D.A., 2008. Future projections of winter rainfall in southeast Australia using a statistical downscaling technique. Climatic Change, 86(1): 165-187. DOI:10.1007/s10584-007-9279-7

Toba, T., Ohta, T., 2005. An observational study of the factors that influence interception loss in boreal and temperate forests. Journal of Hydrology, 313(3–4): 208-220. DOI:10.1016/j.jhydrol.2005.03.003

Tokay, A., Short, D.A., 1996. Evidence from tropical raindrop spectra of the origin of rain from stratiform versus convective clouds. Journal of Applied Meteorology(3): 355-371. DOI:https://doi.org/10.1175/1520-0450(1996)035<0355:EFTRSO>2.0.CO;2

Tomkins, K.M. et al., 2008. Postwildfire hydrological response in an El Niño-Southern Oscillation-dominated environment. J. Geophys. Res., 113(F2): F02023. DOI:10.1029/2007jf000853

Torri, D., Sfalanga, M., Del Sette, M., 1987. Splash detachment: Runoff depth and soil cohesion. CATENA, 14(1): 149-155. DOI:https://doi.org/10.1016/S0341-8162(87)80013-9

Townsend, S.A., Douglas, M.M., 2004. The effect of a wildfire on stream water quality and catchment water yield in a tropical savanna excluded from fire for 10 years (Kakadu National Park, North Australia). Water Research, 38(13): 3051-3058. DOI:10.1016/j.watres.2004.04.009

Truman, C.C., Bradford, J.M., 1990. Effect of antecedent soil moisture on splash detachment under simulated rainfall. Soil Science, 150(5): 787-798.

Tryhorn, L., Lynch, A., Abramson, R., Parkyn, K., 2008. On the Meteorological Mechanisms Driving Postfire Flash Floods: A Case Study. Monthly Weather Review, 136(5): 1778-1791. DOI:10.1175/2007MWR2218.1

Tsiko, C.T., Makurira, H., Gerrits, A.M.J., Savenije, H.H.G., 2012. Measuring forest floor and canopy interception in a savannah ecosystem. Physics and Chemistry of the Earth, Parts A/B/C, 47–48: 122-127. DOI:http://dx.doi.org/10.1016/j.pce.2011.06.009

Úbeda, X., Bernia, S., Simelton, E., Celso, G., Ramon, J.B., 2005. Chapter 6: The long-term effects on soil properties from a forest fire of varying intensity in a Mediterranean environment, Developments in Earth Surface Processes. Elsevier, pp. 87-102.

Ulbrich, C.W., 1983. Natural Variations in the Analytical Form of the Raindrop Size Distribution. Journal of Climate and Applied Meteorology, 22(10): 1764-1775. DOI:10.1175/1520-0450(1983)022<1764:NVITAF>2.0.CO;2

Vacchiano, G. et al., 2014. Fire severity, residuals and soil legacies affect regeneration of Scots pine in the Southern Alps. Science of The Total Environment, 472: 778-788. DOI:https://doi.org/10.1016/j.scitotenv.2013.11.101

Valente, F., David, J.S., Gash, J.H.C., 1997. Modelling interception loss for two sparse eucalypt and pine forests in central Portugal using reformulated Rutter and Gash analytical models. Journal of Hydrology, 190(1–2): 141-162. DOI:10.1016/s0022-1694(96)03066-1

Valentin, C., Poesen, J., Li, Y., 2005. Gully erosion: Impacts, factors and control. CATENA, 63(2-3): 132-153. DOI:https://doi.org/10.1016/j.catena.2005.06.001

van Dijk, A.I.J.M. et al., 2013. The Millennium Drought in southeast Australia (2001–2009): Natural and human causes and implications for water resources, ecosystems, economy, and society. Water Resources Research, 49(2): 1040-1057. DOI:10.1002/wrcr.20123

Venter, Z.S., Cramer, M.D., Hawkins, H.J., 2018. Drivers of woody plant encroachment over Africa. Nat Commun, 9(1): 2272. DOI:10.1038/s41467-018-04616-8

Verdon-Kidd, D.C., Kiem, A.S., 2009. On the relationship between large-scale climate modes and regional synoptic patterns that drive Victorian rainfall. Hydrol. Earth Syst. Sci., 13(4): 467-479. DOI:10.5194/hess-13-467-2009

Vernimmen, R.R.E., Bruijnzeel, L.A., Romdoni, A., Proctor, J., 2007. Rainfall interception in three contrasting lowland rain forest types in Central Kalimantan, Indonesia. Journal of Hydrology, 340(3): 217-232. DOI:http://dx.doi.org/10.1016/j.jhydrol.2007.04.009

Versini, P.-A., Velasco, M., Cabello, A., Sempere-Torres, D., 2013. Hydrological impact of forest fires and climate change in a Mediterranean basin. Natural Hazards, 66(2): 609-628. DOI:10.1007/s11069-012-0503-z

Verstraeten, G., 2006. Regional scale modelling of hillslope sediment delivery with SRTM elevation data. Geomorphology, 81(1-2): 128-140.

Vertessy, R.A., Hatton, T.J., Benyon, R.G., Dawes, W.R., 1996. Long-term growth and water balance predictions for a mountain ash (Eucalyptus regnans) forest catchment subject to clear-felling and regeneration. Tree Physiology, 16(1-2): 221-232. DOI:10.1093/treephys/16.1-2.221

Vertessy, R.A., Watson, F.G.R., O'Sullivan, S.K., 2001. Factors determining relations between stand age and catchment water balance in mountain ash forests. Forest Ecology and Management, 143(1): 13-26. DOI:https://doi.org/10.1016/S0378-1127(00)00501-6

VicEmergency, 2019. Incidents and Warnings: Advice - Bushfire. Accessed 16 Mar 2019 from http://emergency.vic.gov.au/respond/#.

Victoria Country Fire Authority, 2013a. Gippsland Fire Facts, Latest News. Accessed 7 Aug 2017 from http://news.cfa.vic.gov.au/news/gippsland-fire-facts.html.

Victoria Country Fire Authority, 2013b. Summer Fire Wrap-up, Latest News. Accessed 7 Aug 2017 from http://news.cfa.vic.gov.au/news/summer-fire-wrap-up.html.

Victorian Government, 2007. Addendum to Victorian Government Submission to Environment and Natural Resources Committee (ENRC) "Inquiry into the Impacts of Public Land Management Practices on Bushfires in Victoria": The consequent impact of bushfires on the June/July 2007 Gippsland flood. In: Ministry of Environment and Climate Change (Ed.). State Government of Victoria, Melbourne, Victoria, Australia.

Vieira, D.C.S., Malvar, M.C., Fernández, C., Serpa, D., Keizer, J.J., 2016. Annual runoff and erosion in a recently burn Mediterranean forest – The effects of plowing and time-since-fire. Geomorphology, 270: 172-183. DOI:http://dx.doi.org/10.1016/j.geomorph.2016.06.042

Vis, M., 1986. Interception, drop size distributions and rainfall kinetic energy in four colombian forest ecosystems. Earth Surface Processes and Landforms, 11(6): 591-603. DOI:10.1002/esp.3290110603

Vivian, L.M., Cary, G.J., 2012. Relationship between leaf traits and fire-response strategies in shrub species of a mountainous region of south-eastern Australia. Annals of Botany, 109(1): 197-208. DOI:10.1093/aob/mcr263

Wainwright, J., Parsons, A.J., 2002. The effect of temporal variations in rainfall on scale dependency in runoff coefficients. Water Resources Research, 38(12): 1271. DOI:10.1029/2000WR000188

Wainwright, J., Parsons, A.J., Abrahams, A.D., 2000. Plot-scale studies of vegetation, overland flow and erosion interactions: case studies from Arizona and New Mexico. Hydrological Processes, 14(16-17): 2921-2943. DOI:10.1002/1099-1085(200011/12)14:16/17<2921::AID-HYP127>3.0.CO;2-7

Wakiyama, Y. et al., 2010. Estimation of temporal variation in splash detachment in two Japanese cypress plantations of contrasting age. Earth Surface Processes and Landforms, 35(9): 993-1005. DOI:https://doi.org/10.1002/esp.1844

Walker, J., Crapper, P.F., Penridge, L.K., 1988. The crown-gap ratio (C) and crown cover: The field study. Australian Journal of Ecology, 13(1): 101-108. DOI:10.1111/j.1442-9993.1988.tb01419.x

Wang, D., Heckathorn, S.A., Wang, X., Philpott, S.M., 2012. A meta-analysis of plant physiological and growth responses to temperature and elevated CO2. Oecologia, 169(1): 1-13. DOI:10.1007/s00442-011-2172-0

Wang, J., Dong, X., Xi, B., Heymsfield, A.J., 2016a. Investigation of liquid cloud microphysical properties of deep convective systems: 1. Parameterization raindrop size distribution and its application for stratiform rain estimation. Journal of Geophysical Research: Atmospheres, 121(18): 739-760. DOI:10.1002/2016JD024941

Wang, W., Yin, S., Xie, Y., Liu, B., Liu, Y., 2016b. Effects of four storm patterns on soil loss from five soils under natural rainfall. CATENA, 141: 56-65. DOI:http://dx.doi.org/10.1016/j.catena.2016.02.019

Webb, A.A., Kathuria, A., Turner, L., 2012. Longer-term changes in streamflow following logging and mixed species eucalypt forest regeneration: The Karuah experiment. Journal of Hydrology, 464–465: 412-422. DOI:http://dx.doi.org/10.1016/j.jhydrol.2012.07.034

Wellington Shire Council, 2016. Wellington Shire Municipal Flood Emergency Plan: A Sub-Plan of the Municipal Emergency Management Plan.

Wester, T., Wasklewicz, T., Staley, D., 2014. Functional and structural connectivity within a recently burned drainage basin. Geomorphology, 206: 362-373. DOI:http://dx.doi.org/10.1016/j.geomorph.2013.10.011

Whelan, M.J., Anderson, J.M., 1996. Modelling spatial patterns of throughfall and interception loss in a Norway spruce (Picea abies) plantation at the plot scale. Journal of Hydrology, 186(1–4): 335-354. DOI:http://dx.doi.org/10.1016/S0022-1694(96)03020-X

Whelan, R.J., 1995. The ecology of fire. Cambridge studies in ecology. Cambridge ; Melbourne : Cambridge University Press, 1995.

Wilkinson, M.T., Richards, P.J., Humphreys, G.S., 2009. Breaking ground: Pedological, geological, and ecological implications of soil bioturbation. Earth-Science Reviews, 97(1-4): 257-272. DOI:10.1016/j.earscirev.2009.09.005

Wilks, D.S., 2006. Statistical Methods in the Atmospheric Sciences. International Geophysics Series, 91. Elsevier Inc., Burlington, MA, USA, 627 pp.

Williams, C.J. et al., 2015. Structural and functional connectivity as a driver of hillslope erosion following disturbance. International Journal of Wildland Fire: 306-321. DOI:http://dx.doi.org/10.1071/WF14114

Williams, C.J. et al., 2016. Structural and functional connectivity as a driver of hillslope erosion following disturbance. International Journal of Wildland Fire, 25(3): 306-321.

Williams, C.J., Pierson, F.B., Robichaud, P.R., Boll, J., 2014. Hydrologic and erosion responses to wildfire along the rangeland–xeric forest continuum in the western US: a review and model of hydrologic vulnerability. International Journal of Wildland Fire, 23(2): 155-172. DOI:http://dx.doi.org/10.1071/WF12161

Williams, J., Woinarski, J., 1997. Eucalypt Ecology: Individuals to Ecosystems. Cambridge University Press.

Williams, R.J., Bowman, D.M.J.S., 2012. Fire futures for a megadiverse continent. New Phytologist, 196(2): 337-340. DOI:10.1111/j.1469-8137.2012.04342.x

Williams, R.J. et al., 2008. Large fires in Australian alpine landscapes: their part in the historical fire regime and their impacts on alpine biodiversity. International Journal of Wildland Fire, 17(6): 793-808. DOI:https://doi.org/10.1071/WF07154

Williamson, G.J., Murphy, B.P., Bowman, D.M.J.S., 2014. Cattle grazing does not reduce fire severity in eucalypt forests and woodlands of the Australian Alps. Austral Ecology, 39(4): 462-468. DOI:10.1111/aec.12104

Wischmeier, W.H., Smith, D.D., 1978. Predicting Soil Erosion Losses: A Guide to Conservation Planning. USDA Agricultural Handbook No. 537, 58 pp.

Wong, J.C., Gee, A., 2017. California fires: at least 15 killed in 'unprecedented' wine country blaze, The Guardian. The Guardian and News Ltd., San Francisco, USA.

Woodgate, P.W. et al., 1996. Old-growth forest studies in Victoria, Australia Concepts and principles. Forest Ecology and Management, 85(1): 79-94. DOI:http://dx.doi.org/10.1016/S0378-1127(96)03752-8

Wu, L., Jiang, J., Li, G.-x., Ma, X.-y., 2018. Characteristics of pulsed runoff-erosion events under typical rainstorms in a small watershed on the Loess Plateau of China. Scientific Reports, 8(1): 3672. DOI:10.1038/s41598-018-22045-x

Yang, G. et al., 2011. Water quality of throughfall and stemflow in planted forest in Guangxi, China. 9: 947-953.

Yang, S., Smith, E.A., 2006. Mechanisms for Diurnal Variability of Global Tropical Rainfall Observed from TRMM. Journal of Climate, 19(20): 5190-5226. DOI:10.1175/JCLI3883.1

Yang, X. et al., 2018. Near real-time monitoring of post-fire erosion after storm events: a case study in Warrumbungle National Park, Australia. International Journal of Wildland Fire, 27(6): 413-424. DOI:https://doi.org/10.1071/WF18011

Youberg, A., 2013. Hydrologic and geomorphic responses of burned basins in the southwestern U.S.A., AGU Chapman Conference.

Yufang, J. et al., 2015. Identification of two distinct fire regimes in Southern California: implications for economic impact and future change. Environmental Research Letters, 10(9): 094005.

Zeppel, M.J.B., Macinnis-Ng, C.M.O., Yunusa, I.A.M., Whitley, R.J., Eamus, D., 2008. Long term trends of stand transpiration in a remnant forest during wet and dry years. Journal of Hydrology, 349(1): 200-213. DOI:https://doi.org/10.1016/j.jhydrol.2007.11.001

Zhao, X., Huang, J., Gao, X., Wu, P., Wang, J., 2014a. Runoff features of pasture and crop slopes at different rainfall intensities, antecedent moisture contents and gradients on the Chinese Loess Plateau: A solution of rainfall simulation experiments. CATENA, 119: 90-96. DOI:http://dx.doi.org/10.1016/j.catena.2014.03.007

Zhao, Y., Qin, N., Weber, B., Xu, M., 2014b. Response of biological soil crusts to raindrop erosivity and underlying influences in the hilly Loess Plateau region, China. Biodiversity and Conservation, 23(7): 1669-1686. DOI:10.1007/s10531-014-0680-z

Zhou, G., Wei, X., Yan, J., 2002. Impacts of eucalyptus (Eucalyptus exserta) plantation on sediment yield in Guangdong Province, Southern China--a kinetic energy approach. CATENA, 49(3): 231-251. DOI:10.1016/s0341-8162(02)00030-9

Zhou, Y., Zhang, Y., Vaze, J., Lane, P., Xu, S., 2015. Impact of bushfire and climate variability on streamflow from forested catchments in southeast Australia. Hydrological Sciences Journal, 60(7-8): 1340-1360. DOI:10.1080/02626667.2014.961923

Zhu, J.-j., Yu, L.-z., Xu, T.-l., Wei, X., Yang, K., 2018. Comparison of water quality in two catchments with different forest types in the headwater region of the Hun River, Northeast China. DOI:10.1007/s11676-018-0688-4

Zhu, P. et al., 2017. Elevated atmospheric CO_2 negatively impacts photosynthesis through radiative forcing and physiology-mediated climate feedback. Geophysical Research Letters, 44(4): 1956-1963. DOI:10.1002/2016GL071733

Zhu, Z. et al., 2016. Greening of the Earth and its drivers. Nature Climate Change, 6: 791. DOI:10.1038/nclimate3004

Zimmermann, A., Wilcke, W., Elsenbeer, H., 2007. Spatial and temporal patterns of throughfall quantity and quality in a tropical montane forest in Ecuador. Journal of Hydrology, 343(1–2): 80-96. DOI:http://dx.doi.org/10.1016/j.jhydrol.2007.06.012

APPENDIX A: EARLIER STUDIES ON POST-FIRE EROSION IN SOUTHEAST AUSTRALIA

Authors	Location(s) and fire(s)	Focus of study	Vegetation type(s)	Treatment of vegetation factor	Timeframe	Geology and soils	Selected findings
Chessman (1986)	11 streams in East Gippsland: Errinundra, Combienbar, Bemm, West Cann, East Cann, Cann, Thurra, Wingan, Genoa, Fiddlers Green and Drummer; 1983 Ash Wednesday fires of varying burn extents and severities across region	Regional monitoring of post-fire stream water quality along streams from catchments with varying extents and severities of burning. Parameters included: DO, colour, turbidity, TSS, EC, K, P, NO$_3$, NO$_2$, NH$_4$, Total N;	Variable across region; upper Bemm mainly wet sclerophyll forest; upper Cann and Genoa mainly dry sclerophyll forest; Thurra and Wingan mainly lowland sclerophyll forest and heath.	Map of 11 sampling stations across burnt areas of varying extent and severity was presented. Rates and patterns of vegetation recovery one of the many factors affecting severity of wildfire impact on water quality, no detailed analysis of factor; Variable relationships between burn extent and rainfall-runoff and water quality response across catchments	3-month immediate post-fire period	Upper Devonian granites and granodiorites; Ordivician sandstones and mudstones; permeable, red friable gradational earths (upper Bemm and Thurra) and low permeability hard-setting loamy soils with clay subsoils (upper Cann, Wingan and Genoa)	Highest sediment and solute exports in first large storm after fire Highest exports from Cann and Genoa catchments compared to others attributed to differences in catchment topography, soil and surface/subsurface flow partitioning and pathways.
Leitch et al. (1983)	35 ha catchment in Millgrove, Warburton, Victorian Central Highlands; Ash Wednesday Fires of 1983; high-intensity fires	Estimation of post-fire erosion and nutrient loss caused by short duration, high-intensity (17 mm) thunderstorm 6-days post-fire; using field survey measurements of erosion and deposition forms; soil samples across catchment	1/3 area *Eucalyptus regnans* mountain ash wet sclerophyll forest; 2/3 area mix of *Eucalyptus cypellocarpa, sieberi, baxteri, and oblique*; understorey *Acacia, Cassinia, Platylobium, Pteridium esculentum and* tussock grass *Poa spp.*	Visual assessment observed total consumption of ground cover and almost complete (95%) death or destruction of canopy foliage; Some interception attributed to dead foliage in scorched canopy; Lack of ground cover as main cause for high erosion rates; No specific quantitative linkages between vegetation cover and erosion rates.	First 3 months in the immediate post-fire period	Metamorphosed sandstones and siltstones; Shallow, gravelly, stony and acidic sandy loam to clay loams	Estimated ash and soil loss of 22 t ha^{-1}; total loss of 2900 kg of nitrogen and 220 kg of phosphorus. Hydrophobicity and lack of lack of vegetative cover accounted for high erosion rates; Heightened erosion exacerbates fertility differences gradients in dry sclerophyll forests
Burgess et al. (1981)	5 experimental catchments near Eden, south New South Wales; 1979 severe wildfire	Measurement of catchment exports of suspended sediment and solution loads comparing effects of logging and wildfire; runoff monitoring using V-notch weirs, manual and automatic water sampling	Mixed dry sclerophyll forest, mainly *Eucalyptus sieberi* with *E. oblique, muelleriana, consideriana* and *cypellocarpa*. Understorey of *Acacia terminalis, Banksia serrata, Casuarina littoralis, Personia luniaris and levis*.	Noted the ground cover of leaf, branch and bark litter, grasses, sedges and small shrubs; Complete removal of ground cover accounted for higher sediment and solute loads for post-fire than post-logging; Litter in logged catchments attenuated transport of hillslope materials. No specific quantitative relationships drawn between vegetation recovery and measured outcomes for this immediate post-fire period	3 month immediate post-fire period	'[E]asily erodible adamelite' with small areas of rhyolite and granodiorite; Well-developed red and yellow Podsols	Distinct hydrologic and sedimentological responses between post-fire and post-logging treatments; Post-fire streamflow: 0.275 cumecs from 80 mm rainfall; Suspended loads: 196 mg L^{-1} at 0.096 cumecs; 283 mg L^{-1} at 0.277 cumecs; Post-fire suspended loads remained high 6 months after fire whereas post-logging suspended loads recovered to low levels.

APPENDIX B: ANALYSIS OF RAINFALL HOURS

This appendix presents the detailed analysis of: (a) rainfall hours across all times of the day; and correspondingly (b) rainfall percentages, for individual months, organized according to summer (DJF), autumn (MAM), winter (JJA) and spring (SON) seasons.

1. Summer rainfall hours and percentages

Figure B-1 presents the rainfall hours and percentages for the summer months of December, January and February.

<u>December</u>

December had 646 total rainfall hours and 675 mm total rainfall depth. From Figure B-1(i)(a), the modal rainfall time-of-day was 1200 hrs (34 hrs); rather high rainfall hours were also seen in the following early afternoon times of 1300 hrs (31 hrs) and 1400 hrs (32 hrs). Another high rainfall time was also found at late afternoon of 1800 hrs (31 hrs). Additionally, a high was detected in the very early morning at 0300 hrs (32 hrs).

Figure B-1(i)(b) shows that the highest proportion of total rainfall occurred in the early afternoon at 1400 hrs during which 8.2% fell; this was flanked by two "shoulder" times of 1300 hrs (6.8%) and 1500 hrs (6.7%). Another peak rainfall hour was found in the late evening/night at 2100 hrs (7.6%) and preceding it, a high "lead-up" at 2000 hrs (6.5%). The 0300 hrs rainfall hour peak did not translate into a high rainfall percentage, although it was a localized peak amongst the other surrounding hours.

<u>January</u>

January had 432 total rainfall hours and 603.1 mm total rainfall depth. As seen in Figure B-1(ii)(a), January rainfall patterns showed even higher contrasts between the "wet" and "dry" times of the day compared to December. In contrast to Dec there was higher temporal correspondence between the modal rainfall hour of 1600 hrs and the "shoulder" (1500 hrs,

6.8%; 1700 hrs, 10.6%; 1800 hrs, 9.4%; and 1900 hrs, 7.9%) and "peak" (1600 hrs, 11.1%) rainfall times; see Figure B-1(ii).

<u>February</u>

February had 526 total rainfall hours and 912.4 mm total rainfall depth. As seen in Figure B-1(iii)(a), February rainfall hours were more evenly distributed throughout the day compared to January, although two peaks were seen at 1400 hrs and 1700 hrs; see Figure B-1(iii)(b). However, as seen in Figure B-1(iii)(b), the highest percentage of total rainfall was at 1300 hrs (14.7%) followed by 1400 hrs (11.3%). A smaller peak was also seen at 1800 hrs (7.2 %) with a "shoulder" at 1900 hrs (6.2%). Summer rainfall patterns by time-of-day from midnight (0) to 11 PM (23) as (a) Total hours of rainfall occurrence; (b) Percent (%) total rainfall depth, for (i) Dec, (ii) Jan and (iii) Feb. Note that y-axis scales vary according to the range of values calculated.

(a) Total hours of rainfall occurrence

(b) Percent (%) total rainfall depth
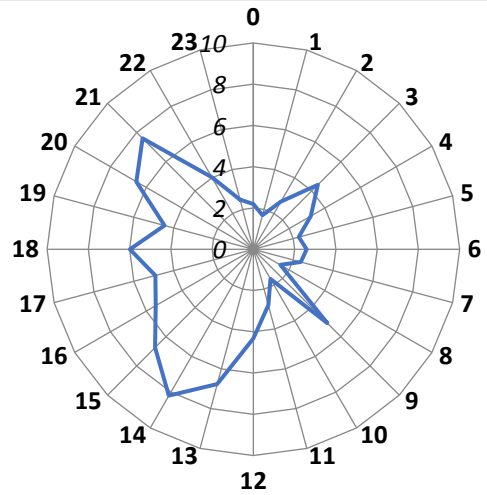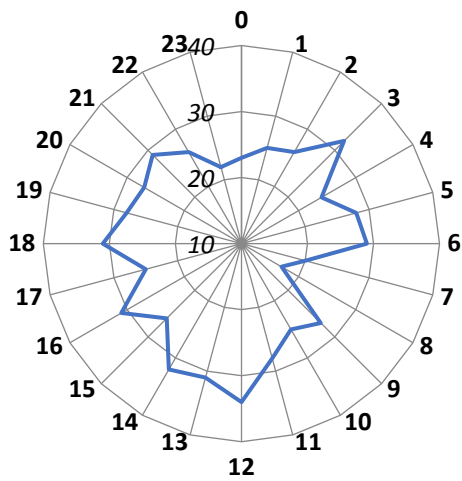
(i) December
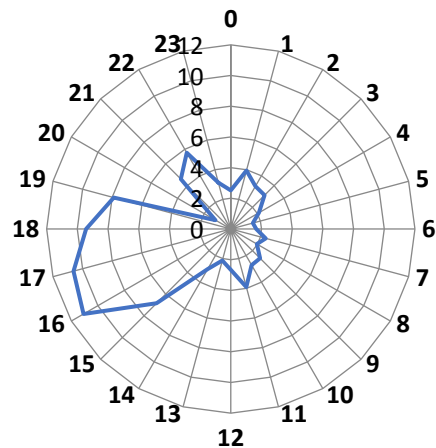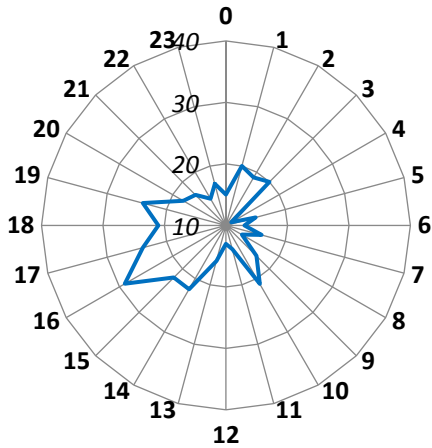
(ii) January
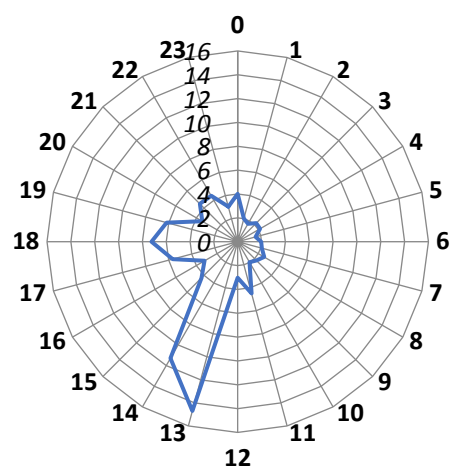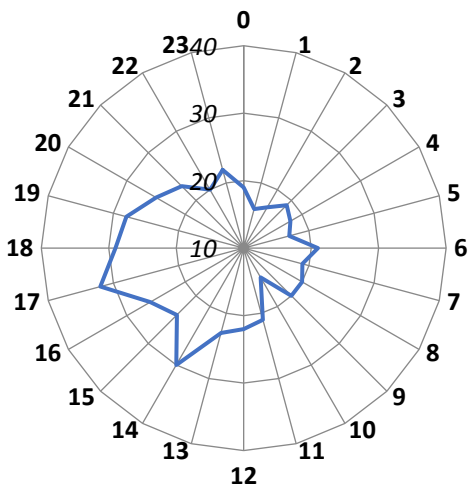
(iii) February

<u>Figure B-1.</u> Summer rainfall patterns by time-of-day (perimeter of each chart) from midnight (0) to 11 PM (23) as: (a) Total hours of rainfall occurrence; (b) Percent (%) total rainfall depth, for (i) Mar, (ii) Apr and (iii) May. Notes: Radial y-axis scales vary according to the range of values calculated.

419

2. Autumn rainfall hours and percentages

Figure B-2 presents the rainfall hours and percentages for the summer months of March, April and May.

March

   March had 474 total rainfall hours and 462 mm total rainfall depth. As seen from Figure B-2(i)(a), March rainfall had highest number of rainfall hours at 1900 hrs; this peak had "shoulder" hours of 2000 hrs (25 hrs) and 1900 hrs (22 hrs). More rainy hours can be found in the morning hours, with another peak is found at 1100 hrs (26 hrs) with some moderate level "lead-up" hours at 0900 hrs (22 hrs) and 1000 hrs (23 hrs). However, very low rainfall hours were recorded at 1200 hrs (14 hrs), just after the 1100 hrs peak. A third high was also found at 0800 hrs (24 hrs). The lowest rainfall hour was at 2300 hrs (12 hrs).

   From Figure B-2(i)(b), rainfall percentage had good temporal correlation to rainfall hours, with the peak at 1900 hrs (7.7 %) and "shoulders" at 1800 hrs (5.9%) and 2000 hrs (5.5%). However, peak rainfall percentages were also found at 0800 hrs (6.6%) and 0900 hrs (6.5%).

April

   April had 601 total rainfall hours and 475.6 mm total rainfall depth. As shown in Figure B-2(ii)(a), peak rainfall hours were just past midday at 1300 hours (33 hrs) with "shoulders" at 1200 hrs (32 hrs) and 1400 hrs (31 hrs). Other high rainfall hours were seen in the early morning hour of 0600 hrs (28 hrs) of 0900 hrs (27 hrs), and the late-night hours of 2100 hrs (28 hrs), 2200 hrs (27 hrs) and 2300 hrs (28 hrs). These appear to be around 2 hours shift of peaks to later hours compared to Mar peaks.

   Peak rainfall percentage time, as seen from Figure B-2(ii)(b), contrasts with rainfall hours, with highest percentage at 0300 hrs (7.1 %) even though rainfall hours at 0300 hrs was only 21 hrs (Figure B-2(b)(i)), indicating that heavy rainfall occurs regularly during these

nocturnal hours. Another peak rainfall percentage was detected mid-day at 1300 hrs (5.5%), correlating closely with the peak rainfall hour of 1300 hrs.

May

      May had 751 total rainfall hours and 654.1 mm total rainfall depth. As seen from Figure B-2(iii)(a), May had modal rainfall in the midnight hour (39 hrs), but this did not translate into a high percentage of rainfall (4.3%). While rainfall hours were generally evenly distributed across all the other times of the day with the exception of 1100 hrs (20 hrs), peaks were found in the late afternoon at 1700 hrs (35 hrs), early evening at 1900 hrs (37 hrs), and late night at 2300 hrs (36 hrs).

      From Figure B-2(iii)(b), peak rainfall percentage was at 1600 hrs (7%) even though the corresponding rainfall hours (32 hrs) was not particularly high. This indicated contribution from late afternoon higher-intensity events. 1700 hrs had the second-highest rainfall percentage (5.9%). This was followed by 1800 hrs (5.4%) and 1900 hrs (5.7%). A lower peak rainfall percentage was found at 0800 hrs (5.7%), despite a moderate 29 rainfall hours, hinting at possible morning heavy rainfall events during this time of day.

(a) Total hours of rainfall occurrence   **(b) Percent (%) total rainfall depth**
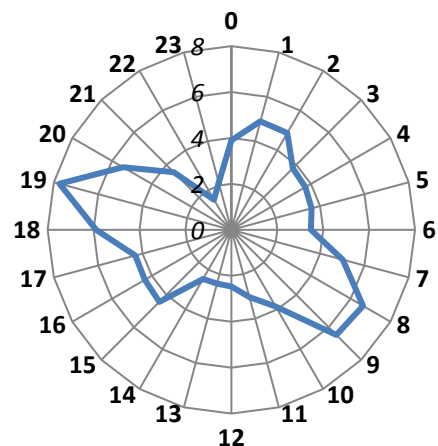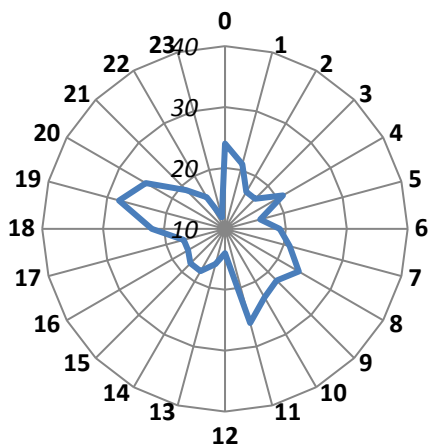
(i) March
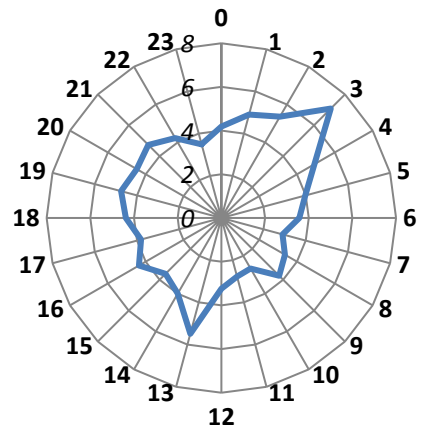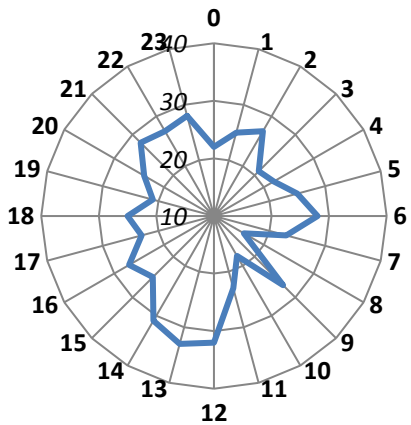
(ii) April
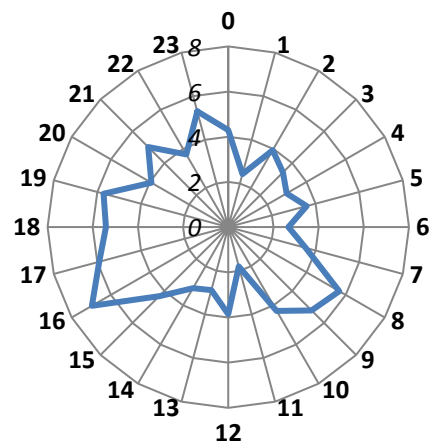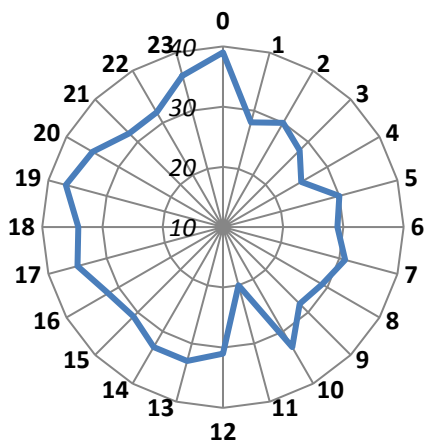
(iii) May

Figure B-2. Autumn rainfall patterns by time-of-day (perimeter of each chart) from midnight (0) to 11 PM (23) as: (a) Total hours of rainfall occurrence; (b) Percent (%) total rainfall depth, for (i) Mar, (ii) Apr and (iii) May. Note: Radial y-axis scales vary according to the range   of   values   calculated.

422

3. Winter rainfall hours and percentages

Figure B-3 presents the rainfall hours and percentages for the summer months of June, July and August.

<u>*June*</u>

June had 982 total rainfall hours and 992.8 mm total rainfall depth. From Figure B-3(i)(a), June had low variation in rainfall hours (s.d. 4.0 hrs), meaning that occurrence of rainfall was relatively evenly distributed through all hours of the day. From Figure B-3(i)(b), there also appeared to be low variation in the rainfall percentages. Nevertheless, slightly higher rainfall percentages were found at mid-morning 1000 hrs (5.0%); mid-day at 1300 hrs (4.9%), late afternoon at 1600 hrs (4.8%) and evening at 1900 hrs (5.0%). Low rainfall percentages were found at the late-night and midnight hours of 2300 hrs (3.0%) and 0000 hrs (2.7%).

<u>*July*</u>

July had 953 total rainfall hours and 684 mm total rainfall depth. As seen in Figure B-3(ii)(a), July saw more variation in rainfall hours than in June (see Figure B-3(i)(a)). Multiple rainfall hour peaks were seen at mid-morning at 1000 hrs (45 hrs), early evening at 1700 hrs (48 hrs), evening at 1900 hrs (48 hrs) and night at 2100 hrs (48 hrs). Lowest rainfall hours were found at noontime 1200 hrs (30 hrs).

As shown in Figure B-3(ii)(b), the rainfall percentages for July showed some contrasts, with peaks found at 1700 hrs (5.6%) and 1800 hrs (5.7%) and 2100 hrs (5.3%), showing some good temporal correlation with rainfall hours. However, moderately high rainfall percentages were also found at 2300 hrs (4.9%) at rather modest rainfall hours (39 hrs) and 0400 hrs (5.6%) for 43 rainfall hours. These indicate the occurrence of slightly higher rainfall rates during these nocturnal hours.
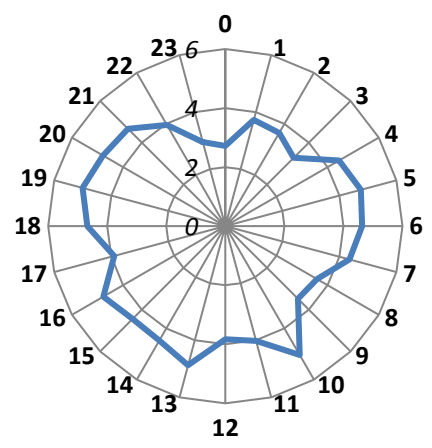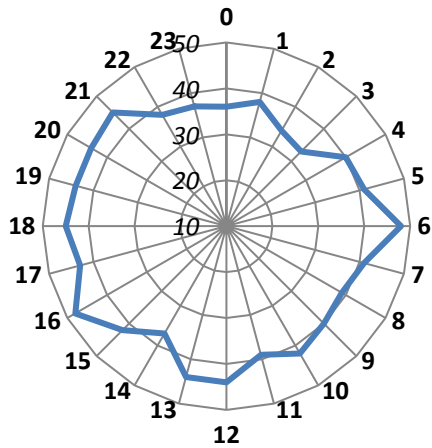
August

August had 1152 total rainfall hours and 1001.8 mm total rainfall depth. From Figure B-3(iii)(a) and (ii), August rainfall, showed more variations in both rainfall hours and rainfall percentages compared to Jul and Jun. A single peak was found at 2000 hrs (71 hrs) with lower "shoulders" at 1900 hrs (60 hrs) and 2100 hrs (57 hrs). Minimum rainfall hours were found at 1200 hrs (25 hours) and preceding it at 1100 hrs (38 hrs).

As seen in Figure B-3(iii)(b), peak rainfall percentage occurred at 1900 hrs (6.6%) with "shoulders" of 1800 hrs (5.8%) and 2000 hrs (6.1%). However, there was another peak rainfall percentage at 2300 hrs (6.4%) which was not reflected in the rainfall hours at the same time (51 hrs), and peaks at 0300 hrs (5.4%) and 0400 hrs (5.1%) that were also not clearly discernible from rainfall hours of 48 hours for both these times. These indicate the occurrence of heavy rainfall events during these late-night and nocturnal hours. The distribution of peak rainfall percentages was somewhat like those for July, albeit with greater variation in values.
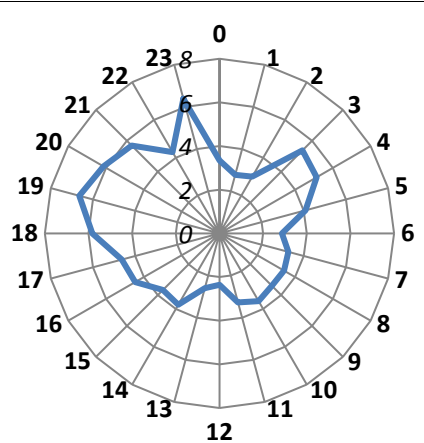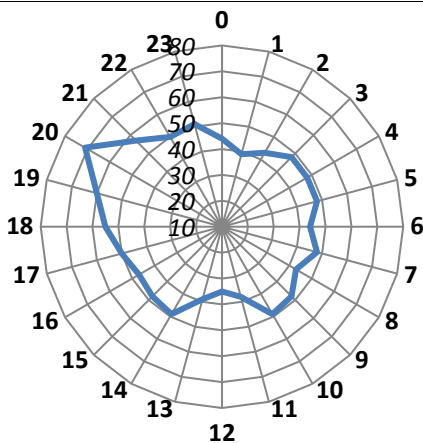
(i) Total hours of rainfall occurrence	(ii) Percent (%) total rainfall depth

(i) June
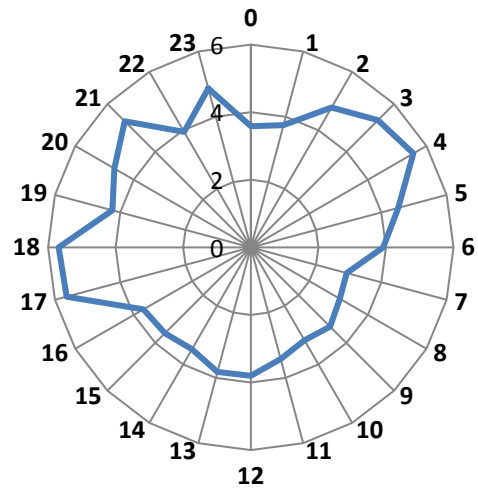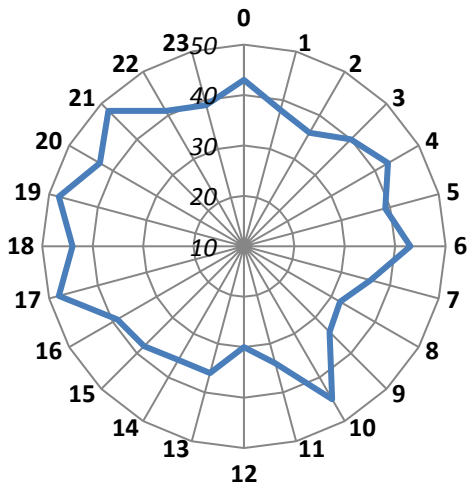
(ii) July

(iii) August

<u>Figure B-3.</u> Winter rainfall patterns by time-of-day (perimeter of each chart) from midnight (0) to 11 PM (23) as: (a) Total hours of rainfall occurrence; (b) Percent (%) total rainfall depth, for (i) Jun, (ii) Jul and (iii) Aug. Note: Radial y-axis scales vary according to the range of values calculated.

4. Spring rainfall hours and percentages

Figure B-4 presents the rainfall hours and percentages for the summer months of September, October and November.

<u>*September*</u>

September had 1200 total rainfall hours and 862.6 mm total rainfall depth. As seen in Figure B-4(i)(a), September rainfall exhibited rather even distribution of rainfall hours with some slight variations. Peak rainfall hour was 1300 hrs (59 hrs) which remained relatively high in the following afternoon hours, at 1400 hrs (57 hrs), 1500 hrs (57 hrs) and late afternoon at 1700 hrs (54 hrs). Moderately high rainfall hours were also seen in the evening time at 1900 hrs (53 hrs), 2000 hrs (54 hrs) and 2100 hrs (52 hrs). Similarly, high values were seen for the nocturnal hours of 0000 hrs (54 hrs) and 0100 hrs (56 hrs). Minimum rainfall hours occurred at 0400 hrs (36 hrs).

From Figure B-4(i)(b), rainfall percentage appeared to vary more compared to rainfall hours. Peak rainfall occurred in the early afternoon hours of 1300 hrs (7.0%), 1400 hrs (6.5%) and 1500 hrs (5.9%). A secondary peak during the evening hours of 1900 hrs (5.6%), 2000 hrs (5.7%) and 2100 hrs (5.2%). Rainfall minima were found just before midnight at 2300 hrs (2.7%) and in the early morning hours at 0400 hrs (2.6%), 0500 hrs (2.7%) and 0600 hrs (2.6%).

<u>*October*</u>

October had 985 total rainfall hours and 917.5 mm total rainfall depth. As seen in Figure B-4(ii)(a), rainfall hours peaks in October appeared later in the day compared to September. While a clear night-time peak at 2100 hrs (58 hrs) followed by a rather high value at 2200 hrs (52 hrs) were found, there was another lower peak earlier in the day during the late afternoon hour of 1800 hrs (54 hrs) that was followed by a high at 1900 hrs (50 hrs).

As seen in Figure B-4(ii)(b), rainfall percentages showed a clustering of peak values in the late afternoon and early evening hours. Peaks at 1600 hrs (6.7%) and 1900 hrs (6.6%) were found, with quite high values seen in the intervening hours as well. A lower peak at 2100 hrs (5.8%) corresponding with the rainfall hours peak was also found. Minimum rainfall percentages were found in the morning at 0800 hrs and 1200 hrs (both 2.4%).
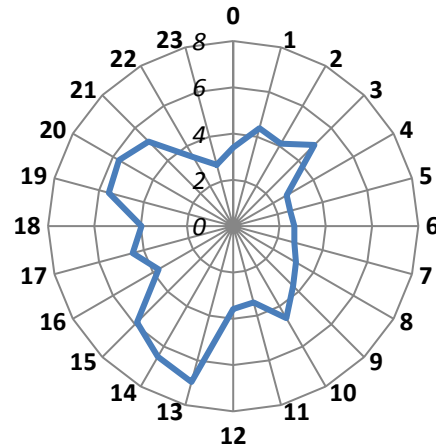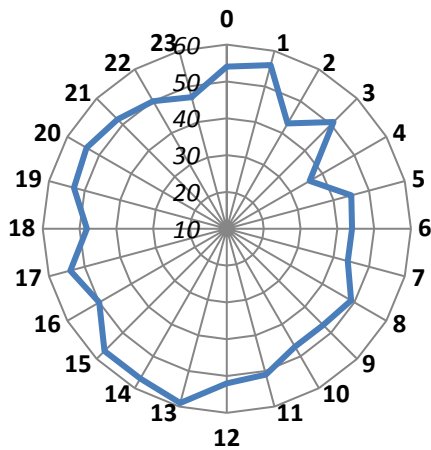
November

November had 851 total rainfall hours and 1045 mm total rainfall depth. As seen from Figure B-4(iii)(a), Nov peak rainfall hours were found in the late morning at 1000 and 1100 hrs (both 44 hrs), in contrast to Sep and Oct. Another peak rainfall hour time was late afternoon; at 1700 hrs (42 hrs) with high "shoulders" at 1600 hrs and 1800 hrs (both 40 hrs). A trio of moderately wetter hours was also seen at 0400 hrs (40 hrs), 0500 hrs (39 hrs) and 0600 hrs (38 hrs). Lowest rainfall hours were found in the early afternoon 1400 hrs (26 hrs) and midnight 0000 hrs (28 hrs).

Examination of Figure B-4(iii)(b) found that the peak rainfall percentages showed some interesting patterns with respect to the rainfall hours. Highest rainfall percentages were found in the morning hours of 0500 hrs (5.8%) and 0600 hrs (5.3%), even though the corresponding rainfall hours were just moderately high, possibly indicating somewhat heavier rainfall events during these times of day. Late-morning peaks in rainfall percentage were also found at 1000 hrs (5.2%) and 1100 hrs (4.9%), corresponding well with the rainfall hour peaks at the same hours. Two other peaks were found in the late afternoon at 1700 hrs (5.2%) and night at 2100 hrs (5.2%). Minimum rainfall percentage of 2.5% was found at 2300 hrs.
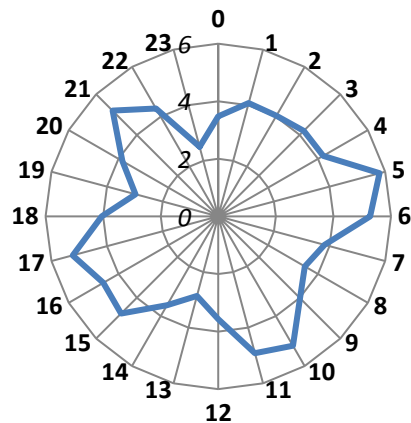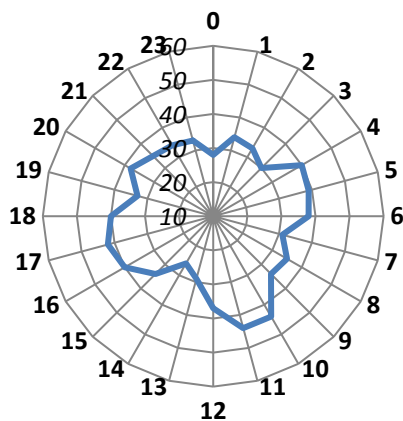
(i) Total hours of rainfall occurrence	(ii) Percent (%) total rainfall depth

(i) September
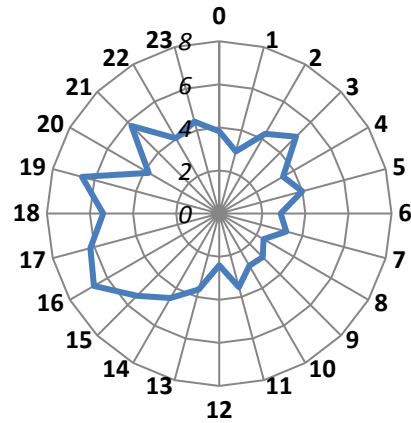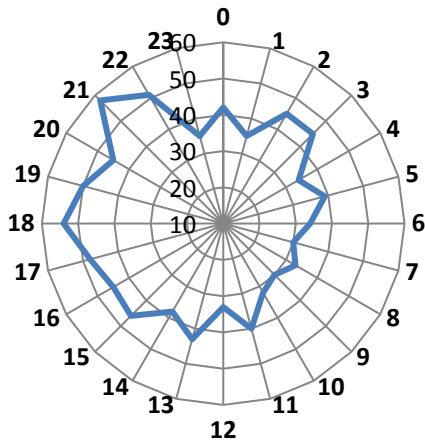
(ii) October

(iii) November

Figure B-4. Spring rainfall patterns by time-of-day (perimeter of each chart) from midnight (0) to 11 PM (23) as (a) Total hours of rainfall occurrence; (b) Percent (%) total rainfall depth, for (i) Sep, (ii) Oct and (iii) Nov. Note: Radial y-axis scales vary according to the range of values calculated.

428